

**Some pages of this thesis may have been removed for copyright restrictions.**

If you have discovered material in AURA which is unlawful e.g. breaches copyright, (either yours or that of a third party) or any other law, including but not limited to those relating to patent, trademark, confidentiality, data protection, obscenity, defamation, libel, then please read our [Takedown Policy](#) and [contact the service](#) immediately

**FUNCTIONALISATION OF ETHYLENE-PROPYLENE  
RUBBER WITH GLYCIDYL METHACRYLATE IN THE  
PRESENCE OF COMONOMER AND *IN SITU*  
COMPATIBILISATION OF PET/*f*-EPR BLENDS**

**AZHAR AHMAD**

**Doctor of Philosophy**

**ASTON UNIVERSITY**

**18 November 2008**

This copy of the thesis has been supplied on condition that anyone who consults it is understood to recognize that its copyright rest with its author and that no quotation from the thesis and no information derivative from it may be published without proper acknowledgment

# ASTON UNIVERSITY

## FUNCTIONALISATION OF ETHYLENE-PROPYLENE RUBBER WITH GLYCIDYL METHACRYLATE IN THE PRESENCE OF COMONOMER AND *IN SITU* COMPATIBILISATION OF PET/*f*-EPR BLENDS

AZHAR AHMAD  
DOCTOR OF PHILOSOPHY

### SUMMARY

The main aim of this work was two fold, firstly to investigate the effect of a highly reactive comonomer, divinylbenzene (DVB), on the extent of melt grafting of glycidyl methacrylate (GMA) on ethylene-propylene rubber (EPR) using 2,5-dimethyl-2,5-bis-(tert-butyl peroxy) hexane (Trigonox 101, T101) as a free radical initiator, and to compare the results with a conventional grafting of the same monomer on EPR. To achieve this, the effect of processing conditions and chemical composition including the concentration of peroxide, GMA and DVB on the extent of grafting was investigated. The presence of the comonomer (DVB) in the grafting process resulted in a significant increase in the extent of the grafting using only a small concentration of peroxide. It was also found that the extent of grafting increased drastically with increasing the DVB concentration. Interestingly, in the comonomer system, the extent of the undesired side reaction, normally the homopolymerisation of GMA (polyGMA) was shown to have reduced tremendously and in most cases the level of polyGMA was immeasurable in the samples. Compared to a conventional EPR-g-GMA<sub>CONV</sub> (in the absence of a comonomer), the presence of the comonomer DVB in the grafting system was shown to result in more branching and crosslinking (shown from an increase in melt flow index (MFI) and torque values) and this was paralleled by an increase in DVB concentration. In contrast, the extent of grafting in conventional system increased with increasing the peroxide concentration but the level of grafting was much lower than in the case of DVB. Homopolymerisation of GMA and excessive crosslinking of EPR became dominant at high peroxide concentration and this reflects that the side reactions were favorable in the conventional grafting system.

The second aim was to examine the effect of the *in-situ* functionalised EPR when used as a compatibiliser for binary blends. It was found that blending PET with functionalised EPR (*f*-EPR) gave a significant improvement in terms of blend morphology as well as mechanical properties. The results showed clearly that, blending PET with *f*-EPR<sub>DVB</sub> (prepared with DVB) was much more effective compared to the corresponding PET/*f*-EPR<sub>CONV</sub> (without DVB) blends in which *f*-EPR<sub>DVB</sub> having optimum grafting level of 2.1 wt% gave the most pronounced effect on the morphology and mechanical properties. On the other hand, blends of PET/*f*-EPR<sub>DVB</sub> containing high GMA/DVB ratio was found to be unfavorable hence exhibited lower tensile properties and showed unfavorable morphology. The presence of high polyGMA concentration in *f*-EPR<sub>CONV</sub> was found to create damaging effect on its morphology, hence resulting in reduced tensile properties (e.g. low elongation at break). However, the use of commercial terpolymers based on ethylene-methacrylate-glycidyl methacrylate (EM-GMA) or a copolymer of ethylene-glycidyl methacrylate (E-GMA) containing various GMA levels as compatibilisers in PET/EPR blends was found to be more efficient compared to PET/EPR/*f*-EPR blends with the former blends showing finer morphology and high elongation at break. The high efficiency of the terpolymers or copolymers in compatibilising the PET/EPR blends is suggested to be partly, higher GMA content compared to the amount in *f*-EPR and due to its low viscosity.

**Keywords:** EPR, GMA, PET, functionalisation, comonomer, divinylbenzene, grafting, blending, terpolymer, copolymer.

## **ACKNOWLEDGEMENTS**

*First, I would like to sincerely acknowledge my supervisor, Dr Sahar Al-Malaika. I am grateful for all her valuable guidance, constructive suggestions and comments I have received whilst researching and writing up this thesis. This thesis could not have been completed without her guidance and constructive criticism.*

*Special thanks go to the Malaysian Rubber Board for awarding a scholarship to me which has enabled me to carry out this research and subsequently complete my thesis.*

*I would also like to extend my sincere and genuine thanks to Dr Hussam Sheena for his useful technical support and discussion at various stages during the research. A special thanks is dedicated to Dr Khalid Doudin for his assistance in performing the NMR analysis for samples produced in this work and his help and guidance for interpreting these results. I wish also to express my thanks to the other members of the Polymer Processing and Performance Research Unit, Dr Eddyanto, Mark Lay, Elizabeth Lakin and Cezary Lewucha for their support and useful discussions.*

*Last but not least, I would like to dedicate this thesis to the memory of my beloved wife Azura Mohamed Ibrahim, to my lovely children, Ikhwan, Ikram, Fatiha, Akmal and Ikhsan and my parents for their support throughout all these years.*

## List of Content

Thesis Title	Page
Summary	i
Acknowledgements	ii
List of Content	iii
List of Schemes	iv
List of Tables	viii
List of Figures	ix
List of Abbreviations	xii
Symbols	xvii
	xix

<b>Chapter 1</b>	<b>Introduction</b>	<b>Page</b>
1.0	Background	1
1.2	Polymer functionalisation with reactive monomers	2
1.2.1	Grafting Glycidyl methacrylate (GMA) onto polymers	2
1.2.2	Grafting Maleic anhydride (MA) onto polymers	5
1.2.3	Grafting Oxazoline (OXA) onto polymers	5
1.3	Free radical grafting reaction process and mechanism	6
1.4	Grafting reactions in the presence of co-monomers	11
1.5	Reactive processing	13
1.6	Polymer blends	14
1.6.1	Compatibilisation of immiscible polymer blends	15
1.7	Types of compatibilisers	19
	(i) <i>In situ</i> formed copolymers	19
	(ii) Copolymers added separately (Non-reactive copolymers)	19
	(iii) Addition of reactive copolymers	19
1.8	Thermodynamic consideration	23
1.9	PET profile	24
1.10	EPR profile	25
1.11	Aim and objectives of this study	26

<b>Chapter 2</b>	<b>Experimental and Analytical Techniques</b>	
2.1	Materials	28
2.1.1	Polymers	28
2.1.2	Monomer and comonomer	29
2.1.3	Initiators	30
2.1.4	Solvents and additives	31
2.2	Processing and sample preparation	32
2.2.1	Polymer functionalisation by reactive processing	32
2.2.2	Functionalisation of EPR with GMA in absence and presence of the comonomer divinyl benzene (DVB)	34
2.2.3	Physical and reactive blending of PET with functionalised EPR or terpolymers	35
2.3	Purification of functionalised EPR	35

2.4	Fractionation of PET/f-EPR blends by sequential solvent extraction for characterisation of interfacial reaction	36
2.5	Films and plaques preparation	36
	(i) Films preparation for FTIR	36
	(ii) Plaques preparation for DMA and tensile measurement	37
2.6	Synthesis of side reaction products	37
2.6.1	Homopolymerisation of GMA in chloroform	37
2.6.2	Homopolymerisation of DVB in hexane	37
2.6.3	Copolymerisation of GMA and DVB in hexane	38
2.7	Characterisation of processed polymers and blends	38
2.7.1	Determination of melt index	38
2.7.2	Determination of insoluble gel	39
2.7.3	Solubility Test	39
2.8	Determination of GMA grafting degree by titration and calibration against IR	40
2.9	Experimental error	42
2.10	FTIR Spectroscopy	45
2.11	$^1\text{H}$ and $^{13}\text{C}$ NMR spectroscopy	46
2.11.1	$^1\text{H}$ NMR	46
2.11.2	$^{13}\text{C}$ NMR	46
2.11.3	2D $^1\text{H}$ - $^{13}\text{C}$ HSQC	47
2.11.4	2D $^1\text{H}$ - $^{13}\text{C}$ HMBC	47
2.11.5	CP/MAS $^{13}\text{C}$ NMR spectroscopy	48
2.12	Testing	48
2.12.1	Tensile test	48
2.12.2	Dynamic Mechanical Properties (DMA)	48
2.12.3	Scanning Electron Microscopy (SEM)	49

### **Chapter 3      Functionalisation of Ethylene-Propylene Rubber with Glycidyl Methacrylate**

3.1	Objective and methodology	68
3.2	Results	72
3.2.1	Separation of reaction products and characterisation on the grafting system	72
3.2.2	Characterisation of side reaction products of EPR-g-GMA in the absence and presence of the comonomer DVB	73
	(i) Characterisation of polyGMA	73
	(ii) Characterisation of polyDVB	78
	(iii) Characterisation of GMA-co-DVB	81
3.2.3	Characterisation of purified EPR-g-GMA by FTIR and NMR method	84
3.2.4	Grafting GMA onto EPR in the absence of DVB	85
3.2.4.1	Effect of Initiator (T101) concentration on the grafting reaction in the absence of DVB	85
3.2.5	Grafting GMA onto EPR in the presence of DVB	87
		87

3.2.5.1	Effect of T101 concentration on grafting system in the presence of DVB	
3.2.5.2	Effect of processing temperature on grafting degree	89
3.3	Discussion	90
3.3.1	Melt grafting of GMA in absence of a comonomer	90
3.3.2	Melt grafting of GMA in EPR in presence of the Comonomer DVB and comparison with grafting in its absence	92
3.3.3	Mechanism of GMA grafting on EPR in the presence of comonomer DVB	99
3.3.4	Characterisation of the synthesised homo and co-polymers	102
3.3.4.1	Integration of $^1\text{H}$ NMR of polyGMA and $f\text{-EPR}_{\text{CONV}}$	103
3.3.4.2	Stereochemical sequence of $1\text{-CH}_2$ and $\alpha\text{-CH}_3$	103
3.3.5	Characterisation of the microstructure of the GMA grafted in $f\text{-EPR}_{\text{CONV}}$	106
3.3.6	Characterisation of purified $\text{EPR-g-GMA}_{\text{DVB}}$ by NMR	110
<b>Chapter 4</b>	<b>Reactive Compatibilisation of PET/EPR Blends</b>	
4.1	Objective and methodology	158
4.2	Results	160
4.2.1	Physical blends of PET/EPR	160
4.2.2	PET/EPR-g-GMA <sub>CONV</sub> (without comonomer)	162
4.2.2.1	Effect of Grafting level on torque characteristics	162
4.2.2.2	Mechanical properties of reactive PET/EPR-g-GMA <sub>CONV</sub> Blends	163
	(i) Morphology observation	164
	(iii) ii) Dynamic Mechanical Analysis (DMA)	164
4.2.2.3	Effect of polyGMA on PET/EPR-g-GMA <sub>CONV</sub> blends	165
4.2.2.4	Effect of PET/EPR-g-GMA <sub>CONV</sub> blend composition on torque characteristics, mechanical properties and morphology	166
4.2.3	PET/EPR-g-GMA <sub>DVB</sub> blends (with comonomer)	168
	(i) Grafting level	168
	(ii) Blend ratio	170
	(iii) DVB concentration	172
4.2.4	Solubility test (Molau Test)	172
4.3	Discussion	174
4.3.1	Effect of grafting level on blend properties	174
4.3.2	Effect of polyGMA in $f\text{-EPR}$ on the blend properties	178
4.3.3	Effect of DVB concentration on the blend properties	180
4.3.4	Effect of blend concentration on the blend properties	182
4.3.5	Interfacial analysis of PET/EPR-g-GMA in blends with FTIR	184
4.3.6	Mechanism of reactive blending in presence of DVB	185

<b>Chapter 5</b>	<b>PET Blends with Terpolymers and Copolymer</b>	
5.1	Objective and methodology	227
5.2	Results	231
5.2.1	Effect of different GMA content on compatibility of PET/EPR/EM-GMA blends	231
5.2.2	Effect of viscosity of the compatibiliser on blends properties	232
5.2.3	The effect of terpolymers compared to a copolymer on the extent of compatibilisation of PET/EPR ternary blends	234
5.2.4	Effect of <i>f</i> -EPR and terpolymer on compatibilisation of PET/EPR ternary blends	236
5.3	Discussion	238
5.3.1	Effect of GMA content in commercial terpolymers on compatibilising efficiency of PET/EPR/compatibiliser ternary blends	239
5.3.2	Effect of viscosity of terpolymers on compatibilising efficiency of PET/EPR blends	240
5.3.3	The effect of a copolymer (E-GMA <sub>8</sub> ) and terpolymer (EM-GMA <sub>8</sub> ) as compatibilisers for PET/EPR blends	241
5.3.4	Comparison of the effect of synthesised <i>f</i> -EPR and the commercial terpolymer on compatibilisation of PET/EPR blends	241
<b>Chapter 6</b>	<b>Conclusions and Recommendation for Further Work</b>	
6.1	Conclusions	259
6.2	Recommendation for further work	263



## List of Schemes

	<b>Page</b>	
Scheme 1.1	Simplified overall scheme of free-radical grafting onto polymer backbone	7
Scheme 1.2	Radical generation reactions from Trogonox-101	10
Scheme 2.1	Methodology for grafting GMA onto EPR in the absence of DVB	50
Scheme 2.2	Methodology for grafting GMA onto EPR in the presence of DVB	51
Scheme 2.3	PET/EPR or terpolymer blends	52
Scheme 2.4	Purification of GMA grafted EPR in the absence or presence of DVB	53
Scheme 2.5	Homopolymerisation of GMA in chloroform	54
Scheme 2.6	Homopolymerisation of DVB in hexane	55
Scheme 2.7	Homopolymerisation of GMA-co-DVB in Hexane	56
Scheme 2.8	Flow chart for analysis of EPR-g-GMA by titration	57
Scheme 3.1	Methodology for Grafting GMA onto EPR in the absence of DVB	116
Scheme 3.2	Methodology for grafting GMA onto EPR in the presence of DVB	117
Scheme 3.3	Mechanism of grafting reactions	101
Scheme 3.4	Graft composition in EPR-g-GMA <sub>CONV</sub>	107
Scheme 3.5	Length of the grafted GMA sequence in EPR-g-GMA <sub>CONV</sub>	108
Scheme 3.6	The structure of the grafted GMA on the EPR-g-GMA <sub>CONV</sub>	110
Scheme 4.1	Methodology for compatibilisation of PET/EPR Blends	189
Scheme 4.2	Sequential solvent fractionation of PET/f-EPR blends	190
Scheme 4.3	Possible reactions during compatibilisation between PET with EPR-g-GMA	188
Scheme 5.1	Methodology for compatibilisation of PET/EPR/compatibiliser blends	243

## List of Tables

<b>Chapter 1</b>		Page
Table 1.1	Functionalisation of GMA onto polymers	3
Table 1.2	Examples of common compatibilising reactions between functionalised blend constituents	20
Table 1.3	Compatibilisation through the reaction of functionalised blend components	22
<b>Chapter 2</b>		
Table 2.1	Polymers used in the experiments	28
Table 2.2	Compatibilisers used in the PET blends	29
Table 2.3	Monomer and comonomer used in the experiments	30
Table 2.4	Peroxides used in the experiments	30
Table 2.5	Solvents and chemical additive used in the experiments	31
Table 2.6	Standard deviation in the grafting degree measurement by titration (conventional system)	44
Table 2.7	Standard deviation in the grafting degree measurement by titration (DVB system)	44
<b>Chapter 3</b>		
Table 3.1A	Composition and processing conditions used in the functionalisation of EPR with GMA (GMA/T101) System,	70
Table 3.1B	Composition and processing conditions used in the functionalisation of EPR with GMA in the presence of comonomer, DVB	71
Table 3.2	Solubility of monomer and comonomers of GMA and DVB, homopolymers and polymerised product typically found in the EPR grafting system.	73
Table 3.3a	<sup>1</sup> H NMR chemical shifts, $\delta$ (ppm), and signal assignments of GMA and polyGMA in CDCl <sub>3</sub> ,	75
Table 3.3 b	<sup>13</sup> C NMR chemical shifts, $\delta$ (ppm), and signal assignments of GMA and polyGMA in CDCl <sub>3</sub>	75
Table 3.4a	<sup>1</sup> H NMR chemical shifts, $\delta$ (ppm), and signal assignments of DVB in CDCl <sub>3</sub>	79
Table 3.4b	<sup>13</sup> C NMR chemical shifts, $\delta$ (ppm), and signal assignments of DVB in CDCl <sub>3</sub> .	79
Table 3.5	IR absorption characteristic of DVB and PolyDVB,	80
Table 3.6	IR absorption characteristic of PolyGMA, PolyDVB and GMA-co-DVB	81
Table 3.7	IR absorption characteristic of PolyGMA, PolyDVB and GMA-co-DVB	82
Table 3.8	<sup>13</sup> C solid state NMR chemical shifts, $\delta$ (ppm), and signal assignments of GMA in polyGMA and in GMA-co-DVB in CDCl <sub>3</sub>	83
Table 3.9	Half life ( $t_{1/2}$ ) of peroxide Trigonox 101	99
Table 3.10	Calculated % of different stereochemical sequences of poly-GMA	105

Table 3.11	Stereochemical sequence calculation based on of 1-CH <sub>2</sub> and α-CH <sub>3</sub> in PolyGMA	105
Table 3.12	Calculated % of different stereochemical sequences of poly-GMA and EPR-g-GMA	107
Table 3.13	Amount of GMA molecule grafted in straight chain at different solvent and temperature	114
<b>Chapter 4</b>		
Table 4.1	Functionalised EPR used in the blends	159
Table 4.2	PET/EPR blends composition	160
Table 4.3	Elongation at break of physical blends	161
Table 4.4	Effect of blend composition of physical PET/EPR blends on dynamic mechanical properties	162
Table 4.5	Elongation at break of PET/EPR-g-GMA <sub>CONV</sub> blends at various GMA content	164
Table 4.6	Effect of MFI values on dynamic mechanical properties of PET/EPR-g-GMA <sub>CONV</sub> 70/30 w/w % blends	165
Table 4.7	Tensile and elongation at break of PET/EPR-g-GMA <sub>CONV</sub> blends at various blend ratios	167
Table 4.8	Effect of blend compositions on dynamic mechanical properties of PET/EPR-g-GMA <sub>CONV</sub> blends	168
Table 4.9	Tensile and elongation at break of PET/EPR-g-GMA <sub>DVB</sub> blends at various blend ratios	169
Table 4.10	Effect of grafting level on dynamic mechanical properties of PET/ <i>f</i> -EPR <sub>DVB</sub> blends	169
Table 4.11	Tensile strength and elongation at break of DVB containing blend at various blend ratios	171
Table 4.12	Effect of blend composition on dynamic mechanical properties of PET/EPR-g-GMA <sub>DVB</sub> blends	172
Table 4.13	Solubility test according to Molau test	273
<b>Chapter 5</b>		
Table 5.1	Chemical structure of polymers used in the PET blends	229
Table 5.2	PET/EPR blends compatibilised with terpolymer with different contents of glycidyl methacrylate (GMA)	130
Table 5.3	Functionalised EPR used in PET blends and the PET blends compatibilised with <i>f</i> -EPR	230
Table 5.4	Elongation at break of PET/EPR-g-GMA <sub>CONV</sub> blends at various GMA content	231
Table 5.5	<i>T<sub>g</sub></i> and storage modulus of PET and EPR phase of PET/EPR compatibilised with EM-GMA <sub>1(8)</sub> and EM-GMA <sub>8(6)</sub> 70/10/20 w/w %	232
Table 5.6	Elongation at break of PET/EPR/terpolymer blends at different terpolymer viscosity	233
Table 5.7	<i>T<sub>g</sub></i> and storage modulus of PET and EPR phase of PET/EPR compatibilised with EM-GMA <sub>8(6)</sub> and EM-GMA <sub>9(85)</sub>	234
Table 5.8	Elongation at break of PET/EPR compatibilised with terpolymer and copolymer	235
Table 5.9	<i>T<sub>g</sub></i> and storage modulus of PET and EPR phase of PET/EPR compatibilised with E-GMA <sub>8(5)</sub> and EM-GMA <sub>8(6)</sub>	235

Table 5.10	Elongation at break of PET/EPR compatibilised with terpolymer and $f$ -EPR <sub>CONV</sub> or $f$ -EPR <sub>DVB</sub>	237
Table 5.11	$T_g$ storage modulus of PET and EPR phase of PET/EPR compatibilised with $f$ -EPR or terpolymer	238
Table 5.12	Characteristics of $f$ -EPR and terpolymer	242

## List of Figures

<b>Chapter 1</b>		Page
Figure 1.1	Chemical structure of Glycidyl methacrylate	1
Figure 1.2	Chemical structure of Maleic Anhydride	5
Figure 1.3	Chemical structure of Oxazoline	6
Figure 1.4	Chemical structure of Ricinoloxazoline maleinate	6
Figure 1.5	Chemical structure of Poly(ethylene terephthalate)	25
Figure 1.6	Chemical structure of Ethylene-propylene rubber	26
<b>Chapter 2</b>		
Figure 2.1	FTIR spectrum of unmodified EPR	58
Figure 2.2	FTIR spectrum of virgin PET	58
Figure 2.3	FTIR spectrum of neat GMA	59
Figure 2.4	FTIR spectrum of neat DVB	59
Figure 2.5	FTIR spectrum of neat peroxide T101	60
Figure 2.6	FTIR spectrum of AIBN	60
Figure 2.7	FTIR spectrum of synthesised polyGMA	61
Figure 2.8	FTIR spectrum of synthesised polyDVB	61
Figure 2.9	FTIR spectrum of synthesised GMA-co-DVB	62
Figure 2.10	Area boundaries for absorption peak area calculation of GMA in functionalised EPR	63
Figure 2.11	FTIR spectrum of pressed film of purified EPR-g-GMA before and after titration	64
Figure 2.12	FTIR spectrum of EPR-g-GMA before and after reaction with trichloroacetic acid	65
Figure 2.13	FTIR spectrum of purified EPR-g-GMA before and after titration	66
Figure 2.14	Calibration curve established from titration against FTIR area ratio	67
<b>Chapter 3</b>		
Figure 3.1	FTIR spectra of synthesised polyGMA and neat GMA	118
Figure 3.2	$^1\text{H}$ NMR Spectra of GMA in $\text{CDCl}_3$	119
Figure 3.3	$^1\text{H}$ NMR Spectra of polyGMA in $\text{CDCl}_3$	120
Figure 3.4	$^{13}\text{C}$ NMR Spectra of GMA in $\text{CDCl}_3\text{H}$ (A) and $^{13}\text{C}$ HMBC NMR of GMA in $\text{CDCl}_3$ (B)	121
Figure 3.5	$^{13}\text{C}$ NMR Spectra of p-GMA in $\text{CDCl}_3$	122
Figure 3.6.	Structures of different possibilities of GMA polymerisation	123
Figure 3.7	$^1\text{H}$ NMR Spectra of DVB in $\text{CDCl}_3$	124
Figure 3.8	HSQC of poly-GMA; expansion of the 1- $\text{CH}_2$ region on bother reigns $^1\text{H}$ and $^{13}\text{C}$ , expansion	125
Figure 3.9	HMBC of poly-GMA; expansion region 1, 1- $\text{CH}_2$ and $\alpha\text{-CH}_3$ $^1\text{H}$ vis $\text{C}=\text{O}$ on $^{13}\text{C}$ , expansion Region 2	126
Figure 3.10	$^1\text{H}$ -NMR Spectra of DVB in $\text{CDCl}_3$	127
Figure 3.11	$^{13}\text{C}$ NMR Spectra of DVB in $\text{CDCl}_3$	127
Figure 3.12	Solid state $^{13}\text{C}$ NMR spectra of polyDVB	128
Figure 3.13	FTIR spectra of neat DVB and polyDVB	129
Figure 3.14	FTIR spectra of neat GMA, neat DVB and GMA-co-DVB	130

Figure 3.15	FTIR spectra of polyGMA, polyDVB and GMA-co-DVB	131
Figure 3.16A	<sup>13</sup> C NMR spectra of polyGMA in solid state	132
Figure 3.16B	<sup>13</sup> C NMR spectra of DVB-co-GMA in solid state	133
Figure 3.17	Comparison of spectra of neat GMA and EPR-g-GMA <sub>DVB</sub>	134
Figure 3.18	Comparison of spectra of purified EPR-g-GMA; purified with acetone and methanol)	134
Figure 3.19	Comparison of spectra of purified EPR-g-GMA <sub>CONV</sub> (blue) and EPR-g-GMA <sub>DVB</sub> (red) GMA/DVB=9/1	135
Figure 3.20	<sup>1</sup> H-NMR spectra of EPR in in CDCl <sub>3</sub>	136
Figure 3.21	<sup>13</sup> C NMR spectra of EPR (ethylene:propylene 8:2) in CDCl <sub>3</sub>	137
Figure 3.22	<sup>1</sup> H-NMR GMA-g-EPR <sub>CONV</sub> (unpurified) in CDCl <sub>3</sub>	137
Figure 3.23	Effect of peroxide concentrations on torque behaviour, MFI and gel content in EPR-g-GMA <sub>CONV</sub>	138
Figure 3.24	Effect of GMA concentration on torque characteristic, MFI value, gel content and GMA grafting level in EPR-g-GMA <sub>CONV</sub> system	139
Figure 3.25	Effect of processing time on GMA grafting and polyGMA level in conventional EPR-g-GMA <sub>CONV</sub> system	140
Figure 3.26	Torque behaviour at various peroxide concentrations in EPR-g- GMA <sub>DVB</sub> system	141
Figure 3.27	Torque behaviour at various DVB concentrations in EPR-g-GMA <sub>DVB</sub> system	142
Figure 3.28	Effect of DVB concentrations on extent of GMA grafting degree and formation of polyGMA in EPR-g-GMA <sub>DVB</sub> samples	143
Figure 3.29	Effect of [GMA] <sub>i</sub> concentrations in EPR-g-GMA <sub>DVB</sub> system on processing characteristic and the extent of grafting and homopolymerisation	144
Figure 3.30	Effect of processing time on grafting degree of EPR-g-GMA <sub>DVB</sub> samples	145
Figure 3.31	Effect of processing temperature on torque, GMA grafting and polyGMA level in EPR-g-GMA <sub>DVB</sub> samples	146
Figure 3.32	Comparison of the effect of peroxide concentration on torque behaviour and MFI values of polymer in the absence or presence of GMA	147
Figure 3.33	Comparison the effect of T-101 concentration on MFI values, gel content, grafting level and polyGMA in grafting systems with DVB and without DVB.	148
Figure 3.34	Comparison of grafting degree, torque and MFI values as a function of peroxide concentration at various comonomer concentrations and without comonomer	149
Figure 3.35	Effect of initial GMA concentrations on GMA grafting level in EPR-g-GMA <sub>CONV</sub> and EPR-g-GMA <sub>DVB</sub>	150
Figure 3.36	Comparison of the kinetic of grafting reaction in conventional and comonomer (DVB) system	151
Figure 3.37	Analysis of EPR-g-GMA <sub>DVB</sub> processed and purified samples, taken out at different processing times	152
Figure 3.38	Schematic representing of stereochemical configuration of GMA grafted on EPR (EPR-g-GMA <sub>CONV</sub> )	153
Figure 3.39	<sup>1</sup> H-NMR of EPR-GMA <sub>DVB</sub> in CDCl <sub>3</sub> at room temperature	154
Figure 3.40	<sup>1</sup> H-NMR of EPR-GMA <sub>DVB</sub> in DMSO-d <sub>6</sub> at room	154

	temperature	
Figure 3.41	<sup>1</sup> H-NMR of EPR-g-DVB in C <sub>2</sub> D <sub>2</sub> Cl <sub>4</sub> at room temperature	155
Figure 3.42	<sup>1</sup> H-NMR of EPR-g-DVB in C <sub>2</sub> D <sub>2</sub> Cl <sub>4</sub> at 135°C	155
Figure 3.43	<sup>1</sup> H-NMR of EPR-g-DVB, in CDCl <sub>3</sub> at 57°C	156
Figure 3.44	<sup>1</sup> H-NMR of EPR-g-GMA <sub>DVB</sub> , in C <sub>6</sub> D <sub>4</sub> Cl <sub>2</sub> at 57°C	156
Figure 3.45	<sup>1</sup> H-NMR of EPR-g-DVB in C <sub>6</sub> D <sub>4</sub> Cl <sub>2</sub> at 135°C	157
<b>Chapter 4</b>		
Figure 4.1	Effect of blend composition in physical blends of PET/EPR on torque characteristics	191
Figure 4.2	Effect of blend composition of physical blends of PET/EPR on tensile properties	191
Figure 4.3	Effect of blend composition of physical blends of PET/EPR on morphology	192
Figure 4.4	Dynamic mechanical properties of PET, EPR and physical blend of PET/ EPR 70/30 w/w	193
Figure 4.5	Tan delta of PET/ EPR physical blend at various blend composition	194
Figure 4.6	Storage modulus of PET/ EPR physical blend at various blend composition	195
Figure 4.7	Torque curves of the PET/ <i>f</i> -EPR <sub>CONV</sub> blends 70/30 w/w	196
Figure 4.8	Stress–Strain (σ/ε) curves of virgin PET (A) and EPR (B) and comparison of physical blend with those of reactive blends of PET/ <i>f</i> -EPR 70/30 w/w %	197
Figure 4.9	Correlation between elongation to break and polyGMA content in the PET/ <i>f</i> -EPR <sub>CONV</sub> blends (70/30 w/w %)	197
Figure 4.10	Effect of grafting level on morphology of PET/ <i>f</i> -EPR <sub>CONV</sub> 70/30 w/w %	198
Figure 4.11	Effect of grafting level of <i>f</i> -EPR <sub>CONV</sub> on dynamic mechanical properties of PET/ <i>f</i> -EPR <sub>CONV</sub> blends 70/30 w/w %	199
Figure 4.12	Effect of polyGMA content in EPR-g-GMA <sub>CONV</sub> on torque, mechanical properties and morphology of PET/EPR-g-GMA <sub>CONV</sub> blends 70/30 w/w%.	200
Figure 4.13	Effect of blend composition on torque and mechanical properties of PET/EPR-g-GMA <sub>CONV</sub> blends	201
Figure 4.14	Effect of blend compositions on morphology of PET/EPR and PET/EPR-g-EPR <sub>CONV</sub>	202
Figure 4.15	Effect of blend composition on thermal properties of the PET/EPR-g-GMA <sub>CONV</sub> blends	203
Figure 4.16	Effect of grafting level on torque curves and tensile properties of PET/ <i>f</i> -EPR <sub>DVB</sub> blends 70/30 w/w	204
Figure 4.17	Effect of GMA grafted level on morphology of PET/ <i>f</i> -EPR <sub>DVB</sub> blends 70/30	205
Figure 4.18	Elongation at break of PET/EPR-g-GMA in both system (with comonomer and without comonomer) at various grafting level and polyGMA concentration	206
Figure 4.19	Effect of grafting level of EPR-g-GMA <sub>DVB</sub> on tan delta of PET/ EPR-g-GMA <sub>DVB</sub> blends 70/30 w/w %	207

Figure 4.20	Torque curves and mechanical properties of PET blended with purified $\text{EPR-g-GMA}_{\text{DVB}}$ and with addition of synthesised polyGMA	208
Figure 4.21	Effect of addition of polyGMA to $\text{PET}/f\text{-EPR}_{\text{DVB}}$ (70/30 w/w %) blend morphology	209
Figure 4.22	Effect of blend composition on torque and mechanical properties of $\text{PET}/f\text{-EPR}_{\text{DVB}}$ blends	210
Figure 4.23	Effect of blend composition on morphology of $\text{PET}/f\text{-EPR}_{\text{DVB}}$	211
Figure 4.24	Effect of blend composition on thermal properties of the $\text{PET}/f\text{-EPR}_{\text{DVB}}$	212
Figure 4.25	Comparison the morphology of reactive blends in the presence of DVB or in the absence of DVB with the physical blend at blend ratio of 70/30 w/w	213
Figure 4.26	Comparison of $\text{EPR-g-GMA}_{\text{CONV}}$ and $\text{EPR-g-GMA}_{\text{DVB}}$ rheology properties, and peroxide concentration used during the grafting reaction on the blends' torque	214
Figure 4.27	Effect of higher GMA grafting level in 70/30 w/w % $\text{PET}/f\text{-EPR}$ blends both in the presence and absence of the comonomer	215
Figure. 4.28	Phase morphology of $\text{PET}/\text{EPR-g-GMA}$ in both system (with comonomer and without comonomer) at various grafting level and polyGMA concentration	216
Figure 4.29 i	Interfacial analysis: Sample virgin EPR and virgin PET	217
Figure 4.29 ii	Interfacial analysis of $\text{PET}/\text{EPR-g-GMA}_{\text{CONV}}$ (BG55) and $\text{PET}/\text{EPR-g-GMA}_{\text{DVB}}$ (BD52) blends 70/30 w/w% by FTIR technique	218
Figure 4.30	Correlation between tensile properties and IR absorption intensity of PET present in the separated EPR fraction from $\text{PET}/f\text{-EPR}_{\text{DVB}}$ 70/30 w/w% blends at different grafting levels	219
Figure 4.31	Dynamic mechanical properties of PET, EPR, physical blend of $\text{PET}/\text{EPR}$ and reactive blends $\text{PET}/f\text{-EPR}$ 70/30 w/w%	220
Figure 4.32	Comparison of $\text{PET}/\text{EPR-g-GMA}_{\text{CONV}}$ and $\text{PET}/\text{EPR-g-GMA}_{\text{DVB}}$ blends 70/30 w/w% in terms of morphology and elongation at break	221
Figure 4.33	Effect of presence of polyGMA (unpurified in conventional or added polyGMA in DVB systems) and its absence (purified) in $\text{PET}/f\text{-EPR}_{\text{CONV}}$ and DVB blends on elongation and morphology	223
Figure 4.34	Effect of DVB concentration in $f\text{-EPR}_{\text{DVB}}$ on tensile properties of $\text{PET}/f\text{-EPR}_{\text{DVB}}$ blends 70/30 w/w%.	223
Figure 4.35	Morphology of PET blended with different type of functionalised EPRs 70/30 w/w%.	224
Figure 4.36	Comparison of PET blended with EPR in physical blends, and $\text{EPR-g-GMA}_{\text{CONV}}$ and $\text{EPR-g-GMA}_{\text{DVB}}$ in reactive blends at various rubber contents	225
Figure 4.37	Correlation between elongation at break and intensity of absorbance of PET present in separated EPR fraction from $\text{PET}/f\text{-EPR}_{\text{DVB}}$ 70/30 blends at different DVB concentrations	226



## Chapter 5

Figure 5.1	Effect of GMA content on PET/EPR/EM-GMA <sub>x</sub> ternary blends properties	244
Figure 5.2	Effect of GMA content on thermal properties of PET/EPR/EM-GMA <sub>x</sub> 70/10/20 w/w%	245
Figure 5.3.	Effect of GMA content on thermal properties (storage modulus) of PET/EPR/EM-GMA <sub>x</sub> 70/10/20 w/w %	246
Figure 5.4.	Effect of viscosity of terpolymer on PET/EPR/EM-GMA <sub>x</sub> ternary blends properties.	247
Figure 5.5	Effect of GMA content on thermal properties of PET/EPR/EM-GMA <sub>x</sub> 70/10/20 w/w %,	248
Figure 5.6	Effect of GMA content on thermal properties (storage modulus) of PET/EPR/EM-GMA <sub>x</sub> 70/10/20 w/w %	249
Figure 5.7	Effect of copolymer and terpolymer on PET/EPR/EM-GMA <sub>x</sub> ternary blends properties	250
Figure 5.8.	Effect of copolymer and terpolymer on thermal properties of PET/EPR/EM-GMA <sub>x</sub> 70/10/20 w/w % ternary blends	251
Figure 5.9	Effect of copolymer and terpolymer on thermal properties (storage modulus) of PET/EPR/EM-GMA <sub>x</sub> 70/10/20 w/w % ternary blends	252
Figure 5.10	Effect of <i>f</i> -EPR and terpolymer on PET/EPR/ <i>f</i> -EPR or EM-GMA <sub>1(8)</sub> ternary blends properties	253
Figure 5.11.	Effect of <i>f</i> -EPR and terpolymer on thermal properties of PET/EPR/ <i>f</i> -EPR or EM-GMA <sub>1(8)</sub> ternary blends properties	254
Figure 5.12	Effect of <i>f</i> -EPR and terpolymer on thermal properties (storage modulus) of PET/EPR/ <i>f</i> -EPR or EM-GMA <sub>1(8)</sub> ternary blends properties	255
Figure 5.13.	Comparison between binary PET/ <i>f</i> -EPR blends and ternary PET/EPR/ <i>f</i> -EPR blend	256
Figure 5.14	Morphology of PET/EPR blends compatibilised with different type of compatibilisers	257
Figure 5.15	Tensile properties of ternary PET/EPR compatibilised with various types of compatibilisers	258

## Abbreviations

ABS	Acrylonitrile-butadiene-styrene terpolymer
ABS-g-MA	Maleic anhydride grafted ABS
AES	Acrylonitrile-Ethylene-Propylene-Diene-Styrene
AIBN	2,2-Azobis(2-methylpropionitrile)
AM	Acrylamide
ASTM	American Society for Testing and Materials
BPO	Benzoyl peroxide
B.P	Boiling point
BR	Polybutadiene rubber
BTP	bis[1-(tert-butylperoxy)-1-methylethyl] benzene
CDCl <sub>3</sub>	Deuterated Chlorform-d1
C <sub>6</sub> D <sub>4</sub> Cl <sub>2</sub>	Deuterated dichlorobenzene-d4
DMSO-d <sub>6</sub>	Deuterated dimethyl sulfoxide-d6
CNBR	Carboxy nitrile rubber
CTC	Charge transfer complex
DHBP	2,5-Di(t-butyl-peroxy)-2,5-dimethylhexane
DTBPIB	1,3-Bis(ter-butylperoxy-isopropyl)benzene
DCM	Dichloromethane
DCP	dicumyl peroxide
DD	Dodecene
DMA	Dynamic mechanical analyser
DMAC	Dimethylacetamide
DVB	Divinylbenzene
EAA	Poly(ethylene-co-acrylic acid)
E-GMA	Ethylene glycidyl methacrylate copolymer
EMA	Poly(ethylene-comethylacrylate)
EM-GMA	Ethylene metharylate glycidyl methacrylate copolymer
EPDM	Ethylene propylene diene terpolymer
EPDM-g-GMA	Glycidyl methacrylate grafted EPDM
EPDM-SH	Mercapto-functionalized EPDM
EPR or EPM	Ethylene Propylene Rubber
EPR-g-GMA	Glycidyl methacrylate grafted Ethylene Propylene Rubber
EPR-g-GMA <sub>CONV</sub>	GMA grafted Ethylene Propylene Rubber (conventional)
EPR-g-GMA <sub>DVB</sub>	GMA grafted Ethylene Propylene Rubber (DVB)
Eqn	Equation
EVA	Poly(ethylene-co-vinyl acetate)
EVA-g-MA	Ethylene-co-vinyl acetate
EVA-SH	Mercapto-modified EVA
f-EPR	Functionalised ethylene-propylene rubber
FTIR	Fourier Transform Infrared Spectroscopy
g-GMA	Grafted GMA
GMA	Glycidyl Methacrylate
GMA-co-DVB	GMA-copolymer-DVB
HDPE	High Density Polyethylene
HI	Hydroxyethyl methacrylate-isophorone diisocyanate
HIPS	High-impact polystyrene
HMBC	Heteronuclear Multiple Bond Coherence
HSQC	Heteronuclear Single Quantum Coherence
iPP	Isotactic-polypropylene

ISO	International Organization for Standardization,
LDPE	Low Density Polyethylene
LLDPE	Linear Low Density Polyethylene
LLDPE-MA	Linear Low Density Polyethylene Maleic Anhydride
MA	Maleic Anhydride
MFI	Melt Flow Index
MI	Melt Index
MMA	Methyl methacrylate
M.P	Melting point
MR	Molar ratio
MW	Molecular Weight
NBR	Nitrile butadiene rubber
NH <sub>2</sub>	Hexamethylenediamine
NHR	N-hexylethylenediamine
NMR	Nuclear Magnetic Resonance
Nd <sub>2</sub> O <sub>3</sub>	Neodymium oxide
OPS	Oxazoline modified PS
OXA	Oxazoline
PA	Polyamide
PA-6	Polyamide 6
PA-6,6	Polyamide 6,6
PBT	Polybutylene terephthalate
PC	Polycarbonate
PCL	Polycaprolactone
PE	Polyethylene
PF	Phenol formaldehyde resin
PET	Poly(ethylene terephthalate)
PET-co-EPR-g-GMA	PET-copolymer-EPR-g-GMA
pGMA	polyGMA
PMMA	Poly(methyl methacrylate)
phr	Part per hundred resin
PPE	Poly(2,6-dimethyl methacrylate)
PP	Polypropylene
PP-g-AA	Acrylic acid grafted PP
PP-g-MA	Maleic anhydride grafted PP
PP-g-NH <sub>2</sub>	(PP-g-MA/hexamethylenediamine)
PP-g-NHR	(PP-g-MA/N-hexylethylenediamine)
PPE	Poly(2,6-dimethyl-1,4-phenylene ether)
ppm	Part per million
PPP	Polymer Processing and Performance Research Unit
PU	polyurethane
PS	Polystyrene
PS-g-MA	Maleic anhydride grafted PS
PTFE	Polytetrafluoroethylene
RSD	Relative Standard Deviation
PSU	Polysulfone
PVC	Polyvinyl chloride
RSD	Relative standard deviation
SAN	Poly(styrene-co-acrylonitrile)
SBR	Styrene butadiene rubber
SEBS	Styrene-ethylene/butadiene-styrene triblock copolymer

SEBS-g-MA	Maleic anhydride grafted SEBS
SEM	Scanning Electron Microscopy
SEP	Styrene-b-(ethylene-co-propylene)
SIS	Styrene-isoprene-styrene
S-I-HDB	Styrene-isoprene-hydrogenated butadiene
SMA	Styrene-maleic anhydride copolymer
St	Styrene
TCA	Trichloroacetic acid
T101	(2,5-dimethyl-2,5-bis-tertiarybutyl peroxide)hexane
THF	Tetrahydrofuran
TMS	Tetramethylsilane
TPE	Thermoplastic elastomer
TRIS	Trimethylol propane triacrylate
TSE	Twin screw extruder
VBB	Vinyl 4- <i>tert</i> -butylbenzoate

### Symbols

$I\cdot$	Free radicals
$IM\cdot$	Monomer radical
$V_n$	Net chamber volume
wt%	Weight percent
w/w%	Weight/weight percent
$\rho$	Melt Density
$t_{1/2}$	half life
$\Delta H_{mix}$	Enthalpy of mixing
$\Delta G_{mix}$	Gibbs free energy of mixing
$E'$	storage modulus
$E''$	loss modulus
$R^*$	Macroradical
$\tan \delta$	Tan <i>delta</i>
$T_g$	Glass transition temperature
$\bar{X}$	arithmetic mean
$\delta$	Chemical shifts
[GMA] <sub>i</sub>	Initial concentration
$\alpha$	Alpha
$\sigma$	Standard derivative

## CHAPTER 1

### INTRODUCTION

#### 1.0 Background

Studies on functionalisation of polyolefins by reactive processing have been carried out widely [1-9]. During this process, functional groups can be incorporated into the polymer backbone by a free radical melt grafting process. The term reactive processing refers to the use of suitable reactive modifiers with polymers and the adoption of conventional polymer processing machinery e.g. a batch mixer or an extruder, as a chemical reactor to perform *in situ* targeted reactions for chemical modification of preformed polymers [1]. The major feature of reactive processing is that it is carried out in the melt without a solvent in the presence of shear at high temperatures, using a high viscosity and heterogeneous polymers. This gives rise to tremendous challenges to melt free radical grafting in terms of reactivity, selectivity and process control. In a typical polymer functionalisation reaction, at least three reactants would be involved including a polymer, functional modifier, e.g. a vinyl-containing monomer, and a free radical initiator. The free radicals formed from the initiator react with the functional monomer to form propagating radicals, which would graft onto the polymer backbone. The efficiency of the grafting reaction depends largely on the reactivity of the free radicals formed as well as the reaction process conditions (e.g. temperature, time, shear). The major advantages of using reactive processing methods are relatively low output costs and is a rapid way of obtaining new polymers without having to search for new monomers. Furthermore, there is no need to use solvents in the melt reactions which would provide post processing cost advantages in term of solvent recovery [1]. However, several limitations have been reported [10] including the use of high temperatures typically required for melt reactions which may promote polymer degradation or crosslinking that would subsequently affect the ultimate product quality and performance.

Work on polymer blends has been carried out extensively in recent years by many researchers [1, 11-13]. Polymer blends are mixtures of two or more polymers with a unique range of properties obtained from both polymer components. The combinations of immiscible polymers that can be compatibilised result in polymer blends that would offer an opportunity to achieve the desired properties at optimum cost [14]. In addition, such polymer blends provide an alternative to designing completely new polymers, and such would satisfy new markets useful in industrial applications [15]. With a proper selection of materials and process conditions, blends with excellent properties can be therefore made. In most cases however, one or both polymer phases do not possess any functional groups and therefore reactive groups are typically incorporated into such blends, through the use of functionalised polymers in order to enhance the compatibility of the immiscible polymer components [16].

## 1.2 Polymer Functionalisation with Reactive Monomers

A number of functional monomers such as glycidyl methacrylate (GMA) [17-20], maleic anhydride (MA) [21-23], and oxazoline [24] have been grafted onto polyolefins by free radical grafting reactions. One of the main problems, however, in grafting these monomers on polymer backbones is the fact that in addition to grafting, they can also homopolymerise, a reaction that competes directly with the grafting process and often results in low grafting [9].

### 1.2.1 Grafting Glycidyl Methacrylate (GMA) onto Polymers

GMA (**Figure 1.1**) is a highly reactive bifunctional monomer, containing an unsaturated group capable of free radical grafting on hydrocarbon polymers, and an epoxy group that can react further with different functional groups e.g. carboxylic, hydroxide and amine group. The use of GMA in reactive processing for polymer functionalisation has gained a great attention from many researchers [2, 9, 25-27] and is summarised in **Table 1.1**.

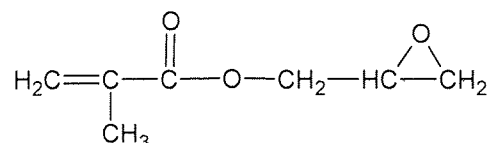


**Figure 1.1.** Chemical structure of glycidyl methacrylate (GMA)

Table 1.1. Functionalisation of GMA onto Polymers

Polymer	Mixer/ extruder	[GMA]i added	Co- monomer	Peroxide type (see abbreviations)	Peroxide conc.	GMA grafted	Ref
EPR	Torque rheometer	10	TRIS	T101	0.003 M.R	3 %	[9]
EPDM	Torque rheometer	10	TRIS	T101	0.0.229 M.R	3.6 %	[28]
EP	Brabender like mixer	6%		DCP	0.2%	0.8 mol%	[25]
EPR	Rheocord Haake mixer	6 phr	Styrene	DCP	0.3 phr	3.5phr	[29]
PE	Haake mixer	5% 10%		DCP	0.6%	1.6% 2.4%	[30]
EPR		10%		DCP	1.1%	2.1%	
PE	Rheocord Haake mixer	10 phr	Styrene	DHBP	0.4 phr	5.2phr	[31]
PP	Haake Rheocord 90 mixer	5%	Styrene	AM	0.5%	4.7%	[20]
PP	Rheocord Haake mixer	6phr	Styrene	DHBP	0.2phr	1.4%	[17]
PP	Rheocord Haake mixer	6phr	Styrene	DHBP	0.2phr	1.4%	[18]
PP	Werner % Pfleiderer	3phr	Styrene	DTBPIB	0.3phr	0.9phr	[18]
	ZSK-30 TSE	3phr	Styrene	DTBPIB	0.3phr	0.3phr	
PP	Haake Rheocord 600 mixer	18%	Styrene	DHBP	1.1phr	3.8%	[16]
PP	Haake Rheocord 600 mixer	11%		DHBP	1.1phr	2.8%	[32]
TRIS	trimethylolpropane triacrylate						
T101	2,5-dimethyl-2,5-bis( <i>t</i> -butylperoxy) hexane						
DCP	Dicumylperoxide						
DHBP	2,5-bis( <i>tert</i> -butylperoxy)-2,5-dimethylhexane						
AM	Acrylamide						
DTBPIB	1,4-diisopropylbenzene						

The grafting level of GMA onto PP in a co-rotating twin screw extruder was studied [18] and the grafting yield was shown to increase with increasing concentration of the initiator, (1,3-bis(*tert*-butylperoxyisopropyl)benzene) but decreased with increasing screw speed or feed rate. Gallucci *et. al* [30] studied the reaction of grafting GMA in the presence of dicumyl peroxide (DCP) as initiator onto low density polyethylene (LDPE) and ethylene propylene rubber (EPR) using a batch mixer (Haake equipped with roller blades). It was found that grafting on EPR could be achieved without significant crosslinking (less than 5% gel was found). On the other hand, the EPR was

found to be more difficult to functionalise compared to polyethylene (PE). It was concluded that epoxy-modified polyolefins could be prepared in the melt by radical melt grafting of GMA. However, when GMA was grafted onto ethylene propylene diene rubber (EPDM), a considerable crosslinking was observed and this was also attributed to the presence of peroxide in the system [28].

Grafting GMA onto low density polyethylene (LDPE) was also carried out by Pracella *et. al.* [26] using bis[1-(tert-butylperoxy)-1-methylethyl] benzene (BTP) in a Brabander internal mixer at 175 °C, 50 rpm, 5 min. In this work, two procedures were applied during the grafting:

- A. *The LDPE was powdered and premixed with GMA and BTP before feeding, then the mixture was charged in mixing chamber at 175°C.*
- B. *LDPE was melted into the mixing chamber at 145°C for 5 min, then the mixture of GMA and BTP were added dropped-wise then the temperature was increased to 175°C for 5 min.*

It was found that the grafting degree was largely affected by the grafting procedure with procedure A giving higher grafting degree ranging from 1-12 wt % compared to that achieved by procedure B. The authors suggested that good absorption of the monomer and initiator onto the LDPE powder facilitated the grafting reaction rate leading to higher grafting yield. The amount of the GMA grafted onto polymers is usually determined by the initial concentration of the monomer and peroxide used in the melt grafting reaction. A study on the effect of monomer (GMA) and peroxide concentrations on the grafting yield of GMA onto EPR using dicumyl peroxide (DCP) showed that an increase in peroxide and GMA concentrations increased the grafting level to 0.7 mol % [25]. However, with constant GMA concentration a higher grafting yield was obtained at peroxide concentration of 0.15%. In fact, an increase in the peroxide concentration resulted in dramatic increase in the melt index due to crosslinking reaction of the PE component of EPR. It was showed that GMA melt free radical grafting onto polypropylene (PP) was accompanied by  $\beta$ -chain scission of the polymer [16]. However, the extent of grafting and the level of PP degradation can be controlled by manipulating both the initiator and monomer concentrations as well as the processing temperature.



### 1.2.2 Grafting Maleic Anhydride (MA) onto Polymers

Maleic anhydride (MA) (Figure 1.2) is also a bifunctional monomer which has been used extensively for grafting onto polyolefins [21, 33-38]. Like other,  $\alpha$ ,  $\beta$ -unsaturated compounds, reactions can take place on the carbonyl groups, the unsaturated site or on both sites. Agnelli *et. al* [23] examined the grafting reaction of MA on PP and concluded that an increase in peroxide concentration caused an increase in the percentage of grafted MA onto PP but with a reduced melt flow index (MFI) values due to excessive degradation of PP. It was shown that an increase in the initial MA concentration and also an increase in the rotor speed resulted in increasing the chance of MA reaction with the PP macroradicals leading to increased extent of grafting but this was also associated with PP degradation [23]. Furthermore, in PE, the extent of crosslinking was found to increase when MA was grafted onto different PE grades using 2,5-dimethyl-2,5-(di-*t*-butylperoxy)hexane as a radical initiator in a internal batch mixer (Haake Buchler Rheomix 600) [21] whereas in EPR, both cross-linking and degradation reaction have been shown to take place to varying extent [21].

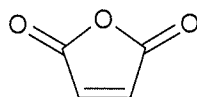
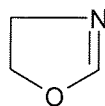


Figure 1.2. Chemical structure of Maleic Anhydride (MA)

### 1.2.3 Grafting Oxazoline onto Polymers

Oxazoline, Figure 1.3, is another monomer which has been used extensively to functionalise polyolefins [39-41]. It was shown that the efficiency of grafting of a monomer containing a terminal oxazoline group with double bond, ricinloxazoline maleinate (OXA), Figure 1.4, onto PE depends strongly on the processing conditions. A sample obtained from processing at a temperature of 180 °C, screw speed of 64 rpm and a mixing time of 7 min, without peroxide was found to give remarkable grafting yield [40]. Oxazolines react fast with carboxyl and amino groups, which make them suitable for use in blends containing these functional group e.g. as end groups in polyester or polyamide [39, 42-44]. The functionalisation of polyolefins and elastomers

with ricinloxazoline maleinate was shown to give an increase in the degree of grafting with increasing the initial monomer concentration [24].



**Figure 1.3.** Chemical structure of oxazoline

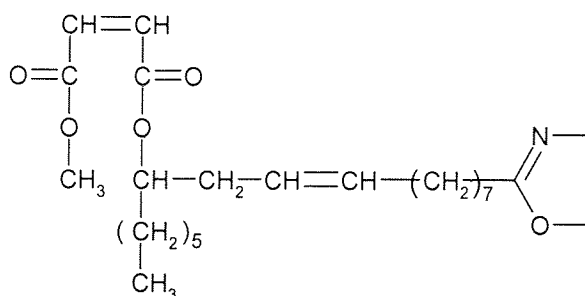


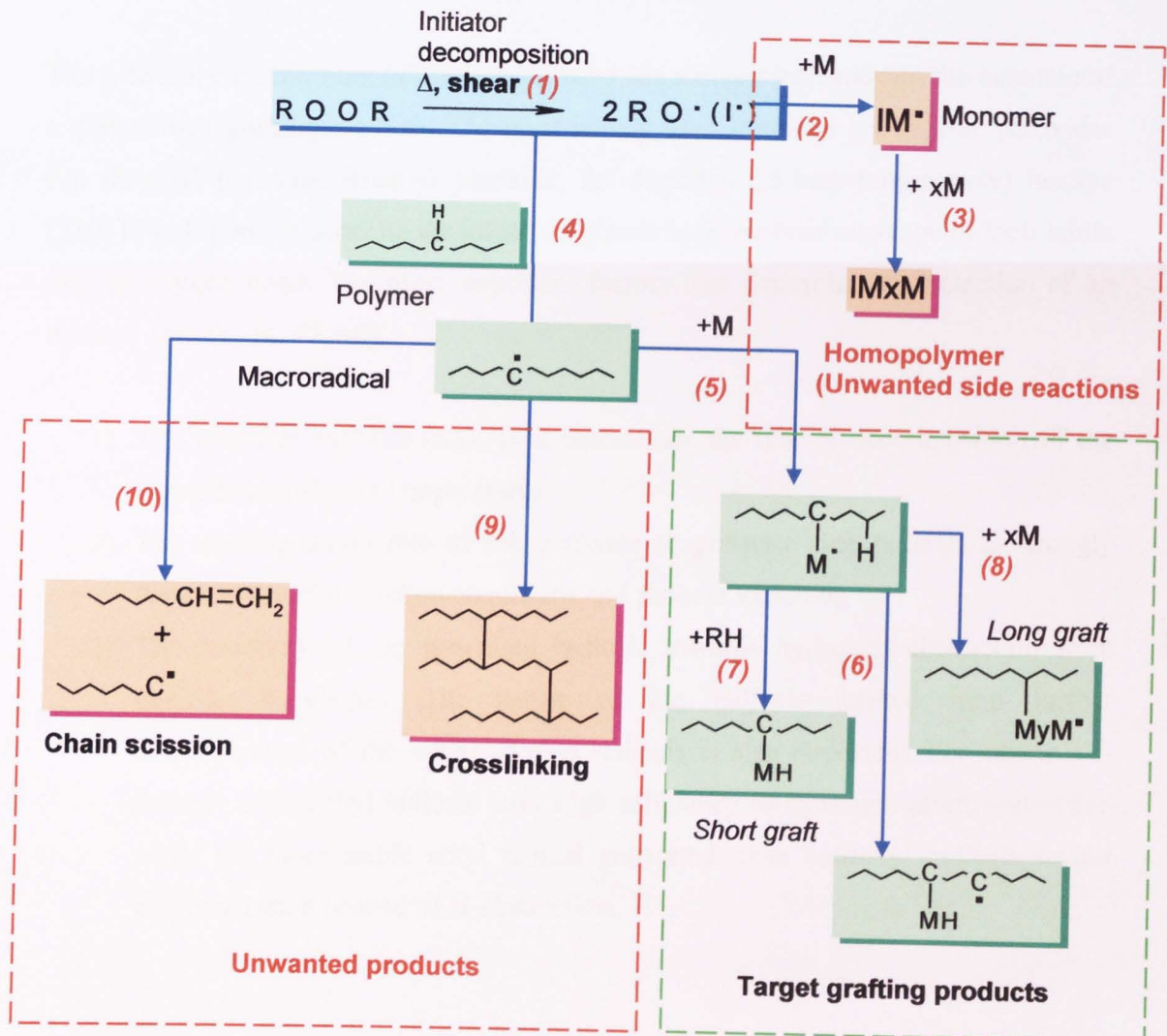
**Figure 1.4.** Chemical structure of ricinloxazoline maleinate (OXA) [45]

However, crosslinking was found also to accompany the grafting reaction in the case of PE even with a low initial monomer and peroxide concentrations. Hu *et. al.* [45] investigated the grafting efficiency of ricinloxazoline maleinate (OXA) onto PP in a batch mixer. It was concluded that the grafting yield varied from about 0.5 to 1.5 phr and was shown that the presence of styrene used as a comonomer, the grafting did not enhance the grafting yield of OXA but it did markedly reduce the extent of PP degradation. The efficiency of grafting was shown to be dependent on the concentration of both monomer and peroxide.

### 1.3 Free Radical Grafting Reaction Process and Mechanism

The main reaction steps involved in a typical melt free-radical grafting process are summarised in **Scheme 1.1**. The initiator decomposes under the effect of shear and high temperature to give free radicals ( $I\cdot$ ) for subsequent reactions (**Scheme 1.1, Rn-1**). In the presence of a polymer or a monomer molecule, the initiator radicals may follow two different reactions. They may attack a monomer molecule generating a monomer radical ( $IM\cdot$ ) via H abstraction (**Scheme 1.1, Rn-2**) and this can continue to react with more

monomer forming a homopolymer (**Scheme 1.1, Rn-3**), which has a limited hydrogen abstraction capacity, thus, reducing the possibility of its grafting onto the polymer backbone [10]. The initiator may also react with the polymer forming macroradicals (**Scheme 1.1, Rn-4**). The grafting of the monomer onto the polymer backbone occurs when the macroradicals react with a monomer followed by H atom abstraction, (**Scheme 1.1, Rn-5 and Rn-6**). The macroradicals however, may continue to react with more monomer molecules leading to the formation of longer grafts (**Scheme 1.1, Rn-8**). Other side reactions such as polymer crosslinking (**Scheme 1.1, Rn-9**) or chain scission (**Scheme 1.1, Rn-10**) may also occur during the grafting process, but their extent would depend on the polymer structure, for example PE undergoes crosslinking while PP is prone to chain scission [10].



**Scheme 1.1** Simplified overall scheme of free-radical grafting onto polymer backbone, M is monomer.

The melt free radical grafting reactions are generally complicated due to the influence of various factors including high temperature, high viscosity and heterogeneity of the reacting medium as well as the formation of unwanted reactions of the monomer and the polymer which would compromise the level of grafting [10] including radical or shear induced crosslinking or chain scission of the polymer, as well as homopolymerisation of the monomer [46]. It was shown that, generally, addition of high concentration of the initial monomer or the initiator would result in an increase in the extent of homopolymerisation of the monomer [9]. Monomers such as GMA and MA have low reactivity toward macroradicals [9], hence low extent of grafting can be expected. To improve the extent of grafting yield both the chemical composition and the processing conditions must be controlled to minimise the extent of the unwanted side reactions. Another approach would be to use a more reactive comonomer that will result in enhanced grafting efficiency, see **Sec 1.4**.

The type and concentration of the initiator used has a major influence on the outcome of a typical melt grafting reaction. The most widely used initiators are organic peroxides e.g. dicumyl peroxide, benzoyl peroxide, 2,5-dimethyl-2,5-bis(*t*-butylperoxy) hexane (T101) [4, 47] which generate the initiator radicals by homolytic cleavage of their labile oxygen-oxygen bond. The most important factors that determine the selection of an initiator include: [4, 47, 48].

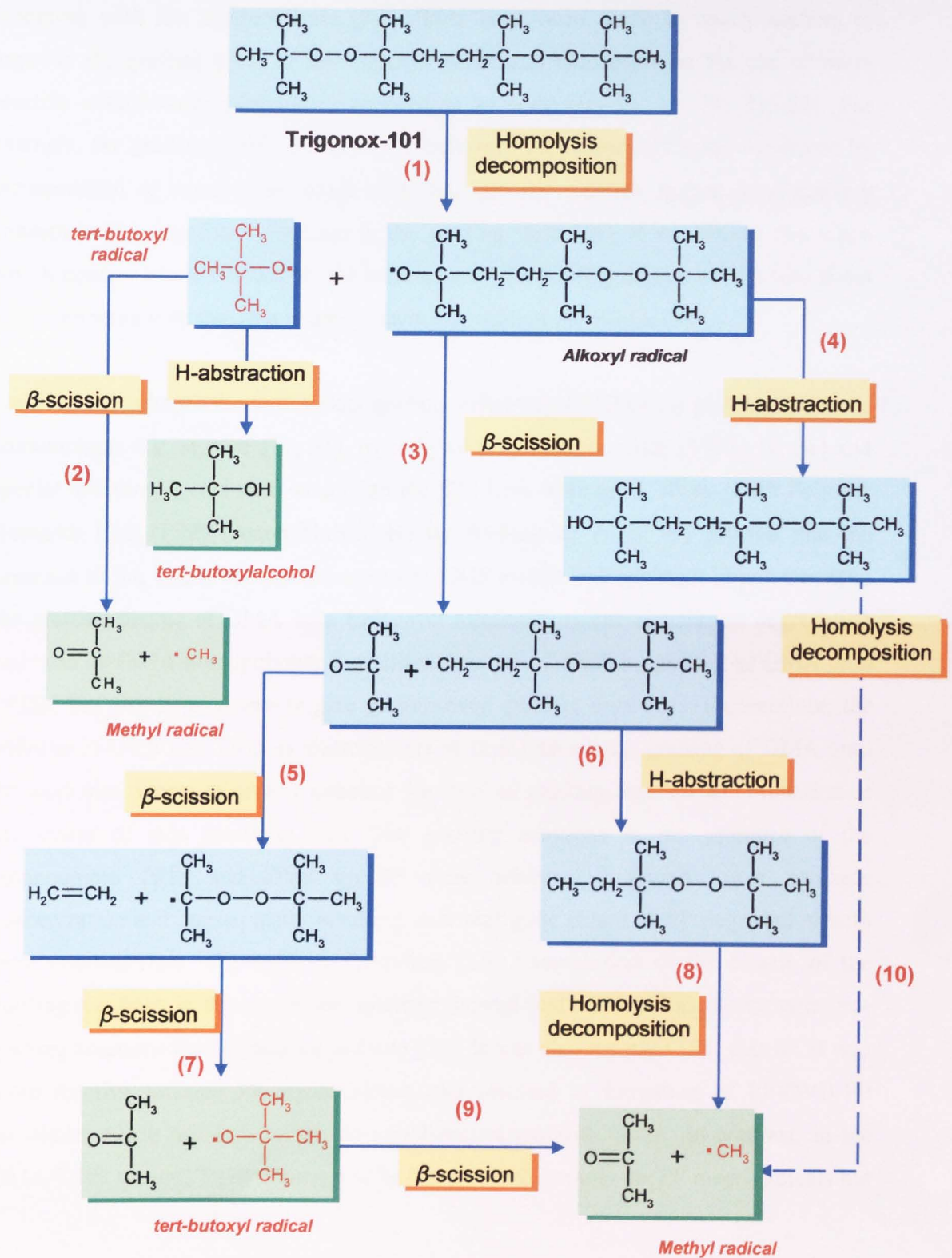
- 1) The peroxide half life ( $t_{1/2}$ ), as it determines the rate of decomposition of the peroxide at different temperatures.
- 2) The decomposition rate of the peroxide to generate free radicals is strongly dependent on the reaction conditions and process variables.
- 3) The reactivity of the generated radicals towards hydrogen abstraction from polymer backbones. The nature of the radicals formed from further decomposition of the initial alkoxy radicals is also important. For example *t*-butoxyl and methyl radicals have high efficiency to hydrogen atom abstraction while the more stable ethyl radical generated from amiloxy radicals favour polymerization instead of H-abstraction.

- 4) High reactivity of the initiating radicals towards monomers would promote homopolymerisation of the monomer leading to lower extent of the desired grafting reaction.
- 5) The physical characteristics of the initiator (solid, liquid absorbed on solid carrier) are also important for the purpose of delivery and mixing and the toxicity of the peroxides is an essential criteria particularly if applications involve human-contact.

The initiator half life represents the time taken for half of the quantity of the initiator originally used to decompose [10]. This is important because if the half life is too long, the initiator may not be completely utilised and thus is inefficient and unattractive from an economical point of view. Ideally, the half life of the initiator should be short compared to the processing time [10]. In many cases, the nature of the peroxide influences the efficiency of the grafting reaction and the degree of macromolecular degradation. Competition between the grafting and side reaction processes, which determines the chemical structure of the product, will largely depend on the nature and concentration of the peroxide used [49]. Other factors are also important and must be considered when selecting an initiator including the solubility of the initiator in the polymer melt and in the case of multiphase polymer melts, its partition coefficient between the phases. The method of introducing the initiator also plays a significant role in determining its efficiency. Initiators can be introduced into polymers through the main hopper of the processing machine either with the monomer or in a separate feed. Alternatively, it can be added directly, by absorbing it onto the polymer, or by adding it as a solution in the monomer or in a solvent. All reactants including the initiator may be added at once or through multipoint addition.

The rate of decomposition and the reactivity of peroxides (ROOR) depend on the peroxide structure and particularly the type of the R group [50]. The mechanism of radical generation from Trigonox 101 (T101), one of the most widely used peroxide for melt grafting reactions and the peroxide used in the work described in this thesis, is illustrated in **Scheme 1.2**. Dissociation of T101 generates *t*-butyl radicals and alkoxy radicals (**Scheme 1.2, Rn-1**). The formation of methyl radical takes place through  $\beta$  scission of *tert*-butoxy radical (**Scheme 1.2, Rn-2**). Further formation of *t*-butyl radicals

and alkoxy radicals take place by H atom abstraction and  $\beta$  scission reactions, (Scheme 1.2, Rn 3, 4, 6 and 7).



Scheme 1.2 Radical generation reactions from Trigonox-101

## 1.4 Grafting Reactions in the Presence of Co-Monomers

It was shown in the **Section 1.2** that generally the grafting efficiency of many functional monomers onto polymers is low, and this depends on the reactivity of the specific monomer with the macroradicals [9]. Efforts have been made by many authors to improve the grafting yield of less reactive functional monomers by the use of more reactive comonomers (sometimes referred to as coagents) [9, 17, 31, 51, 52]. For example, the grafting yield of MA on isotactic-polypropylene (iPP) was improved by incorporation of neodymium oxide ( $\text{Nd}_2\text{O}_3$ ), into the reactive system as a grafting coagent, with a significant increase in the grafting yield [49]. It was shown that when  $\text{Nd}_2\text{O}_3$  content was 4.5 mmol %, the increment of the grafting degree of MA was about 30% compared with that of a related system but without the  $\text{Nd}_2\text{O}_3$  [49].

Similarly, to enhance the free radical grafting efficiency of GMA on polymers, various comonomers e.g. styrene [17, 31], trimethylol propane triacrylate (TRIS) [9, 51] and special initiating agents such as acrylamide [20] have been used. Work in the Polymer Research Unit (PPP) (Aston University) by Al-Malaika *et. al* [9] showed that the presence of the highly reactive comonomer TRIS results in significant improvement in the grafting degree of GMA onto EPR with minimum extent of polymer degradation and with no GMA homopolymer formation. The use of TRIS in grafting of GMA onto EPDM has also been shown to give an improved grafting level [51]. Furthermore, the addition of DVB and TRIS as comonomers in melt free radical grafting of GMA onto PP were also shown to greatly enhance the level of grafting reaction and reduction of the extent of side reactions [53]. The grafting reactions in the presence of the comonomers TRIS and DVB on PP were achieved at much lower peroxide concentration and consequently resulting in a negligible extent of PP degradation with very small amount of polyGMA formation [53]. Examination of the kinetic of the grafting reactions in the commoner systems showed that TRIS led to shorter complete grafting reactions time compared to DVB [53]. It was also reported [53] that DVB was more reactive towards PP macroradicals and resulted in formation of PP-DVB-PP crosslinks which occurred before the copolymerisation with GMA. In contrast, in the GMA/TRIS system, TRIS appeared to be less reactive towards the PP macroradicals but

more reactive towards GMA and copolymerised with GMA before the formation of TRIS assisted PP crosslinking.

The effect of styrene on grafting of GMA onto PP [17] and PE [54] was reported. The presence of styrene as a comonomer increased the GMA grafting yield greatly with reduced PP chain degradation [17]. In contrast, the addition of styrene in the grafting system of GMA on PE increased the efficiency to 30%. However the styrene also caused PE branching reaction [54]. Styrene was shown to act as a mediator where it initially reacted with PP macroradicals to form stable styryl macroradicals which react with GMA to form GMA-grafted PP [17]. However, the high grafting yield in the presence of styrene was suggested to be associated with longer chain grafts and formation of more grafting sites [46]. It is worth noting here that, in the presence of maleate esters, styrene was found to be ineffective at improving their grafting yield on PP inspite of the fact that it was effective in reducing the degradation of PP [46, 55]. The use of styrene with oxazoline for functionalising PP was also shown not to enhance the grafting yield but did reduce the PP degradation [56]. It was illustrated that styrene and oxazoline did not copolymerize easily hence the low extent of grafting.

Other comonomers were reported to enhance the grafting of functional monomer on polymers. Whitney *et. al* [57] investigated the effect of three comonomers, vinyl 4-*tert*butylbenzoate (VBB), styrene and 1-dodecene (DD) on the grafting of MA onto poly(ethylene-co-methylacrylate) (EMA). It was suggested that both styrene and VBB were capable of significantly increasing the amount of MA grafted onto EMA while 1-dodecene appeared to exhibit primarily a plasticiser effect. The styrene was shown to react with the EMA macro-radicals at a greater rate than the MA monomer, thereby producing styryl macroradicals. The MA monomer then reacted readily with the styryl macro-radicals, resulting in an overall synergistic effect. As a result, the EMA polymer grafted with styrene forming MA oligomeric grafts. In this system where VBB was present, the VBB monomer was shown to graft onto EMA radicals, followed by MA grafting onto the new macro-radical sites on the VBB. However, this resulted in reduced MFI values indicating an increased viscosity due to crosslinking. As a result, there may have been less mixing in the VBB system resulting in poorer migration of both VBB and MA to the radical sites, leading to an overall decrease in anhydride incorporation



when compared to the styrene system. The presence of DD however, resulted in a remarkable increase in MFI value. The DD monomer was shown to function mainly as a plasticiser in the melt and did not play a role in the MA grafting, which is the reason why DD was found to be less effective than the other comonomers examined in this study [57].

## 1.5 Reactive Processing

Functionalisation of polymers has been achieved primarily by one of two main routes based either on *in-situ* melt reactions via reactive processing, or in solution [1, 58]. The most widely used technique has been that of reactive processing which is a cost-effective approach for the production of new materials [1, 9, 14]. Some of the main advantage of reactive processing compared to utilisation of solvent is the reduced costs associated with the solvent, recovery and the absence of solvent emission resulting in safety implication, and since the solvent usually comprises 5-20 time the weight of the desired polymer products, the economic advantages are extensive [59]. In a typical reactive processing step, existing commercial polymers are chemically modified in the melt inside an extruder or internal mixer (which act as a chemical reactor) and the functionalised polymers produced can subsequently be used to promote further chemical reactions with other materials e.g. other polymers, resulting in the desired properties of the new materials [14].

For increased grafting level, a good mixing, and more precise internal temperature control would be required [59]. For example, extruders [60, 61] and internal mixer [62, 63] are widely used in reactive processing. When an extruder is used, optimised reaction zone length may possibly increase the grafting level and the use of a twin screws extruder would create a better opportunity for good interfacial reaction to take place for example during reactive blending of immiscible polymers [15]. It was reported that the use of batch reactors for bulk free radical polymerisation of acrylic monomers may be problematic due to poor heat transfer, inadequate mixing, rapid viscosity increase and gel formation. Therefore, high efficiency mixing equipment such as twin screw extruder are normally used for large scale reactive processing [48] and extruders are better sealed against oxygen compared to batch mixers [10].

Batch mixing involves loading a volume of material into the mixer, which must later be unloaded, this contrasts the process of continuous mixing (e.g. in extruder) where the material flows steadily from an upstream process into the mixer and is retained in the mixer for a specified mixing time, and then discharged at the same flow rate for downstream handling [64]. Haake Rheocord or Brabender type batch mixers are the most popular types of mixers used by most researchers for reactive processing for the purpose of studying melt free radical grafting or reactive blending process. Batch mixers are also used to process small quantities of exotic or expensive chemicals and are also capable of processing highly viscous polymers. In order to achieve optimum output, the polymer is normally added first in the empty chamber in order to warm up or before adding other reactant ingredients. For polymer blending, mixing is conducted generally until a homogeneous blend is achieved. However as mentioned earlier, due to its structure, the mixing chamber of batch mixers are not perfectly sealed and this would be unfavourable for low boiling point liquid monomers or other temperature dependent reagents used in reactive processing systems.

## 1.6 Polymer Blends

Work on polymer blends has been carried out extensively in recent years by many researchers [1, 28, 51, 65-68]. Polymer blends are mixtures of two or more polymers that provide unique range of properties obtained from both polymer components. Polymer blends offer cost effective alternative to designing new materials, as they have useful and sometimes unique properties that can satisfy new markets of different applications [15, 69].

Most polymers pairs are immiscible due to thermodynamic reasons and without compatibilisation, the physical properties of such polymer blends are worse than those of either individual polymers due to poor structural integrity [69]. Typically, the dispersed phase agglomerates into large domains when subjected to thermal processing due to phase separation [70]. For example, it was shown that there is no evidence for any interfacial interaction or adhesion in the immiscible PET/PE physical blends and the morphology of these blends showed discrete spherical domains of the minor component within the continuous phase due to immiscibility of PET and PE polymers [71]. The incompatibility of two polymer phases, e.g. the immiscible PET/HDPE blends, results

in a fragile material [72] due to coalescence resulting in gross phase segregation and delaminating on a macroscopic scale thereby increasing the brittleness and giving poor surface appearance in the final molded part [73]. The miscibility of polymer blends have been categorised into [74]: i) Completely miscible blends (minority) ii) partially miscible blends and iii) fully immiscible blends.

### 1.6.1 Compatibilisation of Immiscible Polymer Blends

The immiscible polymer pairs require compatibilisation and an economical way of achieving this would be through reactive blending that gives rise to an *in-situ* copolymer formation by a reaction between functionalities of the polymers [69, 75, 76]. For example, blends of PET and polyurethane (PU) were shown [77] to offer better mechanical and thermal properties due to compatibilisation via association of the carbonyl groups of PET with the hydrogens of –NH groups in PU. Compatibilisation between two immiscible polymers can also be achieved by using a third component in the formation of a block or copolymer which would significantly improve the blends properties [72]. For example, blends of PET and HDPE have been effectively compatibilised using GMA or MA as functionalising monomers with the GMA showing a higher effectiveness [78], due to the slow reactivity of the hydroxyl end groups of PET towards MA. Indeed, blends of poly(butylene terephthalate) (PBT) with poly(styrene-*co*-acrylonitrile) (SAN) using epoxy containing molecules as compatibilisers showed rapid reaction between carboxylic or hydroxyl end groups of PBT with the epoxy groups [79].

The reactively formed block or graft copolymers are able to stabilise the morphology resulting in better adhesion at the interphase [80]. In polymer blends, it has been shown that the size and morphology of the dispersed phase, its stability to coalescence and the interfacial reaction between the two phases determine the overall performance of the blends [81]. It is well established that in addition to composition, rheological properties and type and extent of interaction between the blend components, the processing conditions used may also affect the size and the shape of the dispersed phase [20, 81]. Therefore, overall compatibilisation of immiscible blends results in reduction of the interfacial tension in the melt causing an emulsifying effect and leading to an extremely fine dispersion of one phase in another [82]. This promotes specific interaction and/or

chemical reactions with the blend constituents. The dispersed phase in a compatibilised blends of immiscible polymers pairs is therefore stabilised against agglomeration by interphase adhesion and lowering of the interfacial tension between the two phases [73]. Furthermore, stabilising the dispersed phase against growth during annealing by modifying the phase boundaries of the interface can also be expected to promote compatibilisation of immiscible blends [82].

The effectiveness of added compatibilisers vary significantly, for example diblock copolymers have been shown to be more effective in improving the compatibility of blends than triblock, multiblock, or graft copolymers [83]. This is most probably due to the presence of just one linkage bond, which is necessarily located at the interface, allowing the rest of the chain to penetrate into, and form entanglements in the homopolymer phases. Despite the greater efficiency of diblocks, they have seldom been used in commercial applications since [83].

In commercial reactive blends, graft copolymers are typically formed by reaction between compatibilisers with functional groups randomly distributed along a chain and the end functional groups in polymers like polyamides or polyesters. It was reported [80] that the location of the functional groups plays an important role in determining the kinetic of the reaction in the polymer blends, determined by investigating the kinetics and comparing end-functional polymers versus mid-functional polymers. It was found that coupling with a mid-functional polymer is slower than that with an end-functional polymer and this was attributed to steric hindrance due to the polymer chain [80].

In blends of PP/NBR (nitrile butadiene rubber), where variety of compatibiliser having acidic groups have been used, good compatibilisation was achieved [84]. It was shown that GMA and oxazoline compatibilisers greatly reduced the size of the dispersed phase and the size distribution became uniform, however similar observations were not seen when compatibilisers containing carboxylic acid were used. Blending poly(styrene-*co*-acrylonitrile) (SAN) with EPDM grafted with (methyl methacrylate) MMA improved the miscibility of the blends [85]. Although the presence of compatibilisers in polymer blends help to improve compatibilisation between the polymers, the quantity used has been shown to always influence the degree of compatibility, and thus affect the

properties of the end product. Karger-Kocsis *et. al.* [86] have shown that, at 5 and 10 w/w % modified elastomer used in PET/EPR binary blends gave similar stiffness, but blends with 20 w/w % elastomer reduced the blend performance below that of PET alone.

Enhanced interfacial adhesion with improved fracture toughness has been achieved in polyamide6/ethylene-co-vinyl acetate (PA6/EVA-g-MA) blends [87]. The rate of coalescence of the dispersed phase was lower, producing finer and more stable dispersion of EVA-g-MA domains in the PA6 matrix. Comparison of the effect of the binary and ternary blends of PA6/EVA in the presence of EVA-g-MA as a compatibiliser suggested that the impact strength of the binary blends is slightly increased compared to that of ternary blends [87]. Large differences in viscosity ratio between components in the blends may also influence their compatibilisation. Small viscosity ratios between the polymer components in blends allow easy dispersion in the matrix giving a more uniform dispersion and fine particle size [87]. However, increasing the functional groups of the compatibiliser does not necessarily improve the compatibility. In some cases [88, 89], higher amount of functional groups were shown to deteriorate the compatibility of blends as the interface becomes saturated with the functional groups hence facilitate cross-linking reaction mainly at the interface and as a consequence, the disperse phase will become more viscous and preventing droplet breakup resulting in rough morphology. For example, the phase morphology of PET/EPR showed a finer domain phase when it was compatibilised with EPR-g-GMA containing 1.2 wt% grafted GMA compared to one with 1.5 wt% [90]. Similar findings were also reported in the case of PET/EPR compatibilised with ethylene-glycidyl methacrylate (E-GMA) where at lower GMA content, the blend exhibited finer morphology and better mechanical properties [91]. The incorporation of various grades of ethylene-methacrylate-glycidyl methacrylate (EM-GMA) in polybutylene terephthalate (PBT) blends was found to be capable of improvement of the morphology and mechanical properties of these blends [92-95].

*In-situ* produced copolymers formed at the interphase during reactive blending of immiscible polymers, with one of the phases being functionalised, results in great improvement in morphology and performance. For example, blending PET with GMA-

functionalised ethylene propylene diene terpolymer (EPDM) and GMA-functionalised EPR using batch mixer showed a tremendous improvement in morphology of the blend compared to the corresponding physical blends [96]. Another example is the use of *in-situ* functionalised PP with GMA (PP-g-GMA) as a compatibiliser in PET/PP blends which was shown to promote significant improvement in phase dispersion and adhesion in these blends [97]. The observed increase in mixing torque was attributed to the occurrence of reaction between GMA modified PP and PET leading to formation of PET-co-PP copolymer. In addition, the improvement in physical and mechanical properties and morphology confirmed that PP-g-GMA was successful in acting as a compatibiliser in these blends.

The compatibility of polypropylene/polyethylene terephthalate (PP/PET) blends was further investigated [98] in the presence of glycidyl methacrylate grafted PP (PP-g-GMA) containing either 0.2 or 1.2 wt% GMA. It was observed that the mechanical behavior changed from fragile to ductile improving the tensile strength by 10%. More importantly, the elongation at break increased by 10 to 20 fold while the stiffness remained unchanged. The morphology examination of these blends revealed that the average domain size of PP decreased to the micron/submicron size upon addition of the GMA modified-PP. It is important to point out that a low-GMA graft content on PP was shown to give slightly more efficient performance than higher GMA content on PP [98].

Several compatibilisers used in blending functionalised PP with thermoplastic polyurethane (TPU) were investigated [99], for example the effect of amine functionalized PP (PP-g-NH<sub>2</sub>), secondary amine functionalized PP (PP-g-NHR) was compared with that of a maleated PP (PP-g-MA) on their compatibility with thermoplastic polyurethane and was shown to be in the order: PP-g-NHR > PP-g-NH<sub>2</sub> > PP-g-MA. Improvement in mechanical properties including higher tensile strength and ultimate elongation, and finer and more stable morphologies of the blends resulted from higher reactivity of the amine function (primary and secondary) with the urethane linkages. Similar finding with poly(2,6-dimethyl-1,4-phenylene ether) (PPE)/PBT blends was reported by Nelissen *et. al* [76] which showed that the type and concentration of functionality on PPE, the molecular weight of the polymers and the

presence of a catalyst or chain extending agents would influence the extent of compatibilization of the PPE/PBT blends.

## 1.7 Types of Compatibilisers

An overview of the main types of compatibilisers used for compatibilisation of immiscible polymer blends is outlined below [100]:

### i) *In Situ* Formed Copolymers

In this approach, the blend components are modified in such a way so that a reaction can occur during melt blending. For example, a hydrocarbon polymer would first be functionalised in-situ with a reactive group, for example, with an anhydride, epoxy, or oxazoline function that can react with the second polymer to provide the formation of an interchain block or copolymer through covalent or ionic bonding [100]. **Table 1.2** shows examples of reactions between various functionalised polymers and **Table 1.3** shows compatibilisation reactions that can take place easily across polymer phase boundaries.

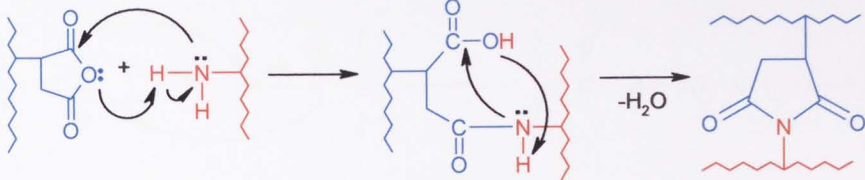
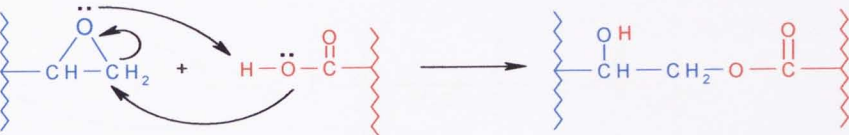
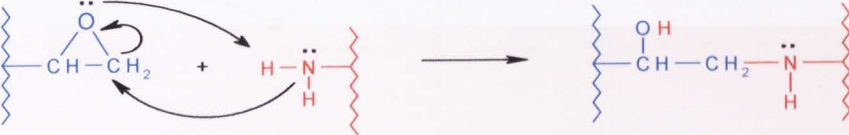
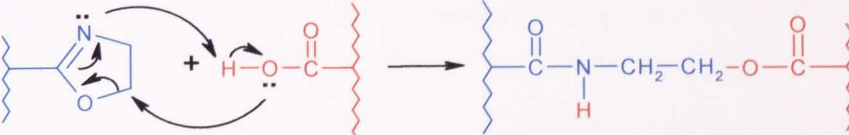
### ii) Copolymers Added Separately (Non-Reactive Copolymers)

Non-reactive copolymers have segments that are capable of specific interactions with each of the blend components, their miscibility is often dictated by their closely matched solubility parameters whereas reactive copolymers, segments are capable of forming stronger covalent or ionic bonds with at least one of the blend components [100]. Interfacially active graft or block copolymers of the type A-B or A-C may compatibilise immiscible polymers A and B provided that C is miscible (at least partly) with B [100].

### iii) Addition of Reactive Copolymers

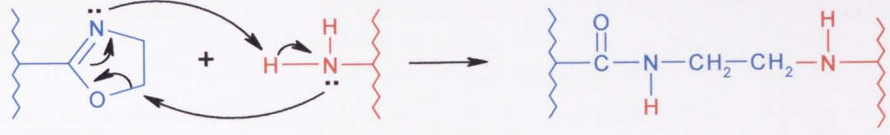
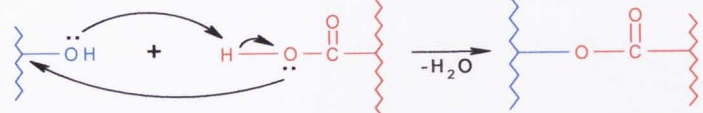
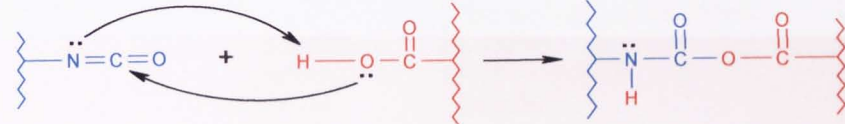
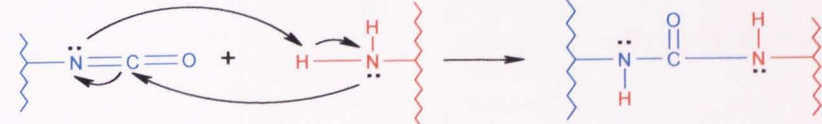
Compatibilisation of immiscible polymer blends can be performed by addition of reactive copolymer during reactive blends. For example, blends of PET with PP can be compatibilised by adding PP-g-GMA in with PP-g-GMA is miscible with PP while the GMA is reactive toward carboxyl or hydroxyl end groups in PET.

**Table 1.2** Examples of common compatibilising reactions between functionalised blend constituents

Code	Reaction Mechanism	Refs.
1	<p><b>Anhydride and amine</b></p> 	[11, 101-105]
2	<p><b>Epoxy and carboxylic acid</b></p> 	[106-108]
3	<p><b>Epoxide and amine</b></p> 	[109-113]
4	<p><b>Oxazoline and carboxylic acid</b></p> 	[114-116]



**Table 1.2** Examples of common compatibilising reactions between functionalised blend constituents (continue)

Code	Reaction Mechanism	Refs.
5	<p><b>Oxazoline and amine</b></p> 	[117]
6	<p><b>Hydroxyl/Carboxylic (Transesterification)</b></p> 	[118-121]
7	<p><b>Isocyanate and Carboxylic acid</b></p> 	[122-125]
8	<p><b>Isocyanate and amine</b></p> 	[124]

**Table 1.3.** Compatibilisation through the reaction of functionalised blend components

Compatibilising Reaction	Polymer Blend	References	
Epoxy and Carboxyl	PP-g-GMA/PET or PBT or CNBR HDPE-g-GMA/PET EP-g-GMA/PET PS-g-GMA/PBT ABS-g-GMA/PBT	[106, 107, 126-128] [129] [91] [108, 130, 131] [89]	
Oxazoline/carboxyl acid or Mercapto (-SH)	PP-g-OXA/PBT PP-g-OXA/PA NBR-g-OXA/EVA-SH or EPDM-SH PS-g-OXA/PBT	[115, 116] [132] [133] [42]	
Anhydride/Amine	PSU-g-MA/PA6 NR-g-MA/PA PE-g-MA/PA6 PA-1010/HIPS-co-MA PP-g-MA/PA-6 and PA-12 EP-g-MA/PA-6	[134] [101] [105, 135, 136] [137] [103, 104, 138-141] [102, 142]	
Anhydride/Carbonyl	HDPE-g-MA/PET SAN-g-MA/PBT SEBS-g-MA/PET EVA-g-MA/PBT or PET ABS-g-MA/PC PP-g-MA/PBT	[143] [144] [145] [65, 146, 147] [148] [149, 150]	
Isocyanate/carboxyl or amine	EPR-g-Isocyanate/PBT LDPE-g-Isocyanate/PA or PBT PP-g-HI/PBT and PET	[151] [124] [122, 151]	
Compatibilising Reaction	Polymer Blend	Compatibiliser	References
Epoxy/Amine	PET/HDPE PET/EPR PBTAES PBT/PC PET/PP PBT/ABS	E-GMA, E-EA-GMA SEBS-g-GMA, E-MA-GMA E-GMA MMA-GMA-EA E-GMA E-GMA, SEBS-g-GMA, SEP-g-GMA S-GMA and MMA-GMA	[78] [152] [90, 153] [154] [155] [156, 157] [158, 159] [160]
Epoxy/Amine	LDPE/PA-6 ABS/PA	E-GMA SEBS-g-GMA MMA-GMA	[161] [67] [162, 163]
Anhydride/carboxylate	PP/PET LLDPE/PBT PET/HDPE	SEBS-g-MA, LLDPE-g-MA EVA-g-MA EPR-g-MA, SEBS-g-MA, E-GMA	[164, 165] [166] [167]
Anhydride/amine	LDPE/PA-6 PP/PA-6 PMMA/PA-6 PP/PA-6	SEBS-g-MA SEBS-g-MA SMA TPE-g-MA	[67] [12, 168, 169] [170, 171] [172]
Oxazoline/carboxyl	PP/PBT	SEBS-g-OXA, EP-g-OXA	[171]

## 1.8 Thermodynamic Consideration

As was mentioned earlier, for thermodynamic reasons, most polymer pairs are immiscible, and few polymers generate a truly homogeneous product. This is generally not detrimental, as often it is desirable to have a two-phase structure. However, the situation at the interface between these two phases would lead to problems. A typical problem would be a high interfacial tension and poor adhesion between the two phases which would contribute, along with high viscosities, to the inherent difficulty of imparting the desired degree of dispersion to immiscible mixtures and to their subsequent lack of stability with gross separation or stratification during later processing or use [18, 19].

Compatibility of polymers from a thermodynamic perspective can be determined by a balance of enthalpy and entropic contributions to the free energy of mixing according to **Eqn 1.1** [173, 174].

$$\Delta G_{\text{mix}} = \Delta H_{\text{mix}} - T\Delta S_{\text{mix}} \quad \text{(Eqn.1.1)}$$

$$\Delta H_{\text{mix}} = VZW\Phi_1\Phi_2/V_s \quad \text{(Eqn.1.2)}$$

$$\Delta S_{\text{mix}} = -K[N_1 \ln\Phi_1 + N_2 \ln\Phi_2] \quad \text{(Eqn. 1.3)}$$

Where

$\Delta G_{\text{mix}}$  – Gibbs free energy of mixing

$\Delta H_{\text{mix}}$  – enthalpy of mixing

$\Delta S_{\text{mix}}$  – entropy of mixing

T – temperature

K - the universal gas constant

$N_1$  - moles of component 1

$\Phi_1$  – volume fraction of component 1

$V_s$  – interacting segment volume

V – the total volume

W – interaction energy

Z – coordination number

For a system to be fully miscible, the mixing free energy  $\Delta G_{\text{mix}}$  must be negative ( $\Delta G_{\text{mix}} < 0$ ) [174]. The condition where  $\Delta G_{\text{mix}} < 0$  can be achieved only if the binary polymer-polymer interaction coefficient  $\chi$  is negative [175]. Interaction coefficient is influenced by three factors; dispersion interaction, free volume and the specific interactions. According to the classical Flory-Huggins theory [173, 174], entropy change on mixing (see **Eqn. 1.3**) is an inverse function of the molecular weight of each component due to the intrinsic order in a system from limited possible arrangement of linked segments. This will make a negligible contribution to the free energy of mixing change associated with the net intermolecular attractions [174]. As a consequence,  $\Delta G_{\text{mix}} \equiv \Delta H_{\text{mix}}$ , and miscibility depends entirely on the energetic of intermolecular interaction between the blend components (e.g. H-bonding, ionic, dispersion). Copolymers may be added as discrete third components or generated in situ during processing via interfacial reaction of blend components. The formation of the appropriate bridging copolymers at the interface in the blends is possible if two co-reactive polymers are incorporated [84].

## 1.9 PET Profile

Poly(ethylene terephthalate) (PET) is a polycondensation polymer that is most commonly produced from a reaction of ethylene glycol with either purified terephthalic acid or dimethyl terephthalate, using a continuous melt-phase polymerisation. PET is a hard, stiff, strong, dimensionally stable material that absorbs very little water [176]. It has good gas barrier properties and good chemical resistance except towards to alkalis (which hydrolyse it). Its crystallinity varies from amorphous to fairly highly crystalline. It can be highly transparent and colourless but thicker sections are usually opaque and off-white. Its melting temperature is about 255°C [177]. The chemical structure of the repeat units of PET is illustrated in **Figure 1.5**. PET chains are relatively stiff due to flexible but short  $(\text{CH}_2)_2$  groups [178]. Generally, PET is recognised to be very slow at crystallisation especially outside temperature range (around 190°C). It is highly transparent if the melt is rapidly cooled to a temperature below its  $T_g$  to form an amorphous solid. However, crystallisation takes place if the amorphous solid is heated above  $T_g$  [178]. PET is the most industrially important polyester and has been principally recognised for its use as fibre [179]. However, PET which is an engineering

plastic, is also widely used for food packaging (mainly for soft drink bottle), in electronics [180] and in a number of other applications [179, 180]. It is well known that the mechanical properties of PET are molecular weight dependent [181, 182]. It is also established that PET can degrade under conditions typically encountered during processing and that the extent of degradation is dependent on temperature and other processing variables [183-186]. It was reported [187] that when poly(ethylene oxide) segments were incorporated into PET, a large drop in  $T_g$  was observed. A major advantage of PET is its excellent permeability and good barrier properties [188]. However, PET has poor impact resistance when it is injection moulded. Blends of PET with other polymers, in particular with polyolefins, may offer an attractive balance of mechanical and barrier properties and improved processability [189].

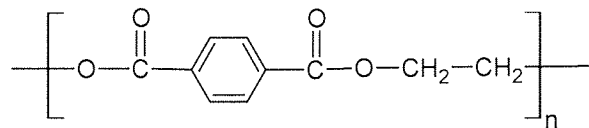


**Figure 1.5.** Chemical structure of poly(ethylene terephthalate)

### 1.10 EPR Profile

EPR (**Figure 1.6**) is formed by copolymerization of ethylene and propylene. Its properties are dependent on various parameters such as structures of the copolymer chains, the content of each of the comonomer units in the copolymer chain, the distribution of the comonomer in the composition of different chain and the average molecular weight and its distribution [176]. The EPR has rubbery properties at room temperature in which vary with the compositions of ethylene (E): propylene (P) ranging from 45:55 to 80:20 w% of E:P composition. EPR demonstrates excellent resistance to degradation by heat, light, oxygen and ozone because EPR does not have unsaturated carbon-carbon bonds [176]. However, their limitations include low resistance to oils and fuels, poor adhesion to many substrates or reinforcements and a generally low compatibility with other rubbers. EP copolymers are widely used for exterior automotive and construction parts including solid and cellular weather strips, wire and cable insulation [74]. While both PE and PP are crystallising plastics, random copolymers of ethylene and polypropylene are non-crystallising and have low  $T_g$ .

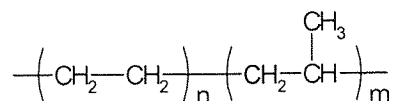


Figure 1.6. Chemical structure of ethylene-propylene rubber

### 1.11 Aim and Objectives of This Study

Conventional melt free radical reactions of GMA onto polymers has been reported in the literature to give rise to low grafting yields. Higher peroxide content would be needed in order to achieve the desired grafting level, but this approach results in severe polymer degradation and promotes homopolymerisation of the monomer. The first aim of this study was to investigate and optimise the grafting reaction of GMA on EPR in the presence of a highly reactive comonomer, and divinyl benzene (DVB) was chosen for this purpose. The *in-situ* melt free radical grafting of GMA in the presence of the reactive comonomer DVB was carried out using a novel approach developed by Aston University PPP research group [3, 9, 51, 190]. The effect of the comonomer DVB on the grafting of GMA onto EPR was conducted using  $\alpha,\alpha$ -dimethyl 2,5-bis(*t*-butylperoxy) hexane (Trigonox T101) as an initiator. The investigation examined the effect of chemical composition and the processing conditions on the grafting reaction. The functionalised polymer products were characterised using various techniques including Fourier Transform Infrared (FTIR) spectroscopy, Nuclear Magnetic Resonance (NMR) spectroscopy and melt flow index (MFI). The grafting level was determined after purification of the reaction products to remove all side reaction products and the grafts extent was then measured using a calibration curve developed through titration and FITR methods. The overall performance of the functionalised rubber in the presence of DVB ( $f$ -EPR<sub>DVB</sub>) was then compared with performance of conventionally functionalised EPR ( $f$ -EPR<sub>CONV</sub>) in absence of DVB.

The second aim of the work was to examine the effect of the synthesised functionalised EPR polymer (both DVB-modified ( $f$ -EPR<sub>DVB</sub>) and the synthesised conventional ( $f$ -EPR<sub>CONV</sub>) on the extent of compatibilisation of binary blends of PET/ $f$ -EPR. The efficiency of these functionalised EPR polymers in compatilising PET/ $f$ -EPR blends was examined using various techniques such as scanning electron microscopy (SEM),

tensile test, dynamic mechanical analyser (DMA) and FTIR spectroscopy of fractionated blend components in order to examine the extent of the reaction at the interphase. Ternary blends based on PET/EPR/*f*-EPR as well as PET/EPR/commercial terpolymer, ethylene-methylacrylate-glycidylmethacrylate (EM-GMA) or copolymer, ethylene-glycidylmethacrylate (E-GMA) containing GMA were also examined and the performance of the ternary PET/EPR/*f*-EPR blends was also compared with that of the corresponding binary PET/*f*-EPR blends.

## CHAPTER 2

## EXPERIMENTAL AND ANALYTICAL TECHNIQUES

## 2.1 Materials

## 2.1.1 Polymers

Two different polymers were used in this work, see **Table 2.1**,

1. Ethylene-propylene Rubber (EPR): Commercial grade Tafmer P-0280, pellet, supplied by Mitsui Chemical.
2. Poly(ethylene terephthalate) (PET): Film grade of PET (Eastapak™ PET9921W), pellets, supplied by Eastman Chemical Limited.

**Table 2-1:** Polymers used in the experiments

Name	Structure (repeat units)	Supplier	Grade, form & properties	FTIR Spectrum
Ethylene-propylene rubber (EPR)	$\left( \text{CH}_2 - \text{CH}_2 \right)_n \left( \text{CH}_2 - \overset{\text{CH}_3}{\text{CH}} \right)_m$	Mitsui Chemical	Tafmer P- 0280 White pellet MFI=4.9 g/10min E:P=8:2	Fig 2.1
Poly(ethylene-terephthalate) (PET)	$\text{HO} - \text{CH}_2 - \text{CH}_2 - \left[ \text{O} - \overset{\text{O}}{\parallel} \text{C} - \text{C}_6\text{H}_4 - \overset{\text{O}}{\parallel} \text{C} - \text{O} - \text{CH}_2 - \text{CH}_2 \right]_n - \text{OH}$	Eastman Chemical Limited	Eastapak 9921W White pellet	Fig 2.2

Four commercial compatibilisers were also used, see **Table 2.2**, as follows:

1. Terpolymer: Ethylene-methylacrylate-glycidylmethacrylate terpolymer (EM-GMA<sub>8(6)</sub>), was a commercial grade (Lotader AX8900), pellets with a ratio of ethylene: methyl acrylate: glycidyl methacrylate: of 67:25:8 w/w and a melt flow index (MFI) of 6g/10min (ASTM 1238-2.1kg load, 190°C, based on the data provided by manufacturer (Atofina Chemical company)). The level of GMA content was 8%.
2. Terpolymer: Ethylene-methylacrylate-glycidyl methacrylate terpolymer (EM-GMA<sub>1(9)</sub>) was a commercial grade (Lotader AX8920), pellets with a ratio of ethylene: methyl acrylate: glycidyl methacrylate: of 71:28:1 w/w and a melt flow index (MFI) of 8g/10min (ASTM 1238-2.1kg load, 190 °C, based on the



data provided by manufacturer (Atofina Chemical company)). The level of GMA content was 1 %.

3. Terpolymer: ethylene-methylacrylate-glycidyl methacrylate terpolymer (EM-GMA<sub>9(85)</sub>) was a commercial grade (Lotader AX8950) pellets with a ratio of ethylene: methylacrylate: glycidylmethacrylate: of 76:15:9 w/w and a melt flow index (MFI) of 85g/10min (ASTM 1238-2.1kg load, 190 °C, based on the data provided by the manufacturer (Atofina Chemical company). The level of GMA content was 9 %.
4. Copolymer: ethylene-glycidyl methacrylate (E-GMA<sub>8(5)</sub>) was a commercial grade (Lotader AX8840) pellets with a ratio of ethylene-glycidyl methacrylate of 92:8 w/w and a melt flow index (MFI) of 5 g/10min (ASTM 1238-2.1kg load, 190 °C), based on the data provided by manufacturer (Atofina Chemical company). The level of GMA content was 8%.

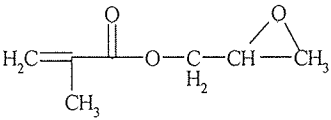

**Table 2.2:** Compatibilisers used in the PET blends

No.	Name	Structure (repeat unit)	Supplier/Grade	GMA% Ester Content MFI	Form
1	Ethylene-methylacrylate-glycidylmethacrylate terpolymer (EM-GMA <sub>8</sub> )		Atofina Chemical Lotader AX8900	GMA=8 % MFI=6g/10min Ester=25 %	White Pellets
2	Ethylene-methylacrylate-glycidylmethacrylate terpolymer (EM-GMA <sub>1</sub> )		Atofina Chemical Lotader AX8920	GMA=1 % MFI=8g/10min Ester=28%	White Pellets
3	Ethylene-methylacrylate-glycidylmethacrylate terpolymer (EM-GMA <sub>9</sub> )		Atofina Chemical Lotader AX8950	GMA=9 % MFI=85g/10min Ester=15	White Pellets
4	Ethylene-glycidyl methacrylate copolymer (E-GMA <sub>8</sub> )		Atofina Chemical Lotader AX8840	GMA=8 % MFI=5g/10min Ester=0	White Pellets

### 2.1.2 Monomer and Comonomer

Glycidyl methacrylate (GMA) (97% purity) and divinylbenzene (DVB) (80% purity) were purchased from Aldrich Chemical Co. Ltd and used as received, see **Table 2.3**.

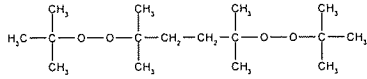
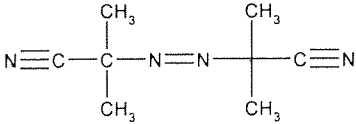
**Table 2.3.** Monomer and comonomer used in the experiments

No.	Name	Structure/ Molecular weight, Half life	Supplier	Colour, Form Boiling Point, Purity	FTIR Spectra
1	Glycidyl methacrylate (GMA) CAS No. 106-91-2	 M.w (142)	Aldrich Chemicals Ltd	Colourless liquid B.P=189°C Purity=97%	Fig. 2.3
2	Divinyl Benzene (DVB) CAS No. 1321-74-0	 M.w (130)	Aldrich Chemicals Ltd.	Mixture of o- and p-isomers Colourless liquid B.P=180°C Purity=80%	Fig. 2.4

### 2.1.3 Initiators

The peroxide, 2,5- dimethyl 2,5-bis(t-butylperoxy)hexane, Trigonox 101 (T101) was provided by Akzo Nobel and used without further purification. The initiator 2,2-azoisobutyronitrile (AIBN) was supplied by Ventron and used without further purification, see **Table 2.4**.

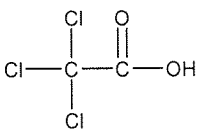
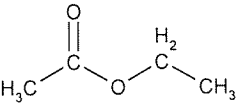
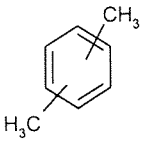
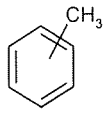
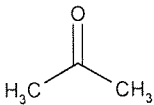
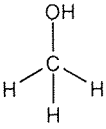
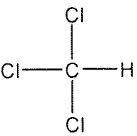
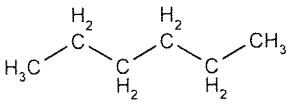
**Table 2.4.** Initiators used in the experiments

No.	Name	Structure (repeat unit)// (Molecular weight)//	Supplier	Colour, form Boiling Point, Melting point, purity	FTIR Spectra
1	$\alpha,\alpha$ - dimethyl 2,5-bis(t-butylperoxy) hexane <b>Trogonox 101 (T101)</b> CAS No. 78-63-7	 M.w (290), Half life=1 min at 190°C	AKZO	Colourless liquid B.P=369.4 °C Purity=98%	Fig. 2.5
2	2,2-azobis(2-methylpropionitrile) (AIBN) CAS No. 78-61-1	 M.w (164), Half life=1.42 min at 180°C	Ventron	White powder M.P=102°C Purity=98%	Fig. 2.6

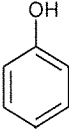
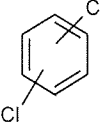
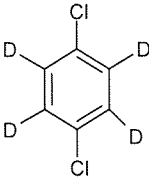
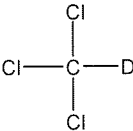
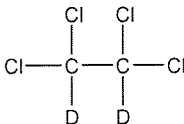
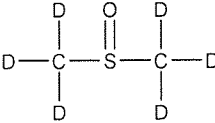
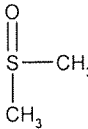
### 2.1.4 Solvents and Additives

Trichloroacetic acid (TCA) and 1.0 N potassium hydroxide (KOH) standard solution in methanol were of analytical grade and were supplied by Aldrich Chemical Co (see **Table 2.5**). Solvents such as xylene, toluene, acetone, methanol, chloroform, hexane and ethyl acetic acid, phenol, dichlorobenzene were of reagent grade and were used without further purification. see **Table 2.5**.

**Table 2.5.** Solvents and chemical additive used in the experiments

No.	Name	Structure (repeat unit)/ (Molecular weight)	Supplier	Colour, Form Boiling Point, Purity
1	Trichloroacetic Acid (TCA)		Aldrich Chemicals Ltd	Crystals with a slight odour M.P.=196°C Purity=98%
2	Potassium hydroxide	K-O-H	Aldrich Chemicals Ltd	White pallet M.P 360 °C
3	Ethyl acetate		Fisher Chemical	Colourless liquid B.P. 77.1 °C
4	Xylene		Fisher Chemical	Colourless liquid B.P. 138-139°C
5	Toluene		Fisher Chemical	Colourless liquid B.P. 110-111°C
6	Acetone		Fisher Chemical	Colourless liquid B.P. 55-56 °C
7	Methanol		Fisher Chemical	Colourless liquid B.P. 64-65 °C
9	Chloroform		Fisher Chemical	Colourless liquid B.P. 60-62 °C
10	Hexane		Fisher Chemical	Colourless liquid B.P. 68-69 °C

**Table 2.5.** Solvents and chemical additive used in the experiments (continue)

11	Phenol		Fisher Chemical	White crystal solid M.P. 40.5 °C
12	Dichlorobenzene		Fisher Chemical	Colorless to light yellow B.P. 179-180 °C
13	1,4-Dichlorobenzene-d4		Sigma-Aldrich	Colorless B.P. 173 °C 98 % deuterated
14	Chloroform-d		Sigma-Aldrich	Colorless B.P. 60.9 °C 99.8 % deuterated
15	1,1,2,2-Tetrachloroethane-d2		Alfa Aesar	Colorless B.P. 147 °C 99.6 % deuterated
16	Dimethyl sulfoxide -d6		Alfa Aesar	Colorless B.P. 190 °C 95.5 % deuterated
17	Dimethyl sulfoxide		Fisher Chemical	Clear, colorless liquid B.P. 189 °C

## 2.2 Processing and Sample Preparation

### 2.2.1 Polymer Functionalisation by Reactive Processing

The reactive processing was carried out using a Thermo-Haake (Rheomix 600) internal mixer using roller rotors. The mixing chamber has three plates which are electrically heated and run with a PolyLab motor drive, equipped with a digital torque displaying unit and a ram which can be pressed down to offer closed chamber system and exerts pressure on the polymer during mixing. The temperature can be controlled up to 400°C and compressed air is used as a cooling system. The torque and temperature of the

chamber were determined by the mixer sensors. The data were monitored and recorded via the associated Polylab software.

The net chamber volume ( $V_n$ ) with the roller rotors in use was  $69 \text{ cm}^3$ . However the amount of the polymer needed to fill the chamber depends on its melt density. The melt density of EPR was measured using Ray Ran Melt Flow Indexer at  $190 \text{ }^\circ\text{C}$ . The EPR was charged into pre-heated cylinder of the Melt Flow Indexer and kept for 4 minutes before introducing a 2.16 kg load on the piston. The amount of extrudate through a standard die (2.095 mm diameter) obtained in a given length of the cylinder was weighed. The melt density of the polymer was calculated using **Eqn. 2.1**.

$$\text{Melt density (Ray Ran)} = \frac{\text{Mass of extrudate}}{\text{Volume of the cylinder at length of 1 cm}} \quad [191] \quad (\text{Eqn. 2.1})$$

Example of calculation:

$$\begin{aligned} \text{Melt density of EPR } (\rho) &= 0.56/0.71 \times 1 \\ &= \mathbf{0.79 \text{ g/cm}^3} \end{aligned}$$

The mass of extrudate = 0.56 g

Area of the barrel (given) =  $0.71 \text{ cm}^2$  [191]

The piston travel distance = 1 cm

Volume of the cylinder =  $0.71 \text{ cm}^3$

The amount of polymer needed to fill the chamber was calculated using **Eqn. 2.2**. Based on the melt density measured, the amount of EPR needed to fill the chamber was found to be about 38 g.

$$\text{Sample weight (mass) (for Haake mixer)} = \frac{\rho \times V_n \times 70\%}{100} \quad (\text{Eqn. 2.2})$$

Where

$$\begin{aligned} \rho &= \text{Melt Density } (0.79 \text{ g/cm}^3) \\ V_n &= \text{Net chamber volume} = 69 \text{ cm}^3 \\ 70\% &= \text{Filling percentage} \end{aligned}$$

The filling percentage of 70% refers to the total percentage of the volume of the chamber

The total weight of the polymer and reagents to fill the chamber was fixed at 43 g and within this total weight, the amount of EPR was around 38 g.

### 2.2.2 Functionalisation of EPR with GMA in Absence and Presence of the Comonomer Divinyl benzene (DVB)

The melt free radical grafting of glycidyl methacrylate (GMA) on ethylene propylene rubber (EPR) was carried out in an internal mixer (Haake Rheomix). The formulations were prepared by initially pre-weighing the appropriate amounts of polymer and modifiers. The mixing chamber was initially preheated and flushed with nitrogen for more than 15 seconds to eliminate oxygen from the chamber and minimise polymer oxidation. The mixing (using roller rotor) was carried out for 15 minutes at the required temperature using rotor speed of 65 rpm with the ram down offering a closed chamber condition. In the absence of DVB, the polymer was first charged into the chamber and processed for one minute followed by injection in the melt of a mixture of neat GMA and peroxide T101 (mixed at different molar ratios) using a syringe. Once the additives were charged, the ram was immediately lowered to keep a closed system during the mixing and to minimise the loss of GMA and T101. The torque and temperature were continuously monitored during the melt processing (see **Scheme 2.1**). The processed polymer was removed from the mixer and quenched in dry ice to prevent further reactions before storage in air tight polyethylene bags.

In the presence of DVB, the polymer was tumble mixed with the DVB before charging into the chamber. This was then processed with the ram down (to homogenise) for one minute followed by injection of a mixture of GMA and peroxide using a syringe (see **Scheme 2.2**). The injection of reagents into the mixing chamber was done carefully in order to minimise their losses through evaporation. Prior to injection, the hopper was removed in order to allow for a better positioning of the syringe for injection of the reagents followed by a rapid return of the hopper to its original position after the reagents were injected. This provided better control in terms of pointing the syringe directly onto the melt and minimising losses. The mixing was allowed to continue for 14 minutes before discharging the product into dry ice to prevent further oxidation. Both

torque and temperature were continuously monitored throughout the processing operation.

### 2.2.3 Physical and Reactive Blending of PET with Functionalised EPR or Terpolymers

Reactive and physical blending were carried out in a Haake mixer either in the presence or absence of the functionalised EPR, see **Scheme 2.3**. PET and EPR were dried at 120°C and at 35°C, respectively in a vacuum oven for 24 hours before use. The pre-weighed PET and EPR were first tumble mixed with EPR-g-GMA or terpolymer at a given ratio in a paper cup and then introduced into the preheated mixing chamber after flushing with nitrogen for half minute, followed by lowering the piston down quickly to keep a closed mixing system. The mixing temperature, rotor speed and mixing time were set at 260°C, 65 rpm and 10 minutes. The torque and temperature of the mixing chamber were recorded using in Polylab software. The molten polymer blends were then removed and quenched in dry ice to avoid oxidation followed by granulation which were kept into air-tight sample bags. The granulated blends were pre-dried in normal oven for 24 hours at 60°C before use.

### 2.3 Purification of Functionalised EPR

GMA functionalised polymers have to be purified before the grafting degree could be evaluated in order to eliminate any unreacted monomer, homopolymers and copolymer which might be formed during the reactive processing step. 3 g of grafted EPR (small film pieces) was placed in a paper thimble (weight known) and Soxhlet extracted for 24 hour with 120 cm<sup>3</sup> xylene under oxygen free nitrogen atmosphere (**Scheme 2.4**). The crosslinked polymer was separated out as xylene insoluble (see **Scheme 2.4A**). The xylene soluble fraction was precipitated in 7 time excess volume of acetone to give a soluble fraction containing the unreacted (free) GMA and polyGMA while the insoluble fraction contained the GMA-grafted-polymer. When the soluble xylene fraction was precipitated in methanol, the unreacted (free) GMA was soluble while the grafted GMA and polyGMA precipitated out. In the presence of DVB, the homopolymer of DVB (polyDVB), the copolymer of DVB with GMA (DVB-co-GMA) and any crosslinked polymer were separated out as xylene insolubles (stayed in the thimble) **Scheme 2.4B**). The soluble fraction was precipitated in acetone or methanol as described above. The

precipitated polymers obtained from both routes were then dried for 24 hr in a vacuum oven at 50°C.

## 2.4 Fractionation of PET/*f*-EEPR Blends by Sequential Solvent Extraction for Characterisation of Interfacial Reaction

The samples in granule form were dissolved in a mixed solvent of phenol/chlorobenzene/xylene (35/35/30 w/w%) at 140°C for 3 hours in the presence of nitrogen gas to prevent oxidation. In principle, phenol/chlorobenzene is a good solvent mixture for PET, whereas xylene is a good solvent for EPR [28]. For precipitation of PET based products, the dissolved PET and PET-co-EPR-g-GMA (in solvents) was added to hot toluene. The PET fraction (containing PET-co-EPR-g-GMA) was filtered off and washed with toluene, dried and its IR spectrum recorded. The clear remaining solutions which contained soluble EPR and any formed EPR-g-GMA-co-PET was then added to methanol to precipitate the EPR and EPR-g-GMA-co-PET. The EPR fraction was then filtered off and subsequently washed with methanol. The polymers obtained from both fractions were dried in a vacuum oven at 70°C for 24 hours. About 0.2 g of both dried polymer samples were pressed into thin films by compression moulding (at 270°C). The films were then analysed using FTIR spectroscopy. The steps of sequential solvent extraction are shown in **Scheme 4.2, Chapter 4, p 189**. From the IR spectrum, the amount of PET present in the EPR fraction (and vice versa) was determined using **Eqn 2.3**.

$$\text{Index} = \frac{\text{Peak Area of a specific absorption}}{\text{Thickness of the film used}} \quad (\text{Eqn. 2.3})$$

## 2.5 Films and Plaques Preparation

### i) Films preparation for FTIR Spectroscopy Analysis

Small amount of processed polymers were used to prepare thin films having thickness of 0.03-0.05mm for FTIR spectroscopic analysis using a Bradleys Hydraulic Press. About 0.2 g of a processed polymer was placed in between two PTFE sheets placed between stainless steel plates assembly. The plates and the polymer were then placed under the platens of the electrically preheated press at 170°C for 2 minutes without applying pressure. In the case of PET and its blends, the films were prepared at the



temperature of 270°C for 7 minutes preheating. A pressure of about 40kg/cm<sup>2</sup> was then applied for 1 minute before cooling the assembly (running waters through press platens) below 70°C under full pressure (40 kg/cm<sup>2</sup>). Once cooled, the assembly was then taken out and the thin films were removed and stored for further analysis.

## ii) Plaques Preparation for DMA and Tensile Measurement

3 mm thick plaques of PET/EPR blends were prepared by compression moulding for tensile property measurement, dynamic mechanical thermal analysis (DMA) and scanning electron microscopy (SEM) analysis. The blends were dried in a normal oven at 60°C for 24 hours before moulding. About 24 gram polymer blend granules were placed uniformly in a square spacer with dimensions 15×15×1.4 mm and covered with two PTFE (polytetrafluoroethylene) sheets and two steel plates. This was placed between the electrically heated platens of the press; the temperature was set at 270°C, and held for 6 minutes under minimum load for preheating. A pressure of 40kg/cm<sup>2</sup> was then applied for 2 minutes and then the heating was switched off and cold water circulated through the plates. The plates were taken out of the press once cooled.

## 2.6 Synthesis of Side Reaction Products

### 2.6.1 Homopolymerisation of GMA in Chloroform

Homopolymerisation of GMA was carried out using AIBN as an initiator in 120 cm<sup>3</sup> chloroform. 8.53 g GMA was mixed with 0.1 molar ratio (AIBN/GMA) of the initiator AIBN to GMA in a 250 cm<sup>3</sup> three-neck round bottom flask. After assembling with thermometer, condenser and purging with nitrogen gas, it was refluxed for 4 hours at 70°C. After cooling to room temperature, the solution was precipitated into 400 cm<sup>3</sup> methanol, filtered and washed thoroughly with methanol. After the filtration, the polyGMA (in powder form) was dried in vacuum oven at 70°C for 24 hours (see **Scheme 2.5**). FTIR spectrum of the polyGMA is shown in **Figure 2.7**. (Full characterisations is described in **Chapter 3** later)

### 2.6.2 Homopolymerisation of DVB in Hexane

Homopolymerisation of DVB was carried out using AIBN as an initiator in 120 cm<sup>3</sup> hexane. 5.0 g DVB was mixed with 0.3 molar ratio (AIBN/DVB) of the initiator AIBN to DVB in a 250 cm<sup>3</sup> three-neck round bottom flask. After assembling with

thermometer, condenser and purging with nitrogen gas, the solution was refluxed for 4 hours. The homopolymerisation of polyDVB took place at temperature of 70 °C with continuous stirring. After cooling down to room temperature, the solution was washed with chloroform and filtered resulting in polyDVB (in powder form) which was then dried in a vacuum oven at 70°C for 24 hours (see **Scheme 2.6**). FTIR spectrum of the polyDVB is shown in **Figure 2.8**. (Full characterisation is given in **Chapter 3**).

### **2.6.3 Copolymerisation of GMA and DVB in Hexane**

Copolymerisation of GMA and DVB at ratio of 6/4 w/w% was carried out on bench using AIBN as an initiator in 120 cm<sup>3</sup> hexane. 5.0 g GMA and 3.3 g DVB were mixed at 0.2 molar ratio of AIBN/(GMA+DVB) in a 250 ml three-neck round bottom flask. After assembling with thermometer, condenser and purging with nitrogen gas, the solution was refluxed for 4 hours at 70°C. After cooling down to room temperature, the solution was washed thoroughly with chloroform and filtered, giving GMA-co-DVB (in powder form) which was then dried in vacuum oven for 24 hours (see **Scheme 2.7**). FTIR spectrum of the GMA-co-DVB is shown in **Figure 2.9**. (Full characterisation is given in **Chapter 3**).

## **2.7 Characterisation of Processed Polymers and Blends**

### **2.7.1 Determination of Melt Index**

The melt flow index (MFI) is a measure of melt viscosity and is related to the molecular weight of the polymer. It is defined as the molten polymer extruded under a weight of 2.16 kg through a 2.095 mm diameter die in a given time. MFI of GMA functionalised EPR samples were measured using a Ray Ran Melt Flow Indexer at a constant extrusion temperature of 230°C and 2.16 kg load in accordance with ASTM D 1238. A standard die of 1 mm diameter was used for all samples. After the samples were granulated, 3 g of each sample was charged into the barrel within one minute. The sample was then preheated for 4 min before placing the load to drive the molten polymer through the die. The time interval for the cut off was 1 to 4 minutes depending on the flow rate of each sample. In this measurement, five samples per each measurement were taken and their averages calculated as shown in **Eqn. 2.4**.

$$\text{MFI (g/10min)} = \frac{m \times 10}{t \text{ (min)}} \quad (\text{Eqn. 2.4})$$

Where ,

$m$  : the average weight of extrudates (g)

$t$  : time of extrusion (min)=10min

### 2.7.2 Determination of Insoluble Gel

The insoluble gel is a measure of the insoluble fraction caused by crosslinking of a modified polymer after being exhaustively extracted with a solvent that dissolves the virgin polymer. A known weight of finely cut processed polymer sample was placed in a known weight paper thimble and was Soxhlet extracted using xylene (b.p=138°C) as a solvent, with the thimble temperature of about 80°C, for 24 hours. Nitrogen was introduced into the system to avoid oxidation during the extraction. The thimble was then dried in a vacuum oven at room temperature for 24 hours and was reweighed. The net weight of the residue was obtained and gel content was calculated as shown in Eqn.2.5.

$$\text{Gel content \%} = \frac{W_1}{W_2} \times 100 \quad (\text{Eqn. 2.5})$$

Where,

$W_1$  is the residue weight of the extracted polymer (insoluble in the thimble)

$W_2$  is the original weight of the polymer used before extraction.

### 2.7.3 Solubility Test

Molau test has been used to qualitatively investigate the compatibility of polymer blends [192, 193]. In this test, 3g polymer (from reactive and physical blends) was dissolved in 90 cm<sup>3</sup> of the mixed solvent of phenol/tetrachloroethene (60/40 w/w%) at a temperature of 90°C for 4 hours. PET dissolves in this solvent mixture whereas the EPR phase is insoluble. The samples were dissolved in a tube containing the mixed solvent and were left at room temperature for a long period. For incompatible blends, the component separated out and floated on top of the clear solution. However if the blend was compatibilised, the solution turned milky and a colloidal suspension arose.

## 2.8 Determination of GMA Grafting Degree by Titration and Calibration Against IR.

The grafting parameters were calculated from the mass of purified reaction products before and after grafting. The grafting degree is defined as the weight percentage of grafted monomer onto a polymer backbone (Eqn. 2.6).

$$\text{Grafting Degree (\%)} = \frac{M (V - V_1) \text{ M.W} \times 100}{1000 \times W} \quad (\text{Eqn. 2.6})$$

(by titration)

Example of calculation:

$$\begin{aligned} \text{Grafting Degree (\%)} &= \frac{0.1(15.2-14.1) \times 142.12 \times 100}{1000 \times 0.5} \\ &= 2.8\% \end{aligned}$$

Where;

M= molar concentration of KOH (0.1M)

V= Volume of KOH consumed by the blank sample (15.2 cm<sup>3</sup>)

V<sub>1</sub>= Volume of KOH consumed by the purified sample (14.1 cm<sup>3</sup>)

W= weight of sample (0.5 g)

M.W=molecular weight of GMA (142.12)

The total amount of grafted GMA and polyGMA was determined from extracted purified samples (precipitate in methanol) (see Scheme 2.4C) using FTIR spectroscopy and titration methods. The GMA grafting level was determined from purified samples precipitated in acetone, see Scheme 2.4D. Thus, the concentration of polyGMA in the purified samples was calculated by subtraction from the total values of grafted GMA and polyGMA, (Eqn. 2.7)

$$\text{PolyGMA (\%)} = (\text{PolyGMA} + \text{Grafted GMA}) - \text{Grafted GMA} \quad (\text{Eqn. 2.7})$$

To determine the degree of grafting of GMA by IR spectroscopy, a calibration curve between IR spectroscopy and titration had to be constructed. For the IR spectroscopy, the carbonyl absorption at 1729 cm<sup>-1</sup> was used in the modified and purified polymer

along with a reference peak at  $719\text{ cm}^{-1}$  corresponding to  $[\sim(\text{CH}_2)_n\text{ (}n>4\text{)}]$  rocking absorption of EPR]. The carbonyl absorption peak area boundaries were defined from  $1786\text{ cm}^{-1}$  to  $1662\text{ cm}^{-1}$  for peak maximum at  $1729\text{ cm}^{-1}$  and the boundaries for the reference peak were defined from  $680\text{-}781\text{ cm}^{-1}$ , (**Figure 2.10**). The amount of grafted GMA was calculated from absorption area ratio of  $1729\text{ cm}^{-1}$  to  $719\text{ cm}^{-1}$  according to **Eqn. 2.8**.

$$\begin{aligned} \text{Index Area Ratio (X)} &= \frac{\text{Peak Area of Carbonyl Absorption}}{\text{Peak Area of Reference Peak}} \\ &= \frac{A_{1662-1786\text{ cm}^{-1}}}{A_{680-781\text{ cm}^{-1}}} \end{aligned} \quad (\text{Eqn. 2.8})$$

To work out the grafting level from the value of index area ratio, calibration curve had to be used (see **Eqn. 2.8**).

A titration method for determining the GMA grafting degree as reported in the literature [9, 20, 23, 55] was used in this work. About 1.0 g of a purified GMA functionalised polymers was completely dissolved in  $75\text{ cm}^3$  hot toluene (around  $110^\circ\text{C}$ ). 5.0 ml of 0.3M trichloroacetic acid (TCA) was then added into the dissolved polymer (see **Scheme 2.8**). The mixture was stirred continuously for over 90 minute at temperature of  $100\text{ -}110^\circ\text{C}$  to drive the ring opening reaction of the epoxy group with the acid (see **Rn-2.1**). The solution was then precipitated into  $100\text{ cm}^3$  ethyl acetate with continuous stirring at ambient temperature. The filtrate containing the residual trichloroacetic acid after reacting with the epoxy group of GMA was then titrated with 0.1M KOH solution in methanol until the first permanent pink end point was achieved (pink color must stay for at least 1 min, see **Rn-2.2**). 0.3% phenolphthalein in methanol was used as an indicator.

For a reference (blank), 1.0 g of unmodified processed polymer was also titrated using a similar procedure. The amount of 0.1M KOH consumed to react with TCA until permanent pink end point achieved was recorded and the degree of grafted GMA onto EPR was determined using **Eqn. 2.6**.

To confirm that the reaction of the epoxy group with the acid has occurred, the precipitated polymer was dried in vacuum oven for 24 hours at 70°C. FTIR spectroscopic characterisation of the samples was carried out and it was shown that the epoxy absorption peaks at 909 cm<sup>-1</sup> and 845 cm<sup>-1</sup> have completely disappeared (see **Figure 2.11**). Furthermore, a new absorption peak at 1772 cm<sup>-1</sup> was observed due to trichloro ester group (see **Figure 2.12**) and a new absorption peak at 3432 cm<sup>-1</sup> corresponding to -OH group formed during the ring open reaction was also observed (see **Figure 2.13**). This confirms the reaction of epoxy group with trichloroacetic has taken place.

A calibration curve (**Figure 2.14**) was established based on a correlation between the grafting degree measured by titration (**Eqn. 2.6**) and the carbonyl absorption area ratio determined by FTIR from a set of purified EPR-g-GMA samples **Eqn. 2.8**. From the calibration curve, the degree of grafting was calculated using **Eqn. 2.9**

$$Y = 0.2812 X \quad (\text{Eqn. 2.9})$$

$$X = \frac{Y}{0.2812} \quad (\text{value of slope of the curve})$$

Where,

X = Grafted GMA (%)

Y = Peak Area Index from FTIR measurement  
( $A_{1662-1786 \text{ cm}^{-1}} / A_{680-781 \text{ cm}^{-1}}$ ) (**Eqn. 2.6**)

0.2812 = Value of slope obtained from the calibration curve (**Figure 2.14**)

## 2.9 Experimental Error

Experimental error, which is generally caused by analytical systems and individual operations, is shown as scatter of the values of experimental results. In this work, the deviation was determined based on statistics derived from replicate measurements of representative samples. The processing variability was determined based on statistics derived from replicate processing runs of representative samples using equations below [194].

The variability of the grafting yield measurement of purified samples from titration results caused by the processing step, was determined from three repeats processing of representative samples to access the batch-to-batch uncertainty and the repeatability of titration measurements from the same representative sample was also carried out (see **Table 2.6** and **Table 2.7**). In addition, the variability the grafting yield measurement of purified samples was also statistically determined from three replicate titration measurement of representative samples. The standard deviation derivation,  $\sigma$  (see **Eqn. 2.12**) and the percentage (%) relative standard derivation, % RSD, (see **Eqn. 2.13**), of the grafting yield are used as quantitative measures of the scatter (reproducibility) of the data. It shows that the average error is low and therefore the titration measurements were considered accurate.

$$\bar{X} = \text{arithmetic mean} = \sum \frac{X_i}{N} \quad (\text{Eqn. 2.10})$$

Where,

$X_i$  = numerical result of the  $i^{\text{th}}$  run

$$\sigma = \sqrt{\frac{\sum (X_i - \bar{X})^2}{N}} \quad (\text{Eqn. 2.11})$$

Where,

$\sigma$  = Standard derivative

$N = 3$  (total number of runs)

$X$  = Arithmetic Mean

$$\text{RSD (\%)} = \text{relative standard deviation} = \frac{\sigma \cdot 100}{\bar{X}} \quad (\text{Eqn. 2.12})$$

$$95\% \text{ CL} = 95\% \text{ confidence limit} = \sigma \cdot [t/N^{1/2}] \quad (\text{Eqn. 2.13})$$

Where,

RSD = Relative standard deviation

CL = Confidence limit

$t$  = Factor which varies with the confidence limit and the value of  $N$

$[t / N^{1/2}] = 8.99$  (for 2 measurements)

$[t / N^{1/2}] = 2.48$  (for 3 measurements) [194]

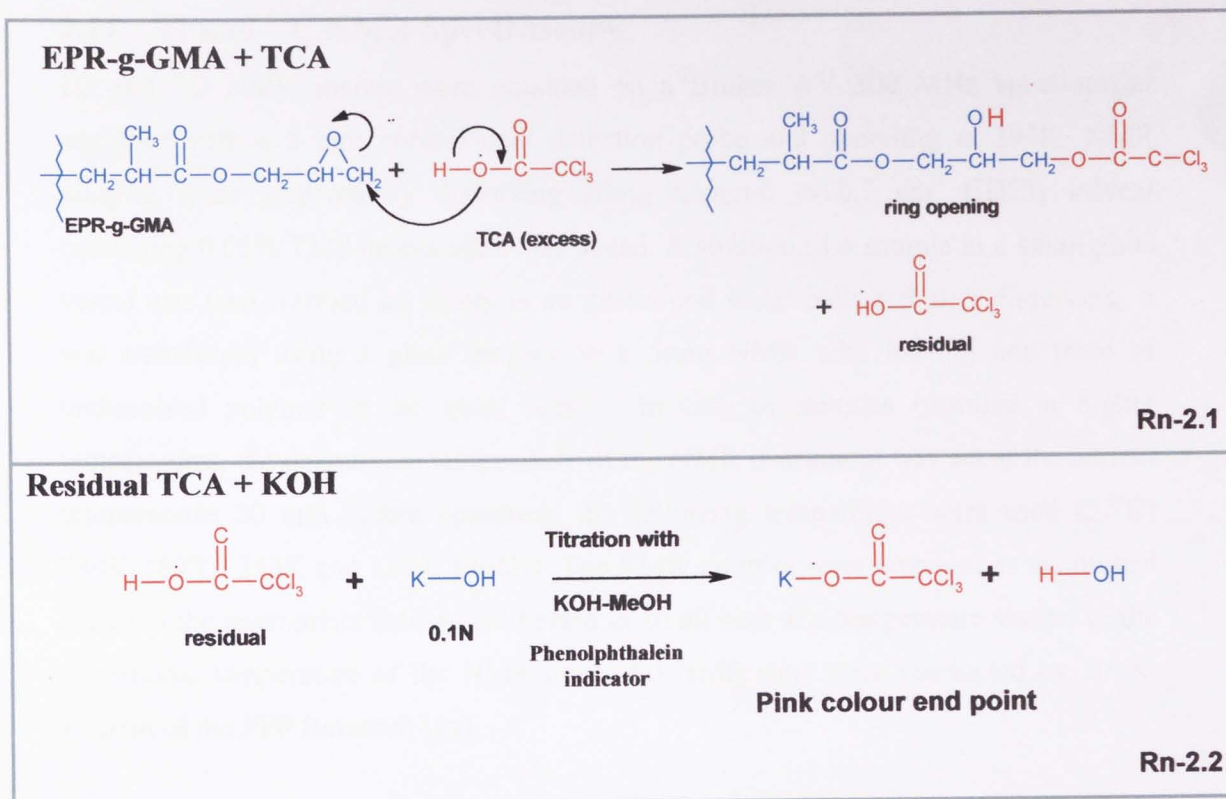
**Table 2.6:** Standard deviation in the grafting degree measurement by titration for samples from triplicate processing of representative sample under the same conditions. Sample-G19 (conventional), see Table 3.1 (Chapter 3 p.70)

Number of RUN (processing)	Volume of 0.1M KOH used (ml) (a)	Grafting yield (%) (b)	Average grafting yields (%)	Mean (X)	Standard Deviation	RSD (%)	95% CL
1	V <sub>1</sub> = 14.4	2.04	2.07	2.07	0.03	1.4	0.072
	V <sub>1</sub> = 14.4	2.06					
	V <sub>1</sub> = 14.4	2.10					
2	V <sub>1</sub> = 14.4	2.03	1.99	1.99	0.04	2.01	0.099
	V <sub>1</sub> = 14.4	1.95					
	V <sub>1</sub> = 14.5	1.99					
3	V <sub>1</sub> = 14.4	2.06	2.04	2.04	0.06	2.89	0.147
	V <sub>1</sub> = 14.4	1.98					
	V <sub>1</sub> = 14.3	2.09					
Average			2.033	2.033	0.043	2.033	0.106
Volume KOH used for the blank sample = 15.2 ml							

**Table 2.7:** Standard deviation in the grafting degree measurement by titration for samples from triplicate processing of representative sample under the same conditions. Sample-DG13 (comonomer DVB), see Table 3.1 (Chapter 3 p.71)

Number of RUN (processing)	Volume of 0.1M KOH used (ml) (a)	Grafting yield (%) (b)	Average grafting yields (%)	Mean (X)	Standard Deviation	RSD (%)	95% CL
1	V <sub>1</sub> = 14.1	3.00	3.05	3.05	0.04	1.47	0.111
	V <sub>1</sub> = 14.1	3.05					
	V <sub>1</sub> = 14.0	3.09					
2	V <sub>1</sub> = 14.0	2.95	2.95	2.95	0.02	0.67	0.049
	V <sub>1</sub> = 14.0	3.02					
	V <sub>1</sub> = 14.1	2.97					
3	V <sub>1</sub> = 14.2	2.97	2.98	2.98	0.04	1.25	0.092
	V <sub>1</sub> = 14.1	2.94					
	V <sub>1</sub> = 14.1	2.94					
Average			2.993	2.993	0.033	1.113	0.084
Volume KOH used for the blank sample = 15.2 ml							





## 2.10 FTIR Spectroscopy

Fourier Transform Infrared (FTIR) spectroscopic investigation of blends was used to characterize the reaction of the glycidyl epoxy groups of the grafted GMA in EPR with the -OH and -COOH groups in PET. FTIR measurements were performed on a Perkin Elmer Spectrum One over the range of 4000-400  $\text{cm}^{-1}$  and spectral collection was taken over 16 scans with resolution of 4  $\text{cm}^{-1}$ . For solid samples which are not able to form a film, they were analysed in form of pressed potassium bromide (KBr) discs. The samples were mixed (0.5 g sample in 0.1 g KBr) with dry KBr (dried in oven at 120°C to remove moisture) and were then ground to form a homogenous mixture. The mixture was pressed for 3 minutes to form a thin disc. The FTIR spectra of liquid samples were recorded as thin films held between two KBr windows. In the case of polymer, films which were prepared as described in **Section 2.5(i)**, and were clamped onto a metal plate having a 25x14 mm aperture and the samples were presented to the beam in the usual position.

## 2.11 $^1\text{H}$ and $^{13}\text{C}$ NMR Spectroscopy

1D and 2D NMR spectra were obtained on a Bruker AV 300 MHz spectrometer equipped with a 5 mm normal dual detection probe and operating at 293K. NMR samples were prepared by dissolving 20mg material in 0.7 cm<sup>3</sup> CDCl<sub>3</sub> solvent containing 0.05% TMS unless otherwise stated. A solution of a sample in a small glass vessel was then warmed up gently in an ultrasound water bath and after dissolving, it was transferred using a glass dropper to a 5mm NMR tube leaving any trace of undissolved polymer in the glass vessel. In case of samples recorded at higher temperatures, the operational temperature of the NMR instrument was set at the correct temperatures 30 min before operation, the following temperature were used (57°C) 330K, (80°C) 353K and 135°C (408K). The NMR samples were prepared as mentioned above in the appropriate solvent but heated in an oil bath at a temperature similar to the operational temperature of the NMR once. All NMR runs were conducted by Dr K. Doudin of the PPP Research Unit.

### 2.11.1 $^1\text{H}$ NMR Spectroscopy

For  $^1\text{H}$ , the spectrometer was operated at 300.13 MHz employing a high-resolution dual ( $^1\text{H}$   $^{13}\text{C}$ ) gradients probe. Spectra were recorded using the zg30 pulse program with  $P_{90} = 12 \mu\text{s}$  covering a sweep width of 12 ppm with 64k time domain data points giving an acquisition time of 9 seconds, with number of scans, (NS) of 128 or 1k. It was Fourier transformed using 32k data points and referenced to an internal TMS standard at 0.0 ppm.

### 2.11.2 $^{13}\text{C}$ NMR Spectroscopy

PENDANT  $^{13}\text{C}$  NMR spectra were obtained on the spectrometer operating at 75 MHz for carbon. The pendant pulse program was used with waltz16 decoupling during acquisition, using a delay, d4, of 1.64 ms (145 Hz), and a relaxation delay, d1, of 3 second. The spectra were recorded over a sweep width of 250 ppm with 32k time domain data points giving an acquisition time of 0.9 seconds, with number of scans, NS of 12K. Fourier transformed using 32k data points phased for CH<sub>3</sub>/CH positive and CH<sub>2</sub> negative and referenced to an internal TMS standard at 0.0 ppm.

### 2.11.3 2D $^1\text{H}$ - $^{13}\text{C}$ HSQC

2D  $^1\text{H}$ - $^{13}\text{C}$  HSQC (Heteronuclear Single Quantum Coherence) spectra correlate  $^1\text{H}$  and  $^{13}\text{C}$  chemical shifts through one-bond heteronuclear scalar coupling ( $^1J_{\text{CH}}$ ). The cross peaks in the  $^1\text{H}$ - $^{13}\text{C}$  HSQC spectrum show the chemical shift of  $^1\text{H}$  one axis (horizontal) correlated  $^{13}\text{C}$  on the other axis (vertical) that belongs to the **H-C atoms directly bonded to each others**. The pulse sequence utilizes several polarization transfer steps that increase the overall sensitivity of the experiment, the sequence includes inverse detection i.e.  $^1\text{H}$  detection rather than  $^{13}\text{C}$  detection. The following acquisition parameters were used for: F2; spectral width (F2 350 Hz), (588 Hz); time domain points, 512 (2 K); relaxation delay, 1.5 s; number of scans, 8 (24); and q delay, 1.923 ms, corresponding to a heteronuclear coupling constant of 130 Hz. The BIRD delay was optimized for each experiment separately and was ca. 0.4 s (1.3 s); 90 (128) time increments were acquired in the indirect dimension (F1 with a  $^{13}\text{C}$  spectral window of 60 Hz (2705 Hz).)

The HSQC spectra (64 scans, with the FID time domain F2 having a digital acquisition of 2048 data points and the time domain F1 having 256 data points) were acquired using a relaxation delay of 1.5 s with phase-sensitive states-time proportional phase incrementation (TPPI). Approximately 12 h of spectrometer time was usually necessary to acquire the data for each sample. The data were processed with a  $90^\circ$  shifted squared sine multiplication (QSINE) window function in the F1 dimensions ( $^{13}\text{C}$ ) and a Gaussian function in the F2 dimensions ( $^1\text{H}$ ), and a 1 Hz line broadening in both dimensions.

### 2.11.4 2D $^1\text{H}$ - $^{13}\text{C}$ HMBC

2D  $^1\text{H}$ - $^{13}\text{C}$  HMBC (Heteronuclear Multiple Bond Coherence) spectra correlate  $^1\text{H}$  and  $^{13}\text{C}$  chemical shifts through multiple-bond heteronuclear scalar coupling ( $^nJ_{\text{CH}}$ ,  $n = 2$  or 3). The cross peaks in the  $^1\text{H}$ - $^{13}\text{C}$  HMBC spectrum show the chemical shift of  $^1\text{H}$  one axis (horizontal) correlated  $^{13}\text{C}$  on the other axis (vertical) that belong to H and C atoms that are separated by two or three chemical bonds. Just like the HSQC, the HMBC pulse sequence utilizes  $^1\text{H}$  to  $^{13}\text{C}$  polarisation transfer and inverse ( $^1\text{H}$ ) detection for optimum sensitivity. HMBC spectra were optimized for a long range  $J_{\text{H-C}}$  of 7Hz ( $d_6=0.07\text{s}$ ).

### 2.11.5 CP/MAS $^{13}\text{C}$ NMR Spectroscopy

The solid-state CP/MAS  $^{13}\text{C}$  NMR spectroscopy experiments were performed on the same Bruker Avance-300 spectrometer operating at frequencies of 75 MHz for  $^{13}\text{C}$ . All the experiments were carried out at ambient temperature using a Bruker 4-mm MAS probe. The samples were packed in 4-mm ZrO rotors and spun at 4.5 or 6 kHz and  $^{13}\text{C}$  CP/MAS data were acquired with 400 scans accumulated/sample.

## 2.12 Testing

### 2.12.1 Tensile Test

The tensile properties were measured on a Tinius Olsen Tensile Tester H25KS. The computer software collected the selected tensile data and carried out a statistical analysis automatically. Five replicates per sample were required to get an accurate confidence limit. The test specimens were cut from the 1mm thick plaque which was prepared before by using a dumb-bell shape cutter. The dimension of the cutter and specimens was 4mm in width and 30mm in length. A pair of grips were used to grip the ends of the dumb-bell shape specimens. All the tensile tests were carried out at a crosshead speed of 10mm/min in accordance with ISO 527 to measure the strain at room temperature. The tensile strength, elongation at break and energy to break were recorded.

### 2.12.2 Dynamic Mechanical Properties

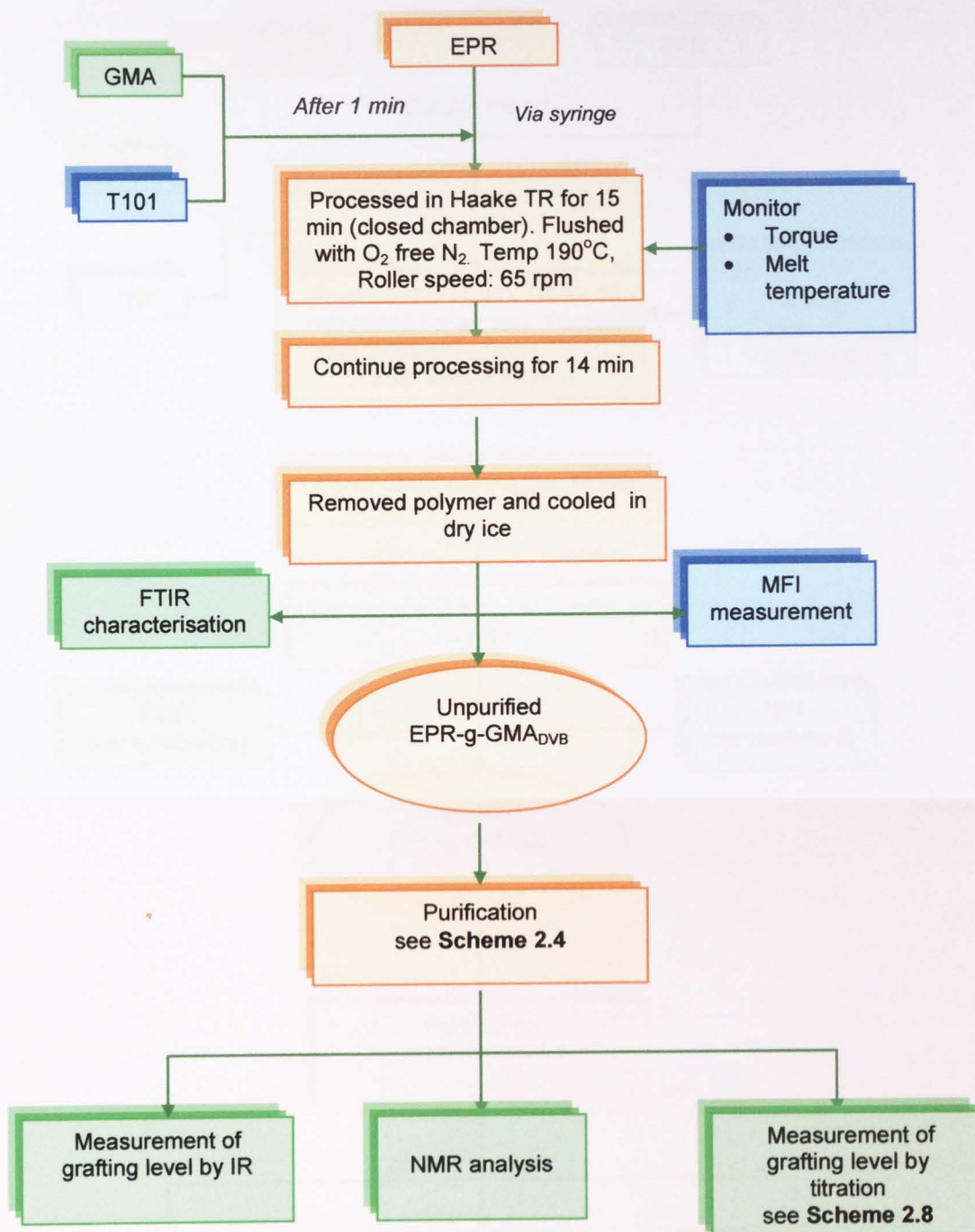
Perkin Elmer Pyris Diamond dynamic mechanical analyser (DMA) was used to measure the dynamic mechanical properties of the PET blends. The dynamic mechanical properties include storage modulus  $E'$ , loss modulus  $E''$  and the internal friction  $\tan \delta$  ( $\tan \delta = E''/E'$ ). DMA is a good technique to study the compatibilisation of blends. Generally, for an incompatible blend, the  $\tan \delta$  vs temperature curve shows two  $\tan \delta$  (or damping peaks) corresponding to the glass transition temperatures of the individual polymers. For highly miscible blends the curves show only a single peak in between the transition temperatures of the component polymers, whereas there are two separate peaks corresponding to the individual polymers in the case of partially compatible polymer blends, but the position of the peaks normally is shifted to higher or lower temperatures as a function of composition [1]. DMA analysis of PET blends or the virgin components was carried out at a fixed frequency of 1 Hz in a bending mode over

the temperature range of  $-80^{\circ}\text{C}$  to  $180^{\circ}\text{C}$  at a  $2^{\circ}\text{C}/\text{min}$  temperature rise, using liquid nitrogen as a cryogenic medium. The dimension of the test specimens which was cut from compression moulded plaques were  $50\times 10\times 3\text{mm}$ , see **Sec. 2.5(ii)**. The data were processed by a dedicated computer and the storage modulus and  $\tan \delta$  were plotted against temperature.

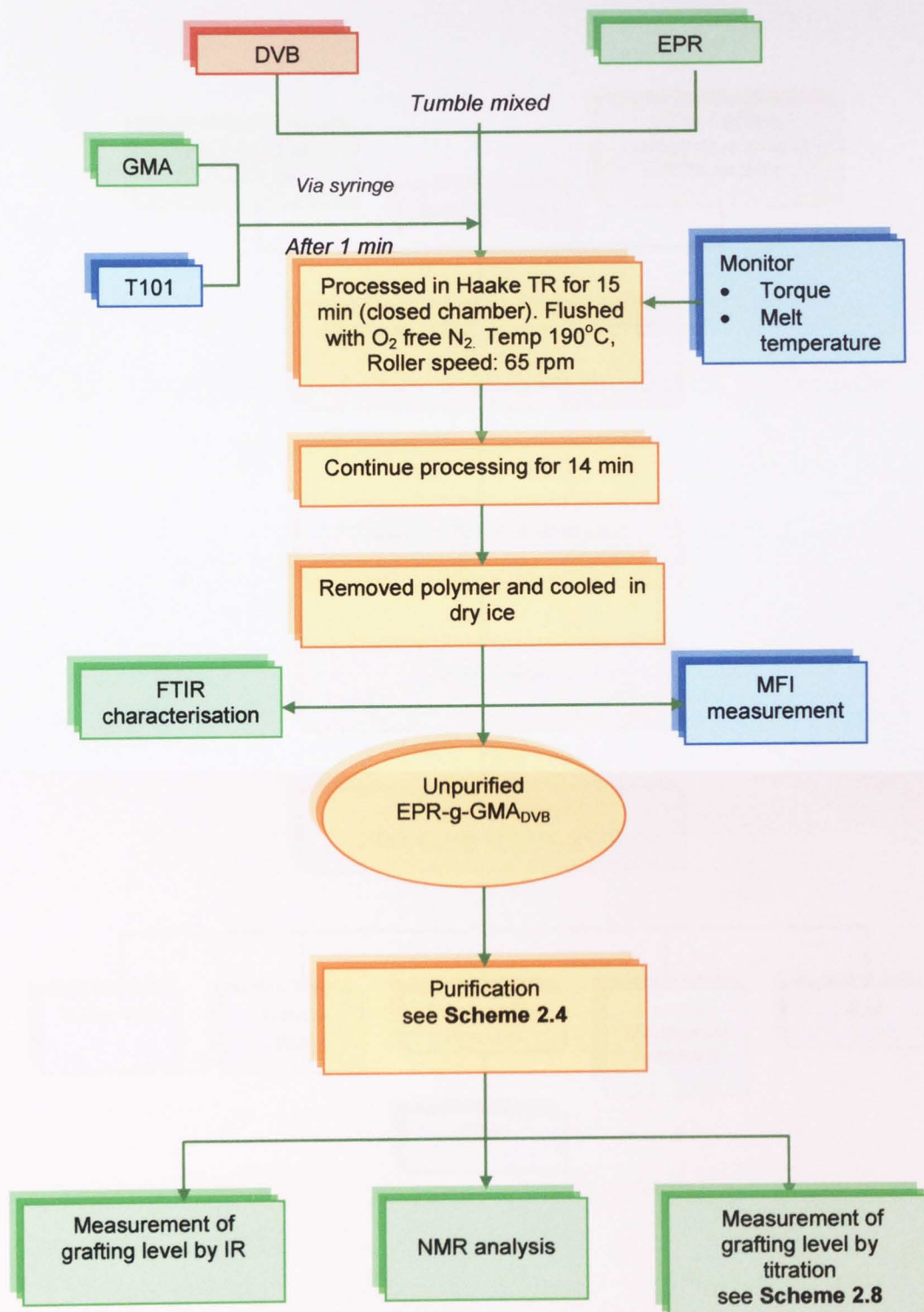
### **2.12.3 Scanning Electron Microscopy (SEM)**

Scanning electron microscopy (SEM) was used to characterise the morphology of blends including surface roughness, fracture surface, and adhesive failure [195]. In this study, the samples were characterized from a cross-section of cryogenically fractured surfaces of the compression-moulded plaques by using a Cambridge Instruments Stereoscan 90 Scanning Electron Microscope. Strips cut out from 1mm compression moulded plaques were placed in liquid nitrogen for 20 minutes and bended (by clamping from one end) at  $180^{\circ}\text{C}$  until fracture. For better observation of any adhesion between the phases, the cryogenically fractured surfaces were etched with boiling xylene for 5 hours in order to remove the EPR or/and terpolymers. The samples were washed with acetone and then dried in a normal oven at  $50^{\circ}\text{C}$ . The ends of samples with fractured surfaces were cut with a sharp blade and attached to a metal stub using a double sided sticky carbon pad with the fractured surface facing up. The samples were sputter coated with gold using an Emscope SM300 Coater prior to SEM examination.

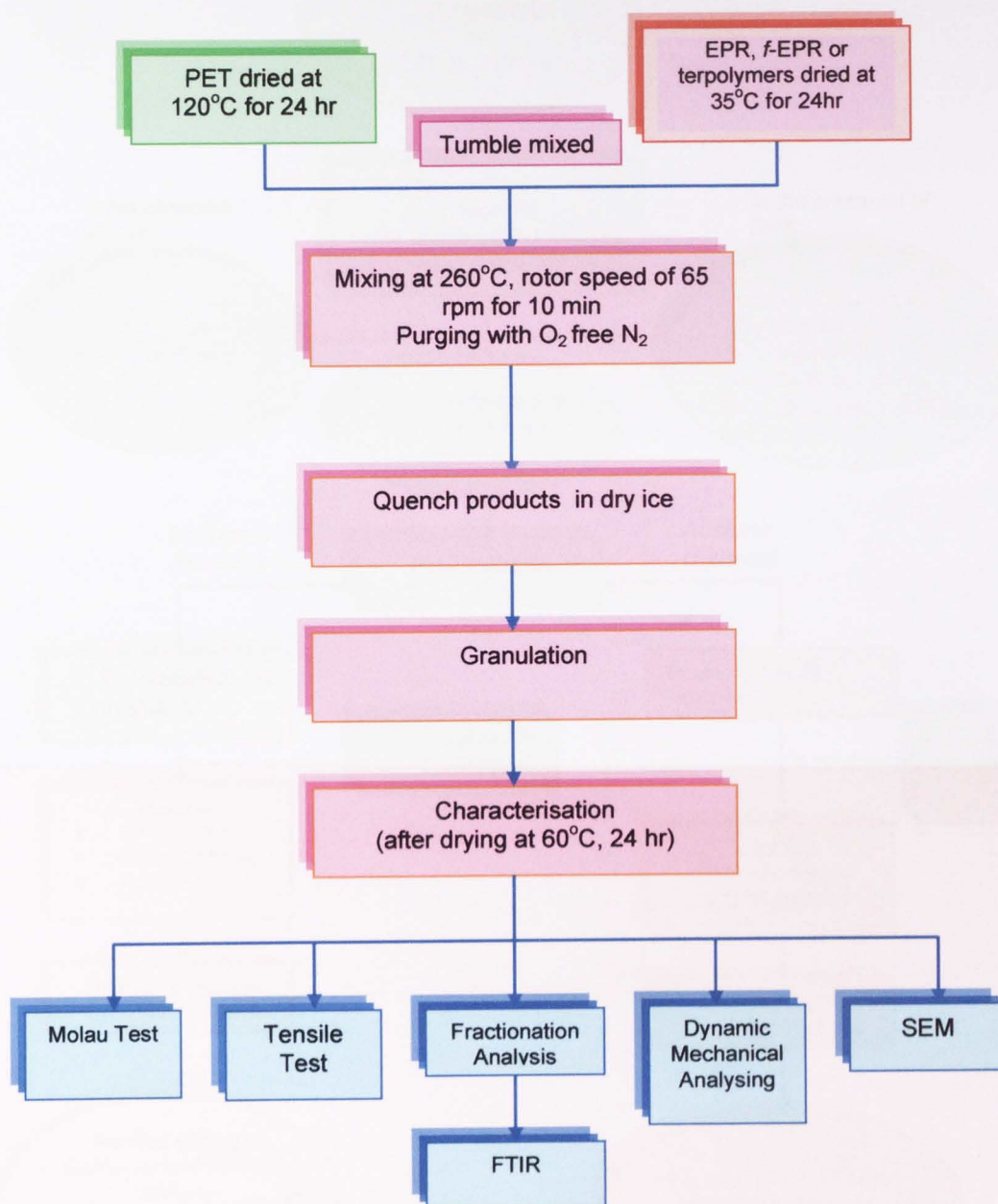
Scheme 2.1: Methodology for Grafting GMA onto EPR in the Absence of DVB



Scheme 2.2: Methodology for Grafting GMA onto EPR in the Presence of DVB

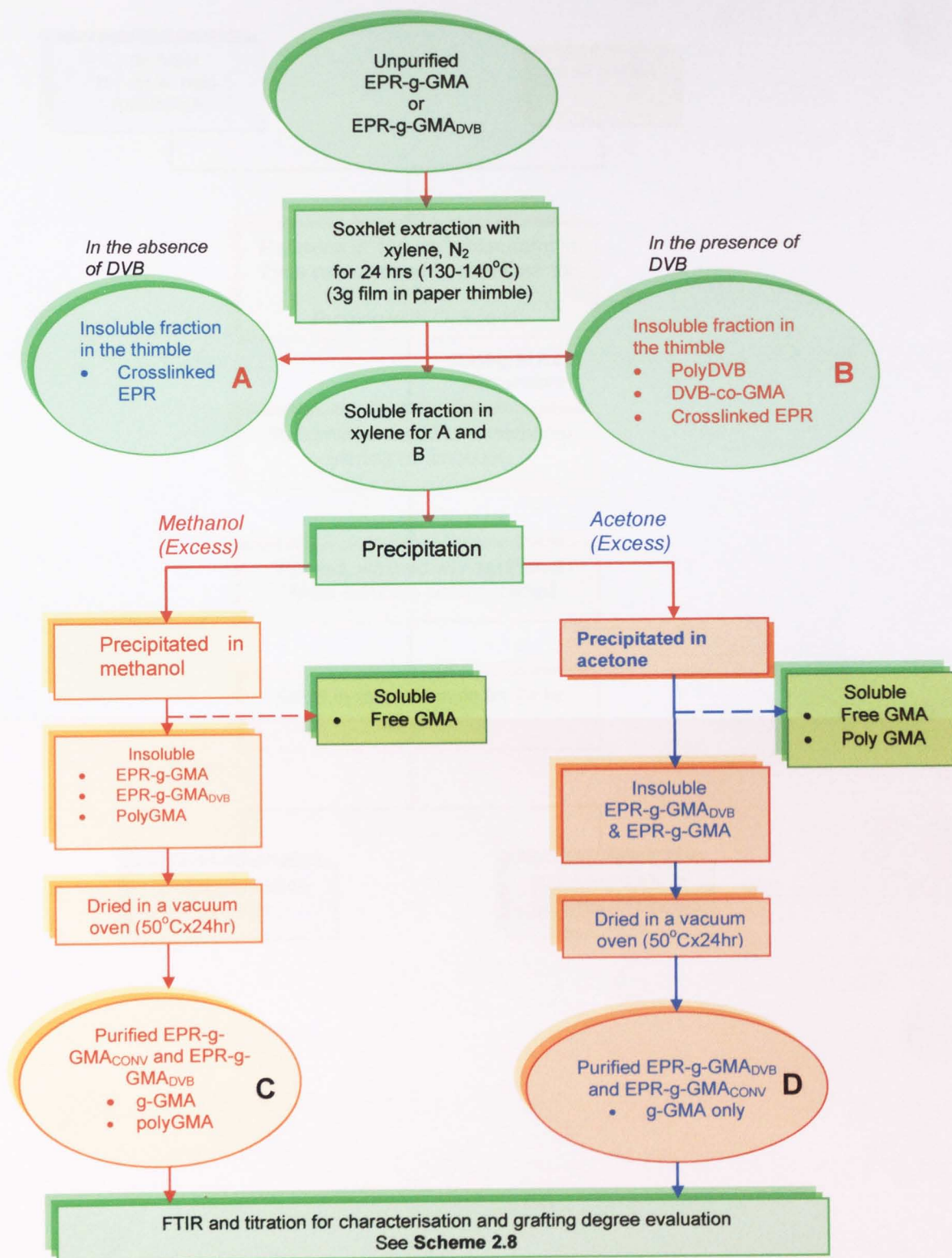


Scheme 2.3. PET/EPR or terpolymer blends

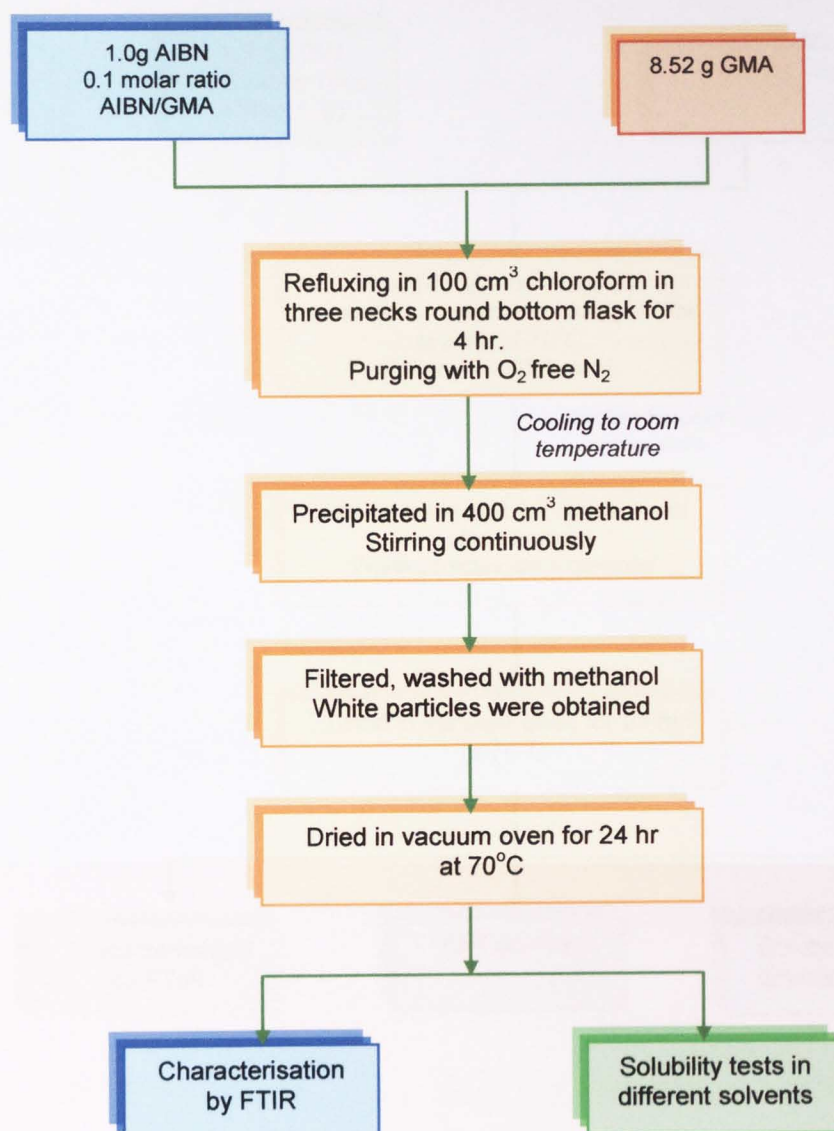




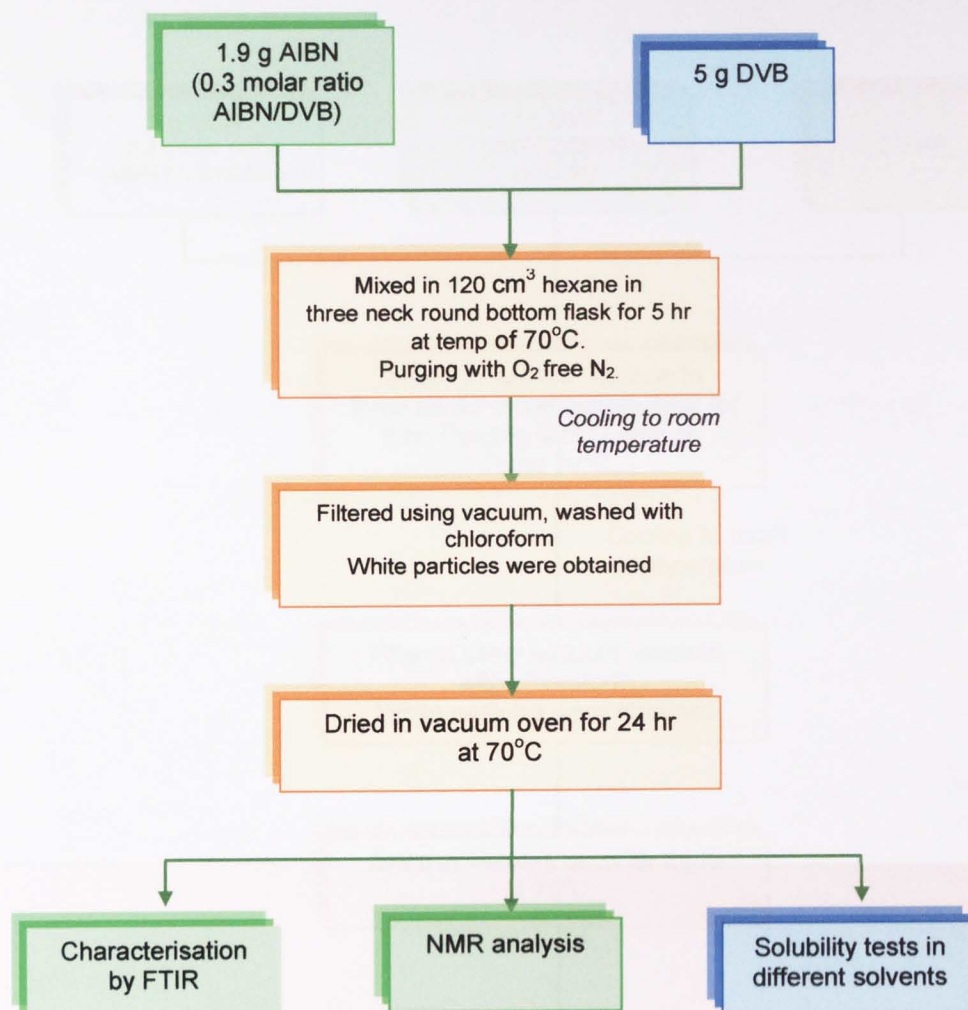
Scheme 2.4: Purification of GMA grafted EPR in the absence or presence of DVB



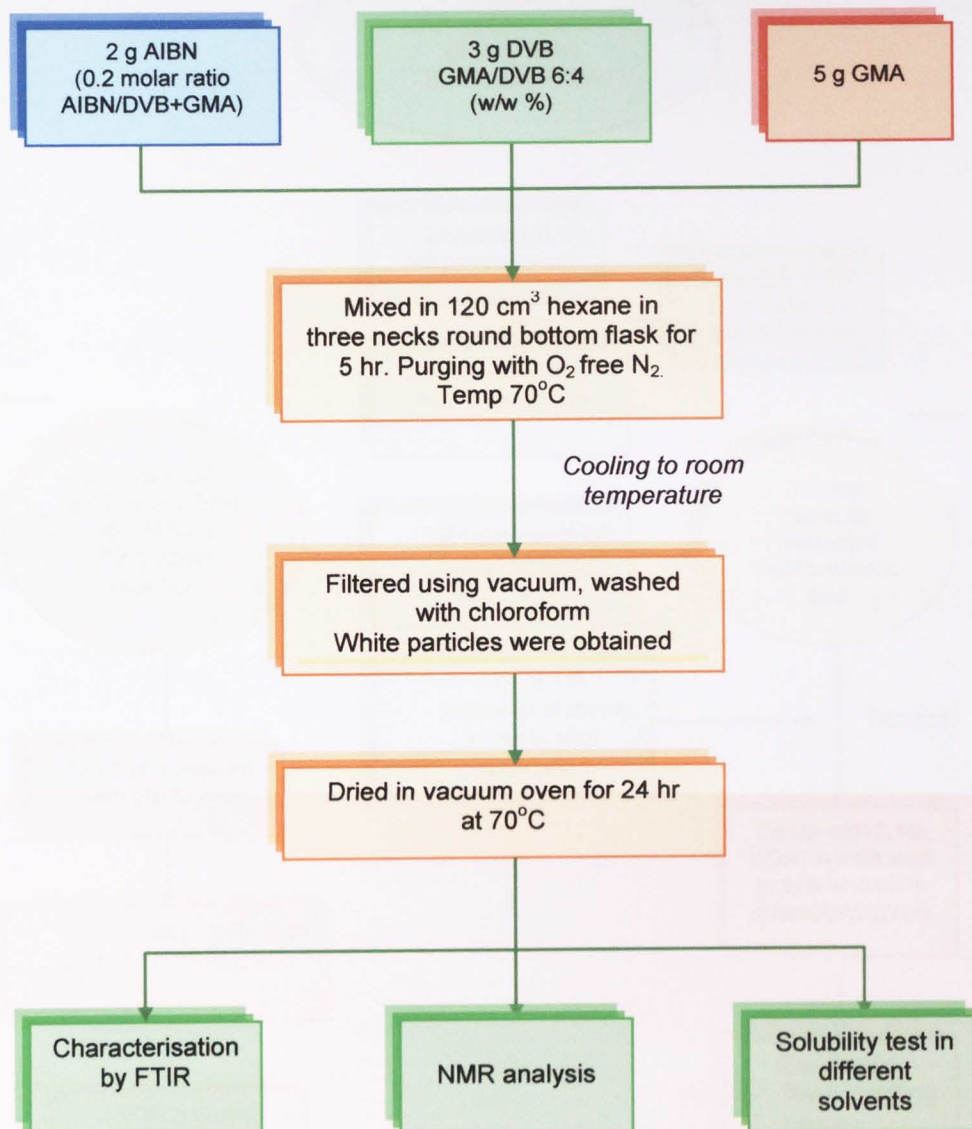
Scheme 2.5: Homopolymerisation of GMA in Chloroform



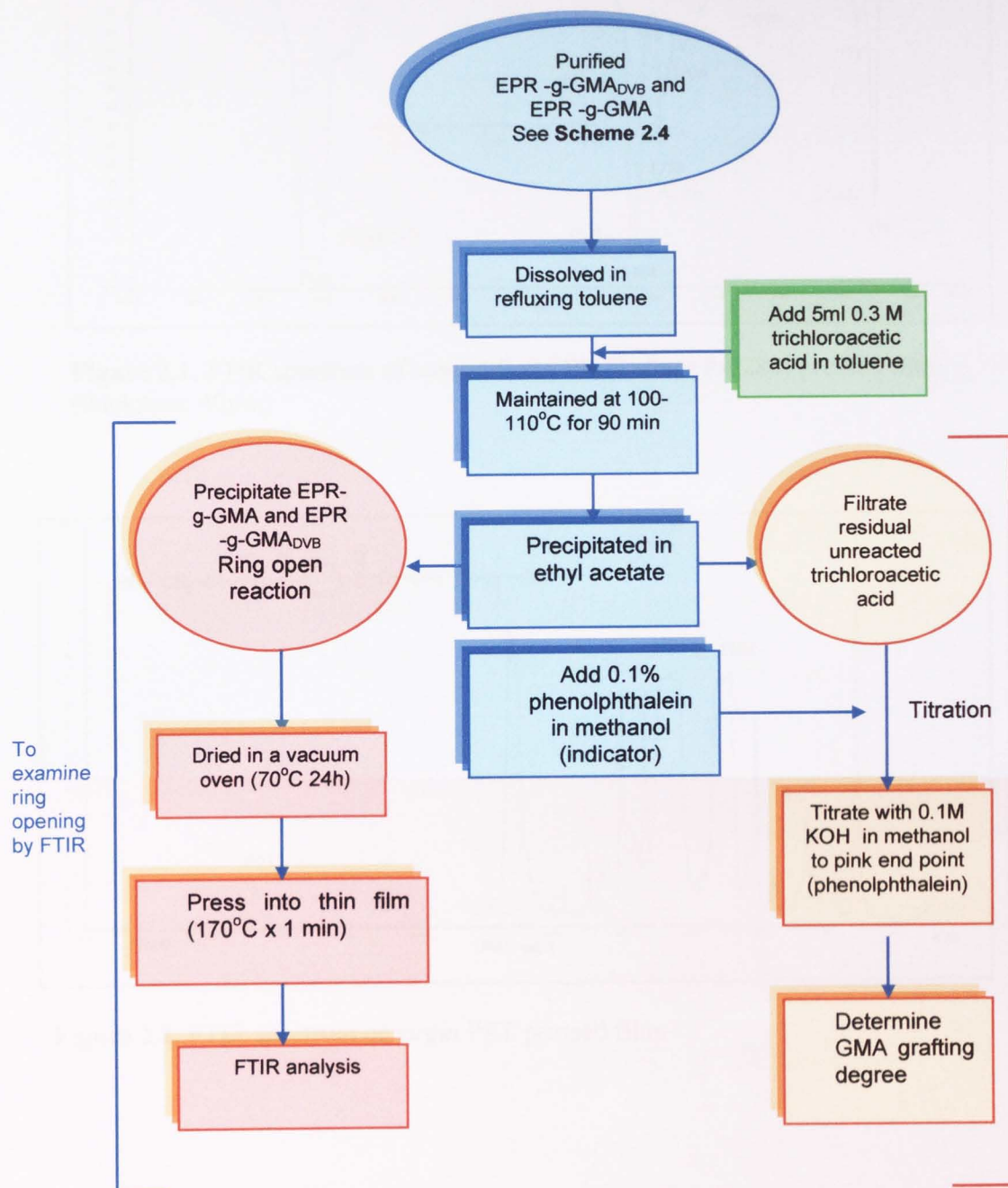
Scheme 2.6: Homopolymerisation of DVB in Hexane



Scheme 2.7: Homopolymerisation of GMA-co-DVB in Hexane



Scheme 2.8: Flow Chart for Analysis of EPR-g-GMA by Titration



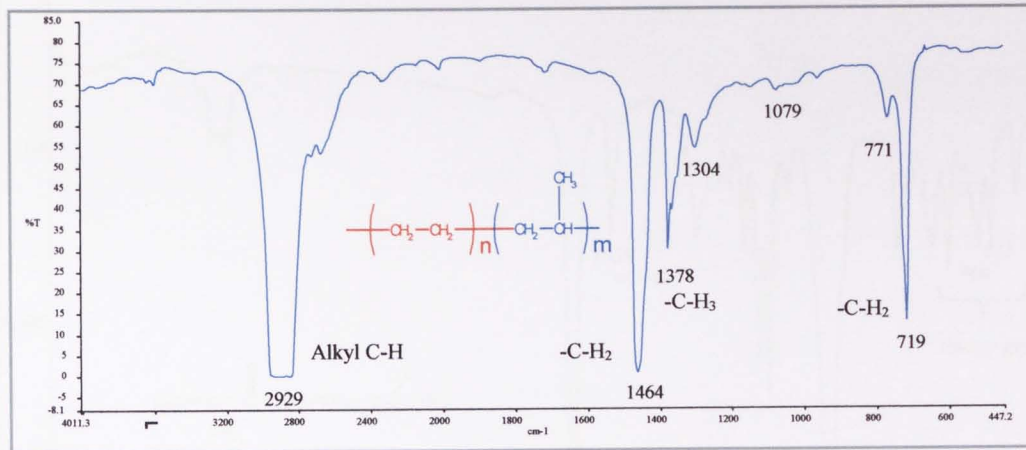


**Figure 2.1.** FTIR spectrum of unmodified EPR (Tafmer P-0280) pressed film (thickness: 40 $\mu$ m)

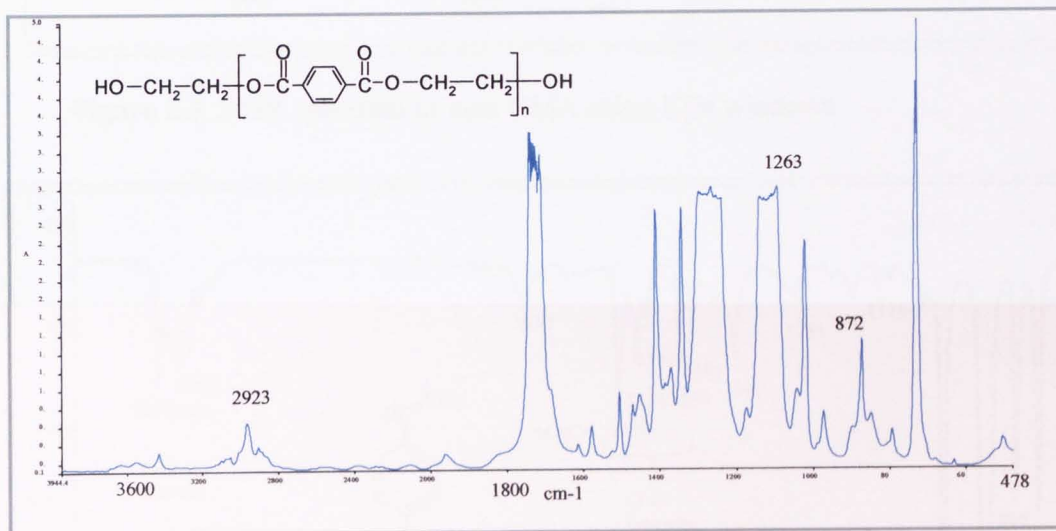


**Figure 2.2.** FTIR spectrum of virgin PET pressed film.

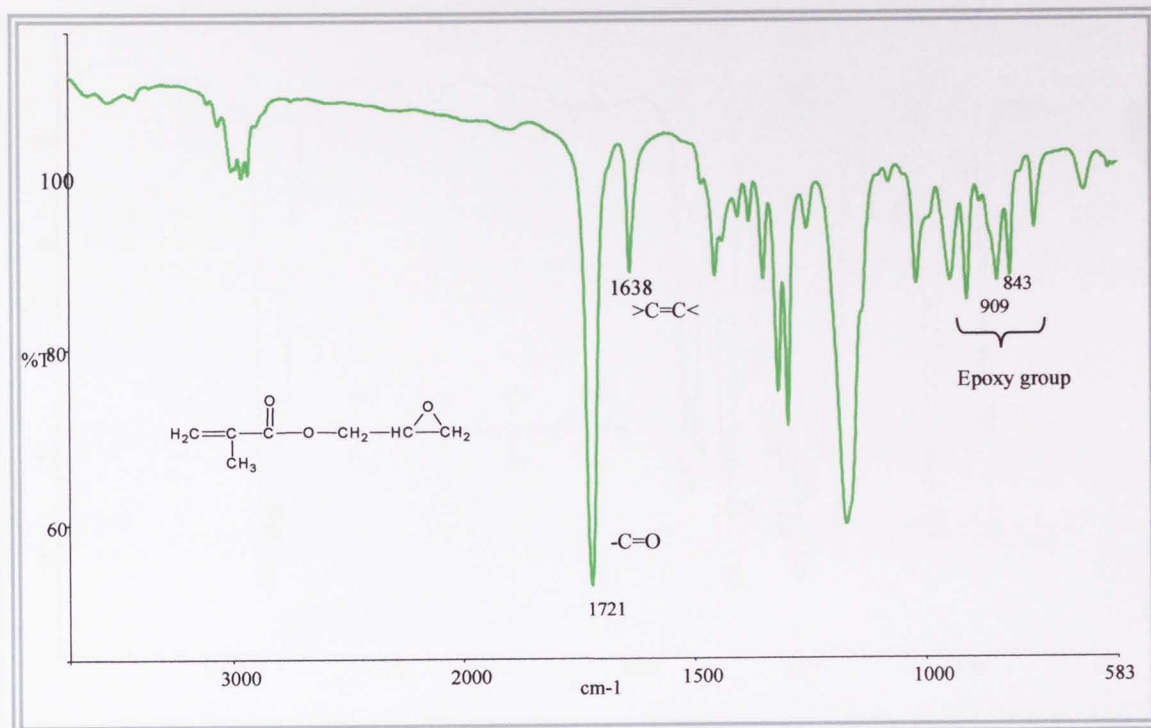


Figure 2.3. FTIR spectrum of neat GMA using KBr windows

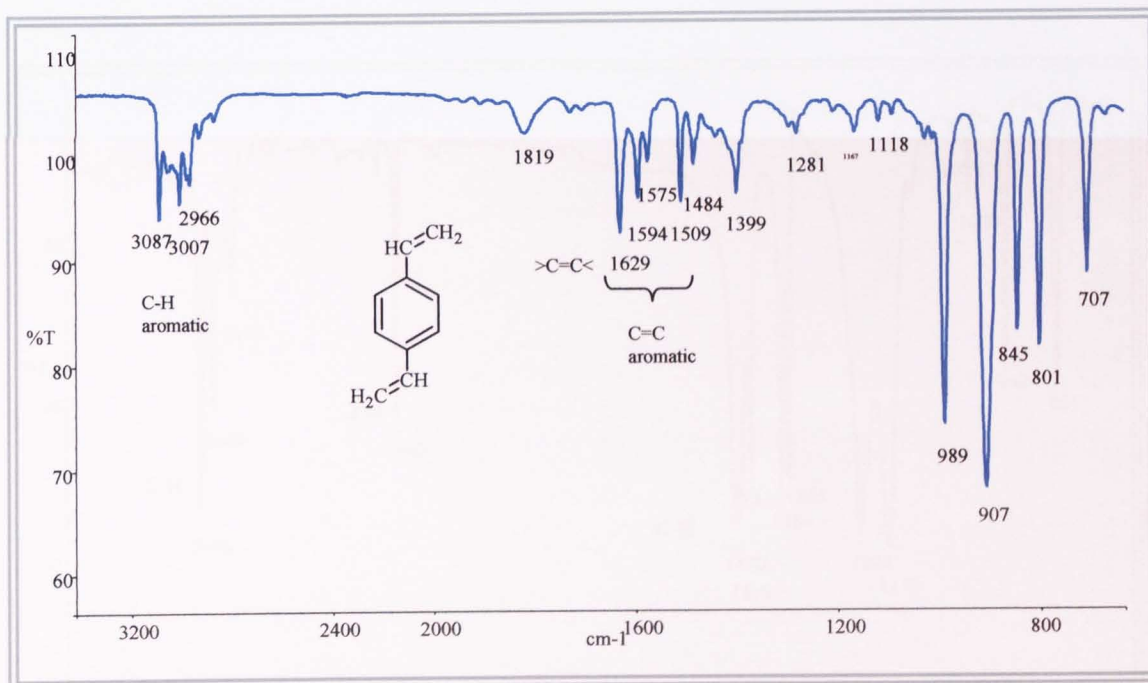
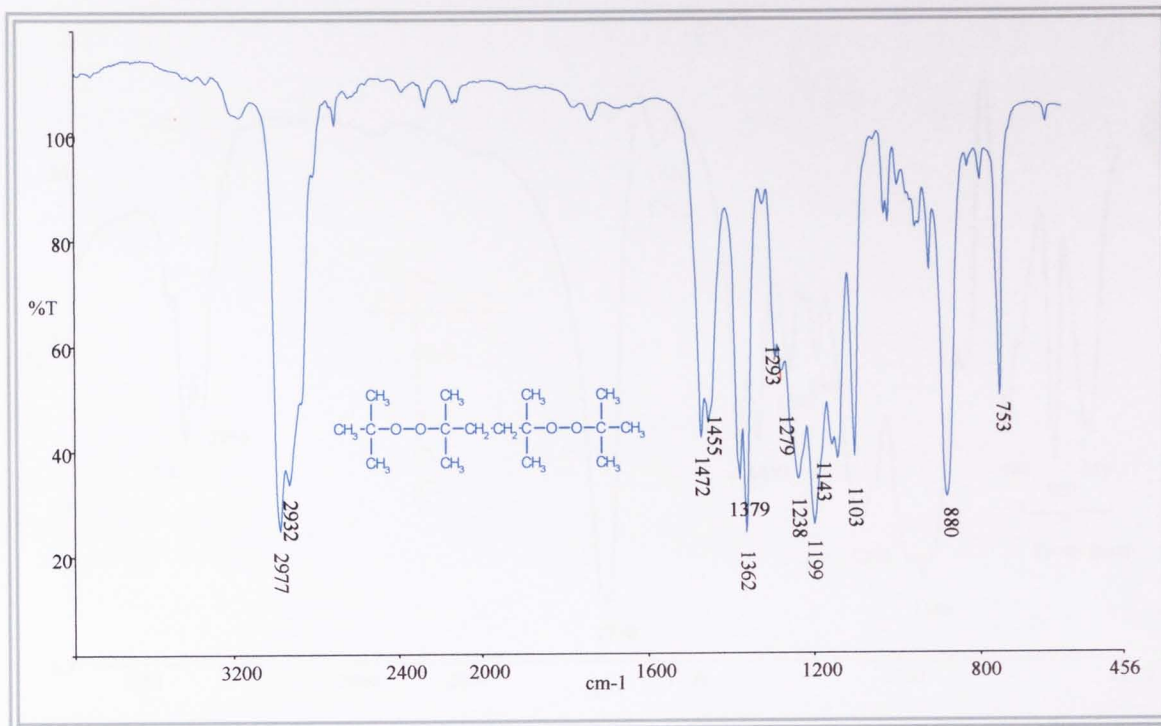
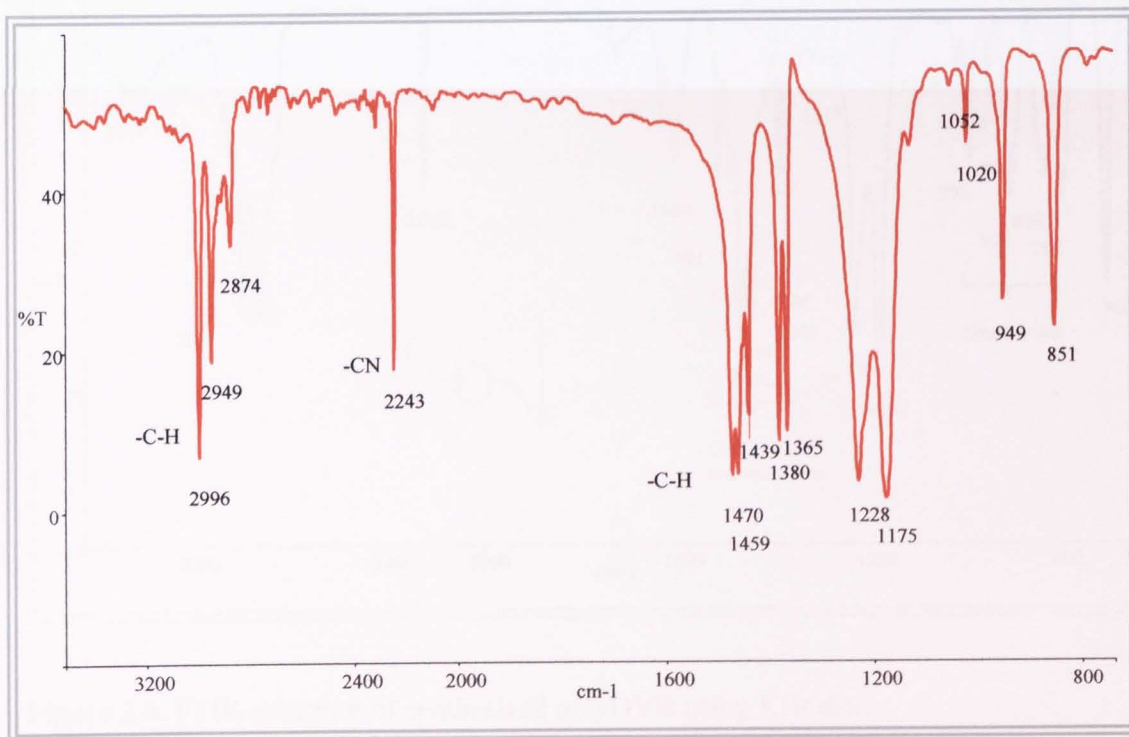


Figure 2.4. FTIR spectrum of neat DVB using KBr windows.



**Figure 2.5.** FTIR spectrum of neat peroxide T101 using KBr windows.



**Figure 2.6.** FTIR spectrum of AIBN using KBr windows.



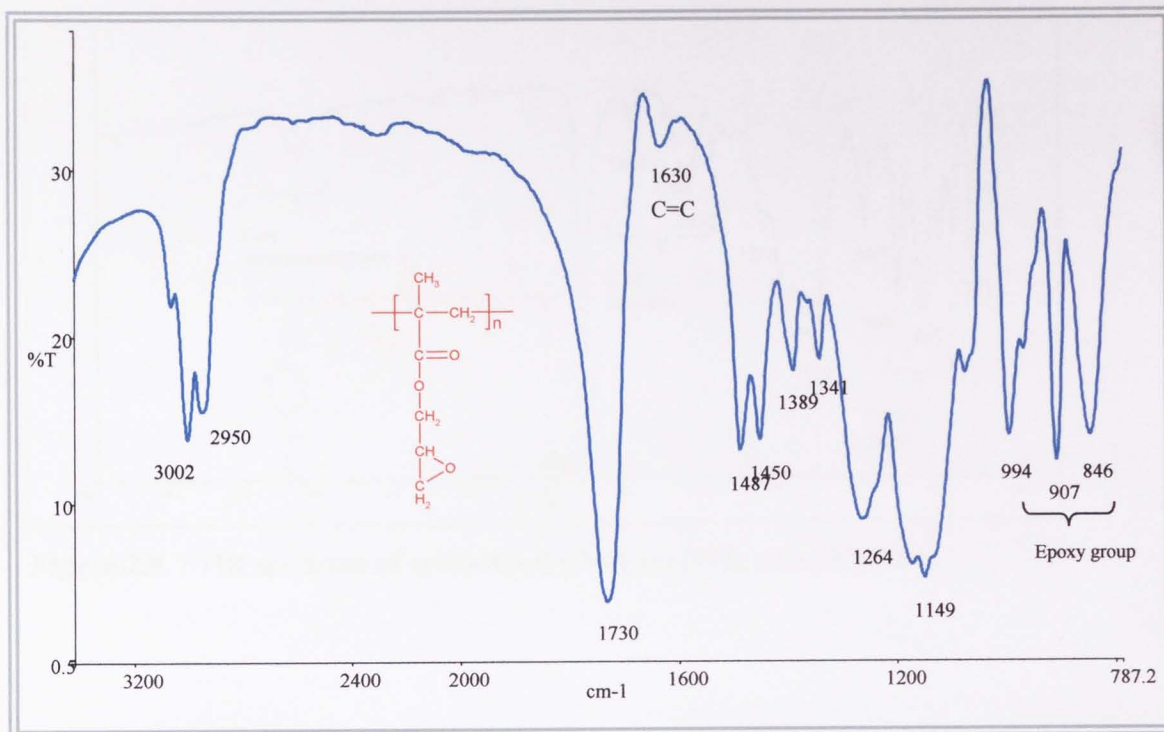


Figure 2.7. FTIR spectrum of synthesised polyGMA using KBr disc.

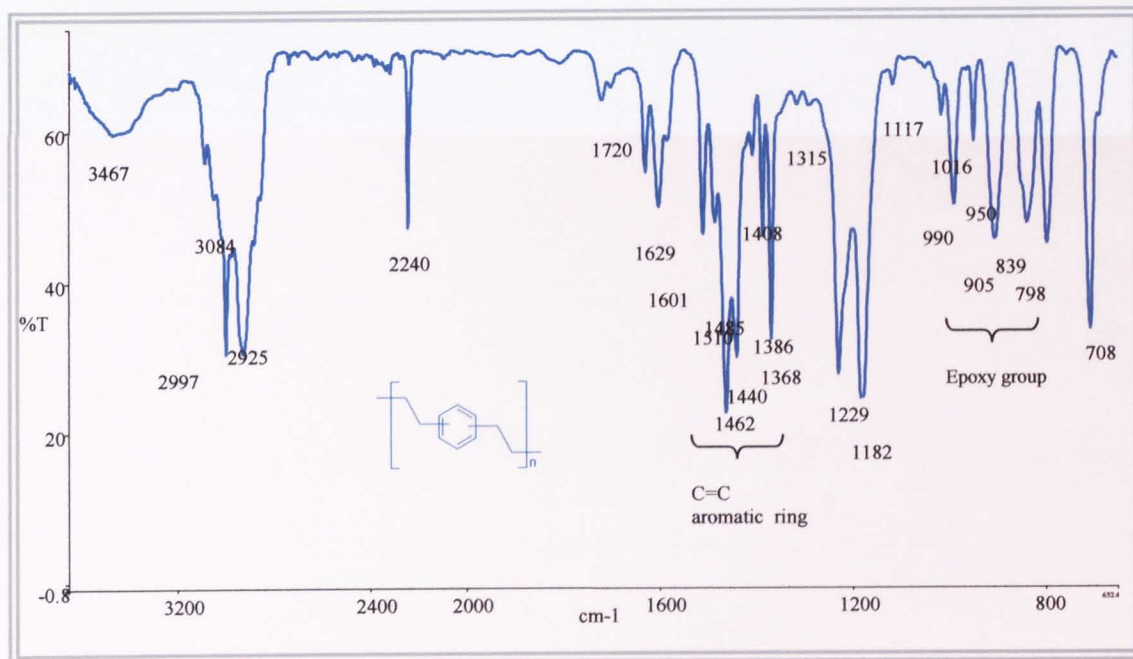


Figure 2.8. FTIR spectrum of synthesised polyDVB using KBr disc.

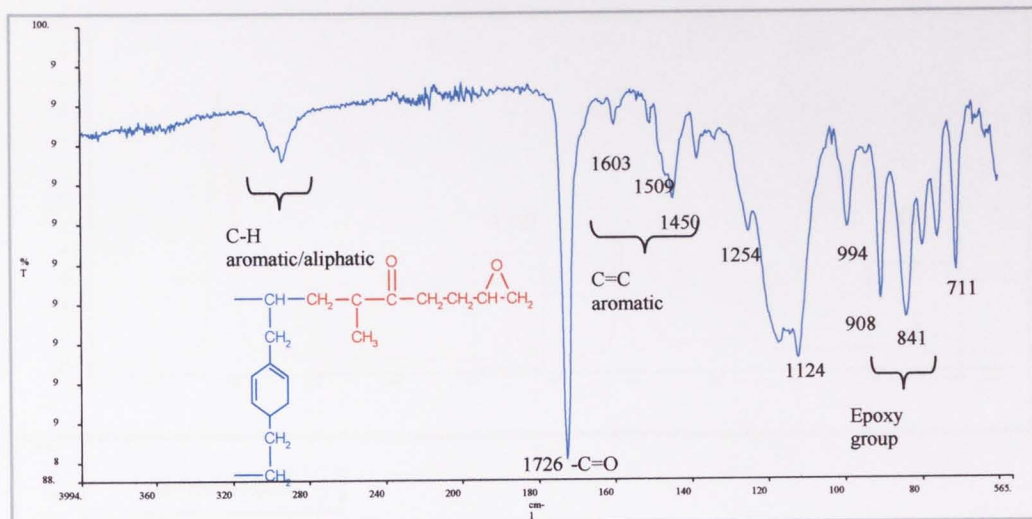
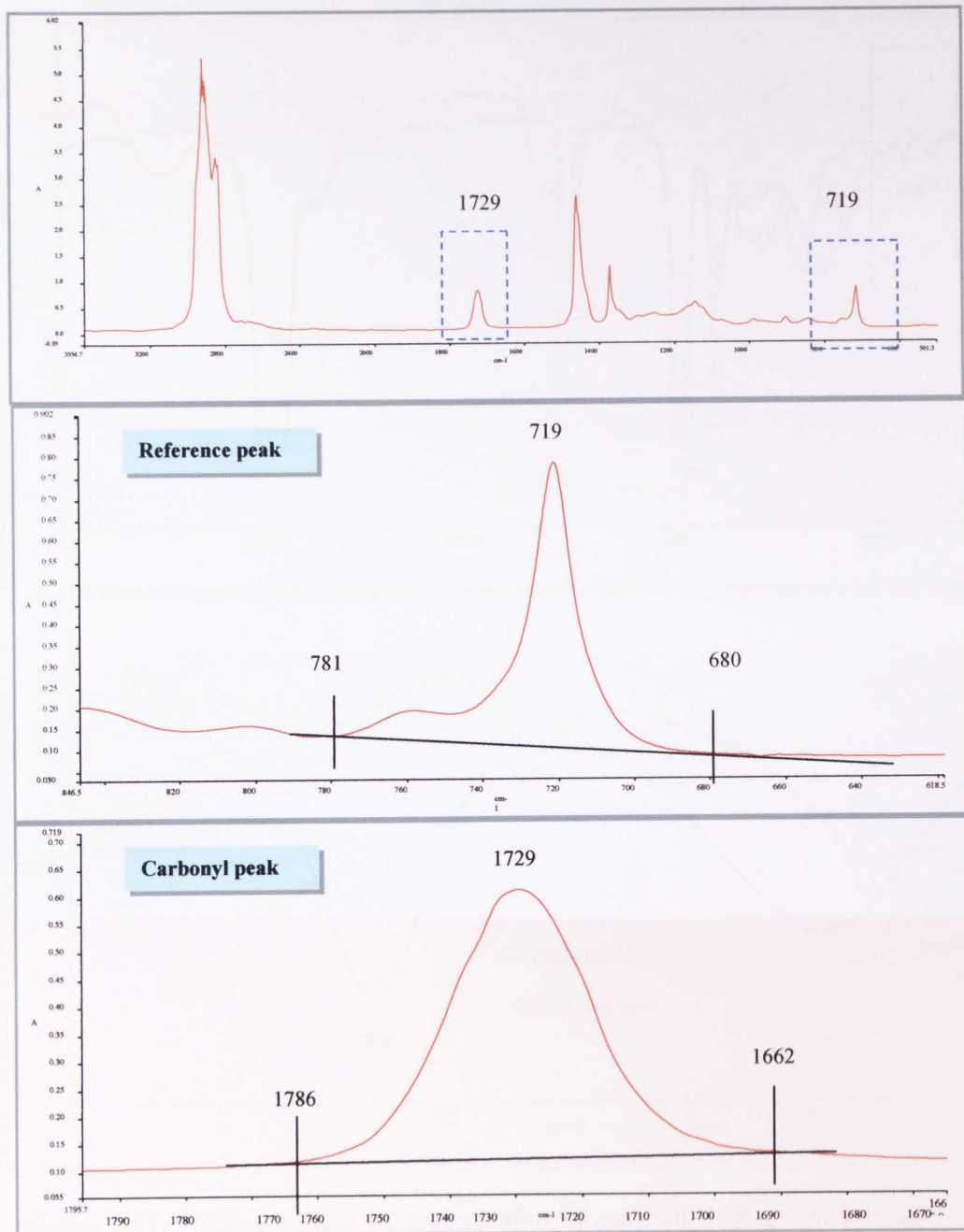
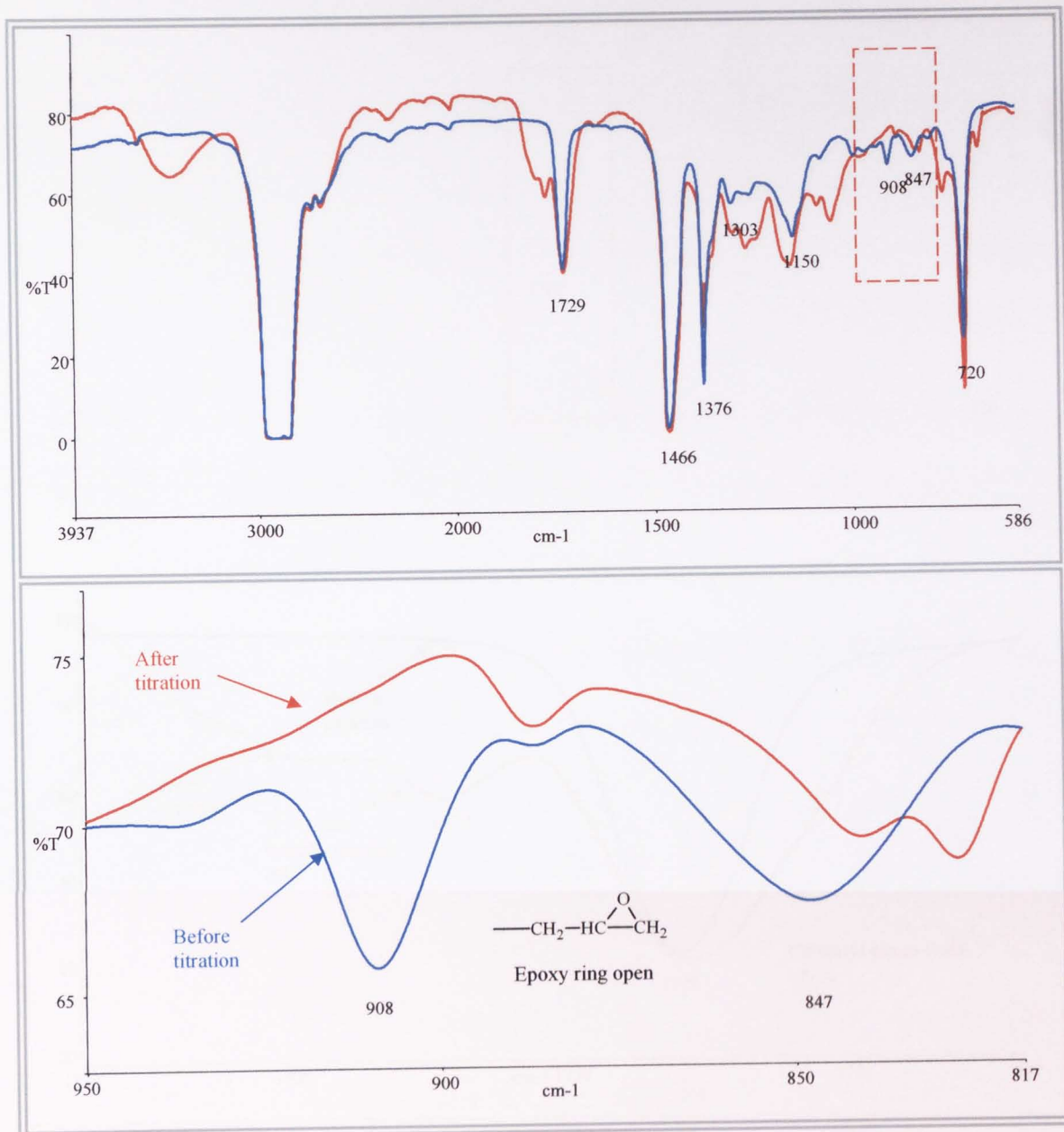


Figure 2.9. FTIR spectrum of synthesised GMA-co-DVB using KBr discs



**Figure 2.10.** Area boundaries for absorption peak area calculation of GMA in functionalised EPR. Film thickness is 40  $\mu\text{m}$ . Reference peak at 719  $\text{cm}^{-1}$  (b) Carbonyl group peak at 1729  $\text{cm}^{-1}$ .



**Figure 2.11.** FTIR spectrum of pressed film of purified EPR-g-GMA before and after titration. Thickness: 40 $\mu$ m

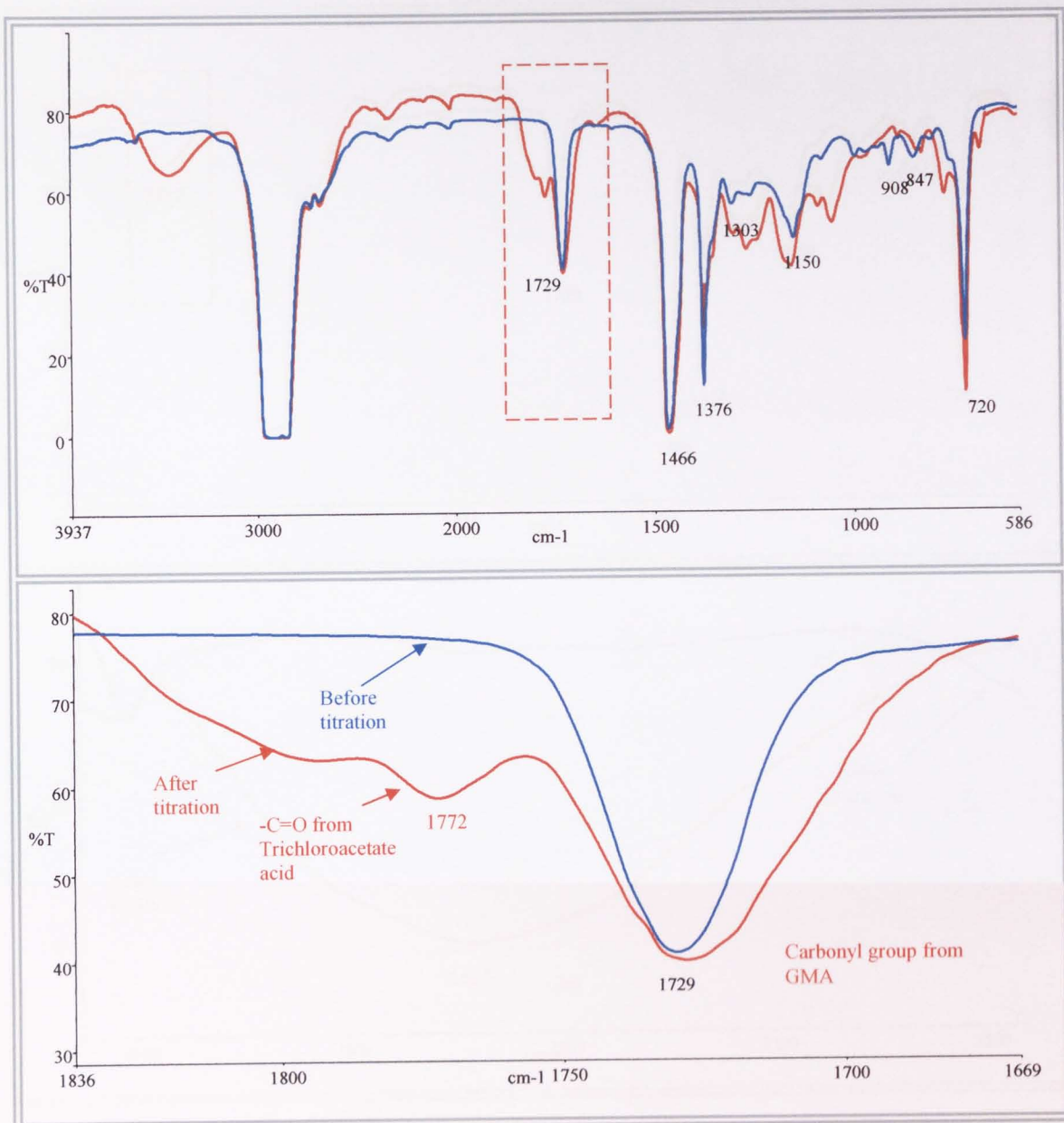


**Figure 2.12.** FTIR spectrum of press film of EPR-g-GMA before and after reaction with trichloroacetic acid. Thickness: 40  $\mu\text{m}$

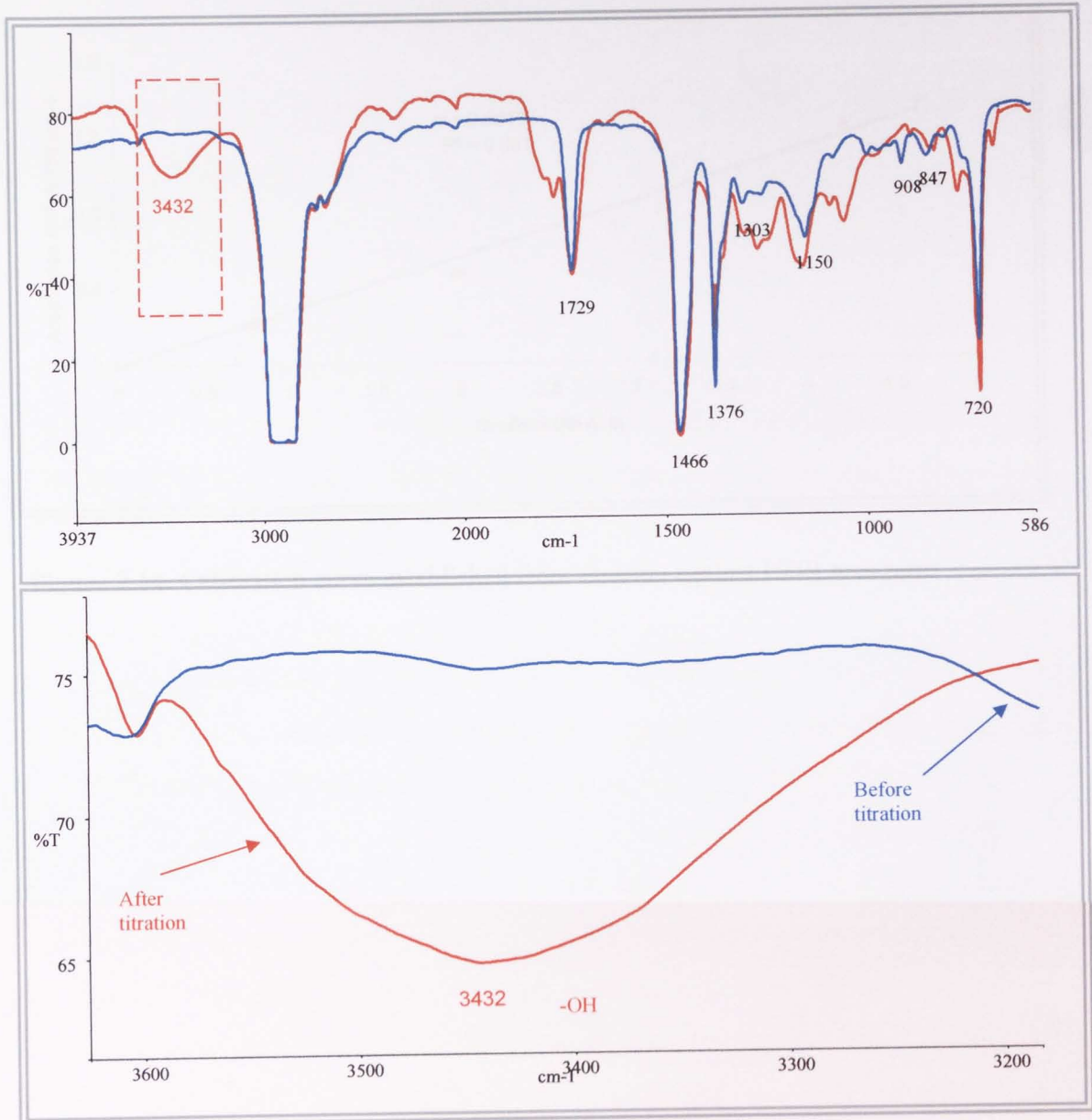


**Figure 2.13.** FTIR spectrum of press film of purified EPR-g-GMA before and after titration. Thickness: 40  $\mu\text{m}$

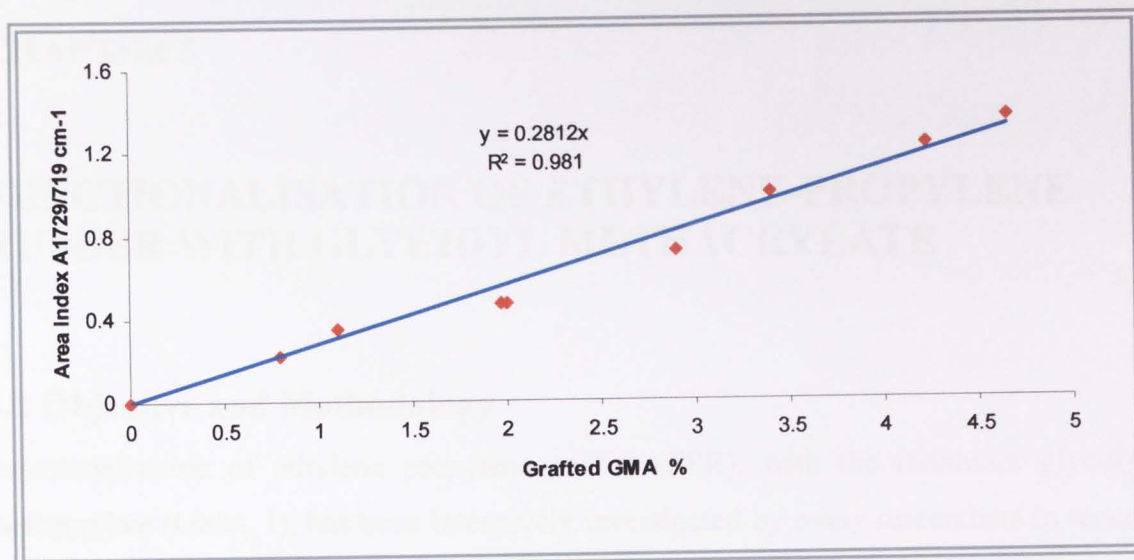


Figure 2.14. Calibration curve established from titration against FTIR area ratio

## CHAPTER 3

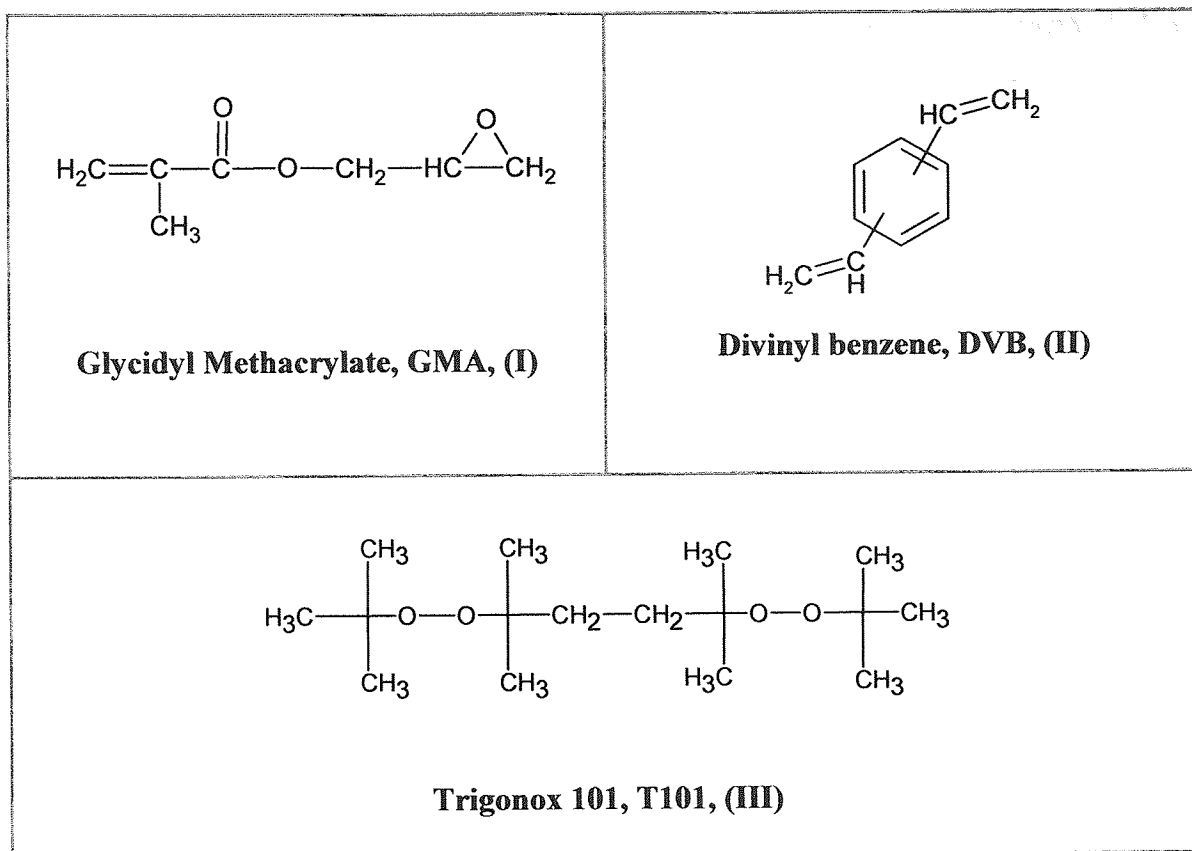
# FUNCTIONALISATION OF ETHYLENE-PROPYLENE RUBBER WITH GLYCIDYL METHACRYLATE

### 3.1 Objective and Methodology

Functionalisation of ethylene propylene rubber (EPR), with the monomer glycidyl methacrylate (GMA, I), has been intensively investigated by many researchers in recent years [9, 19, 20, 25, 31, 196, 197]. GMA has both a free radical reactivity via its double bond as well as reactivity via its epoxy group towards many functional groups such as carboxyl, hydroxyl, anhydride, amide. GMA has therefore been used for functionalising many hydrocarbon polymers e.g. PE [54, 198], PP [16], EPR [9], EPDM [51, 199] via melt grafting reactions using reactive processing methods by reaction of the polymers via the GMA double bond without destroying the epoxy group [200]. However, GMA was shown [9, 10] to have low reactivity towards macroradicals leading to low grafting yield in these polymers. Thus higher initiator concentration has been used in order to increase the grafting yield, but the problem with this approach is that it also results in higher extent of competing side reactions such as homopolymerisation of the monomer and degradation of the polymer via crosslinking or chain scission reactions. In order to increase the grafting yield and avoid or minimise these side reactions, different highly reactive comonomers such as styrene [29, 201], trimethylolpropane triacrylate (TRIS) [3, 9], have been used with GMA and other functional monomers during the reactive processing stage in order to enhance the grafting efficiency.

In this study, divinylbenzene (DVB, II) was used as a reactive comonomer to enhance the extent of grafting of GMA on EPR in the presence of the peroxide initiator Trigonox 101 (T101, III). DVB has been conventionally used as a crosslinking agent and therefore it can be expected to influence the physical properties of the polymer product such as molecular weight and viscosity [202, 203].





The main objective of the work described in this chapter was to investigate the effect of the reactive bifunctional comonomer divinyl benzene on the efficiency of the free radical (T101) initiated melt grafting reaction of GMA onto EPR conducted in an internal (Haake) batch mixer, and to optimise the reaction conditions, with the aim of increasing the grafting level and minimising the extent of side reactions. The effect of varying the processing temperature and the chemical composition of the system (viz. the concentration of GMA, DVB, and peroxide, T101) on the grafting degree and the nature and extent of the different side reactions was therefore examined and compared with that of a conventional (no comonomer) GMA-grafted-EPR system processed under the same conditions. The nature and distribution of the graft on the polymer backbone in both the GMA and GMA-DVB systems was also examined using NMR spectroscopy.

The melt free radical grafting of GMA onto EPR in the absence and presence of the comonomer was carried out in a Haake Rheomix 600 at a given processing temperature for 15 minutes at 65 rpm using closed system as described in **Schemes 3.1** and **3.2**. **Table 3.1** presents the composition and processing conditions for samples reported in this section. The functionalised EPR (*f*-EPR) products were purified and the side

reaction products were separated using sequential extraction-precipitation method. The grafting degree was determined by titration and FTIR spectroscopy (see **Chapter 2, Sec. 2.7, p.40**), using a calibration curve set up from a plot of the IR absorption area index ( $1720\text{ cm}^{-1}$  over  $720\text{ cm}^{-1}$ , the latter was used as a reference) versus the titration values (see **Chapter 2, Figure 2.14, p.67**). The melt index and gel content of the functionalised polymers were also determined.

**Table 3.1A:** Composition and processing conditions used in the functionalisation of EPR with GMA (GMA/T101) system, No comonomer-conventional system)

Code	Compositions				Processing Conditions			MFI g/10 min	g- GMA %	P- GMA %
	EPR phr	T101 phr	T101 /GMA Molar ratio	GMA phr	Temp °C	Time (min)	Speed (rpm)			
G1	100	0.017	-	-	190	15	65	1	-	-
G2	100	0.078	-	-	190	15	65	0.2	-	-
G3	100	0.13	-	-	190	15	65	0	-	-
G4	100	0.078	0.0038	10	180	3	65	4.4	0.6	0
G5	100	0.078	0.0038	10	180	5	65	4.3	0.6	0
G6	100	0.078	0.0038	10	180	10	65	4.3	0.9	0
G7	100	0.078	0.0038	10	180	15	65	4.3	0.6	0
G8	100	0.13	0.0042	15	190	3	65	3.5	0.6	1.2
G9	100	0.13	0.0042	15	190	5	65	3.6	1.4	2.4
G10	100	0.13	0.0042	15	190	10	65	3.7	1.6	2.7
G11	100	0.13	0.0042	15	190	15	65	3.7	1.4	2.6
G12	100	0.30	0.0147	10	190	3	65	2.8	1.3	0
G13	100	0.30	0.0147	10	190	5	65	2.9	1.5	0.9
G14	100	0.30	0.0147	10	190	10	65	2.9	1.5	0.5
G15	100	0.30	0.0147	10	190	15	65	2.9	1.5	0.4
G16	100	0.078	0.0038	10	190	15	65	4.3	0.7	0
G17	100	0.13	0.0064	10	190	15	65	3.7	1.3	0.1
G19	100	0.80	0.0392	10	190	15	65	0.95	1.7	0.6
G20	100	1.50	0.0728	10	190	15	65	0.2	1.5	0.5
G21	100	0.8	0.0783	5	190	15	65	0.9	0.8	0.2
G23	100	0.8	0.0301	13	190	15	65	1.0	2.5	2.0
G24	100	0.8	0.0261	15	190	15	65	1.2	1.9	3.0
G25	100	0.8	0.0261	15	190	3	65	1	1.7	2.82
G26	100	0.8	0.0261	15	190	5	65	1.1	1.9	3.18
G27	100	0.8	0.0261	15	190	10	65	0.9	2.0	3.30

**Table 3.1B:** Composition and processing conditions used in the functionalisation of EPR with GMA in the presence of comonomer, DVB ,(EPR-GMA-T101-DVB)

Code	Compositions				GMA/DVB		Processing Conditions			MFI g/10 min	g-GMA %	P-GMA %
	EPR (phr)	T101 phr	T101/DVB +GMA (MR)	GMA phr	DVB phr	w/w %	Temp °C	Time (min)	Speed (rpm)			
EP	100	0	0	0	0	0	190	15	65	4.9	0	0
DG1	100	0.017	0.0007	10	1.1	9:1	170	15	65	3.3	3.3	0
DG2	100	0.039	0.0015	10	1.1	9:1	170	15	65	3.1	2.6	0
DG3	100	0.078	0.0034	10	1.1	9:1	170	15	65	2.4	3.0	0
DG4	100	0.130	0.0057	10	1.1	9:1	170	15	65	2.5	3.6	0
DG5	100	0.017	0.0007	10	1.1	9:1	180	15	65	3.5	3.0	0
DG7	100	0.078	0.0034	10	1.1	9:1	180	15	65	2.3	2.8	0
DG8	100	0.130	0.0057	10	1.1	9:1	180	15	65	2.0	3.5	0
DG9	100	0	0	10	1.1	9:1	190	15	65	4.1	0.8	0
DG10	100	0.017	0.0007	10	1.1	9:1	190	15	65	3.7	2.3	0
DG11	100	0.078	0.0034	10	1.1	9:1	190	15	65	3.2	2.8	0
DG12	100	0.130	0.0102	5	1.1	9:1	190	15	65	2.6	1.4	0
DG13	100	0.130	0.0057	10	1.1	9:1	190	15	65	2.3	2.7	0
DG14	100	0.130	0.0039	15	1.1	9:1	190	15	65	2.1	4.7	0.1
DG15	100	0.130	0.0057	10	1.1	9:1	190	3	65	2.1	2.5	0
DG16	100	0.130	0.0057	10	1.1	9:1	190	5	65	2.1	2.7	0.04
DG17	100	0.130	0.0057	10	1.1	9:1	190	10	65	2.1	2.7	0
DG19	100	0.017	0.0007	10	1.1	9:1	200	15	65	3.8	1.6	0
DG21	100	0.078	0.0034	10	1.1	9:1	200	15	65	2.0	1.8	0
DG23	100	0.130	0.0057	10	1.1	9:1	200	15	65	1.8	2.1	0
DG24	100	0.017	0.0006	10	2.5	8:2	170	15	65	2.3	4.2	0
DG25	100	0.078	0.0030	10	2.5	8:2	170	15	65	1.6	4.1	0
DG26	100	0.130	0.0050	10	2.5	8:2	170	15	65	1.1	4.2	0
DG27	100	0.017	0.0006	10	2.5	8:2	180	15	65	2.5	3.7	0
DG28	100	0.078	0.0030	10	2.5	8:2	180	15	65	1.8	4.5	0
DG29	100	0.130	0.0050	10	2.5	8:2	180	15	65	1.5	3.8	0
DG31	100	0.078	0.0030	10	2.5	8:2	180	10	65	1.8	3.8	0
DG32	100	0.078	0.0030	10	2.5	8:2	180	5	65	1.6	3.9	0.1
DG33	100	0.078	0.0030	10	2.5	8:2	180	3	65	1.5	3.7	0
DG34	100	0.008	0.0006	10	2.5	8:2	190	15	65	2.9	1.9	0
DG35	100	0.017	0.0006	10	2.5	8:2	190	15	65	2.1	3.5	0
DG36	100	0.078	0.0030	10	2.5	8:2	190	15	65	1.5	3.9	0
DG37	100	0.130	0.0050	10	2.5	8:2	190	15	65	1.0	3.6	0
DG38	100	0.017	0.0006	10	2.5	8:2	200	15	65	3.0	2.7	0
DG39	100	0.078	0.0030	10	2.5	8:2	200	15	65	1.9	3.4	0
DG40	100	0.130	0.0050	10	2.5	8:2	200	15	65	1.1	3.2	0
DG41	100	0.130	0.0043	10	4.3	7:3	180	15	65	0.5	4.5	0
DG42	100	0.017	0.0006	10	4.3	7:3	180	15	65	1.0	3.2	0
DG43	100	0.078	0.0026	10	4.3	7:3	180	15	65	0.7	3.5	0
DG44	100	0.13	0.0043	10	4.3	7:3	180	15	65	0.7	3.7	0

**Table 3.1B:** Composition and processing conditions used in the functionalisation of EPR (P-0280) with GMA in the presence of comonomer, DVB, (EPR-GMA-T101-DVB). (continue)

Code	Compositions				GMA/DVB		Processing Conditions			MFI g/10 min	g-GMA %	p-GMA %
	EPR (phr)	T101 phr	T101/DVB +GMA (MR)	GMA phr	DVB phr	w/w %	Temp °C	Time (min)	Speed (rpm)			
DG45	100	0	-	10	4.3	7:3	190	15	65	3.3	1.0	0
DG46	100	0.008	0.00027	10	4.3	7:3	190	15	65	2.6	3.6	0
DG47	100	0.017	0.0006	10	4.3	7:3	190	15	65	1.1	4.1	0
DG48	100	0.078	0.0026	10	4.3	7:3	190	15	65	0.7	5.0	0
DG49	100	0.130	0.0043	10	4.3	7:3	190	3	65	0.04	0.2	0
DG50	100	0.130	0.0043	10	4.3	7:3	190	4	65	0.25	2.9	0
DG51	100	0.130	0.0043	10	4.3	7:3	190	6	65	0.38	4.0	0
DG52	100	0.130	0.0043	10	4.3	7:3	190	15	65	0.5	4.5	0
DG53	100	0.130	0.0039	15	1.1	9:1	190	3	65	2.1	4.2	0.38
DG54	100	0.130	0.0039	15	1.1	9:1	190	5	65	2.1	4.6	0.56
DG55	100	0.130	0.0039	15	1.1	9:1	190	10	65	2.1	4.7	0.30
DG56	100	0.130	0.0039	15	1.1	9:1	190	15	65	2.1	4.6	0.1
DG57	100	0	-	-	1.1	-	190	15	65	-	-	-
DG58	100	0.13	-	-	1.1	-	190	15	65	-	-	-

## 3.2. Results

### 3.2.1 Separation of Reaction Products and Characterisation of the Grafting System

The reaction products of the EPR-g-GMA<sub>CONV</sub> (conventional-without DVB) and EPR-g-GMA<sub>DVB</sub> (with DVB) systems are expected to contain not only the desired grafted GMA but also a number of undesired side reaction products including crosslinking and chain scission of EPR, ungrafted GMA, polyGMA and in the presence of DVB additional products can also be formed, namely polyDVB and GMA-co-DVB. In order to identify suitable solvents for extraction and purification of the functionalised polymers, the solubility of synthesised polyGMA, polyDVB and GMA-co-DVB was examined in different solvents (see **Table 3.2**). It was found that GMA and DVB were soluble in all solvents examined (acetone, methanol, xylene, toluene, chloroform, tetrahydrofuran (THF), dichloromethane (DCM)), dichlorobenzene and dimethyl sulfoxide (DMSO). PolyGMA was insoluble in methanol but soluble in all other solvents, whereas polyDVB and GMA-co-DVB were insoluble in all the solvents examined here. The grafted-GMA was found to be soluble in hot xylene and hot toluene but insoluble in acetone and methanol.

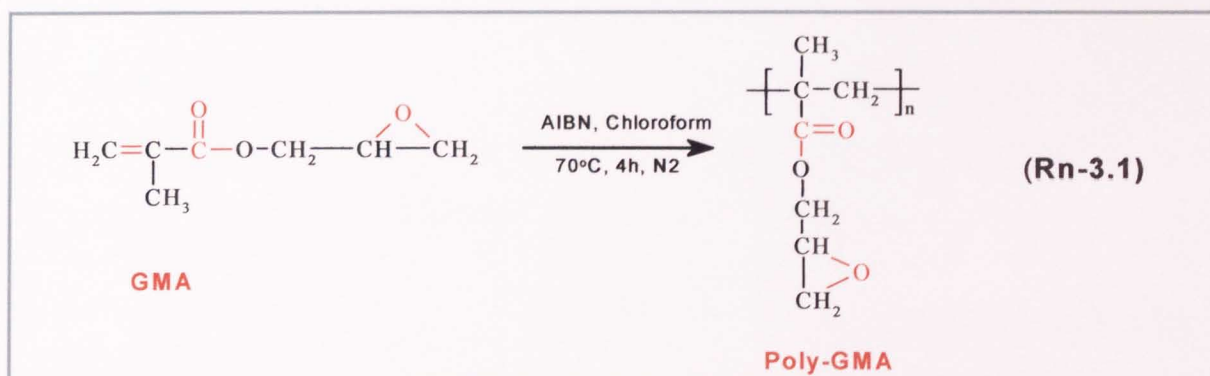
**Table 3.2.** Solubility of monomer and comonomers of GMA and DVB, homopolymers and polymerised product typically found in the EPR grafting system.

COMPOUND	SOLUBILITY										
	Acetone	Methanol	Xylene	Toluene	Chloroform		DCM		THF	Chloro- benzene	DMSO
	Cold	Cold	Hot	Hot	Cold	Hot	Cold	Hot	Hot	Hot	Hot
GMA	Y	Y	Y	Y	Y	Y	Y	Y	Y	-	-
DVB	Y	Y	Y	Y	Y	Y	Y	Y	Y	-	-
PolyGMA	Y	N	Y	Y	-	-	-	-		-	-
PolyDVB	N	N	N	N	N	N	N	N	N	N	N
GMA-co-DVB	N	N	N	N	N	N	N	N	N	N	N
EPR-g-GMA	N	N	Y	Y	Y	Y	-	-		-	

### 3.2.2 Characterisation of Side Reaction Products of EPR-g-GMA in the Absence and Presence of the Comonomer DVB

#### i) Characterisation of PolyGMA

Figure 3.1 shows the FTIR spectra of neat GMA and synthesised polyGMA, see Rn 3.1. The formation of a saturated carbonyl group in polyGMA is evident from the observed shift from unsaturated carbonyl absorption at  $1721\text{cm}^{-1}$  to saturated and broad carbonyl peak at  $1730\text{cm}^{-1}$  and from the substantial reduction of the acrylic double bond absorption at  $1638\text{cm}^{-1}$ , whereas the epoxy group absorptions at  $909\text{cm}^{-1}$  and  $843\text{cm}^{-1}$  were still clearly present.

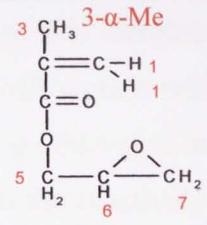
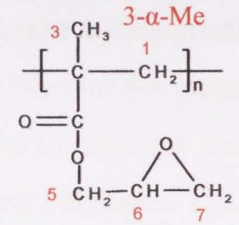


$^1\text{H}$ -NMR and  $^{13}\text{C}$  NMR chemical shifts for GMA and polyGMA are given in Table 3.3. The  $^1\text{H}$  spectra for GMA and polyGMA are given in Figures 3.2 and 3.3. It is clear from these figures and Tables 3.3a and 3.3b that the chemical shifts and the protons and

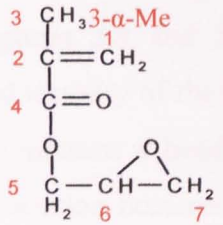
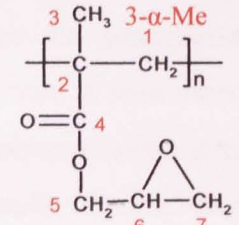
carbons of the epoxy ring are very similar in both GMA and polyGMA confirming that the epoxy ring is not affected by the polymerisation of GMA, see atoms 5,6 and 7 in **Table 3.3**. On the other hand, the acrylate group shows clear shifts in both the  $^1\text{H}$  and  $^{13}\text{C}$  signals from being unsaturated to becoming saturated indicating the loss of the  $\text{C}=\text{C}$  double bonds due to polymerisation, see **Figures 3.4 and 3.5** and **Table 3.3b**. For better understanding of the difference between the spectra of GMA and polyGMA, ( $^1\text{H}$  and  $^{13}\text{C}$  NMR spectra in  $\text{CDCl}_3$ ) are compared, see **Figure 3.2 and 3.3**. First the HMBC NMR spectrum for GMA (shown in **Figure 3.4**) is analysed, it shows the following characteristic:

- The carbon C3 is directly bonded to H3, and H1's are connected to C3 through long range coupling.
- The carbon C7 has H7's directly bonded to it and H's 5 and 6 are connected to C7 through long range coupling.
- The carbon C6 has H6 directly bonded to it, and H's 5 and 7 are connected to C6 through long range coupling.
- The carbon C5 has H5's directly bonded to C5, and H's 6 and 7 are connected to C5 through long range coupling
- The carbon C1 has H1,s directly bonded to C1, and H3 is connected to C1 through long range coupling
- The carbon C2 has H's 1 and 3 connected to it through long range coupling
- The carbon C4 has H's 1, 5 and 3 connected to it through long range coupling

**Table 3.3a.**  $^1\text{H-NMR}$  chemical shifts,  $\delta$  (ppm), and signal assignments of GMA and polyGMA in  $\text{CDCl}_3$ , see **Figures 3.2** and **3.3**

Group	Position	$\delta$ , ppm (multiple)	
		(s=single, m=multiple, b=broad)	
			
GMA	PolyGMA		
CH <sub>2</sub> unsaturated in GMA CH <sub>2</sub> saturated in polyGMA	H1, H2	6.1 (s) 5.5 (s)	1.8 (rrr <sub>I</sub> ), 1.95[mrr <sub>I</sub> ] 2.00[mrm <sub>I</sub> ], 2.05[rmr <sub>I</sub> ] 2.10 [mmr <sub>II</sub> ], 1.49 [mmr <sub>III</sub> ] 1.45 [mmr <sub>III</sub> ]
CH <sub>3</sub>	H3	1.9 (s)	0.91 [rm] (br), 1.06 [rm, mr] (br) 1.26 [mm] (br)
CH <sub>2</sub>	H5	4.4 (m) 3.9 (m)	4.2 (m) 3.9 (m)
CH of epoxy group	H6	3.2 (m)	3.2 (b)
CH <sub>2</sub> of epoxy ring	H7	2.8 (m) 2.6 (m)	2.8 (b) 2.6 (b)

**Table 3.3 b.**  $^{13}\text{C NMR}$  chemical shifts,  $\delta$  (ppm), and signal assignments of GMA and polyGMA in  $\text{CDCl}_3$ , **Figure 3.4** and **3.5**

Group	Position	$\delta$ , ppm	
		Sign: 1° and 3° (+), 2° and 4° (-)	
			
GMA	PolyGMA		
CH <sub>2</sub> , unsaturated CH <sub>2</sub> , saturated	C1 (-) C1 (-)	126.2 (-) -	- 52.1(-) 53.7 (-), 54.0(-)
C, unsaturated C, saturated	C2(-) C2(-)	136 (-) -	- 45 (-)
$\alpha$ -CH <sub>3</sub> , unsaturated $\alpha$ -CH <sub>3</sub> , saturated	C3(+) C3(+)	18.3 (+) -	- 20.5[mm] (+), 18.7 [rm, mr] (+), 16.7 [rr] (+)
C=O	C4 (-)	167 (-)	177.2 [rr] (-), 176.3 [mr] (-), 176.5 [mmr] (-), 176 [mm] (-)
CH <sub>2</sub>	C5 (-)	65.3 (-)	65.7 (-)
CH of epoxy ring	C6 (+)	49.5 (+)	48.8 (+)
CH <sub>2</sub> of epoxy ring	C7	44.7 (-)	44.5 (-)

Returning now to the  $^1\text{H}$  and  $^{13}\text{C}$  NMR of polyGMA, (**Figures 3.3** and **3.5**), it is clear that the signal of the  $^1\text{H}$  and  $^{13}\text{C}$  of the  $\text{CH}_3$  group in polyGMA (position 3) splits up into a complex peak structure and this is attributed to different stereochemical configurations in the polymer, see also **Figure 3.6**. Since the epoxy part of polyGMA shows similar peaks to that of neat GMA, it is therefore not affected by the grafting or polymerisation reaction. Therefore its NMR signals will be used here for the purpose of investigating the microstructure of EPR-g-GMA and in particular to calculate the graft distribution and the graft composition in the reactively processed polymers. The other part of the GMA, the methacrylate group, has shown shifts in both of the  $^1\text{H}$  and  $^{13}\text{C}$  peaks from the alkenes to aliphatic regions, indicating the loss of the  $\text{C}=\text{C}$  double bonds due to polymerisation, see **Table 3.3** and **Figures 3.3** and **3.5**. **Figure 3.3** shows clearly that for polyGMA, the Hs that are located on C1 and C3 (the  $\alpha\text{-CH}_3$ ) (and similarly in the  $^{13}\text{C}$ 's spectrum, **Figures 3.5**), these carbons (i.e. C1 of  $\text{CH}_2$  and C3 of  $\text{CH}_3$  as well as C4 (the  $\text{C}=\text{O}$ ) gave several peaks, see also the expanded spectra in this region (**Figure 3.3b** and **3.5b**). The complex peaks pattern observed here is due to the chemical complexities and tacticity of polyGMA [204, 205].

The assignment of the  $^1\text{H}$  and  $^{13}\text{C}$  NMR spectra of polyGMA (which is shown more clearly in the expansion of the NMR region given in **Figure 3.3b** and **3.5b**) is based on the structures shown in **Figures 3.6** and **3.7** and the 2D NMR spectra (both HSQC and HMBC of polyGMA) shown in **Figures 3.8** and **3.9**. **Figure 3.6** summarises the different stereochemical sequences and tacticity of the homopolymer. A four repeat unit structure is chosen in this figure to represent a head-to-tail polymerisation structure. Four repeat units were chosen for illustration because of the results obtained based on the calculated length of the grafted GMA sequence in  $\text{EPR-g-GMA}_{\text{CONV}}$  which was shown, (see later) to consist of four molecules.

**Figure 3.6** focuses is on the H's of the  $\text{CH}_2$  of the second GMA repeat unit e.g. **Figure 3.6a** ( $\text{CH}_2$  labelled I). The  $^1\text{H}$  NMR chemical shift of these two H's is affected by the environment around them; when the two surrounding similar groups are located opposite to each other (*racemic, r*) as shown in **Figure 3.6a**, the two H's of this  $\text{CH}_2$ , I, appears at the same chemical shift,  $\delta = 1.87$  ppm, see **Figure 3.3b**. When similar groups around the  $\text{CH}_2$  are located at the same side (*meso, m*), see **Figure 3.6d**, the two H's (II



and III) have appeared at different chemical shifts, *rmr-II* at 2.05 ppm and *rmr-III* at 1.45 ppm, see **Figure 3.3b**. Furthermore, the chemical shifts of these 3H's (I, II and III) seem to be affected by the groups surrounding the CH<sub>2</sub> groups on both sides; the H's of (*r*) surrounded by (*r*) from both side (see **Figure 3.6a**) are different from the H's of (*r*) surrounded by an (*r*) from one sides and (*m*) from the other side (see **Figure 3.6b** appearing at 1.95ppm in **Figure 3.3b**). Therefore, based on the NMR results and the stereochemical configuration presented in **Figure 3.6**, there are at least five different peaks observed for the H's of the 1-CH<sub>2</sub> of poly-GMA in the <sup>1</sup>H NMR spectrum. Those peaks are labelled in **Figure 3.3** as *rrr*, *mrr*, *mr*m**, *rmr* and *mmr* and also there is a possibility of *mmm*.

The effect of the stereochemical sequences on the α-CH<sub>3</sub> is illustrated in **Figure 3.7**. It is important to note here that the stereochemical configuration given in **Figure 3.7** is similar to that shown in **Figure 3.6**, but the focus in **Figure 3.7** is on the α-CH<sub>3</sub>. Here again the *racemic* and *meso* configurations are presented with respect to the CH<sub>2</sub> as in **Figure 3.6**. Hence the α-CH<sub>3</sub> is labelled as *rr* when located between *r* and *r* configured methylene groups, see **Figure 3.7a**, or *mr* when located between *m* and *r*, see **Figure 3.7d** or *mm* being between *m* and *m* as in **Figure 3.7f**. Therefore the α-CH<sub>3</sub> is affected by the surrounding two GMA units on both sides. When the α-CH<sub>3</sub> is positioned between *r* and *r*, it is labelled *rr<sub>i</sub>* (as in (**Figure 3.7a** and in one structure shows in **Figure 3.7b**), it becomes more shielded and appears at lower chemical shift of 0.91 ppm, see **Figure 3.3B**. On the other hand, when the α-CH<sub>3</sub> is located between *m* and *m*, *mm<sub>iii</sub>*, (see **Figure 3.7e** and **f**), it will be less shielded and appears at higher chemical shift, 1.26 ppm, see **Figure 3.3D**. When one of the esters is on the CH<sub>3</sub> side and the other ester group is on the other side *m* and *r*, *mr<sub>ii</sub>*, see **Figure 3.7b, c, d** and **e**, it would appear in the middle of the chemical shifts at 1.06 ppm, see **Figure 3.3B**. Therefore, there are at least three types of α-CH<sub>3</sub> in the polymer as presented in **Figure 3.7** which correspond to the formation of the three different chemical shifts observed for the α-CH<sub>3</sub>, assigned as *rr*, *mr/rm* and *mm*. The <sup>13</sup>C shows similar results for the α-CH<sub>3</sub> where three peaks assigned for the *rr*, *mr* and *mm* appear at 16.7, 18.7 and 20.5 ppm, respectively, (**Figure 3.5**). Similar results are also seen for the 3-C and 4-C where at least three peaks are observed for each carbon, see **Figure 3.9**.

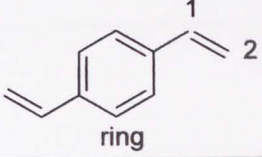
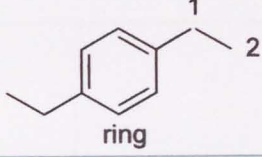
**Figure 3.8B** presents the 2D  $^1\text{H}$ - $^{13}\text{C}$  HSQC NMR spectrum of poly-GMA which shows a correlation between the carbon and the hydrogen which are directly bonded to each carbon. The peaks indicated with the solid lines show the correlations between the protons and the carbons of 3- $\text{CH}_3$ . The dashed lines show the correlations between the protons and the carbons of 1- $\text{CH}_2$ . The rest of the atoms are indicated by the dotted lines. **Figure 3.9A** shows the 2D  $^1\text{H}$ - $^{13}\text{C}$  HMBC NMR spectrum of poly-GMA which shows a correlation between the carbon and the hydrogens that are two or three bonds away from that carbon. There are too many correlations here; but the most important are the two regions which have been expanded in **Figure 3.9B and C**. **Figure 3.9B** shows that the protons of 1-*rrr* and 1-*mrr* are associated with the carbon of 3-*rr* (red arrows), It also shows that the protons of 1-*mrr*, 1-*mrm* and 1-*rmr* are associated with the carbons of 3-*rm* (blue arrows), which confirm the structures presented in **Figures 3.6 and 3.7**. This confirms that the 3- $\text{CH}_3$  *rr* is associated only with *rrr* and *mrr* structures as shown in the structures of **Figure 3.6a and b**. The 3- $\text{CH}_3$  *rm* is associated with the structures *mrr*, *mrm* and *rmr*, see **Figure 3.6b, c and d**. The part of the spectrum shown in **Figure 3.9C** focuses on the correlation with C4, C=O. **Figure 3.9C** shows that the protons of 1-*rrr* and the protons of 3-*rr* are associated with one carbonyl group 4-*rr* at 177.2 ppm, also the protons of 1-*mrr* has a correlation with this carbonyl group, 4-*rr*. The protons of 1-*mrr* and 1-*mrm* and the protons of 3-*mr* are associated with a carbonyl group 4-*mr* at 176.3ppm. The protons of 1-*mmr* are associated with a carbonyl group, 4-*mmr* at 176.5 ppm. The protons of 1-*mrr* are associated with a carbonyl group, 4-*mrr* at 177.6 ppm. Furthermore, the protons of the 3-*mm* show a weak correlation with the carbonyl group, 4-*mmm* at about 175.2 ppm

## ii) Characterisation of PolyDVB

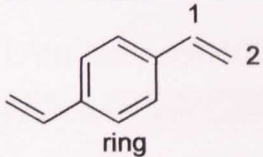
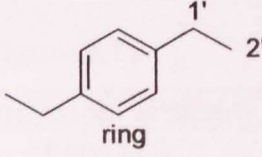
The  $^1\text{H}$  and  $^{13}\text{C}$  NMR spectra of DVB are shown in **Figures 3.10 and 3.11** respectively, and the data are also summarised in **Tables 3.4a and 3.4b**. The results show that there is about 10% diethyl benzene present with the DVB. The  $^{13}\text{C}$  solid state NMR spectrum, (**Figure 3.12**) of polyDVB shows that polymerized DVB, un-reacted DVB and ethylstyrene are all present in the sample (as polyDVB was not soluble in any common solvent, its solid state spectra was examined instead). The peak at 65 ppm has shifted

when the spinning frequency was changed from 4500 to 6000Hz (marked "X") suggesting that it is an artificial and not a real peak.

**Table 3.4a.**  $^1\text{H-NMR}$  chemical shifts,  $\delta$  (ppm), and signal assignments of DVB in  $\text{CDCl}_3$ , see **Figure 3.10**

Group	Position	$\delta$ , ppm (multiplicity) (s=single, m=multiplet, b=broad)	
			
		<b>DVB</b>	<b>Diethyl benzene</b>
CH, unsaturated CH <sub>2</sub> , saturated	H1	6.6 (m)	2.5 (m)
CH <sub>2</sub> , unsaturated CH <sub>3</sub> , saturated	H2	5.6 (m) 5.1 (m)	1.1 (m)
CH	ring	7.2 (m)	7.2 (m)

**Table 3.4b.**  $^{13}\text{C-NMR}$  chemical shifts,  $\delta$  (ppm), and signal assignments of DVB in  $\text{CDCl}_3$ , see **Figure 3.11**

Group	Position	$\delta$ ppm, Sign: 1° and 3° (+), 2° and 4° (-)	
			
		<b>DVB</b>	<b>Diethyl benzene</b>
CH, unsaturated CH <sub>2</sub> , saturated	C1 C1'	135.4 (+) -	- 29 (-)
CH <sub>2</sub> , unsaturated CH <sub>3</sub> , saturated	C2 C2'	114 (-) -	- 15.8 (+)
Ring	C-H C quart	123 to 128 (+) 137 (-)	

**Figure 3.13** shows the FTIR spectra of neat DVB and synthesised polyDVB, see **Rn 3.2**. In polyDVB, the absorption peak of the vinyl double bond of DVB (at  $1629\text{cm}^{-1}$ ) had decreased though not completely disappeared (see **Figure 3.13C**). This suggests that the polymerisation of polyDVB may not have gone to completion or some free

DVB may be trapped in the polymerised DVB network. The absorption peaks of the  $>C=C<$  of the aromatic ring of the benzene are however, all present in the polyDVB spectrum and are shown at  $1602\text{ cm}^{-1}$ ,  $1594\text{ cm}^{-1}$ ,  $1510\text{ cm}^{-1}$  and  $1486\text{ cm}^{-1}$ . Similarly, the characteristic strong C-H out of plane of the aromatic ring absorption at  $837\text{ cm}^{-1}$  and  $796\text{ cm}^{-1}$  are clearly seen in the polyDVB. The characteristic infrared absorptions of polyDVB are summarised in **Table 3.5**.

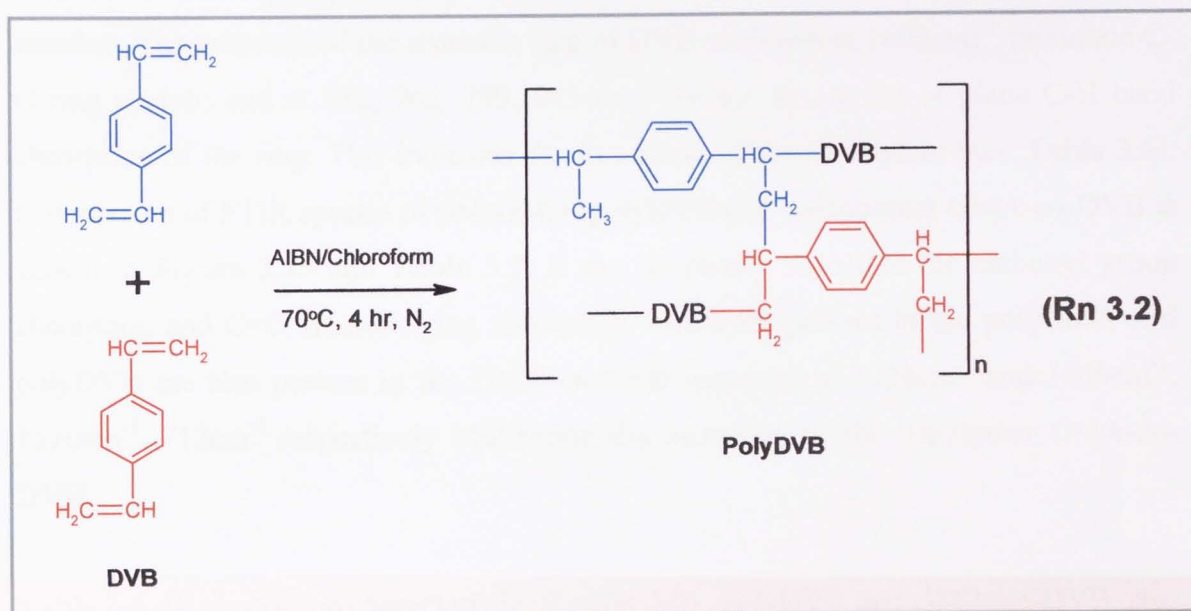


**Table 3.5.** IR absorption characteristic of DVB and polyDVB, see **Figure 3.13**

	Assignment and region expected, $\text{cm}^{-1}$	Frequency, $\text{cm}^{-1}$ , and intensity from spectra	
		DVB	PolyDVB
A	Aromatic C-H stretch 2100-3000	3087, 3007	3085, 3007
B	Aliphatic C-H stretch 3000-2840	-	2988, 2921
C	Vinyl C=C stretch 1640	1629	1629 (reduced in intensity)
D	Aromatic C---C ring stretch 1600-1400 (often appear in duplicates)	1594, 1575 1509, 1485	1602, 1590 1510, 1486
E	-(C-H) out of plane bend of the ring for p-substitute	801, 845	837, 796
F	C=C out of plane ring bonding	709	710
G	Para substitute benzene	1704	1703

## iii) Characterisation of GMA-co-DVB

**Figure 3.14** shows FTIR spectra of neat DVB, neat GMA and that of the synthesised copolymer GMA-co-DVB, see **Rn 3.3**. The IR spectrum of the GMA-co-DVB shows clearly a shift in the carbonyl group of the GMA from  $1721\text{ cm}^{-1}$  (unsaturated  $>\text{C}=\text{O}$  in GMA) to  $1729\text{ cm}^{-1}$  (broad weak) due to the formation of saturated  $>\text{C}=\text{O}$  group. The absorption of  $>\text{C}=\text{C}<$  at  $1630$  and  $1638\text{ cm}^{-1}$  in GMA and in DVB, respectively, have reduced in intensity significantly due to reaction of  $>\text{C}=\text{C}<$  in the copolymerisation reaction. The presence of the aromatic ring of DVB is shown at  $1606\text{ cm}^{-1}$  (aromatic C-C ring stretch) and at  $712, 762, 799, 843\text{ cm}^{-1}$  for the strong out of plane C-H bend absorption of the ring. This indicates the formation of the copolymer (see **Table 3.6**). Comparison of FTIR spectra of polyGMA, polyDVB and comonomer GMA-co-DVB is shown in **Figure 3.15** and **Table 3.7**. It can be clearly seen that the carbonyl group absorption and C=C aromatic ring absorption which are present in the polyGMA and polyDVB are also present in the GMA-co-DVB spectrum at  $1728\text{ cm}^{-1}$  and  $1606\text{ cm}^{-1}$ ,  $1510\text{ cm}^{-1}$ ,  $712\text{ cm}^{-1}$  respectively confirming the formation of the copolymer GMA-co-DVB.

**Table 3.6.** IR absorption characteristic of polyGMA, polyDVB and GMA-co-DVB, see **Figure 3.14**

Label	Assignment and region expected, $\text{cm}^{-1}$ [37]	Actual frequency, $\text{cm}^{-1}$ , and intensity		
		GMA	DVB	GMA-co-DVB
U	Vinyl C=C stretch 1640	1638	1630	1629 (low intensity)
V	Aromatic C—C ring stretch 1600-1400 (often appear in duplicates)	-	1602 1510-1487	1606, 1510
Y	-(C-H) out of plane bend of the ring for p-substitute	-	801	799
Z	C=C out of plane ring bonding	-	707	712
U	Carbonyl group C=O 1720-1730	1721	-	1729
X	Epoxy group -CH-O-CH <sub>2</sub> 909-845	909, 843	-	909, 843

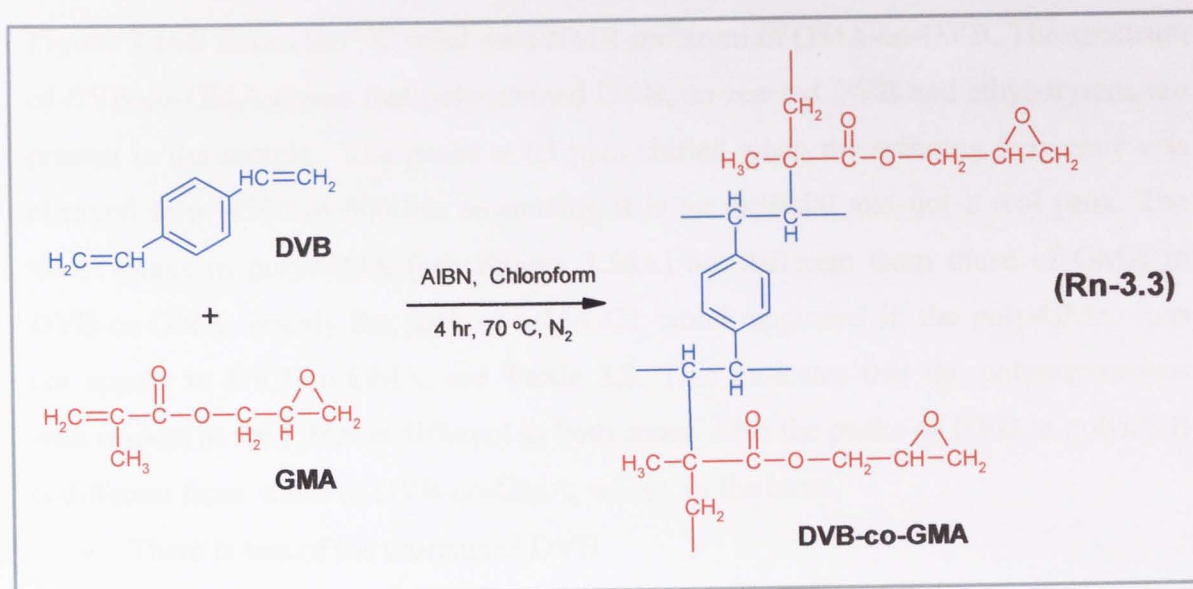


**Table 3.7.** IR absorption characteristic of polyGMA, polyDVB and GMA-co-DVB, see **Figure 3.15**

Label	Assignment and region expected, $\text{cm}^{-1}$ [37]	Actual frequency, $\text{cm}^{-1}$ , and intensity		
		PolyGMA	PolyDVB	GMA-co-DVB
K	Aromatic C-H stretch 2100-3000	-	3085, 3007	
L	Aliphatic C-H stretch 3000-2840	-	2980, 2937	2937
M	Vinyl C=C stretch 1640	1630	1629	1629 (low intensity)
N	Aromatic C—C ring stretch 1600-1400 (often appear in duplicates)	-	1606 1510-1447	1606
P	-(C-H) out of plane bend of the ring for p-substitute	-	795	799
Q	C=C out of plane ring bonding	-	701	712
R	Carbonyl group C=O 1720-1730	1729	-	1729
S	Epoxy group -CH-O-CH <sub>2</sub> 909-845	907, 846	-	909, 843

**Figure 3.16B** shows the  $^{13}\text{C}$  solid state NMR spectrum of GMA-co-DVB. The spectrum of DVB-co-GMA shows that polymerized DVB, un-reacted DVB and ethyl-styrene are present in the sample. The peaks at 65 ppm shifted when the spinning frequency was changed from 4500 to 6000Hz suggesting it is an artificial and not a real peak. The GMA peaks in poly-GMA (see **Figure 3.16A**) are different from those of GMA in DVB-co-GMA, mainly the peak of GMA-C1 which appeared in the poly-GMA does not appear in DVB-co-GMA, see **Table 3.8**. This indicates that the polymerizations with respect to the GMA is different in both cases. Also the peaks of DVB in polyDVB is different from those of DVB-co-GMA, where, in the latter,

- There is less of the un-reacted DVB
- Broad peaks around 26ppm appeared indicating different types of polymerization form, which produced an aliphatic groups.

**Table 3.8.**  $^{13}\text{C}$  solid state NMR chemical shifts,  $\delta$  (ppm), and signal assignments of GMA in polyGMA and in GMA-co-DVB in  $\text{CDCl}_3$ , see **Figures 3.16A and 3.16B**

Group	Position	$\delta$ , ppm	
		GMA in polyGMA	GMA in GMA-co-DVB
$\text{CH}_2$ ,	C1	55	Not seen
C	C2	45	With other peaks
$\text{CH}_3$ ,	C3	16	Broad not clear
C=O	C4	177	177
$\text{CH}_2$	C5	67	67
CH of epoxy ring	C6	49	49
$\text{CH}_2$ of epoxy ring	C7	45	45

### 3.2.3 Characterisation of Purified EPR-g-GMA by FTIR and NMR

Films of the purified GMA-grafted polymer were prepared for characterisation by FTIR, see Schemes 3.1 and 3.2. Figure 3.17 shows a comparison of FTIR spectra of EPR-g-GMA<sub>DVB</sub> (functionalised EPR) and neat GMA. The shift in the ester carbonyl absorption from 1721 cm<sup>-1</sup> to 1729 cm<sup>-1</sup> is clearly seen and this is due to the formation of saturated ester groups whereas the acrylic double bond at 1638 cm<sup>-1</sup> has completely disappeared. Furthermore, the absorption peaks of the epoxy group remained unchanged as shown at 908 cm<sup>-1</sup> and 847 cm<sup>-1</sup> confirming the grafting of GMA onto EPR. The concentration of GMA in the methanol-purified sample is expected to be higher than that of a sample purified in acetone due to the presence of both grafted GMA and polyGMA in the former case, see Figure 3.18. When DVB was added to the GMA grafting system, the spectrum of the purified EPR showed additional absorption peaks at 1602, and 1510 cm<sup>-1</sup> due to the presence of aromatic >C=C< ring stretch of DVB (see Figure 3.19A-B). Similarly, the strong out-of-plane aromatic C-H bend absorptions at 761, 802, 843, 909 cm<sup>-1</sup> are also present and are similar to those seen in GMA-co-DVB (see Figure 3.19C). In addition, the absorption peak at 1638 cm<sup>-1</sup> due to vinyl >C=C< was not observed in the spectrum of EPR-g-GMA<sub>DVB</sub>. This indicates that DVB has reacted with GMA and GMA-co-DVB is grafted on the EPR backbone.

The <sup>1</sup>H and <sup>13</sup>C NMR spectra of EPR (E:P=8:2) are shown in Figures 3.20 and 3.21. Further expansion of the <sup>1</sup>H spectrum of the EPR, see Figure 3.20B shows the presence of minor peaks at 1.9, 2.2, 4.0, 4.6 and 4.9 ppm. In the EPR polymer, there are only aliphatic groups with minor differences in their chemical shifts. In the <sup>1</sup>H NMR spectrum there are three peaks, labelled 1, 2 and 3. Peak 1 being the minor peak corresponding to the CH (no.1) at the branched carbon which appears at 1.05ppm, the second peak, 2, (the main peaks) for the -CH<sub>2</sub> (no.2) backbone of the polymer appearing at 1.2ppm and the third peak, 3, at 0.8ppm, for the -CH<sub>3</sub> (no.3). The <sup>13</sup>C NMR peaks were assigned for the propylene peaks 1, 3 and 4 and for the ethylene peaks 2 mainly and peak 5 for the carbons away from the branched site, see EPR structure in Figure 3.21.

The <sup>1</sup>H-NMR spectrum of a purified EPR-g-GMA<sub>CONV</sub> (sample G24 containing 1.9 wt% GMA, see Table 3.1A) is shown in Figure 3.22, as in the poly-GMA, the



epoxide region is not affected by the grafting while the methylacrylate group has been converted completely to a polymerised methylpropanoate group. The  $^1\text{H}$  NMR peaks of the methyl group  $\alpha\text{-CH}_3$  of the GMA in the  $\text{EPR-g-GMA}_{\text{CONV}}$  (should appear at about 1ppm) are in the same region as the EPR peaks, thus the analysis will be based on  $1\text{-CH}_2\text{-}$  of the GMA, where its peaks appeared resolved in the 2.0 ppm region (EPR does not show signals in this region). As was assigned for the poly-GMA in **Figure 3.3**, similarly in the case of  $\text{EPR-g-GMA}_{\text{CONV}}$ , there are three peaks for the  $\text{-CH}_2\text{-}$  in the 2.0 ppm region, those peaks are assigned for sequences *rrr*, *mrr* and *mrmm* as shown in **Figure 3.22** and illustrated later in **Figure 3.38**.

Integration of  $^1\text{H}$  NMR was used to estimate the nature and the distribution of GMA grafts in samples of  $\text{EPR-g-GMA}_{\text{CONV}}$  (sample G24). The calculation is based on the fact that the EPR used in this work has 8 ethylene  $\text{-(CH}_2\text{-CH}_2\text{)}_8\text{-}$  groups and 2 propylene groups  $\text{-(CH(CH}_3\text{)-CH}_2\text{)}_2\text{-}$  in each repeat unit. Since all the polymer H's are located in chemical shift region between 0.7 to 1.5 ppm, they were summed up (total of 44 H's in one repeat unit) and their integration was counted for all 44 H's. The GMA has two parts, the epoxide has 5H's (H's no. 4,5,6) and the part bonded to the polymer has 5H's (no. 1 and 3).

### 3.2.4 Grafting GMA onto EPR in the absence of DVB

#### 3.2.4.1 Effect of Initiator (T101) and Initial GMA Concentration on the Grafting Reaction

The effect of the peroxide concentration on the torque behaviour of conventional  $\text{EPR-g-GMA}_{\text{CONV}}$  is shown in **Figure 3.23**. It is clear that higher peroxide concentration results in higher torque maximum and final torque values and requires longer time to reach the torque maximum. This is almost certainly due to an intense reaction at the initial stages of processing between the EPR-macroradicals and GMA together with the formation of polyGMA. This is supported by the observed decrease in MFI values and increase in xylene-insoluble gel content at higher peroxide concentrations. At peroxide concentration of 1.50 phr (0.07 MR) the MFI became immeasurable and up to 8 % xylene insoluble crosslinked polymer was formed. The EPR used in this study had a ratio of PE:PP of 8:2 thus, it can be expected that PE crosslinking reactions will dominate during processing [206] and the contribution of chain scission (PP undergoes

mainly chain scission) becomes less important. The extent of grafted GMA was also shown to increase with increasing peroxide concentration but this is concomitant with an increase in the concentration of polyGMA (Figure 3.23E).

The effect of the initial GMA concentration on the grafting reaction in the conventional system was also examined using a fixed T101 concentration of 0.8 phr and processing temperature of 190°C. Figure 3.24 shows that the final torque is slightly lower at higher initial GMA concentration. This is paralleled by a slight increase in the MFI (lower viscosity) and decrease in the gel content (when increasing the GMA concentration from 5 % to 15 %, see Figure 3.24B). At the same time, increasing the initial GMA concentration to 15% resulted in the grafting degree to increase from 0.6 % to 1.9 % but with a significant increase in the extent of polyGMA formation which became the predominant reaction product at 15% initial GMA concentration, see Figure 3.24C.

The kinetics of the conventional melt grafting reaction system was examined by sampling out at time intervals during processing. Two samples processed at 190 °C and which contained 15 % GMA and different amounts of initiator (0.8 and 0.13 phr) were examined by analysing the extent of the graft and homopolymerisation reactions at different times. Figure 3.25 and 3.25B show that the grafting reaction was complete in the first 3 minutes when 0.8 phr T-101 was used and at ~ 5min at the lower T101 concentration of 0.13 phr. It is shown that in presence of initial GMA concentration of 15%, polyGMA was formed at faster rate and its amount was higher, compared to the level of grafted GMA at both peroxide concentrations, see Figure 3.25A and 3.25B. This indicates that under these conditions the GMA homopolymerisation reaction dominated from the start of the melt reaction. As may be expected, at a lower peroxide concentration of 0.13 phr, the initial rates of both the grafting and the polymerisation reactions were slower and the overall concentrations of g-GMA and polyGMA formed were also lower, see Figure 3.25C and 3.25D. The use of lower peroxide and initial GMA concentrations  $[T101]=0.3$  phr and  $[GMA]_i=10$  % in the conventional grafting process gave rise to a faster grafting reaction compared to the formation of polyGMA examined at two peroxide concentrations of 0.3 and 0.078 phr and in the former case the amount of polyGMA decreased with processing time, see Figure 3.25E and 3.25F.

These results confirm the fact that peroxide concentration influences strongly the formation of polyGMA.

### 3.2.5 Grafting GMA onto EPR in the presence of DVB

#### 3.2.5.1 Effect of T101 and Initial GMA Concentration on the Grafting System

In the GMA/DVB grafting system, the concentration of T101 that was required to achieve grafting was much lower than that used in the conventional grafting system (in absence of DVB) and was therefore varied between 0.017 to 0.13 phr (using GMA concentration of 10 phr). **Figure 3.26A** shows the torque behaviour during the melt grafting process in the presence of DVB (at GMA:DVB=8:2 w/w). It is clear that a higher peroxide concentration gives rise to an increase in the torque peak and the final torque suggesting an increased extent of the reactions which occurs at a faster rate, i.e. shorter time to peak maximum, see **Figure 3.26B** and **3.26C**. The suggestion that higher peroxide concentrations in the DVB system give rise to higher extent of crosslinking is supported by the observed decay in MFI values (see **Figure 3.26D**) but no measurable amount of xylene-insoluble gel was formed under these conditions, see **Figure 3.26E**.

It was reported [9, 21, 207] that the presence of reactive comonomers such as trimethylolpropane triacrylate (TRIS) or styrene in grafting systems would significantly improve the grafting degree and reduce the extent of monomer homopolymerisation. Similar observations were seen in this work when DVB was introduced in the GMA grafting system. **Figure 3.26D** shows clearly that the GMA grafting level in the presence of DVB increases significantly compared to that in the conventional system and this high level of grafting was achieved at only a fraction of the peroxide concentration used in the conventional system with the consequence of undermining the GMA homopolymerisation reaction so that no measurable polyGMA was detectable when DVB was present at all peroxide concentrations examined, see later.

It is important to mention here, that the presence of other possible products from side reactions such as polyDVB and GMA-co-DVB could not be quantified here because these products which were separated out during purification were insoluble during the hot xylene-extraction and remained together with the insoluble gel, see **Scheme 3.2**.

However, based on the fact that the total amount of insolubles was unmeasurable (Figure 3.26E) and based on literature findings with other multifunctional comonomers such as TRIS [9], the amount of these products may not be expected to be significant. Increasing the DVB concentration at a constant T101 concentration of 0.13 phr in the EPR-g-GMA<sub>DVB</sub> system resulted in an increase in the torque maximum and the final torque, (Figure 3.27) indicating reaction of DVB with the polymer and with itself resulting in branching and crosslinking reactions (increased polymer viscosity) which became more dominant at higher DVB concentration. In fact, without peroxide or GMA, the presence of DVB alone can cause crosslinking in EPR backbone giving rise to increased torque values compared to EPR alone, (see Figure 27A, EPR+DVB curve). This is supported by the observed reductions in MFI values (reflecting increase in molecular weight) and increase in gel content (Figure 3.27B). Further, the increase in the torque peak values was paralleled by an increase in the time required to reach the torque maximum at the higher DVB concentrations, see Figure 3.27C. It can also be seen that the amount of DVB grafted onto EPR increased at higher initial DVB concentrations as reflected in the higher IR absorbance area index of the >C=C< of the benzene ring of DVB measured in purified samples where any unreacted DVB would have been removed, see Figure 3.27E and 3.27F.

Figure 3.28 shows the effect of DVB concentration on the extent of GMA grafting and polyGMA formation. These results illustrate the significant improvement in the GMA grafting level with increasing DVB concentration and when compared to the conventional system. It is important to note that at all DVB concentrations used (with T101=0.13 phr) no measurable amount of polyGMA was detected (see Figure 3.28 B). The high reactivity of DVB is clearly illustrated from the fact that even in the absence of any peroxide initiator, some GMA grafting has still taken place, (up to 1%), see Figure 3.28B whereas in the conventional system no GMA grafting takes place in the absence of peroxide. These results contradict literature findings [57] involving the use of other comonomers such as vinyl 4-*tert*butylbenzoate (VBB), styrene and 1-dodecene (DD) were used in grafting of maleic anhydride (MA) onto poly(ethylene-*co*-methyl acrylate) (EMA) where no measurable grafted MA onto EMA was found.

The effect of GMA concentration on the GMA grafting level in the presence of DVB was also examined. The concentration of GMA was varied from 5 phr to 15 phr and used at a constant T101 concentration of 0.13 phr and the GMA/DVB ratio was fixed at 9/1 w/w. **Figure 3.29** shows clearly that the torque values were not much affected by varying the GMA concentration which suggests that the amount of GMA in the grafting systems has a negligible influence on the melt viscosity. However increasing the initial GMA concentration gave rise to a decrease in the MFI values of the EPR-g-GMA<sub>DVB</sub> system but with no detectable gel formation (see **Figure 3.29C**). The level of GMA grafting, on the other hand, increased with increasing the initial amount of GMA up to 5% and more importantly, this occurred with no polyGMA formation, **Figure 3.29D**, illustrating again the effectiveness of DVB in enhancing the melt grafting efficiency at the expense of the homopolymerisation reaction.

The kinetics of the GMA grafting in the presence of DVB at various initial GMA concentrations is presented in **Figure 3.30**. The grafting rate increased rapidly to a maximum level after 2 minutes at both GMA concentrations of 10 and 15 phr but with the reaction rate being much faster at initial GMA concentration of 15 phr (**Figure 3.30C**). No polyGMA was formed during the reaction when 10% initial GMA concentration, but with  $[GMA]_i = 15\%$ , a small concentration ( $\sim 0.1\%$ ) of polyGMA was formed in the earlier stages of the reactions and this occurred rapidly in the first 5 minutes but decreased gradually with further processing (**Figure 3.30D**).

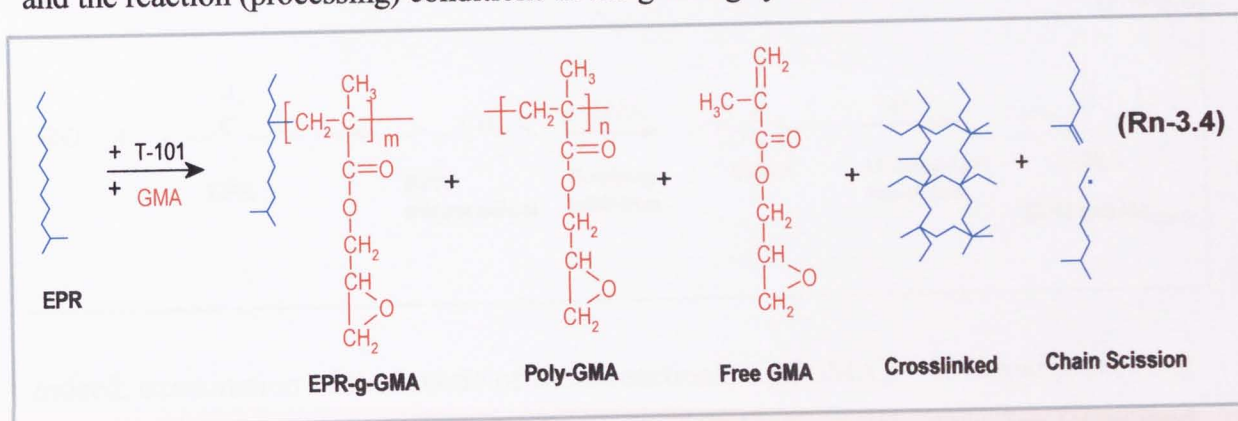
### 3.2.5.2 Effect of Processing Temperature on Grafting

The effect of the processing temperature on the GMA/DVB melt grafting system was also investigated at a fixed GMA concentration of 10 phr, and a GMA:DVB ratio of 9:1. **Figure 3.31** shows clearly that the overall high grafting degree in the DVB systems decreases with increasing processing temperature at all peroxide concentrations examined, but in all cases, no polyGMA was measurable. The processing temperature has a great influence on the overall free radical grafting process as both the kinetic and thermodynamic aspects of all the elementary reactions involved are temperature dependent. The torque behaviour shows a slower onset of reaction at lower processing temperatures (e.g. at 170°C) thus a shorter time to torque maximum was observed at higher temperatures.

### 3.3 Discussion

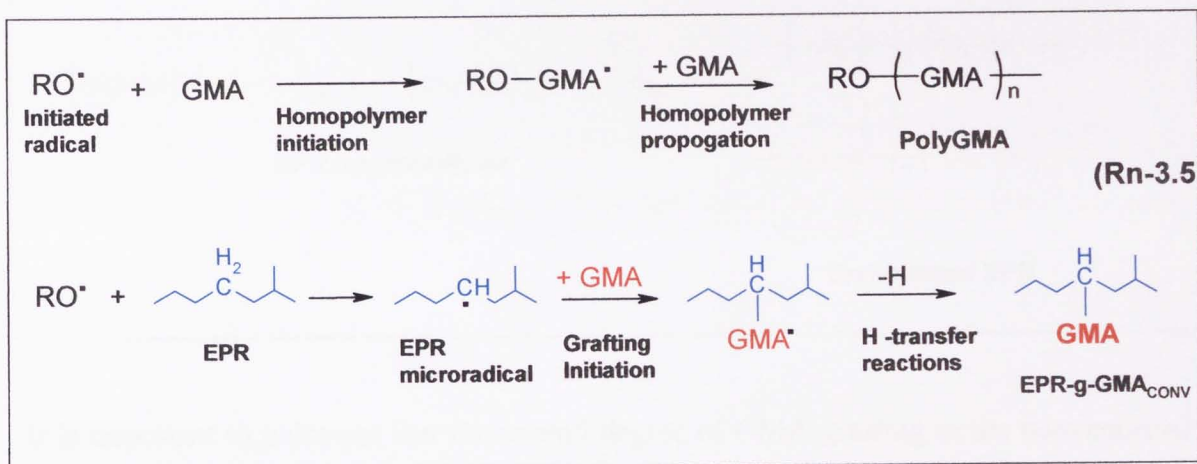
#### 3.3.1 Melt Grafting of GMA in Absence of a Comonomer

Grafting reactions of GMA on polymers in presence of a free radical initiator (conventional system) are always accompanied by a number of competing undesirable side reactions such as homopolymerisation of the monomer and formation of crosslinking or chain scission as a result of radical-induced degradations reactions in the polymer backbone [9, 29, 51, 206], see **Rn 3.4** as an example in EPR. The relative contribution of each of these competing reactions depends on the chemical composition and the reaction (processing) conditions of the grafting system.



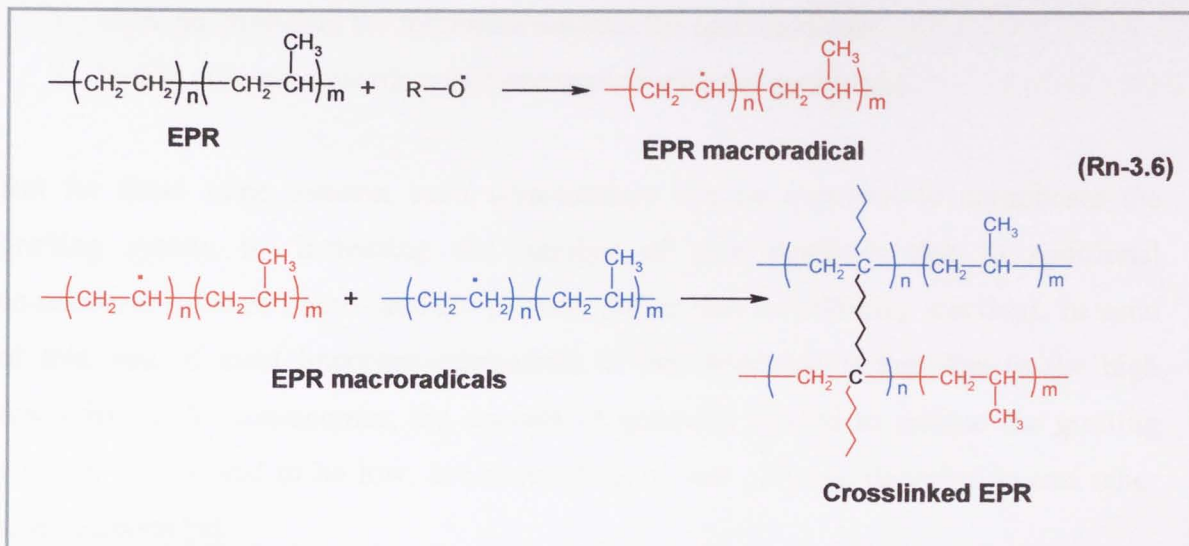
The work reported here shows that increasing the initiator concentration in the conventional GMA/peroxide (T101)–EPR grafting system would increase the level of GMA grafting but at the same time the system gives rise to a substantial increase in the extent of polymer degradation by branching and crosslinking (EPR used here has ethylene:propylene ratio of 8:2) as evidenced from the observed major increase in the gel concentration found and the torque values of the melt reaction along with a dramatic reduction in the MFI values reflecting an increase in polymer viscosity and molecular weight, see **Figures 3.23B** and **3.23C**. Moreover the observed increase in the grafting level is also paralleled by an increase in the level of GMA-homopolymerisation, see **Figure 3.23E**. The importance of the homopolymerisation reaction becomes even more evident when higher initial GMA concentrations are used, e.g. going from 10% to 15%, where it becomes evident that the GMA-homopolymerisation becomes the dominant reaction in the grafting system (higher concentration of polyGMA compared to that of g-GMA), see **Figure 3.24C**.

It is clear therefore that the strategy for increasing the GMA-grafting level in the conventional system, by increasing concentration of either the peroxide or the initial GMA content, is not a successful one as this approach also results in favouring the competition from unwanted side reactions and in particular it would increase the importance of radical-initiated GMA-homopolymerisation (propagation) at the expense of graft-initiation reaction, see **Rn 3.5**.



Indeed, examination of the kinetic of these reactions, e.g.  $[\text{GMA}]_i = 15\%$  and processing temperature =  $190^\circ\text{C}$ , show clearly that the rate of GMA homopolymerisation (examined at two different T101 concentrations of 0.13 and 0.8 phr) is faster than the rate of the graft-reaction giving rise to the formation of a higher (compared to g-GMA) amounts of polyGMA that are formed throughout the melt reaction, see **Figure 3.25A-D**. The importance of the polymer degradation (via crosslinking) reactions at higher peroxide concentrations is further evident when examining the behaviour of EPR processed with different concentrations of peroxide (in absence of GMA). **Figure 3.32** shows clearly that in the absence of GMA and at higher T101 concentrations, the higher torque values are paralleled by a drastic reduction in the MFI confirming an increase in molecular weight due to branching and crosslinking of the polymer. Of course the presence of GMA in the EPR-T101 system does reduce the extent of reduction in MFI as seen clearly in **Figure 3.32B** and **3.33B**, but it still gives rise to a considerable reduction in MFI at higher peroxide concentrations confirming the favourable competition from polymer degradation reactions. Literature studies [9, 208] have shown that degradation of PE in the melt is dominated by crosslinking whereas in PP chain scission reactions

predominate due to stability of the tertiary PP radical, thus predominance of crosslinking reactions in the case of EPR used in this study, see **Rn 3.6**.



It is important to point-out that the overall degree of GMA-grafting in the conventional system remained low (max~1.9%) under all conditions examined, and this clearly reflects the low reactivity of GMA towards the EPR macroradicals. The low reactivity of GMA in grafting reactions on other polymers has also been described in the literature and has been attributed [17, 209, 210] to the relatively low electron density of the acrylate double bond (which is the polymer reactive moiety) due to the electron withdrawing capability of the adjacent carbonyl group and the presence of the bulky substituent on the double bond, hence its low free radical reactivity.

### 3.3.2 Melt Grafting of GMA in EPR in Presence of the Comonomer DVB and Comparison with Grafting in Its Absence

The low grafting efficiency of GMA onto EPR in the conventional grafting system and the problems associated with attempts to increasing the grafting level by increasing the peroxide concentration, a reaction which also gives rise to severe extent of polymer degradation and formation of high level of GMA homopolymer, was clearly illustrated in the above discussion (**Sec. 3.3.1**).

The use of highly reactive comonomers to enhance the grafting efficiency of less reactive monomers on polymer melts has been described in the literature for the case of,



for example, TRIS [3, 9] and styrene [32, 57, 89, 211] comonomers. However, for a comonomer to be useful in improving the grafting efficiency of other monomers, it must be:

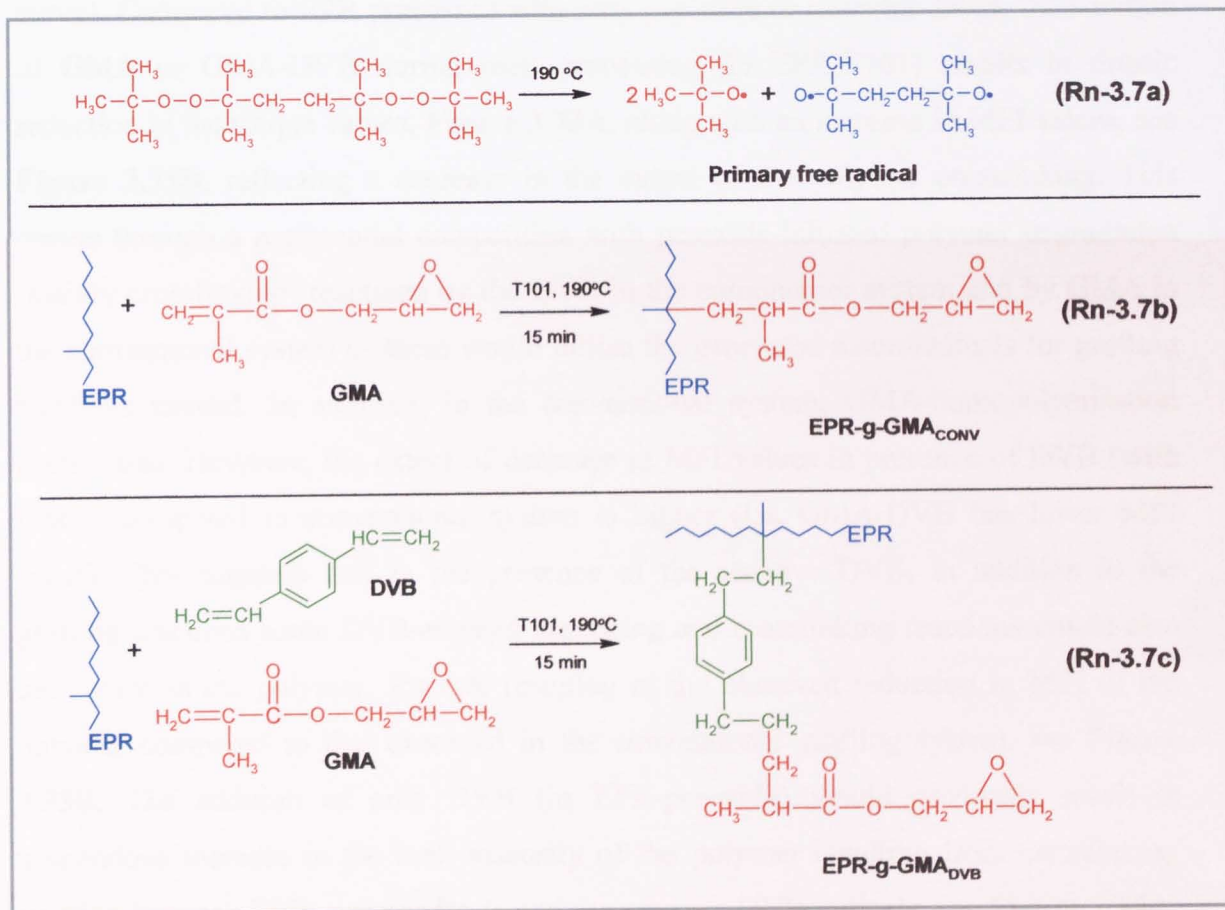
1. more reactive than the monomer towards the macroradicals
2. highly efficient towards copolymerisation with the monomer.

But for these same reasons, such comonomers can be expected to complicate the grafting system by increasing the number of side reactions due to additional comonomer-initiated homo- and co- polymerisation and crosslinking reactions. In spite of this, one of most important-advantages of this approach is that due to the high reactivity of the comonomer, the amount of peroxide needed to initiate the grafting reaction is expected to be low, hence resulting in less polymer degradation and other side reactions [9].

Indeed, the need for only a small fraction of the total amount of peroxide in the presence of a reactive comonomer, compared to the amount required in a conventional grafting system, is confirmed in this work when the highly reactive comonomer DVB is used in the GMA-grafting system on EPR. **Figure 3.28A** shows that in a 10% GMA grafting system, replacing only 1 % of the total GMA by DVB (i.e. GMA:DVB=9:1 w/w ) results in an increase in the extent of grafting by over 4 times and this is achieved at a much lower peroxide concentration compared to the conventional (in absence of DVB) system (e.g [T101]=0.02 phr against 0.8 phr, respectively). The extent of GMA-grafting can be further increased up to 5 % by increasing the proportion of DVB in the GMA:DVB system, see **Figure 3.28A**, this clearly contrasts with the low extent of GMA grafting in the conventional system which even at the highest concentration of peroxide used of 0.13 phr gave rise to less than 1 % grafting.

A second major advantage in using the comonomer DVB is the fact that no (or very low) GMA homopolymer is formed in the grafting system, see **Figures 3.34B** and **3.29D**. These results confirm the high reactivity of DVB towards both the polymer macroradical and GMA thus undermining the chance for the GMA radicals to propagate and produce polyGMA, and in turn increasing the extent of g-GMA formation. The higher reactivity of DVB towards EPR macroradical, compared to that of GMA/macroradical, is further illustrated from the observation that even in the complete

absence of a peroxide, i.e. in a shear-initiated reaction, GMA-grafting can still be achieved (up to 1 %), see **Figure 3.28B**, whereas no grafting was obtained in conventional system processed in the absence of peroxide. Also the DVB-containing system shows a distinctive torque behaviour during melt reactive processing where a clear torque peak occurs at the early part of the reactions with its height increasing with an increase in the DVB concentration in the system, see **Figure 3.27A**, and takes place at shorter times in presence of higher peroxide concentrations, see **Figures 3.26A** and **3.26C**. These results suggest therefore, that the highly reactive DVB can be expected to first become grafted onto the polymer chains, followed by its reaction with GMA, see **Rn 3.7**, thus giving rise to high grafting of DVB-GMA on the polymer backbone without any polyGMA formation.

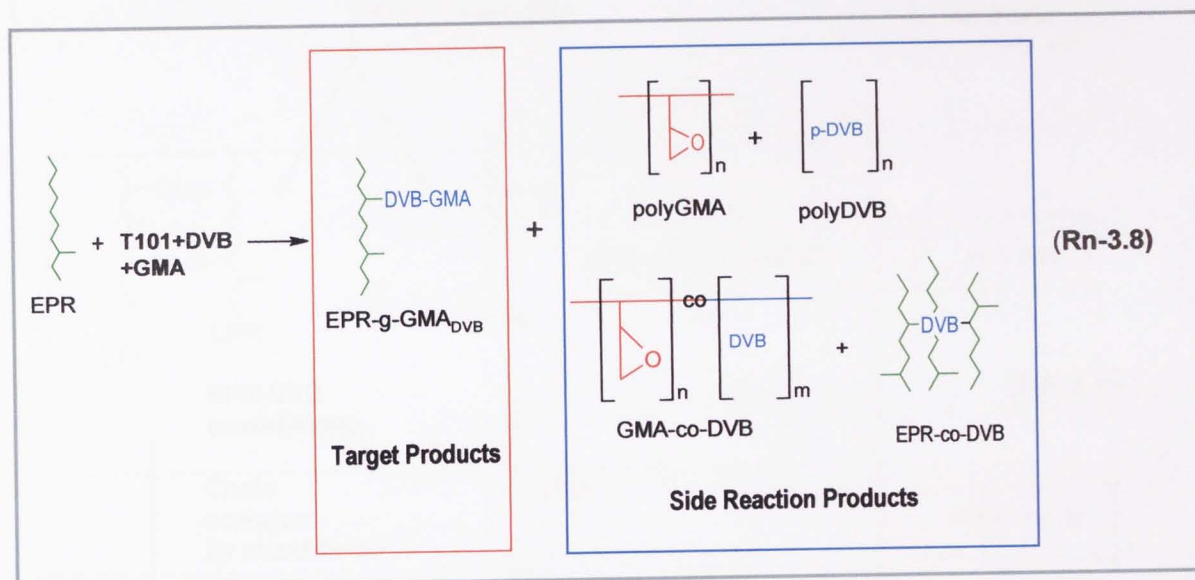


This is supported by results obtained from the kinetics of the EPR-g-GMA<sub>DVB</sub> grafting system, where the extent of grafting and homopolymerisation reactions were determined (in purified samples) at time intervals during the melt reaction. **Figure 3.30** shows

clearly that in GMA:DVB system of 9/1 w/w, the rate of GMA grafting is very fast (reaction is complete in the first 2-3 minutes) and the amount grafted is high with almost complete disappearance of the homopolymer (no measurable amount throughout the reaction time when 10% initial GMA concentration is used and with less than 0.1% formed at the end of reaction in the presence of 15% [GMA]<sub>i</sub>). This contrasts with the corresponding conventional system (in absence of DVB), which gives a much higher extent of GMA-homopolymer formation (e.g at 15 phr initial GMA concentration, 3% polyGMA was found) and a consequent lower rate and amount of graft-GMA yield, see **Figure 3.36**.

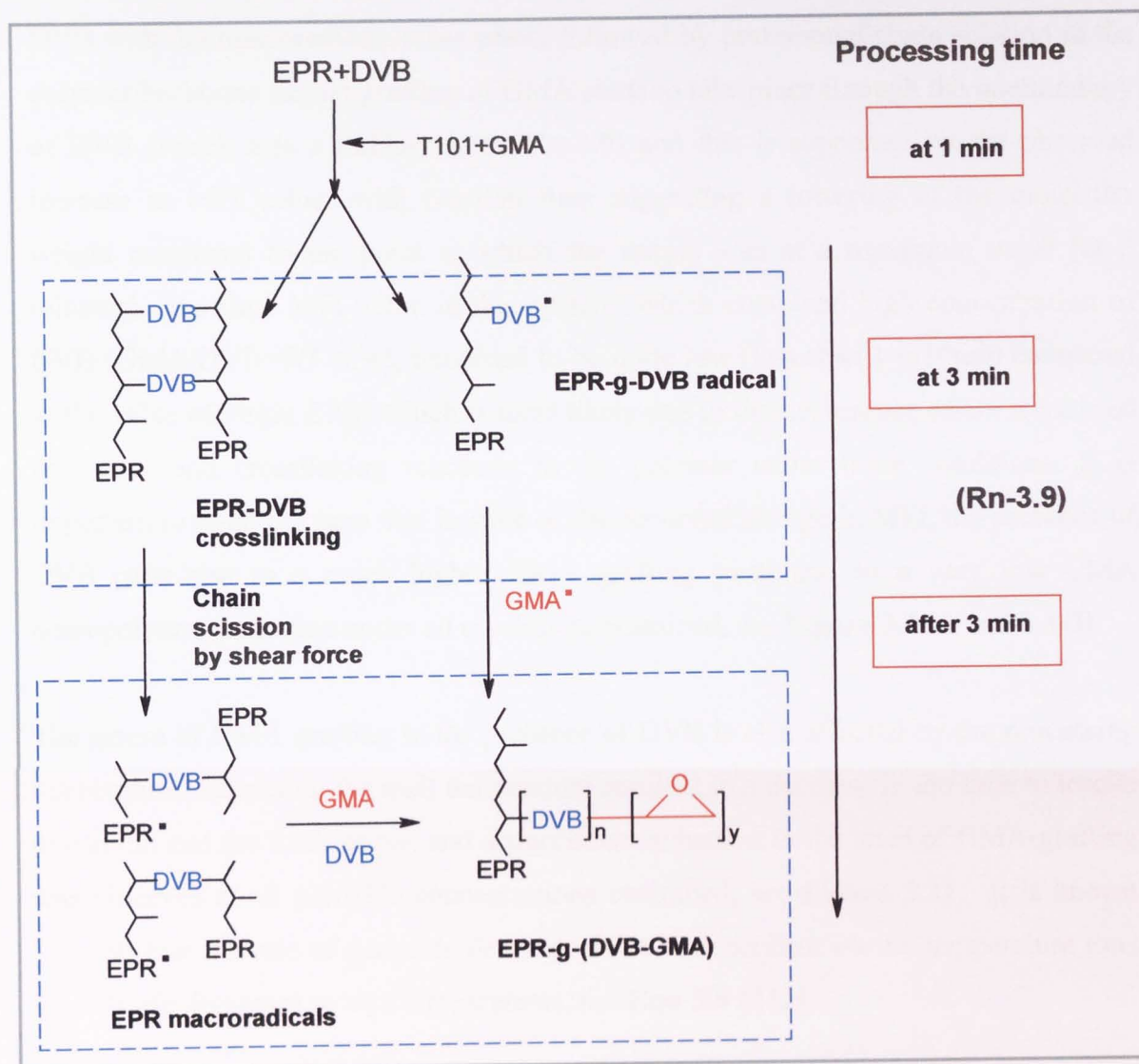
It was mentioned earlier that processing of EPR with peroxide, e.g.T101, resulted in crosslinking of the polymer, as illustrated from the observed increase in torque values as well as the drastic reduction in the MFI values (see **Figures 3.32A and B**, EPR-T101 curve). Compared to EPR processed with only peroxide or peroxide DVB, the addition of GMA or GMA-DVB during melt processing (in EPR-T101) results in drastic reduction in the torque values, **Figure 3.33A**, along with an increase in MFI values, see **Figure 3.33B**, reflecting a decrease in the extent of the polymer crosslinking. This occurs through a preferential competition with peroxide-initiated polymer degradation (mainly crosslinking) reactions by the DVB in the comonomer system and by GMA in the conventional system as these would utilise the generated macroradicals for grafting reactions instead. In addition, in the conventional system, GMA-homopolymerisation occurs also. However, the extent of decrease in MFI values in presence of DVB (with GMA) compared to conventional system is higher (i.e. GMA-DVB has lower MFI value). This suggests that in the presence of the reactive DVB, in addition to the grafting reactions some DVB-assisted branching and crosslinking reactions would also take place in the polymer, **Rn 3.8**, resulting in the observed reduction in MFI of the polymer compared to that observed in the conventional grafting system, see **Figure 3.33B**. The addition of only DVB (in EPR-peroxide) would obviously result in tremendous increase in the melt viscosity of the polymer resulting from crosslinking reaction between EPR macroradicals and the reactive DVB radicals, see **Figure 3.33A**. This explains the fact that, with the addition of GMA the extent of crosslinking can be reduced because the ERP-DVB radicals formed will also react rapidly with GMA, hence reducing the amount of DVB radicals available for recombination reaction

(crosslinking) and homopolymerisation. Furthermore, the torque behaviour shown in **Figure 3.33A** suggests that the reaction of EPR-DVB with GMA occurs much faster than the reaction of DVB with EPR and DVB with DVB as seen from the shorter time torque maximum in the EPR-DVB-GMA sample.



Analysis of the xylene-insoluble fractions of the EPR-g-GMA<sub>DVB</sub> (GMA/DVB ratio of 7/3 w/w) sample at time intervals during processing has shown that at the point of torque maximum (after 3 min processing) the sample contained 32 % insoluble gel, whereas at the end of the reaction (15 min) the gel content has decreased substantially to 1.0 %, see **Figure 3.37B**. The IR absorption spectrum of the insoluble fraction at 3 min processing showed a clear and large benzene absorption corresponding to DVB, see **Figure 3.37D**. The very high amount of gel (32 %) present at the early stages of the reaction and particularly at the point of torque maximum (at 3 min) and the presence of IR absorption peak characteristic of DVB supports the suggestion of a higher extent of DVB-assisted crosslinking reactions in the earlier stages of the melt grafting process due to the high reactivity of DVB towards EPR macroradicals. From these results, it can be concluded that the high reactivity of the formed DVB-EPR radicals results in DVB-assisted crosslinking EPR or/and the formation of EPR-g-DVB (see **Rn-3.9**) giving rise to the observed increase in the melt viscosity (the torque peak) and extensive reduction in MFI almost down to zero at 3 min (see **Figure 3.37C**) supported by the very high

extent of insoluble gel measured at this point of maximum torque of the melt processing.



The extensive initial reaction between DVB and EPR dominated by the high reactivity of DVB inhibits initial involvement of the GMA in the reaction at the early stages of the melt reaction due to the difficulty of diffusion in the highly viscous polymer medium. However, as the reaction progresses (e.g. 4-15 minutes), the torque started to decrease and this was concomitant with a sharp increase in the measured GMA-grafting level and the appearance of an increasing amount of DVB (determined through IR absorption peak of its benzene ring in the soluble fractions) the overall amount of DVB determined in these soluble fractions with increasing processing time is still smaller than that measured at the point of maximum DVB-assisted crosslinking (at 3 min), see **Figure**

**3.37D2** due to reduction in the extent of crosslinking which is supported by the dramatic reduction in the amount of gel present at 15 min processed (dropped from 32% at 3 min to 1% at 15 min), see **Figure 3.37B**. This indicates clearly that once the reaction of DVB with the macroradicals takes place, followed by preferential chain scission in the polymer backbone further grafting of GMA starts to take place through the intermediary of DVB (which acts a linking agent, **Rn-3.9**) and this is supported by the observed increase in MFI values with reaction time suggesting a lowering of the molecular weight compared to the point at which the torque was at a maximum value (at 3 minutes). The final MFI value in this system, which contained high concentration of DVB (GMA/DVB=7/3 w/w), remained to be quite low (less than 1 g/10min compared to the value of virgin EPR) which is most likely due to the occurrence of DVB-assisted branching and crosslinking reactions in the polymer under these conditions. It is important to point out here that in spite of the observed change in MFI, the presence of DVB gave rise to a much higher GMA grafting yield and to a very low GMA homopolymer formation under all conditions examined, see **Figure 3.34A** and **3.34B**.

The extent of GMA grafting in the presence of DVB is also affected by the processing temperature. Increasing the melt temperature resulted in a decrease in the time to torque maximum and the final torque, and a significant reduction in the level of GMA-grafting was observed at all peroxide concentrations examined, see **Figure 3.31**. It is known [10, 29] that the rate of peroxide decomposition is dependent on the temperature thus the half life decreases at high temperatures, see **Eqn 3.4** [212].

$$k_d = A.e^{-\Delta E_a/RT} \quad \text{Eqn 3.3}$$

$$t_{1/2} = (\ln 2)/k_d \quad \text{Eqn 3.4}$$

$t_{1/2}$ =time at which half of the peroxide decomposes (a measure of rate of decomposition)

$\Delta E$ = activation energy 155.49 kJ/mole [212]

$k_o$ = prefactor in Arrhenius equation for the peroxide T101 ( $1.68 \times 10^{16} \text{ s}^{-1}$ ) [212]

$R$ = Arrhenius Constant (8.3142 J/mole.K) [212]

$T$ =temperature

**Table 3.9** shows the calculated  $t_{1/2}$  for the peroxide T101 at different temperatures (from Eqn 3.1 and 3.2) and **Figure 3.31D** shows that the decrease in grafting yield with processing temperature is paralleled by decrease in the half time of the peroxide at the higher processing temperatures, but with no GMA homopolymer being formed over the whole temperature range examined. At higher temperatures e.g. 200°C, the half life of T101 is so short that there may not be enough free radicals generated to promote grafting resulting in a lower g-GMA yield.

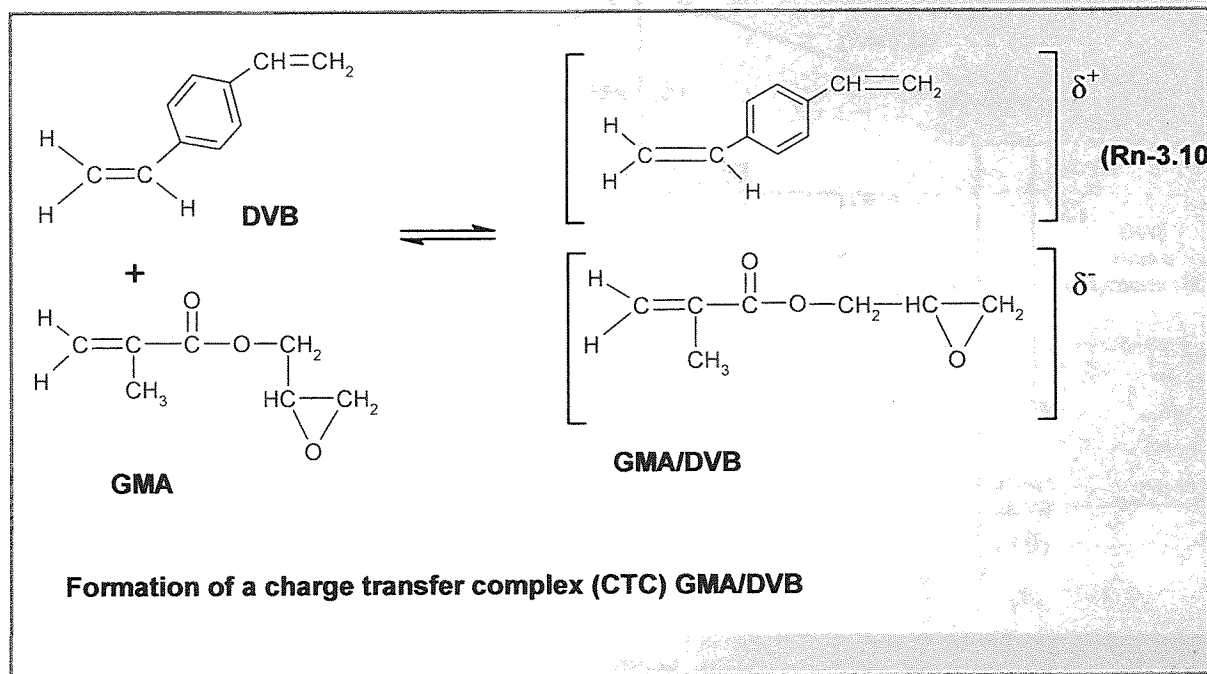
**Table 3.9.** Half life ( $t_{1/2}$ ) of peroxide Trigonox 101

Temperature (°C)	Trigonox 101 Half life $t_{1/2}$ [min]
110	1090
120	310
130	96
140	31
150	11
160	4
170	1.5
180	0.60
190	0.20
200	0.10
210	0.00

### 3.3.3 Mechanism of GMA-Grafting on EPR in the Presence of Comonomer DVB

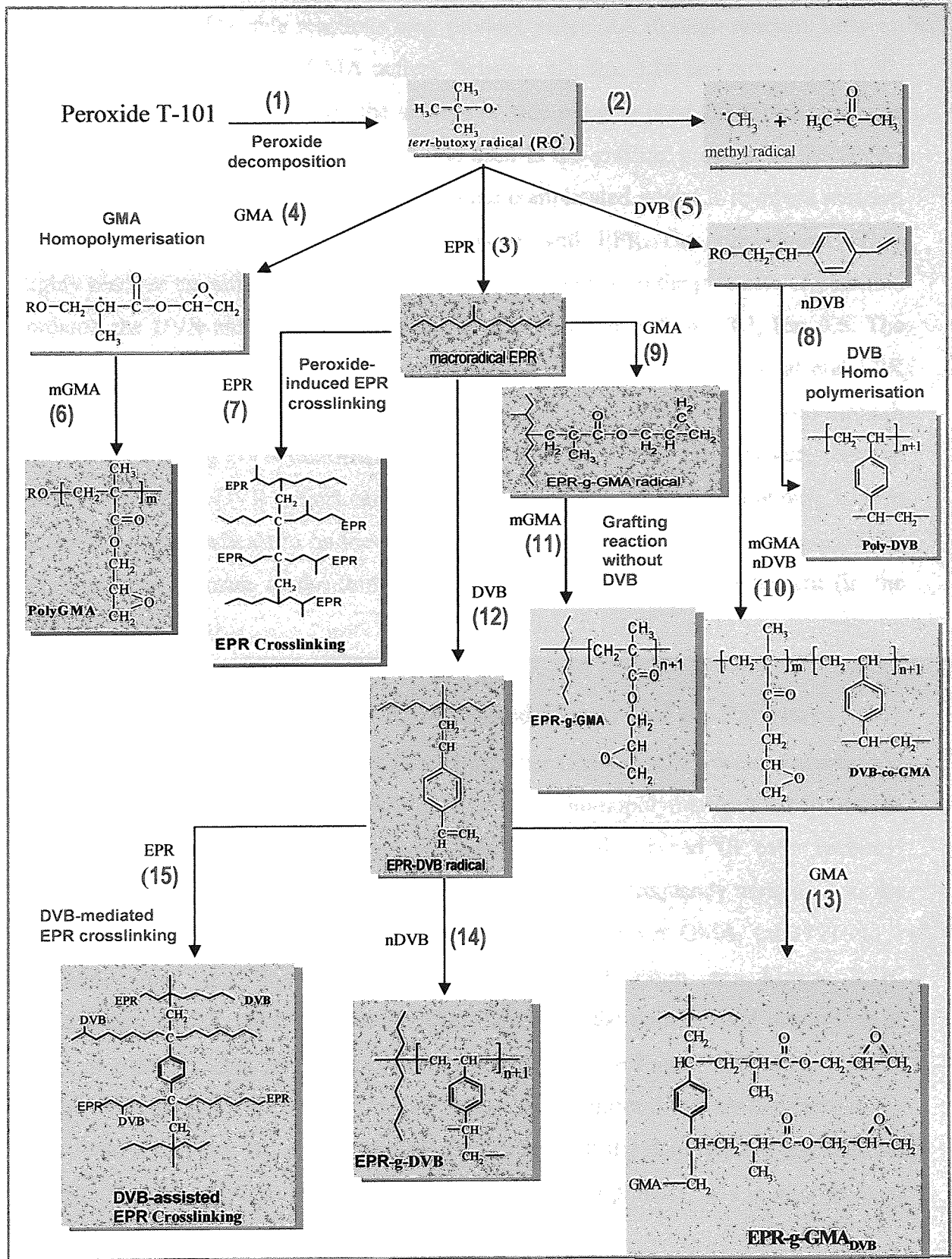
It is clear from the above discussion that compared to the conventional EPR-GMA grafting system, the presence of the comonomer DVB gives rise to a substantial increase in the extent of GMA grafting with no polyGMA formation. The enhanced grafting efficiency of GMA in presence of DVB can be attributed to a number of reasons. Firstly, due to the high reactivity of DVB towards the EPR macroradical compared to that of GMA and this is clearly illustrated from the much higher torque peak observed in the presence of DVB compared with its absence, see **Figure 3.27A** and **3.33A**. This also suggests that DVB must graft first onto the EPR backbone then copolymerises with GMA resulting in EPR-g-(DVB-co-GMA). The DVB may also contribute to increasing the solubility of GMA in the polymer, thus increases its grafting yield. Similar

suggestion were given in the literature in presence of other comonomers such as TRIS [9, 51] and styrene [197]. The electron rich DVB may also enhance the reactivity of the more electron-deficient GMA through a donor-acceptor charge transfer complex route (CTC) similar to that described for styrene-GMA [10], see **Rn 3.10**.



The mechanism of the melt free radical grafting of GMA on EPR in the conventional and the DVB systems is shown in **Scheme 3.3**. The thermal decomposition of the peroxide initiator gives rise to alkoxy radicals (see **Scheme 3.3**, **Rn 3.1**) with further decomposition through  $\beta$  chain scission of the alkoxy radical to form methyl radicals, (see **Scheme 3.3**, **Rn 3.2**). These radicals are very reactive towards H-abstraction giving EPR macroradicals (see **Scheme 3.3**, **Rn. 3.3**). The grafting reaction in the conventional system takes place through the reaction of GMA with EPR macroradical to form GMA grafted EPR, see **Scheme 3.3**, **Rn. 3.11**. Since the EPR used in this study consists of high PE to PP ratio of 8:2, the polymer degradation through crosslinking becomes important, see **Scheme 3.3**, **Rn. 3.17**. In the case of DVB system, the grafting reaction is initiated by the addition of DVB on the EPR macroradical giving rise to a propagating EPR-DVB macroradical, (see **Scheme 3.3**, **Rn. 3.12** and **3.14**). Copolymerisation of the EPR-DVB macroradicals with GMA results in the EPR-g-(DVB-co-GMA).





Scheme 3.3. Mechanism of grafting reactions

In the conventional grafting system, two main side reactions always accompany the grafting reaction. The side reactions may produce polyGMA through reaction between GMA radicals with another GMA radical, **Scheme 3.3, Rn. 3.16** and crosslinked EPR, **Scheme 3.3, Rn. 3.7**. However, the amount of side reaction products formed depends on the concentration of GMA and peroxide used in the grafting process. In the GMA-DVB grafting system, the side reaction is quite complicated where it involves reaction of comonomer and monomer and also comonomer with EPR. The comonomer DVB is highly reactive toward EPR macroradical and GMA radical. In the presence of peroxide initiator, the DVB radical is formed through H abstraction, **Scheme 3.3, Rn. 3.5**. The formation of EPR-DVB radical is formed through reaction of DVB radical and EPR macroradical, **Scheme 3.3, Rn. 3.12**. The formation of polyDVB takes place through the reaction among DVB radicals, **Scheme 3.3, Rn. 3.8**. Since DVB is very reactive towards GMA, the DVB radical can easily react with GMA radical by trapping it. This causes the GMA radicals to be less available for coupling reactions to form polyGMA resulting in a decrease in the formation of polyGMA when DVB is present (in the GMA-DVB system).

### 3.3.4 Characterisation of the Synthesised Homo and co-Polymers

Synthesised polyGMA, polyDVB and the copolymer GMA-co-DVB were characterised by IR and  $^1\text{H}$  and  $^{13}\text{C}$  NMR spectroscopy. The GMA-homopolymer (polyGMA) which was synthesised by free radical polymerisation showed a broad IR ester carbonyl absorption peak at  $1730\text{ cm}^{-1}$  which was shifted to higher frequency compared to the corresponding conjugated carbonyl absorption in the monomer GMA, (at  $1721\text{ cm}^{-1}$ ) confirming the formation of saturated ester carbonyl group, see **Figure 3.1B**. Furthermore, the IR spectrum of polyGMA shows that the double bond absorption of GMA at  $1638\text{ cm}^{-1}$  has almost completely disappeared, see **Figure 3.1B** and, whereas the epoxide ring absorptions at  $843$  and  $909\text{ cm}^{-1}$ , (see **Figure 3.1C**) remain completely intact confirming that the polymerisation occurs through the double bond and that the epoxide ring does not get involved in the polymerisation process, this is in agreement with literature findings [9, 51].

It is clear from the  $^1\text{H}$  and  $^{13}\text{C}$  NMR spectra of polyGMA when compared to the NMR results of GMA, (see **Figures 3.3** and **3.5** versus **Figure 3.2** and **3.4**) that the epoxide

ring remains intact during the polymerisation. Also the unsaturated methylene protons of the double bond of GMA (H1 and H2) which appear at 5.5 ppm and 6.1 ppm have shifted upfield to the saturated protons region in polyGMA indicating the loss of the  $>C=C<$ , but they have shown a more complex pattern, see **Figure 3.3**. Similarly, the protons of the  $\alpha$ -CH<sub>3</sub> side group in polyGMA (H3, see **Figure 3.3**) and the corresponding carbon of the  $\alpha$ -CH<sub>3</sub> (see **Figure 3.5**, C3) gave complex spectral pattern which is due to different stereochemical sequences in the polymer chains. The resonance signals of the protons of the  $\alpha$ -CH<sub>3</sub> group (H3) of polyGMA are shown (see **Figure 3.3**) to split-up into three clear broad peaks (due to high molecular weight) at 1.22, 1.06 and 0.97 ppm. Similarly, the methylene protons (H1) signals, which originated from the double bond of GMA, are shown also to split up to three peaks appearing at 2.0, 1.95 and 1.87 ppm confirming that the methylene group is also sensitive to the stereochemical configuration in the sequence of triads. The different peaks for H1 and  $\alpha$ -CH<sub>3</sub> hydrogens indicate different type of GMA polymerization which will shed light on the characterisations of the microstructure of GMA grafting on EPR.

#### 3.3.4.1 Integration of <sup>1</sup>H-NMR for Poly-GMA to Determine the Nature and Distribution of the GMA Grafts

<sup>1</sup>H-NMR integration was employed to calculate and confirm the following:

- To calculate and confirm the stereochemical sequence based on 1-CH<sub>2</sub> and  $\alpha$ -CH<sub>3</sub> in the polymer.
- To calculate the graft composition, i.e. the length of the GMA sequence in EPR-g-GMA<sub>CONV</sub>.
- To work out the graft distribution i.e. the frequency of grafting of the GMA sequences on the EPR polymer chain.
- To work out the stereochemical configuration of the grafted GMA sequence in the EPR-g-GMA<sub>CONV</sub> polymer.

#### 3.3.4.2 Stereochemical Sequence Calculation Based on of 1-CH<sub>2</sub> and $\alpha$ -CH<sub>3</sub> in PolyGMA

For further confirmation of the results presented in the previous sections, calculation based on integration of the <sup>1</sup>H-NMR spectra for each of the 1-CH<sub>2</sub> and 3-CH<sub>3</sub> groups

having individual stereochemical sequences is performed here. To find out the extent of different sequences in the polyGMA polymer based on the 1-CH<sub>2</sub>, the integration of each sequence is divided by their total integration for 2 units (which is the number of protons in this methylene group) and multiplied by 100 to convert the value to a percentage:

For the CH<sub>2</sub> of the *rrr* sequence (see **Figure 3.6a**) at 1.87 ppm (**Figure 3.3**) it is integrated for 0.84 units which is  $(0.84 \times 100 / 2) = 42\%$  of the polymers sequences.

- The *mrr* peak at 1.95 ppm (**Figure 3.3**) is integrated for 0.47 units which is  $(0.47 \times 100 / 2) = 24\%$ .
- The *mrm* peak (**Figure 3.6c**) at 2.00 ppm (**Figure 3.3**) is integrated for 0.24 units which is  $(0.24 \times 100 / 2) = 12\%$ .
- The *mmr* peak (**Figure 3.6e**) at 1.49 ppm (**Figure 3.3**) is an integration of one of the CH<sub>2</sub> H's III, to calculate the percentage (there is no need here to multiply by 2), hence the integration is 0.13 unit and the formula used is  $(0.13 \times 100) = 13\%$ .
- The *rmr* peak (**Figure 3.6d**) at 1.45 ppm (**Figure 3.3**) is an integration of one of the CH<sub>2</sub> H's III, therefore the calculation is done as for *rmr*, hence the integration is 0.09 unit and the formula used is  $(0.09 \times 100) = 9\%$ .

The results show therefore that the *rrr* sequence is the dominant structure, see **Table 3.10**. To calculate the extent of different sequences in the poly-GMA based on the polymer  $\alpha$ -CH<sub>3</sub> (no 3) group, the integration of each sequence is divided by their total integration which is 3 units (the number of protons in this CH<sub>3</sub> group) and multiplied by 100 to convert to percentages:

- For the CH<sub>3</sub> of the *rr* sequence (see **Figure 3.6a** and **b**) at 0.91 ppm in **Figure 3.3**, it is integrated for 1.85 units which is  $(1.85 \times 100 / 3) = 62\%$  of the polymers sequences.
- The *mr* peak at 1.06 ppm in **Figure 3.3** is integrated for 1.05 units which is  $(1.05 \times 100 / 3) = 35\%$ .
- The *mm* peak at 1.26 ppm in **Figure 3.3** is integrated for the rest of the percentages which is 3%.

**Table 3.10.** Calculation of the % of different stereochemical sequences of poly-GMA

Stereochemical Configuration			
Type	Calculation based on CH <sub>2</sub> (1) (%)	Type	Calculation based on α-CH <sub>3</sub> (%)
rrr	42	rr	62
mrr	24	mr	35
mrm	12	mm	3
mmr	13		
rrr	9		

In the poly-GMA, presented in Figure 3.7, the *rr* of the α-CH<sub>3</sub> corresponds to Figure 3.7A and B, which is composed of all of the *rrr* configurations (Figure 3.7A) and half of the *mrr* configurations (Figure 3.7A). This suggests that the percentage of *rr* which is 62% should be equal to the percentage of *rrr* which is 42% and half of the *mrr* which is ½\* 24% which is 54%. The rest of the sequences are calculated as follow

$$rr \equiv rrr + \frac{1}{2} mrr$$

$$rm/mr \equiv \frac{1}{2} mrr + mrm + rmr + \frac{1}{2} mmr$$

$$mm \equiv \frac{1}{2} mmr + mmm$$

**Table 3.11.** Stereochemical Sequence Calculation Based on of 1-CH<sub>2</sub> and α-CH<sub>3</sub> in PolyGMA

CH <sub>3</sub>	CH <sub>2</sub>
<i>rr</i> 62%	<i>rrr</i> + ½ <i>mrr</i> 42 + 12 = 54%
<i>rm/mr</i> 35%	½ <i>mrr</i> + <i>mrm</i> + <i>rmr</i> + ½ <i>mmr</i> 12 + 12 + 13 + 4 = 41%
<i>mm</i> 3%	½ <i>mmr</i> 4%

The similarity in the sequence calculation based on 1-CH<sub>2</sub> and α-CH<sub>3</sub> further confirms the accuracy of the proposed stereochemical configurations of the synthesised poly-GMA.

### 3.3.5 Characterisation of the Microstructure of the GMA Grafted in *f*-EPR<sub>CONV</sub>

A purified EPR-g-GMA<sub>CONV</sub> sample was chosen for NMR investigation of its microstructure (sample G24). The sample contained 1.9 wt% g-GMA with all the free and polyGMA being removed during the purification step. The microstructure of the *f*-EPR<sub>CONV</sub> sample was compared with that of polyGMA and calculation of the different stereochemical sequences was done as described earlier for polyGMA.

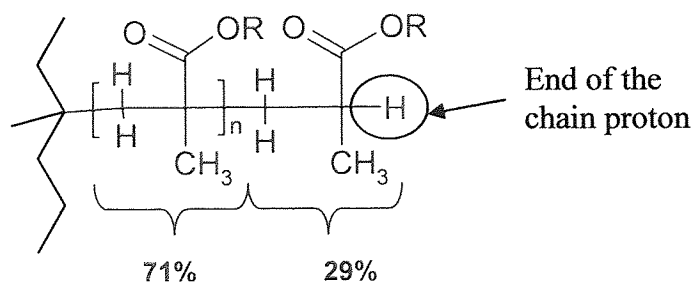
The <sup>1</sup>H-NMR of the purified EPR-g-GMA<sub>CONV</sub> sample measured in CDCl<sub>3</sub> at room temperature (Figure 3.22) shows that the signals of the three protons of the (α-CH<sub>3</sub>) which should appear at about 1 ppm is overlapped by the EPR signals in this region, thus, all calculations of the stereochemical sequences were based on the protons of the methylene group (CH<sub>2</sub>, labelled number 1 in the structure show in Figure 3.22) with signals that appear resolved in the 2 ppm region (EPR signals do not overlap in this region). Similar to the characterisation made earlier for the same CH<sub>2</sub> in polyGMA the signals of this CH<sub>2</sub> in EPR-g-GMA<sub>CONV</sub> polymer show three peaks assigned for the stereochemical sequences rrr, mrr and mrm (see Figure 3.22 and Figure 3.38). A comparison of the -CH<sub>2</sub> signals in the <sup>1</sup>H-NMR spectra of polyGMA (Figure 3.3) and EPR-g-GMA<sub>CONV</sub> (Figure 3.22) shows that the grafted polymer have less sequence isomers with only rrr, mrr/rm and mrm structure appearing in its <sup>1</sup>H-NMR spectrum.

Table 3.12 compares the calculated percents of each of the stereochemical structures that appear in the EPR-g-GMA<sub>CONV</sub> with those in the homopolymerised polyGMA. It is clear that in the case of the grafted polymer, while rrr sequence shows the same amount (42%) that of the rrr sequence in polyGMA (see calculation in Table 3.12), the amount of the mrr/rm sequences are higher at 56 % of the total compared to only 24 % in polyGMA (see also Figure 3.22). The remaining stereochemical sequences which are less apparent in the polymer spectrum counts for only 2 % of the total.

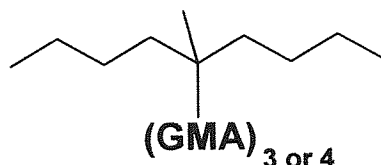
**Table 3.12.** Calculated % of different stereochemical sequences of poly-GMA and EPR-g-GMA<sub>CONV</sub>

Stereochemical Sequences	Calculation based on CH <sub>2</sub> (no.1) in poly-GMA (%)	Calculation based on CH <sub>2</sub> (no.1) in EPR-g-GMA <sub>CONV</sub> (%)
rrr	42	42
mrr/rrm	24	56
Others	34	2
<b>Based on Fig 3.22</b>	e.g. Calculation based on CH <sub>2</sub> for EPR-g-GMA <sub>CONV</sub>	
<b>rrr</b>	the <sup>1</sup> H peak of CH <sub>2</sub> group which appears at 1.9 ppm is integrated for 0.85 units, thus: $\frac{0.85}{2} \times 100 = 42 \%$	
<b>mrr/rrm</b>	the <sup>1</sup> H peaks are integrated for 1.12 units, thus: $\frac{1.12}{2} \times 100 = 56 \%$	

In order to investigate the graft composition (i.e. the number of the GMA units in a typical graft in the EPR-g-GMA<sub>CONV</sub>), a further examination of **Figure 3.22** shows the appearance of a new peak at 2.2 ppm which has been assigned to the H on a carbon at the end of the GMA branch (labelled H2) and this has been integrated for 0.29 units, thus 29 % of the GMA molecules in the graft have this end of chain proton (this is because the unit of integration accounts for one proton only hence it is directly converted to percentage) and the remaining 71 % constitute the chain itself, see **Scheme 3.4**.

**Scheme 3.4** Graft Composition in EPR-g-GMA<sub>CONV</sub>

A simple mathematical calculation (see Eqn 3.5) shows therefore that the length of the grafted GMA sequence is either a 3 or 4 GMA molecules long, the percentages of the three and four sequences is about the same i.e 48% of three GMA molecules in the chain and 52% of four GMA molecules in a chain, see Scheme 3.5.



Scheme 3.5 Length of the grafted GMA sequence in EPR-g-GMA<sub>CONV</sub>

This was calculated as follows:

Eqn: 3.5

For a chain of 3 molecules it is represented as X and for a chain made of 4 molecules it is represented as Y, then

$$X + Y = 100 \quad \text{from the total percentage of different types}$$

$$\frac{1}{3} X + \frac{1}{4} Y = 29 \quad \text{from the end of the chain}$$

$$Y = 4(29 - \frac{1}{3}X)$$

$$Y = 116 - \frac{4}{3}X$$

$$\text{Then } X + (116 - \frac{4}{3}X) = 100 \Rightarrow X = 48 \text{ and } Y = 52$$

To examine the graft distribution, i.e. the frequency of grafting of the GMA sequence in the EPR-g-GMA<sub>CONV</sub>, the <sup>1</sup>H NMR spectrum in Figure 3.22 was used to calculate the ratio of the number of GMA grafts in a given number of carbons on the main EPR polymer chain. Each of the grafted GMA functions, the epoxide side and the acrylate side has 5 protons with the <sup>1</sup>H-NMR peaks of the epoxide side (protons 5, 6 and 7) being completely resolved at 4.3, 3.8, 3.2, 2.8 and 2.6 ppm, see Figure 3.22. Each peak was integrated for one proton and the integration for each was about one unit. Therefore, the average of their integral is accounted for as the integral of each proton in the GMA-g-EPR<sub>CONV</sub> system and is used to calculate the ratio of the GMA graft sequence to the EPR polymer chain as shown in the example calculation below:



**Example 1**, see NMR spectrum in **Figure 3.22**:

Integral per proton = the average GMA integral for the epoxide end =

$$\frac{\text{Sum of proton integral of epoxide side of GMA}}{\text{Number of protons in this side of GMA}} \quad \text{Eqn-3.6}$$

$$= \frac{1.01 + 1.03 + 1.0 + 0.98 + 1.07}{5} = 1.02 \text{ area unit / proton in GMA molecule}$$

In the EPR (ethylene: propylene, 8:2) polymer a one E:P sequence of 8:2 contains 44 protons ( $-\text{[CH}_2\text{-CH}_2\text{]}_8\text{-}$  and  $-\text{[CH}_2\text{-CH(CH}_3\text{)]}_2\text{-}$ ,  $= 4 \times 8 + 6 \times 2 = 44$  protons). The  $^1\text{H-NMR}$  peaks for the EPR have chemical shifts in the region 1.7 to 0.5 ppm with an integration of 418 units, see **Figure 3.22**. The proton signal for the  $\alpha\text{-CH}_3$  of the GMA overlaps with the main NMR signals of EPR therefore it had to be subtracted, hence the following formula was applied to calculate the number of 8:2-EPR sequences for every 1 GMA molecule (i.e the frequency of grafting in the polymer chain).

Number of EPR units/ GMA = **Eqn-3.7**

$$\frac{[\text{Integral of the EPR peaks at (1.7 to 0.5ppm)}] - [\text{integral of three H's of } \alpha\text{-CH}_3 \text{ of GMA}]}{[\text{No of EPR protons}] \times [\text{integral per proton value}]}$$

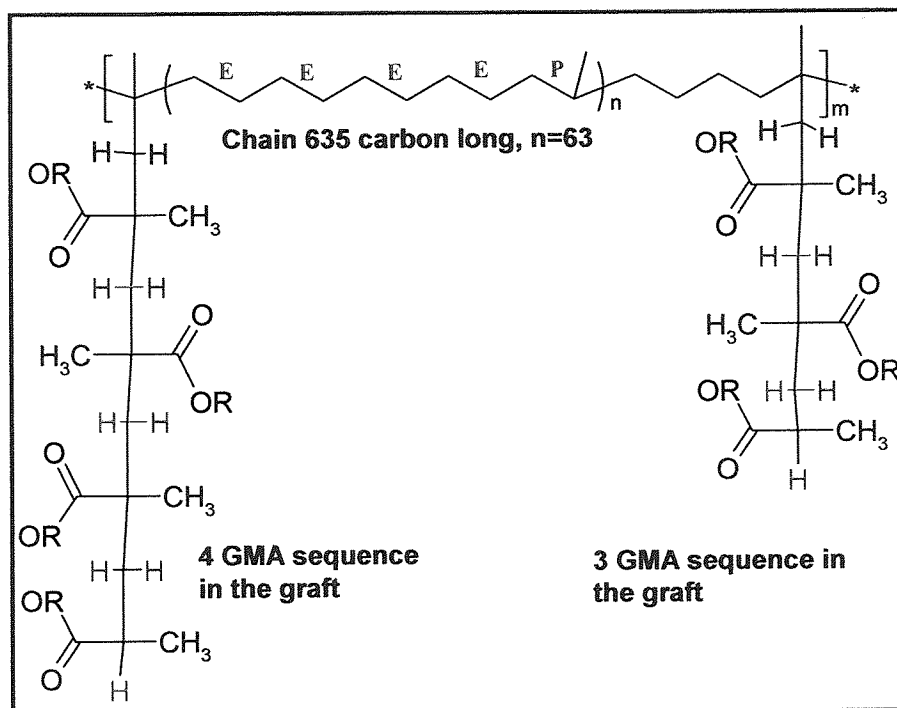
$$\text{Example 1: } \frac{[ \begin{array}{c} 418 \\ [ \quad ] \end{array} ] - [ \begin{array}{c} 3 \times 1.02 \\ [ \quad ] \end{array} ]}{[ \begin{array}{c} 44 \\ [ \quad ] \end{array} ] \times [ \begin{array}{c} 1.02 \\ [ \quad ] \end{array} ]} = \frac{[ \begin{array}{c} 415 \\ [ \quad ] \end{array} ]}{[ \begin{array}{c} 45 \\ [ \quad ] \end{array} ]}$$

$$= 9.2 \text{ (EPR units of 8:2 per 1 GMA molecule)}$$

The 8:2 EPR unit has a straight chain of 20 carbon atoms; therefore the results in example 1 show that there is 1 GMA grafted molecule per  $20 \times 9.2 = 184$  carbon atom of the chain, (or there is 5 to 6 GMA grafted molecules for a straight chain of 1000 carbon atoms).

The results therefore show that the grafted GMA is a sequence of three or four molecules, (based on the 0.29 ppm proton at end of chain of the GMA units used in the calculation shown earlier), and the frequency of the grafting is one in every 635 carbons of the polymer chain ( $184/0.29 = 635$ ), which means there is a graft composed of four

GMA molecules followed by another graft of three GMA molecules after 635 carbons on the EPR straight chain as illustrated in Scheme 3.6.



**Scheme 3.6.** The structure of the grafted GMA on the EPR-g-GMA<sub>CONV</sub> (sample G24 in Table 3.1a) (GMA=15%, T101=0.8 phr, temp=190°C, g-GMA=1.9 %, polyGMA=3%, the sample was purified to remove polyGMA before NMR analysis.

In summary in EPR-g-GMA<sub>CONV</sub> each graft has 3 or 4 GMA molecules (i.e 1 GMA in a polymer chain of ~184 carbons) with similar percentages of the 3 or 4 sequences. The distribution or frequency of the GMA grafts is one graft in every 635 carbons in the straight EPR chain (not counting the CH<sub>3</sub> groups in the propylene unit of the polymer structure which corresponds only to 1 GMA-graft per 32 EPR units of 8:2 (E:P).

### 3.3.6 Characterisation of Purified EPR-g-GMA<sub>DVB</sub> by NMR

A purified sample of EPR-g-GMA<sub>DVB</sub> (sample DG14 in Table 3.1b) containing 4.7 wt% g-GMA (GMA/DVB= 9/1) was chosen for the purpose of characterisation of its microstructure because of its high level of grafted GMA. It is worth noting here that the DVB-containing *f*-EPR<sub>DVB</sub> samples were generally more highly branched than the *f*-EPR<sub>CONV</sub> as reflected from their MFI values.

The  $^1\text{H}$  NMR spectrum of the  $\text{EPR-g-GMA}_{\text{DVB}}$  was recorded at different temperatures in four different solvents: deuterated chloroform- $\text{d}_1$  ( $\text{CDCl}_3$ ), deuterated dichlorobenzene- $\text{d}_4$  ( $\text{C}_6\text{D}_4\text{Cl}_2$ ), deuterated dimethyl sulfoxide- $\text{d}_6$  ( $\text{DMSO-d}_6$ ) and deuterated tetrachloroethane ( $\text{C}_2\text{D}_2\text{Cl}_4$ ). Higher temperatures solvents were chosen in order to increase the solubility of polymer. It was found that  $^1\text{H}$ -NMR spectrum of  $\text{EPR-g-GMA}_{\text{DVB}}$  in  $\text{CDCl}_3$  at room temperature (**Figure 3.39**) was more complicated than that of the  $\text{EPR-g-GMA}_{\text{CONV}}$  (see **Figure 3.22**) due to the presence of DVB. However the main epoxide peaks (H 5, 6 and 7) of the GMA in the  $\text{EPR-g-GMA}_{\text{DVB}}$  sample appeared (**Figure 3.39**) at chemical shifts similar to the corresponding ones in  $\text{EPR-g-GMA}_{\text{CONV}}$  (**Figure 3.22**). However, the peaks for the grafted DVB (aromatic peaks) are not expected to be seen in this spectrum, as its CH and  $\text{CH}_2$  proton signals would appear at 1.8 and 1.3 ppm [213], which is a region overlapped by the major EPR peaks. Moreover, the aromatic peaks of substituted polystyrene appear above 7 ppm a region also masked by peaks of the  $\text{CDCl}_3$  solvent. Similar findings were reported in the case of polystyrene which contain similar aromatic protons [213-217]. A different NMR solvent was therefore used to resolve the peaks of the aromatic ring of the grafted DVB.  $^1\text{H}$ -NMR spectrum of  $\text{EPR-g-GMA}_{\text{DVB}}$  sample was recorded therefore in deuterated dimethyl sulfoxide ( $\text{DMSO-d}_6$ ) which shows a broad peaks around 7.2 ppm which confirm the fact that in  $\text{CDCl}_3$  the DVB aromatic peaks are overlapped by the chlorinated solvent, see **Figure 3.40**.

However, the solubility of the polymer in dimethyl sulfoxide was very low and therefore deuterated tetrachloroethane ( $\text{C}_2\text{D}_2\text{Cl}_4$ ) was chosen as a possible NMR solvent in which the polymer may be more soluble at higher temperatures. The  $^1\text{H}$ -NMR spectrum of  $\text{EPR-g-GMA}_{\text{DVB}}$  in  $\text{C}_2\text{D}_2\text{Cl}_4$  at  $135^\circ\text{C}$  revealed the aromatic proton peaks of DVB in the 7 ppm region but they appeared to be much broader than when the run was carried out at ambient temperature of  $\sim 22^\circ\text{C}$ , see **Figures 3.41** and **3.42**. An even more important finding in this high temperature run (**Figure 3.42**) is that the epoxide group peaks for H5 and H6 became less resolved (closer to each other). This latter complication in the NMR spectra of the DVB-containing polymer would make it difficult to investigate the microstructure of the  $\text{EPR-g-GMA}_{\text{DVB}}$ .

To overcome this complexity therefore, the three unresolved peaks of the epoxide [2 x (H5) + 1 x H6] were integrated as one unit and used to account for the GMA in the polymer structure, while the methyl (CH<sub>3</sub>) group i.e. the propylene units in the EPR structure, was used to account for the EPR part of the grafted polymer. Since each of these units account for 3 H's, then dividing the integral of the methyl (CH<sub>3</sub>) group by the integral of the three epoxide peaks would give directly the number of the propylene units in the polymer per GMA molecule. In order to confirm the accuracy of this method, it was used to re-calculate the number of polymer carbons in a straight chain (not counting the CH<sub>3</sub> group in the propylene unit of EPR) available for every one GMA molecule in the conventional EPR-g-GMA<sub>CONV</sub> polymer sample (**G24**) which gave a much better resolved NMR spectra, (see Sec. 3.3.5). In sample **G24**, the integral of CH<sub>3</sub> was 57 units, dividing this by 3 (the integral of the 3 epoxide H's) gives 19 this means that there is 1 GMA molecule for every 19 propylene units of the EPR. The EPR has an 8:2 E:P units, thus there is one propylene molecule for every 10 carbons in the straight chain of the polymer, which means that there is 1 GMA molecule for every 190 (19x10) carbons in the EPR straight chain. This result is remarkably similar to the result calculated earlier by Eqns 3.6 and 3.7 for the same polymer which gave a 1 GMA molecule for every 184 carbon in the straight chain. This calculation method was therefore used for EPR-g-GMA<sub>DVB</sub> to calculate the ratio of GMA molecules to EPR carbons (samples **DG14**).

Based on the above calculation, the integration of the GMA (epoxide 1H peaks) to the EPR of the DVB-containing **DG14** sample when run in CDCl<sub>3</sub> at ambient temperature, **Figure 3.39**, it showed a very low percentage of the GMA molecules compared to the EPR polymer (1 GMA molecule for every 400 propylene molecule or 1 GMA molecule for 4000 carbons in straight chain of EPR), see **Table 3.13**. This very low frequency of appearance of GMA molecules in the polymer chain is almost certainly a direct consequence of the low solubility of this polymer in CDCl<sub>3</sub> at ambient temperature (NMR spectra was recorded for the solvent-soluble part of the sample only). Increasing the temperature to 57°C in the same solvent (**Figure 3.43**). gave rise to an increased frequency of GMA appearance resulting in 1 GMA molecule for every 191 propylene molecules, or 1 GMA molecule for 1910 carbons in a straight chain of EPR, see **Table 3.13**, which is due to a higher solubility of the polymer at higher temperature, but it was

clear that the polymer was still far from being completely soluble under these conditions. Dissolving the polymer in a higher temperature solvent such as deuterated dichlorobenzene  $C_6D_4Cl_2$  and running the spectra at  $57^\circ C$  (Figure 3.44) and at  $135^\circ C$  (Figure 3.45) gave 1 GMA molecule in 700 and in 390 carbons of the EPR straight chain, respectively (Table 3.13). It is clear from these results that the polymer becomes more soluble at higher temperatures, thus one can see higher frequency of the GMA appearance in the polymer. However, it was clear again that the polymer was not completely soluble even at  $135^\circ C$  in these solvents. Another problem with the NMR spectra recorded in these solvents is the fact that the DVB aromatic protons could not be seen since it was overlapped by solvent peaks, hence the 'real' DVB-GMA structure of the grafts could not be investigated in these solvents.

As a last attempt for finding out the DVB-GMA graft structure in the EPR-g-GMA<sub>DVB</sub> polymer, one final solvent, deuterated tetrachloroethane, was tried since the aromatic proton region at 7.00 ppm is clear in this solvent, the polymer spectra were then recorded both at ambient temperature and at  $135^\circ C$  (Figure 3.41 and 3.42). Calculation of the number of GMA and DVB molecules in EPR has shown that at  $135^\circ C$  there is 1 GMA molecule for every 480 carbons in the polymer straight chain which is less than the number in the solvent d-dichlorobenzene where the NMR spectrum was recorded at the same temperature (this gave 1 GMA molecule for every 390 carbons of EPR). This suggest that the polymer is less soluble in tetrachloroethane than in dichlorobenzene. However, the former solvent was the only one out of all those examined here in which signals of both the DVB and GMA can be detected and thus it would give an idea of the microstructure of the (EPR-g-GMA<sub>DVB</sub>) polymer in the presence of the comonomer DVB.

In the solvent  $C_2D_2Cl_4$ , the aromatic H's peaks for DVB (appearing at around 7.2 ppm) were used to account for the frequency of appearance of DVB in the EPR-g-GMA<sub>DVB</sub> sample. The results show a very low percentage of DVB to the GMA, with the results from the room temperature run giving 1 DVB for every 10 GMA molecules and that recorded at  $135^\circ C$  giving 1 DVB for every 14 GMA molecules in a run of 10,000 carbons of the straight polymer chain, Table 3.13. However, these calculation results

must be treated with caution as the polymer was still not fully soluble in this solvent even at 135 °C.

**Table 3.13.** The frequency of GMA molecule appearance in EPR straight carbon chain in purified EPR-g-GMA<sub>DVB</sub> sample **DG14** calculated from its <sup>1</sup>H-NMR spectra in different deuterated solvents recorded at different temperatures

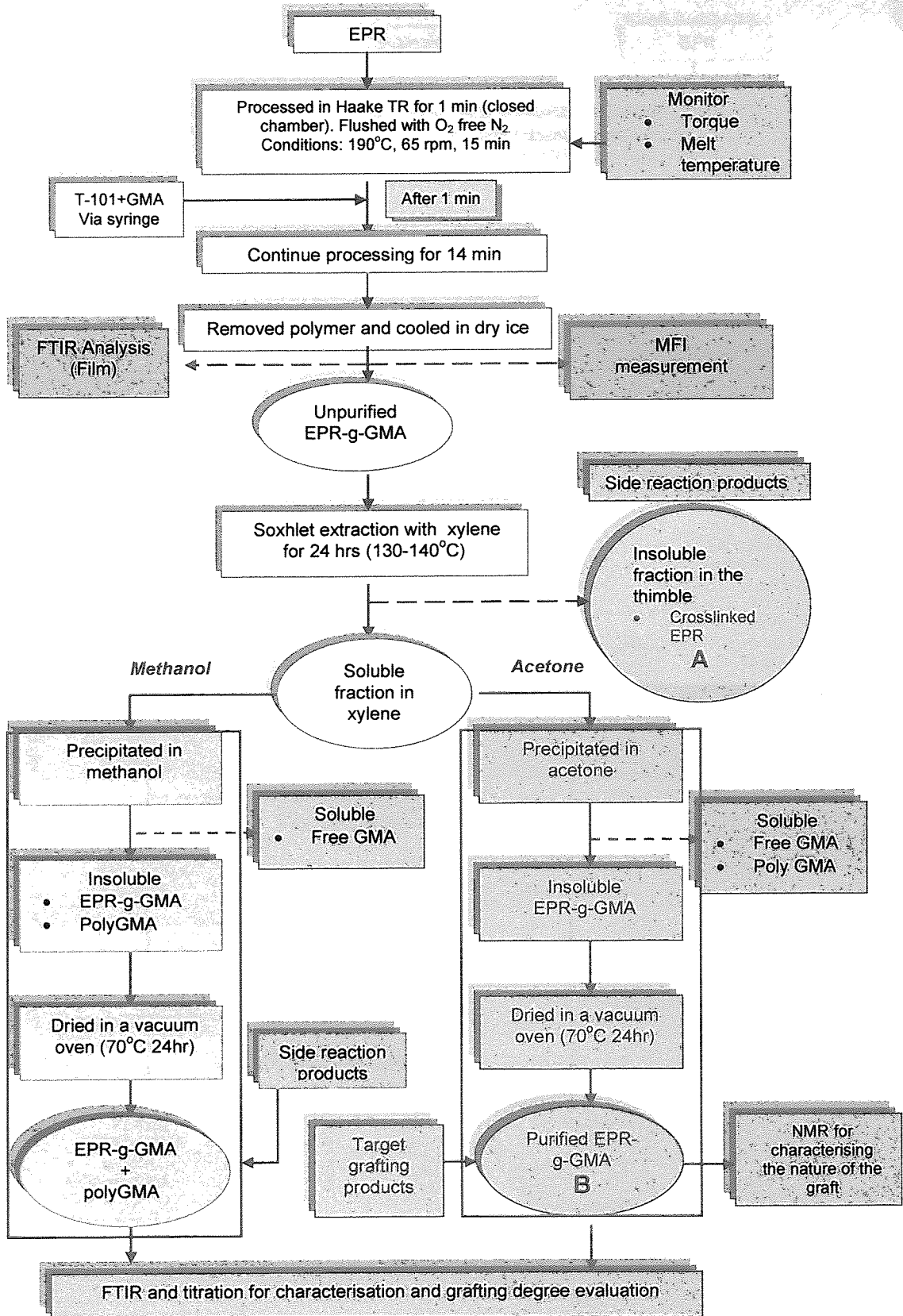
<i>f</i> -EPR	Sample code	Figure No.	Solvent	NMR Run Temperature °C	1 GMA in Number of Carbon (X) in EPR chain	Number of GMA (Y) molecules in 10,000 carbon chain
					X	Y
EPR-g-GMA <sub>CONV</sub>	G24	Fig. 3.22	CDCl <sub>3</sub>	RT	190	53
EPR-g-GMA <sub>DVB</sub>	DG14	Fig. 3.39	CDCl <sub>3</sub>	RT	4000	2.5
EPR-g-GMA <sub>DVB</sub>	DG14	Fig. 3.43	CDCl <sub>3</sub>	57	1910	5
EPR-g-GMA <sub>DVB</sub>	DG14	Fig. 3.44	C <sub>6</sub> D <sub>4</sub> Cl <sub>4</sub>	57	700	14
EPR-g-GMA <sub>DVB</sub>	DG14	Fig. 3.45	C <sub>6</sub> D <sub>4</sub> Cl <sub>4</sub>	135	390	26
						GMA/DVB in 10,000 Cs/EPR
EPR-g-GMA <sub>DVB</sub>	DG14	Fig. 3.41	C <sub>2</sub> D <sub>4</sub> Cl <sub>4</sub>	RT	710	14:1.4, or 10:1
EPR-g-GMA <sub>DVB</sub>	DG14	Fig. 3.42	C <sub>2</sub> D <sub>4</sub> Cl <sub>4</sub>	135	480	21:1.5, or 14:1

Based on the above discussion, it is possible to suggest that the microstructure of this *f*-EPR<sub>DVB</sub> would possibly contain long rather than short graft lengths composed of 1 DVB molecule and 14 GMA molecules. However, due to the complexity of the <sup>1</sup>H-NMR spectra of this polymer and the solubility problems associated with the use of the solvents mentioned above (for the purpose of NMR), the above suggestion has to be treated with caution and certainly further work would be required to confirm this or otherwise.

One interesting observation however, has to be made here, and that is the results from this work on the use of *f*-EPR based on EPR-g-GMA<sub>DVB</sub> containing high concentration of GMA (e.g 3.5 wt%) in polymer blends of PET/EPR-g-GMA<sub>DVB</sub> have shown a deterioration of the blends mechanical properties (e.g. elongation at break) giving rise to poor morphology when compared to similar *f*-EPR<sub>DVB</sub> containing lower levels of GMA, see Chapter 4, Sec. 4.2.3, Figure 4.16. Although the specific EPR-g-EPR<sub>DVB</sub> polymer

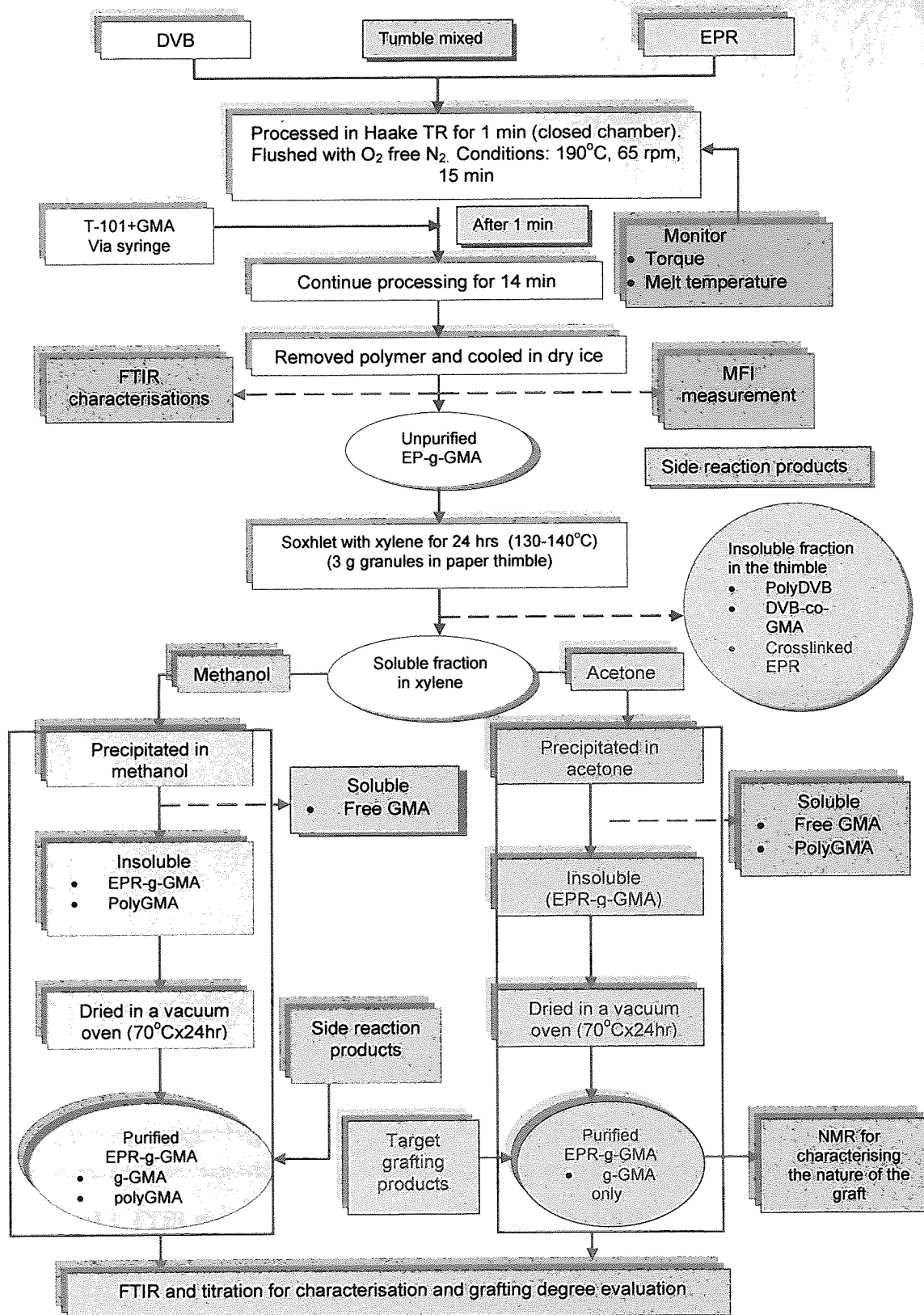
sample (containing 4.7 wt % g-GMA) used for the NMR analysis above itself was unfortunately not used in the polymer blending work, the argument that a similar sample containing high g-GMA content (3.5 wt%) gave inferior characteristics could be used to substantiate the above suggestion that these high g-GMA functionalised polymers in the presence of DVB could have long graft lengths. Copolymers containing long graft lengths are known not to offer good overall properties.

Scheme 3.1: Methodology for Grafting GMA onto EPR in the absence of DVB





Scheme 3.2: Methodology for Grafting GMA onto EPR in the presence of DVB



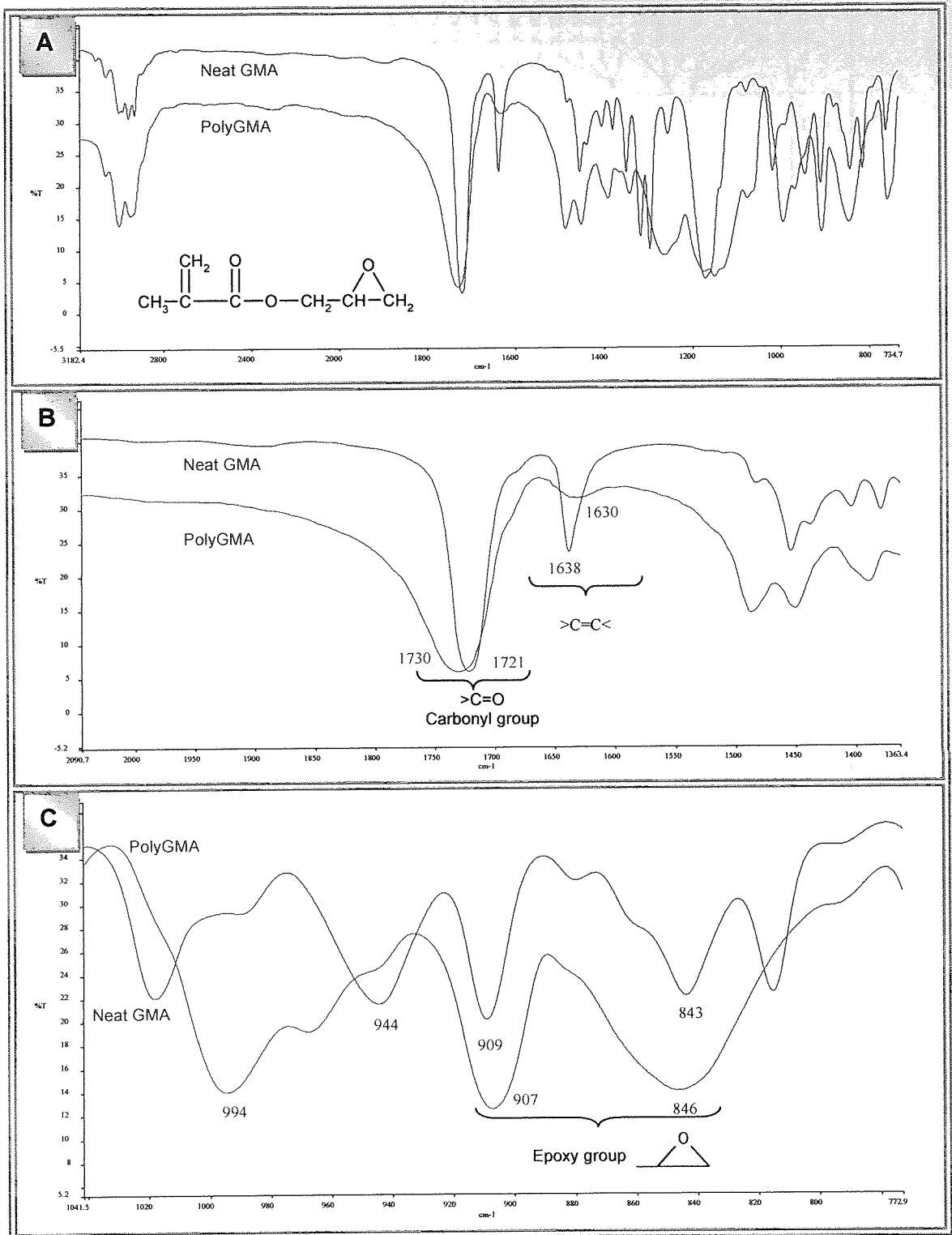


**Figure 3.1.** FTIR spectra of synthesised polyGMA (red) in KBr disc and neat GMA (blue) between KBr windows.

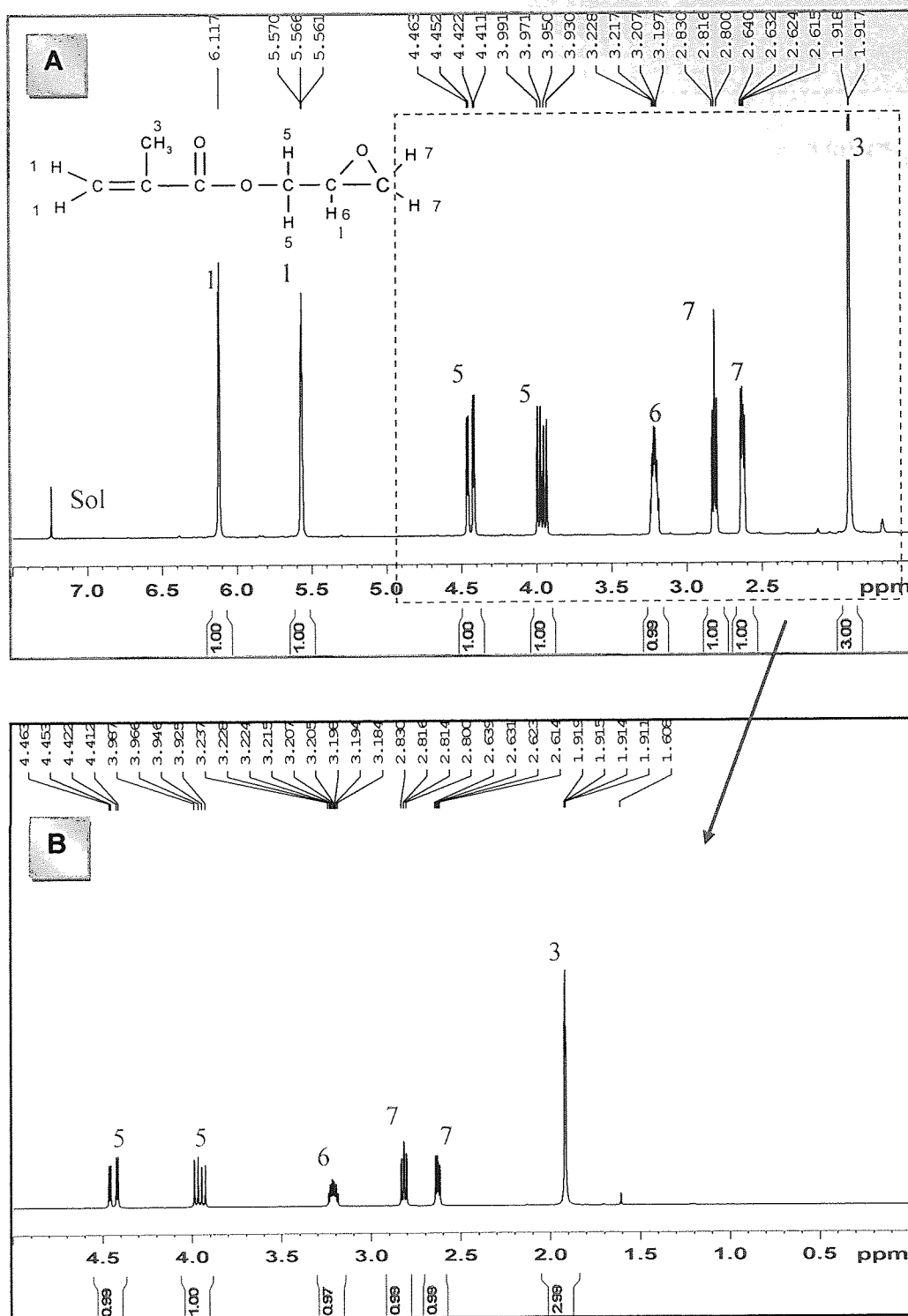


Figure 3.2:  $^1\text{H}$  NMR Spectra of GMA in  $\text{CDCl}_3$  at room temperature.

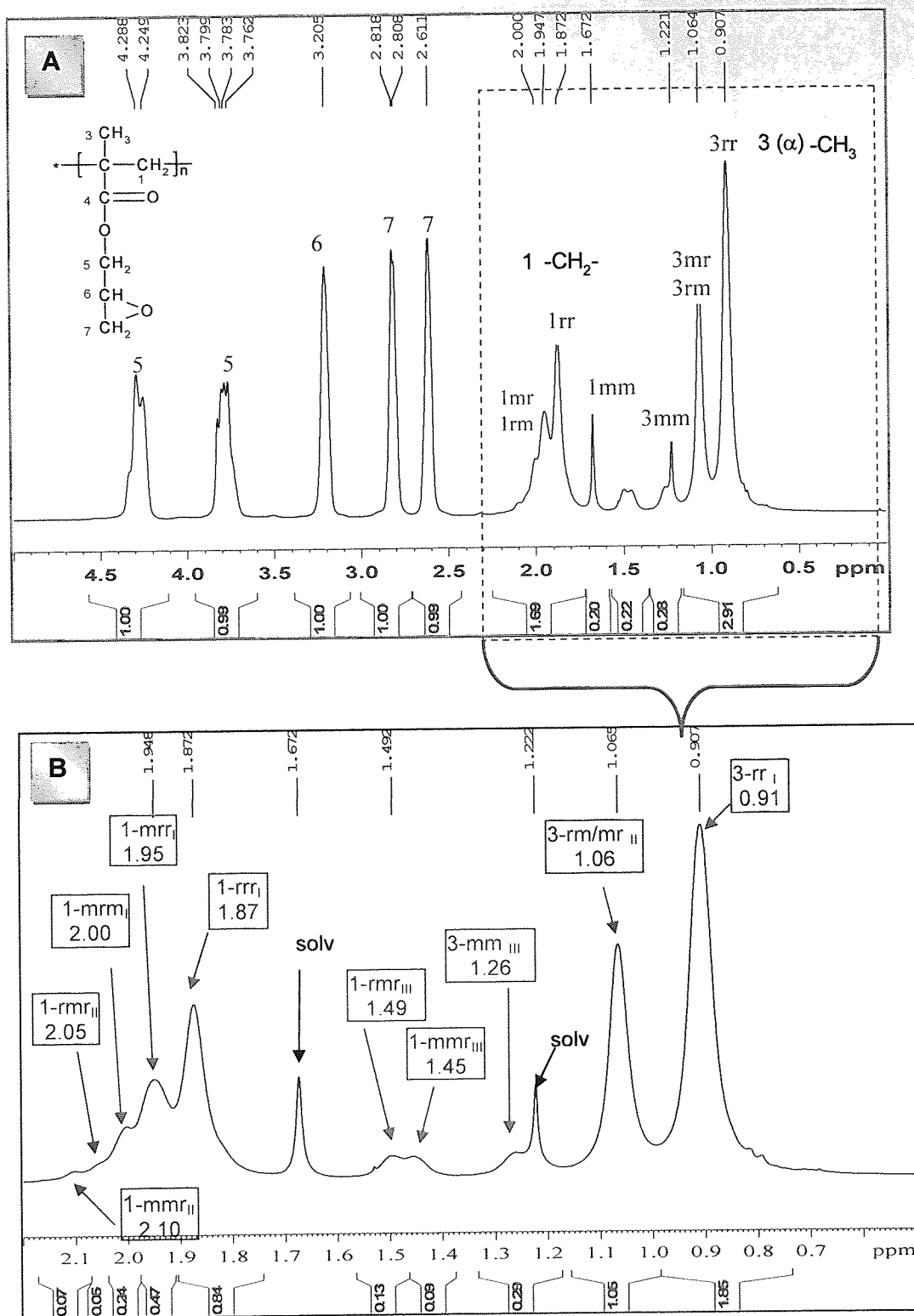


Figure 3.3:  $^1\text{H-NMR}$  spectrum of poly-GMA in  $\text{CDCl}_3$  (A) at room temperature, expansion of the  $\text{CH}_2$  and  $\alpha\text{-CH}_3$ , regions is shown in B,.

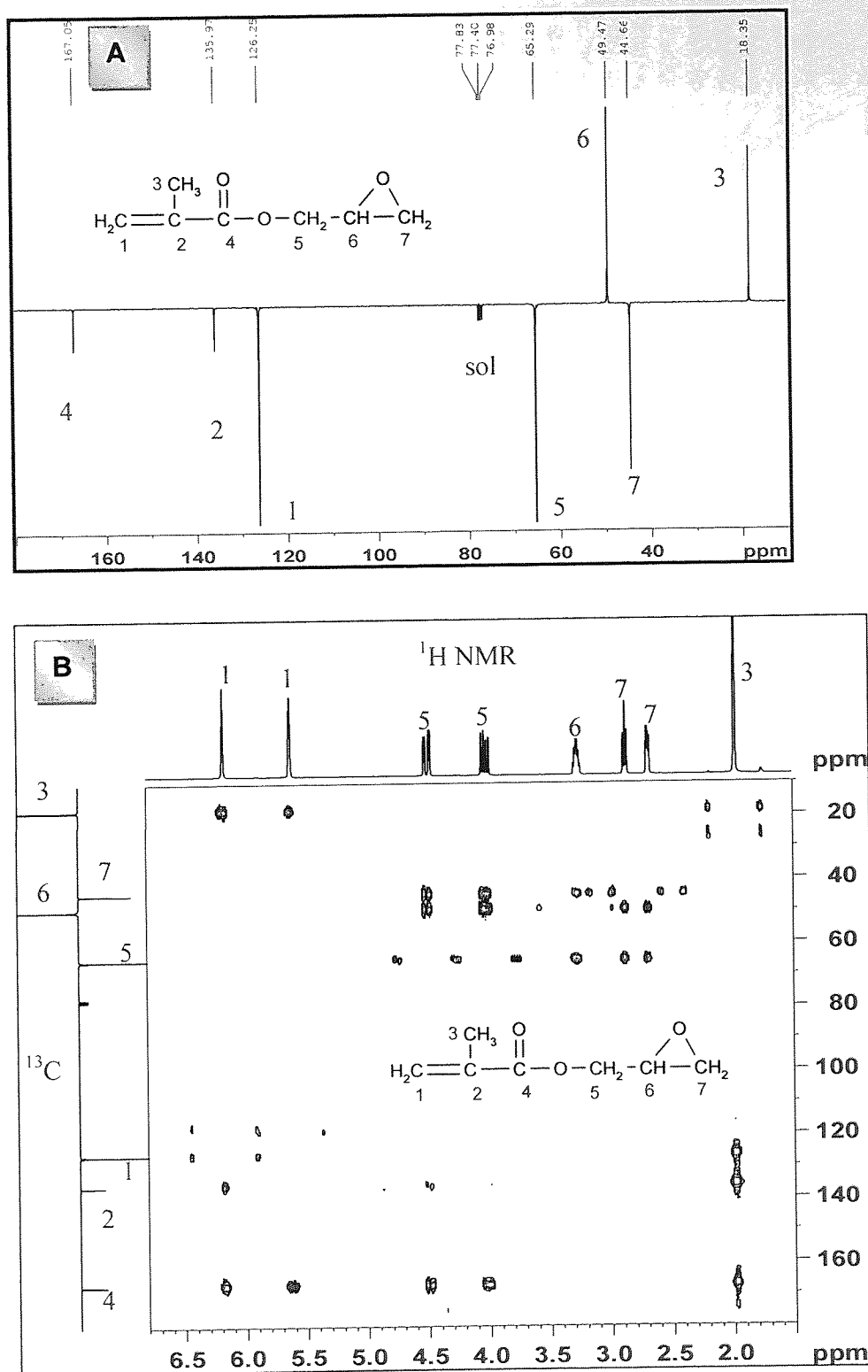


Figure 3.4:  $^{13}\text{C}$  NMR Spectra of GMA in  $\text{CDCl}_3$  (A),  $^{13}\text{C}$  HMBC NMR of GMA in  $\text{CDCl}_3$  (B), all measurements were done at room temperature.

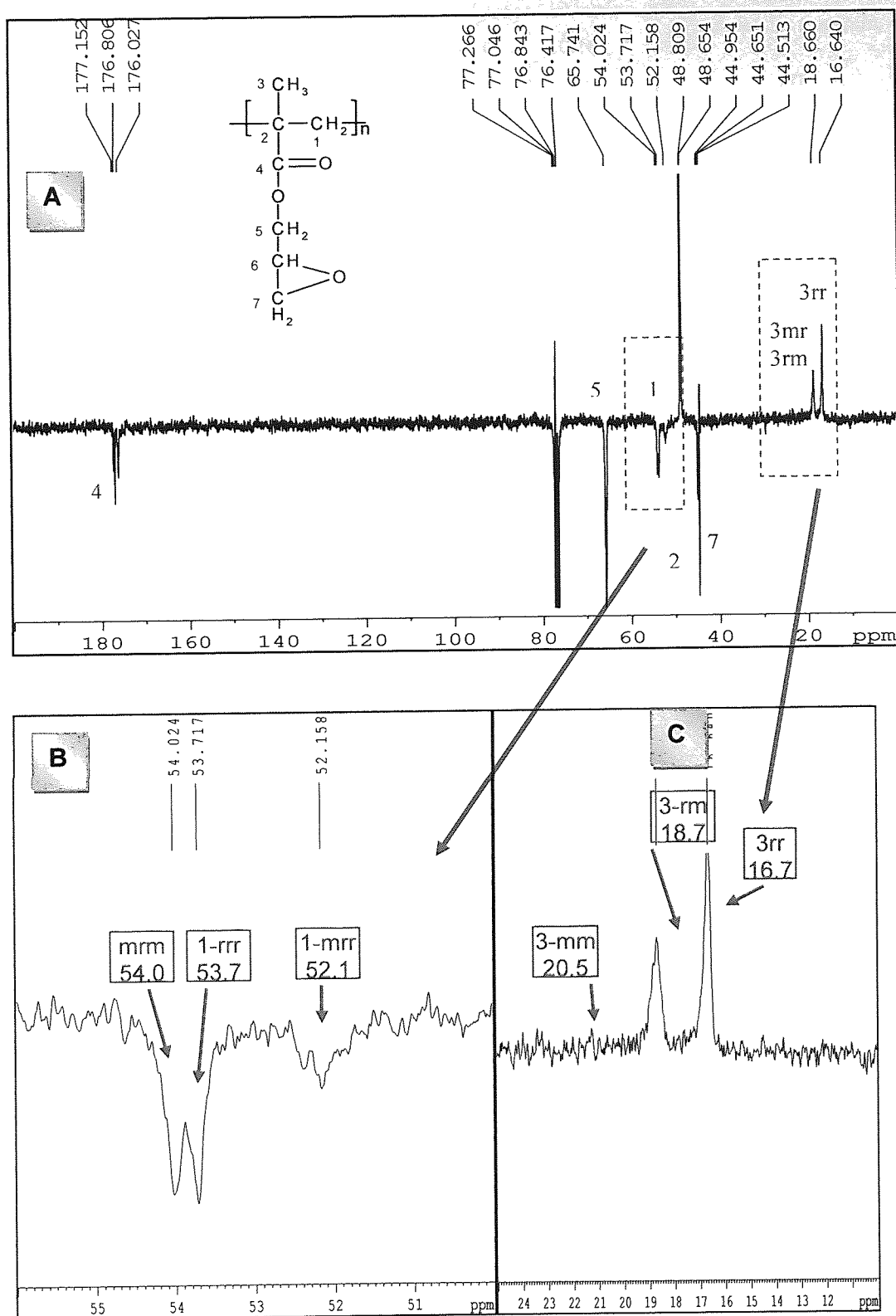


Figure 3.5. <sup>13</sup>C NMR spectrum of p-GMA in CDCl<sub>3</sub> (A), expansion of the CH<sub>2</sub> and α-CH<sub>3</sub> regions are shown in B and C. All measurements were done at room temperature.

a		<p>Syndiotactic (racemic, r)</p> <p>rrr</p>
b		<p>Atactic</p> <p>mrr</p>
c		<p>Atactic</p> <p>mrm</p>
d		<p>Atactic</p> <p>rmr</p>
e		<p>Atactic</p> <p>mmr</p>
f		<p>Isotactic (meso, m)</p> <p>mmm</p>

Figure 3.6: Stereochemical configuration of poly-GMA units (with respect to CH<sub>2</sub>) along the methacrylate polymer chain.

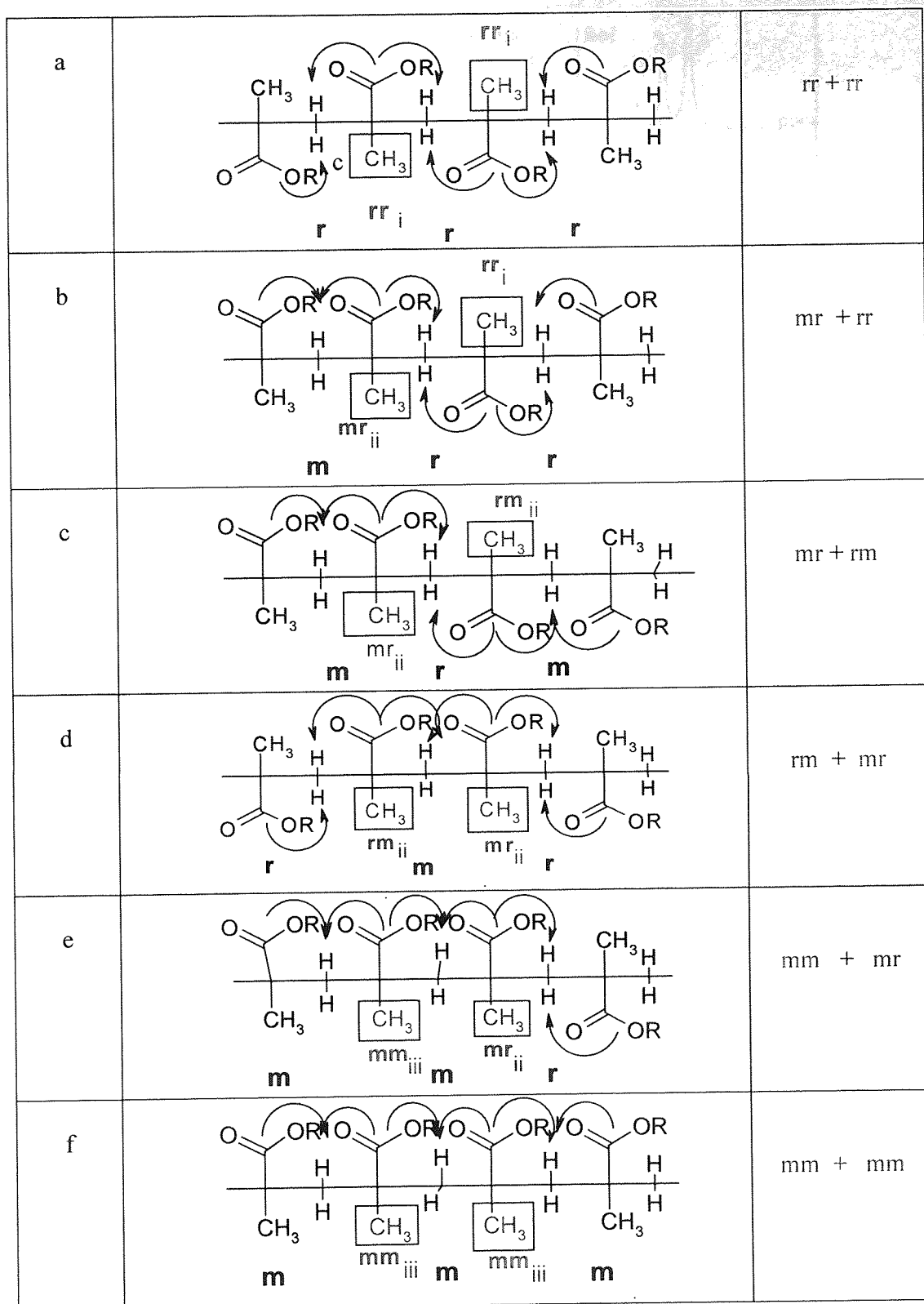
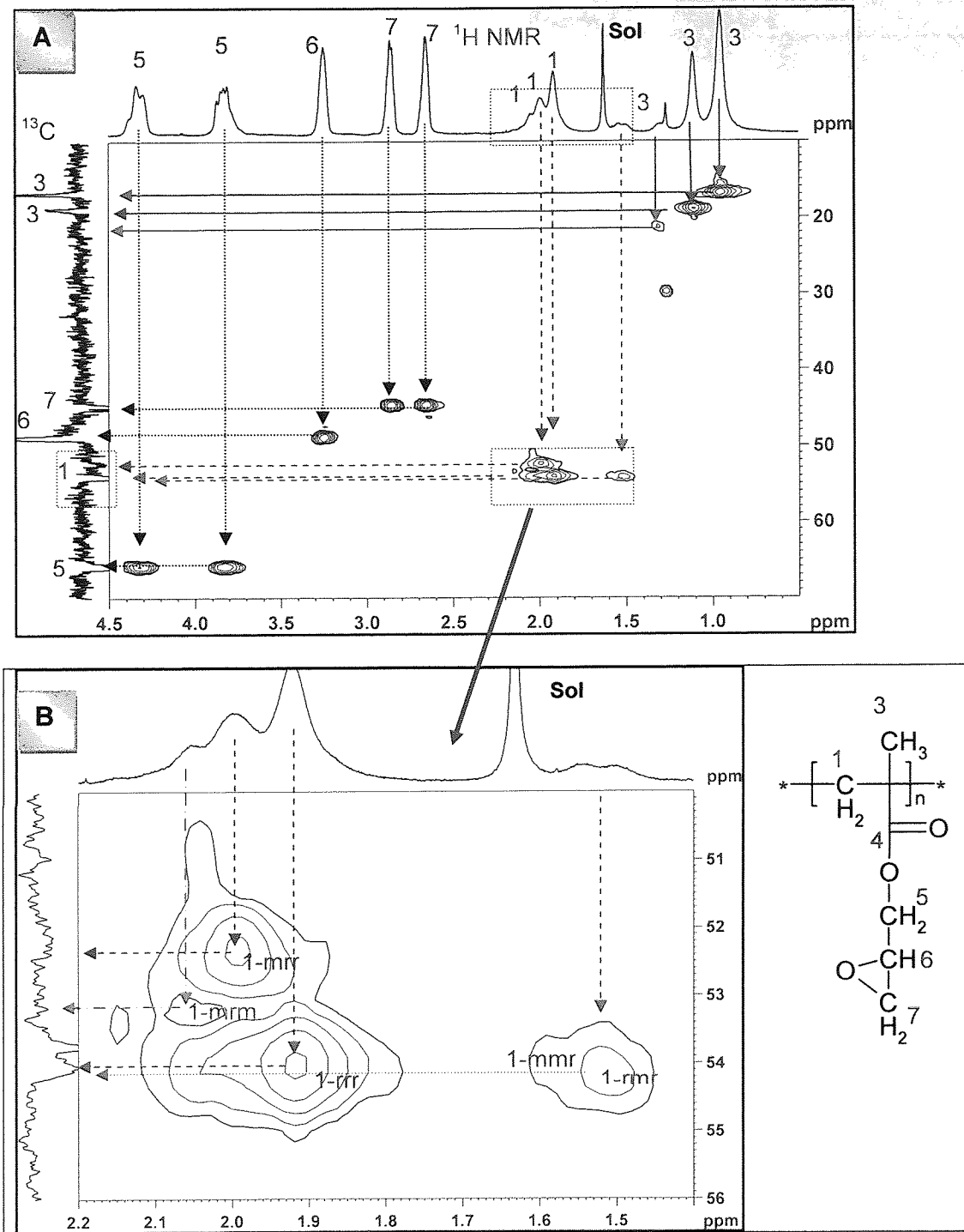
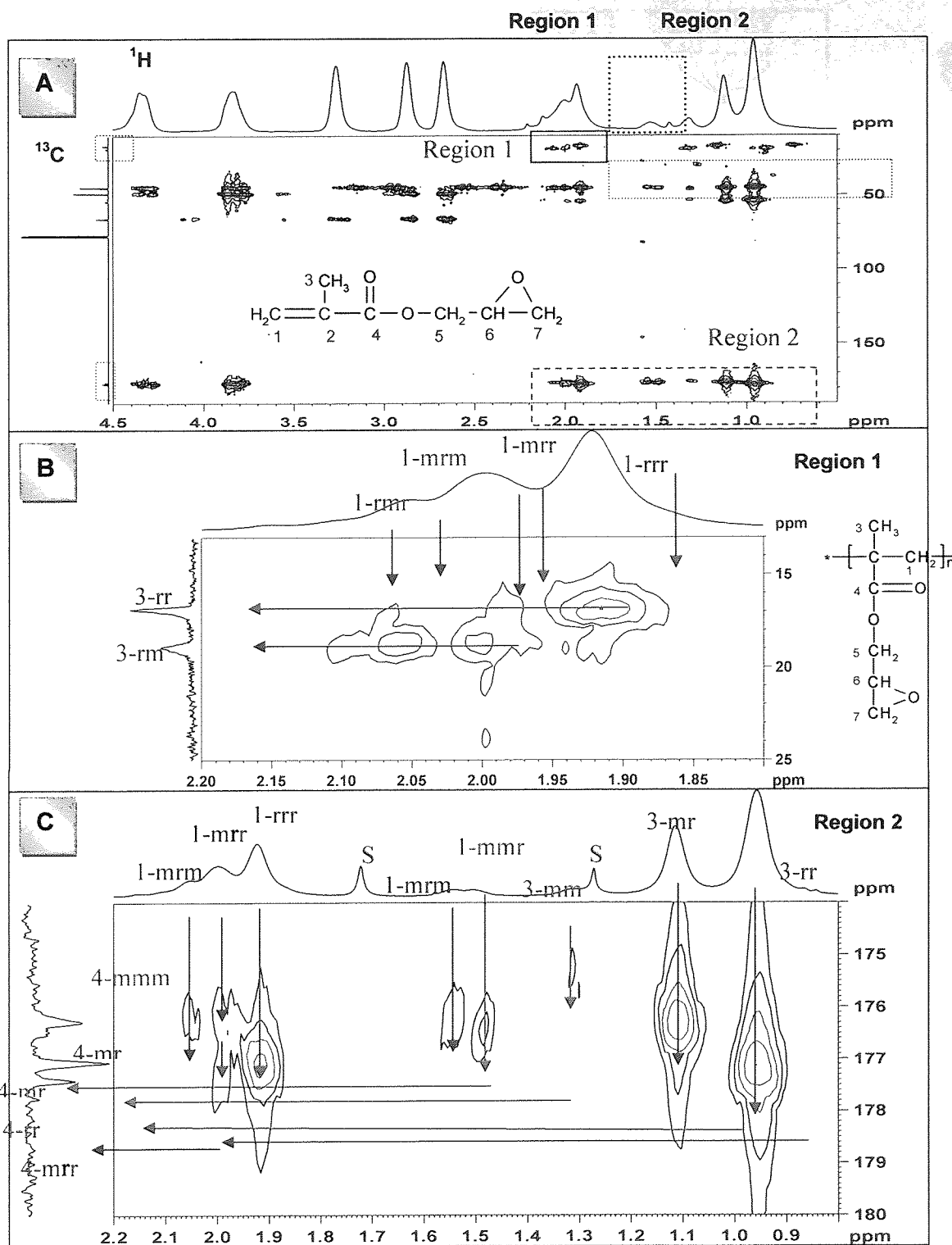


Figure 3.7 Stereochemical configuration of polymerised GMA with respect to  $\alpha$ -CH<sub>3</sub>





**Figure 3.8.** HSQC 2D-NMR spectra of poly-GMA in  $\text{CDCl}_3$  (A); expansion of the 1- $\text{CH}_2$  region is also shown in (B), all measurements were done at room temperature.



**Figure 3.9.** HMBC of poly-GMA in CDCl<sub>3</sub> (A); expansion of region 1 for 1-CH<sub>2</sub> and α-CH<sub>3</sub> is shown in B and expansion of region 2 to include the C=O carbon is shown in C. (S is solvent), all measurements were done at room temperature.

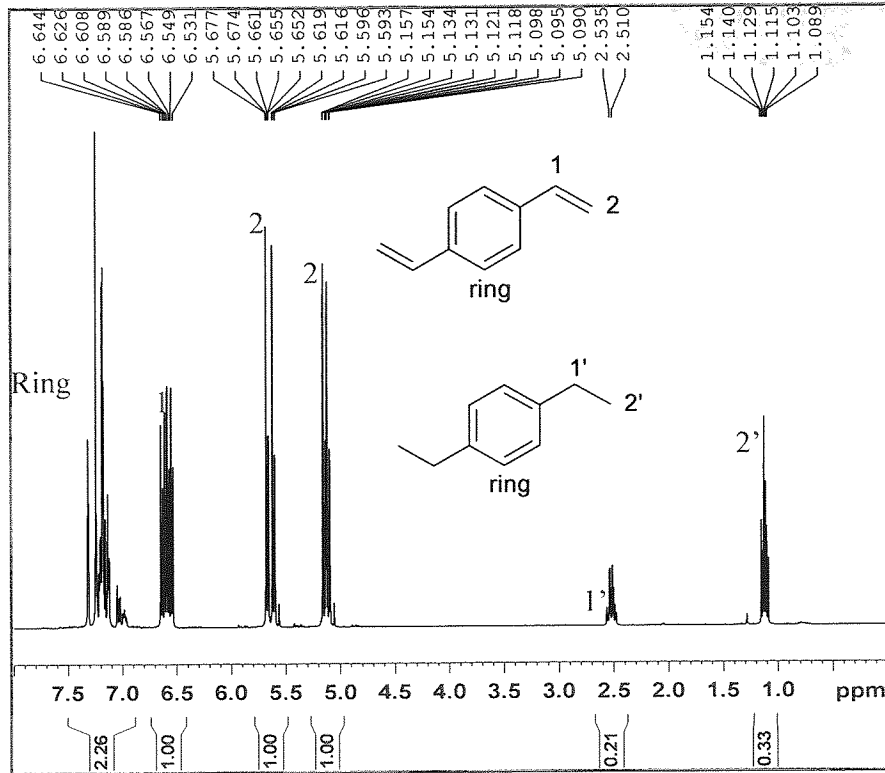


Figure 3.10  $^1\text{H}$  NMR Spectra of DVB in  $\text{CDCl}_3$  at room temperature

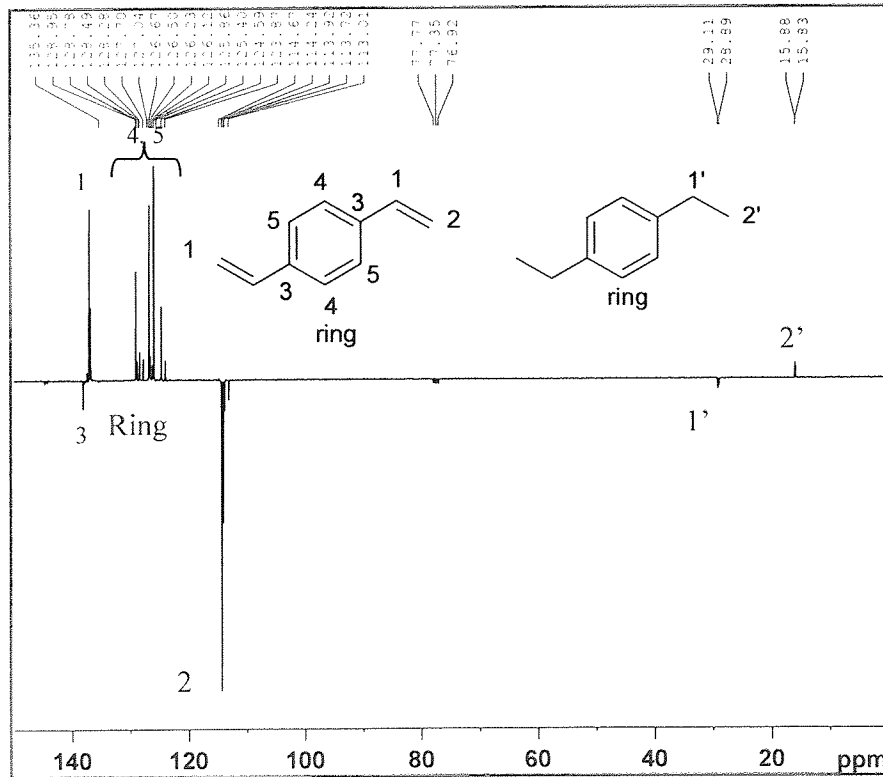
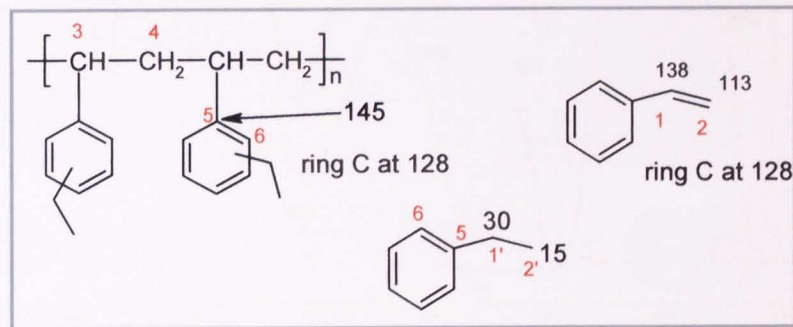
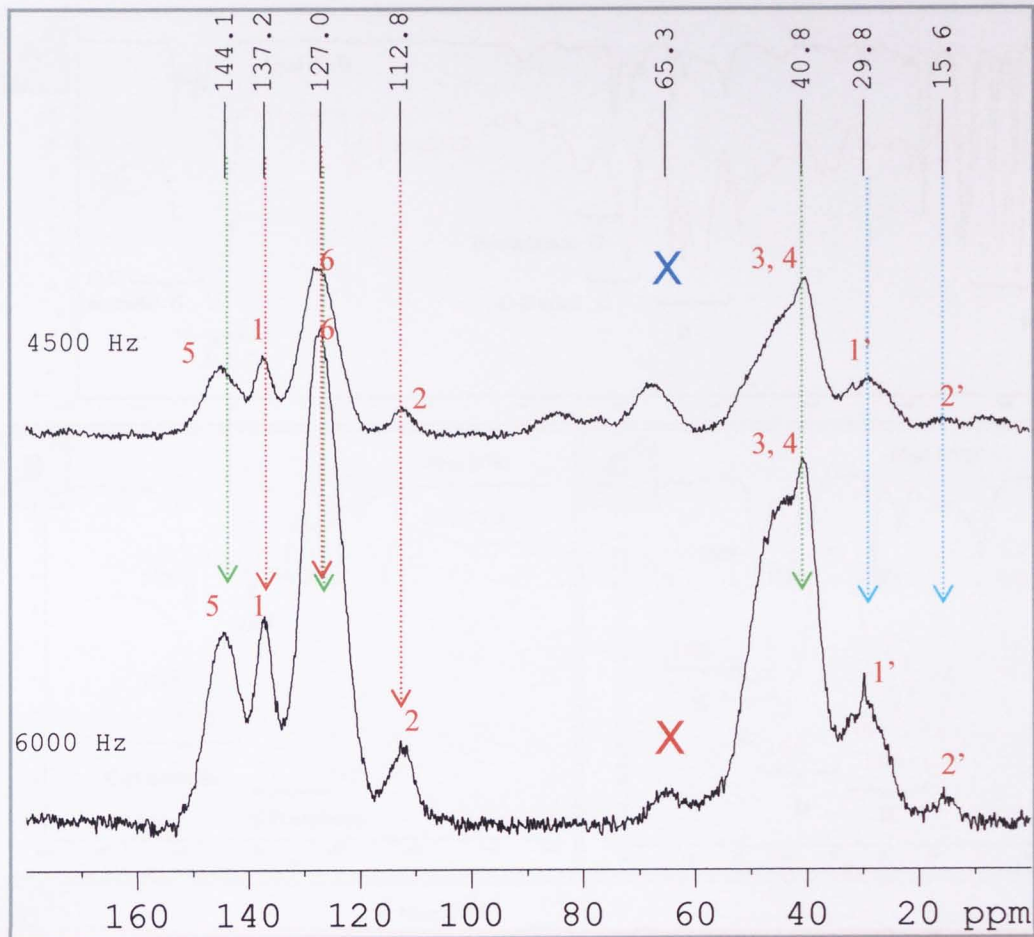


Figure 3.11:  $^{13}\text{C}$  NMR Spectra of DVB in  $\text{CDCl}_3$  at room temperature.



**Figure 3.12.** Solid state  $^{13}\text{C}$  NMR spectra of polyDVB in solid state. The peaks for polyDVB marked with the green lines, free DVB marked with red lines and the saturated ethyl group on styrene marked with blue lines.

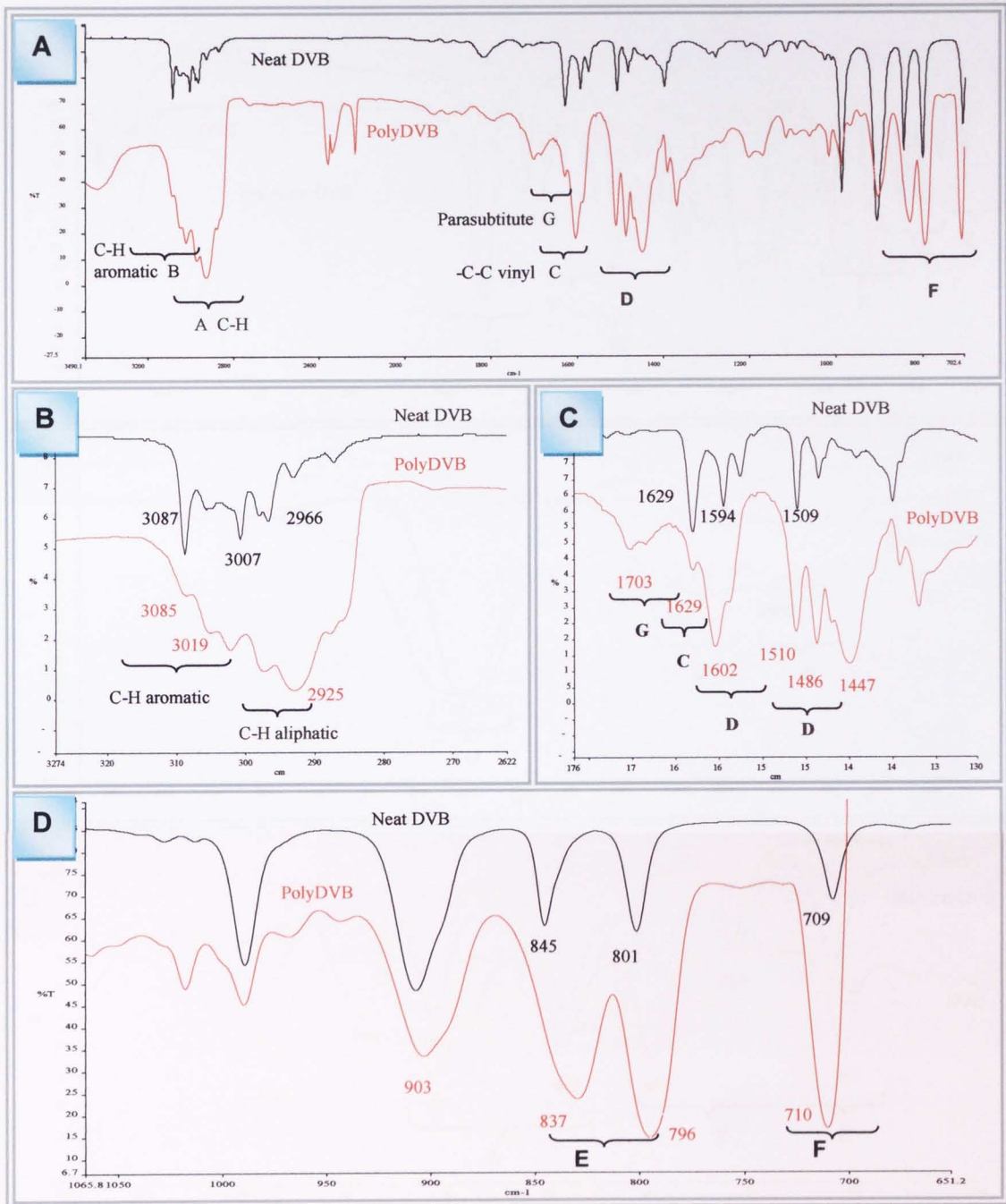


Figure 3.13. FTIR spectra of neat DVB (black) and polyDVB (red) in KBr discs and between KBr windows respectively.

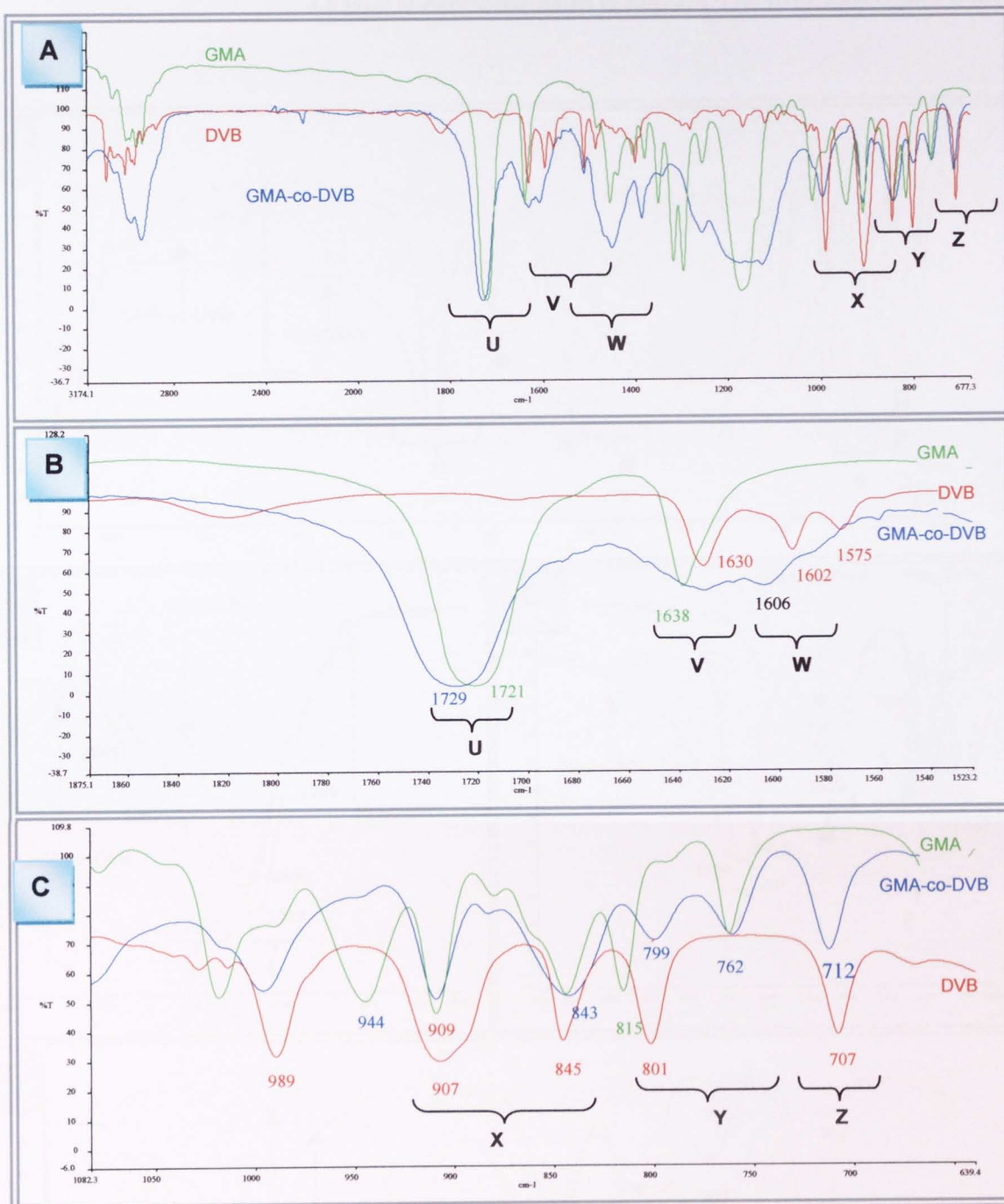


Figure 3.14. FTIR spectra of neat GMA (green), neat DVB in KBr windows (blue) and GMA-co-DVB in KBr disc (red), see Table 3.6.

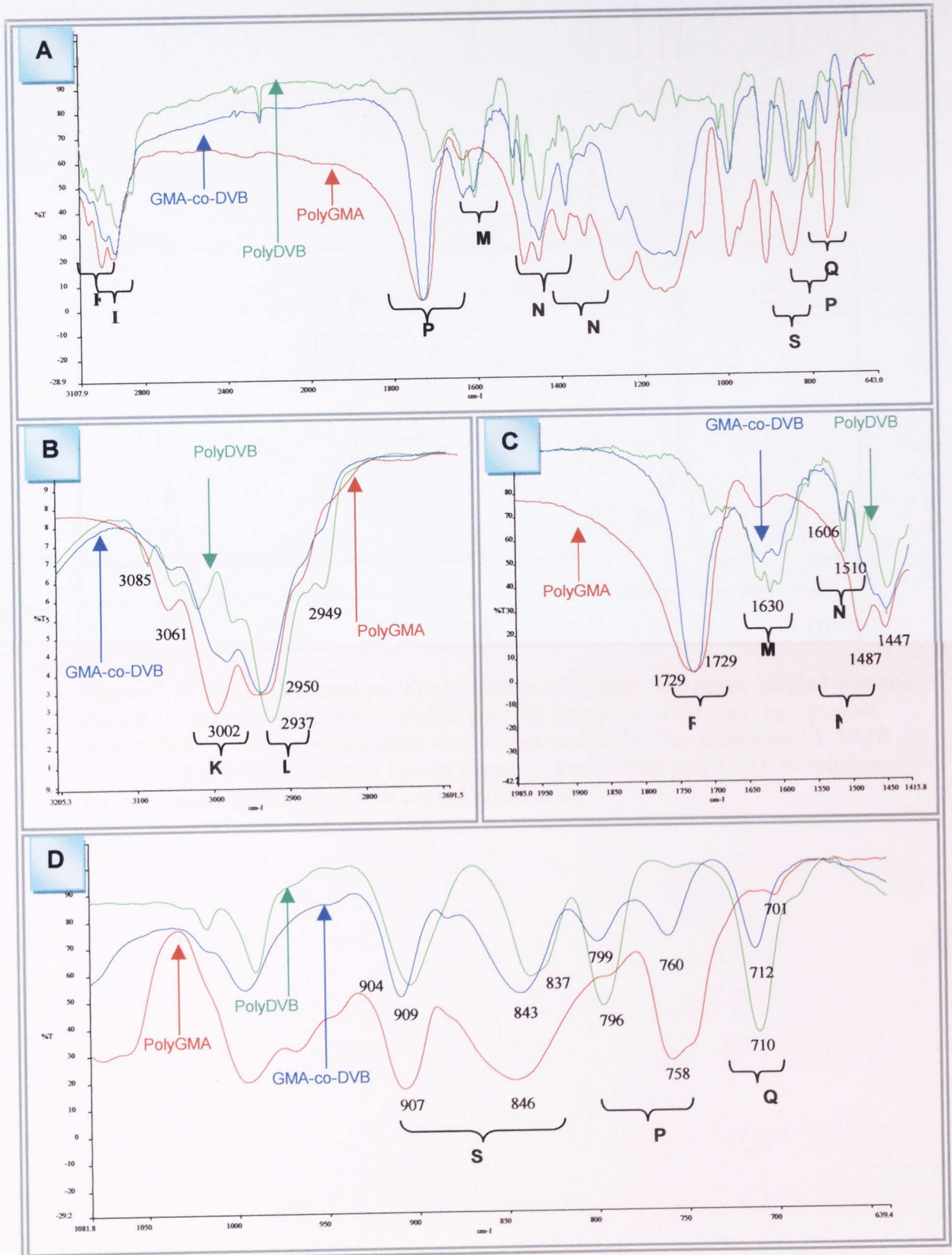
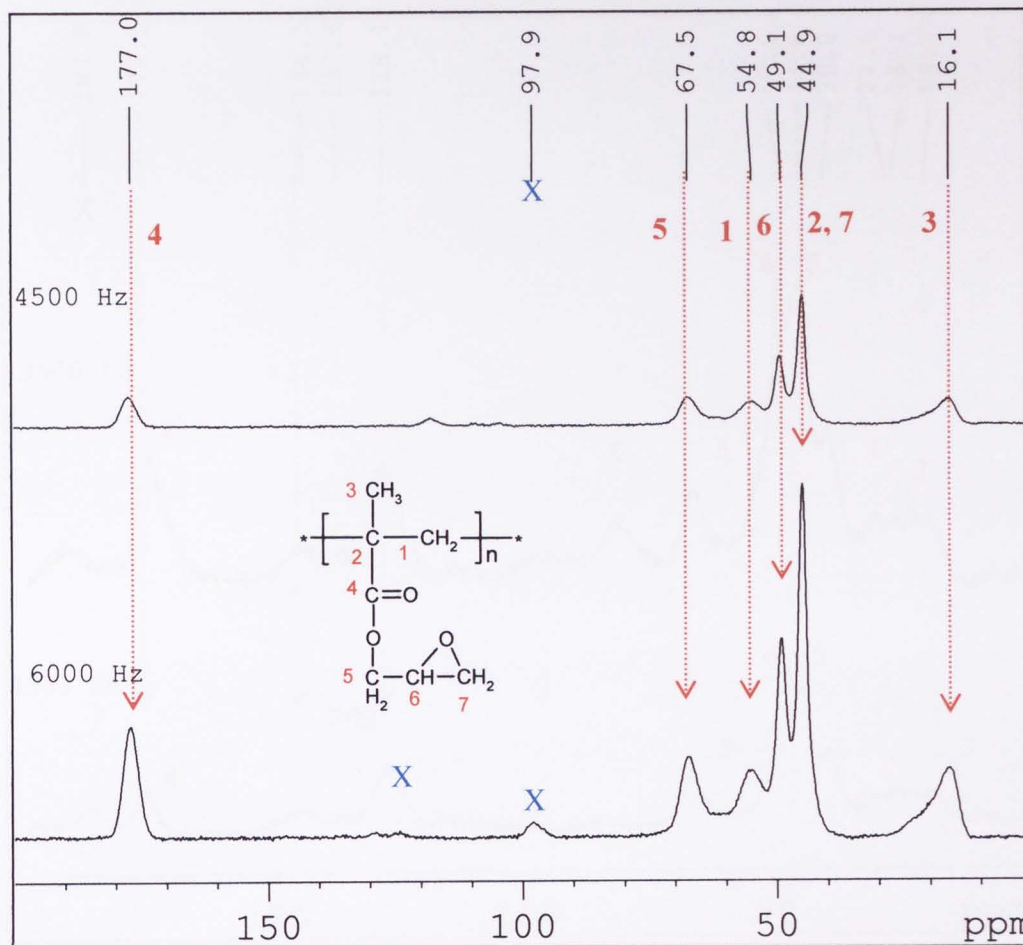
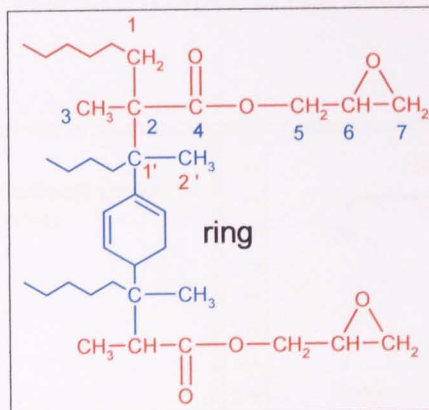
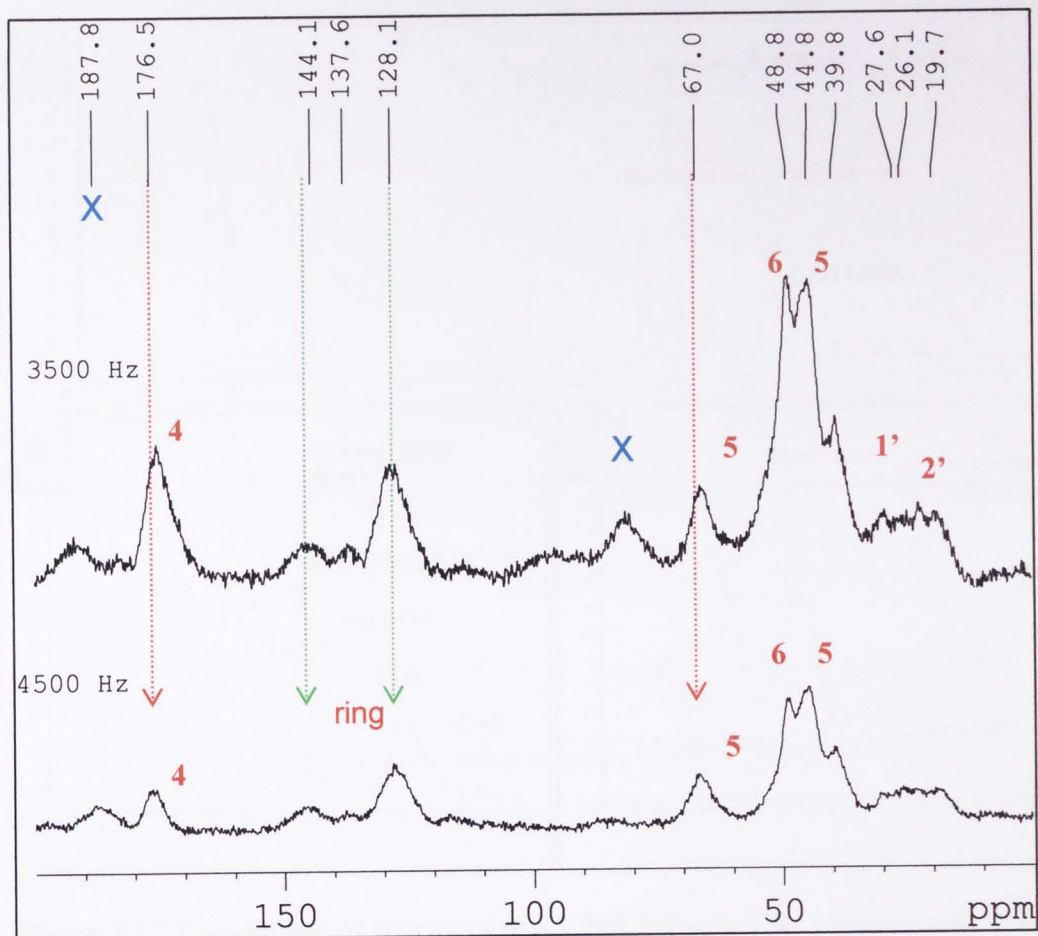


Figure 3.15 FTIR spectra of polyGMA (green) polyDVB (blue) and GMA-co-DVB in KBr discs (red), see Table 3.7.



**Figure 3.16A.**  $^{13}\text{C}$  NMR spectra of polyGMA in solid state. The peaks labelled with the Blue X are artificial peaks which shifted with the frequency of the spinning changed from 4500Hz to 600Hz, which mean they are not real peaks. The solid state  $^{13}\text{C}$  NMR spectrum of poly-GMA showed similar signals to those of the poly-GMA in solution, the main peaks are indicated with the red dotted lines,





**Figure 3.16B.** <sup>13</sup>C NMR spectra of DVB-co-GMA in solid state. The peaks for DVB are marked with green lines, GMA marked with red lines and the saturated ethyl group on styrene marked with blue lines.

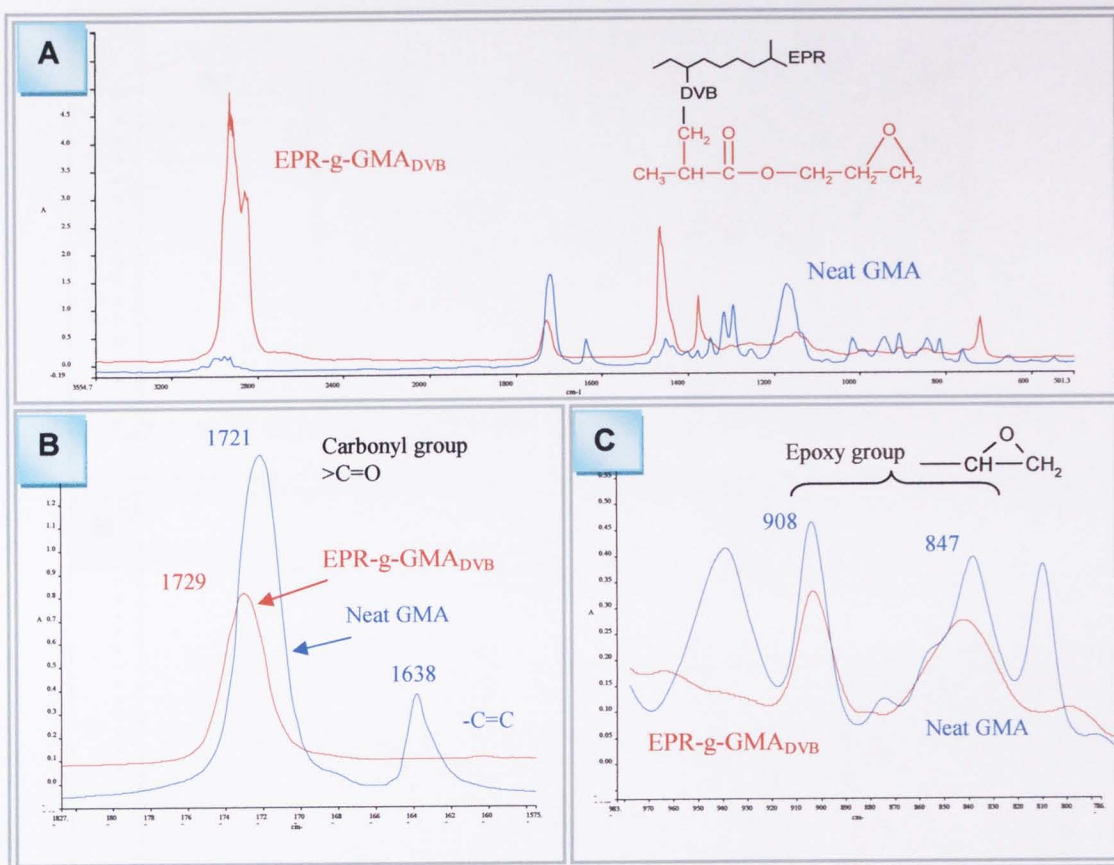


**Figure 3.17.** Comparison of spectra of neat GMA between KBr windows and EPR-g-GMA<sub>DVB</sub> Sample DG14, Table 3.1B (GMA= 15 phr, T101= 0.13phr, GMA/DVB=9/1, temp= 180 °C)

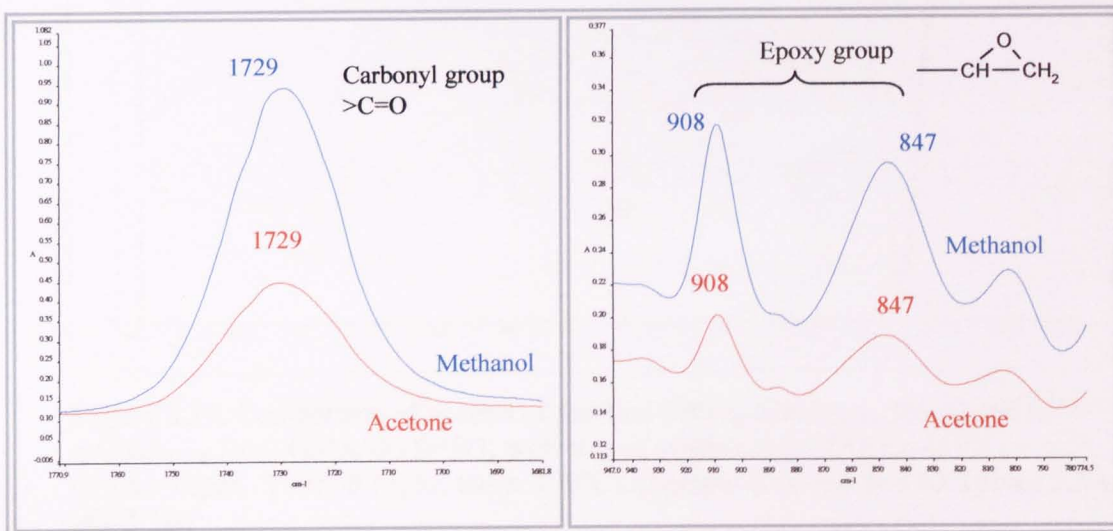


**Figure 3.18.** Comparison of spectra of purified EPR-g-GMA; purified with acetone (red) and methanol (blue). (Sample DG36, Table 3.1B) (GMA=10phr, T101=0.078 phr, GMA:DVB=8:2, temperature 190°C).

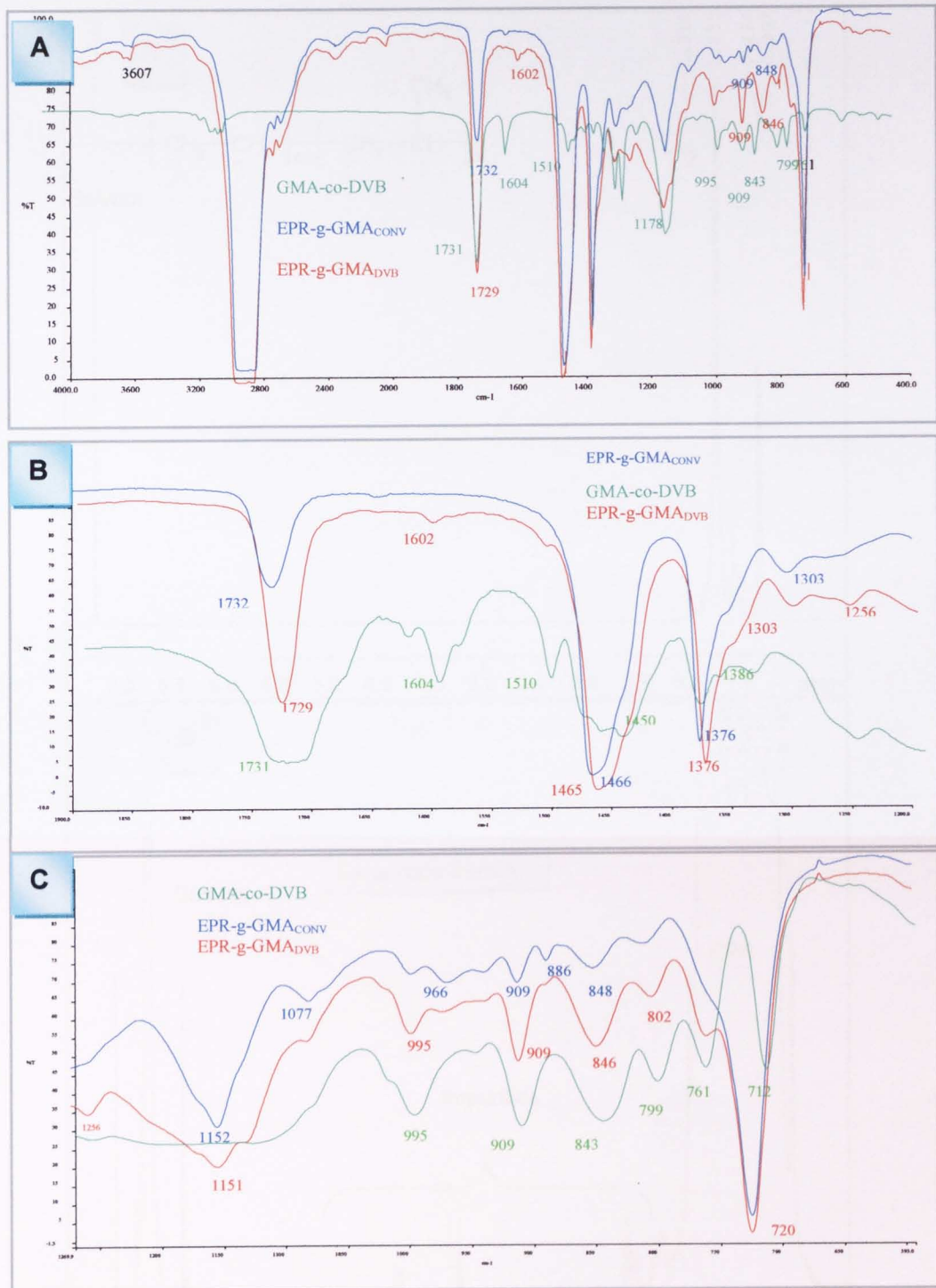


**Figure 3.19.** Comparison of spectra of purified EPR-g-GMA<sub>CONV</sub> (blue) and EPR-g-GMA<sub>DVB</sub> (red) GMA/DVB=9/1, with that of synthesised GMA-co-DVB (green), GMA=10phr, T101=0.13phr, temp. 190°C), (Sample G10 and DG 13 Tables 3.1A and 3.1B)

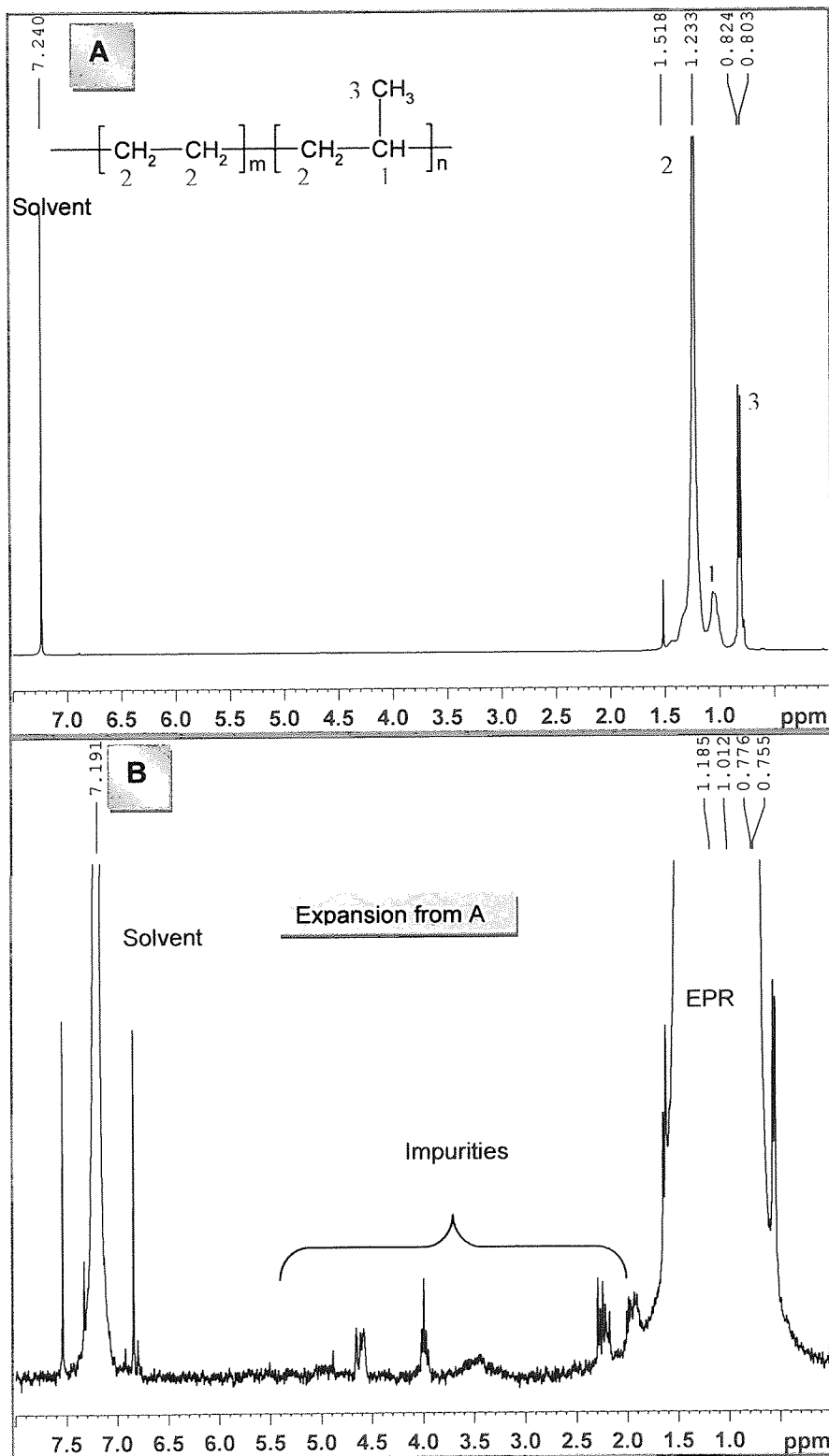


Figure 3.20: <sup>1</sup>H-NMR spectra of EPR in in CDCl<sub>3</sub> at room temperature.

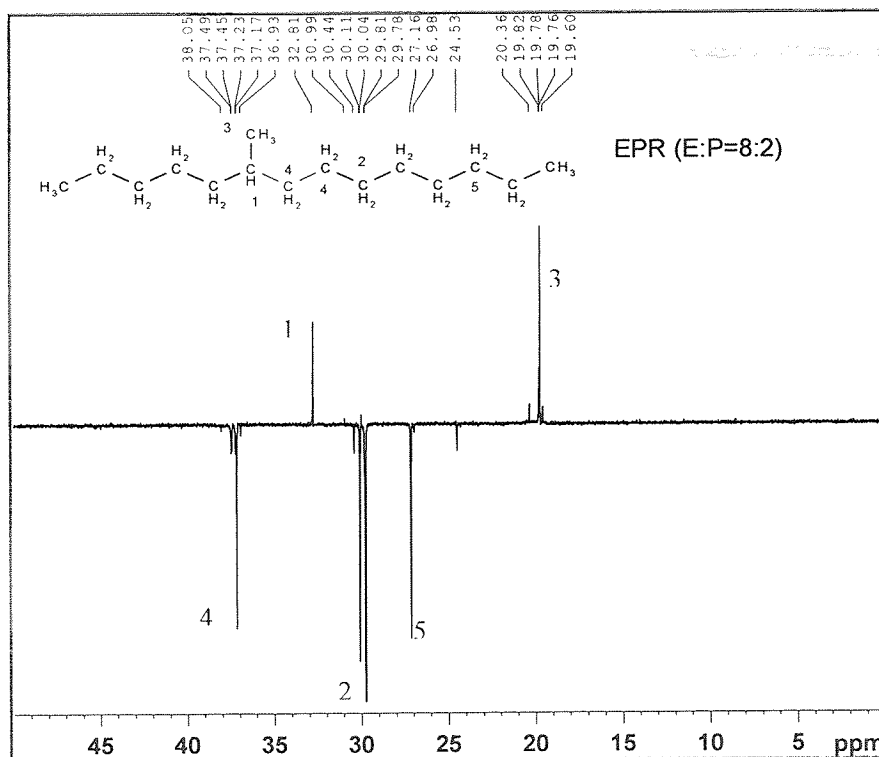


Figure 3.21:  $^{13}\text{C}$  NMR spectra of EPR (ethylene:propylene 8:2) in  $\text{CDCl}_3$  at room temperature.

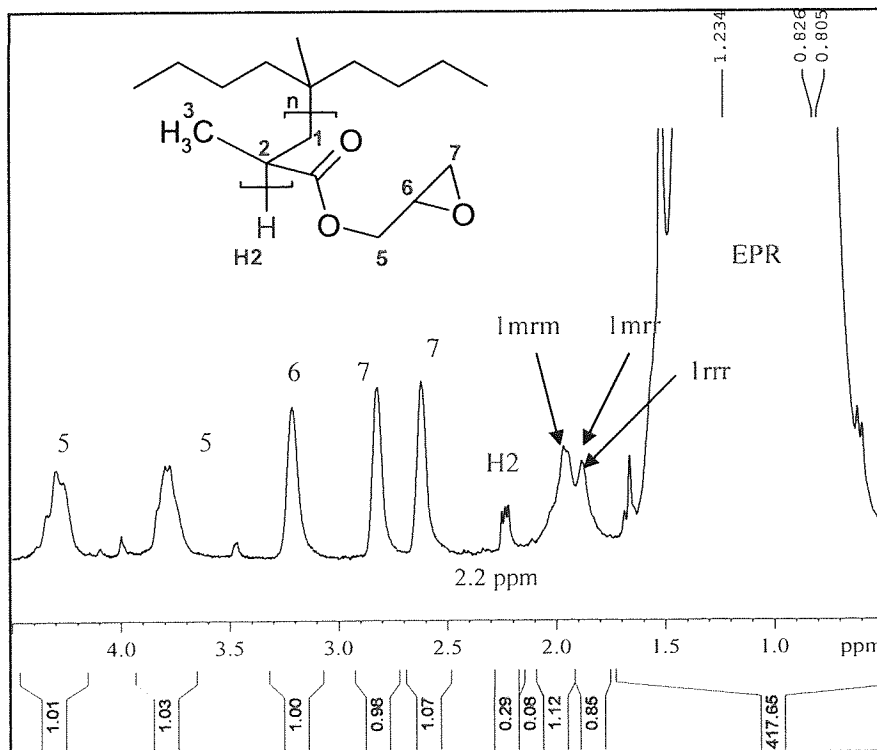


Figure 3.22:  $^1\text{H}$  NMR GMA-g-EPR<sub>CONV</sub> (purified) in  $\text{CDCl}_3$  (sample G24), Table 3.1A, GMA=15%, T101=0.8 phr, temp=190°C, g-GMA=1.9 %, polyGMA=3 %, all polyGMA was removed by purification.

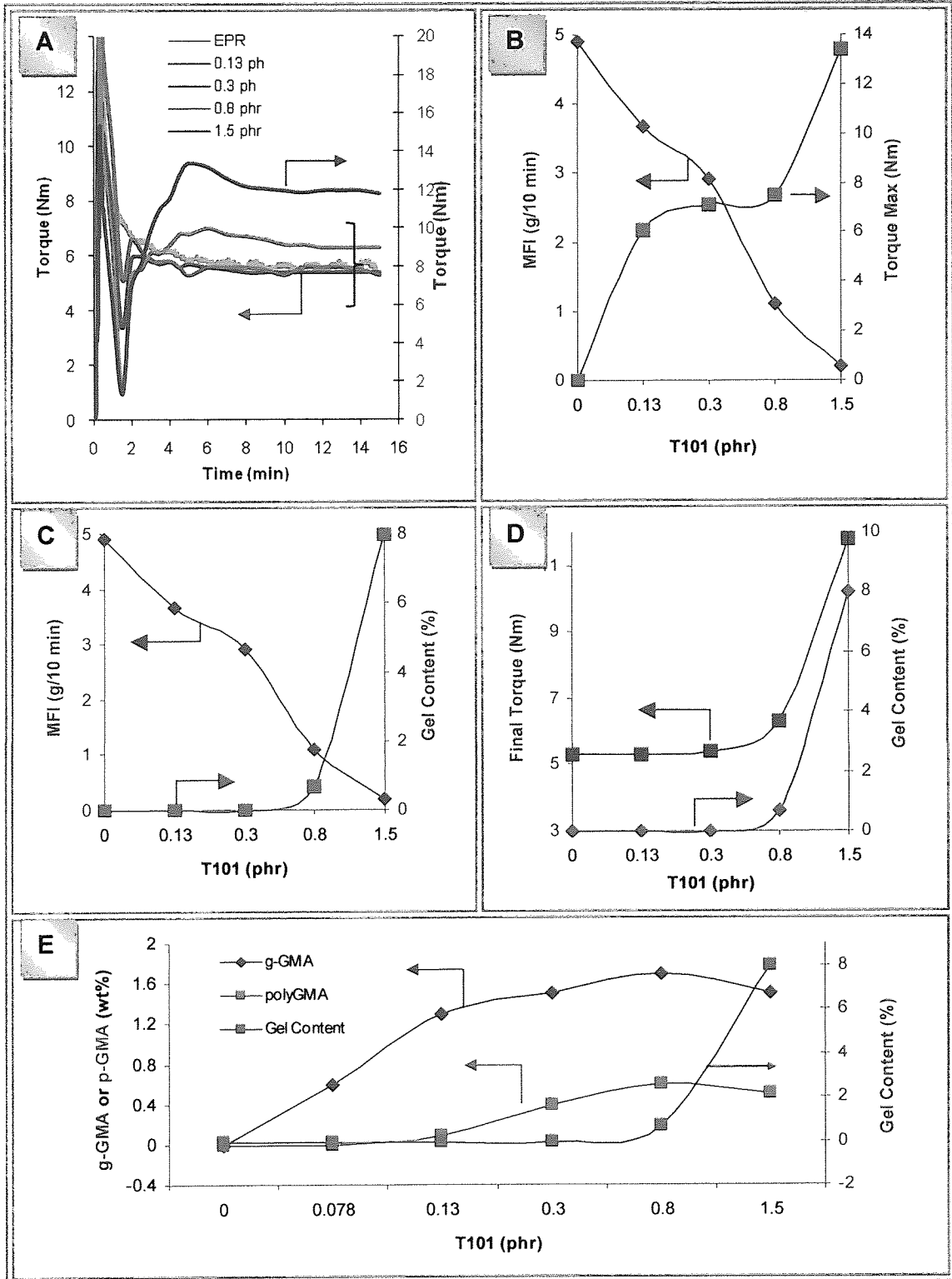
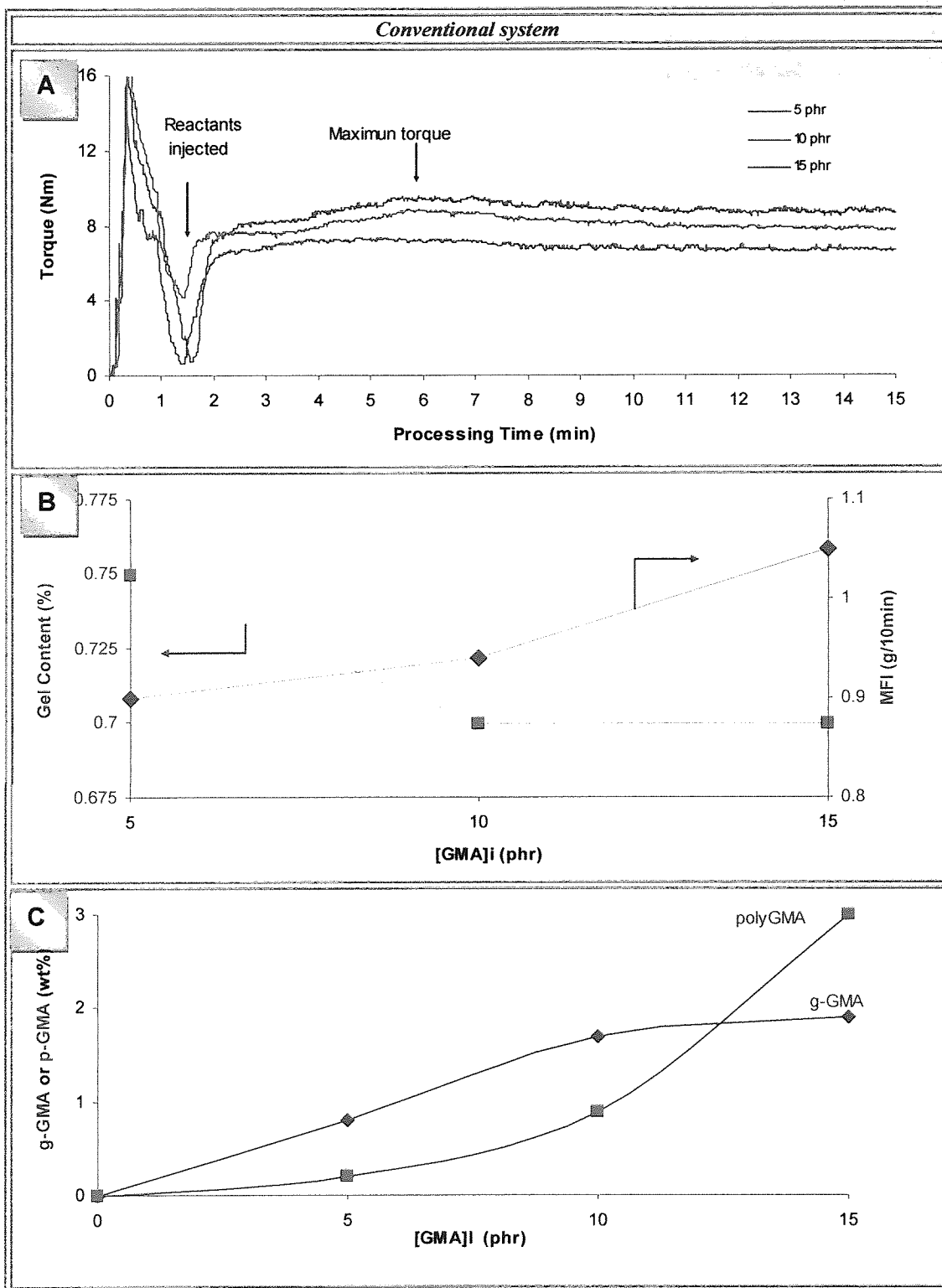
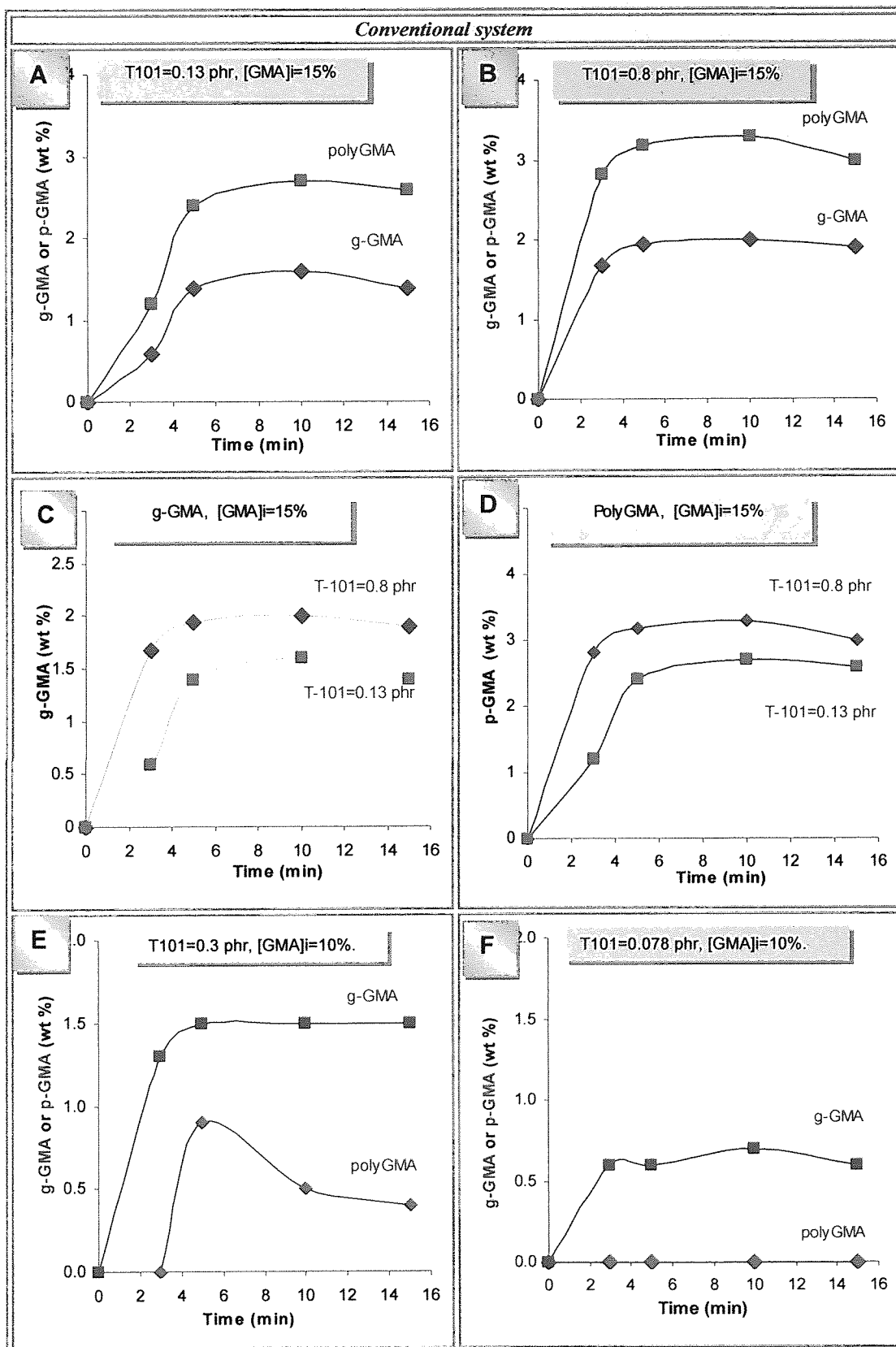


Figure 3.23. Effect of peroxide concentrations on torque behaviour, MFI and gel content in EPR-g-GMA<sub>CONV.</sub> (GMA=10 phr and 190°C). Samples G16, 17, 18, 19, 20, Table 3.1A.



**Figure 3.24.** Effect of GMA concentration on torque characteristic, MFI value, gel content and GMA grafting level in conventional EPR-g-GMA<sub>CONV</sub> system. (T101=0.8 phr and 190°C). Samples G21, 22, 24, Table 3.1A.



**Figure 3.25.** Effect of processing time on GMA grafting and polyGMA level in conventional EPR-g-GMA<sub>CONV</sub> system. (GMA=15 phr A-D, and 190°C). Samples G8, 9, 10, 11, 25, 26, 27, 28, in A-D, samples G4, 5, 6, 7, 12, 13, 14, 15 in E-F, Table 3.1A.



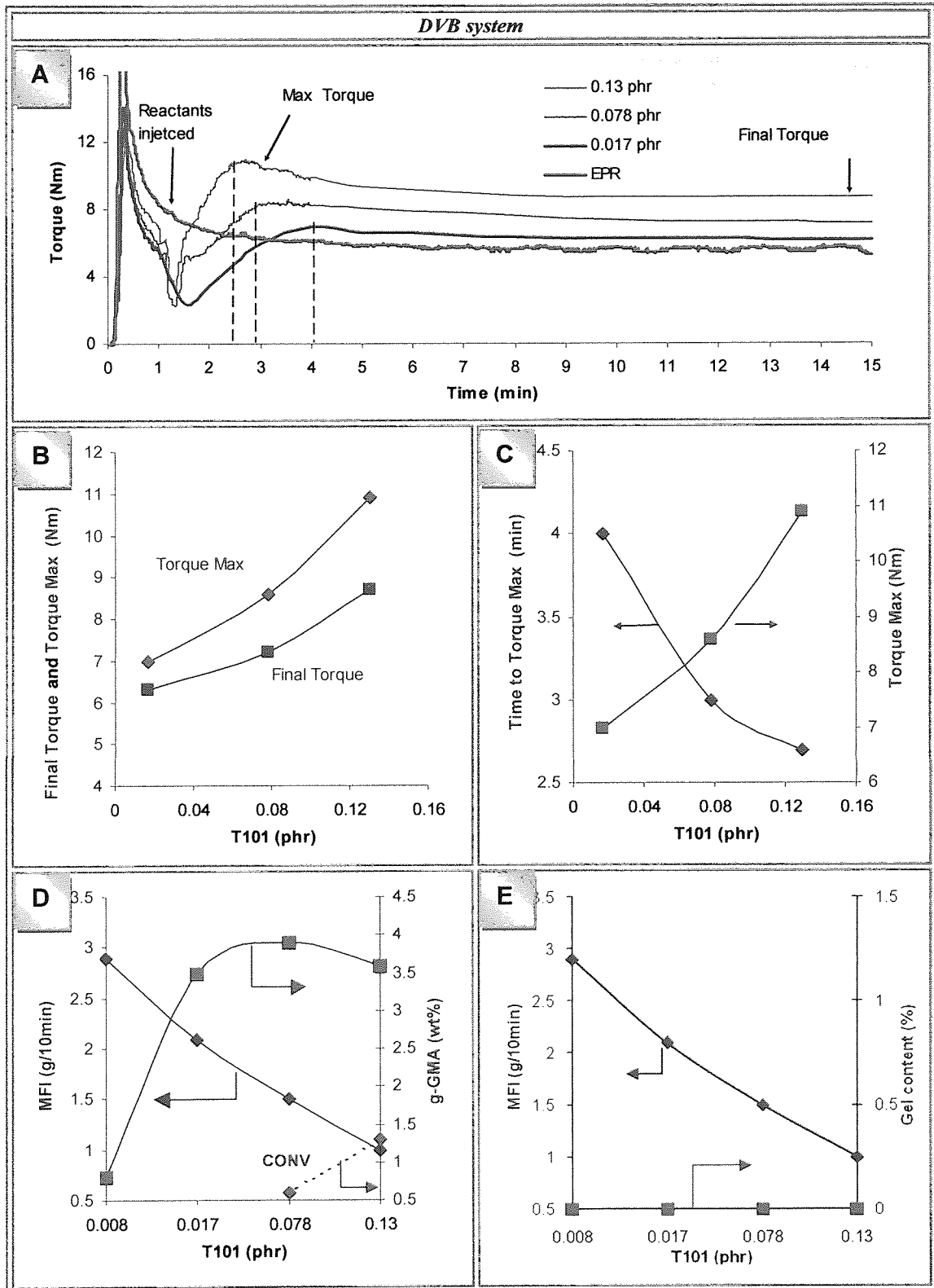


**Figure 3.26.** Torque behaviour at various peroxide concentrations in EPR-g-GMA<sub>DVB</sub> system, (GMA=10 phr, GMA:DVB=8:2 and 190°C). Samples **DG34, 35, 36, 37**, Table 3.1B

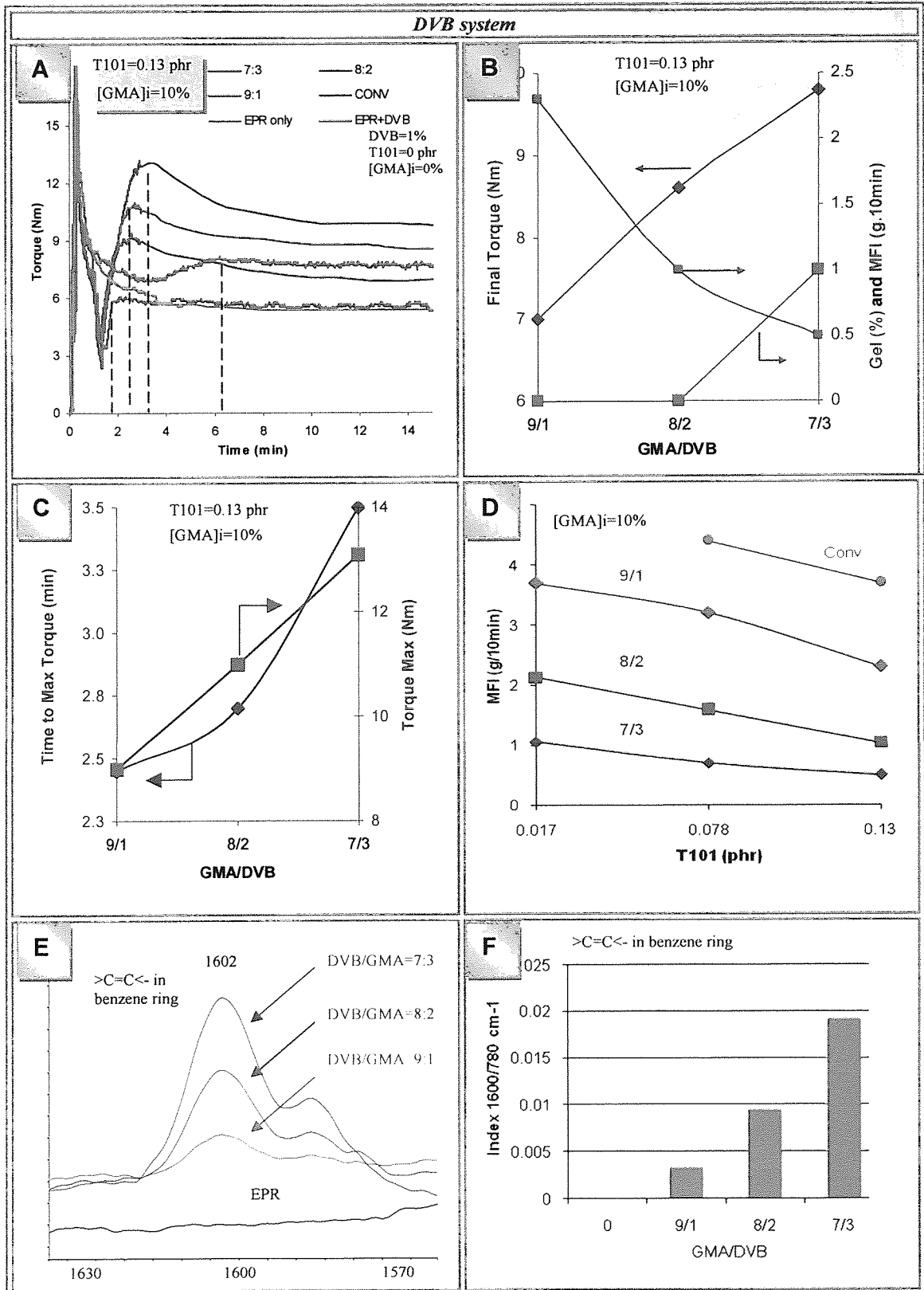


**Figure 3.27.** Torque behaviour at various DVB concentrations in EPR-g-GMA<sub>DVB</sub> system. (T101=0.13 phr, GMA=10 phr and 190°C). Samples G17 (CONV) Table 3.1A and, DG18, D35-37 (D), DG42-44., DG37, DG52, Table 3.1B. E-all purified samples at end of reaction, F-quantified of E.

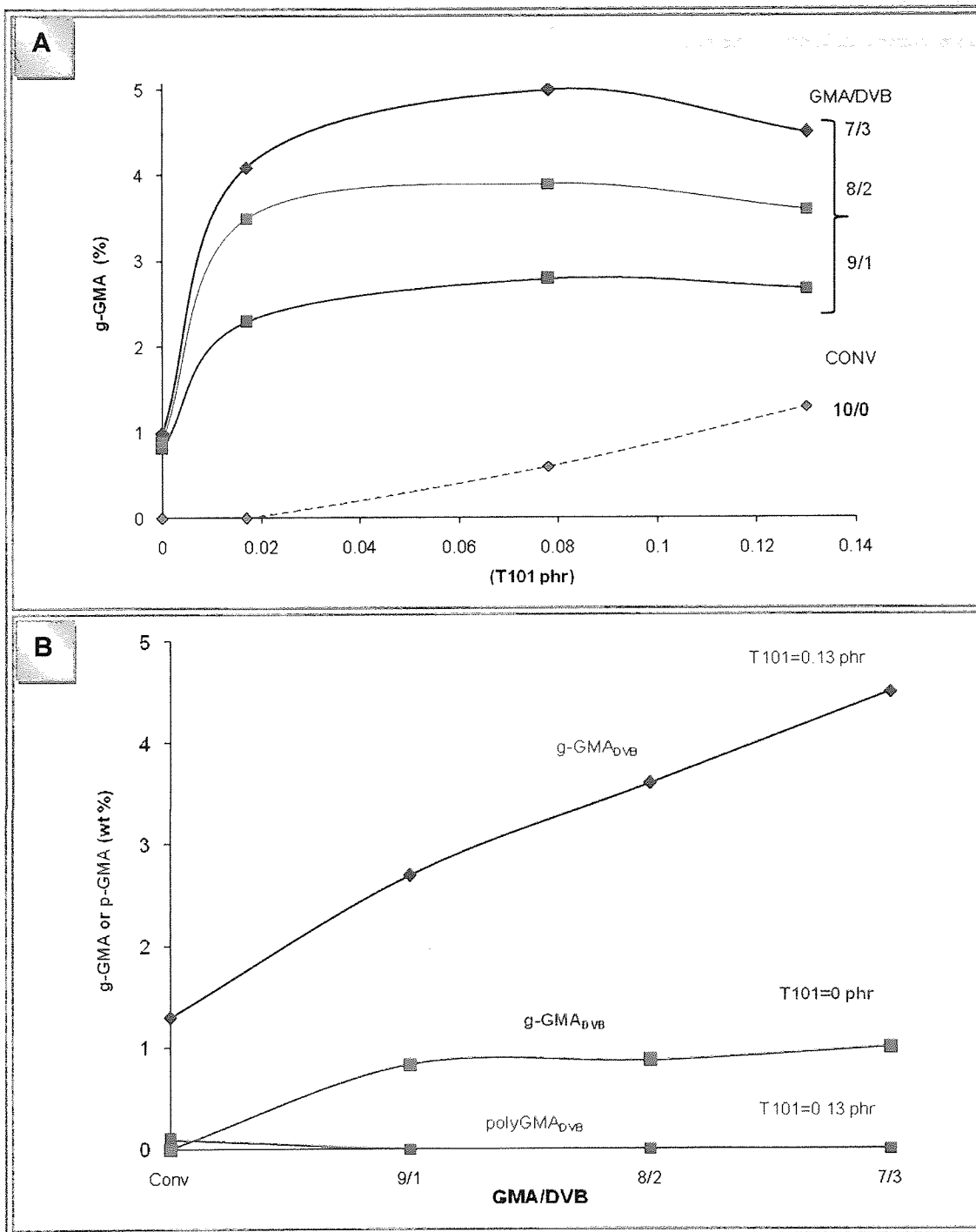
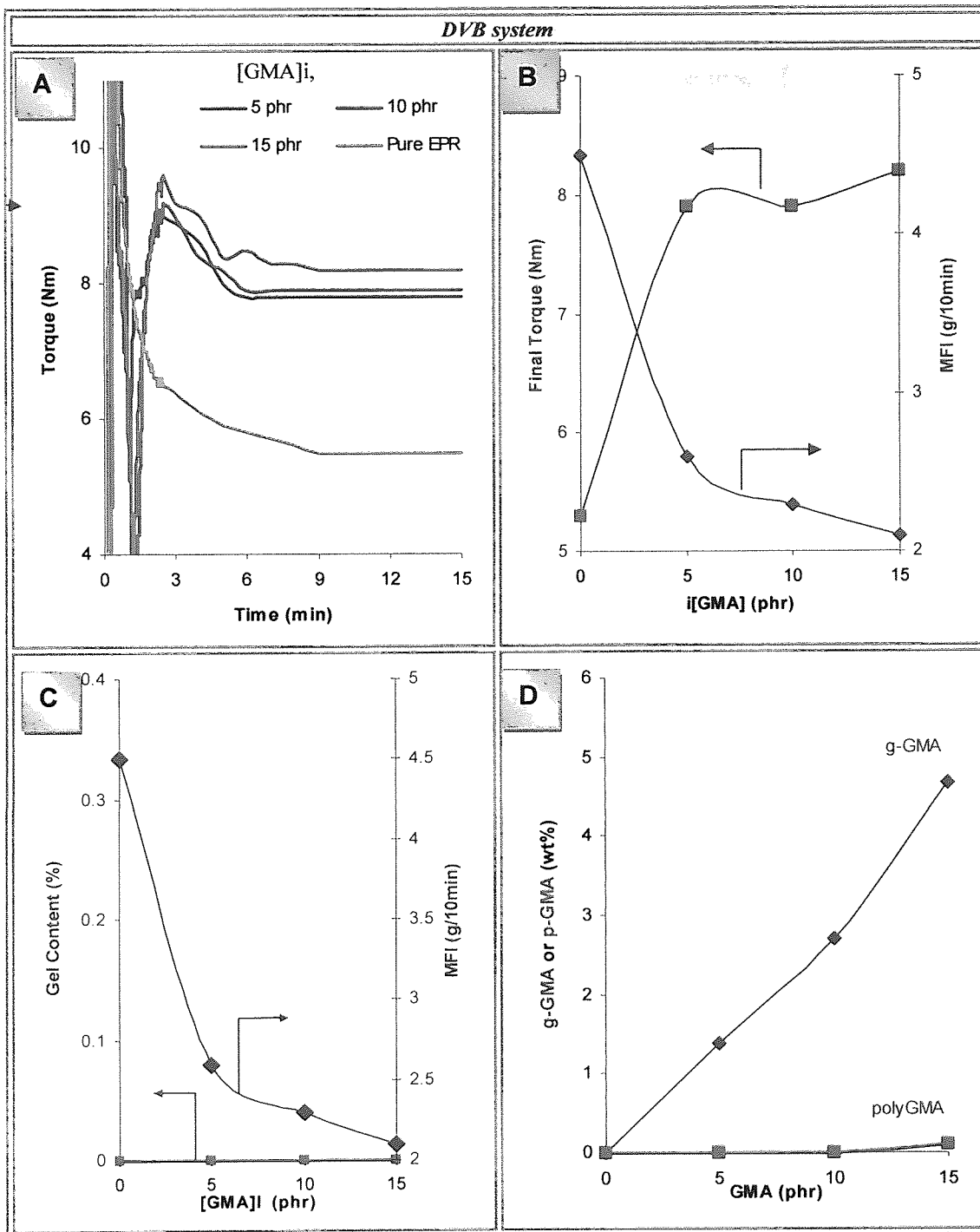
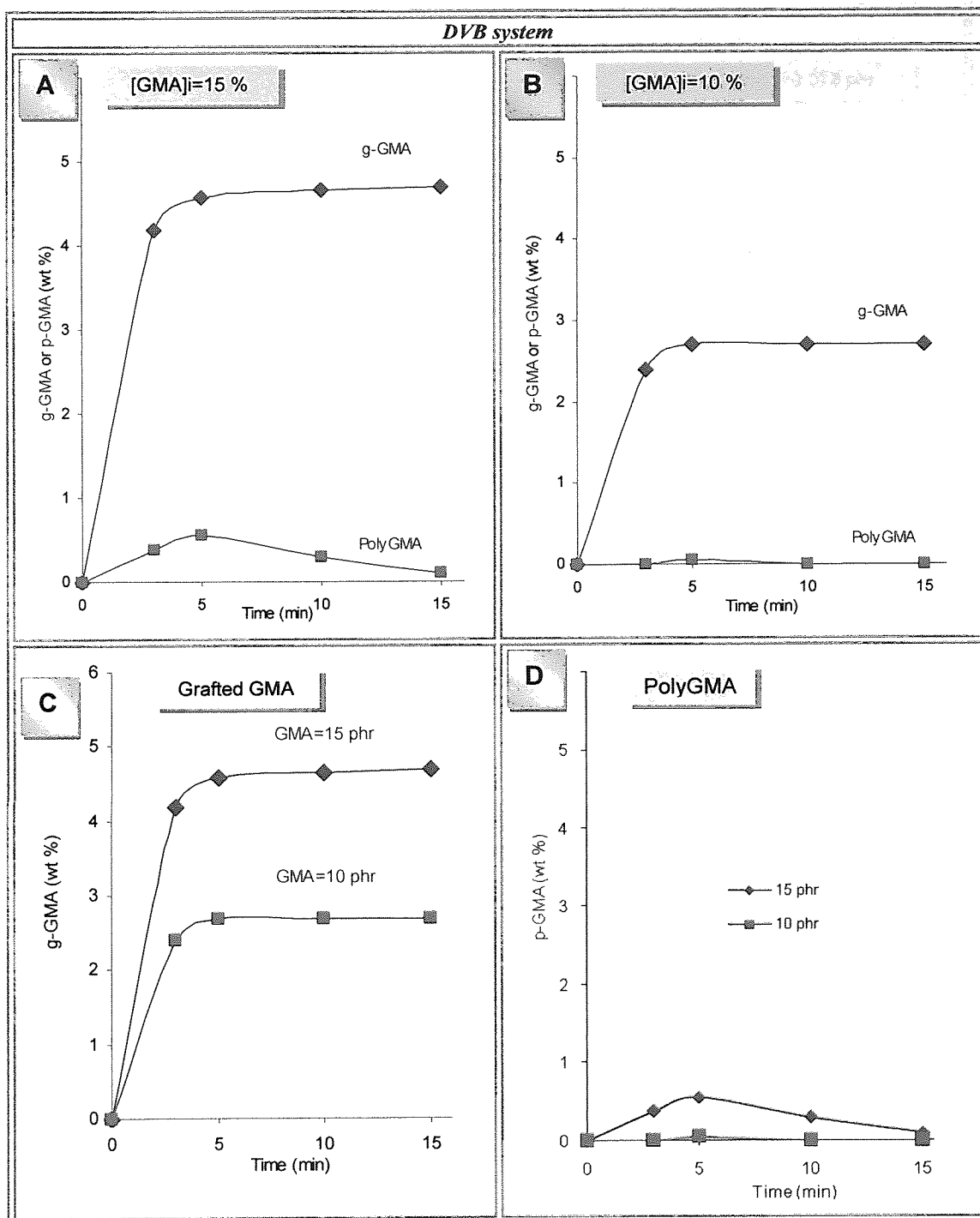


Figure 3.28. Effect of DVB concentrations on extent of GMA grafting degree and formation of polyGMA in EPR-g-GMA<sub>DVB</sub> samples. in B: T101= 0.13 phr,/ in A and B: GMA=10 phr, and 190°C).



**Figure 3.29.** Effect of [GMA]<sub>i</sub> concentrations in EPR-g-GMA<sub>DVB</sub> system on processing characteristic and the extent of grafting and homopolymerisation. T101= 0.13 phr, GMA/DVB=9/1, 190°C). Samples DG12, 13, 14, Table 3.1B.



**Figure 3.30.** Effect of processing time on grafting degree of EPR-g-GMA<sub>DVB</sub> samples. Reagents were added 1 minute after EPR was processed (T101 = 0.13 phr, GMA = 10 and 15 phr, GMA/DVB = 9/1, 190°C). Samples **DG15, 16, 17, 18, 53, 54, 55, 56**, Table 3.1B

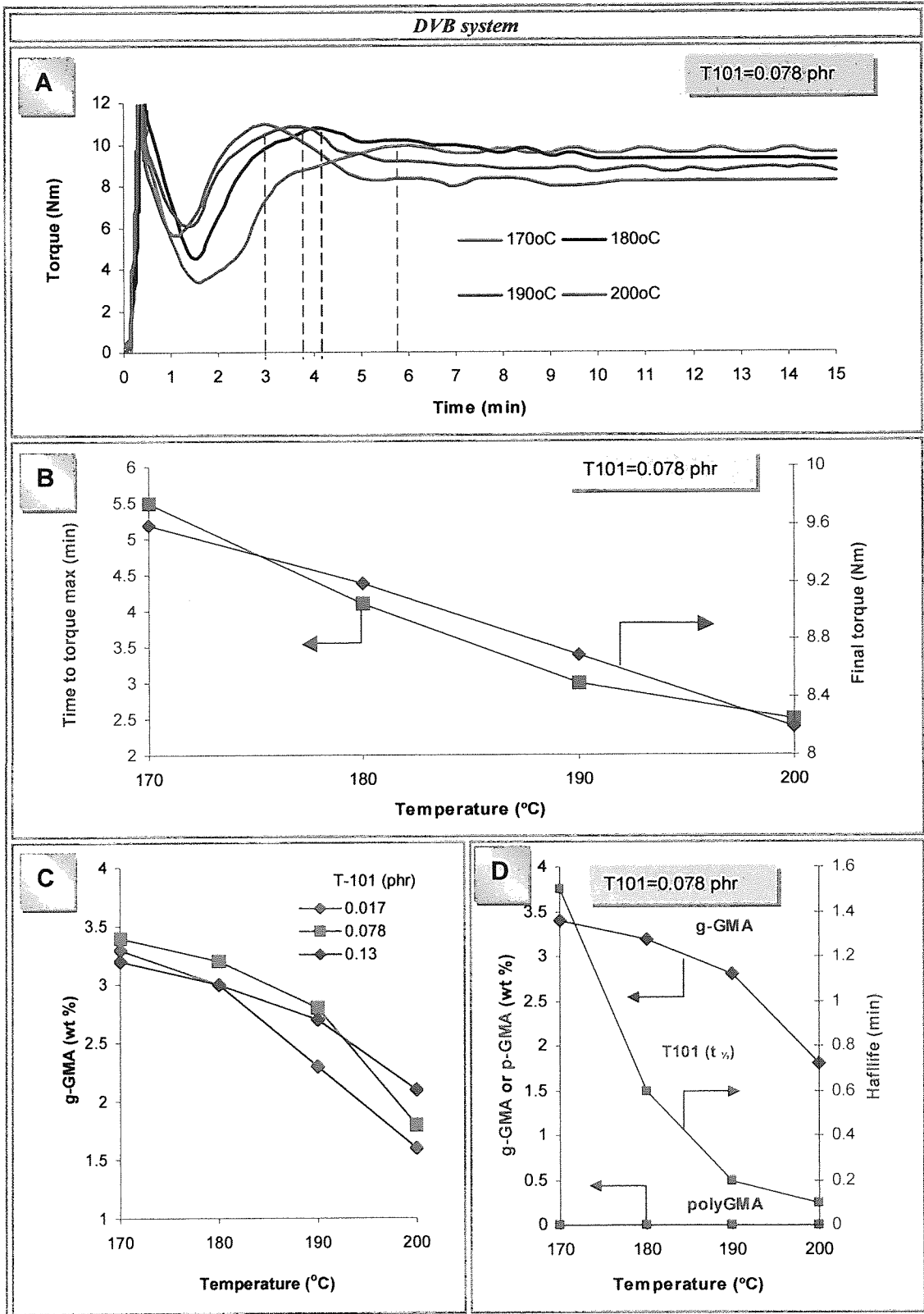


Figure 3.31. Effect of processing temperature on torque, GMA grafting and polyGMA level in EPR-g-GMA<sub>DVB</sub> samples. Also the effect of temperature on peroxide half live. (GMA=10 phr, GMA/DVB= 9/1)

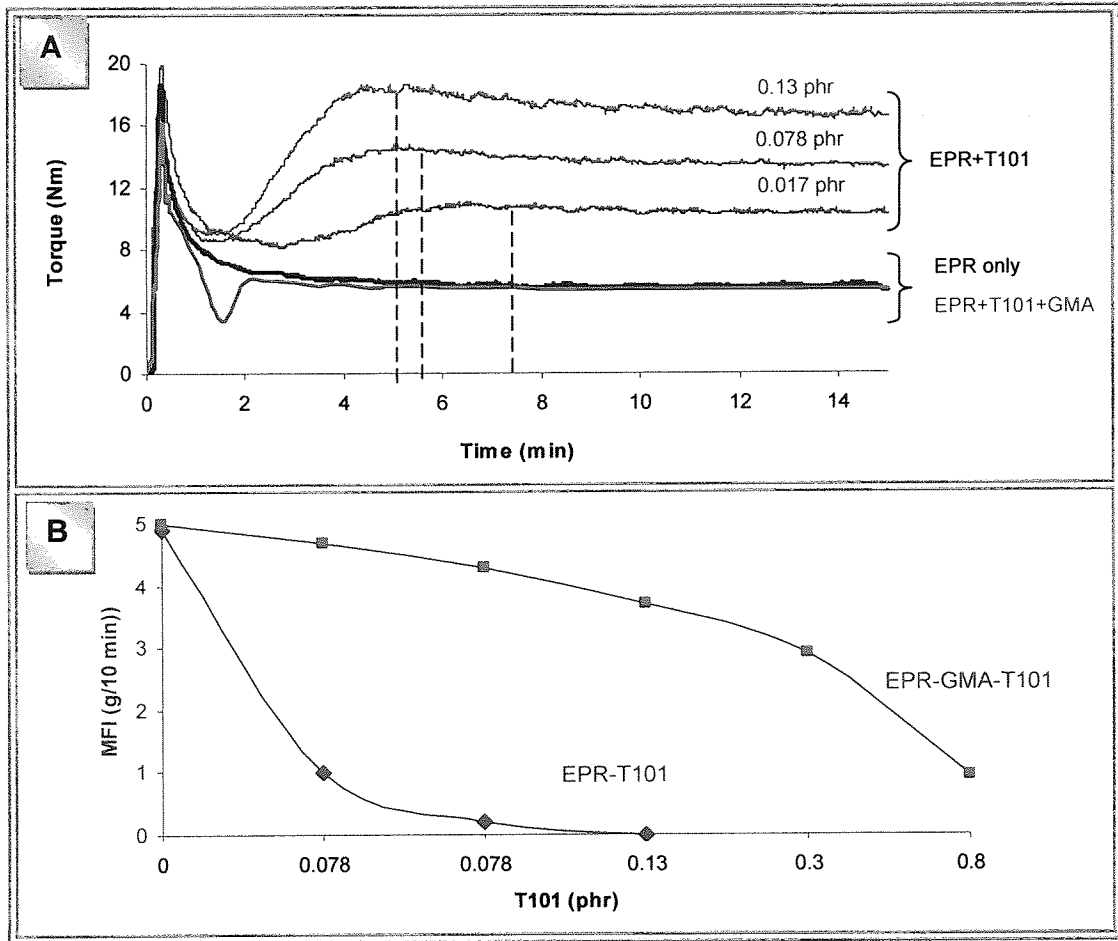


Figure 3.32. Comparison of the effect of peroxide concentration on torque behaviour and MFI values of polymer in the absence or presence of GMA. Temp=190°C. EPR-g-GMA<sub>CONV</sub> containing 10 phr GMA. Samples G1-3, 16-19, Table 3.1A.

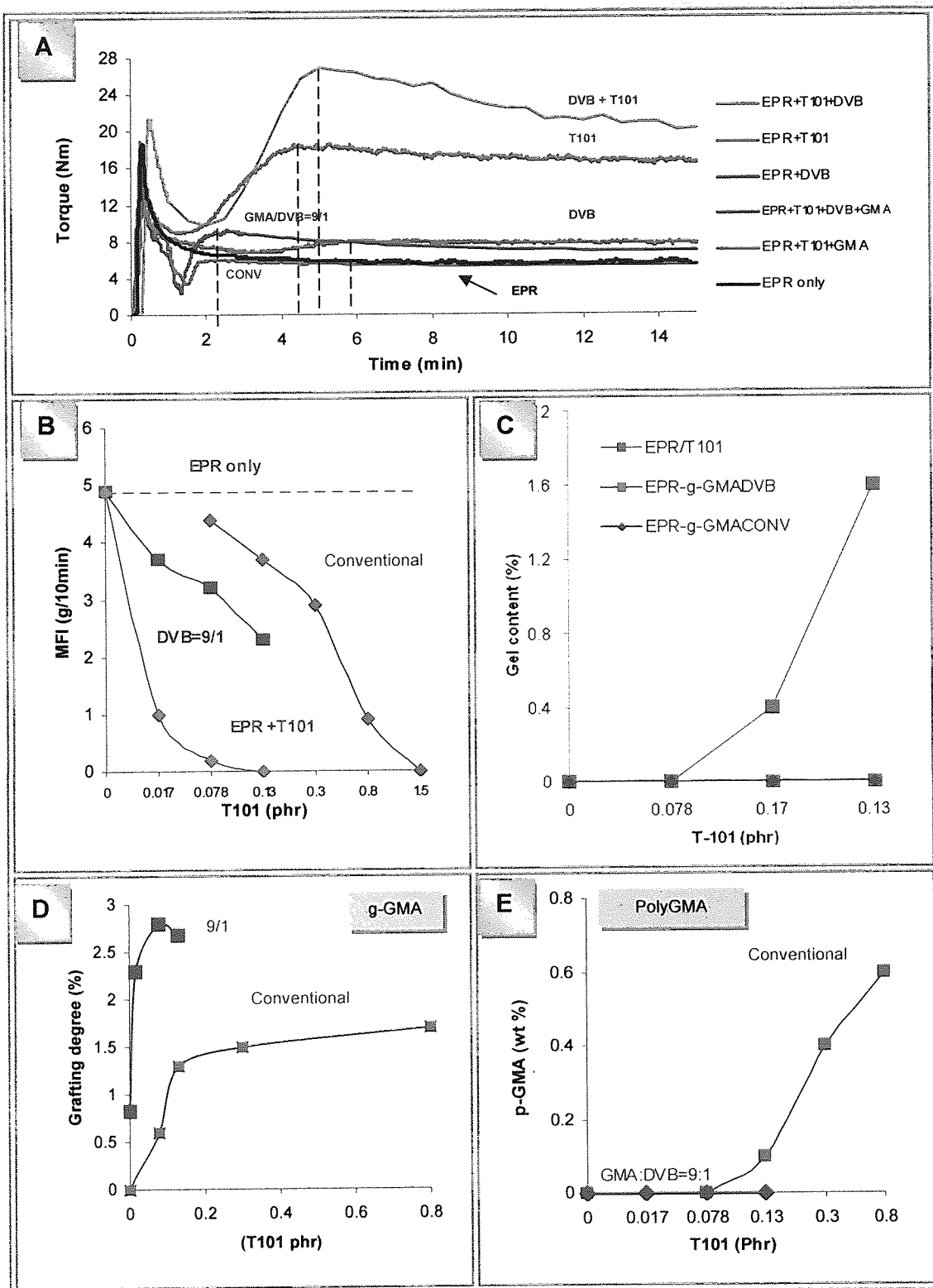


Figure 3.33. Comparison the effect of T-101 concentration on MFI values, gel content, grafting level and polyGMA in grafting systems with DVB and without DVB. GMA/DVB=9/1, GMA=10 phr, temp=190°C. (T-101=0.13 phr in A) Samples G15-19, Table 3.1A. (CONV), Samples DG9-11, 18, 56, 57, Table 3.1B (DVB).



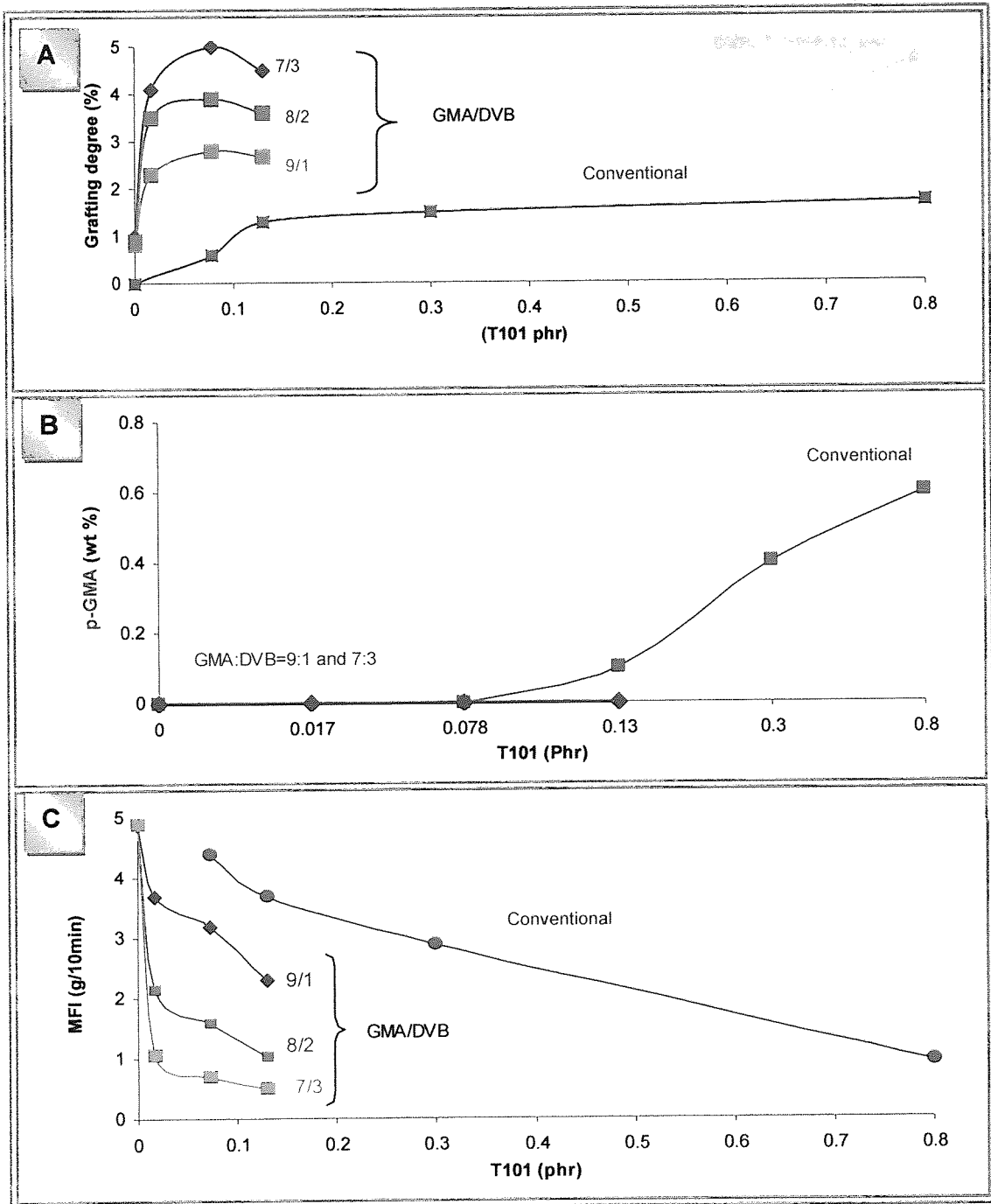
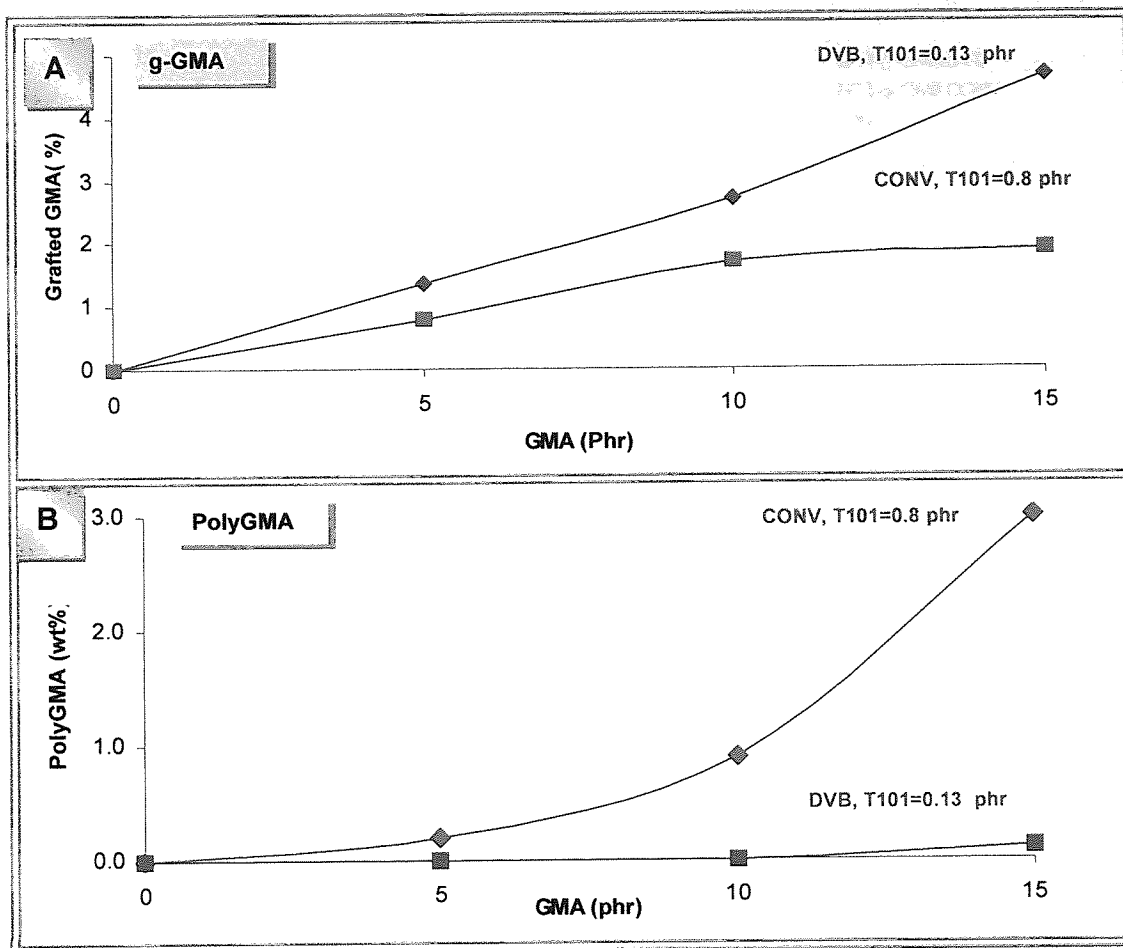
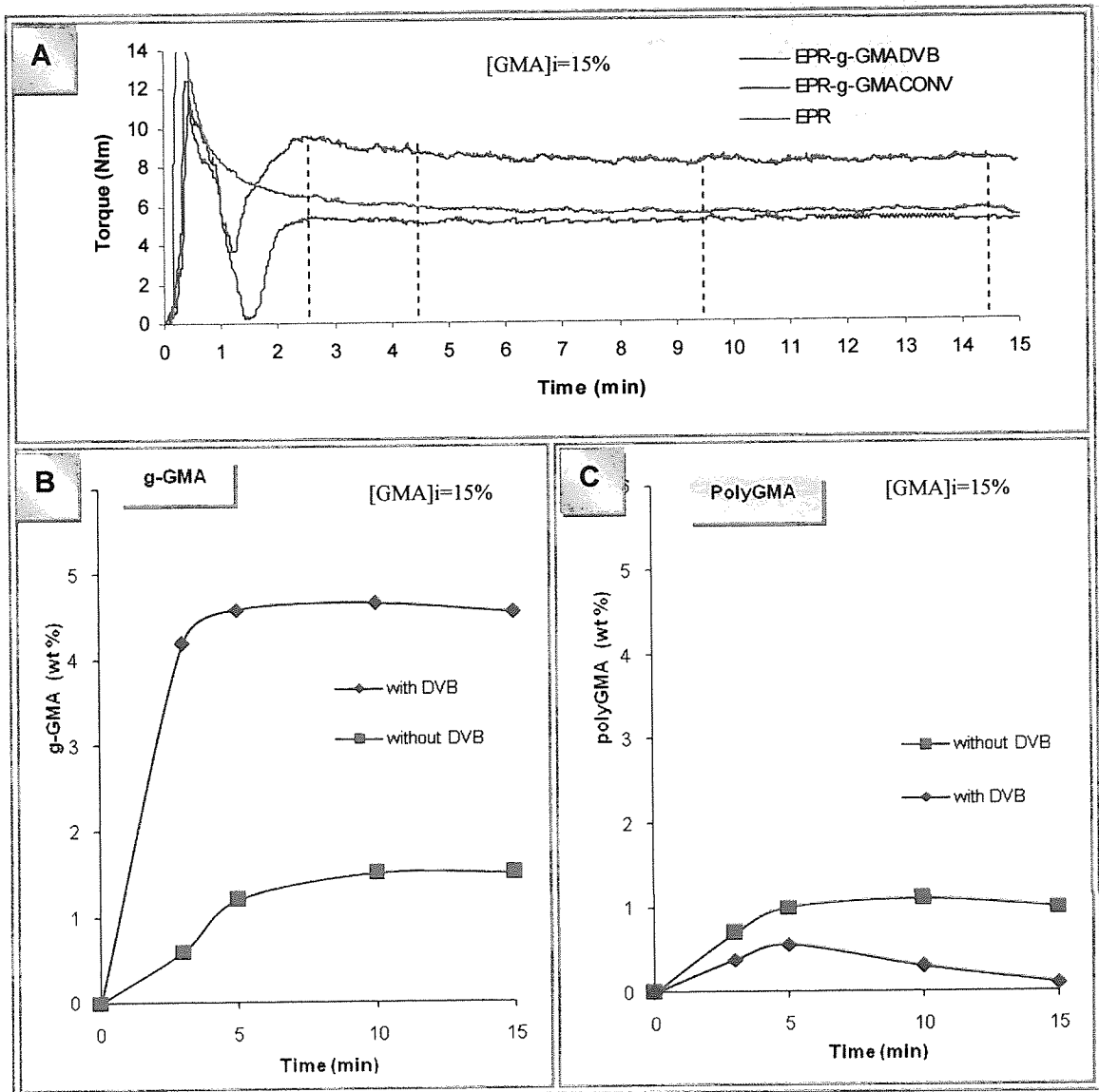


Figure 3.34. Comparison of grafting degree, torque and MFI values as a function of peroxide concentration at various comonomer concentrations and without comonomer. GMA=10 phr, 190°C. For the torque curves of this graph see Figure 3.27A.



**Figure 3.35.** Effect of initial GMA concentrations on GMA grafting level in EPR-g-GMA<sub>CONV</sub> and EPR-g-GMA<sub>DVB</sub>. T101=0.13 phr for GMA/DVB system, GMA:DVB=9:1 w/w, T101=0.8 phr for conventional system, 190°C. Samples G, 19 21, 24, Table 3.1A (CONV), Samples DG 12-14, Table 3.3B (DVB).



**Figure 3.36.** Comparison of the kinetic of grafting reaction in conventional and comonomer (DVB) system. T101= 0.13 phr, GMA:DVB=9:1 w/w, GMA=15 phr, Temperature=190°C. Samples **G24, 25, 26, 27, Table 3.1A (CONV)**, Samples **DG13, 15, 16, 17, Table 3.1B (DVB)**: Sampling was taken at the times shown in dotted lines in A.

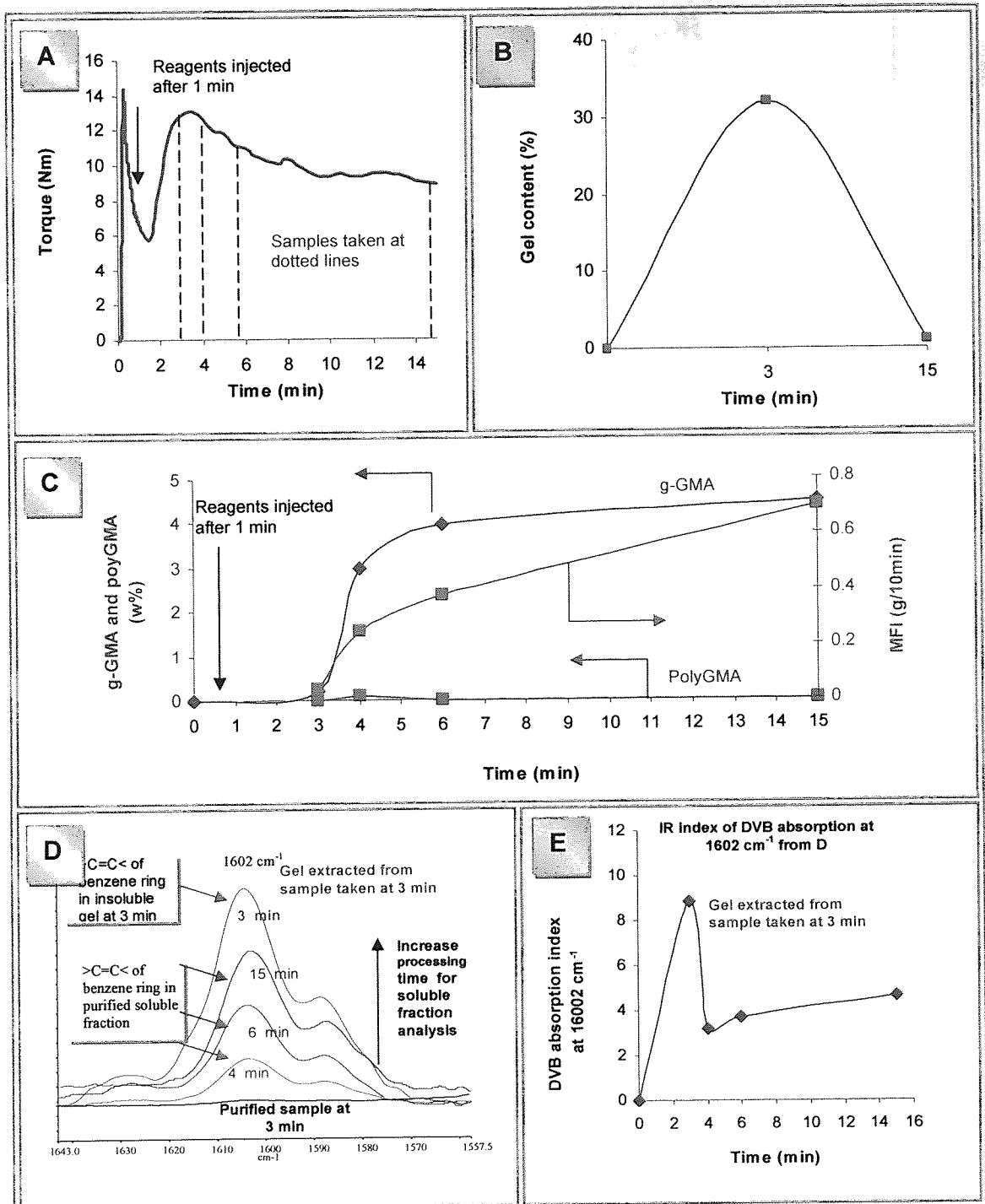


**Figure 3.37.** Analysis of EPR-g-GMA<sub>DVB</sub> processed and purified samples, taken out at different processing times. GMA=10 phr, T101=0.13 phr, GMA/DVB=7/3 w/w, 190°C. Samples DG49, 50, 51, 52, Table 3.1B. Sampling was taken at the times shown in dotted lines in A.

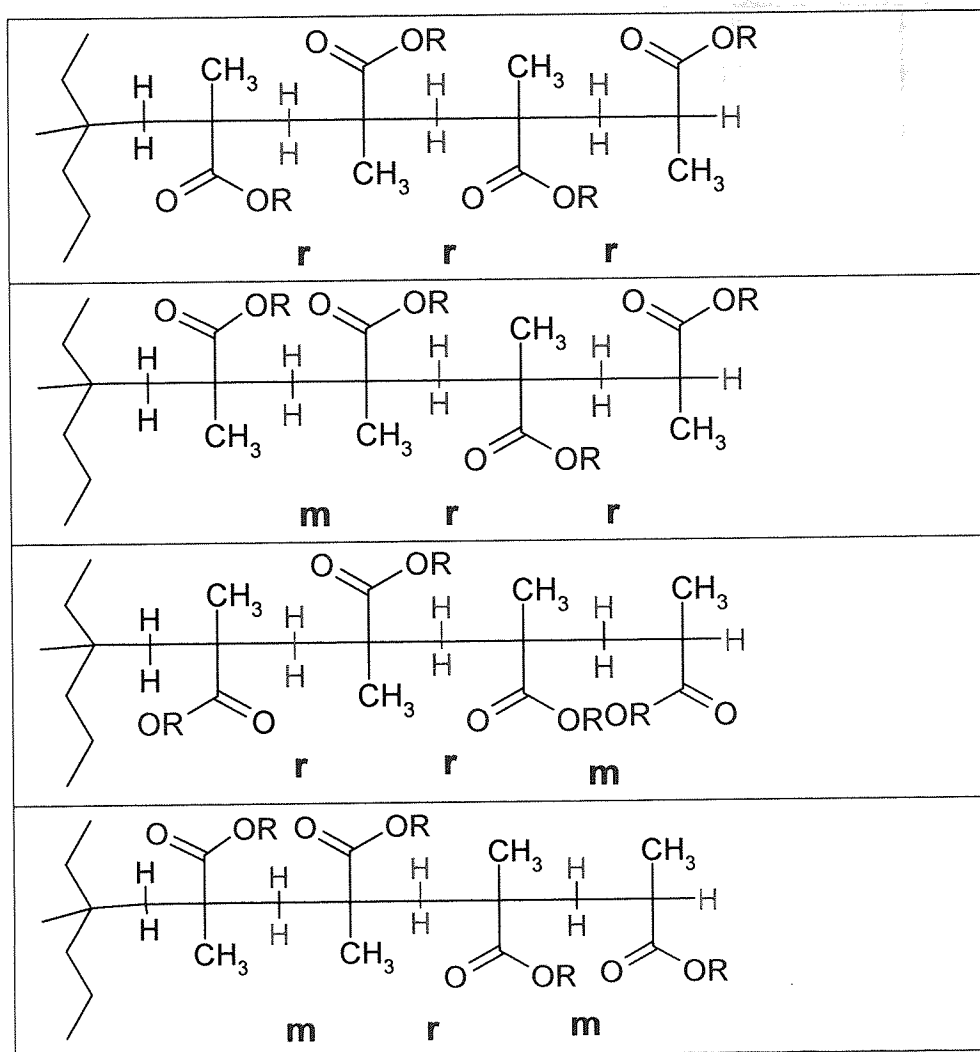


**Figure 3.38.** Schematic representing of stereochemical configuration of GMA grafted on EPR (EPR-g-GMA<sub>CONV</sub>) (sample G24 in Table 3.1a), GMA=15 phr, T101=0.8 phr, temp=190°C, g-GMA=1.9 wt%, polyGMA=3 wt%, all polyGMA was removed by purification.

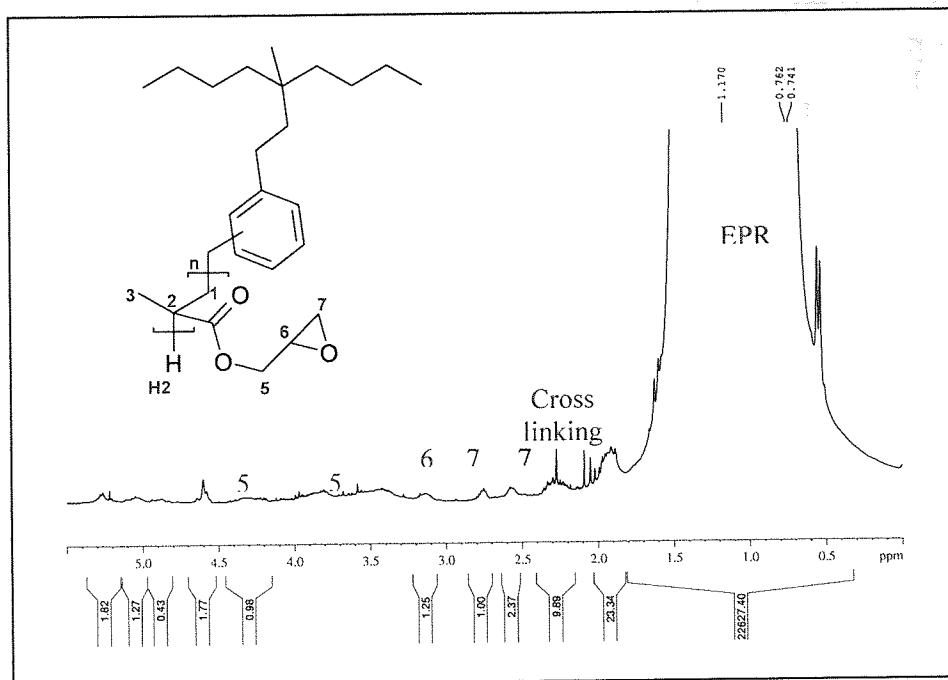


Figure 3.39:  $^1\text{H}$  NMR of purified EPR-GMA<sub>DVB</sub> (sample DG14 in Table 3.1b) in  $\text{CDCl}_3$  at room temperature. T101= 0.13 phr, GMA= 15 phr, GMA/DVB= 9/1, 190°C, g-GMA=4.7 wt%, polyGMA=0.1%, MFI=2.1 g/10min, all polyGMA was removed by purification.

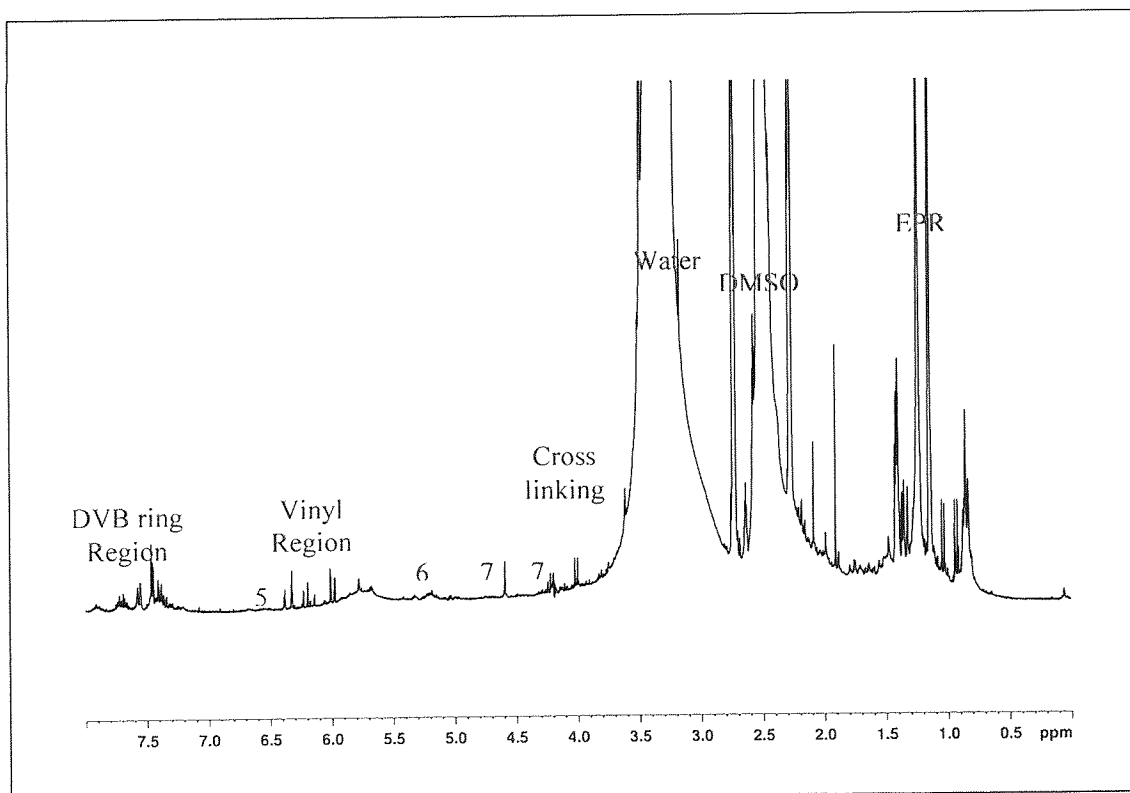


Figure 3.40:  $^1\text{H}$ -NMR of purified EPR-GMA<sub>DVB</sub> (sample DG14 in Table 3.1b) in  $\text{DMSO-d}_6$  at room temperature. T101= 0.13 phr, GMA= 15 phr, GMA/DVB= 9/1, 190 °C, g-GMA=4.7 wt%, polyGMA=0.1%, MFI=2.1 g/10min, all polyGMA was removed by purification.

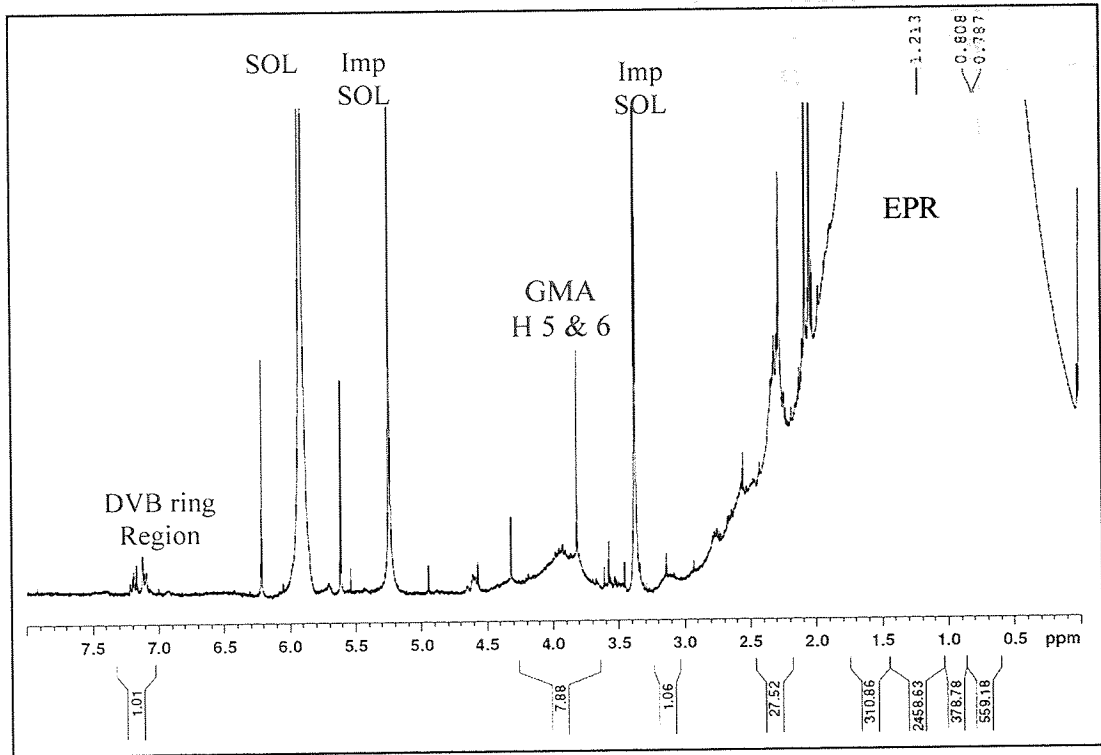


Figure 3.41:  $^1\text{H}$  NMR EPR-g-DVB, (sample DG14 in Table 3.1b) in  $\text{C}_2\text{D}_2\text{Cl}_4$  at room temperature. (T101= 0.13 phr, GMA= 15 phr, GMA/DVB= 9/1,  $190^\circ\text{C}$ ), g-GMA=4.7 wt%, polyGMA=0.1%, MFI=2.1 g/10min

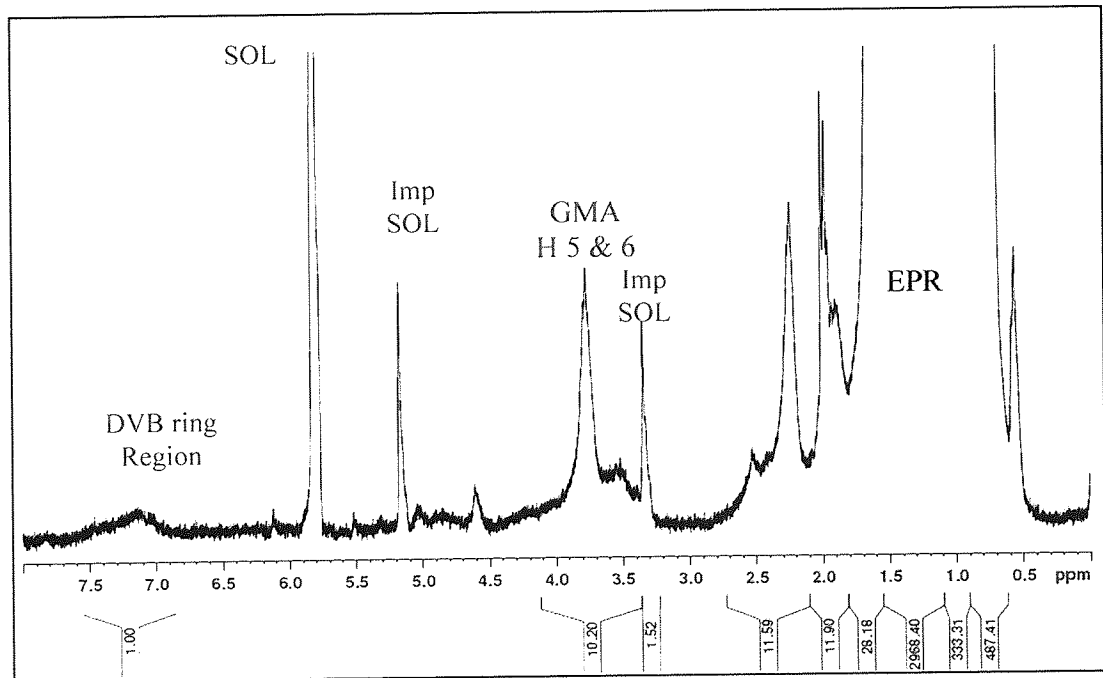


Figure 3.42:  $^1\text{H}$  NMR EPR-g-DVB, (sample DG14 in Table 3.1b) in  $\text{C}_2\text{D}_2\text{Cl}_4$  at  $135^\circ\text{C}$ . (T101= 0.13 phr, GMA= 15 phr, GMA/DVB= 9/1,  $190^\circ\text{C}$ ), g-GMA=4.7 wt%, polyGMA=0.1%, MFI=2.1 g/10min

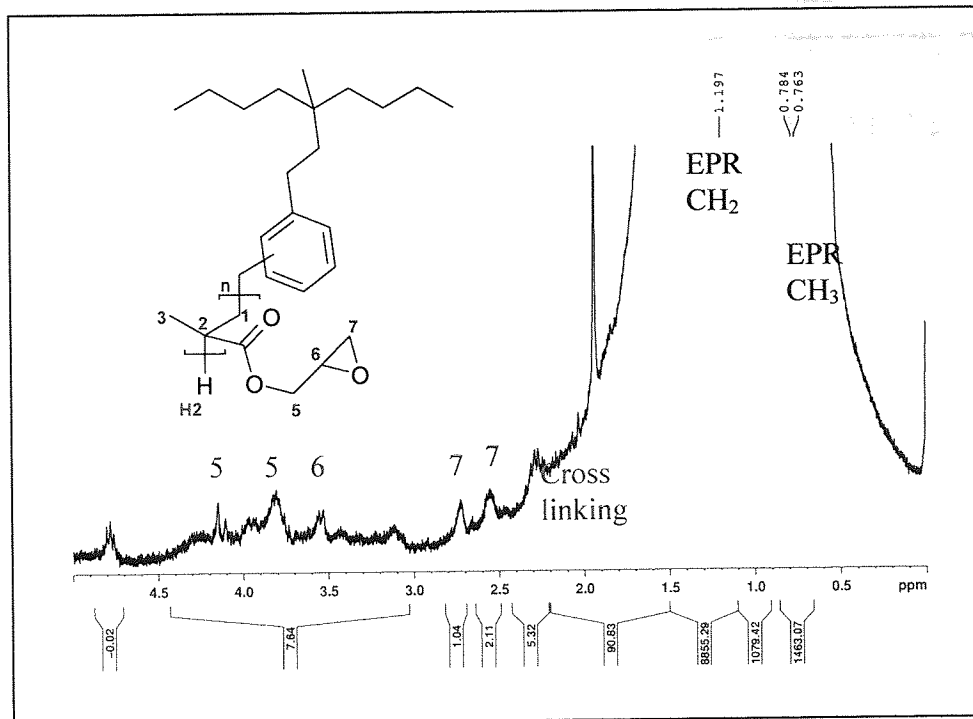


Figure 3.43:  $^1\text{H}$  NMR EPR-g-DVB, (sample DG14 in Table 3.1b) in  $\text{CDCl}_3$  at  $57^\circ\text{C}$ . (T101= 0.13 phr, GMA= 15 phr, GMA/DVB= 9/1,  $190^\circ\text{C}$ ), g-GMA=4.7 wt%, polyGMA=0.1%, MFI=2.1 g/10min

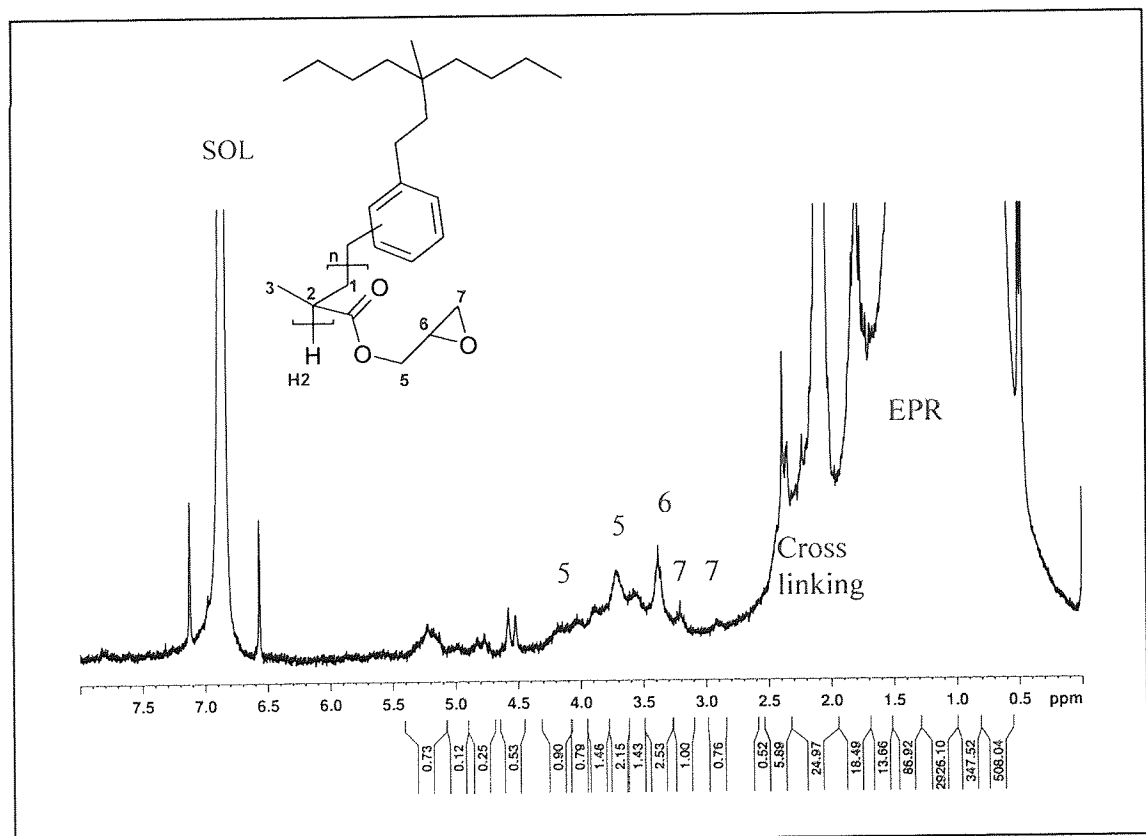


Figure 3.44:  $^1\text{H}$  NMR of EPR-g-GMA<sub>DVB</sub>, (sample DG14 in Table 3.1b) in  $\text{C}_6\text{D}_4\text{Cl}_2$  at  $57^\circ\text{C}$ . (T101= 0.13 phr, GMA= 15 phr, GMA/DVB= 9/1,  $190^\circ\text{C}$ ), g-GMA=4.7 wt%, polyGMA=0.1%, MFI=2.1 g/10min



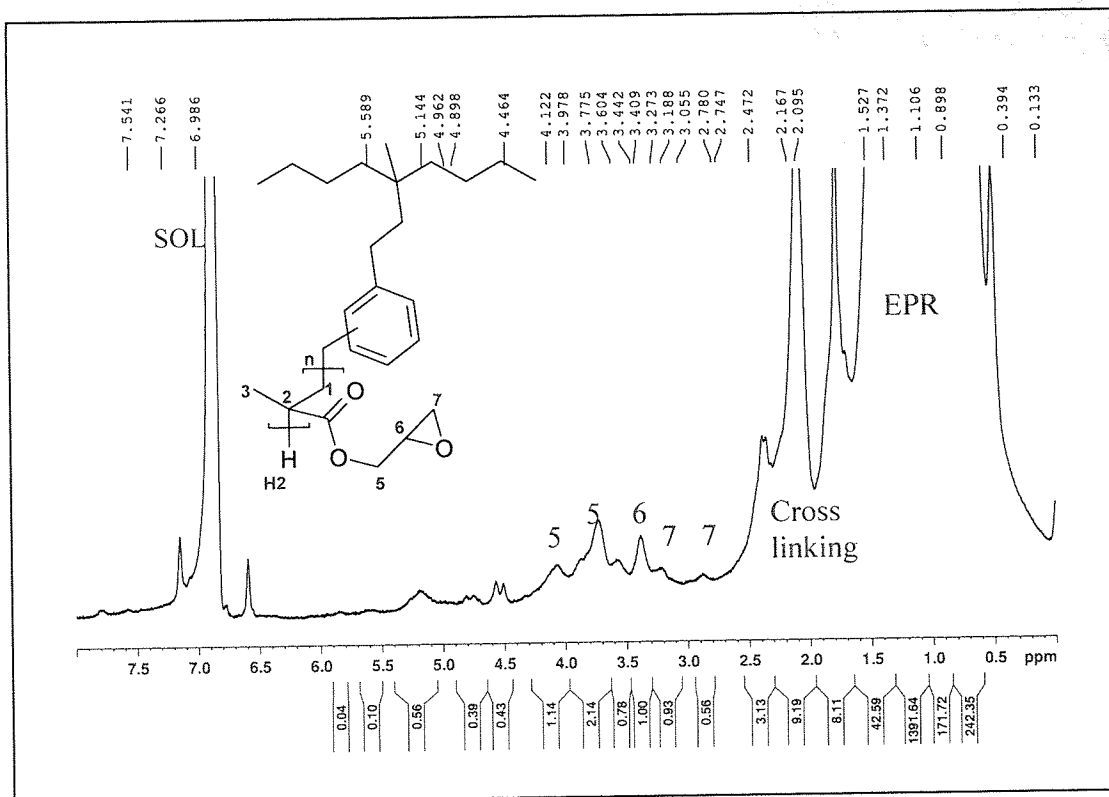


Figure 3.45: <sup>1</sup>H NMR in EPR-g-DVB, (sample DG14 in Table 3.1b) in dichlorobenzene, C<sub>6</sub>D<sub>4</sub>Cl<sub>2</sub> at 135°C. (T101= 0.13 phr, GMA= 15 phr, GMA/DVB= 9/1, 190°C), g-GMA=4.7 wt%, polyGMA=0.1%, MFI=2.1 g/10min

## CHAPTER 4

# REACTIVE COMPATIBILISATION OF PET/EPR BLENDS

### 4.1 Objective and Methodology

Research on blending of two or more polymers has received considerable attention in recent years [15, 28, 47, 51, 85, 192, 218, 219]. PET is an engineering semicrystalline plastic that has excellent properties such as high stiffness, strength and dimensional stability, as well as good chemical and electrical resistant but it also has poor impact properties which can limit some of its possible applications [13, 90]. Blending PET with other polymers especially polyolefins and elastomers has been an attractive route and cost effective way for production of new polymers with the desired mechanical and chemical properties. However, blends of polymers such as PET/polyolefins are, as would be expected, incompatible and require compatibilisation if useful properties are to be obtained. This can be achieved by, first functionalising the polyolefins or olefin elastomer polymers, for example through *in-situ* reactions with polar molecules before subsequently compatibilising the blends through interfacial reactions between the reactive functionalities of the two polymers during the blending process [28, 51]. The *in-situ* compatibilisers act to reduce the interfacial tension between the dispersed phase and the continuous matrix resulting in fine phase morphology. PET is capable of both chemical reactions with polar polymers and of specific polar interactions, like H-bonding [72, 220]. This occurs typically via the reaction of its terminal groups (carboxylic and hydroxyl (-COOH, -OH) ) which are capable for reacting with a number of functional groups (e.g anhydride, epoxy, oxazoline, isocyanate) that may be attached onto the second polymer leading to graft copolymer formation during melt blending.

The main objective of the work described in this chapter was to gain a better understanding of the effect of the comonomer DVB used in the melt grafting of GMA on EPR on the extent of compatibilisation of PET/*f*-EPR blends, compared to EPR-*g*-GMA prepared in a conventional system (without a comonomer).

The compatibilisation was achieved by reactive blending of PET with EPR-g-GMA<sub>CONV</sub> (conventional) or EPR-g-GMA<sub>DVB</sub> samples (both functionalised EPR samples were produced in work described in **Chapter 3**). The composition of the *f*-EPR used in the blend work is summarised in **Table 4.1**. The blending were carried out in a Haake batch mixer at temperature of 260 °C, see **Scheme 4.1**. The rotor speed and mixing time were fixed at 65 rpm and 10 minutes, respectively. The characteristics of the PET blends were investigated in terms of the processing torque behaviour, tensile properties, morphology (SEM after xylene etching of the rubber phase), dynamic mechanical properties and the extent of the interfacial reactions. The composition of the blend samples is presented in **Table 4.2**. The effect of structural differences in the grafted GMA (amount of g-GMA, amount of polyGMA present, the MFI of the modified rubber and the different structures of the graft, i.e. the conventional versus DVB-containing GMA grafts) on the compatibilisation of PET/EPR blends was also investigated.

**Table 4.1.** Functionalised EPR used in the blends

	Code	Compositions					Conditions Temp/ Speed/time (°C)/(rpm)/ (min)	g- GMA (%)	Poly GMA (%)	MFI g/10mi n
		GMA (phr)	DVB (phr)	T101 (phr)	GMA/ DVB	[T101]/ [GMA+ DVB] MR				
Without DVB (CONV)	G17	10	0	0.13	-	0.0038	190/65/15	1.3	0.1	3.7
	G15	10	0	0.3	-	0.0147	190/65/15	1.5	0.4	2.9
	G19	10	0	0.8	-	0.0392	190/65/15	1.7	0.6	0.9
	G20	10	0	1.5	-	0.0728	190/65/15	1.5	0.5	0
	G23	13	0	0.8	-	0.0301	190/65/15	2.5	2.0	1.0
	G24	15	0	0.8	-	0.0261	190/65/15	1.9	3.0	1.0
With DVB	DG1	10	1.1	0.017	9/1	0.0007	170/65/15	3.3	0	3.3
	DG2	10	1.1	0.039	9/1	0.0015	170/65/15	2.6	0	3.1
	DG4	10	1.1	0.13	9/1	0.0057	170/65/15	3.2	0	2.5
	DG8	10	1.1	0.13	9/1	0.0057	180/65/15	3.5	0	2.0
	DG10	10	1.1	0.017	9/1	0.0007	190/65/15	2.3	0	3.7
	DG13	10	1.1	0.13	9/1	0.0057	190/65/15	2.7	0	1.8
	DG19	10	1.1	0.017	9/1	0.0007	200/65/15	1.6	0	3.8
	DG23	10	1.1	0.13	9/1	0.0057	200/65/15	2.1	0	1.8
	DG28	10	2.5	0.078	8/2	0.0030	180/65/15	4.4	0	1.8
	DG34	10	2.5	0.003	8/2	0.0057	190/65/15	1.9	0	2.9
	DG38	10	2.5	0.017	8/2	0.0006	200/65/15	2.7	0	2.9
	DG42	10	4.3	0.017	7/3	0.0006	180/65/15	3.2	0	0.7
	DG43	10	4.3	0.017	7/3	0.0006	180/65/15	3.5	0	0.7
	DG45	10	4.3	0	7/3	0.0030	190/65/15	1.0	0	1.0
DG48	10	4.3	0.017	7/3	0.0006	190/65/15	4.9	0	0.7	

Table 4.2. PET/EPR blends composition

Code		Compositions		Blending Conditions	Feature of EPR-g-GMA components					
Blends	f-EPR	Components PET/EPR from Table 4.1	Weight ratio PET/EPR, PET/f-EPR	Temp (°C)/speed (rpm)/time (min)	g-GMA (wt%)	Poly GMA (wt%)	MFI g/10min	Remarks about EPR		
P1	PET	PET	100						Physical	
E1	EPR	EPR	100							
P91	EPR	PET/EPR	90/10	260/65/10				Virgin EPR		
P82	EPR	PET/EPR	80/20	260/65/10				Virgin EPR		
P73	EPR	PET/EPR	70/30	260/65/10				Virgin EPR		
P64	EPR	PET/EPR	60/40	260/65/10				Virgin EPR	Conv. (Without DVB)	
BG1	G17	PET/G17	70/30	260/65/10	1.3	0.1	3.7	GMA+T101		
BG2	G15	PET/G15	70/30	260/65/10	1.5	0.4	2.9	GMA+T101		
BG3 (9:1)	G19	PET/G19	90/10	260/65/10	1.7	0.6	0.9	GMA+T101		
BG3 (8:2)	G19	PET/G19	80/20	260/65/10	1.7	0.6	0.9	GMA+T101		
BG3 (7:3)	G19	PET/G19	70/30	260/65/10	1.7	0.6	0.9	GMA+T101		
BG3 (6:4)	G19	PET/G19	60/40	260/65/10	1.7	0.6	0.9	GMA+T101		
BG4	G20	PET/G20	70/30	260/65/10	1.5	0.5	0	GMA+T101		
BG5	G23	PET/G23	70/30	260/65/10	2.5	2.0	1.2	GMA+T101		
BG6-UP	G24P	PET/G24P	70/30	260/65/10	1.9	0	1	GMA+T101		
BG7-P	G24UP	PET/G24UP	70/30	260/65/10	1.9	3	1	GMA+T101		
BD1	DG19	PET/DG19	70/30	260/65/10	1.6	0	3.8	GMA+ DVB+T101		With DVB
BD2	DG1	PET/DG1	70/30	260/65/10	3.3	0	3.3	GMA+ DVB+T101		
BD3	DG8	PET/DG8	70/30	260/65/10	3.5	0	2.0	GMA+ DVB+T101		
BD4	DG4	PET/DG4	70/30	260/65/10	3.2	0	2.5	GMA+ DVB+T101		
BD5	DG13	PET/DG13	70/30	260/65/10	2.7	0	1.8	GMA+ DVB+T101		
BD6	DG23	PET/DG23	70/30	260/65/10	2.1	0	1.8	GMA+ DVB+T101		
BD7	DG45	PET/DG45	70/30	260/65/10	1.0	0	1.0	GMA+ DVB+T101		
BD8	DG48	PET/DG48	70/30	260/65/10	4.9	0	0.7	GMA+ DVB+T101		
BD9	DG42	PET/DG42	70/30	260/65/10	3.2	0	0.7	GMA+ DVB+T101		
BD10	DG34	PET/DG34	70/30	260/65/10	1.9	0	2.9	GMA+ DVB+T101		
BD11	DG28	PET/DG28	70/30	260/65/10	4.4	0	1.8	GMA+ DVB+T101		
BD12	DG38	PET/DG38	70/30	260/65/10	2.7	0	2.9	GMA+ DVB+T101		
BD13(9:1)	DG10	PET/DG10	90/10	260/65/10	2.3	0	3.7	GMA+ DVB+T101		
BD13(8:2)	DG10	PET/DG10	80/20	260/65/10	2.3	0	3.7	GMA+ DVB+T101		
BD13(7:3)	DG10	PET/DG10	70/30	260/65/10	2.3	0	3.7	GMA+ DVB+T101		
BD13(6:4)	DG10	PET/DG10	60/40	260/65/10	2.3	0	3.7	GMA+ DVB+T101		
BD14	DG43	PET/DG43	70/30	260/65/10	3.5	+2.5	0.7	GMA+ DVB+T101		
BD15-UP	DG43UP	PET/DG43UP	70/30	260/65/10	3.5	0	0.7	GMA+ DVB+T101		
BD16-P	DG43P	PET/DG43P	70/30	260/65/10	3.5	0	0.7	GMA+ DVB+T101		
BD17	DG2	PET/DG2	70/30	260/65/10	2.6	0	3.1	GMA+ DVB+T101		

UP-unpurified, P-purified, T101 was used in functionalisation work, sample BD14: 2.5% synthesised poly GMA was added

## 4.2 RESULTS

### 4.2.1 Physical Blends of PET/EPR

The torque characteristics reflect the viscosity changes during the reactive blending process. In PET/EPR physical blends, the rubber composition influences the torque-time curves behaviour. The virgin PET has the lowest viscosity (as reflected from its torque characterisation) compared to that of EPR and the physical blends, see **Figure 4.1**. Addition of increasing amounts of rubber results in an increased final torque values, **Figure 4.1B**. Since no interfacial reaction is expected in PET/EPR physical blends, the increase in torque of these blends must be due to the higher viscosity of the EPR phase. The tensile strength and elongation at break values of the physical blends were found to decrease with increasing the rubber content, see **Figure 4.2** and **Table 4.3**.

**Table 4.3.** Elongation at break of physical blends (see **Figure 4.2**)

Samples Code	PET/EPR w/w%	Tensile strength at yield (MPa)	Elongation at break (%)
P91	90/10	39.3 ± 3.2	7.5 ± 0.4
P82	80/20	36.8 ± 2.7	6.5 ± 1.1
P73	70/30	22.2 ± 1.7	4.7 ± 0.4
P64	60/40	12.5 ± 1.5	4.4 ± 0.9

The morphological characteristics obtained from scanning electron microscopy (SEM) of these physical blends reflect their incompatibility, see **Figure 4.3**, showing typical morphology of immiscible blends characterised by very large, coarse and irregular domains. It is also clear that the particles size of the dispersed EPR phase increases with increasing amounts of EPR in the blends and the shape of the holes (the holes are where the rubber phase was etched with xylene before the SEM analysis) is round and clean indicating that the particles are easily pulled out, because of poor adhesion between the two phases.

The dynamic mechanical properties of the physical blends including those of the virgin PET and EPR were also determined. The storage modulus ( $E'$ ), and  $\tan \delta$  were measured from  $-80^{\circ}\text{C}$  to  $180^{\circ}\text{C}$ . The glass transition temperature ( $T_g$ ) of the blends was determined from the  $\tan \delta$  peak. **Figure 4.4** shows the  $\tan \delta$ -temperature and storage modulus ( $E'$ )- temperature curves of these blends. The two  $\tan \delta$  peaks shown in the thermograph of the physical blend (70/30 w/w %) correspond to the glass transition temperatures of EPR and PET. It can be seen clearly (**Figure 4.4**, **Table 4.4**) that the peak corresponding to the virgin EPR is broader and higher compared to the peak of the EPR phase in the PET/EPR blend, see **Figure 4.4C**. The  $\tan \delta$  of EPR phase in the blends has shifted to lower temperature with respect to that of the virgin EPR. For the pure PET, the glass transition temperature was measured at  $92.8^{\circ}\text{C}$ .

The effect of the blend composition on  $\tan \delta$  is shown in **Figure 4.5** and **Table 4.5**. It is clear that the size and height of the rubber phase peak changes proportionately to the rubber content in the blends. As the rubber content increases, the  $\tan \delta$  of the rubber

phase shifts to higher temperature closer to that of the virgin EPR. Similarly, the  $\tan \delta$  of the PET phase decreases with increased PET content (i.e shifts closer to that of virgin PET) but overall the blend composition has lower effect on the  $\tan \delta$  of the PET phase, compared to that of the rubber phase. Only one peak was observed in the PET/EPR 50/50 w/w % blend which corresponded to the EPR phase; the glass transition of the PET phase could not be measured [28]. The storage modulus of the PET/EPR blends was also strongly influenced by the rubber composition. Its value at 25°C decreased steadily (closer to that of virgin EPR) with increasing the rubber content. The storage modulus of the blends dropped drastically above the glass transition of EPR between -40°C to -20°C, see **Figure 4.6** and **Table 4.4**. The high modulus of PET, (see **Figure 4.4D**) in this region confirms that PET is a tough material and this is also reported in the literature [28].

**Table 4.4.** Effect of blend composition of physical PET/EPR blends on dynamic mechanical properties, (see also **Figures 4.5** and **4.6**)

Physical Blends (PET/EPR)		EPR Phase		PET phase		E' (Pa) at 25°C
Code	PET/EPR w/w%	T <sub>g</sub> (°C)	Shift(°C)	T <sub>g</sub> (°C)	Shift(°C)	
Virgin polymer	-	-35	-	92.8	-	-
P91	90/10	-45.3	-	95	-	2.40x10 <sup>8</sup>
P82	80/20	-43.6	-	94.2	-	2.00 x10 <sup>8</sup>
P73	70/30	-42.4	-	93.8	-	1.20 x10 <sup>8</sup>
P64	60/40	-40.6	-	92.1	-	9.50 x10 <sup>7</sup>

## 4.2.2 PET/EPR-g-GMA<sub>CONV</sub> (without comonomer)

### 4.2.2.1 Effect of Grafting level on Torque Characteristics

To improve the blends compatibility, *in-situ* reactive blending of PET and the GMA-functionalised EPR (*f*-EPR<sub>CONV</sub>), (conventional, i.e. no comonomer) was carried out. The effect of the grafting level on the torque characteristics of the compatibilised PET/EPR-g-GMA<sub>CONV</sub> blends was investigated. **Figure 4.7A** presents the torque-time curves of PET/*f*-EPR<sub>CONV</sub> 70/30 w/w% blends in which the *f*-EPR<sub>CONV</sub> contained various GMA grafting levels. The torque-time curves of all PET/EPR-g-GMA<sub>CONV</sub> blends regardless of the grafting level increased initially sharply and after a couple of

minutes decreased and then levelled off due to melting of the polymers. The final torque of the blends is seen to be strongly influenced by the MFI values of the functionalised rubber phase (*f*-EPR), see **Figure 4.7B**. The increase in the final torque of the blends with increasing amount of *g*-GMA<sub>CONV</sub> is paralleled by a decrease in MFI values of EPR-*g*-GMA<sub>CONV</sub> indicating that the samples have higher molecular weight giving rise to an increase in the viscosity of the blends. The torque of virgin EPR is seen to be much higher than that of virgin PET. At low MFI values of functionalised EPR (e.g. 0.9 g/10min), the final torque of the blends increased dramatically to well above the final torque value of the virgin EPR.

#### 4.2.2.2 Mechanical Properties of Reactive PET/EPR-*g*-GMA<sub>CONV</sub> Blends

The stress-strain curves of virgin PET and virgin EPR are shown in **Figures 4.8A** and **4.8B** respectively. It was found that the modulus and tensile strength of virgin PET was very high, up to 100 MPa, and the elongation at break was measured at 80 %, characteristics of a semicrystalline polymer [90]. The high modulus measured in the virgin PET sample indicates that the polymer has high strength and stiffness. In contrast, EPR shows very high elongation at break but low overall strength illustrating typical properties of an elastomeric material. **Figure 4.8C** compares the tensile strength curves of reactive PET/EPR-*g*-GMA<sub>CONV</sub> with that of the corresponding physical PET/EPR blend at 70/30 w/w %, shows clearly that the elongation at break values of the reactive blends are much higher than that of the corresponding physical blend.

A series of EPR-*g*-GMA<sub>CONV</sub> samples which contained various grafting levels were blended with PET at a ratio of 70/30 w/w %. **Figure 4.9** and **Table 4.5** show clearly that elongation at break of these blends increased with increasing the GMA grafting level with a maximum value achieved at a grafting level of 1.5 wt %. Further increase in grafting value to 1.7 wt %, results in no further increase in elongation at break. A significant decrease in elongation at break was observed however, at a grafting level of 1.9 wt % and this is shown to be paralleled by a sharp increase in the amount of poly-GMA (3 wt %) present in the *f*-EPR phase of the blend, see **Figure 4.9** (a polyGMA concentration below 1 wt%, no substantial effect was observed on the tensile properties of the blends).

**Table 4.5.** Elongation at break of PET/EPR-g-GMA<sub>CONV</sub> 70/30 w/w% blends at various GMA content (see **Figure 4.9**)

Samples Code	g-GMA wt-%	polyGMA wt%	Tensile strength at yield (MPa)	Elongation at break (%)
P73 (Physical blend)	-	-	22.2 ± 1.7	4.7 ± 0.4
BG1	1.3	0.1	39.3 ± 3.2	7.5 ± 0.4
BG2	1.5	0.4	36.8 ± 2.7	6.5 ± 1.1
BG3(7:3)	1.7	0.6	22.2 ± 1.7	4.7 ± 0.4
BG4	1.9	3	12.5 ± 1.5	4.4 ± 0.9

**i) Morphology Observation**

Examination of the SEM micrographs of these PET/*f*-EPR<sub>CONV</sub> blend samples revealed that the GMA grafting level has a major influence on their morphology, see **Figure 4.10**. Compared to the physical blends, the morphology of all compatibilised PET/*f*-EPR blends became more stable and the size of the dispersed rubber particles was much finer, with the blend containing a grafting level of 1.5 wt% showing the smallest particle size suggesting that this grafting level in this series of blends gives rise to the best compatibilising effect. This is supported by the improvement observed in mechanical properties (e.g. elongation at break), see **Figure 4.9**. At higher GMA grafting level (1.9 wt%), the morphology became unstable and inhomogeneous with the dispersed rubber particles becoming much larger and coarser (large holes), see **Figure 4.10E**.

**ii) Dynamic Mechanical Analysis (DMA)**

To get better understanding of the effect of grafting level on PET/EPR-g-GMA<sub>CONV</sub> 70/30 w/w % samples, blends containing different GMA grafting levels were prepared for dynamic mechanical properties analysis. The  $\tan \delta$  and storage modulus as a function of temperature for both PET and EPR phases in these blends are shown in **Figure 4.11A-D** (see also **Table 4.6**). Two peaks corresponding to the glass transition temperatures ( $T_g$ ) of PET and EPR phases were observed with the position of  $\tan \delta$  corresponding to the  $T_g$  of PET phase or *f*-EPR<sub>CONV</sub> phase having shifted to a certain extent. The  $T_g$  of PET phase in the physical blend was recorded at 93.8°C. All the  $T_g$ s of PET in PET/EPR-g-GMA<sub>CONV</sub> blends shifted towards the temperature of the EPR



phase with the  $T_g$  of the sample containing grafting level of 1.5 wt% showing the largest shift at about 7°C compared to the  $T_g$  of PET in the physical blend.

The storage modulus ( $E'$ ) curves of the PET/EPR-g-GMA<sub>CONV</sub> are shown in **Figure 4.11E** and **4.11F**. The samples of PET/EPR-g-GMA<sub>CONV</sub> containing 1.3 wt% and 1.5 wt% grafted GMA gave the lowest  $E'$  values measured at temperature of 25°C. Whereas an increase in grafting level to 1.7 wt% resulted in an increase in modulus approaching the value of the physical blend. The lower value of  $E'$  for the sample PET/EPR-g-GMA<sub>CONV</sub> containing lower grafting level (e.g 1.5 wt%) is most likely to be due to the elastomeric effect of the rubber component which changes the blend properties to becoming more rubbery. For the sample containing higher grafting level of 1.7 wt%, the higher  $E'$  values, which is similar to that of the physical blend, may be due to the effect of the rubber component on the blend properties due to low compatibility between the two components. The higher elongation at break obtained for PET/EPR-g-GMA<sub>CONV</sub> containing 1.5 wt % (sample **BG2** in **Table 4.1**) support the suggestion that this sample of PET/EPR-g-GMA<sub>CONV</sub> has more rubbery influence on its properties compared to the other samples chosen in this series, see **Figure 4.9**.

**Table 4.6.** Effect of MFI values on dynamic mechanical properties of PET/EPR-g-GMA<sub>CONV</sub> 70/30 w/w % blends, (see also **Figure 4.11**); shifts are relative to values of physical blend

Blend ratio PET/EPR (or PETEPR-g-GMA)		MFI of rubber (g/10min)	g-GMA (%)	PET/EPR-g-GMA <sub>CONV</sub>				$E'$ (MPa) at 25°C
				EPT Phase		PET phase		
				$T_g$ (°C)	Shift (°C)	$T_g$ (°C)	Shift (°C)	
Physical blend	P73	4.9	0	-43.2	-	93.8	-	171
Reactive blends	BG1	3.8	1.3	-43.9	0.7-	88.6	-5.2	146
	BG2	2.9	1.5	-43.1	0.1+	84.5	-9.3	146
	BG3(7:3)	0.9	1.7	-45.3	2.1-	87.5	-6.3	169

#### 4.2.2.3 Effect of polyGMA on PET/EPR-g-GMA<sub>CONV</sub> Blends

Formation of polyGMA always accompanies the melt grafting process giving rise to a decrease in the grafting level, see **Chapter 3, Sec. 3.2.4, p.85**. It is important to investigate the effect of polyGMA on the blend characteristics. A sample of  $f$ -EPR<sub>CONV</sub>

containing 3 wt% polyGMA (sample **G24** in **Table 4.1**) was used for blending with PET. To get a better understanding of the effect of polyGMA on the blend properties, part of the same *f*-EPR sample was purified with excess acetone in order to eliminate all the formed polyGMA. Both unpurified samples (*f*-EPR<sub>CONV-UP</sub>) and purified sample (*f*-EPR<sub>CONV-P</sub>) were then blended with PET at 70/30 w/w % ratio. The torque curve for the blend containing the unpurified *f*-EPR (PET/*f*-EPR<sub>CONV-UP</sub>) was higher than that of the purified (PET/*f*-EPR<sub>CONV-P</sub>) sample, see **Figure 4.12A**. Al-Malaika *et.al* [28] showed that the presence of polyGMA in reactive PET blends could cause branching and increase in the viscosity of the PET blend, and this may also be responsible for the observed increase in the torque of the sample PET/*f*-EPR<sub>CONV-UP</sub> sample which contained 3.0 wt% polyGMA.

#### **4.2.2.4 Effect of PET/EPR-g-GMA<sub>CONV</sub> Blend Composition on Torque Characteristics, Mechanical Properties and Morphology**

The torque values PET/EPR-g-GMA<sub>CONV</sub> blends at 80/20 and 70/30 w/w % were found to be higher than that of the pure EPR, but a further increase in the *f*-EPR<sub>CONV</sub> content up to 40 w% (in 60/40 w/w % blends) gave a decrease in torque values below those of the molten virgin EPR, see **Figure 4.13A**. Examination of the mechanical properties shows that the tensile strength and elongation at break of all PET/*f*-EPR<sub>CONV</sub> (compatibilised) blends are higher than those of the corresponding physical blends having the same sample composition, see **Figures 4.13B, 4.13C** and **Table 4.7**. It is also clear that the effect of the rubber content is to decrease the tensile strength and increase elongation at break with the highest value obtained for blend composition of 70/30 w/w % (a further increase in the rubber phase content up to 40% results in a lowering of the elongation at break).

**Table 4.7.** Tensile and elongation at break of PET/EPR-g-GMA<sub>CONV</sub> blends at various blend ratios (see **Figure 4.13**)

Samples Code	PET/EPR-g-GMA <sub>CONV</sub> w/w%	Elongation at break (%)
BG3 (9:1)	90/10	11.5 ± 0.9
BG3 (8:2)	80/20	13.6 ± 0.9
BG3 (7:3)	70/30	15.4 ± 0.3
BG3(6:4)	60/40	13.0 ± 1.6

† 'yeild' – measured at maximum tensile strength as some sample did not show a true yield point.

The effect of the conventional PET/EPR-g-GMA<sub>CONV</sub> blend composition on their morphology was investigated by examining the dispersion behaviour of the rubber phase in the PET matrix. The morphology seen from the SEM of these reactive (conventional) blends, **Figure 4.14** shows that increasing the rubber content in the composition gives rise to an increase the EPR particles size with the 90/10 w/w % blend giving the smallest particle size but this is still much finer than in the case of the physical blends. Similar observations were reported in other blends [221].

The effect of blend compositions on dynamic mechanical properties is shown in **Figure 4.15** and **Table 4.8**. At below the  $T_g$  of EPR (below  $-60^\circ\text{C}$ ), the modulus of all samples was high indicating stiffness of blends containing lower rubber phase. The storage modulus dropped drastically in the glass transition region between  $-50^\circ\text{C}$  to  $-20^\circ\text{C}$ . The rubbery state was maintained from  $-20^\circ\text{C}$  to  $80^\circ\text{C}$ . The effect of blend composition on storage modulus at  $25^\circ\text{C}$  was determined and at blends ratio of 90/10 w/w %, it was 253 MPa. This value dropped to 117 MPa as the composition of EPR increased to 60/40 w/w %. The drop in  $E'$  occurred when the amount of rubber component increased due to softening of the EPR phase in the blends.

**Table 4.8.** Effect of blend compositions on dynamic mechanical properties of PET/EPR-g-GMA<sub>CONV</sub> blends. The shift is with respect to values of the corresponding physical blends

Blend Ratio PET/ f-EPR	PET	f-EPR	Physical Blends		PET/EPR-g-GMA <sub>CONV</sub>				E' (MPa) at 25°C
			EPR Phase T <sub>g</sub> (°C)	PET phase T <sub>g</sub> (°C)	EPR Phase		PET phase		
					T <sub>g</sub> (°C)	Shift (°C)	T <sub>g</sub> (°C)	Shift (°C)	
BG3 (9:1)	90	10	-45.3	95	-46.1	-0.8	91.7	-3.3	253
BG3 (8:2)	80	20	-43.6	94.2	-43.8	-0.2	90.4	-3.8	202
BG3 (7:3)	70	30	-42.4	93.8	-45.3	-2.9	86.1	-7.7	134
BG3 (6:4)	60	40	-40.6	92.1	-42.6	-2.0	82.6	-9.5	117

### 4.2.3 PET/EPR-g-GMA<sub>DVB</sub> Blends (with comonomer)

#### i) Grafting level

The effect of the grafting level on torque behaviour of PET/EPR-g-GMA<sub>DVB</sub> (70/30 w/w %) blends using samples containing different extent of GMA grafting, (grafted in presence of DVB e.g. 2.1 wt%, 2.7 wt%, 3.5 wt%) and having similar MFI values was examined. **Figure 4.16** shows that the torque values of these blends increased with increasing the grafting level to a final torque value above that of EPR at the highest GMA grafting level, see **Figure 4.16B**.

In phase separated systems, the mechanical properties especially elongation at break are very sensitive to interface adhesion or partial miscibility at the interface of blend components [222]. The very strong adhesion necessary from efficient stress transfer is usually achieved by chemical coupling of the second phase with the polymer matrix [223]. The influence of the grafting level on the mechanical properties of PET/EPR-g-GMA<sub>DVB</sub> particularly the elongation at break is shown in **Figures 4.16 C** and **4.16D** and **Table 4.9** where a grafting level of 2.1 wt% gave rise to the highest elongation at break but a further increase in the grafting level resulted in a decrease in the elongation at break. This suggests that grafting levels above a certain extent may not be efficient in compatibilising the PET blends with EPR-g-GMA<sub>DVB</sub>. Similar influence of the grafting level on the tensile properties of PET/EPDM-g-GMA blends was reported [51] where a moderate grafting level resulted in the best tensile properties. The observed increase in the elongation at break at grafting level of 2.1 wt% was associated with a very fine

dispersed rubber particles and stable morphology, see **Figure 4.17B**, but with a further increase in extent of GMA grafting is clearly shown not to result in any further reduction in the size of the EPR particles any further, see **Figure 4.17D**. As shown in **Figure 4.18** the grafting level 2.1 to 2.6 wt % seem to be very effective in enhancing the elongation at break for PET/EPR-g-GMA<sub>DVB</sub> blends which is much higher than that of the maximum values achieved in the conventional system.

**Table 4.9.** Tensile and elongation at break of PET/EPR-g-GMA<sub>DVB</sub> blends 70/30 w/w% at various blend ratios (see **Figure 4.16**)

Samples Code	g-GMA wt %	polyGMA wt%	Elongation at break (%)
P73 (Physical blend)	-	-	4.74 ± 0.4
BD6	2.1	0	21.3 ± 1.6
BD5	2.7	0	17.3 ± 1.4
BD3	3.5	0	17.4 ± 1.4

The dynamic mechanical properties of these blends are shown in **Figure 4.19** and **Table 4.10**. The  $\tan \delta$  values of PET phase and EPR phases were measured in the temperature range of  $-80^{\circ}\text{C}$  to  $180^{\circ}\text{C}$ . At a grafting level of 2.1 wt%, the  $\tan \delta$  value of the PET phase has shown a significant shift to a lower temperature moving towards that of the EPR phase, and similarly, the  $T_g$  of the EPR phase in this blend has shifted towards the PET phase. A further increase in the grafting level to 3.5 wt% resulted in a smaller difference in the  $\tan \delta$  values compared to values of the physical blend.

**Table 4.10.** Effect of grafting level on dynamic mechanical properties of PET/*f*-EPR<sub>DVB</sub> blends. The shift is with respect to values of the corresponding physical blend, (see also **Figure 4.19**).

Blend ratio PET/EPR (or PET/EPR-g-GMA)		MEI of rubber (g/10min)	g-GMA (%)	PET/EPR-g-GMA <sub>DVB</sub>				E' (MPa) at 25°C
				EPR Phase		PET phase		
				$T_g$ (°C)	Shift (°C)	$T_g$ (°C)	Shift (°C)	
Physical blend	BP73	-	0	-43.2	-	93.8	-	171
Reactive blends	BD6	1.8	2.1	-42.7	+0.5	89.6	-4.2	114
	BD5	1.8	2.7	-44.1	-0.9	91.5	-2.3	144
	BD3	2.0	3.5	-44.0	-0.8	91.3	-2.5	138

This blend having grafting level of 2.1 wt% also showed the lowest  $E'$  value indicating that the sample was more rubbery. This is in agreement with the observation that this sample also gave the highest elongation at break, see **Figure 4.16C**. It was shown earlier, (see **Chapter 3, Sec 3.2.5, p.87**) that the functionalised ( $f$ -EPR<sub>DVB</sub>) rubber contains very low or no polyGMA. However, other undesired side reaction products such as polyDVB, copolymer DVB-co-GMA or crosslinked polymer gel could be formed in the rubber sample. To determine the effect of these products on the blend properties, an EPR-g-GMA<sub>DVB</sub> rubber sample which was functionalised with GMA/DVB at a ratio of 7/3 w/w % and had a grafting level of 3.5 wt% was blended with PET (PET/EPR-g-GMA<sub>DVB</sub> 70/30 w/w %). Half of the  $f$ -EPR sample was purified by Soxhlet extraction to remove the undesired side reaction products (polyGMA, polyDVB, DVB-co-GMA and gel content) and this purified GMA-grafted rubber sample was then blended with PET (PET/EPR-g-GMA<sub>DVB-P</sub>). Close examination of the torque-time curves shown in **Figure 4.20A** reveals that at the early stages of mixing, the torque of the blend containing purified rubber is slightly lower than that of the corresponding blend sample containing unpurified rubber, but reached the same value at the end of the blending process. However, when a 2.5 wt% of a synthesised polyGMA was added during the reactive blending to the PET/EPR-g-GMA<sub>DVB-UP</sub> blend, the torque was found to be much higher. Furthermore, the purified blend sample containing added synthesised polyGMA showed a substantial decrease in its elongation and tensile strength compared to the corresponding samples (both purified and unpurified) without polyGMA, see **Figure 4.20B** and **4.20C**. These results suggest that the presence of polyGMA affect the polymer blends compatibility, resulting in the observed poor mechanical properties (similar observation was reported in other blend systems) [96]. This is further supported by examining the morphology of the sample containing added polyGMA, see **Figure 4.21C**, which shows a much larger particles size and inhomogeneous morphology compared to the corresponding blends containing no polyGMA.

#### ii) Blend ratio

To study the effect of blend composition on the torque behaviour, PET was reactively blended with EPR-g-GMA<sub>DVB</sub> (rubber sample **DG10, Table 4.1**). Increasing the rubber content in the blends gave rise to a gradual increase in the torque above the value of the

pure PET and those of the corresponding physical blends, see **Figure 4.22A** and **4.22B**. Similar trends were observed in mechanical properties of PET/EPR-g-GMA<sub>DVB</sub> blends, whereby the tensile strength decreased with decreasing the amount of PET in the blends, see **Figure 4.22C** and is almost certainly associated with the crystallinity of PET. Similar effect of crystallinity on tensile properties in blend of PP/EPR [224] and PET/PE-g-GMA [86] were reported. Similarly, the elongation at break of these blends increased with increasing EPR content with a composition of 70/30 giving the highest value, **Figure 4.22D**, **Table 4.11**. Similar behaviour was observed in binary blends of PP/EPR-g-GMA containing more than 60 % EPR where the mechanical properties of the blends decreased significantly [224].

**Table 4.11:** Tensile strength and elongation at break of DVB containing blend at various blend ratios, see **Figure 4.22**.

Samples Code	PET/EPR-g-GMA <sub>DVB</sub> w/w%	Elongation at break (%)
BD13 (9:1)	90/10	13.2 ± 1.5
BD13 (8:2)	80/20	21.2 ± 1.2
BD13 (7:3)	70/30	22.7 ± 0.3
BD13 (6:4)	60/40	21.5 ± 1.6

The morphology of the different blend ratios of PET/EPR-g-GMA<sub>DVB</sub> is shown in **Figure 4.23**. The size of the dispersed phase rubber particles is shown to increase with increasing the rubber content in the blends but in all cases the particle size in the reactive PET/EPR-g-GMA<sub>DVB</sub> blends, which is strongly influenced by the blend composition, are much smaller than in the corresponding physical blends.

The effect of the blend composition on the dynamic mechanical properties was also examined, see **Table 4.12** and **Figure 4.24**. Two peaks appeared at temperature between  $-50^{\circ}\text{C}$  to  $-20^{\circ}\text{C}$  and  $70^{\circ}\text{C}$  to  $100^{\circ}\text{C}$  corresponding to EPR phase and PET phase respectively. At a blend composition of PET/EPR-g-GMA 90/10 w/w %, the  $\tan \delta$  of PET was  $92.9^{\circ}\text{C}$  and the  $\tan \delta$  shifted to lower temperature of  $87.7^{\circ}\text{C}$  when the EPR content increased to 60/40 w/w %. The increase of EPR content in the composition of the blends was paralleled by an increase in peaks heights. Investigation of  $E'$  as a

function of blend composition shows that at temperature of 25°C, there is a decrease in  $E'$  values with increasing the rubber content.

**Table 4.12.** Effect of blend composition on dynamic mechanical properties of PET/EPR-g-GMA<sub>DVB</sub> blends. The shift is with respect to values of the corresponding physical blend, (see also **Figure 4.24**)

Blend Ratio PET/ f-EPR	Blend Ratio		Physical Blends		PET/EPR-g-GMA <sub>CONV</sub>				$E'$ (MPa) at 25°C
	PET w %	EPR w %	EPR Phase	PET phase	EPR Phase		PET phase		
					$T_g$ (°C)	Shift (°C)	$T_g$ (°C)	Shift (°C)	
BD13 (9:1)	90	10	-45.3	95	-45	+0.3	92.8	-2.2	253
BD13 (8:2)	80	20	-43.6	94.2	-44.2	-0.6	92.2	-2.0	177
BD13 (7:3)	70	30	-42.4	93.8	-43.0	-0.6	87.6	-6.2	120
BD13 (6:4)	60	40	-40.6	92.1	-41.2	-0.6	86.8	-5.3	106

### iii) DVB Concentration

The effect of DVB concentration used for functionalisation of EPR on tensile properties of PET/f-EPR<sub>DVB</sub> blends was determined. As discussed in **Chapter 3**, the presence of the comonomer gives rise to a significant improvement in the GMA grafting level. Moreover, the grafting degree was shown to increase with increasing the DVB concentration and a GMA/DVB ratio of 7/3 w/w % gave the highest grafting level, (see **Chapter 3, Sec 3.2.5, p87**). In order to examine the effect of the DVB concentration on the tensile properties, binary blends PET/EPR-g-GMA<sub>DVB</sub> (70/30 w/w%) having the best tensile properties in each series of samples containing different DVB concentration are compared. **Figure 4.25** shows that PET/f-EPR<sub>DVB</sub> blend with GMA/DVB ratio of 9/1 w/w % gave the highest elongation at break but the elongation decreased slightly with further increase in the DVB concentration. Furthermore, PET/EPR-g-GMA<sub>DVB</sub> blends prepared in the presence of DVB displayed higher elongation at break compared to a corresponding conventional blend.

## 4.2.4 Solubility Test (Molau Test)

It was suggested [28, 44, 75] that the Molau solubility test could be used to qualitatively test for the graft formation due to an *in-situ* copolymerisation reaction between functional groups of the polymer components in the blends that occur during the



reactive blending process. A mixture of phenol and tetrachloroethane was prepared in a 60:40 weight ratio in which the virgin PET was completely soluble and the EPR was not. Three samples of virgin PET, non-reactive (physical) PET/EPR at 80/20, 70/30 w/w% and reactive blends of PET/EPR-g-GMA<sub>DVB</sub> at 80/20, 70/30 w/w% were prepared for the solubility test. In each case, 0.5g fine granular sample was added to the solvent mixture for 4 hours at temperature of 90°C with continuous stirring.

**Table 4.13** summarises the observation made during the solubility test. It was observed that PET had completely dissolved in the solvent mixture. For the non reactive physical blends, a slightly milky solution formed with white flakes that floated on top of the solution. This demonstrated that the PET phase, which formed as the continuous phase in this case, had dissolved in the mixture of solvents whereas the EPR formed white flakes floating on top of the solvent mixture suggesting that the EPR remained as an insoluble separate phase. For the reactive blends of PET/EPR-g-GMA<sub>DVB</sub>, a white milky colloidal suspension was observed which had completely dissolved with no floating flakes confirming the formation of a reactive copolymer at the interphase. Unfortunately, the effect of blend composition on the degree of solubility during the test could not be determined accurately due to the absence of a quantitative turbidity test.

**Table 4.13.** Solubility test according to Molau test in a mixture of solvents (phenol/tetrachloroethene) 60/40 w/w%. Samples P73, BD2, (g-GMA=3.3 wt%, MFI=3.3 g/10min) in **Table 4.2**.

Samples		Observation
Virgin polymer	PET and EPR	Sample soluble in the solvents
Physical blend	Non-reactive (physical) blends of PET/EPR 80/20 w/w%	Sample partially soluble. Flake floating on the top of the solvent mixture
	Non-reactive blends of PET/EPR 70/30 w/w%	Sample partially soluble. Flakes floating on the top of the solvent mixture
Reactive blends (GMA+DVB)	Reactive blends of PET/EPR-g-GMA <sub>DVB</sub> 70/30 w/w%	White milky and colloidal suspension formed. No flakes were observed
	Reactive blends of PET/EPR-g-GMA <sub>DVB</sub> 80/20 w/w %	White milky and colloidal suspension formed. No flakes were observed

### 4.3 Discussion

#### 4.3.1 Effect of Grafting Level on Blend Properties

Blending PET with EPR and functionalised EPR (*f*-EPR) was carried out. Functionalised EPR samples were first prepared both in the presence of a highly reactive comonomer (DVB) and in the absence of the comonomer as described in **Chapter 3**. The effects of the amount of grafted GMA, DVB concentration and the microstructure on properties of EPR-g-GMA<sub>DVB</sub> blends were compared with those of the corresponding EPR-g-GMA<sub>CONV</sub> (in the absence of DVB) blend properties. Processing behaviour was characterised by examining the torque values as it is related to the viscosity of the blends [89]. Higher melt viscosity of the reactive PET/EPR-g-GMA<sub>DVB</sub> 70/30 w/w % blends compared to the corresponding physical blend was demonstrated by an increase in their torque values, see **Figures 4.16A** and **4.16B**. By increasing the GMA grafting level in EPR-g-GMA<sub>DVB</sub> from 2.1 to 3.5 wt%, a steady increase in final torque values of the reactive blends was observed approaching and exceeding that of the virgin EPR, see **Figure 4.26A**. Similar observation was also made for the final torque values of PET/EPR-g-GMA<sub>CONV</sub> 70/30 w/w% blend which also increased steadily with increasing the grafting levels, see **Figure 4.26A**. This may be either due to an increase in the extent of interfacial reaction or/and due to branching via a reaction between the PET end groups and the higher concentration of the epoxy moiety present in EPR-g-GMA<sub>DVB</sub> containing highest amount of grafted GMA. Similar observation was reported in the literature where higher GMA content (of 8 wt %) in PBT/ABS-g-GMA gave highest torque values compared to those with lower GMA content in the same blend composition [89, 97, 225].

It has been shown (**Chapter 3. Sec. 3.2.4, p.85.** and **Figure 4.26B**) that grafting GMA onto EPR in the conventional system required higher concentration of peroxide (to achieve high grafting level), compared to the comonomer system. This will inevitably give rise to some branching and crosslinking of the rubber which is associated with the higher torque observed in the absence of DVB, see **Figure 4.26B**. As a result, the MFI values of EPR-g-GMA<sub>CONV</sub> reduced drastically with increasing level of GMA grafting compared to the value of virgin EPR, see **Figure 4.26C**. In contrast, only small peroxide concentration was required in the comonomer system, hence the MFI values of EPR-g-GMA<sub>DVB</sub> remained almost unchanged with increasing grafted GMA level. However, the

overall low MFI values in the comonomer system may be due to some DVB-assisted branching of the rubber due to the bifunctionality of DVB. The differences in the ultimate blend properties, tensile properties and morphology, would therefore be due to differences in the microstructure of the EPR-g-GMA<sub>CONV</sub> and EPR-g-GMA<sub>DVB</sub>. The results suggest that conventional blends have lower extent of interfacial reaction supported by both the observed morphology which shows larger dispersed rubber particles (compared to that of comonomer system), see **Figures 4.27A-C**, and the observed lower elongation at break, see **Figures 4.27D**. Therefore, this suggests that the significant increase in torque observed in the PET/EPR-g-GMA<sub>CONV</sub> containing 1.7 wt% GMA grafting degree (see **Figure 4.26A**) is most likely to be due to high viscosity of the rubber phase as shown in its lower MFI value rather than to a high interfacial reaction whereas the high torque values at higher grafted GMA (e.g. at 2.1 wt%) in the DVB system, (see **Figure 4.26A**) must be due, at least in part, to increased extent of interfacial reaction.

Examination of the SEM results demonstrates that the shape and domain size of the rubber phase is controlled by the GMA grafting level, see **Figure 4.28**. Different phase morphology can be observed showing that the domain size became larger with an uneven distribution at levels higher than 2.1 wt % GMA grafting level in the EPR-g-GMA<sub>DVB</sub> blends. At grafting level of 2.1 wt % in the DVB-containing blend, the SEM showed a very fine and uniform distribution of the dispersed rubber particles when compared to higher grafting levels (e.g. at 2.7 and 3.5 wt %), see **Figures 4.28A-C**. Unfavourable morphology obtained in EPR-g-GMA<sub>DVB</sub> blends having higher grafting levels is most likely due to branching and cross-linking resulting from reactions of the higher extent of epoxy rings of the GMA (present at higher grafted GMA level) with both the hydroxyl and the carboxyl end groups of PET [226]. The occurrence of the branching in these blends is supported by the higher torque values observed for example for the blend containing 3.5 wt% grafted GMA compared to that having lower grafting levels, see **Figure 4.26A**.

Changes in the mechanical properties were consistent with morphology observations for these samples. **Figure 4.18A** shows that maximum elongation at break is observed for the EPR-g-GMA<sub>DVB</sub> blend having GMA grafting level of 2.1 wt%, while at higher

grafting levels (e.g. 2.7 wt %), the elongation at break decreased. These results suggest that the significant improvement observed in the phase morphology, which suggests good interfacial adhesion, is responsible for the higher elongation at break for blends containing lower grafting levels of 2.1 wt % and this seems to be the critical optimum concentration of grafted GMA in the DVB-containing blends [226].

To obtain a better understanding of the effect of GMA on the interfacial reaction in the reactive blends, the PET and EPR phases were separated from both reactive blends (conventional containing 1.7 wt % g-GMA, and DVB system containing different concentrations of g-GMA) and physical (70/30 w/w%) blend by a sequential solvent extraction method capable of separating the individual phases of the blends [28], see **Chapter 2, Sec. 2.4, p. 36** and **Scheme 4.2**.

**Figure 4.29** which shows IR spectral region for the separated EPR fractions from reactive and physical blends (see **Figures 4.29iiB** and **C**), see also separated PET fraction, **Figure 29iiA**) provides clear evidence of the formation of interfacial reaction in the reactive blends, shown by the presence of PET absorptions in the separated EPR fraction (e.g. at 872 and 1263  $\text{cm}^{-1}$ ) due to formation of EPR-g-PET copolymer at the interphase compared to the complete absence of such PET absorptions in the separated EPR fraction of the physical blend due to the absence of any interfacial reaction in this blend. This figure (**Figures 4.29iiD** and **E**) further shows that the extent of the interfacial reaction (quantified from measurement of normalised IR absorptions, see **Chapter 2, Eqn 2.3. in Sec. 2.4, p.36**), is higher in the DVB blends containing the optimum g-GMA concentration of 2.1 wt % compared to the conventional blend containing its optimum g-GMA concentration of 1.7 wt%. This confirms that the DVB-containing blend is compatibilised to a higher extent compared to the 'best' conventional blend system (with 1.7 wt% g-GMA) and this is further supported by the higher elongation at break and better morphology, i.e. for DVB-containing blend with 2.1 wt % g-GMA (see also **Figure 4.25**). However, higher GMA grafting levels in the DVB-containing blends, which showed lower elongation at break (see **Figure 4.18**) and worse morphology (see **Figures 4.17** and **4.25**), have also given lower extent of interfacial reaction (shown from the normalised IR), see **Figure 4.29iiD** and **E** and **4.30**,

confirming that higher extent of GMA-grafting has an adverse effect on compatibilisation.

The reason for this, is most likely to be due to a higher extent of branching or crosslinking reaction that would take place in the presence of higher concentration of grafted GMA present in the blend samples e.g. with 3.5 wt% g-GMA, (see **Figure 4.16**) due to reactions of the GMA moieties with PET end groups resulting in more difficult dispersion of the rubber phase in the PET matrix as supported by the coarser morphology of, for example PET/*f*-PER<sub>DVB</sub> blend containing 3.5 wt % g-GMA, see **Figure 4.25**. Similar findings were also shown for polyester/LLDPE blends explained as a saturation of the interfacial area with the LLDPE-g-GMA copolymer formed through reaction of the GMA and PET end groups [54] and also by Al-Malaika *et. al* for PET/EPR functionalised in presence of the comonomer TRIS [51].

Another explanation for the observed lower improvement in mechanical properties and compatibility where high g-GMA concentrations (higher than the optimum level) are present in the blends is that the large concentrations of the reactive sites may not distribute well across the entire polymer chains, thus become constrained in certain places and therefore are unable to reduce the domain size [227]. It can be concluded from the above discussion that high a content of g-GMA is not necessary for achieving better compatibilisation of blends. Similar results were observed in PET/*f*-EPR<sub>CONV</sub> blends where higher grafting levels gave also lower compatibilising extent leading to lower elongation at break (see **Figure 4.18**) and larger domain sizes and unstable morphology when compared to similar blends with lower grafting GMA, see **Figure 4.10**. The finer morphology and higher elongation at break obtained for PET/EPR-g-GMA<sub>DVB</sub> containing optimum amount of grafted GMA compared to the conventional systems is almost certainly due to the absence of polyGMA and to a different microstructure of the *f*-EPR in which higher grafting of GMA takes place at much lower peroxide concentration. see **Figures 4.18B** and **4.26B**.

The shifts observed in the  $T_g$  of PET (from DMA measurement) in compatibilised blends (compared to the physical blend) are due to interaction between the two phases with stronger interface giving rise to reduced  $T_g$  values of the matrix in the blends

[228]. The  $\tan \delta$  of PET and EPR phase in a PET/EPR-g-GMA<sub>DVB</sub> (70/30 w/w %) blend having 2.1 wt% grafted GMA exhibited broad peaks compared to those of the corresponding physical, see **Figures 4.31B** and **4.31C**. The PET/EPR-g-GMA<sub>CONV</sub> (70/30 w/w %) blend showed a larger shift in its matrix (see **Table 4.6**) and this may be explained by the absence of a bulky structure (the benzene ring in the case of DVB), thus a lower energy is needed for segmental motion of the molecule in the blend compared to corresponding PET/EPR-g-GMA<sub>DVB</sub> blend. A lower storage modulus of PET/EPR-g-GMA<sub>DVB</sub> blend at all temperatures examined (**Figure 4.31D**) was observed compared to PET/EPR-g-GMA<sub>CONV</sub> blend suggesting more elastomeric behaviour from the highly compatibilised PET/EPR-g-GMA<sub>DVB</sub> blend. This result is consistent with the higher elongation at break observed for this blend compared to that of the blend produced in the absence DVB, see **Figure 4.32E**.

The compatibility of PET/EPR blends was supported by the “Molau solubility test”. **Table 4.13**, where a blend sample of PET/EPR-g-GMA<sub>DVB</sub> produced a milky (emulsion) solution when it was dissolved in the mixture of ‘Molau solvent’ at high temperature. By contrast, a clear solution was observed for the corresponding PET/EPR physical blend. Since there is no interfacial reaction between the components in the physical blend, the EPR dissolved easily in the solvents while the PET separated out and floated on the top. Similar solubility observation in compatibilised blends of other polymers were reported [75, 92, 152, 192, 229, 230] where emulsion solutions were formed resulting in turbid solution indicating the compatibility of the blends.

### 4.3.2 Effect of polyGMA in *f*-EPR on the Blend Properties

As reported in **Chapter 3**, the functionalisation of GMA onto EPR in the absence of comonomer was low due to low reactivity of GMA towards macroradicals and competition from homopolymerisation of GMA. Thus, high peroxide and high initial GMA concentrations were necessary to achieve enhanced extent of grafting in the conventional system. In this system, the amount of peroxide used ranged from 0.13 to 1.5 phr with the maximum grafting level achieved at 1.9 wt% only for an initial GMA concentration of 10% (peroxide=1.5 phr) but this was paralleled by a significant decrease in the MFI values of the *f*-EPR due to crosslinking reactions, see **Chapter 3**.

An increase in the initial GMA concentration to 15 %, (peroxide =0.8 phr) resulted in a slight increase in the grafting level from 1.7 to 1.9 wt% but this resulted in substantial increase in the formation of polyGMA content up to 3.0 wt%. By contrast, very small peroxide concentration was needed (i.e 0.078 to 0.13 phr), and no measurable polyGMA was found, when similar initial GMA concentrations were used in the GMA-DVB containing system.

Lambla *et. al.* [231] have shown in PBT/PP-g-GMA blends that an increase in the initial GMA concentration increased the extent of polyGMA and free GMA (unreacted GMA in the GMA functionalised PP) and resulted in lowering of the elongation at break and impact strength of the blends. Poor compatibility between PBT and PP-g-GMA was attributed to reaction of the epoxy groups from free the GMA with -COOH end groups of PBT and was suggested that the unreacted GMA reacted faster with PBT than its reaction with grafted GMA due to its greater mobility, thus decreased the possibility of grafted GMA reaction with PBT. In this work, higher level of polyGMA formed in PET with EPR-g-GMA<sub>CONV</sub> blends has also shown adverse effect on the compatibility of the blends where the dispersed rubber particle sizes became larger than in similar blends having much lower polyGMA content or when compared to the DVB-containing blends which have no polyGMA, see **Figure 4.28**. Closer examination of the effect of polyGMA on blend properties revealed that the presence of high polyGMA in the rubber phase gave severe deterioration to the blend properties. For example, the presence of 3.0 wt% polyGMA in a PET/EPR-g-GMA<sub>CONV</sub> blend (containing [GMA]<sub>i</sub>=15%) showed a damaging effect to its mechanical properties (e.g. lower elongation at break) and morphology (coarse particle size) compared to a similar blend where the polyGMA was removed by purifying the *f*-EPR before blending with PET, see **Figure 4.33A**. Furthermore, a higher torque was observed in the PET/EPR-g-GMA<sub>CONV</sub> blend containing polyGMA (**Figures 4.12A-B**) compared to that where the polyGMA was removed suggesting that polyGMA can cause crosslinking in PET blends. The lower elongation at break obtained from the PET/EPR-g-GMA<sub>CONV</sub> blend containing polyGMA is supported by the observed poor morphological characteristics (**Figure 4.33C**) where the rubber phase in the unpurified blend sample (containing 3.0 wt% polyGMA) is seen to have much larger and coarser particle size suggesting a poor interfacial adhesion between the PET and rubber phase. On the other hand, the phase

morphology of the same sample but purified to remove completely the polyGMA gave smaller particle size (of the dispersed EPR phase) and much finer morphology with more uniform distribution of the EPR phase in the PET matrix, see **Figure 4.33D**. This adverse effect of polyGMA can also be seen if synthesised polyGMA is added to PET/*f*-EPR<sub>DVB</sub> (which originally contains no polyGMA, see **Figures 4.33E-G**), and this is almost certainly due to a reaction between the added polyGMA with carboxylic acid end groups of PET which reduce the possibility of the epoxy groups in the grafted GMA to react with the PET end groups, consequently decreasing the desired interfacial reaction between the PET phase and the rubber phase. The effect of polyGMA on the blends of PET with EPR-GMA<sub>TRIS</sub> (in the presence of comonomer TRIS) was also shown by Al-Malaika *et. al* [28] to reduce the compatibilising effect of EPR-GMA<sub>TRIS</sub> reflected in poor blend's morphology.

The above discussion is supported by the fact that the PET/EPR-g-GMA<sub>DVB</sub> blends which contained no polyGMA showed no significant difference before and after purification in terms of blends' morphology (**Figures 4.33E and F**) and mechanical properties (e.g. elongation at break) (**Figure 4.33B**). In fact, the blends of the PET/EPR-g-GMA<sub>DVB</sub> (unpurified) exhibited higher elongation at break compared to that of the purified PET/EPR-g-GMA<sub>CONV</sub> blend where all the polyGMA was removed, see **Figures 4.33A-B**. SEM micrographs of PET/EPR-g-GMA<sub>DVB</sub> blend where a 2.5 wt% of synthesised polyGMA was added has shown a significant difference compared to purified or unpurified corresponding blends, where poor morphology with large and coarse particle sizes are clearly seen (see **Figures 4.33E-G**) confirming that the added polyGMA reduces significantly the compatibilisation efficiency and this is consistent with the observed large decrease in elongation to break for this sample, see **Figure 4.33B**.

### 4.3.3 Effect of DVB Concentration on the Blend Properties.

The effect on blend properties of EPR-g-GMA<sub>DVB</sub> containing various comonomer concentrations was examined and then compared with the corresponding EPR-g-GMA<sub>CONV</sub>. As was shown in **Chapter 3, Sec 3.2.5, p.87**, the presence of high DVB content increased the grafting level significantly. However the presence of high DVB



concentration also reduced the MFI values of the functionalised EPR due to high crosslinking and branching. The changes in the microstructure of the rubber sample may influence the blend properties [51]. EPR-g-GMA<sub>DVB</sub> containing various GMA/DVB ratios but similar grafting levels and MFI values were chosen to be blended with PET. The presence of high GMA/DVB ratio (7/3 w/w) and higher grafting level in EPR-g-GMA<sub>DVB</sub> seems to be unfavourable for improving the elongation at break for the PET/EPR-g-GMA<sub>DVB</sub> blends as shown in a GMA/DVB ratio of 7/3 w/w, see **Figure 4.25E**. Further, the SEM results (**Figures 4.25**) demonstrated that a blend with higher DVB content exhibited a rough morphology with larger dispersed particles, (see **Figure 4.25D**) compared to one with lower DVB concentration (GMA/DVB=9/1w/w %), (see **Figure 4.25C**) but it is important to point out here that the morphologies in these DVB blends are still better than in the case of conventional blends, see **Figure 4.25B**. Although the amount of unreacted GMA and copolymer GMA-co-DVB present in the functionalised rubber samples processed in the presence of DVB could not be quantified, it is expected that the decrease in elongation at break for the blend samples having higher DVB content and higher grafting level would possibly be due to competition from free GMA-co-DVB copolymer and possibly some polyDVB which would reduce the possibility of reaction of grafted GMA with the end groups of PET. DVB has been widely used [232] as a crosslinking agent for example in PP branching process, thus the presence of higher DVB concentration in the grafting system has led to an increase in melt viscosity of EPR-g-GMA<sub>DVB</sub> possibly due to crosslinking and branching of EPR-g-GMA<sub>DVB</sub> compared to *f*-EPR<sub>DVB</sub> having lower DVB concentration, see **Figure 4.34C**. Champagne *et. al.* [98] has suggested that residues of polyGMA, unreacted GMA or copolymer of styrene-GMA which are present in GMA-grafted PP systems are also reactive and might compete with grafted GMA in PP for PET end-groups. Deactivation of PET end groups by these species would decrease the availability for PP-g-GMA for PP/PET compatibilisation. Another possibility that could affect the compatibilisation and the reduced elongation at break in blends containing higher DVB content may be due to steric hindrance of the bulky benzene groups in the DVB unit whereby the epoxy groups of the GMA units may not be able to easily access the carboxyl groups the PET as freely as those without or with lower level of DVB. Similar effect of microstructure of PP-g-GMA-styrene in PP blends with NBR on impact strength was also reported [16] where the presence of styrene reduced the impact

strength of the blends. The decrease in impact strength was suggested to be caused by steric hindrance of the bulky benzene groups in the styrene unit. At the same grafted GMA level, it is clear that blends containing DVB, even at higher DVB content, gave higher elongation at break compared to conventional blends, see **Figure 4.34A**, supported by better morphology seen in **Figure 4.33**.

The higher amount of peroxide needed for the conventional system to achieve grafting level of 2.5 % caused drastic reduction in MFI of the *f*-EPR (see **Figure 4.34A**) causing increase in its melt viscosity and this would adversely affect the migration of the reactive sites to the interface, hence decrease the possibility of the reaction of epoxide groups with carboxylic or hydroxyl groups in PET. Furthermore, the presence of higher polyGMA content in the *f*-EPR<sub>CONV</sub> compared to DVB-containing blends having the same level of grafted GMA reduces the possibility of the reaction of the epoxy groups with the end groups in PET in the former due to competition between polyGMA for the end groups and grafted GMA, resulting in the observed low elongation at break of this conventional blend containing 2.5 wt% g-GMA, (see **Figure 4.34A**).

#### 4.3.4 Effect of Blend Composition on the Blend Properties.

There are several factors that could potentially influence the morphology of the blends such as the composition, the compatibility-interfacial tension and the viscosity ratio [233]. The phase morphologies of PET/EPR, PET/EPR-g-GMA<sub>CONV</sub> (optimised sample used) and PET/EPR-g-GMA<sub>DVB</sub> (non-optimised sample used) blends at different blend compositions are shown in **Figure 4.35**. It is clear that the amount of rubber used in the blends has a main influence on the phase morphology. At lower rubber content (90/10 w/w%), the rubber particles in the dispersed phase of PET/EPR-g-GMA<sub>DVB</sub> (also in the other blends) are shown to be smaller when compared to those with the higher rubber content, see for e.g. **Figure 4.35D**. For lower rubber content, the smaller sizes is most likely due to particles having little chance to undergo coalescence and not due to improvement in compatibilisation between the two components. It was reported [228] that increasing the rubber fraction from 15 to 20 phr in PET/SBR-g-MAH blends resulted in coalescence characterised by increasing the size of the dispersed rubber

particles in the matrix phase. Similar finding was also reported in poly(trimethylene terephthalate) (PPT)/acrylonitrile–butadiene–styrene (ABS) blends in which the domain size of ABS increased with increasing its content in the blends due to particle coalescence [234].

However, the fine morphology observed in these blends (e.g. 90/10 w/w%) is unfavourable for mechanical properties. The low elongation at break observed for these blends is due to the low rubber content and thus lower elastomeric effect, see **Figure 4.36B**. On the other hand, a further increase in the content of *f*-EPR above 30 w% results in no additional enhancement in the elongation at break. Similar observation has been reported in the case of carboxy nitrile rubber (CNBR)/PP/PP-*g*-GMA where addition of more than 5 % of PP-*g*-GMA resulted in no further improvement in the elongation at break of the blending system [235].

Close examination of the final torque characteristics for different blend ratios of PET/EPR-*g*-GMA<sub>CONV</sub> (based on *f*-EPR<sub>CONV</sub> samples with 1.7 wt% grafted GMA and 0.9 g/10min MFI) revealed that the resulting torque values were higher, especially at 80/20 and 70/30 ratios, than those of PET/EPR-*g*-GMA<sub>DVB</sub> (based on *f*-EPR samples with 3.3 wt% grafted GMA and 3.3 g/10min MFI), see **Figure 4.22B** which may be due to two factors, i) better interfacial reaction, ii) high viscosity of the functionalised rubber sample used in the blends. It was reported [236] that the rheological properties in the case of ethylene propylene copolymer (EPR) and EPDM blends depended on the individual blend composition such as molecular weight and viscosity. However, the lower elongation at break (**Figure 4.36B**) for PET/EPR-*g*-GMA<sub>CONV</sub> blends compared to blends containing DVB would rule out an increased in reaction between the PET and *f*-EPR. The increase in torque values of these blends at these compositions is therefore most likely to be due to higher viscosity of the *f*-EPR rather than an increased interfacial reaction.

Examination of the shifts in  $T_g$  of blends with different composition revealed that in general  $T_g$  of the PET phase decreased while the  $T_g$  of the EPR phase increased with increasing rubber content in the blends, see **Figure 4.24A**. The  $T_g$  of the PET phase of the physical blends showed higher values when compared to those of both reactive

blends (conventional and DVB). In the case of PET/EPR-g-GMA<sub>DVB</sub> blends, higher  $T_g$  values of their PET phase at all blend compositions was observed compared to those of the corresponding blends in the absence of DVB, see **Figure 4.24A**, which may be due to the presence of the bulky DVB structure thus reducing the mobility of the molecule in the PET phase as discussed earlier. Similarly, the substantial shift of  $T_g$  PET phase in the PET/EPR-g-GMA<sub>CONV</sub> blends toward  $T_g$  of their EPR phase can also be attributed to easier movement of the chains. Similar results were reported [237] where increasing the EPR content in polypropylene/ethylene-propylene rubber blends increased the  $T_g$  of EPR to higher temperatures. As for the rubber transition in these blends, which all show increase with increasing rubber content, there is no significant difference in the EPR  $T_g$  of the different blends in the presence or absence of DVB. Similarly, the storage modulus ( $E'$ ) showed generally higher value (determined at lower temperatures below  $T_g$  of EPR at  $-40^\circ\text{C}$ ) at lower rubber content, see **Figures 4.24E and 4.24F**, since low rubber content (high PET content) would result in blends with more stiff characteristics.

#### 4.3.5 Interfacial Analysis of PET/EPR-g-GMA in Blends with FTIR

The compatibilisation of PET/EPR-g-GMA blends could lead to very efficient interfacial reactions between the carboxyl groups of PET with epoxy groups of the grafted GMA in the rubber samples. It was shown in **Sec. 4.3.1** that the extent of formation of graft copolymer in the different blends was determined from separation of the phases of both physical PET/EPR and reactive PET/ $f$ -EPR blends (70/30 w/w %) and their analyses by FTIR. The best reactive blend samples (**BG3, BD6, BD12, BD15, Table 4.2**) in terms of elongation at break were chosen for examination of their interfacial reaction. Again  $f$ -EPR<sub>DVB</sub> (**sample BD6, Table 4.2**) prepared in the presence of DVB at 9/1 w/w GMA/DVB ratio gave higher reactivity towards the end group of PET. **Figure 4.37** shows the differences in terms of the amount of a specific IR absorption corresponding to PET in the separated EPR fractions of blends (IR was normalised with sample thickness) containing various DVB concentrations. The blend samples were chosen based on the best elongation at break obtained in each case. It is clear that the PET-normalised IR absorption in the separated EPR from PET/ $f$ -EPR<sub>DVB</sub> blends is higher than in the conventional blend. The GMA modified EPR becomes

chemically linked to the PET through a reaction between the epoxide groups in the modified EPR with the end groups in PET forming interfacial EPR-g-PET copolymer observed in IR of fractionated samples. The formation of similar graft copolymers at the interface in reactive blends has been shown to offer efficient compatibilisation [28, 51, 154]. The interfacial reaction also improves the interfacial adhesion giving rise to the observed reduction in the dispersed rubber particles size in the continuous PET matrix, see **Figure 4.25**. The importance of the graft copolymer in stabilising the morphology has been reported in the literature [80]. During reactive blending, the copolymer would disperse at the interfaces acting as a linker between the immiscible phases resulting in reduction in the interfacial tension [98]. It is worth noting that the effectiveness of the functionalised EPR in compatibilising an immiscible polymer blend depends strongly on the mobility of the copolymer to enable it to get to the interface and how much of it is located at the interface [16]. Further, it is known that the morphology of compatibilised blends is controlled by the interfacial tension, which is in turn controlled by the structure of compatibiliser [129].

#### 4.3.6 Mechanism of Reactive Blending in Presence of DVB

Based on the evidence discussed above a mechanism of reactive blending of PET/EPR-g-GMA in presence of DVB (and its absence), is suggested in **Scheme 4.3**. The presence of EPR-g-GMA in blend systems reduces the surface tension through interfacial reactions between the epoxy group of GMA with the carboxylic and hydroxyl end groups of PET leading to the formation of a copolymer of PET-co-EPR [97, 238]. The compatibilisation that involves reaction between the epoxy groups of EPR-g-GMA<sub>DVB</sub> and carboxyl and the hydroxyl end groups of PET is shown in **Rn 4.1** and **4.2** which gives rise to the observed formation of PET-co-*f*-EPR copolymer at the blend interface. This copolymer is expected to increase the interfacial strengths giving rise to improved interfacial adhesion. Sun *et. al.* [89] suggested that the compatibilisation effect of blending of PBT/ABS-g-GMA was improved by two ways. First the dispersed phase coalescence rate is reduced through steric repulsion. Secondly, dispersed phase breakup rate is increased through lowering of the interfacial tension. These factors are responsible for the finer distribution of the dispersed phase and the better morphological characteristics observed in PET/EPR-GMA<sub>DVB</sub> blends as described earlier. The size of

the dispersed particles has been shown to be strongly influenced by the microrheology process that takes place during blending [239]. It was shown [239] that the coalescence occurs when two droplets moving in an externally applied flow field collide and the duration of the collision is sufficient to allow completion of the coalescence process. An effective way to inhibit the coalescence is by introducing a compatibiliser with different “tails” that are compatible with either the matrix or the dispersed phase [239], thus reducing the coalescence by reducing the interfacial mobility and apart from that it may also introduce repulsive interactions.

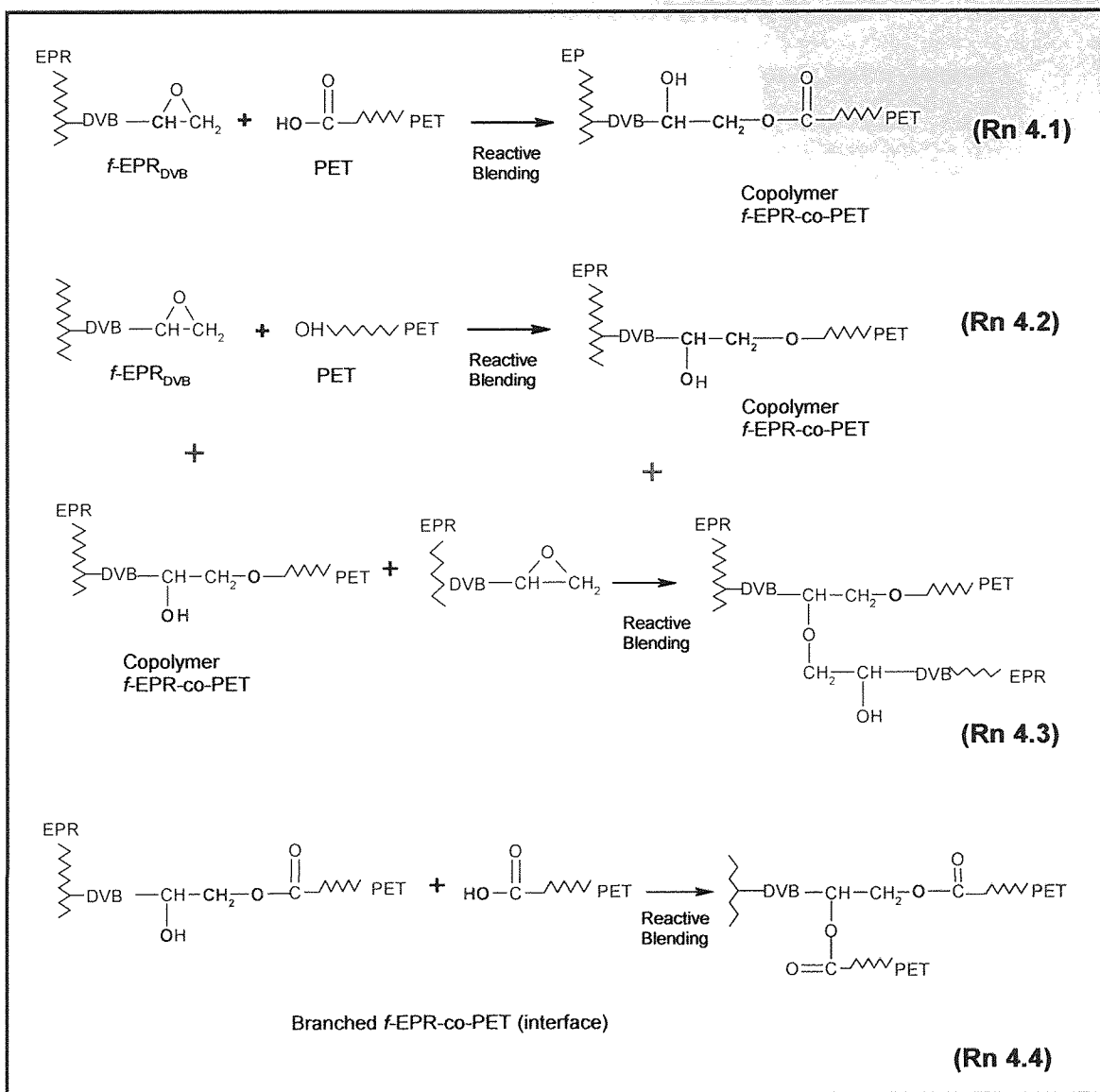
Branching reactions in the presence of a compatibiliser in these blend systems can result in two side reactions based on the epoxy groups of the EPR-g-GMA reacting with the hydroxyl group of the formed copolymer (Rn 4.3), or with the PET matrix when the carboxyl groups react with the hydroxyl groups of the copolymer, (Rn 4.4) [90]. It was suggested [89] that such branching or crosslinking reactions could interfere with the phase morphology formation. As a result the dispersed phase becomes more viscous and the dispersed particles become irregular giving rise to rougher morphology.

In PET/EPR-g-GMA blends, the ratio between the available epoxy groups and PET end groups plays an important role in ensuring high efficiency of compatibilisation effect in the blends. The functional group location is also important and this determines the kinetic of the reaction between the compatibiliser and the functional groups during the reactive blending. The reaction of functional groups with the reactive sites located at the middle of the molecular chain of polymers is slower than that located at the end [80]. In the case of PBT/PS-g-GMA blends, the rate of reaction between carboxylic acid in PBT and the epoxy group was shown to be much higher than that between the hydroxyl groups in PBT and the epoxy group [225]. According to several authors [89, 92], the rate of interfacial reaction in case of epoxide/carboxyl pair can be defined as:

$$\gamma = k_{AB}[A][B] \qquad \text{Eqn 4.1}$$

where  $k_{AB}$  is the kinetic constant for the reaction between the chemical functions A and B, and [A] and [B] are the concentrations of these reactive functions; respectively.

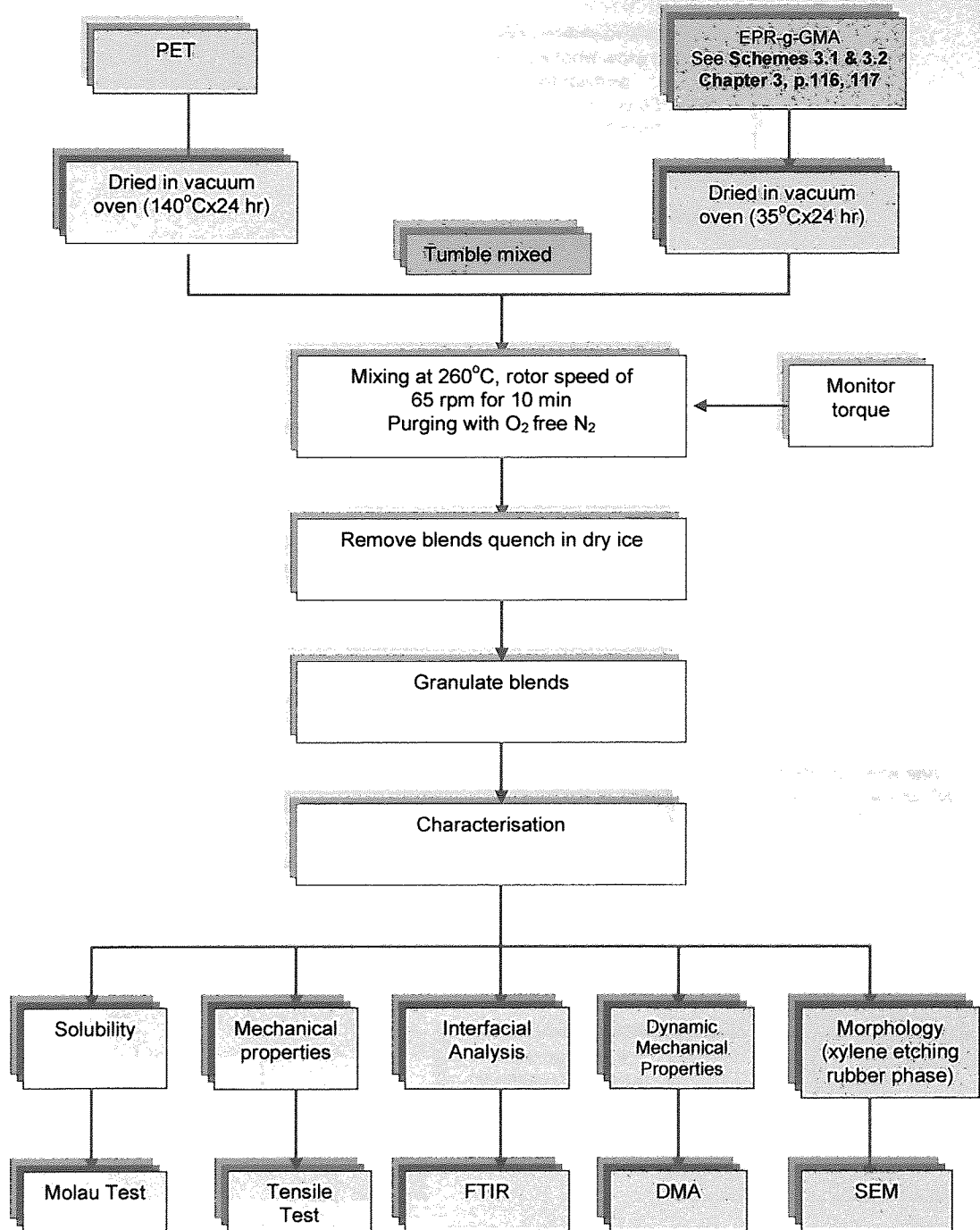
In this study, the amount of carbonyl and hydroxyl groups in the blend systems was the same (the same PET grade was used in all blends) while the concentration of GMA in EPR-g-GMA was varied. According to Eqn 4.1, the formation of PET-co-EPR-g-GMA copolymer and the subsequent crosslinking of the rubber phase is expected to take place more rapidly in the case PET//EPR-g-GMA blends containing high GMA content, thus, the compatibilisation reaction between GMA and the end groups of PET, **Rn 4.1** and **4.2** would occur at a high rate. As a result, the concentration of carboxyl, hydroxyl and epoxy groups would decrease due to the compatibilisation reaction. This would result in an increase in the viscosity of the blends due to formation of in situ copolymer, which would subsequently reduce the diffusion rate of the dispersed phase to the interface. On the other hand, the reaction of EPR-g-GMA with hydroxyl groups present in PET-co-EPR-g-GMA copolymer (**Rn 4.3**) can still occur at high rate because the EPR-g-GMA can disperse easily in the dispersed phase itself. The epoxy group in EPR-g-GMA contains high GMA content capable of reacting with the hydroxyl groups present in the PET-co-EPR-g-GMA copolymer giving rise to an increase in the crosslinking reaction rate in the blends. Similar mechanism in the case of PBT/ABS-g-GMA blends was also reported [89].



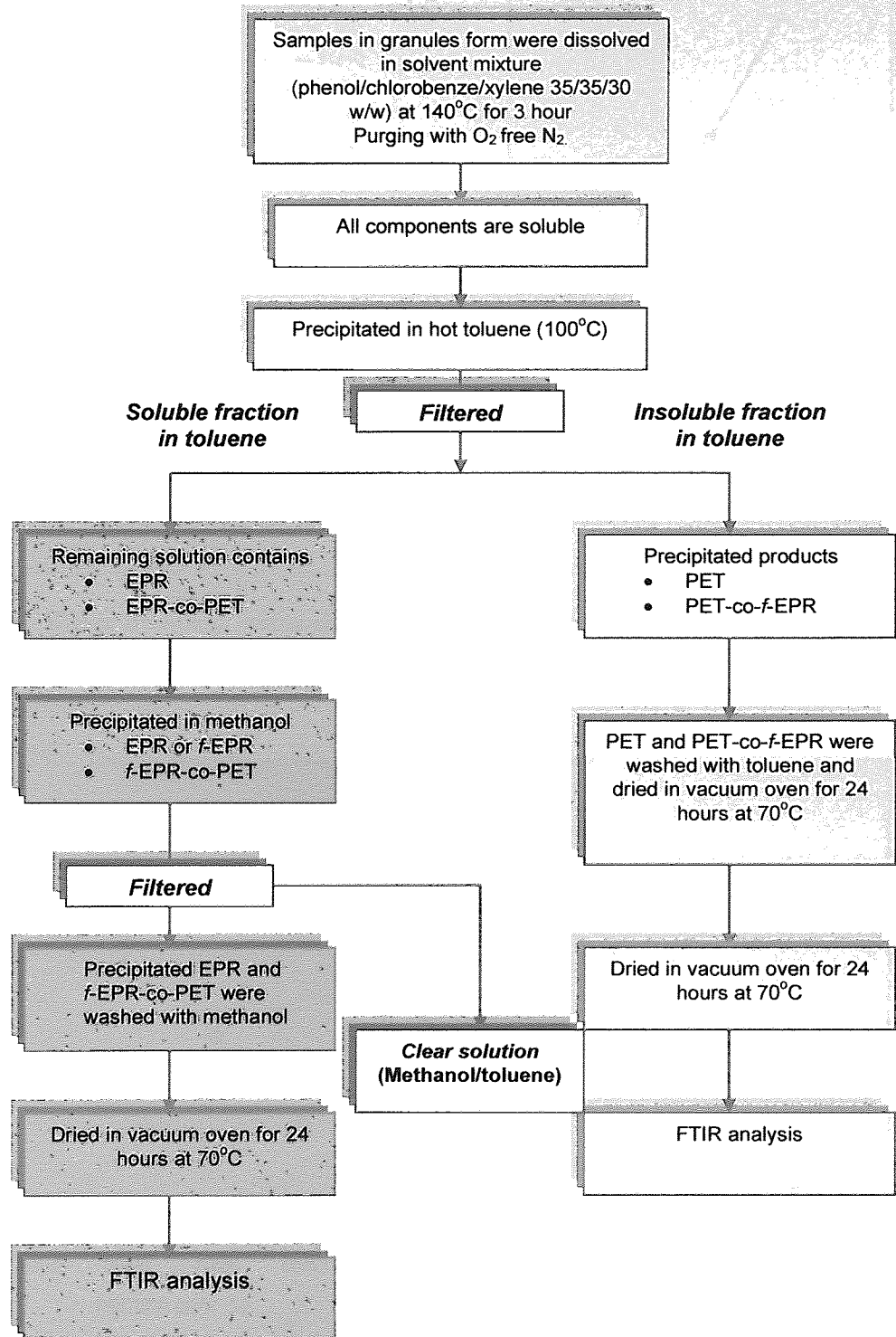
Scheme 4.3. Possible reactions during compatibilisation between PET with EPR-g-GMA.



Scheme 4.1. Methodology for Compatibilisation of PET/EPR Blends



Scheme 4.2: Sequential Solvent Fractionation of PET/*f*-EPR blends



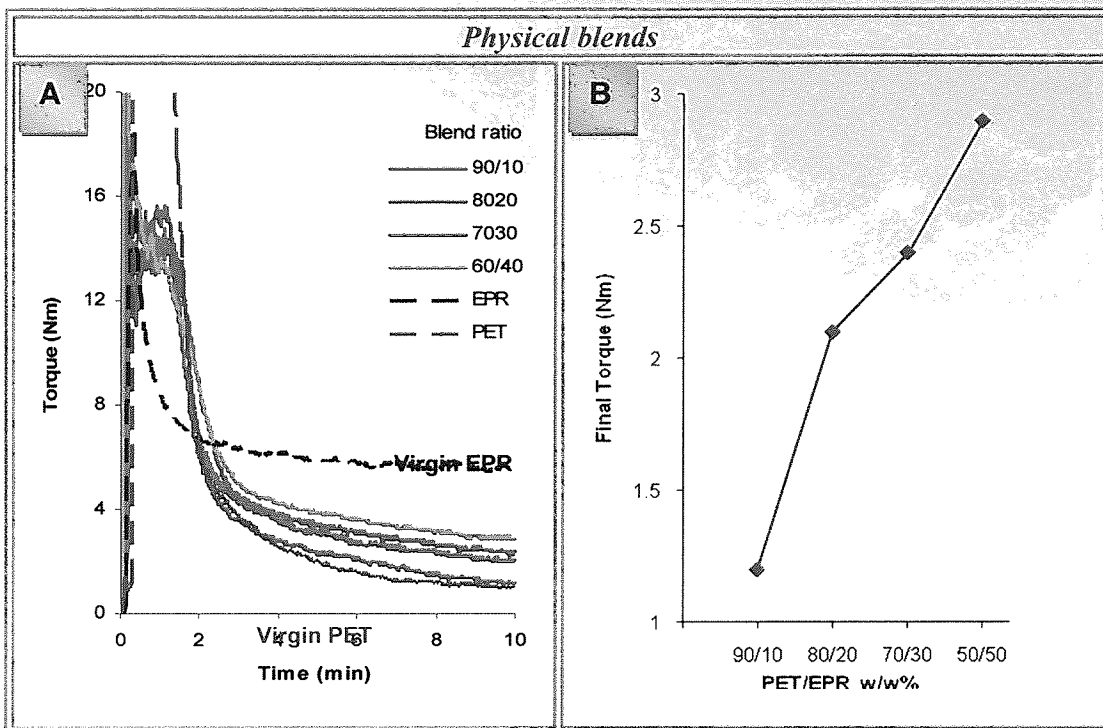


Figure 4.1. Effect of blend composition in physical blends of PET/EPR on torque characteristics. Samples P91, P82, P73, P64 in Table 4.2.

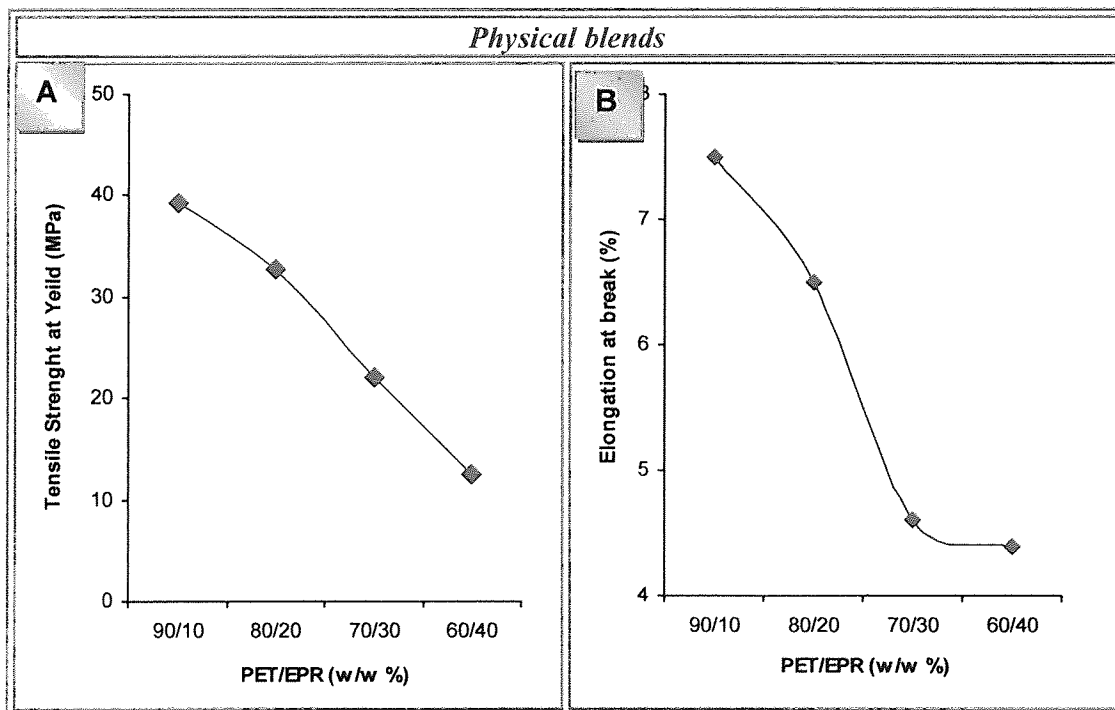
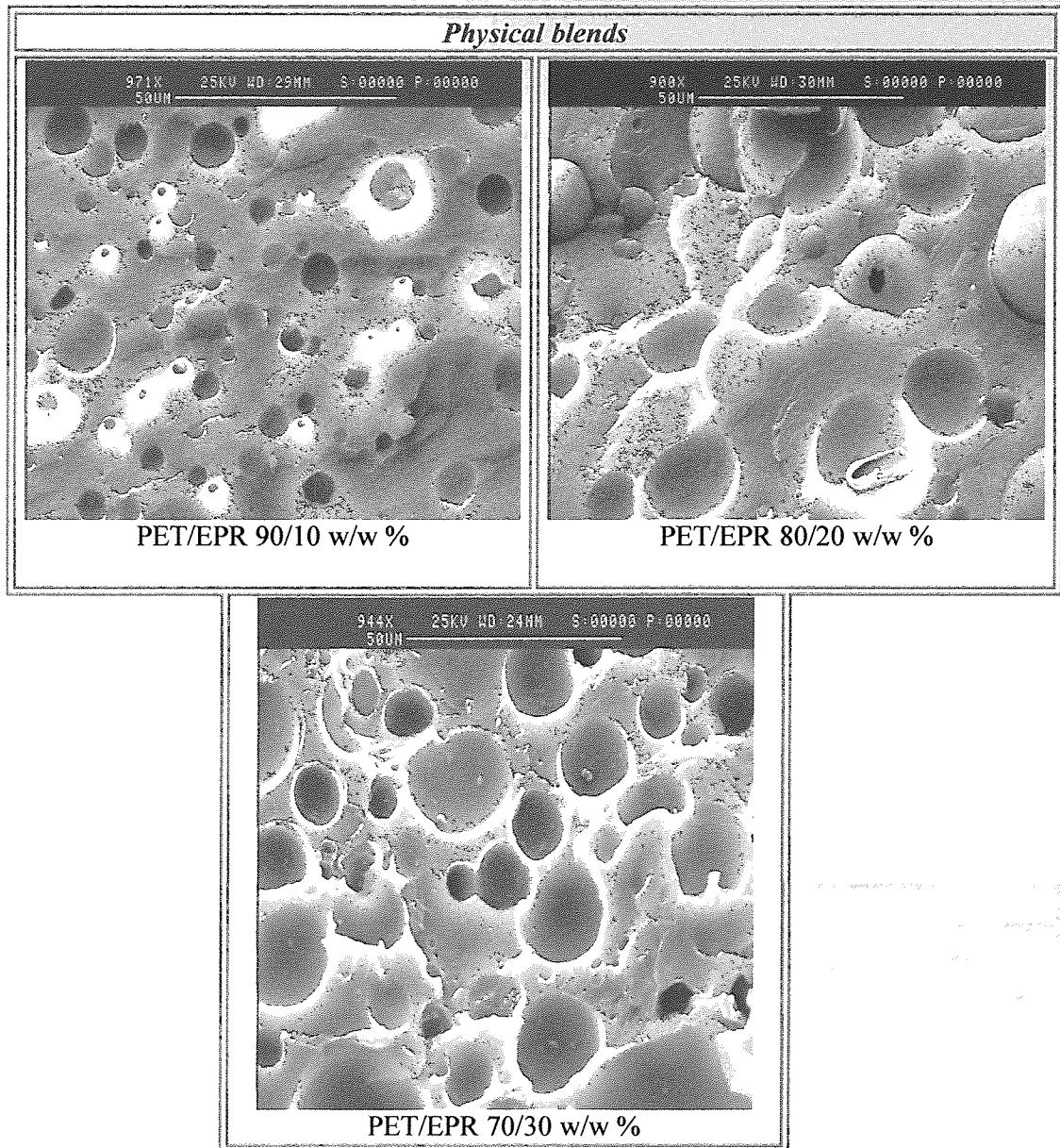


Figure 4.2. Effect of blend composition of physical blends of PET/EPR on tensile properties. Samples P91, P82, P73, P64 in Table 4-2.



**Figure 4.3.** Effect of blend composition of physical blends of PET/EPR on morphology. Samples P91, P82, P73, **Table 4.2.**

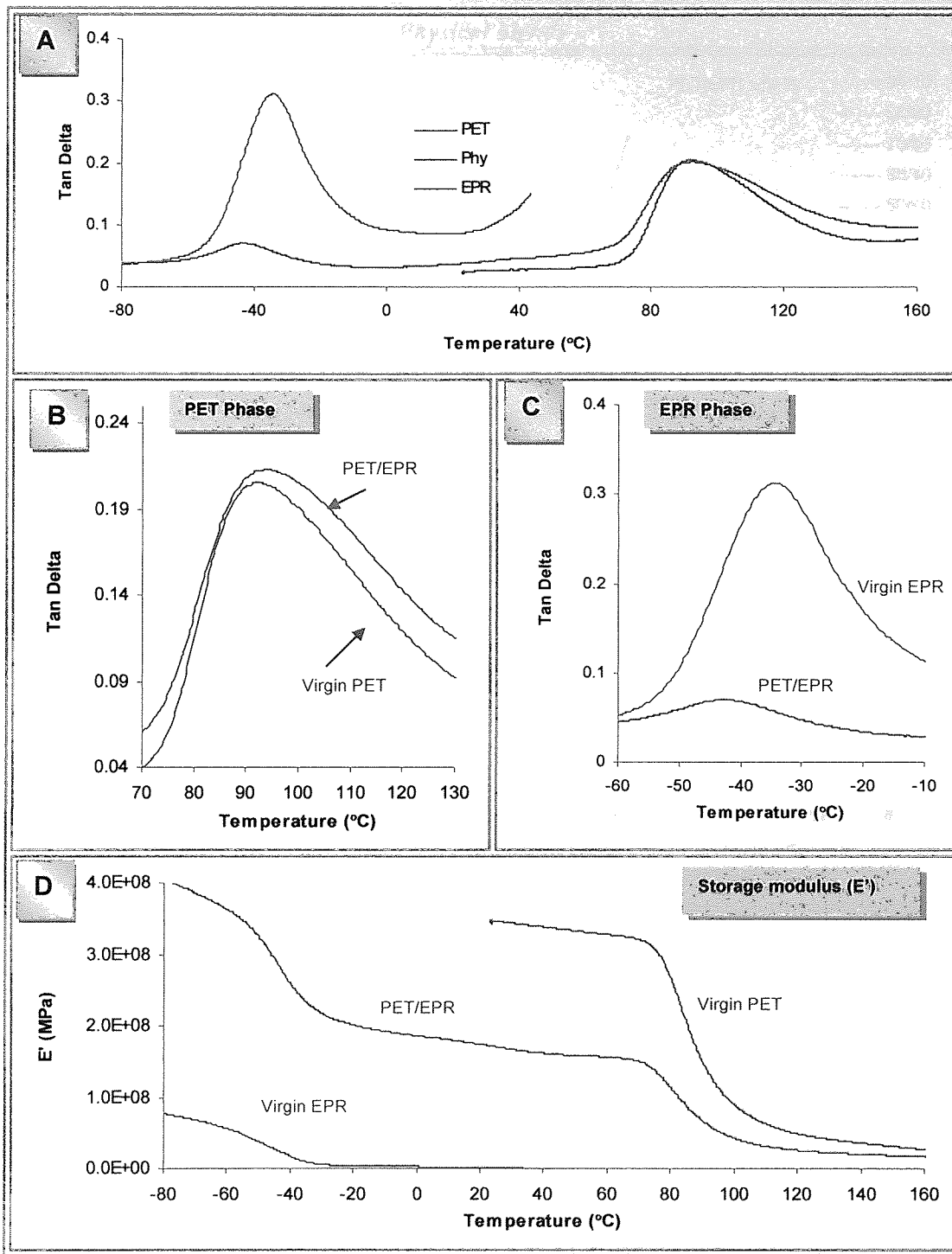


Figure 4.4. Dynamic mechanical properties of PET, EPR and physical blend of PET/EPR 70/30 w/w%. Samples P1, E1, P73 in Table 4.2.

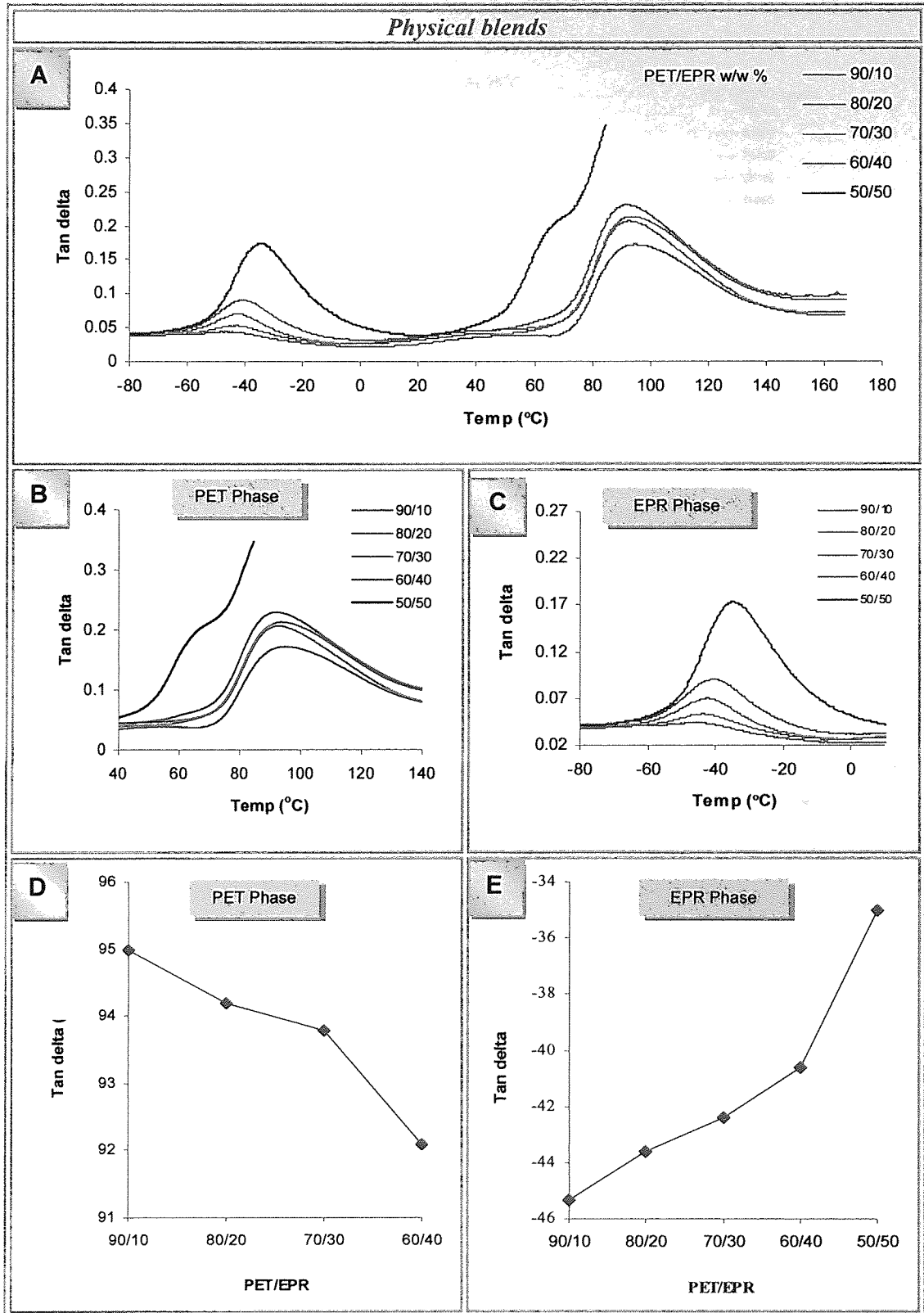


Figure 4.5. Tan delta of PET/ EPR physical blend at various blend composition. Samples P91, P82, P73, P64, P55 in Table 4.2.

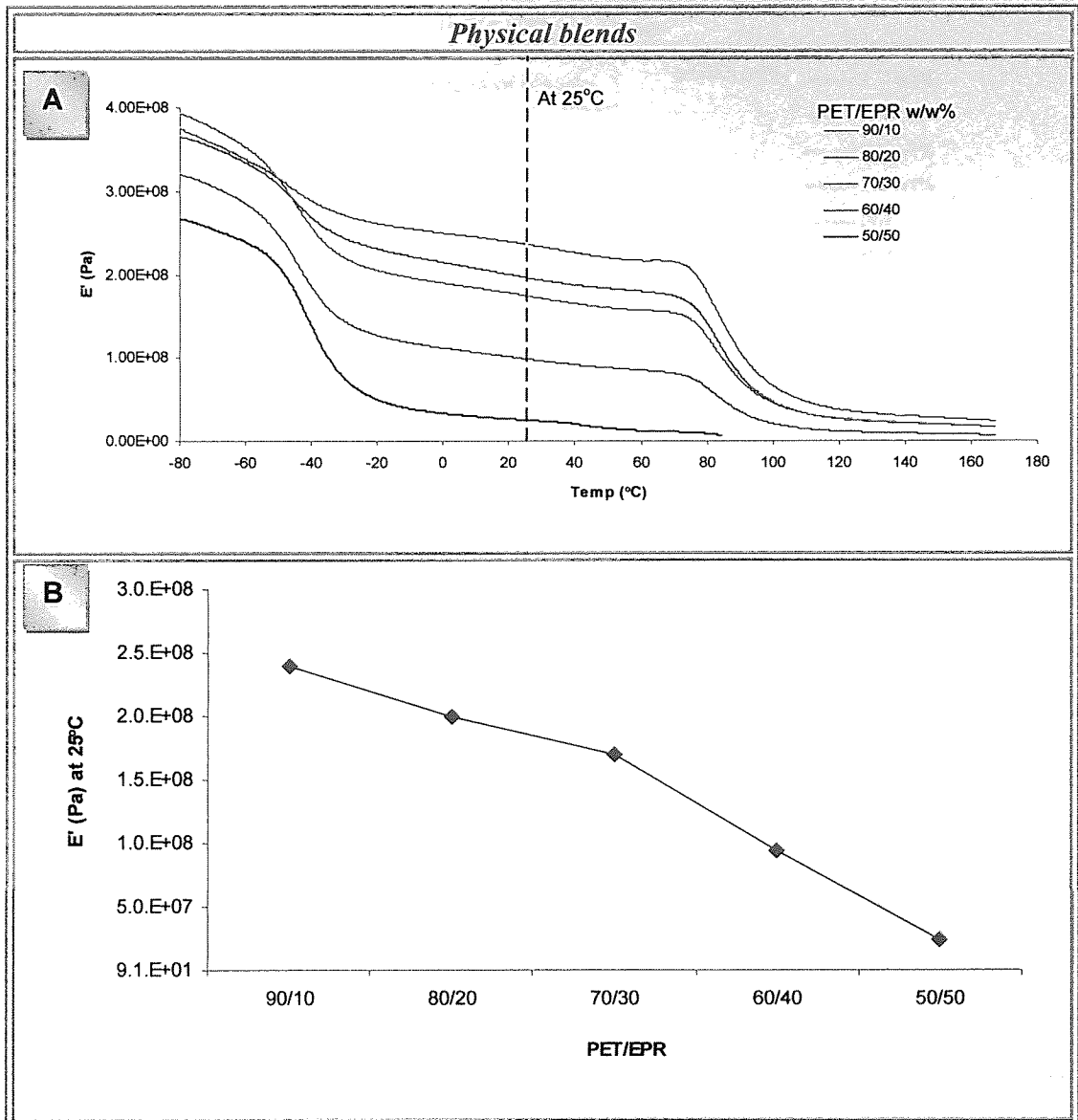


Figure 4.6. Storage modulus of PET/EPR physical blends at various blend composition. Samples P91, P82, P73, P64, P55 in Table 4.2.

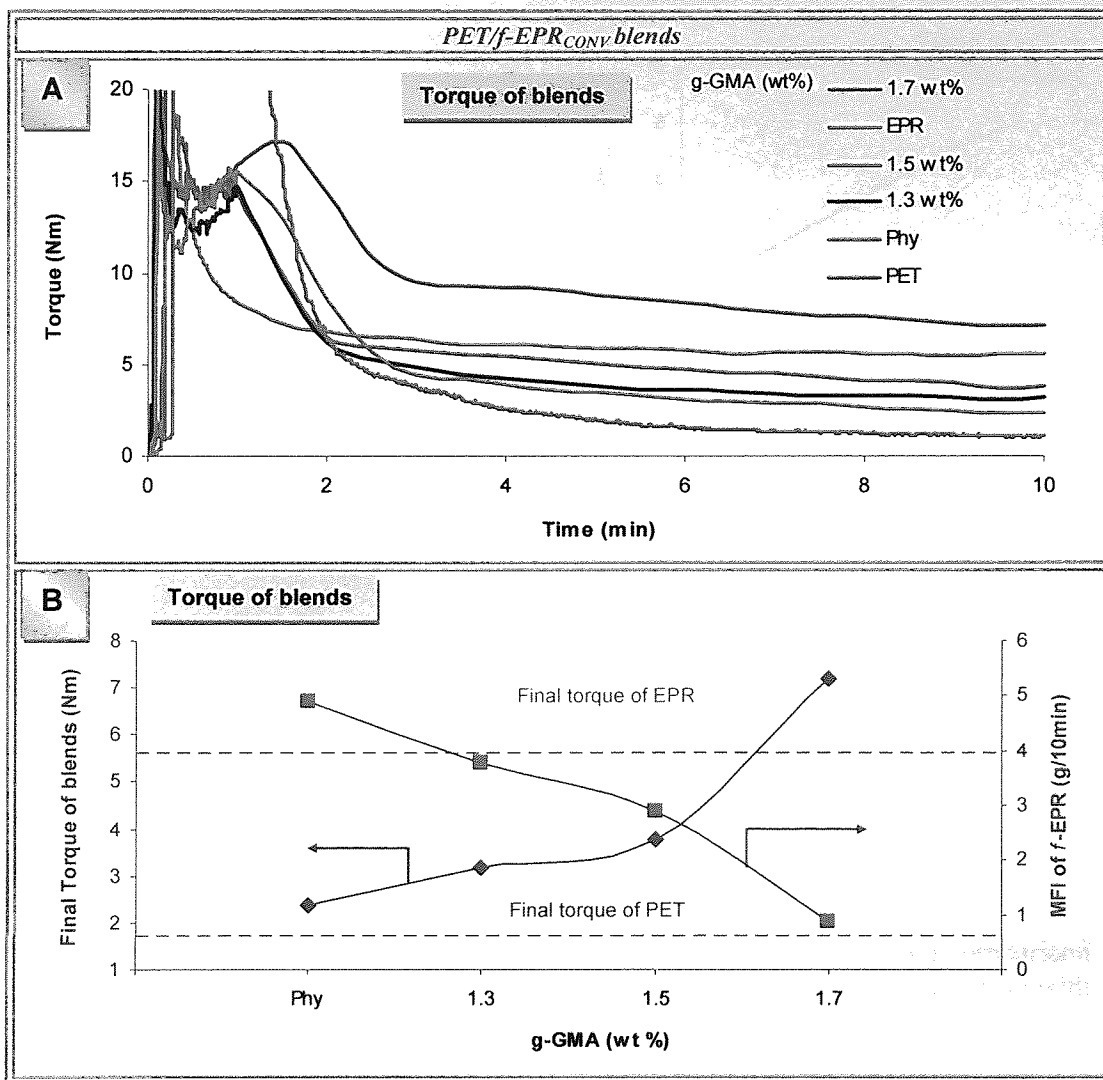


Figure 4.7. Torque curves of the PET/f-EPR<sub>CONV</sub> blends 70/30 w/w%. Samples P73, BG1 BG2, BG3 in Table 4.2. All contain 10 % [GMA]i.



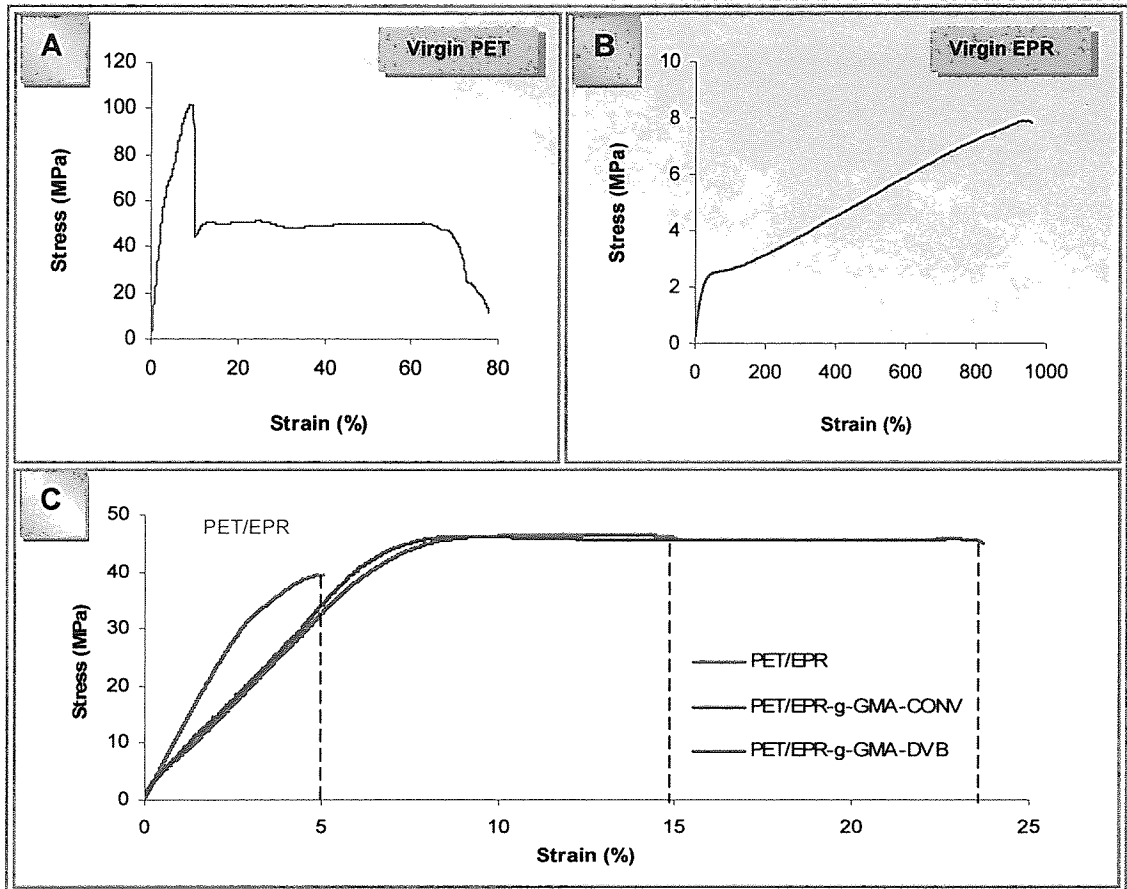


Figure 4.8. Stress–Strain ( $\sigma/\epsilon$ ) curves of virgin PET (A) and EPR (B) and comparison of physical blend with those of reactive blends of PET/*f*-EPR 70/30 w/w% (sample with DVB BD13(7:3) and without DVB (CONV) BG3(7:3), Table 4.2).

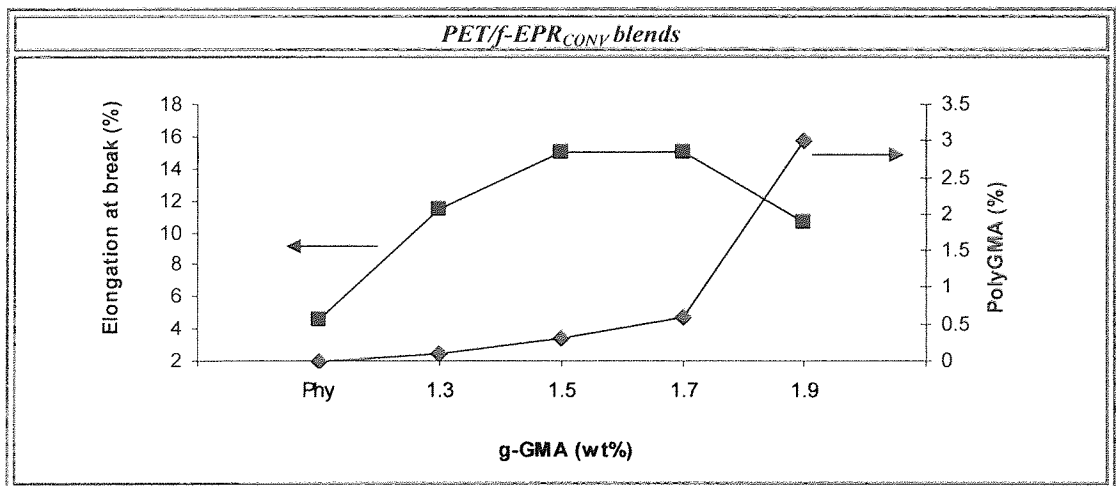
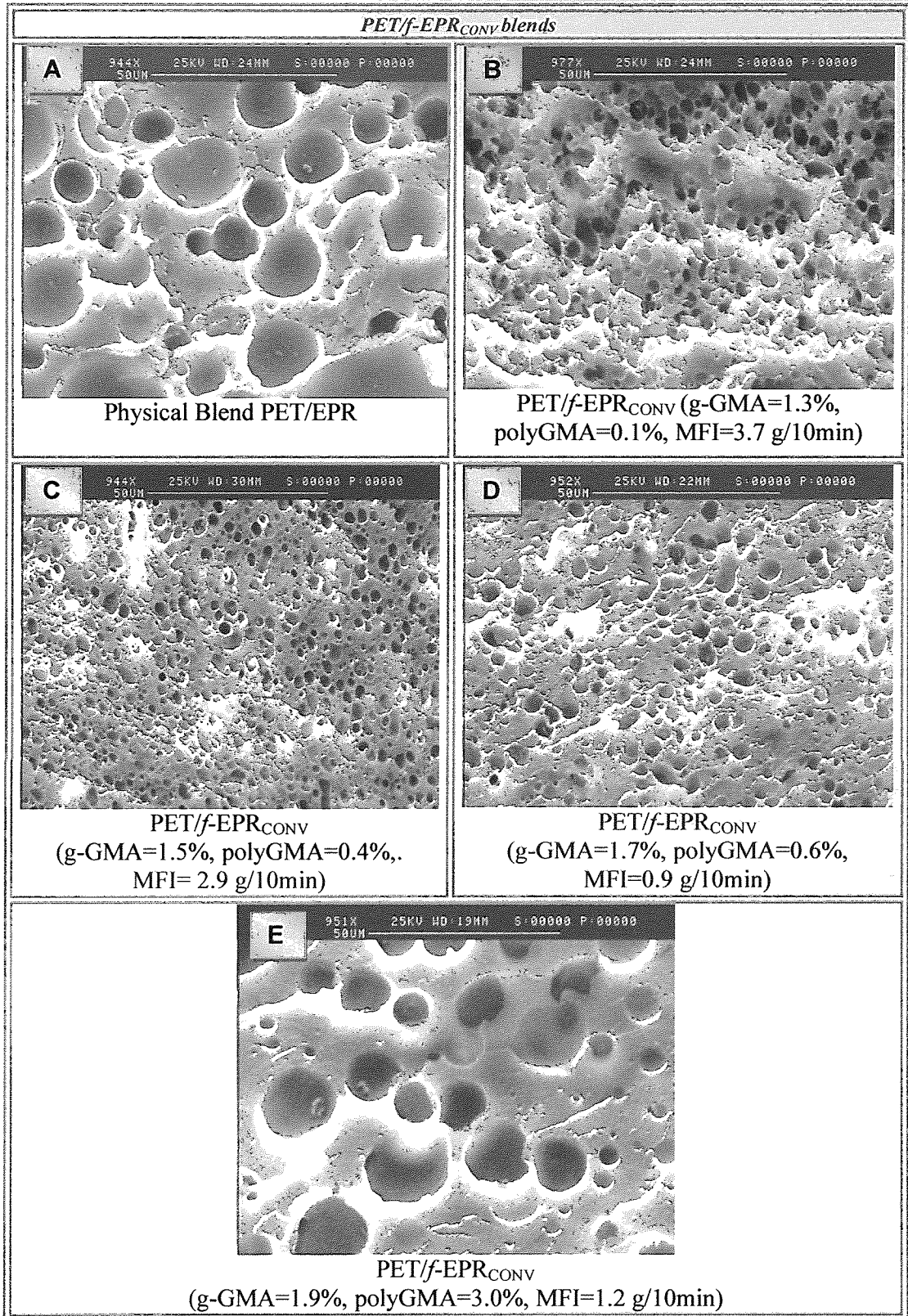
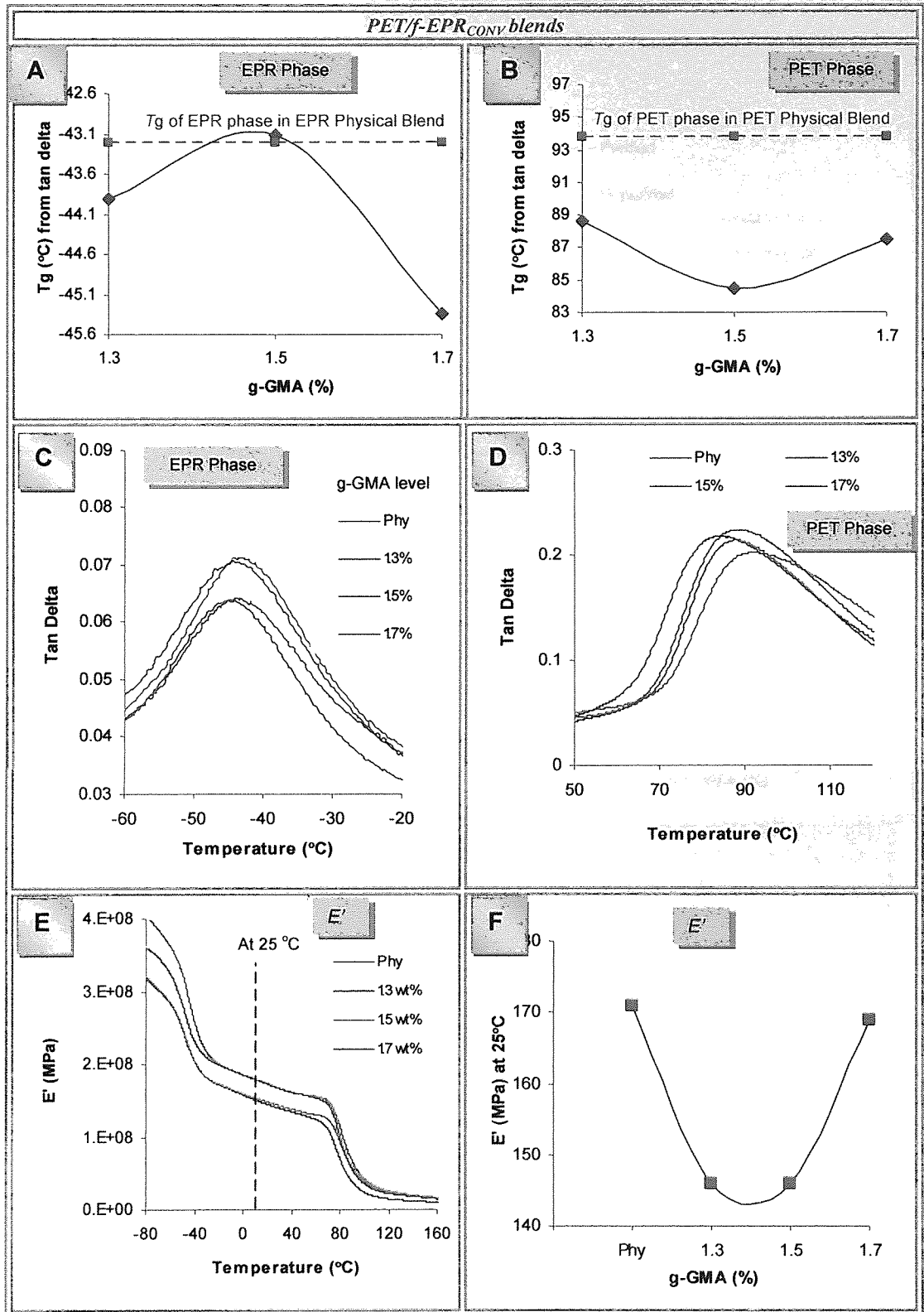


Figure 4.9. Correlation between elongation at break and polyGMA content in the PET/*f*-EPR<sub>CONV</sub> blends (70/30 w/w%). Samples P73, BG1, BG2, BG3(7:3), BG6 in Table 4.2.



**Figure 4.10.** Effect of grafting level on morphology of PET/f-EPR<sub>CONV</sub> 70/30 w/w%. Samples P73, BG1, BG2, BG3(7:3), BG6 in Table 4.2



**Figure 4.11.** Effect of grafting level of  $f$ -EPR<sub>CONV</sub> on dynamic mechanical properties of PET/ $f$ -EPR<sub>CONV</sub> blends 70/30 w/w%. Samples P73, BG1, BG2, BG3(7:3) in Table 4.2

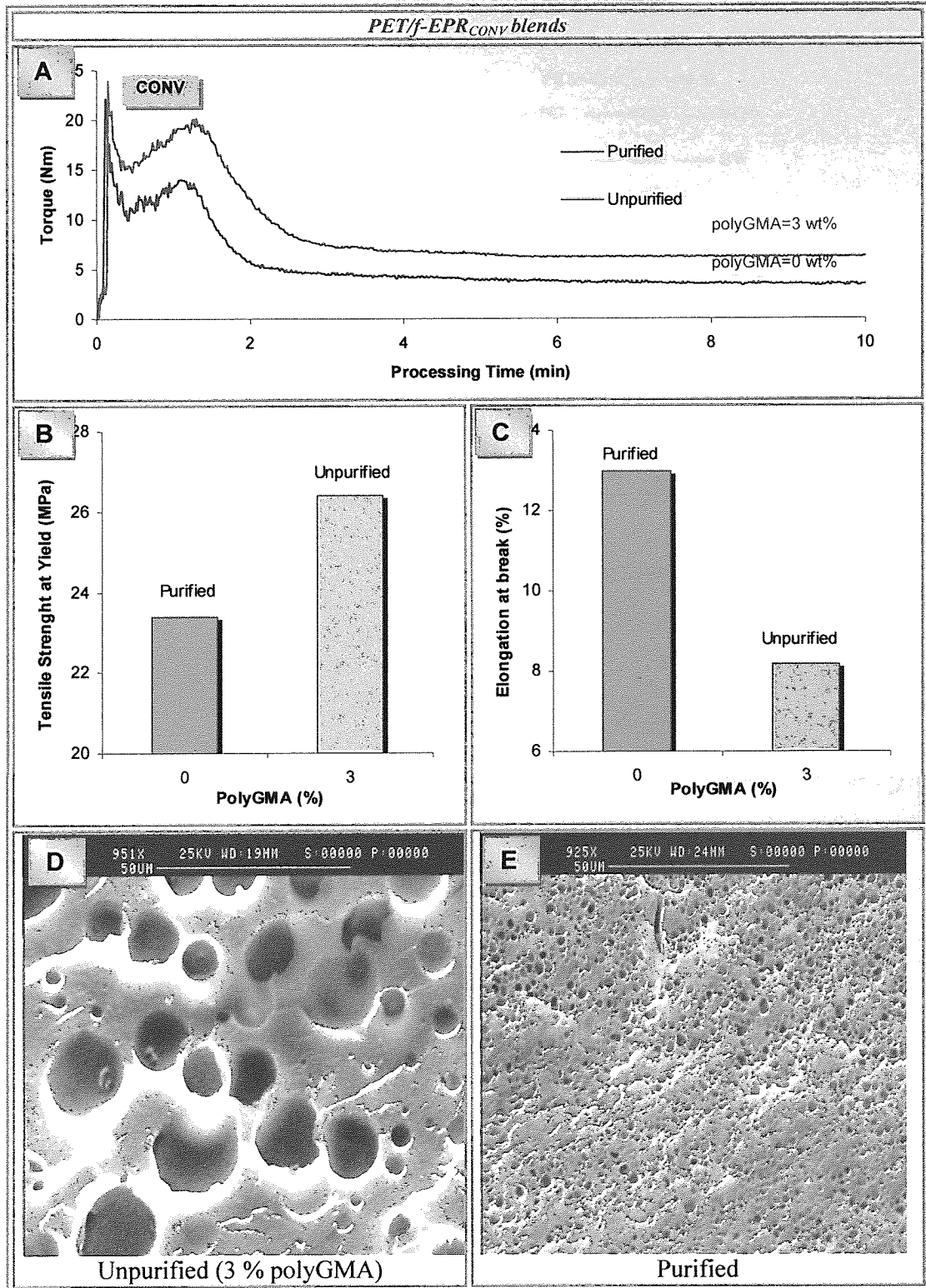


**Figure 4.12.** Effect of polyGMA content in EPR-g-GMA<sub>CONV</sub> on torque, mechanical properties and morphology of PET/EPR-g-GMA<sub>CONV</sub> blends 70/30 w/w%. Samples BG6, BG7 (g-GMA=1.9 %, polyGMA=3.0 %, MFI of *f*-EPR<sub>CONV</sub>=1.2 g/10min) in Table 4.2. Sample BG7 used purified *f*-EPR<sub>CONV</sub> sample (no polyGMA).

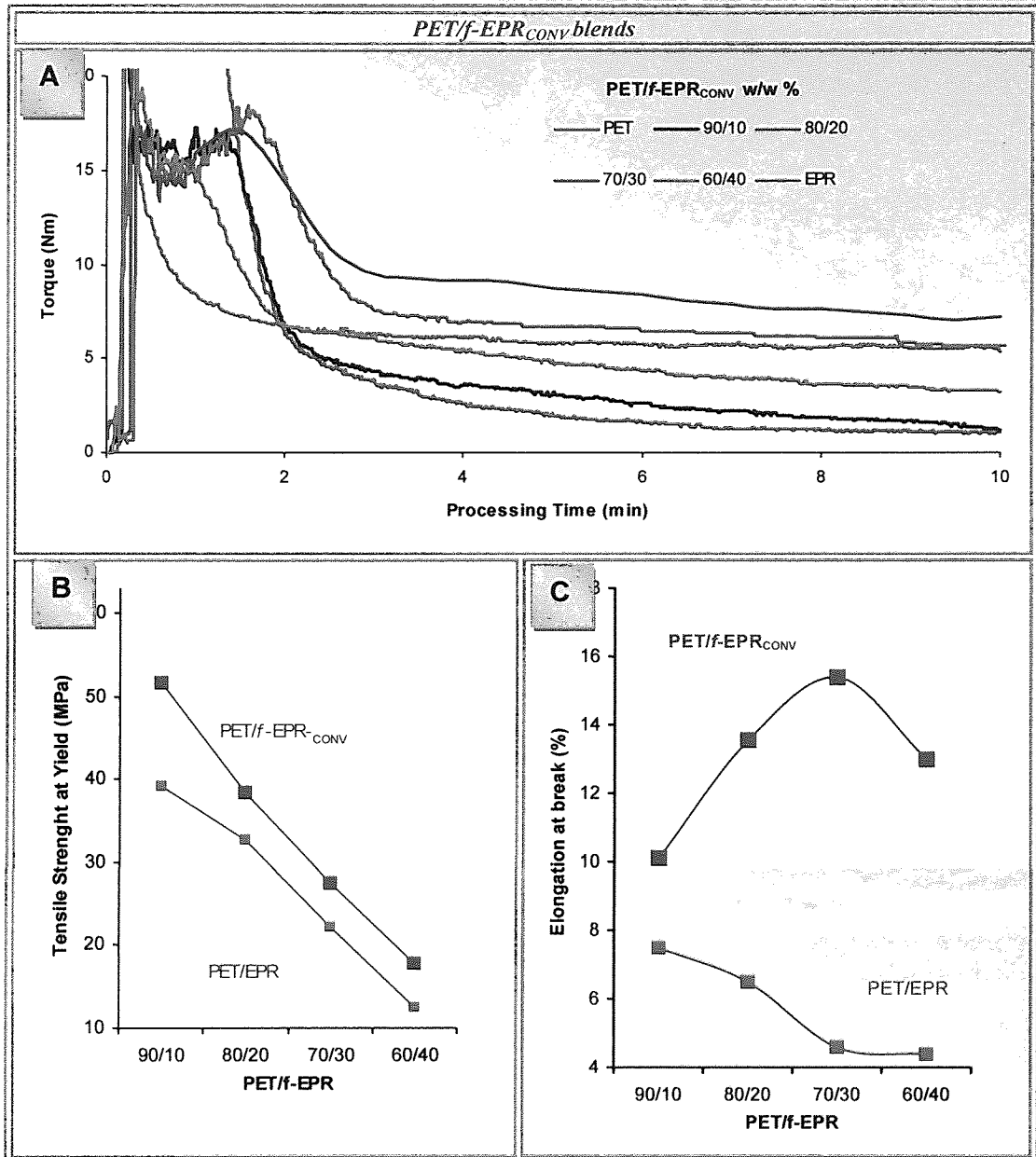
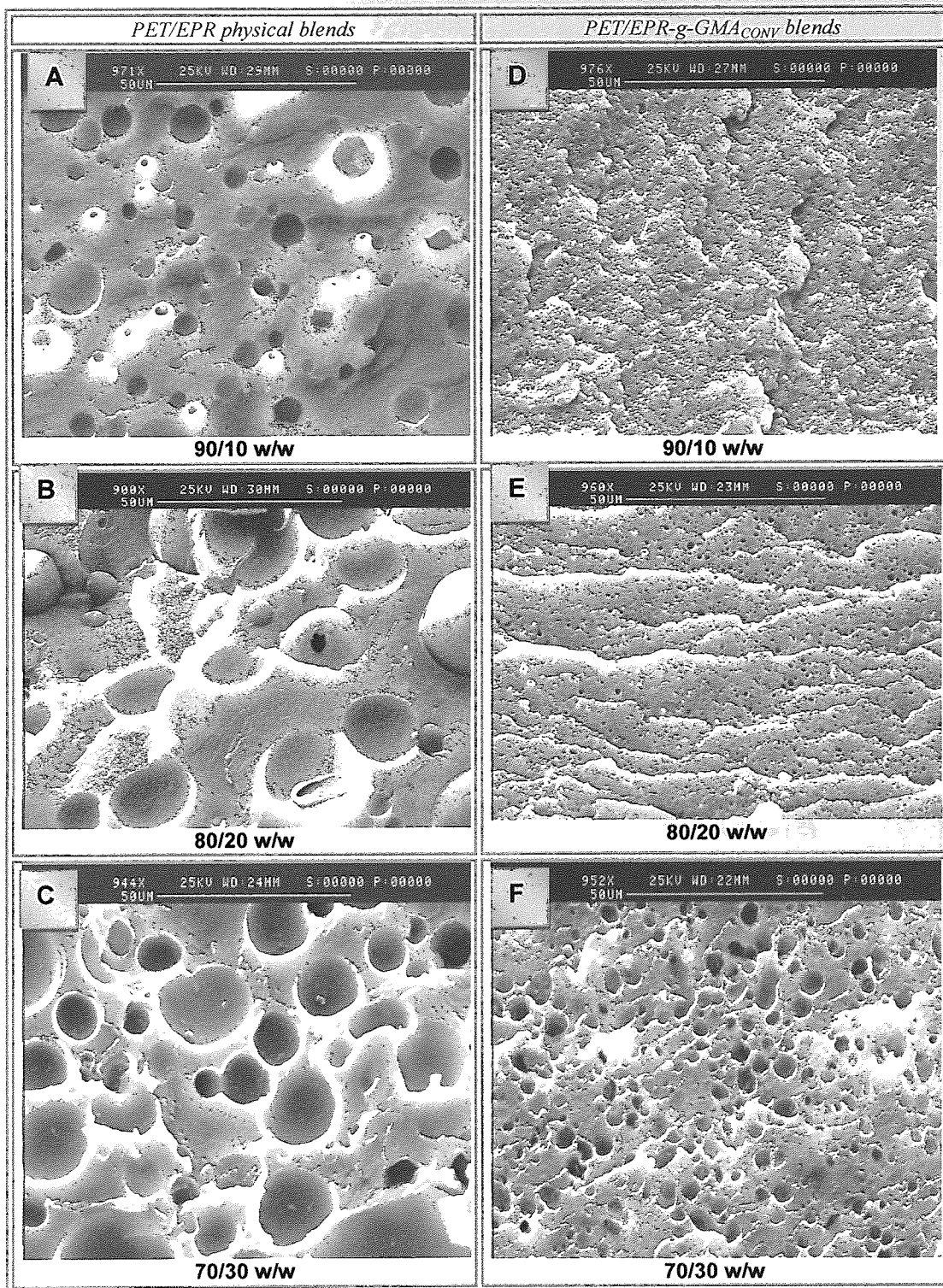
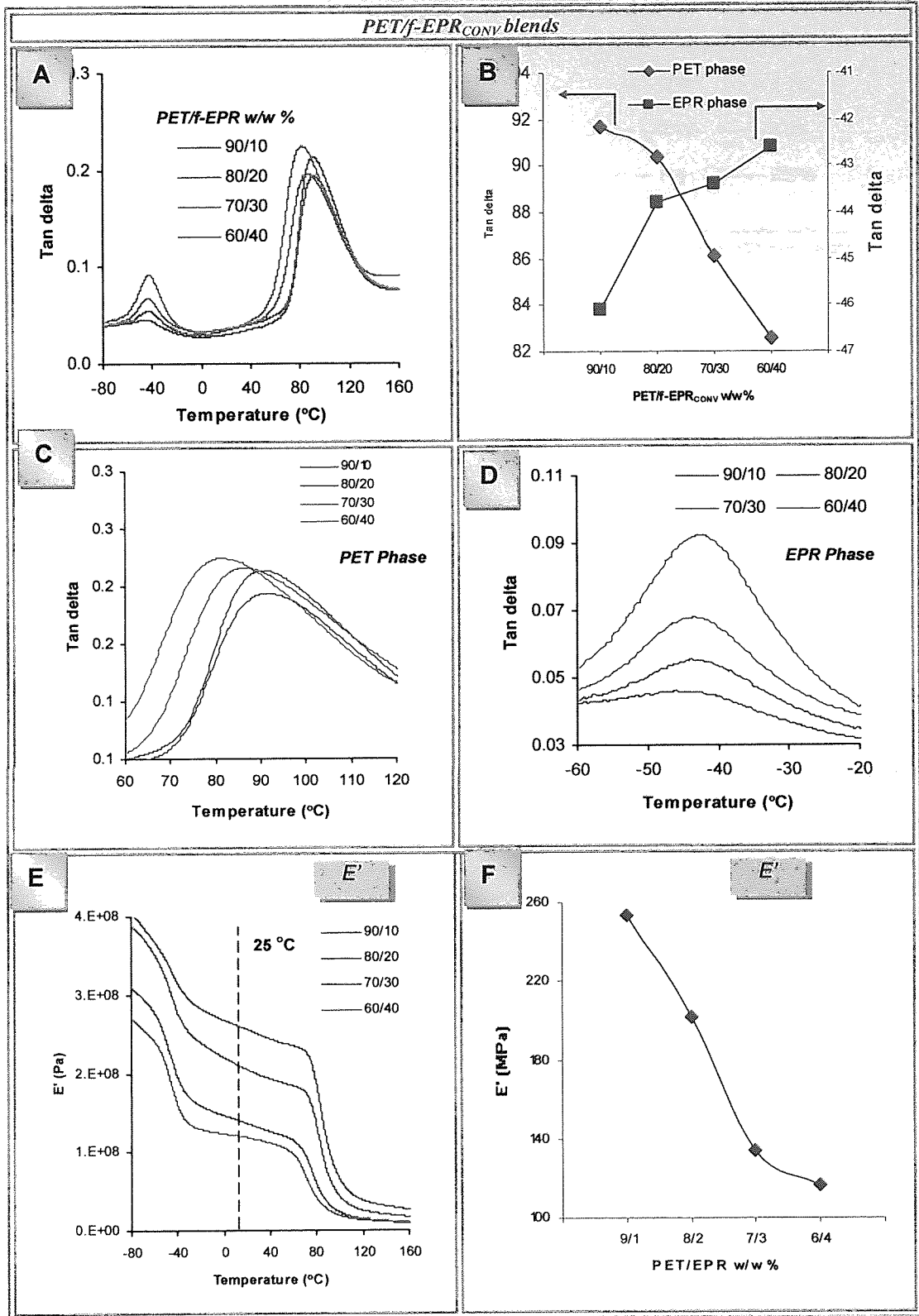


Figure 4.13. Effect of blend composition on torque and mechanical properties of PET/EPR-g-GMA<sub>CONV</sub> blends. Samples BG3(9:1)-(6:4), f-EPR<sub>CONV</sub>: g-GMA=1.7 wt%, polyGMA=0.6 wt%, MFI=0.9 g/10min) in Table 4.2.



**Figure 4.14:** Effect of blend compositions on morphology of PET/EPR and PET/EPR-g-EPR<sub>CONV</sub>. Samples BG3(9:1)-(6:4),  $f$ -EPR<sub>CONV</sub>: g-GMA=1.7 wt%, polyGMA=0.6 wt%, MFI=0.9 g/10min) in Table 4.2.



**Figure 4.15.** Effect of blend composition on thermal properties of the PET/EPR-g-GMA<sub>CONV</sub> blends. Samples BG3(9:1)-(6:4) (*f*-EPR<sub>CONV</sub>: g-GMA=1.7 wt%, polyGMA=0.6 wt%, MFI=0.9 g/10min) in Table 4.2.

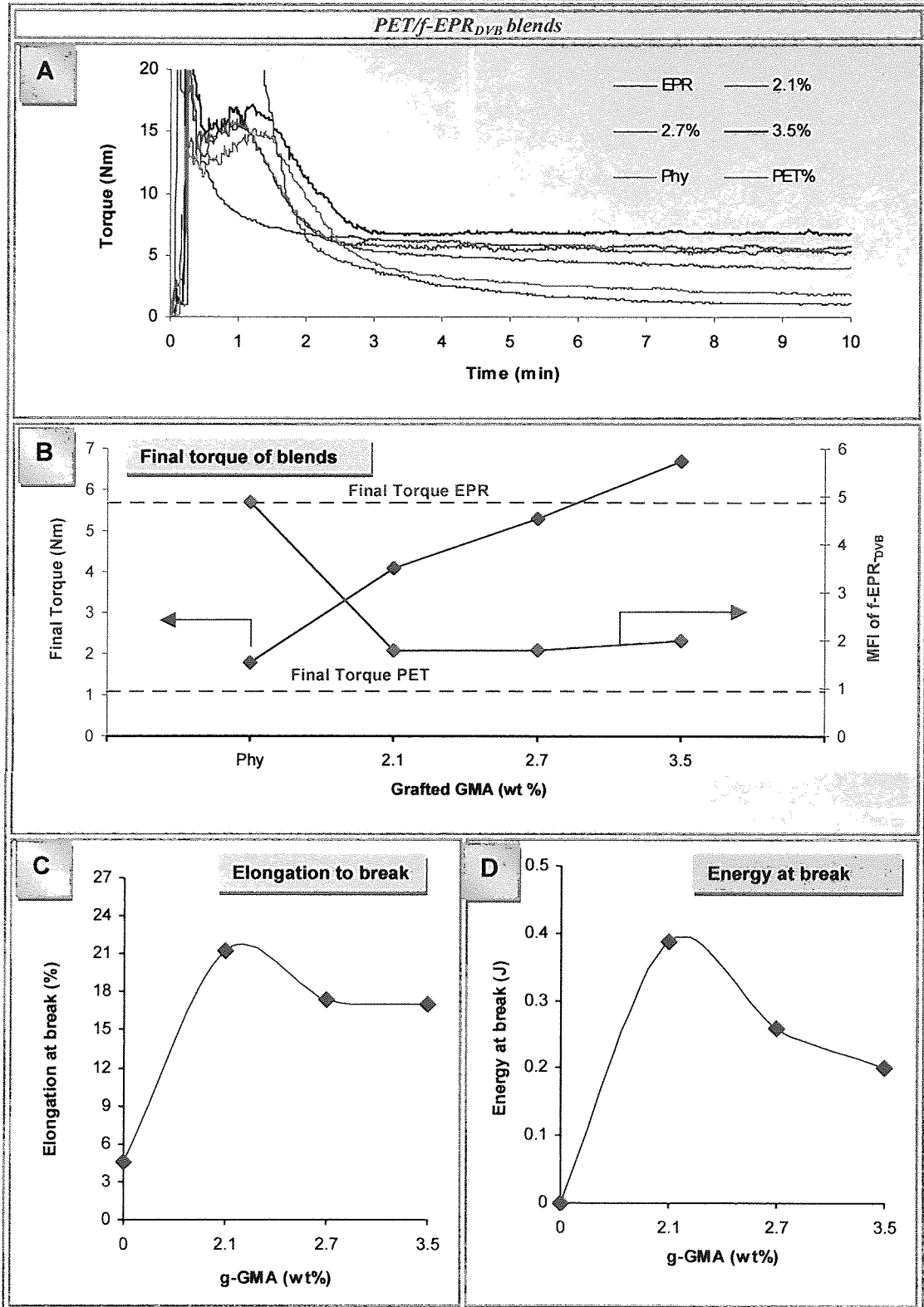


**Figure 4.16.** Effect of grafting level on torque curves and tensile properties of PET/*f*-EPR<sub>DVB</sub> blends 70/30 w/w%. Samples P73, BD6, BD5, BD3 Samples BD6 (*f*-EPR<sub>DVB</sub>: g-GMA=2.1 wt%, MFI=1.8 g/10min), BD5 (*f*-EPR<sub>DVB</sub>: g-GMA=2.7 wt%, MFI=1.8 g/10min), BD3 (*f*-EPR<sub>DVB</sub>: g-GMA=3.5 wt%, MFI=2.0 g/10min) in **Table 4.2**.



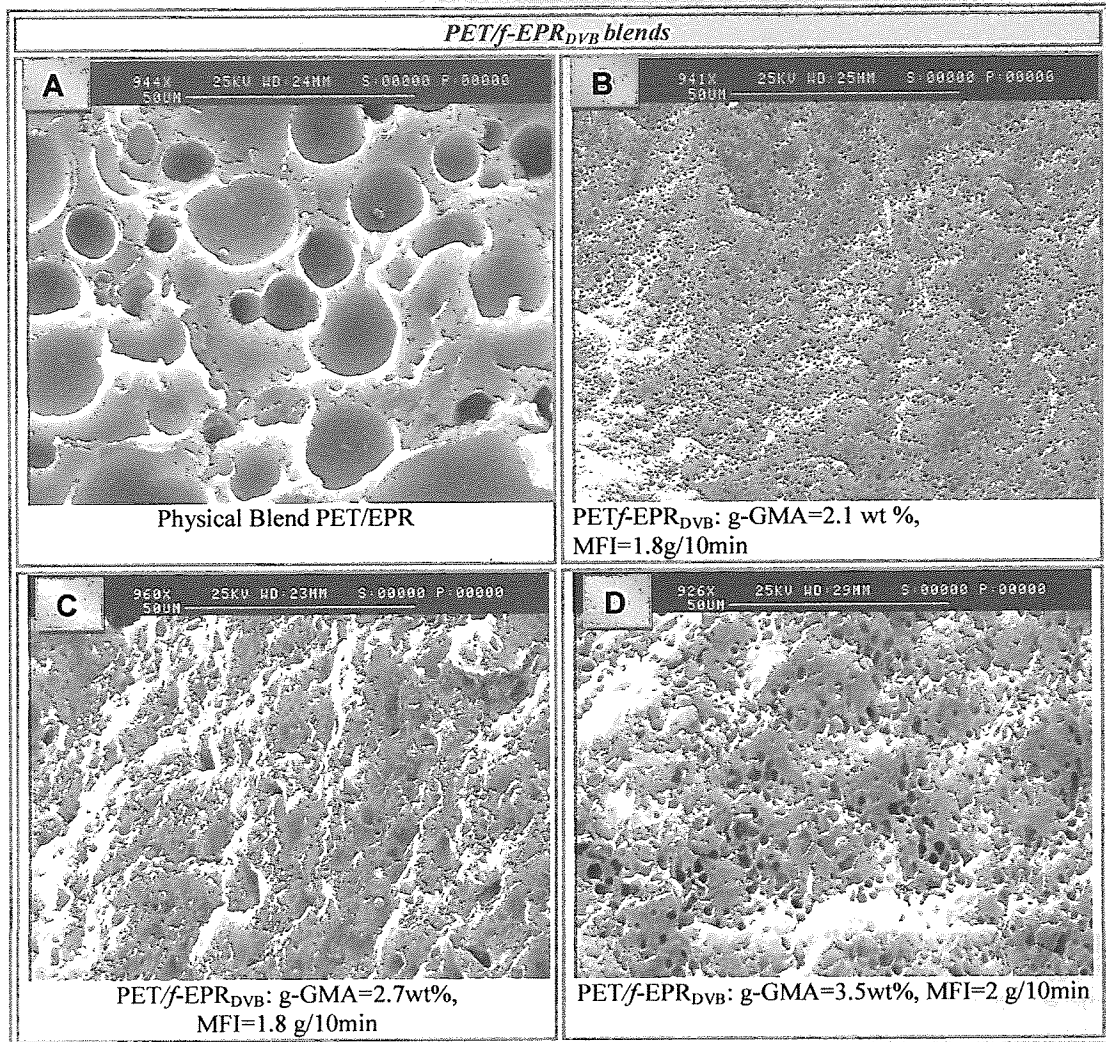


**Figure 4.17.** Effect of GMA grafted level on morphology of PET/f-EPR<sub>DVB</sub> blends 70/30 w/w. Samples P73, BD6, BD5, BD3 in Table 4.2.

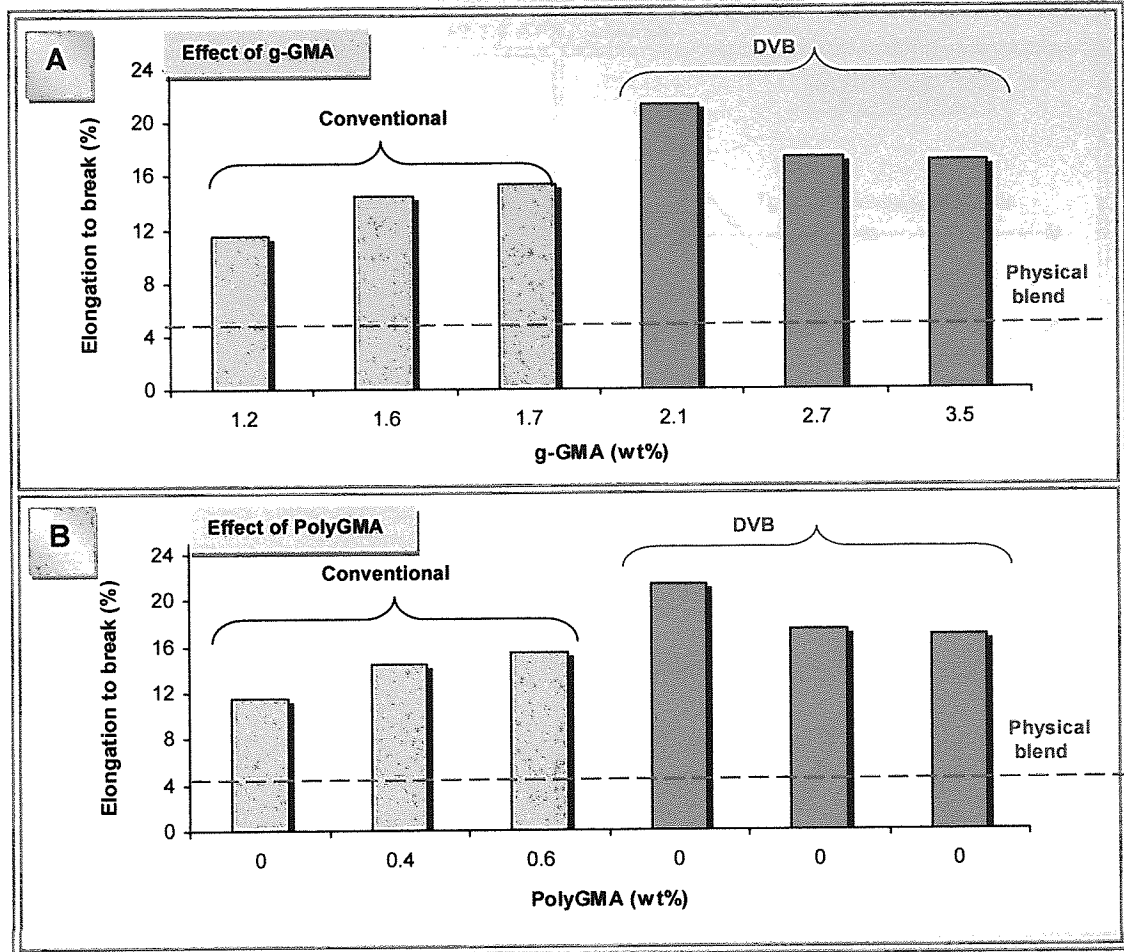
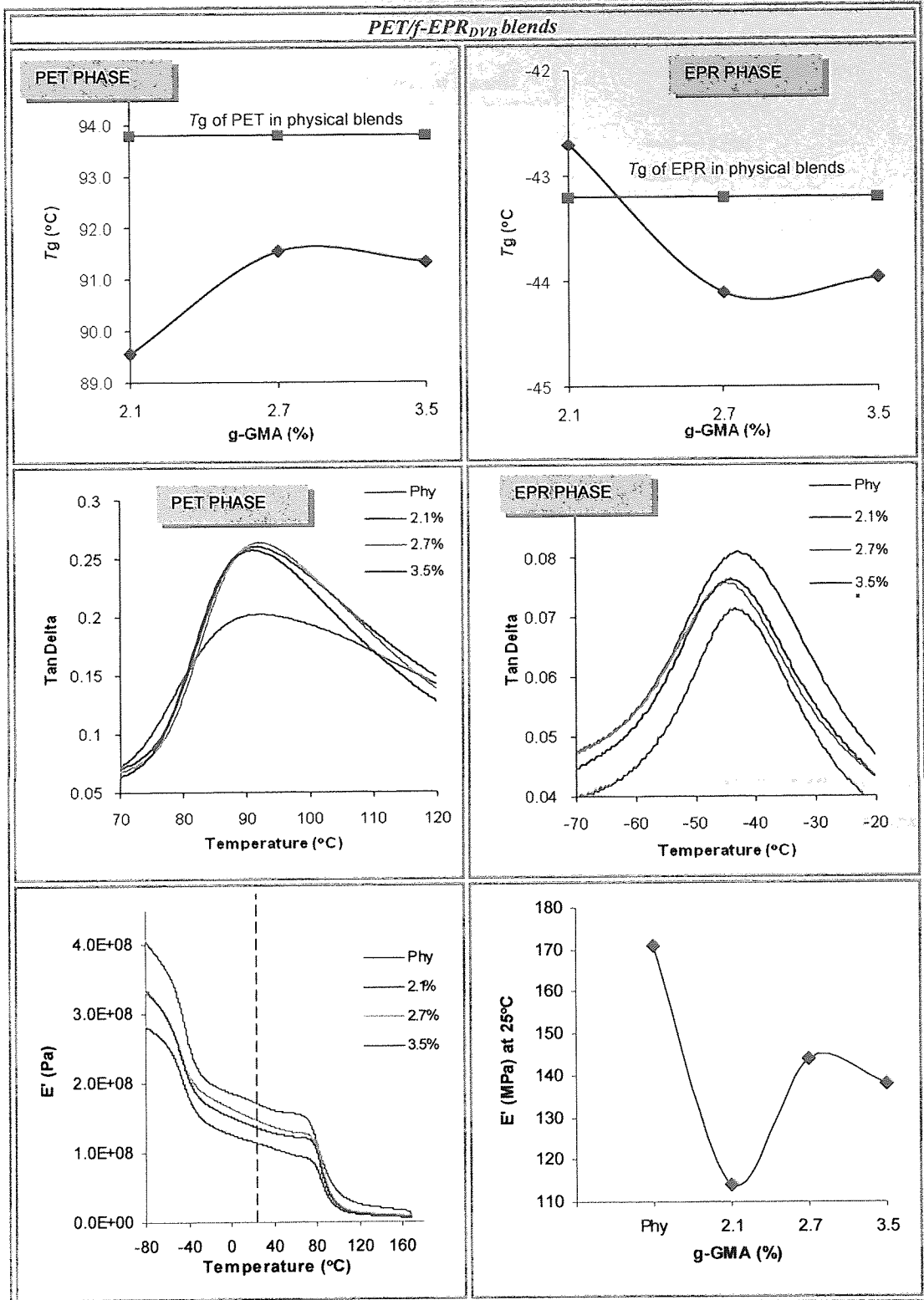
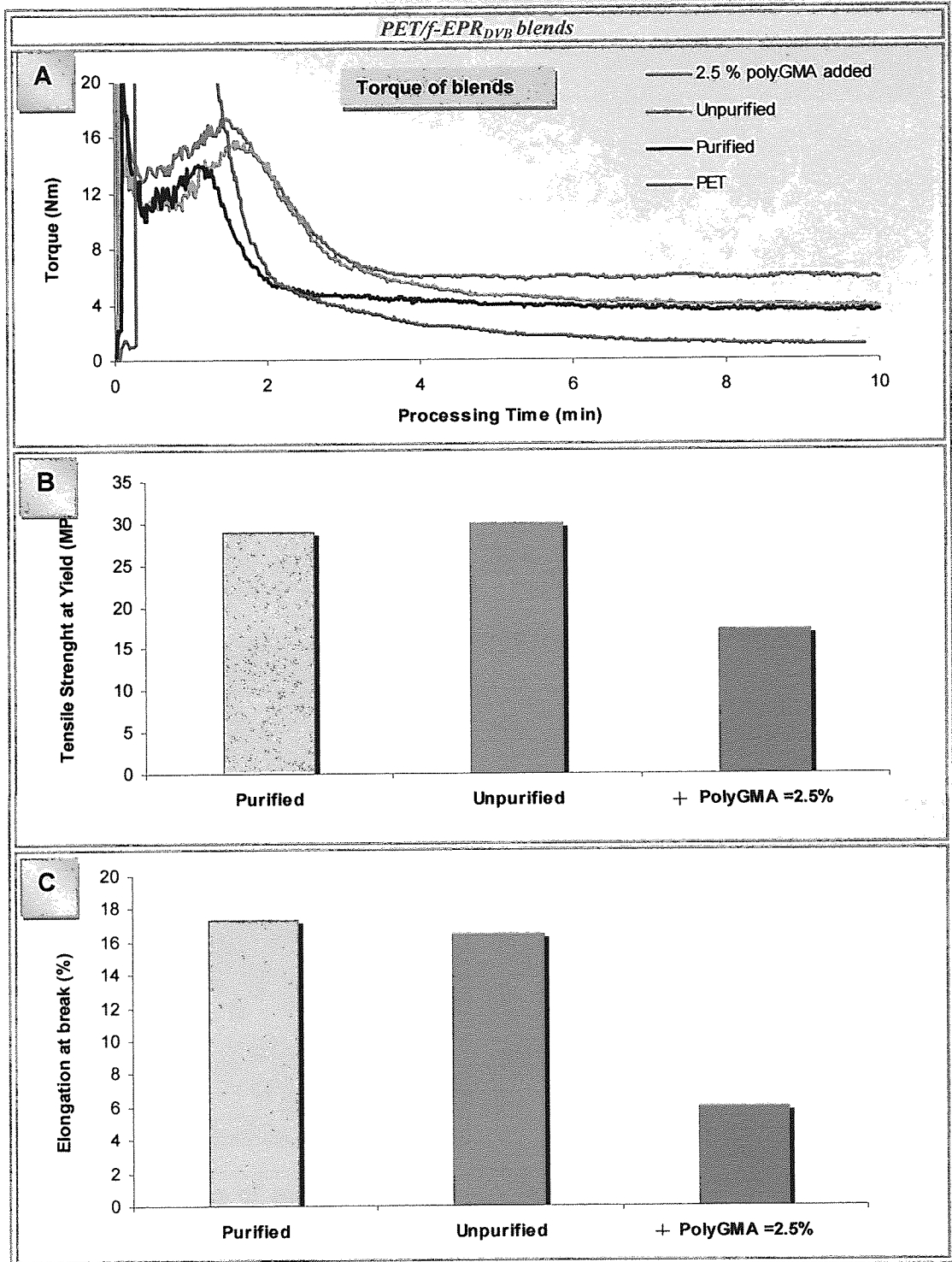


Figure 4.18. Elongation at break of PET/EPR-g-GMA in both system (with comonomer and without comonomer) at various grafting level and polyGMA concentration



**Figure 4.19.** Effect of grafting level of EPR-g-GMA<sub>DVB</sub> on tan delta of PET/ EPR-g-GMA<sub>DVB</sub> blends 70/30 w/w%. Samples BD6 (*f*-EPR<sub>DVB</sub>: g-GMA=2.1 wt%, MFI=1.8 g/10min), BD5 (*f*-EPR<sub>DVB</sub>: g-GMA=2.7 wt%, MFI=1.8 g/10min), BD3 (*f*-EPR<sub>DVB</sub>: g-GMA=3.5 wt%, MFI=2.0 g/10min) in Table 4.2.



**Figure 4.20.** Torque curves and mechanical properties of PET blended 70/30 w/w% with purified EPR-g-GMA<sub>DVB</sub> and with addition of synthesised polyGMA. Samples BD14, BD15, BD16 in Table 4.2. (f-EPR<sub>DVB</sub>: g-GMA=3.5 wt %, polyGMA=0%, MFI=0.7 g/10min).

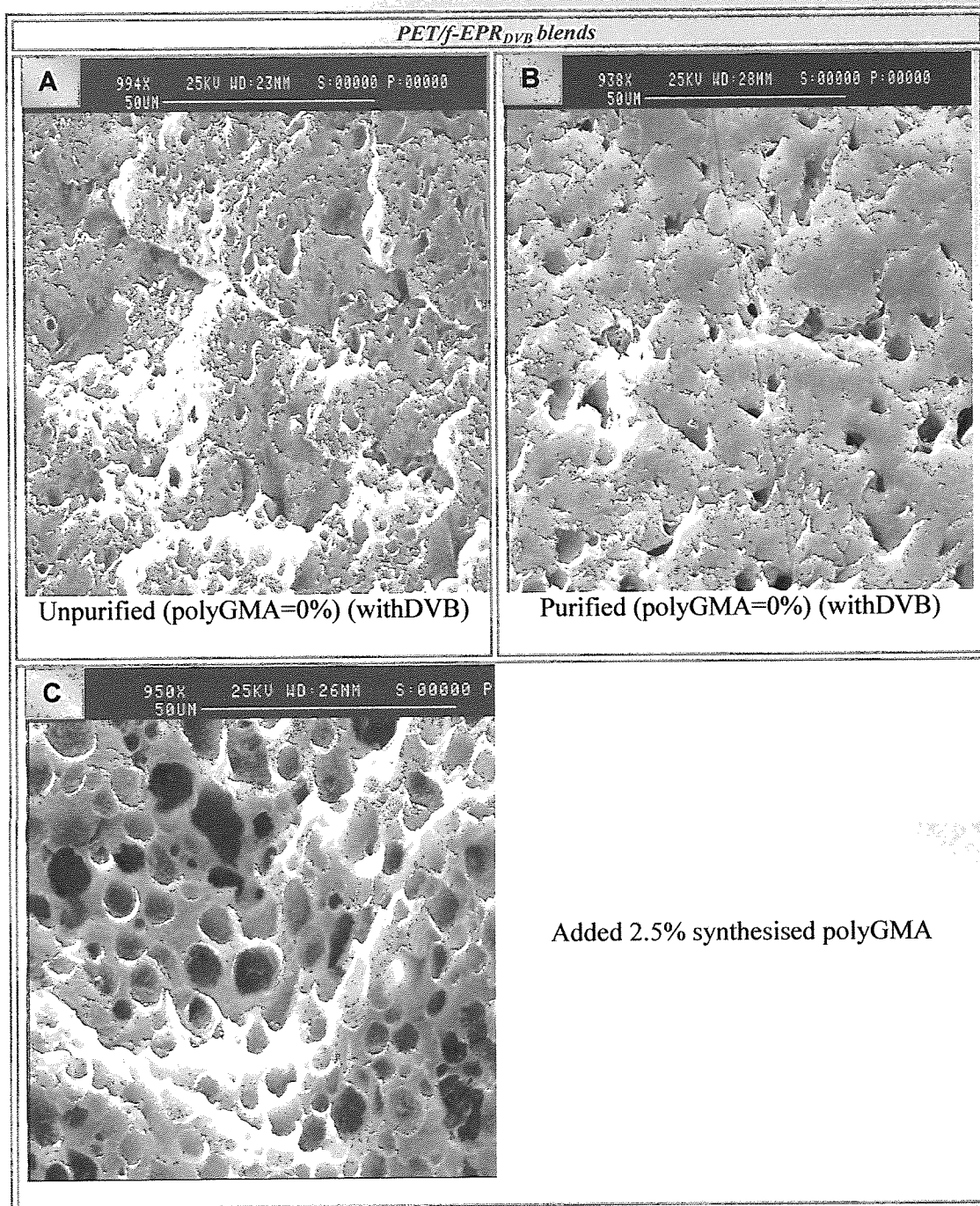


**Figure 4.21.** Effect of addition of polyGMA to PET/f-EPR<sub>DVB</sub> (70/30 w/w%) blend morphology, samples BD14, BD15, BD16 in **Table 4.2.** (f-EPR<sub>DVB</sub>: g-GMA=3.5 wt%, MFI=0.7 g/10min, BD14-added 2.5% synthesised polyGMA).

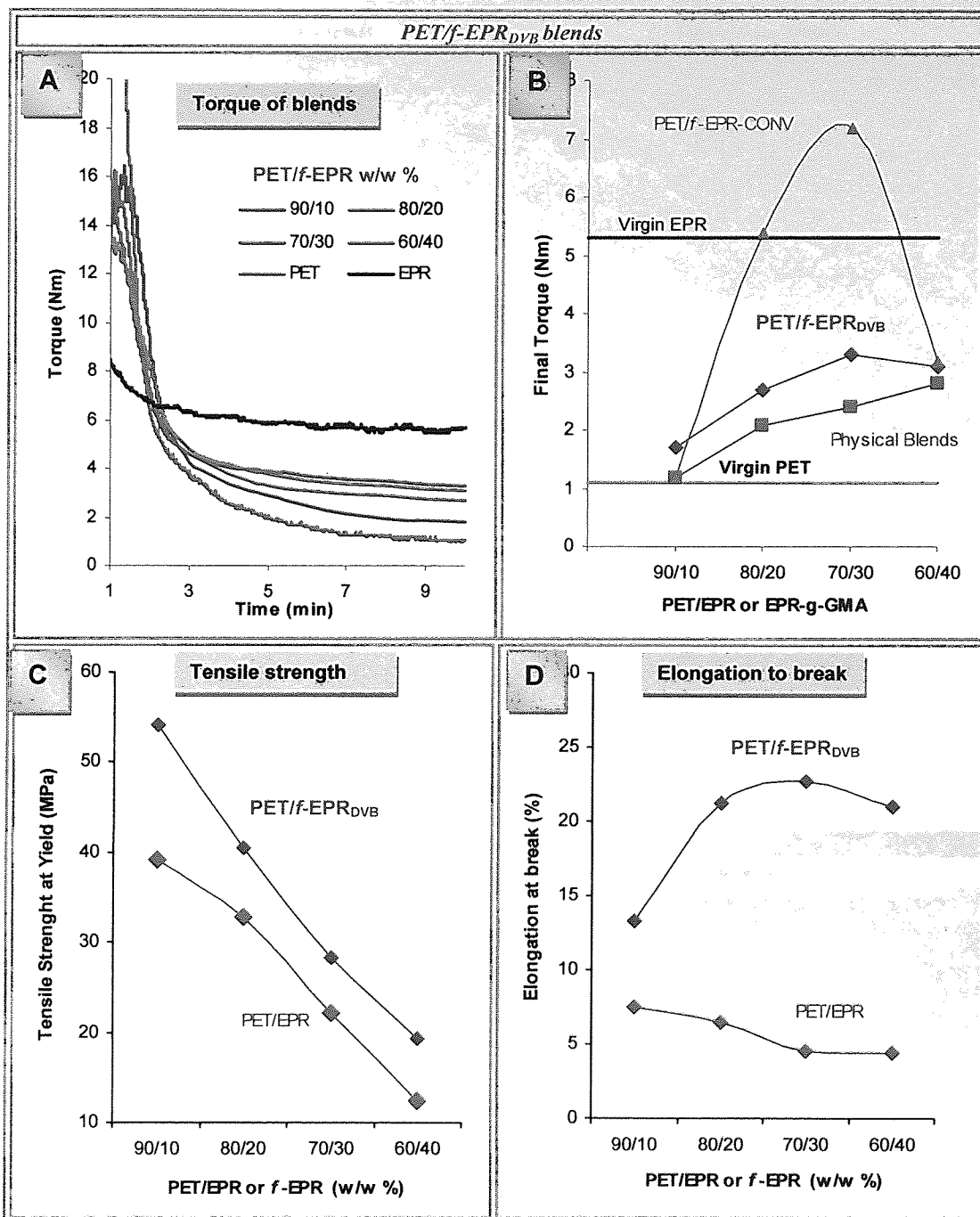


Figure 4.22. Effect of blend composition on torque and mechanical properties of PET/f-EPR<sub>DVB</sub> blends. Samples BD13(9;1)-(6;4) in Table 4.2, (f-EPR<sub>DVB</sub>-DG10-g-GMA=2.3 wt%, MFI=2.3 g/10min)

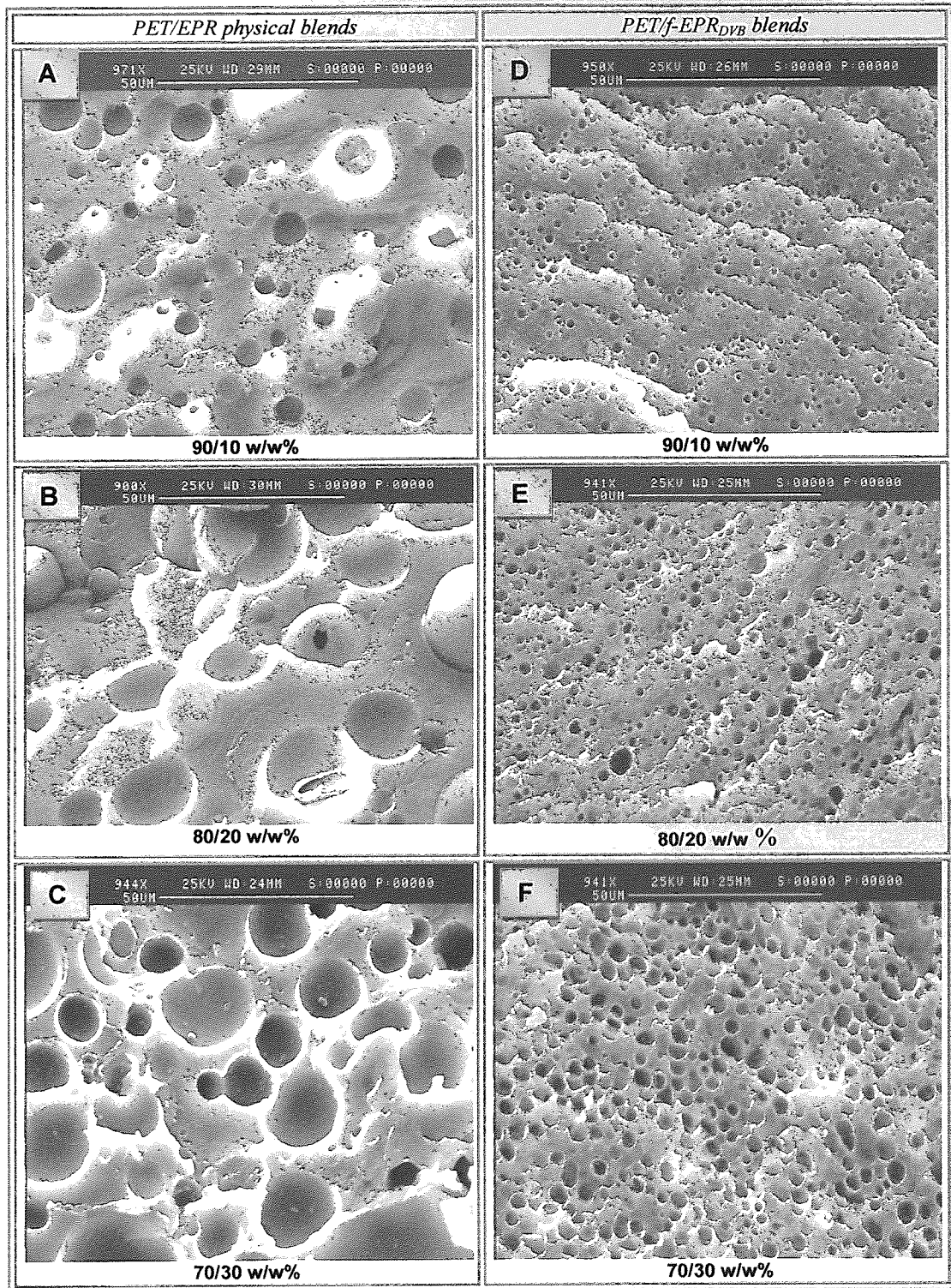
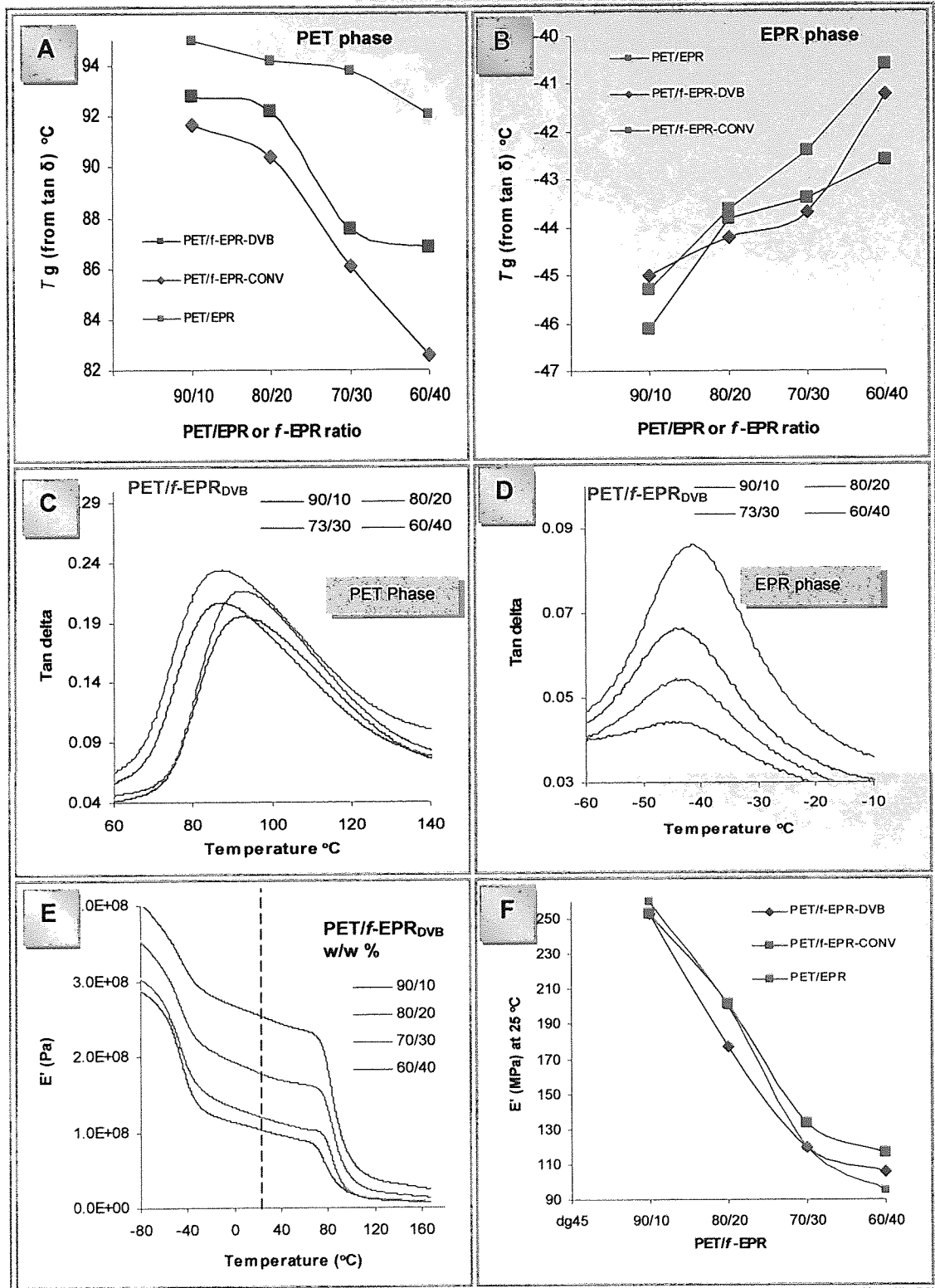


Figure 4.23: Effect of blend composition on morphology of PET/*f*-EPR<sub>DVB</sub>. Samples BD13(9;1)-(6;4) in Table 4.2 (*f*-EPR<sub>DVB</sub>-*g*-GMA=2.3 wt%, MFI=2.3 g/10min)



**Figure 4.24.** Effect of blend composition on thermal properties of the PET/f-EPR<sub>DVB</sub>. Sample BD13(9:1)-(6:4), BG3(9:1)-(6:4), **Table 4.2**. The f-EPR<sub>DVB</sub> is sample DG10-(g-GMA=2.3 wt%, MFI=2.3 g/10min) and that of f-EPR<sub>CONV</sub> is sample G19-(g-GMA=1.7 wt%, polyGMA=0.6 wt%, MFI=0.9 g/10min)



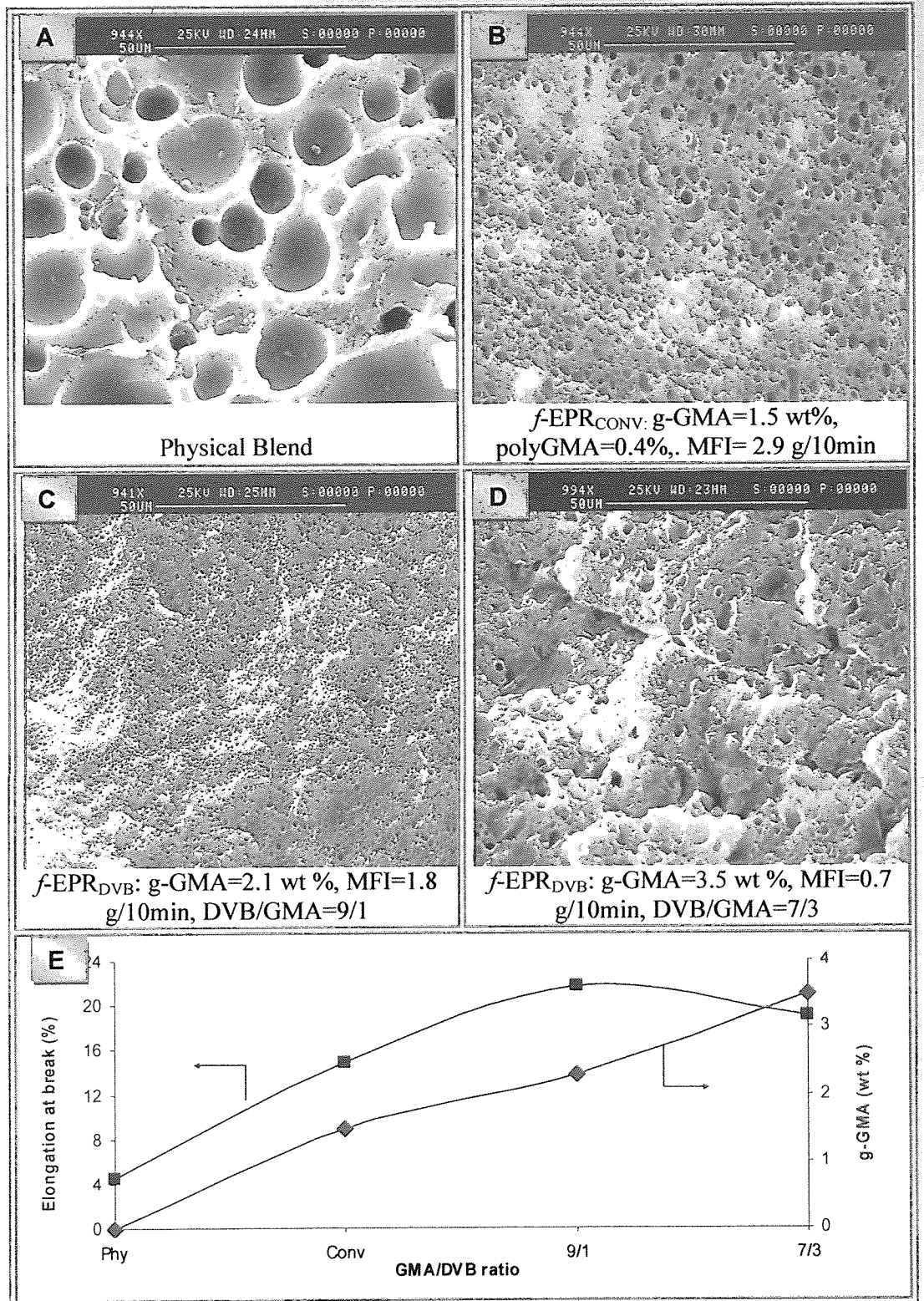


Figure 4.25. Comparison the morphology of reactive blends in the presence of DVB or in the absence of DVB with the physical blend at blend ratio of 70/30 w/w%.

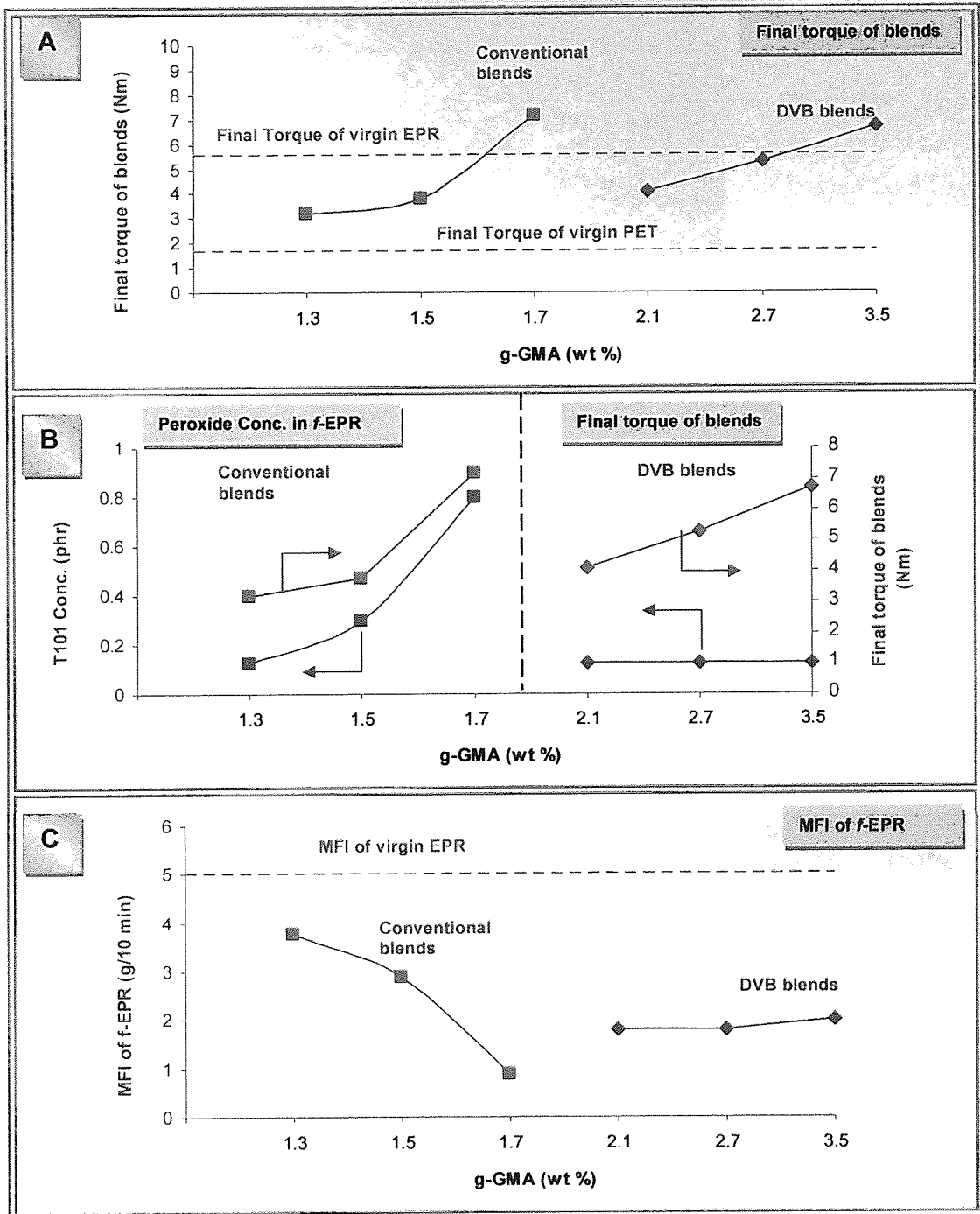
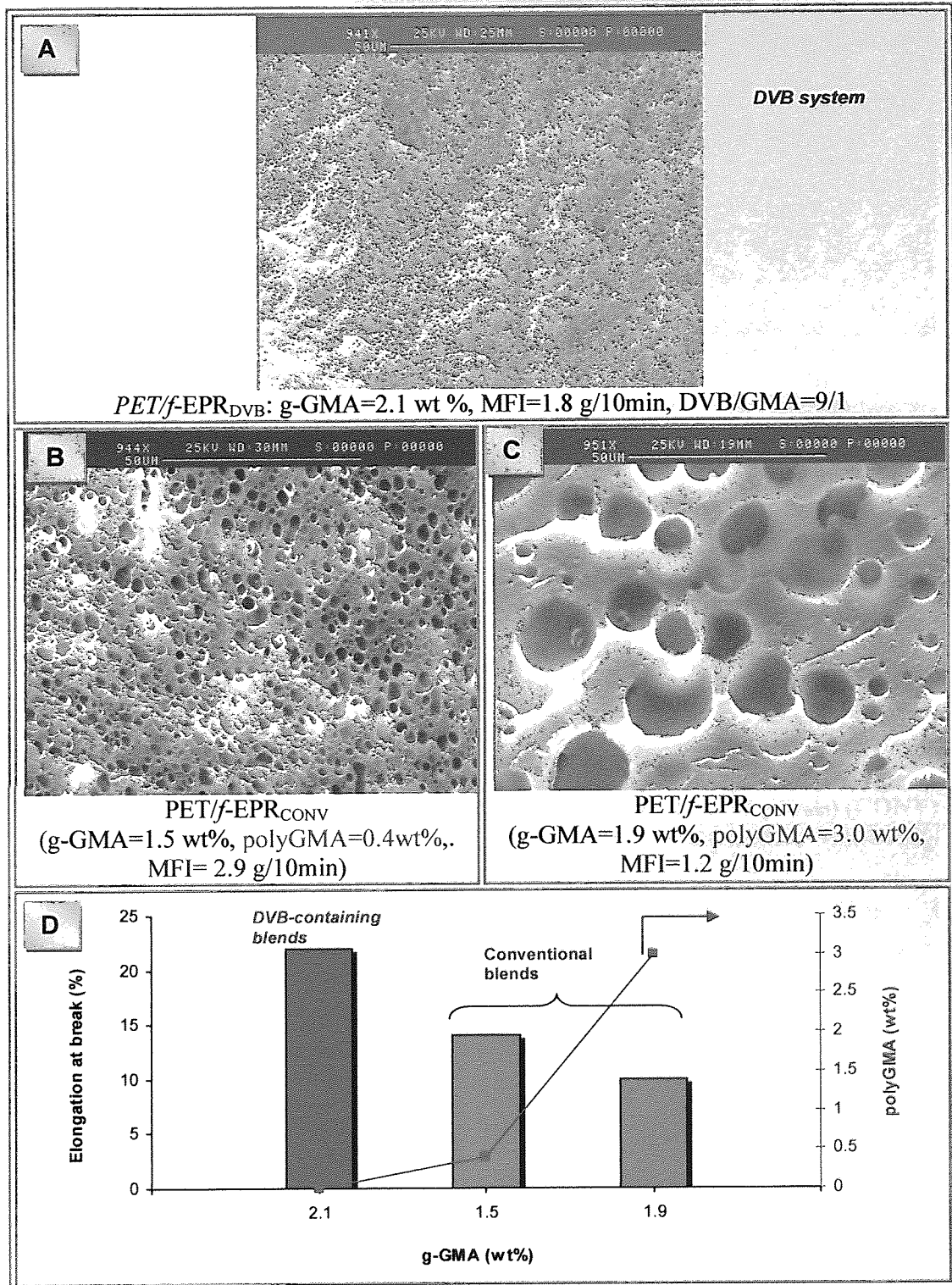
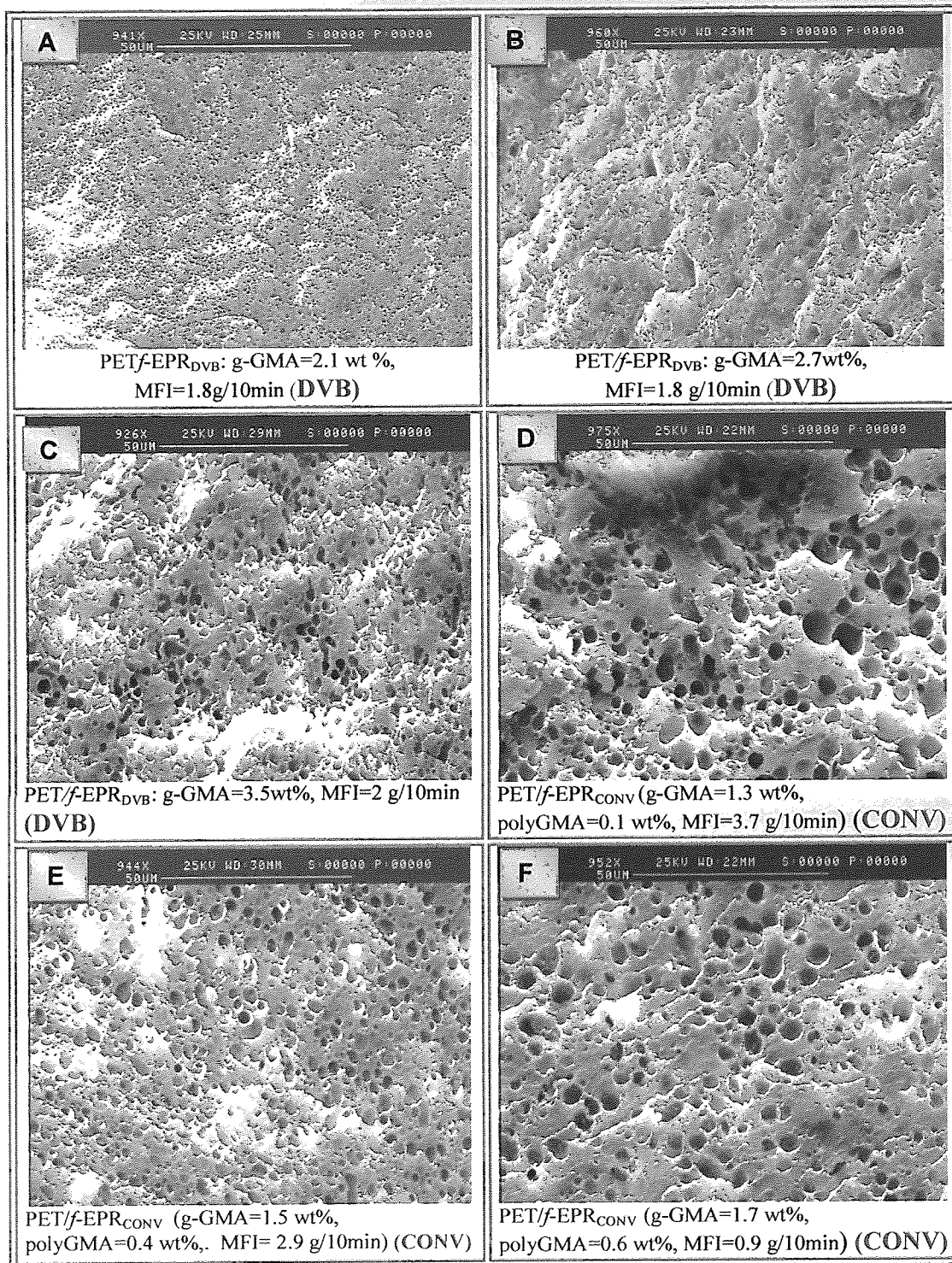


Figure 4.26. Comparison of EPR-g-GMA<sub>CONV</sub> and EPR-g-GMA<sub>DVB</sub> rheology properties, and peroxide concentration used during the grafting reaction on the blends' torque. Sample BD6, BD5, BD3(7:3), BG1, BG2, BG3(7:3) in Table 4.2.



**Figure 4.27.** Effect of higher GMA grafting level in 70/30 w/w% PET/f-EPR blends both in the presence and absence of the comonomer. Sample BD6 (DVB), BG2, BG6 (CONV) in **Table 4.2**.



**Figure 4.28.** Phase morphology of PET/EPR-g-GMA in both system (with comonomer and without comonomer) at various grafting level and polyGMA concentration.

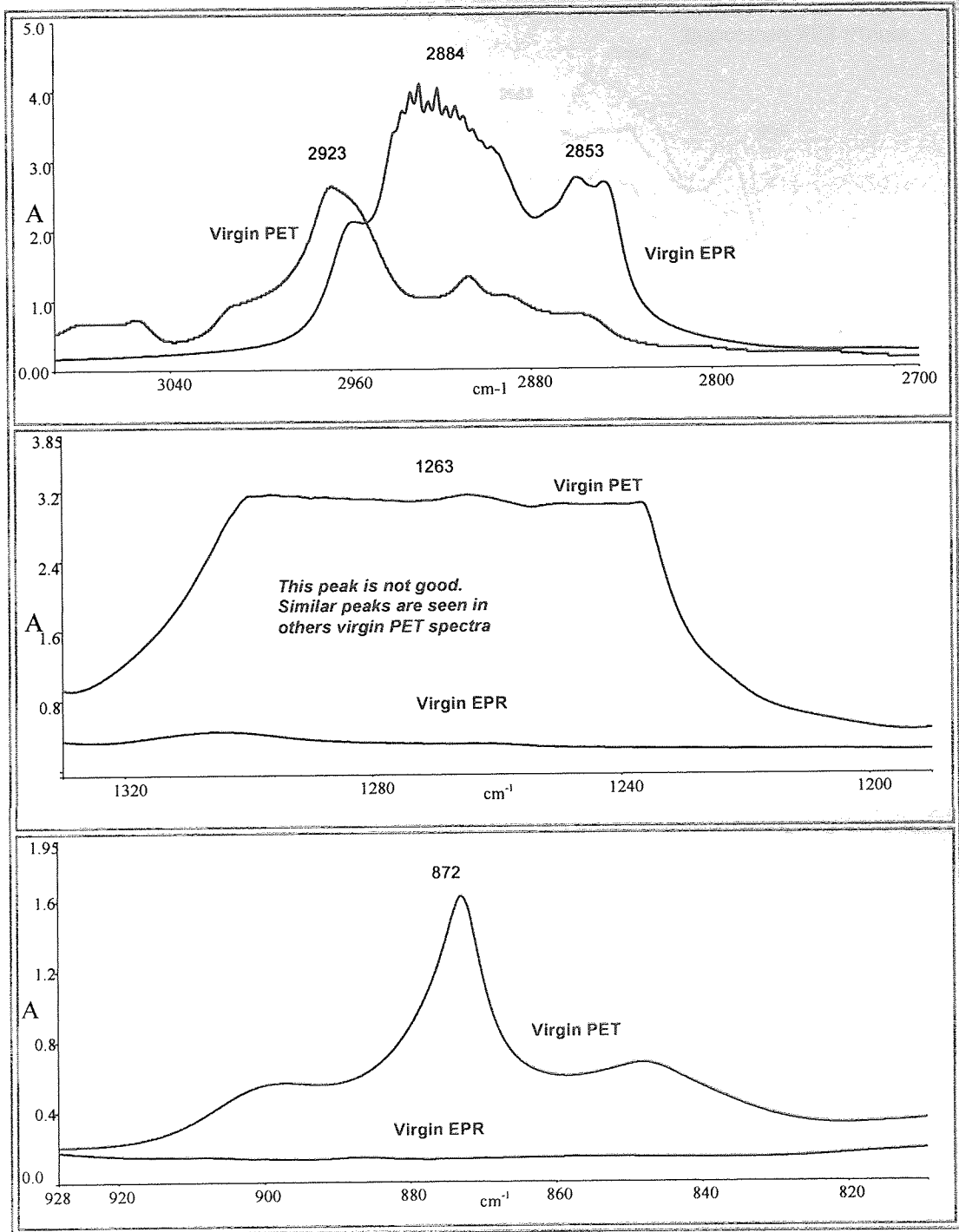
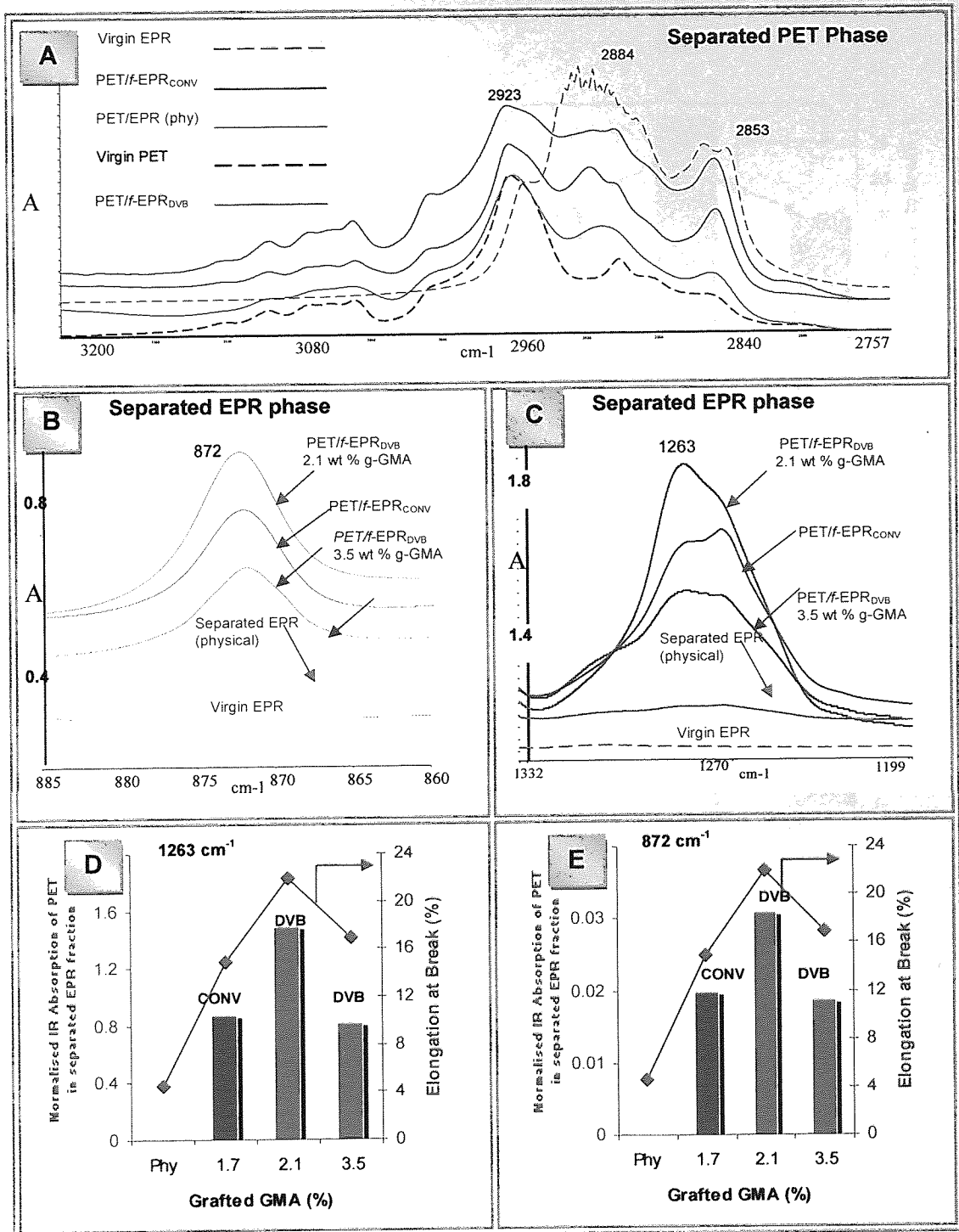
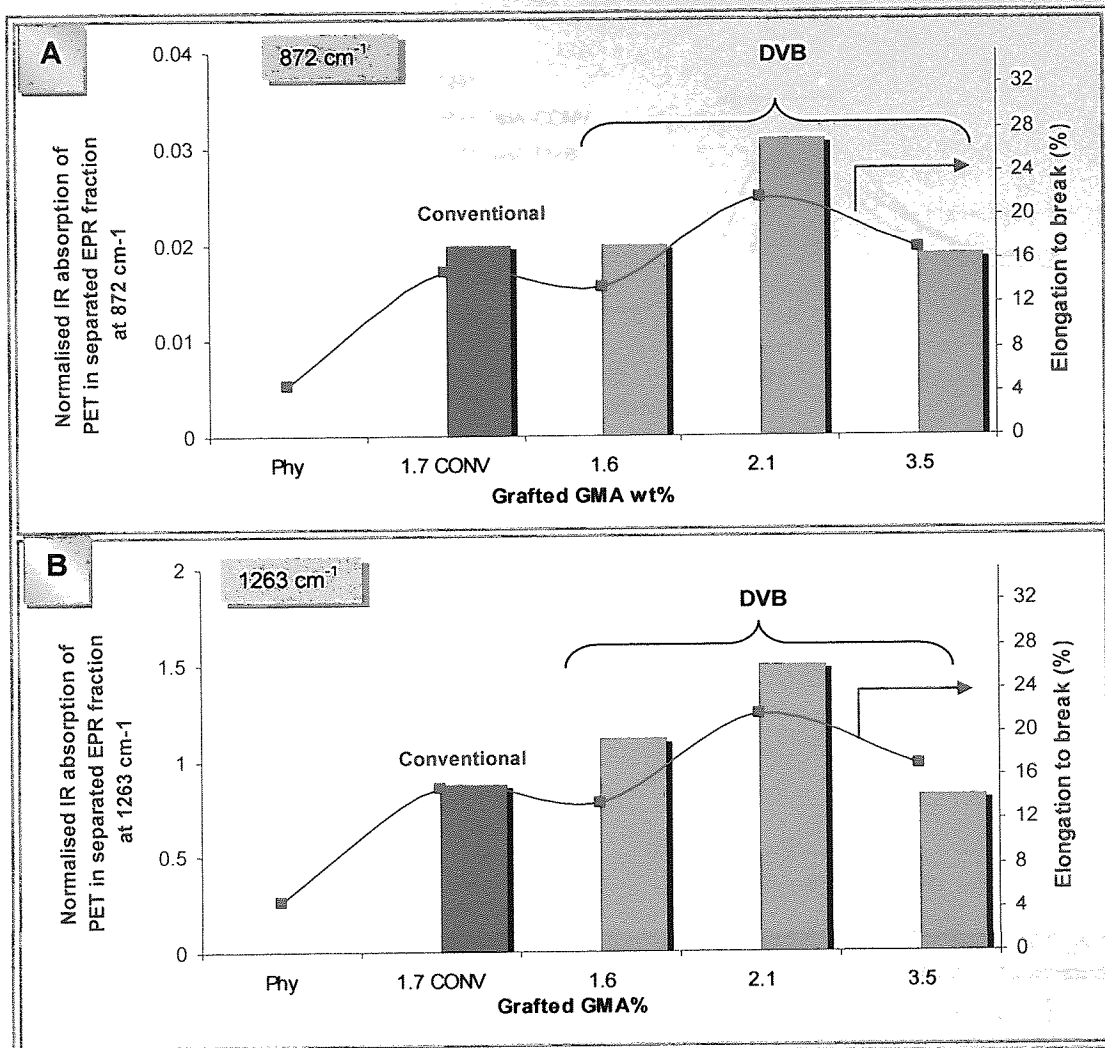


Figure 4.29(i). Interfacial analysis: Sample virgin EPR and virgin PET.



**Figure 4.29(ii).** Interfacial analysis of PET/EPR-g-GMA<sub>CONV</sub> (BG3(7:3)) and PET/EPR-g-GMA<sub>DVB</sub> (BD6, BD15) blends 70/30 w/w% by FTIR technique. Sample *f*-EPR<sub>DVB</sub>, DG23 (g-GMA=2.1 wt%, MFI=1.8 g/10min), DG43 (g-GMA=3.5 wt%, MFI=0.7 g/10min). Sample *f*-EPR<sub>CONV</sub>, G19 (g-GMA=1.7 wt%, MFI=0.9 g/10min), **Table 4.2**, see **Figure 4.29a** for virgin polymers IR spectra.



**Figure 4.30.** Correlation between tensile properties and IR absorption intensity of PET present in the separated EPR fraction from PET/*f*-EPR<sub>DVB</sub> 70/30 w/w% blends at different grafting levels. Result for conventional blend (BG3(7:3)) containing 1.7 wt% g-GMA is also compared. Samples BD1 (*f*-EPR<sub>DVB</sub>: g-GMA=1.6 wt%, MFI=3.8 g/10min), BD6 (*f*-EPR<sub>DVB</sub>: g-GMA=2.1 wt%, MFI=1.8 g/10min), BD3 (*f*-EPR<sub>DVB</sub>: g-GMA=3.5 wt%, MFI=2.0 g/10min), see **Table 4.2**. See also **Scheme 4.2**.

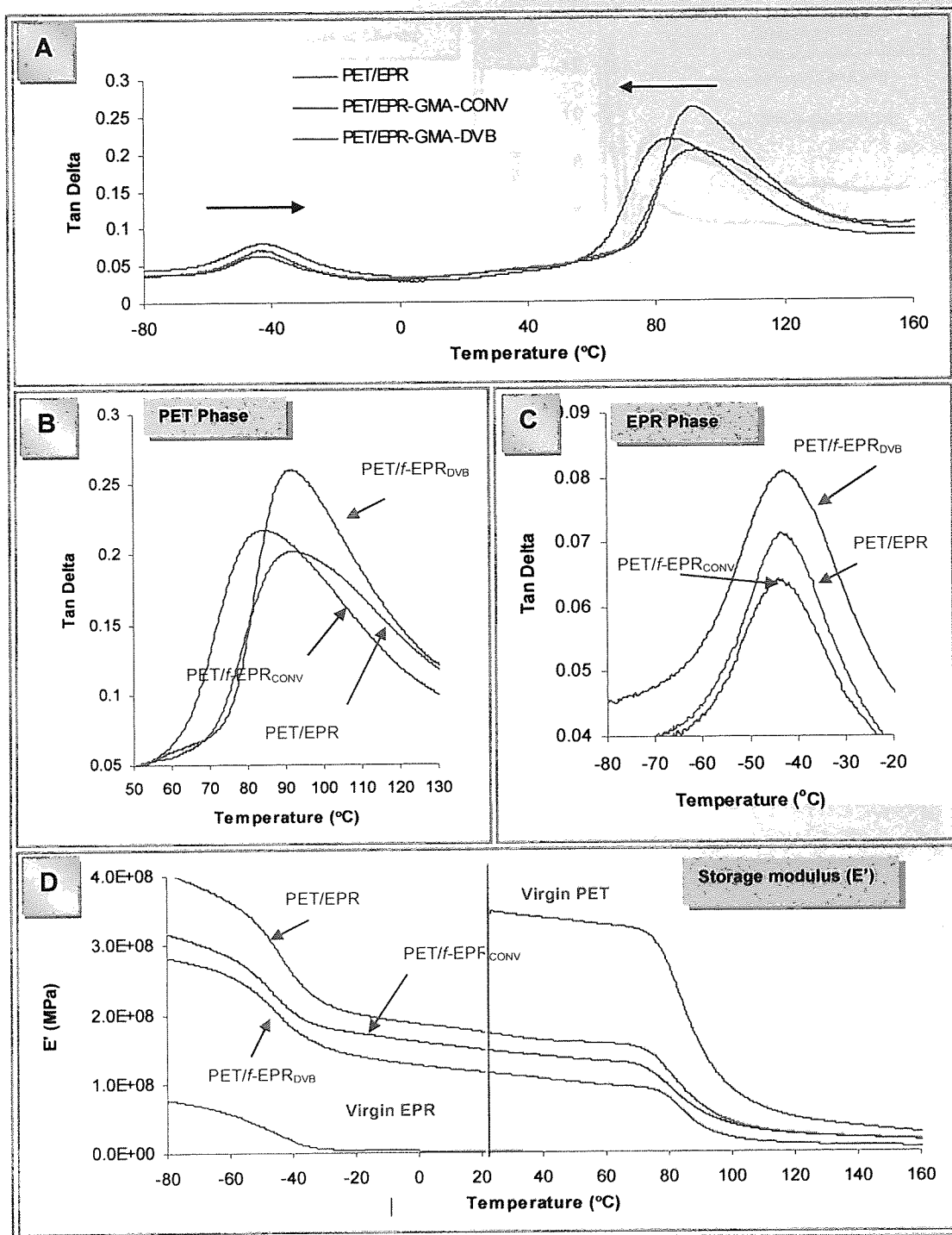


**Figure 4.31.** Dynamic mechanical properties of PET, EPR, physical blend of PET/EPR and reactive blends PET/f-EPR 70/30 w/w%. Samples P1, E1, P73, BD6 (DVB) (g-GMA=2.1 wt%) and BG2 (CONV) (1.5 wt%) in **Table 4.2**.



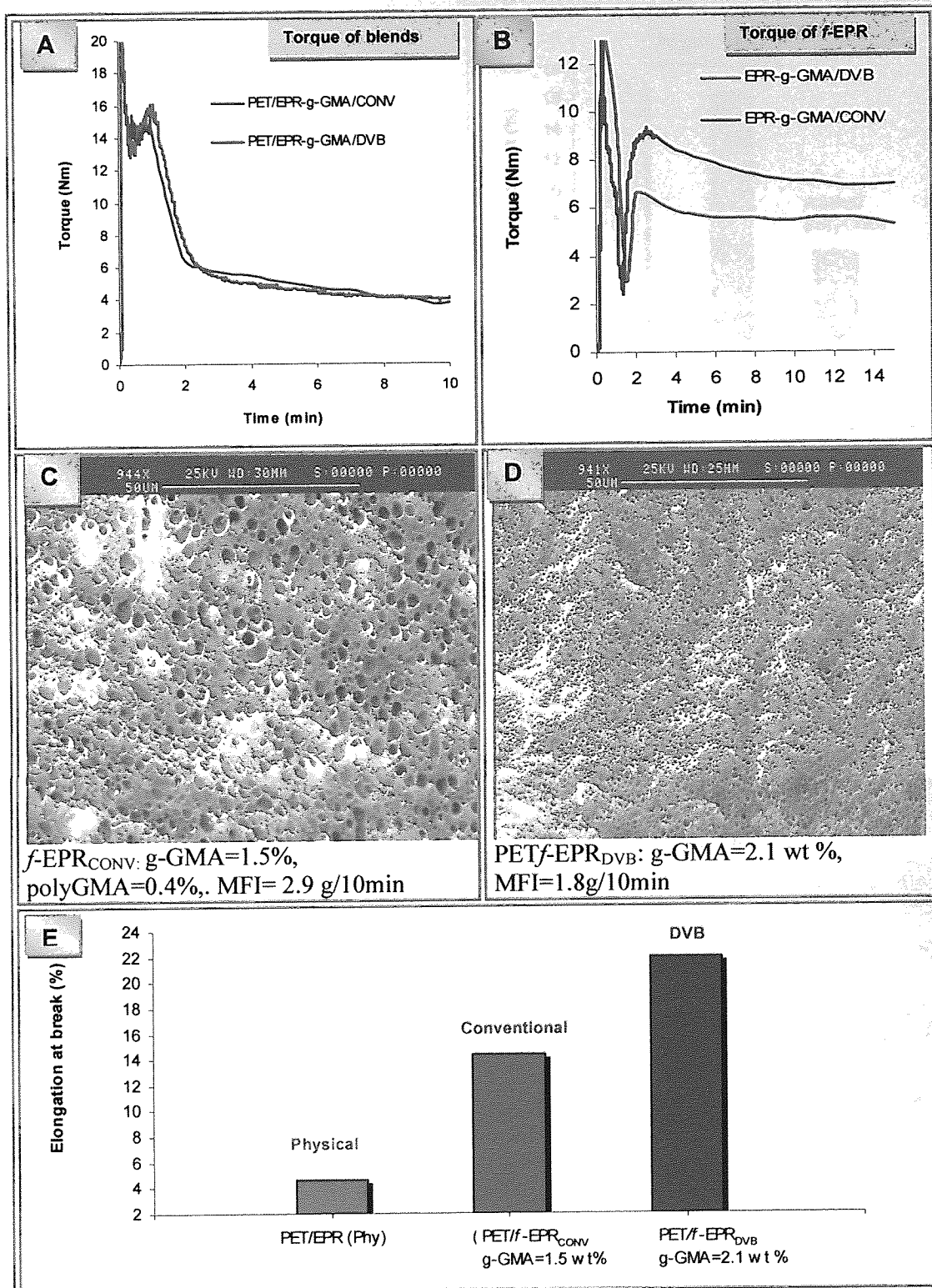


**Figure 4.32.** Comparison of PET/EPR-g-GMA<sub>CONV</sub> and PET/EPR-g-GMA<sub>DVB</sub> blends 70/30 w/w% in terms of morphology and elongation at break. These blends provide the best blend properties in their respective series.

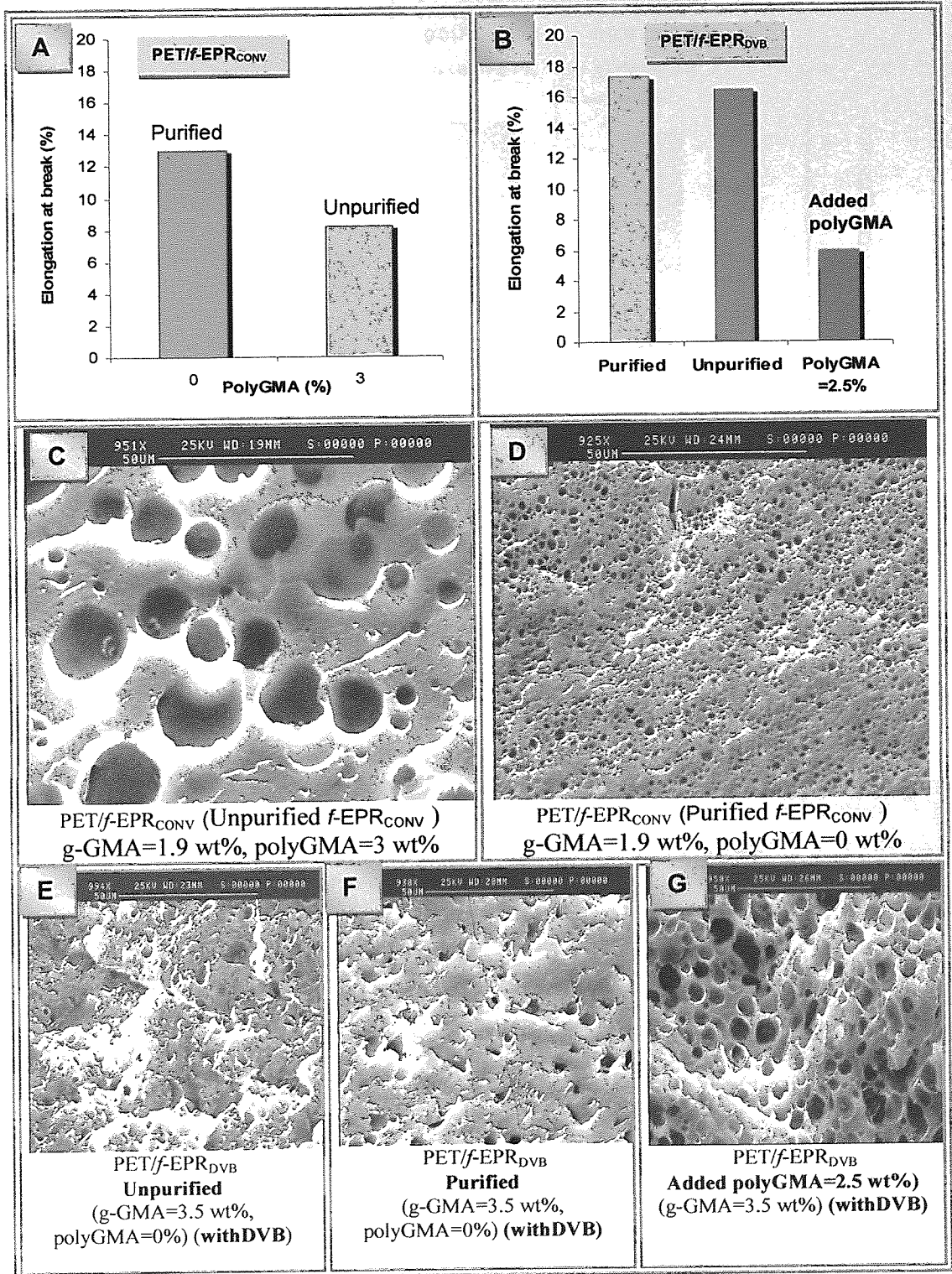


**Figure 4.33.** Effect of presence of polyGMA (unpurified in conventional or added polyGMA in DVB systems) and its absence (purified) in PET/f-EPR<sub>CONV</sub> (BG6-BG7) and PET/f-EPR<sub>DVB</sub> (BD15-BD16) 70/30 w/w% blends on elongation and morphology. f-EPR<sub>DVB</sub> is samples DG43 (g-GMA=3.5 wt%, MFI=0.7 g/10min), f-EPR<sub>CONV</sub> is sample G24 (g-GMA=1.9 wt%, polyGMA=3.0 wt%, MFI=1.2 g/10min), **Table 4.2.**

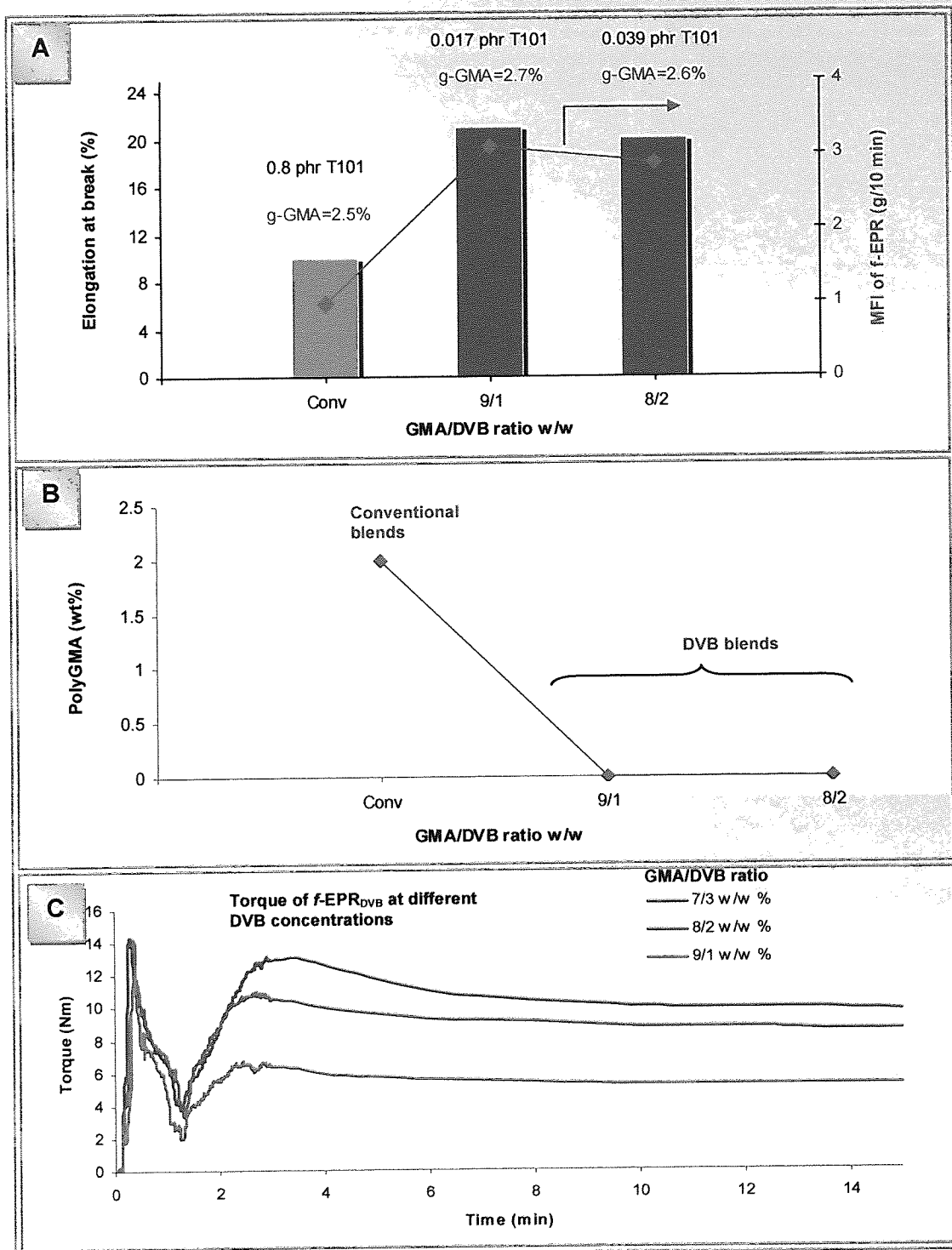


**Figure 4.34.** Effect of DVB concentration in  $f\text{-EPR}_{\text{DVB}}$  on tensile properties of PET/ $f\text{-EPR}_{\text{DVB}}$  blends 70/30 w/w%. Samples BG5 (G23- $f\text{-EPR}_{\text{CONV}}$ : MFI=1.0 g/10min), BD12 (DG38- $f\text{-EPR}_{\text{DVB}}$ : MFI=2.9 g/10min), BD17 (DG2- $f\text{-EPR}_{\text{DVB}}$ : MFI=3.1 g/10min), BD15 ( $f\text{-EPR}_{\text{DVB}}$ : MFI=0.7g/10min), see **Table 4.2** for A and B.  $f\text{-EPR}$  samples were processed at different T101 concentrations (A). Sample DG38, DG13, DG43 in **Table 4.1** were used in C

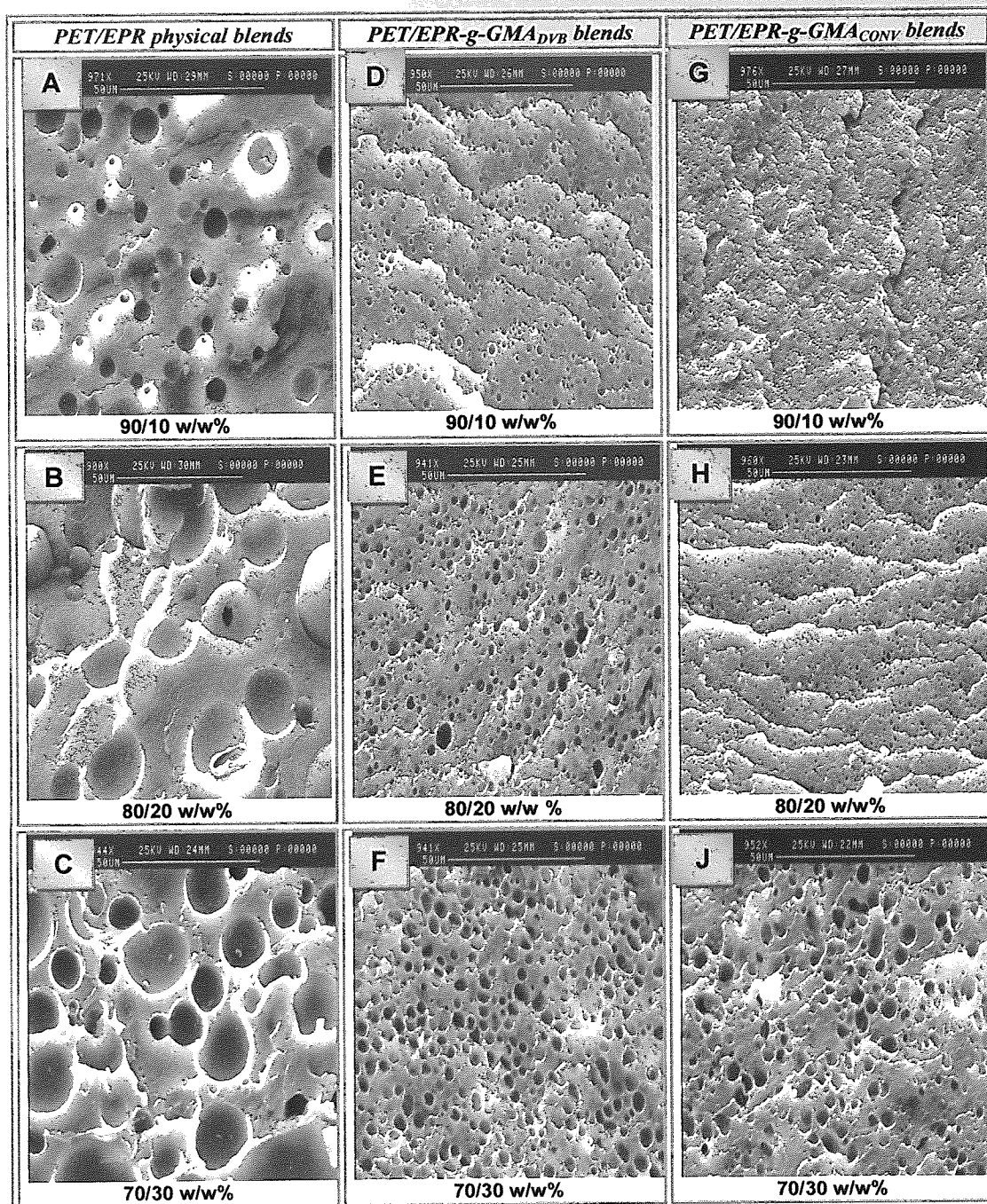


**Figure 4.35.** Morphology of PET blended with different type of *f*-EPR 70/30 w/w%. Sample conventional blends based on *f*-EPR<sub>CONV</sub> sample G19 (0.8 phr T101, 1.7 wt% g-GMA, 0.9 g/10min MFI) and DVB blend based on *f*-EPR<sub>DVB</sub> sample DG10 (0.017 phr T101, 2.3 wt% g-GMA, 3.7 g/10min MFI, **Table 4.1**). Note: The DVB blend is not one of the optimised samples whereas conventional blend is the optimised sample in the conventional series of samples.

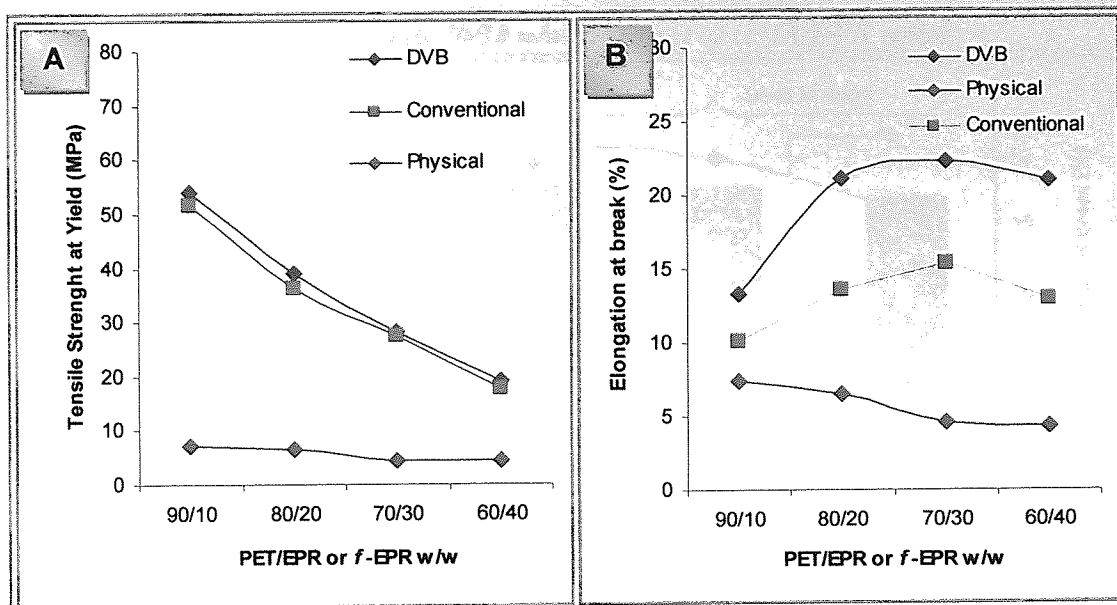


**Figure 4.36.** Comparison of PET blended with EPR in physical blends, and EPR-g-GMA<sub>CONV</sub> and EPR-g-GMA<sub>DVB</sub> in reactive blends at various rubber contents. Sample, P91, P82, P73, Samples based on conventional are BG3(9:1)-(6:4) (1.7 wt% g-GMA and 0.9 g/10min MFI), samples based on DVB are BG13(9:1)-(6:4) (2.3 wt% g-GMA and 3.7 g/10min MFI), **Table 4.2**.

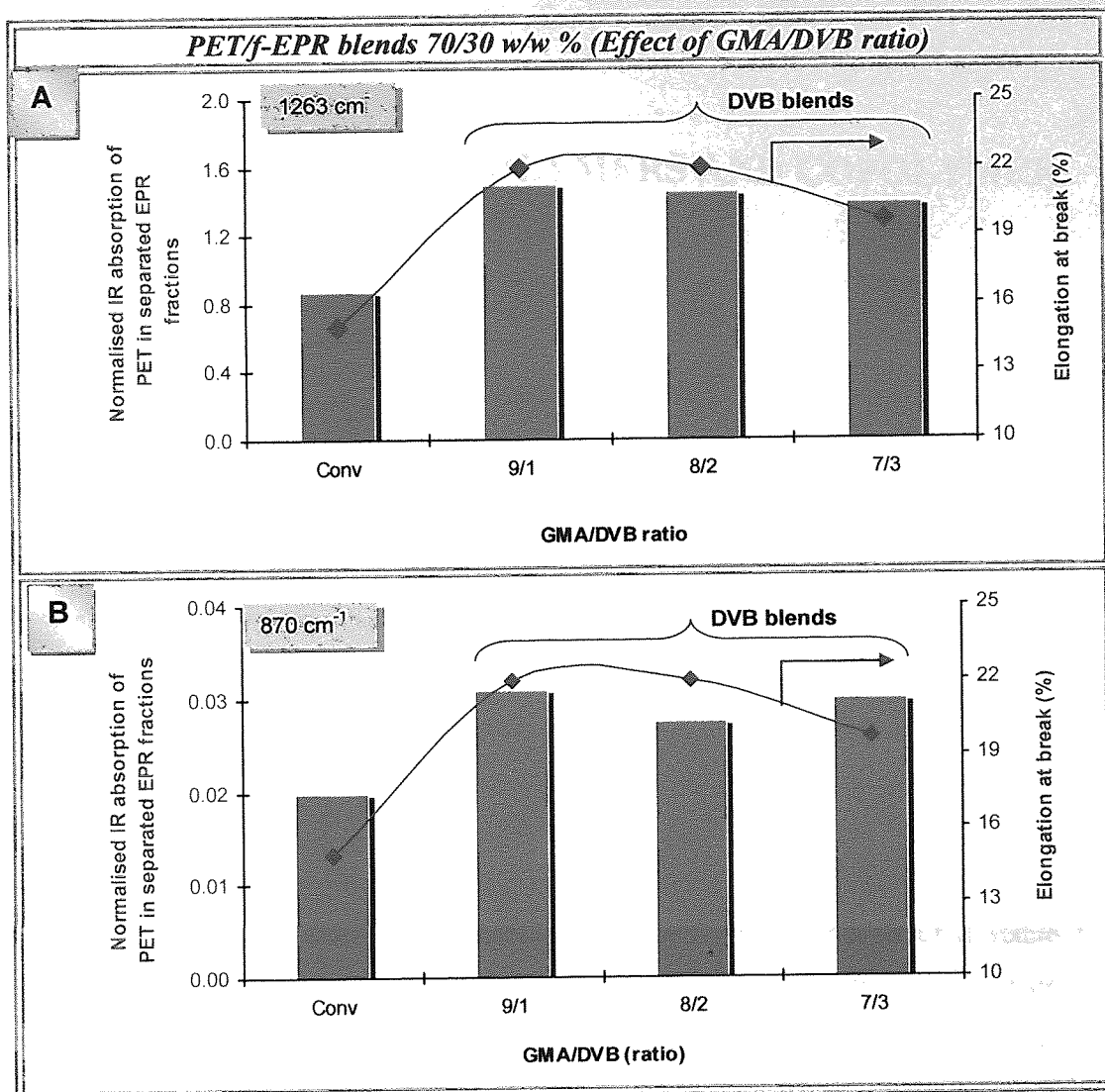


**Figure 4.37.** Correlation between elongation at break and intensity of absorbance of PET present in separated EPR fraction from PET/*f*-EPR<sub>DVB</sub> 70/30 blends at different DVB concentrations. Samples BG3(7:3) (*f*-EPR<sub>CONV</sub>: g-GMA=1.7 wt%, MFI=0.9 g/10min), BD6 (*f*-EPR<sub>DVB</sub>: g-GMA=2.1 wt%, MFI=1.8 g/10min), BD12 (*f*-EPR<sub>DVB</sub>: g-GMA=2.7 wt%, MFI=2.9 g/10min), BD15 (*f*-EPR<sub>DVB</sub>: g-GMA=3.5 wt%, MFI=0.7 g/min), see **Table 4.2**.

## CHAPTER 5

## PET BLENDS WITH TERPOLYMERS AND COPOLYMER

## 5.1 Objective and Methodology

Blending two polymers with different mechanical or chemical properties offers advantages over the individual components as the performance of the blends is generally enhanced and the economic viability of the new products is increased [240, 241]. Blends or alloys offer an attractive strategy for achieving specified portfolio of physical properties, without the need for synthesising specialised polymer systems. The miscibility of such polymer blends is determined by the specific interactions that occur between the two polymers. Incompatible polymer blends are likely to promote a weak interfacial adhesion, give a coarse and unstable morphology leading to poor adhesion between the two phases thus, the addition of a compatibiliser would improve their compatibility [242]. Compatibilisers which are either block or graft copolymers act by reducing the surface tension at the interface leading to the formation of a stable morphology. Common reactive functional groups present in compatibilisers include epoxide, anhydride, amine, oxazoline. **In this work**, a commercial copolymer of ethylene-glycidyl methacrylate (E-GMA, I) and three commercial terpolymers of ethylene-methacrylate-glycidyl methacrylate containing different GMA content (EM-GMA, II) were used as compatibilisers for PET/EPR in ternary blends of PET/EPR/co(ter)polymer (**Table 5.1** gives the full characteristics of the different compatibilisers used in this work). Both E-GMA and EM-GMA have been used extensively as compatibilisers in different polymer blends [91, 95, 156, 243-245].

Blends of PET with the different commercial co(ter)polymer compatibilisers (see **Table 5.2**) were prepared and the effect of their GMA content and viscosity on the blend properties was determined. The *f*-EPR samples, prepared in this work in the presence and absence of DVB (see **Chapter 3**), were also used as compatibilisers in ternary blends (presented in this chapter) and are listed in **Table 5.3**. The efficiency of compatibilisation of the commercial co(ter)polymer and the *f*-EPR in the ternary blends

was examined and compared. For all the ternary blends (PET/EPR/co(ter)polymer or *f*-EPR blends), the PET content was fixed at 70 wt% of the total weight of the blends. The weight ratio between EPR and the co(ter)polymer or the *f*-EPR was varied (i.e 25/5, 20/10, 15/15 and 10/20 w/w %) with the total rubber weight content being kept at 30 wt%, see **Tables 5.2** and **5.3**.

The objectives of the work described in this chapter were to investigate the compatibilising efficiency of these commercial co(ter)polymers when used in ternary PET/EPR blends, and, to compare their efficiency with ternary blends containing the in-home made modified GMA-EPR (*f*-EPR) containing similar grafting level prepared in this work. It is important to point out here, however, that the comparison is only a qualitative one as the commercial ter(co)polymers are very different in their structure and characteristics compared with those synthesised (*f*-EPR) in this work. The blending work was carried out using an internal Haake mixer at a temperature of 260 °C for 10 minutes. **Scheme 5.1** shows a diagram illustrating the methodology used.



Table 5.1. Chemical structure of polymers used in the PET blends

$\text{HO}-\text{CH}_2-\text{CH}_2-\left[\text{O}-\text{C}(=\text{O})-\text{C}_6\text{H}_4-\text{C}(=\text{O})-\text{O}-\text{CH}_2-\text{CH}_2\right]_n-\text{OH}$						
Poly(ethylene terephthalate) PET						
$\left(\text{CH}_2-\text{CH}_2\right)_n \left(\text{CH}_2-\overset{\text{CH}_3}{\text{CH}}\right)_m$						
Ethylene-propylene rubber (EPR) (E:P =8:2)						
$\left[\text{CH}_2-\text{CH}_2\right]_m \left[\text{CH}_2-\overset{\text{O}-\text{C}(=\text{O})-\text{CH}_2}{\underset{\text{CH}_3}{\text{C}}}\right]_n$						
Ethylene/glycidyl methacrylate (E-GMA) (I)						
$\left(\text{CH}_2-\text{CH}_2\right)_x \left(\text{CH}_2-\overset{\text{CH}_3}{\underset{\text{O}-\text{C}(=\text{O})}{\text{C}}}\right)_y \left(\text{CH}_2-\overset{\text{O}-\text{C}(=\text{O})-\text{CH}_2}{\underset{\text{CH}_3}{\text{C}}}\right)_z$						
Ethylene/methacrylate/glycidyl methacrylate (EM-GMA) terpolymer (II)						
Compatibiliser		GMA content (%)	MFI (g/10min)	Ester Content (%)	Type	Supplier
Code †	Grades					
EM-GMA <sub>9(85)</sub>	Lotader AX8950	9	85	15	Terpolymer	Alf-Atochem
EM-GMA <sub>8(6)</sub>	Lotader AX8900	8	6	25		
EM-GMA <sub>1(8)</sub>	Lotader AX8920	1	8	28		
E-GMA <sub>8(5)</sub>	Lotader AX8840	8	5	0	Copolymer	

†EM-GMA<sub>9(85)</sub>, 9 is % amount of GMA and (85) is the MFI of the co(ter)polymer

**Table 5.2.** PET/EPR blends compatibilised with terpolymer with different contents of glycidyl methacrylate (GMA)

Sample code		Blends Composition w/w			GMA content %	MFI g/10min	Ester content %
		PET	EPR	Terpolymer/copolymer			
EM-GMA <sub>9(85)</sub> (Terpolymer)	TT-GMA9-5	70	25	5	9	85	15
	TT-GMA9-10	70	20	10	9	85	15
	TT-GMA9-15	70	15	15	9	85	15
	TT-GMA9-20	70	10	20	9	85	15
	BT-GMA9-30	70	0	30	9	85	15
EM-GMA <sub>8(6)</sub> (Terpolymer)	TT-GMA8-5	70	25	5	8	6	25
	TT-GMA8-10	70	20	10	8	6	25
	TT-GMA8-15	70	15	15	8	6	25
	TT-GMA8-20	70	10	20	8	6	25
	BT-GMA8-30	70	0	30	8	6	25
EM-GMA <sub>1(8)</sub> (Terpolymer)	TT-GMA1-5	70	25	5	1	8	28
	TT-GMA1-10	70	20	10	1	8	28
	TT-GMA1-15	70	15	15	1	8	28
	TT-GMA1-20	70	10	20	1	8	28
	BT-GMA1-30	70	0	30	1	8	28
E-GMA <sub>8(5)</sub> (Copolymer)	TC-GMA8-5	70	25	5	8	5	0
	TC-GMA8-10	70	20	10	8	5	0
	TC-GMA8-15	70	15	15	8	5	0
	TC-GMA8-20	70	10	20	8	5	0
	BC-GMA8-30	70	0	30	8	5	0

**Table 5.3.** Functionalised EPR used in PET blends and the PET blends compatibilised with *f*-EPR

Code		<i>f</i> -EPR Compositions					Conditions Temp. °C/rpm/ min	g-GMA (%)	Poly GMA (%)	MFI g/10min
		GMA (phr)	DVB (phr)	T101 (phr)	GMA/DVB w/w	[T101]/[GMA+DVB] MR				
CONV	G19	10	0	0.8	-	0.039	190/65/15	1.7	0.6	0.9
DVB	DG10	10	1.1	0.017	9/1	0.0007	190/65/15	2.3	0	3.7
Blend sample code		Ternary Blends Composition w/w				GMA Content (%)	GMA/DVB w/w	MFI g/10min		
<i>f</i> -EPR		PET	EPR	<i>f</i> -EPR						
CONV	G19	TG1	70	25	5	1.7	-	0.9		
		TG2	70	20	10	1.7	-	0.9		
		TG3	70	15	15	1.7	-	0.9		
		TG4	70	10	20	1.7	-	0.9		
		TG5	70	0	30	1.7	-	0.9		
DVB	DG10	TD1	70	25	5	2.3	9:1	3.7		
		TD2	70	20	10	2.3	9:1	3.7		
		TD3	70	15	15	2.3	9:1	3.7		
		TD4	70	10	20	2.3	9:1	3.7		
		TD5	70	0	30	2.3	9:1	3.7		
Physical Blend		P73	70	30	-	-	-	-		

## 5.2 RESULTS

### 5.2.1 Effect of Different GMA Content on Compatibility of PET/EPR/EM-GMA Blends

In order to understand the effect of different GMA content in the EM-GMA terpolymers on the compatibility of PET/EPR/EM-GMA ternary blends, two types of terpolymers were used containing GMA at 1 wt% (EM-GMA<sub>1(8)</sub>) and 8 wt% (EM-GMA<sub>8(6)</sub>) with similar MFI values (shown in subscript bracket). The processing torque behaviour of these blends (PET/EPR/EM-GMA 70/10/20 w/w %) are shown in **Figure 5.1A**. It is clear that the presence of a high GMA content in the terpolymer gives rise to a tremendous increase in the torque values of the blend to values well above that of the virgin EPR, compared to the blend containing EM-GMA<sub>1(8)</sub> (lower GMA content). The elongation at break of the ternary blends containing different amounts of the two terpolymers is shown in **Figure 5.1B** and **Table 5.4**. At low EM-GMA content (<10 wt %), the blends compatibilised with both terpolymers showed similar and low elongation at break. At EM-GMA<sub>8(6)</sub> content above 10 w/w%, however a substantial increase in elongation at break up to 40 % (at 20 w%) was observed. In contrast, the EM-GMA<sub>1(8)</sub> was found to be less effective in improving the elongation at break of the blends even when 20 w% was added. **Figure 5.1C** and **D** compare the phase morphology of PET/EPR/EM-GMA<sub>8(6)</sub> and PET/EPR/EM-GMA<sub>1(8)</sub> 70/10/20 w/w% blends, respectively. It can be seen clearly that PET/EPR/EM-GMA<sub>8(6)</sub> blend shows finer dispersed particles which are well distributed in the continuous phase compared to the larger dispersed particle size with irregular shapes observed in the ternary blend containing EM-GMA<sub>1(8)</sub>.

**Table 5.4.** Elongation at break of PET/EPR-g-GMA<sub>CONV</sub> blends at various GMA content (see **Figure 5.1**)

Samples Code	Elongation at break
TT-GMA8-5	7.8 ± 0.5
TT-GMA8-10	8.3 ± 1.0
TT-GMA8-15	30.5 ± 0.5
TT-GMA8-20	40.0 ± 0.2
TT-GMA1-5	6.5 ± 0.5
TT-GMA1-10	8.2 ± 0.5
TT-GMA1-15	13.4 ± 0.5
TT-GMA1-20	11.6 ± 0.4

The effect of GMA content in the terpolymer on the dynamic mechanical properties of the blends can be seen in **Figure 5.2A**. This figure gives an overview of the  $\tan \delta$ -temperature curves as a function of temperature for PET/EPR/EM-GMA at 70/10/20 w/w % blends ratio. The blend containing EM-GMA<sub>8(6)</sub> shows three  $\tan \delta$  peaks which correspond to the glass transition temperatures ( $T_g$ ) of the rubber phases (including EPR and EM-GMA) as well as the PET phase. The  $T_g$  of PET shifted away from the  $T_g$  of PET in the physical blend (about  $-3.9^\circ\text{C}$ ) to lower temperature, see **Figure 5.2B** and **5.2D**, **Table 5.5**. Only two  $\tan \delta$  peaks were observed in blends containing EM-GMA<sub>1(8)</sub> and these can be linked to the  $T_g$  of PET and EM-GMA<sub>1(8)</sub>. On the other hand, the peak corresponding to the  $T_g$  of EPR was not clear, it appeared as a shoulder. In this blend, the  $T_g$  of PET phase has shifted away from the  $T_g$  of PET in the physical blend by  $-2.3^\circ\text{C}$  to lower temperature. The storage modulus values for both compatibilised PET blends showed similar values at room temperature (e.g.  $25^\circ\text{C}$ ) and they were lower than that of the physical blend, see **Figure 5.3A** and **B**, **Table 5.5**.

**Table 5.5.**  $T_g$  and storage modulus of PET and EPR phase of PET/EPR compatibilised with EM-GMA<sub>1(8)</sub> and EM-GMA<sub>8(6)</sub> 70/10/20 w/w %. The shift is with respect to values of the corresponding physical blend, (see also **Figures 5.2** and **5.3**).

Blend ratio PET/EPR (or PET/EPR-g- GMA) 70/10/20 w/w%	Blend Ratio PET/EPR/EM-GMA <sub>x</sub>						$E'$ (MPa) at $25^\circ\text{C}$
	Compatibiliser	PET phase		EPR phase		Compatibiliser $T_g$ ( $^\circ\text{C}$ )	
		$T_g$ ( $^\circ\text{C}$ )	Shift ( $^\circ\text{C}$ )	$T_g$ ( $^\circ\text{C}$ )	Shift ( $^\circ\text{C}$ )		
PET/EPR	-	93.8		-43.2	-	-	171
PET/EPR/ EM-GMA <sub>8(6)</sub>	EM-GMA <sub>8</sub>	89.9	-3.9	-42.5	+0.7	-15.0	114
PET/EPR/ EM-GMA <sub>1(8)</sub>	EM-GMA <sub>1</sub>	91.5	-2.3	-	-	-27.2	127

### 5.2.2 Effect of Viscosity of the Compatibiliser on Blends Properties

To understand the effect of viscosity of the compatibilisers, two terpolymers with different rheological properties were chosen: (EM-GMA<sub>8(6)</sub> and EM-GMA<sub>9(85)</sub>) having MFI values of 6 and 85 g/10min and a close GMA content of 8 and 9 wt%. The torque values of these ternary blends (PET/EPR/EM-GMA 70/10/20 w/w %), **Figure 5.4A**,

shows the blend containing a terpolymer with lower MFI value to give lower torque values.

The elongation at break of these blends (with different amount of the terpolymer), **Figure 5.4B**, **Table 5.6** increased steadily with increasing the terpolymer content in the blends. The blends compatibilised with terpolymer having higher MFI giving a higher overall elongation at break. The SEM micrographs of blends containing 20 w% of the compatibiliser showed no significant difference in morphology in the presence of EM-GMA<sub>9(85)</sub> or EM-GMA<sub>8(6)</sub>, where both showed stable morphology with rough surfaces and no large holes, see **Figure 5.4C** and **D**.

**Table 5.6.** Elongation at break of PET/EPR/terpolymer blends at different terpolymer viscosity (see **Figure 5.4**).

Samples Code	PET/EPR/terpolymer (w/w-%)	Elongation at break (%)
TT-GMA9-5	70/25/5	16.6 ± 0.6
TT-GMA9-10	70/20/10	26.1 ± 0.9
TT-GMA9-15	70/15/15	53.9 ± 2.2
TT-GMA9-20	70/10/20	75.2 ± 1.4
TT-GMA8-5	70/25/5	7.8 ± 0.5
TT-GMA8-10	70/20/10	8.3 ± 0.1
TT-GMA8-15	70/15/15	30.5 ± 0.5
TT-GMA8-20	70/10/20	40.0 ± 0.2

**Figure 5.5A** shows the dynamic mechanical analysis of the blends where the  $T_g$  of the PET phase of a blend compatibilised with EM-GMA<sub>9(85)</sub> had shifted to lower temperature by  $-3.9^\circ\text{C}$  compared to that of the physical blend whereas a blend compatibilised with EM-GMA<sub>8(6)</sub> showed a larger shift of  $-4.6^\circ\text{C}$  (moving closer to  $T_g$  of EPR), see **Figure 5.5B** and **5.5D**, **Table 5.7**. On the other hand, the  $T_g$  of the EPR phase of the PET/EPR/EM-GMA<sub>9(85)</sub> blend showed only a slight shift ( $-0.1^\circ\text{C}$ ) towards lower temperature while the  $T_g$  of the EPR phase of a PET/EPR blend compatibilised with EM-GMA<sub>8(6)</sub> showed a larger shift of  $-0.7^\circ\text{C}$  to lower temperature. Close examination of the storage modulus showed that the PET/EPR/EM-GMA<sub>9(85)</sub> blend gave a lower value compared to PET/EPR/EM-GMA<sub>8(6)</sub> blend, see **Figure 5.6**, **Table 5.7**. In fact, the storage modulus values of all compatibilised blends are shown to be lower than that of the corresponding physical blend.

**Table 5.7.**  $T_g$  and storage modulus of PET and EPR phase of PET/EPR compatibilised with EM-GMA<sub>8(6)</sub> and EM-GMA<sub>9(85)</sub> 70/10/20 w/w.% The shift is with respect to values of the corresponding physical blend, (see also **Figures 5.5 and 5.6**).

Blend ratio PET/EPR (or PET/EPR-g- GMA)	Blend Ratio PET/EPR-g-GMA <sub>DVB</sub>						$E'$ (MPa) at 25°C
	Compatibiliser	PET phase		EPR phase		Compatibiliser	
		$T_g$ (°C)	Shift (°C)	$T_g$ (°C)	Shift (°C)		
PET/EPR	-	93.8		-43.2	-	-	171
PET/EPR/ EM-GMA <sub>8(6)</sub>	EM-GMA <sub>8(6)</sub>	89.9	-3.9	-42.5	+0.7	-15.0	114
PET/EPR/ EM-GMA <sub>9(85)</sub>	EM-GMA <sub>9(85)</sub>	89.2	-4.6	-43.3	-0.1	-14.3	92

### 5.2.3 The Effect of Terpolymers compared to a Copolymer on the Extent of Compatibilisation of PET/EPR Ternary Blends

The effect of the commercial copolymer and terpolymer on the blend properties was examined. Two compatibilisers with “similar” GMA content (8 wt%) and MFI values of 5 and 6 g/10min (copolymer E-GMA<sub>8(5)</sub> and terpolymer EM-GMA<sub>8(6)</sub>) were compared. **Figure 5.7A** shows that the copolymer (E-GMA<sub>8(5)</sub>) containing blend gives lower torque values compared to that containing the terpolymer. However, the torque values of both reactive ternary blends seem to be much higher than those of the virgin EPR, virgin PET and the physical blends.

The mechanical properties of these compatibilised ternary blends are presented in **Figure 5.7B, Table 5.8**. The elongation of PET/EPR/E-GMA<sub>8(5)</sub> blends increased with increasing the content of the copolymer E-GMA<sub>8(5)</sub>. Addition of 10 w % of the copolymer E-GMA<sub>8</sub> was found to be sufficient to promote the compatibilisation in the blends observed through the clear increase in elongation at break, whereas in the blends compatibilised with the corresponding terpolymer EM-GMA<sub>8(6)</sub> required more than 10 w% to observe an improvement in elongation at break. The morphology of the PET/EPR/E-GMA<sub>8(5)</sub> and PET/EPR/EM-GMA<sub>8(6)</sub> blends showed no significant difference as shown in **Figure 5.7C and 5.7D**, respectively.

**Table 5.8.** Elongation at break of PET/EPR compatibilised with terpolymer and copolymer (see **Figure 5.7**)

Samples Code	PET/ERP/terpolymer (w/w-%)	Elongation at break (%)
TT-GMA8-5	70/25/5	7.8 ± 0.5
TT-GMA8-10	70/20/10	8.3 ± 0.1
TT-GMA8-15	70/15/15	30.5 ± 0.5
TT-GMA8-20	70/10/20	40.0 ± 0.2
TC-GMA6-5	70/25/5	9.1 ± 0.8
TC-GMA6-10	70/20/10	22.7 ± 1.3
TC-GMA6-15	70/15/15	30.4 ± 0.7
TC-GMA6-20	70/10/20	53.1 ± 2.5

A comparison the copolymer and terpolymer in terms of their influence on the dynamic mechanical properties of the PET/EPR blends is shown in **Figure 5.8**, **Table 5.9**. For both compatibilised blends, besides the peak of EPR phase, an additional peak was observed around -15°C which is attributed to the  $T_g$  of the terpolymer or the copolymer respectively, see **Figure 5.8C**. However the additional peak for PET/EPR compatibilised with the copolymer E-GMA<sub>8(5)</sub> was found to be broad, thus the exact temperature of the peak could not be measured. The storage modulus (at temperature of 25°C), revealed that the compatibilised blends have lower values compared to the physical blend, see **Figure 5.9**.

**Table 5.9.**  $T_g$  and storage modulus of PET and EPR phase of PET/EPR compatibilised with E-GMA<sub>8(5)</sub> and EM-GMA<sub>8(6)</sub> 70/10/20 w/w.%. The shift is with respect to values of the corresponding physical blend, (see also **Figures 5.8 and 5.9**).

Blend ratio PET/EPR (or PET/EPR-g- GMA)	Blend Ratio PET/EPR-g-GMA <sub>DVB</sub>						E' (MPa) at 25°C
	Compatibiliser	PET phase		EPR phase		Compatibiliser $T_g$ (°C)	
		$T_g$ (°C)	Shift (°C)	$T_g$ (°C)	Shift (°C)		
PET/EPR	-	93.8	-	-43.2	-	-	171
PET/EPR/ EM-GMA <sub>8(6)</sub>	EM-GMA <sub>1(8)</sub>	89.9	-3.9	-42.5	+0.7	-15.0	114
PET/EPR/ E-GMA <sub>8(5)</sub>	E-GMA <sub>8(5)</sub>	89.4	-4.4	-41.4	+1.8	-	110

#### 5.2.4 Effect of *f*-EPR and terpolymer on compatibilisation of PET/EPR ternary blends.

Ternary PET/EPR blends compatibilised with the terpolymer EM-GMA<sub>1(8)</sub> containing 1 % GMA, and with *f*-EPR<sub>CONV</sub> (without DVB) and *f*-EPR<sub>DVB</sub> (with DVB) containing grafted GMA of 1.7 wt% and 2.3 wt%, respectively were compared. The EM-GMA<sub>1(8)</sub> terpolymer was chosen because of its low GMA content which is quite close to the amount of grafted GMA in the *f*-EPR prepared in this work. All polymer blends were prepared under similar processing conditions and compositions. The processing characteristics were determined by analysing the torque behaviour. The torque-time curves of the reactive ternary blends (70/10/20 w/w %) show that their torque fall between that of the virgin PET and virgin EPR, see **Figure 5.10A**. The resulting torque curves of all the PET/EPR/*f*-EPR<sub>CONV</sub> blends however, was found to be higher compared to that of the other ternary blends containing the commercial compatibilisers.

The elongation at break of the ternary blends containing 2.3 wt% *f*-EPR<sub>DVB</sub> (PET/EPR/*f*-EPR<sub>DVB</sub>) was highest compared to those containing *f*-EPR<sub>CONV</sub> with 1.7 wt% (PET/EPR/*f*-EPR<sub>CONV</sub>) and containing the terpolymer (PET/EPR/EM-GMA<sub>1(8)</sub>), see **Figure 5.10B** and **Table 5.10**. The figure also shows that increasing the compatibiliser content increases the elongation at break of these blends, with the PET/EPR/*f*-EPR<sub>CONV</sub> and PET/EPR/EM-GMA<sub>1(8)</sub> blends showing very close elongation at break values at all compatibiliser contents and both gave lower elongation compared to DVB-containing blend system.

Compatibilised ternary PET/EPR blends with either terpolymers or *f*-EPR used at ratio of 70/10/20 w/w% exhibited different morphological characteristics, with the PET/EPR/*f*-EPR<sub>DVB</sub> blend demonstrating fine rubber phase particles dispersion, see **Figure 5.10E**. It is clear that the addition of *f*-EPR<sub>DVB</sub> is effective in reducing the domain size of the matrix phase in the ternary blend. In contrast, morphology of PET/EPR/*f*-EPR<sub>CONV</sub> blend showed large and deep holes with sharp edges and rough surface, see **Figure 5.10D**. The morphology of PET/EPR/EM-GMA<sub>1(8)</sub> on the other hand was found to be different from that of PET/EPR/*f*-EPR<sub>DVB</sub> and PET/EPR/*f*-EPR<sub>CONV</sub> showing irregular shapes with smaller “clean” holes, see **Figure 5.10F**.



**Table 5.10.** Elongation at break of PET/EPR compatibilised with terpolymer and  $f$ -EPR<sub>CONV</sub> or  $f$ -EPR<sub>DVB</sub> (see **Figure 5.10**)

Compatibiliser	Samples Code	PET/EPR/compatibiliser (w/w %)	Elongation at break (%)
TERPOLYMER EM-GMA <sub>1(8)</sub>	TT-GMA1-5	70/25/5	6.5 ± 0.48
	TT-GMA1-10	70/20/10	8.2 ± 0.50
	TT-GMA1-15	70/15/15	13.4 ± 0.5
	TT-GMA1-20	70/10/10	11.6 ± 0.4
	TT-GMA1-30	70/0/30	19.0 ± 1.2
CONV	TG1	70/25/5	8.3 ± 1.5
	TG2	70/20/10	10.2 ± 0.6
	TG3	70/15/15	12.4 ± 1.3
	TG4	70/10/20	10.7 ± 1.6
	TG5	70/0/30	15.4 ± 0.3
DVB	TD1	70/25/5	13.5 ± 0.2
	TD2	70/20/10	14.2 ± 1.0
	TD3	70/15/15	16.7 ± 2.0
	TD4	70/10/20	19.4 ± 0.6
	TD5	70/0/30	21.7 ± 3.2

**Figure 5.11** and **Table 5.11** show the  $\tan \delta$  ( $T_g$  of PET and EPR phases) of PET/EPR ternary blends compatibilised with  $f$ -EPR and EM-GMA<sub>1(8)</sub>, see **Figure 5.11B and C**, **Table 5.11**. The  $T_g$  of the PET phase in PET/EPR/EM-GMA<sub>1(8)</sub> displayed a large shift (compared to the physical blend) towards that of the EPR, while the  $T_g$  of PET/EPR/ $f$ -EPR<sub>CONV</sub> blend demonstrated the smallest shift towards the temperature of the rubber phase. The PET/EPR/ $f$ -EPR<sub>DVB</sub> blend showed the lowest storage modulus value (at 25°C) compared to the rest of the blends, see **Figure 5.12**. Higher storage modulus values at lower temperature (below the  $T_g$  of the rubber phase) are attributed to a high stiffness at this temperature. These values are shown to drop drastically when the temperature exceeds the  $T_g$  of the rubber phase as the blend samples enter the rubbery region before further decrease at higher temperatures above the  $T_g$  of PET phase.

**Table 5.11.**  $T_g$  storage modulus of PET and EPR phase of PET/EPR compatibilised with  $f$ -EPR or terpolymer (70/10/20 w/w.%), The shift is with respect to values of the corresponding physical blend, (see also **Figures 5.11 and 5.12**).

PET/ $f$ -EPR <sub>CONV</sub> or $f$ -EPR <sub>DVB</sub> blend		Blend Ratio PET/EPR-g-GMA <sub>DVB</sub>						$E'$ (MPa) at 25°C
		Compatibiliser	PET phase		EPR phase		Compatibiliser $T_g$ (°C)	
			$T_g$ (°C)	Shift(°C)	$T_g$ (°C)	Shift(°C)		
Physical	PET/EPR	-	93.8	-	-43.2	-	-	171
CONV	PET/EPR/ $f$ -EPR <sub>CONV</sub>	$f$ -EPR <sub>CONV</sub>	92.5	-1.3	-40.6	+2.6	-	170
DVB	PET/EPR/ $f$ -EPR <sub>DVB</sub>	$f$ -EPR <sub>DVB</sub>	91.9	-1.9	-42.5	+0.7	-	99
Terpolymer	PET/EPR/ EM-GMA <sub>1(8)</sub>	EM-GMA <sub>1(8)</sub>	91.5	-2.3	-	-	-27.2	127

### 5.3 Discussion

#### 5.3.1 Effect of GMA Content in Commercial Terpolymers on Compatibilising Efficiency of PET/EPR/Compatibiliser ternary Blends

The effect of the terpolymer compatibilisers having different GMA content on blend properties was examined. The significant increase in the torque values observed for the blend that contain a higher GMA content (PET/EPR/EM-GMA<sub>8(6)</sub>) at 70/10/20 w/w%), see **Figure 5.1A**, may be attributed to higher melt viscosity (lower MFI) of the EM-GMA<sub>8(6)</sub> resulting in higher extent of interfacial chemical reaction via a reaction between the PET end groups and the higher concentration of the epoxy moiety present in the EM-GMA<sub>8(6)</sub> or/and due to branching and crosslinking reaction that may also take place between the epoxy group and the secondary hydroxyl group formed during the formation of the copolymer PET/EM-GMA [93]. Similar observation was reported [89, 97, 225] where higher GMA content (of 8 wt %) in PBT/ABS-g-GMA which was shown to give highest torque values compared to those with lower GMA content in the same blend composition.

The SEM results support a higher level of compatibilisation in blends containing terpolymer with higher GMA content as demonstrated by finer and more uniform distribution of the dispersed rubber particle, see **Figure 5.1C**. Unfavourable morphology obtained in EM-GMA<sub>1(8)</sub> blend, (**Figure 5.1D**) having low GMA content is

most likely due to the presence of smaller amount of GMA for reaction with  $-\text{COOH}$  or  $-\text{OH}$  end groups in the PET resulting in reduced extent of interfacial reaction, thus lower compatibilisation efficiency (a similar interfacial reaction mechanism was illustrated and discussed in **Scheme 4.3.1, Chapter 4, p.173**). The significant improvement observed in the phase morphology is responsible for the higher elongation at break observed in these blends (**Figure 5.1B**). Examination of PBT/EM-GMA blends [92], has also shown a low extent of interfacial reaction in EM-GMA with low GMA content that could not prevent coalescence compared to EM-GMA with high GMA level which would in turn prevent the dispersed phase from being distributed evenly in the PET matrix.

The suggested higher extent of compatibilisation achieved in the PET/EPR/EM-GMA<sub>8(6)</sub> blend is further supported by a larger shift in its matrix  $T_g$  (**Table 5.5**) (compared to the physical blend) which is due to interaction between the two phases with stronger interface giving rise to higher extent of reduction in the  $T_g$  values of the matrix [228]. A lower storage modulus of the PET/EPR/EM-GMA<sub>8(6)</sub> blend at all temperatures examined (**Figure 5.3**) was observed compared to PET/EPR/EM-GMA<sub>1(8)</sub> blend suggesting more elastomeric behaviour in the latter blend.

### 5.3.2 Effect of Viscosity of Terpolymers on Compatibilising Efficiency of PET/EPR Blends

Although two of the terpolymers used in this work contained similar GMA content (8 and 9 wt%), they had very different viscosity (different in MFI value) and their ternary blends (70/10/20 w/w%) showed very different torque behavior, see **Figure 5.4A**. Different extent of interfacial reaction may occur in blends compatibilised with these two terpolymers due to the difference in their MFI values.

The higher torque values shown by a blend containing EM-GMA<sub>8(6)</sub> (**Figure 5.4A**), must be due to its much higher viscosity, compared to blend containing EM-GMA<sub>9(85)</sub>, and is most likely not to be due to a better extent of compatibilisation. This is supported by both the lower elongation at break at all ratios of blends containing the higher viscosity (MFI=6 g/10min) terpolymer (**Figure 5.4B**) and by the slightly larger dispersed particle size observed from its SEM micrograph (**Figure 5.4D**) compared to a

similar blend but with a lower viscosity terpolymer, EM-GMA<sub>9(85)</sub>. The viscosity ratio of the blend components has been shown [234] to have a major effect on the mobility of the interface and the interfacial tension making it difficult for the interfacial copolymer, in the blend containing EM-GMA<sub>8(6)</sub>, to diffuse to the interface hence the observed coarse morphology of this blend. The effect of MFI values of the modified rubber on blend compatibilisation was also discussed by Al-Malaika *et. al* [28]. It was also demonstrated [28] that for blends of PET with EPR-g-GMA<sub>TRIS</sub> (in the presence of the comonomer trimethylol propane triacrylate, TRIS) having higher MFI values (lower viscosity) a finer morphology and better performance was observed.

The suggestion of a better compatibilisation in the PET/EPR/EM-GMA<sub>9(85)</sub> blends is further supported from results of their dynamic mechanical analysis, see **Figure 5.5** which show a sharp increase in  $\tan \delta$  of the PET phase possibly due to the high mobility of PET chain segments [246], see **Figure 5.5B**. A greater shift of  $T_g$  towards the  $T_g$  of the second component in blends is attributed to higher extent of compatibilisation [28]. The lower storage modulus observed for the PET/EPR/EM-GMA<sub>9(85)</sub> blend at all temperatures examined (**Figure 5.6**) indicates also a more elastomeric behaviour for this low viscosity terpolymer containing blend.

### 5.3.3 The Effect of a copolymer (E-GMA<sub>8(5)</sub>) and terpolymer (EM-GMA<sub>8(6)</sub>) as compatibilisers for PET/EPR blends.

The effect of the copolymer (E-GMA<sub>8(5)</sub>) and the terpolymer (EM-GMA<sub>8(6)</sub>) containing the same amount of GMA (8 wt%) and a close MFI values (5 and 6 g/10 min) on the extent of compatibilisation in ternary blends of PET/EPR/compatibiliser was compared. The only difference between the copolymer and terpolymer is the presence of the methacrylate ester unit in terpolymer. **Figure 5.7** shows clearly that the copolymer containing blend gives a higher elongation at break, even at only 10% composition, and finer morphology compared to the terpolymer. The higher torque curve observed for the terpolymer containing blend (EM-GMA<sub>8(6)</sub>) suggests therefore the possibility of occurrence of higher extent of branching and crosslinking in the presence of the ester groups which would be responsible for the observed lower elongation, and the less favourable morphology observed in **Figure 5.7**. Further, the more bulky structure of the terpolymer compared to the copolymer would give rise to a more difficult migration to

the interface, thus a lower efficiency of compatibilisation can be expected in blends containing the terpolymer (EM-GMA<sub>8(6)</sub>). A further support for a good compatibilisation and performance in the case of the copolymer E-GMA<sub>8(5)</sub>, is the observed larger shift in the  $T_g$  of its EPR phase towards the  $T_g$  of PET (by +1.8°C) compared to the terpolymer (+0.7°C), see **Table 5.9** and the lower (than the physical blend) storage modulus values.

#### 5.3.4 Comparison of the Effect of Synthesised $f$ -EPR and the Commercial terpolymer on Compatibilisation of PET/EPR Blends

Comparing the effect of two of the synthesised  $f$ -EPR with the commercial ternary terpolymer EM-GMA<sub>1(8)</sub>, which is the closest one in terms of the amount of GMA grafted content, on the performance and extent of their compatibilisation in the ternary blends (PET/EPR/compatibiliser) is complex due to the differences in the microstructure of each of these compatibilisers. **Table 5.12** shows some of their major differences in terms of the g-GMA content and their MFI. The synthesised  $f$ -EPR chosen was an optimised sample (sample **G19**, see **Table 4.1**, **Chapter 4**, p.159) whereas the  $f$ -EPR<sub>DVB</sub> was not the best optimised sample (sample **DG10**) but is one that has still out-performed the optimum blend sample based on conventional  $f$ -EPR when used in binary blends, see **Chapter 4**, **Figure 4.22**, p.210 and **Figure 4.36**, p.225.

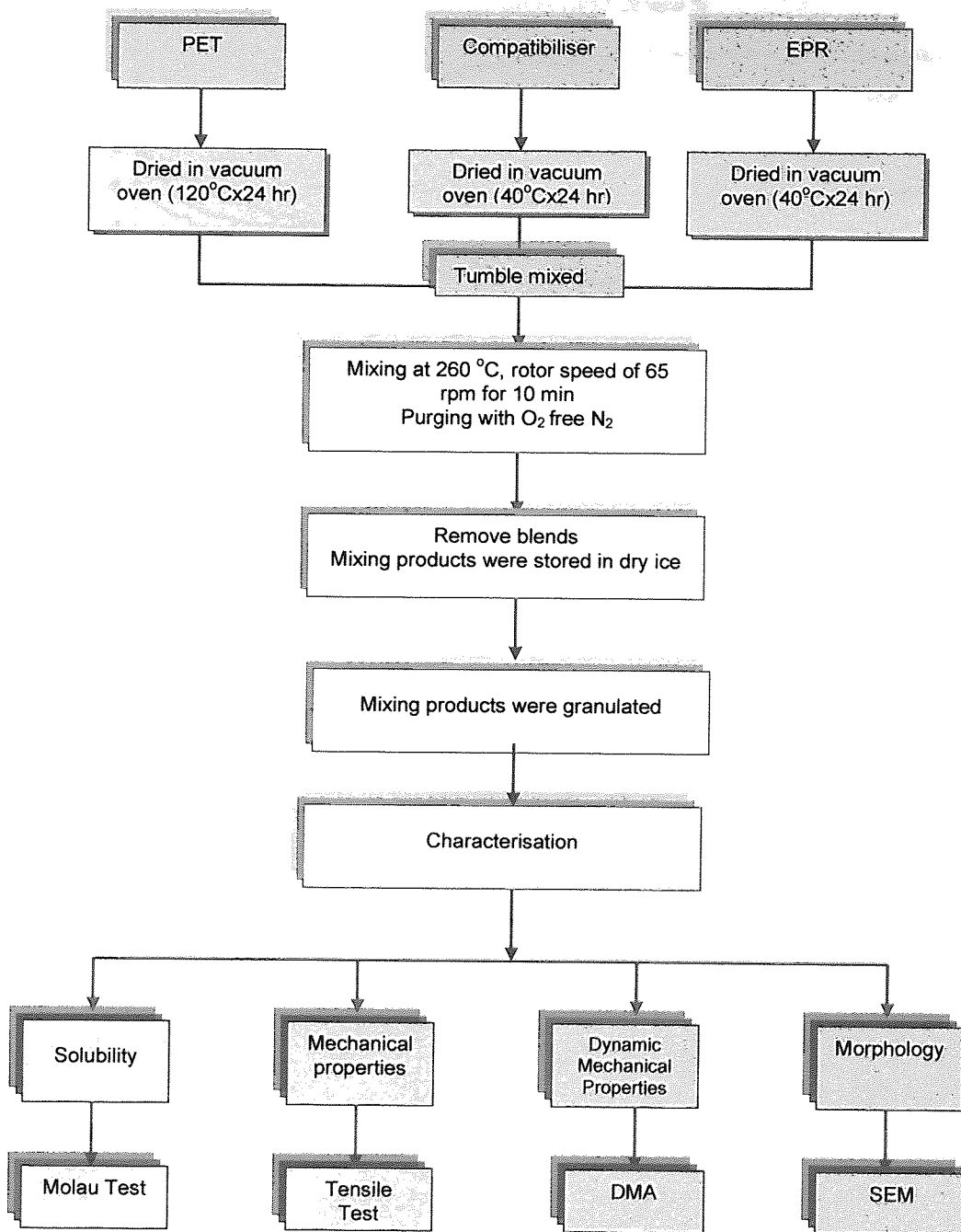
Although it is difficult to make a direct comparison between ternary PET/EPR blends (optimised) containing the three compatibilisers in **Table 5.12**, the comparison would be a useful one. At all concentrations of the compatibilisers used in the blend composition (from 5-20 w%), the blend containing  $f$ -EPR<sub>DVB</sub> showed the highest elongation at break compared to the commercial terpolymer EM-GMA<sub>1(8)</sub> having 1 wt% GMA, (**Figure 5.10B**) and the lowest storage modulus (**Figure 5.12B**) suggesting better elastic properties. The morphology of this sample seems also to be stable, and is finer than that for the ternary blend containing  $f$ -EPR<sub>CONV</sub>, though it is not too different from that containing the terpolymer (**Figure 5.10 C-F**).

**Table 5.12.** Characteristics of *f*-EPR and terpolymer.

	<i>f</i> -EPR <sub>CONV</sub>	<i>f</i> -EPR <sub>DVB</sub>	EM-GMA <sub>1(8)</sub>
g-GMA (wt%)	1.7	2.3	1
MFI (g/10min)	0.9	3.7	6
polyGMA (wt%)	0.6	0	Not available

Comparing the binary with the ternary PET/EPR blends in the presence of the synthesised *f*-EPR shows that in both cases the binary blends of PET/*f*-EPR (70/30 w/w%) gave finer morphology and higher elongation at break compared to the corresponding ternary blends (all blends have a total rubbers content of 30 w%), with blends containing *f*-EPR<sub>DVB</sub> showing better overall performance in terms of both elongation and morphology, see **Figure 5.13**. The use of the terpolymers containing a much higher GMA content of 8-9 wt% and the corresponding copolymer (E-GMA) with 8 wt% GMA in the ternary blends resulted in much higher elongation at break at all concentrations (5-20 wt%) used in this work, see **Figure 5.15** (see also **Figure 5.14** for corresponding morphology). There are several factors that may be responsible for these observations including the much lower grafted GMA content in the *f*-EPR and the terpolymer containing 1 wt % as well as the much lower MFI values. In addition, the presence of polyGMA particularly in the *f*-EPR<sub>CONV</sub> and the bulky DVB structure in *f*-EPR<sub>DVB</sub> may contribute to the lower elongation at break in blends containing these as compatibiliser. Similar findings were reported in literatures [90, 91, 247] suggesting that the commercial copolymers and terpolymers are more effective in improving PET/EPR blend properties compared to home made modified rubber compositions.

Scheme 5.1. Methodology for Compatibilisation of PET/EPR/Compatibiliser Blends



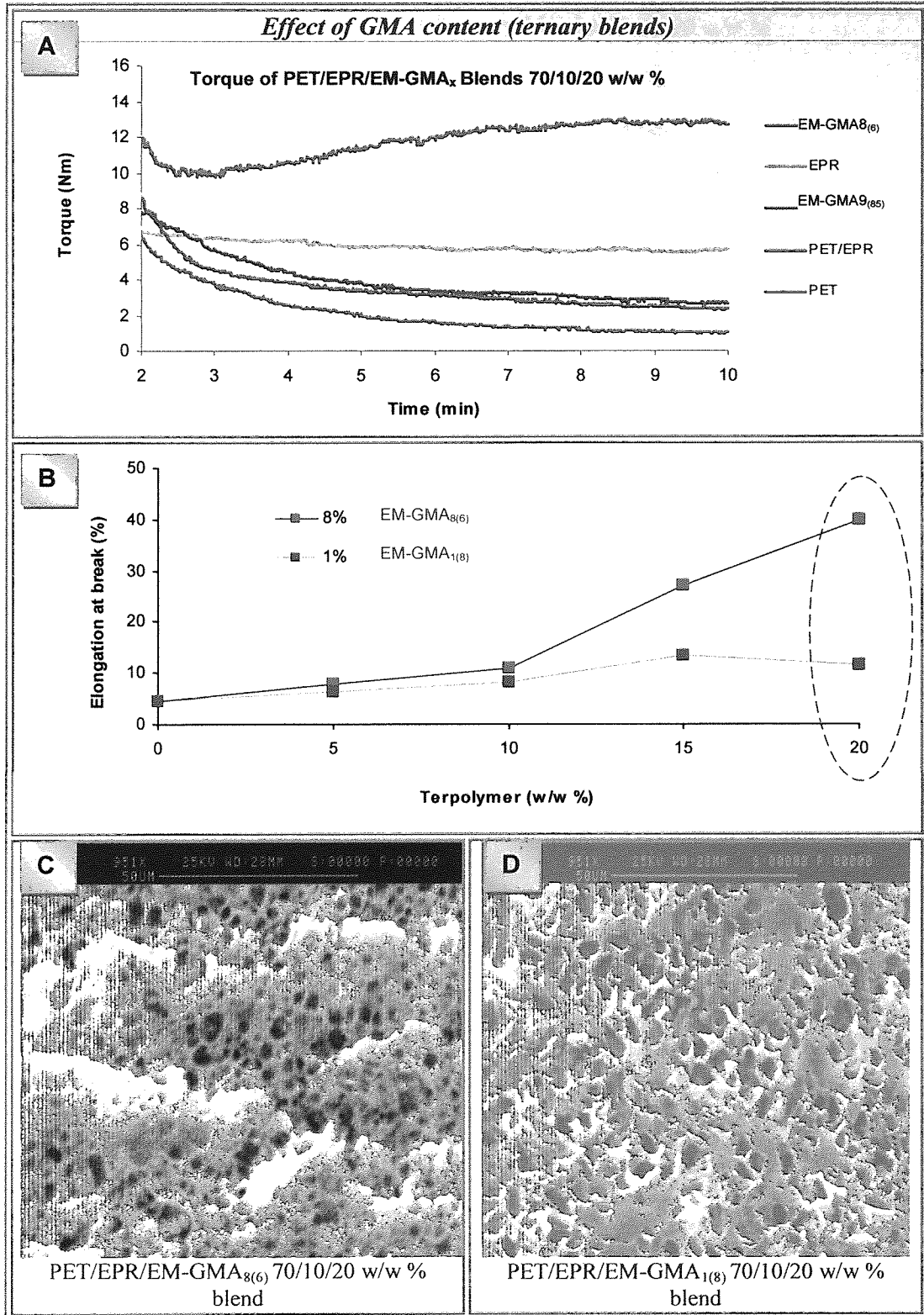


**Figure 5.1.** Effect of GMA content on PET/EPR/EM-GMA<sub>x</sub> ternary blends properties. EM-GMA<sub>1(8)</sub>, GMA=1 %, MFI=8 g/10min, EM-GMA<sub>8(6)</sub>, GMA=8 %, MFI=6 g/min.



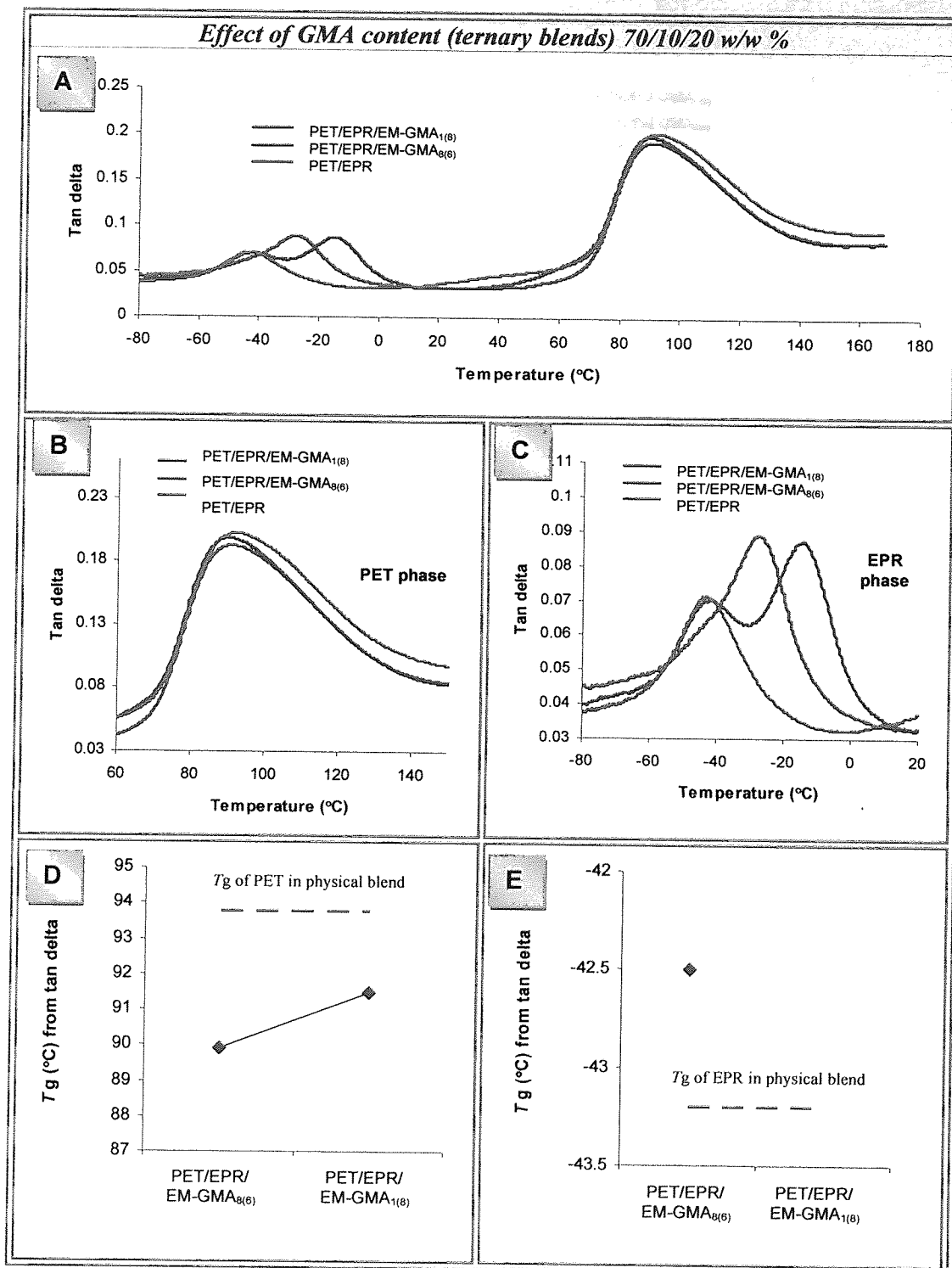


**Figure 5.2.** Effect of GMA content on thermal properties of PET/EPR/EM-GMA<sub>x</sub> 70/10/20 w/w %, see **Table 5.5**. (EM-GMA<sub>8(6)</sub>: GMA=8 %, MFI=6 g/10min, EM-GMA<sub>1(8)</sub>: GMA=1 %, MFI=8 g/10min).

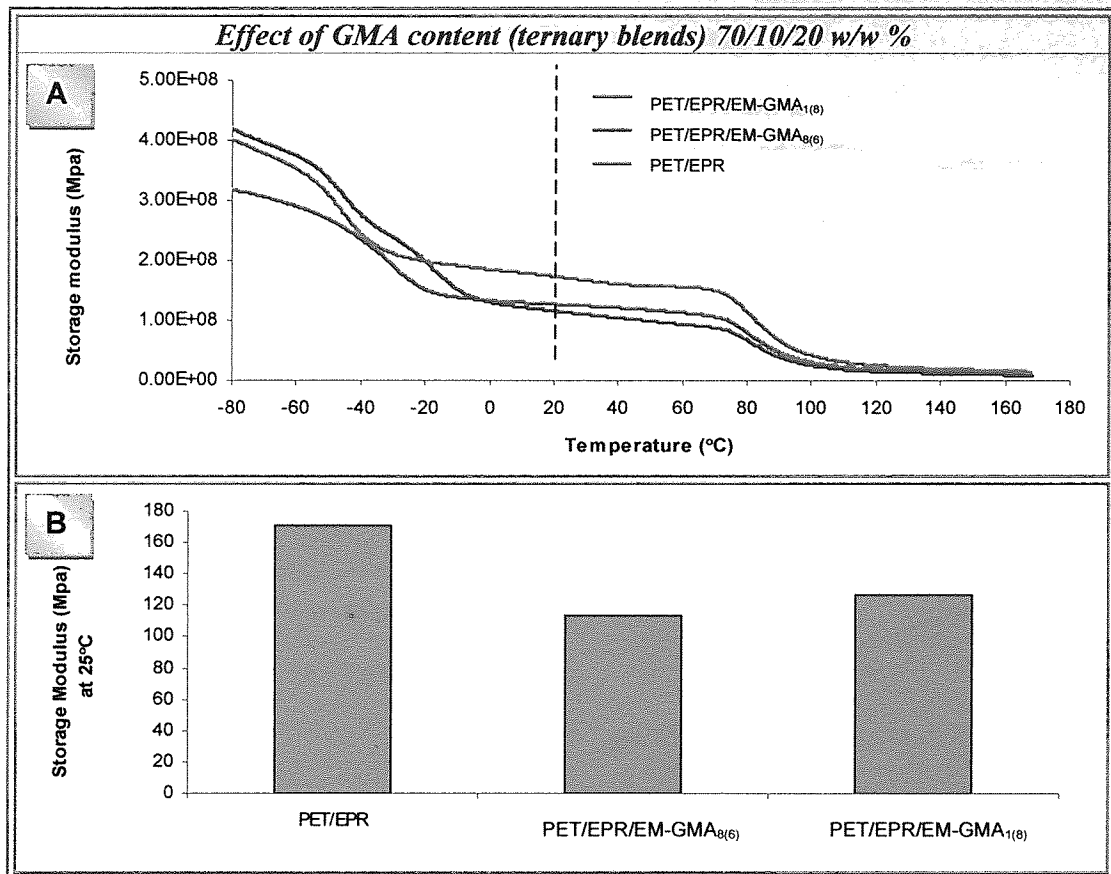


**Figure 5.3.** Effect of GMA content on thermal properties (storage modulus) of PET/EPR/EM-GMA<sub>x</sub> 70/10/20 w/w %, see **Table 5.5**. (EM-GMA<sub>8(6)</sub>: GMA=8 %, MFI=6 g/10min, EM-GMA<sub>1(8)</sub>: GMA=1 %, MFI=8 g/10min).

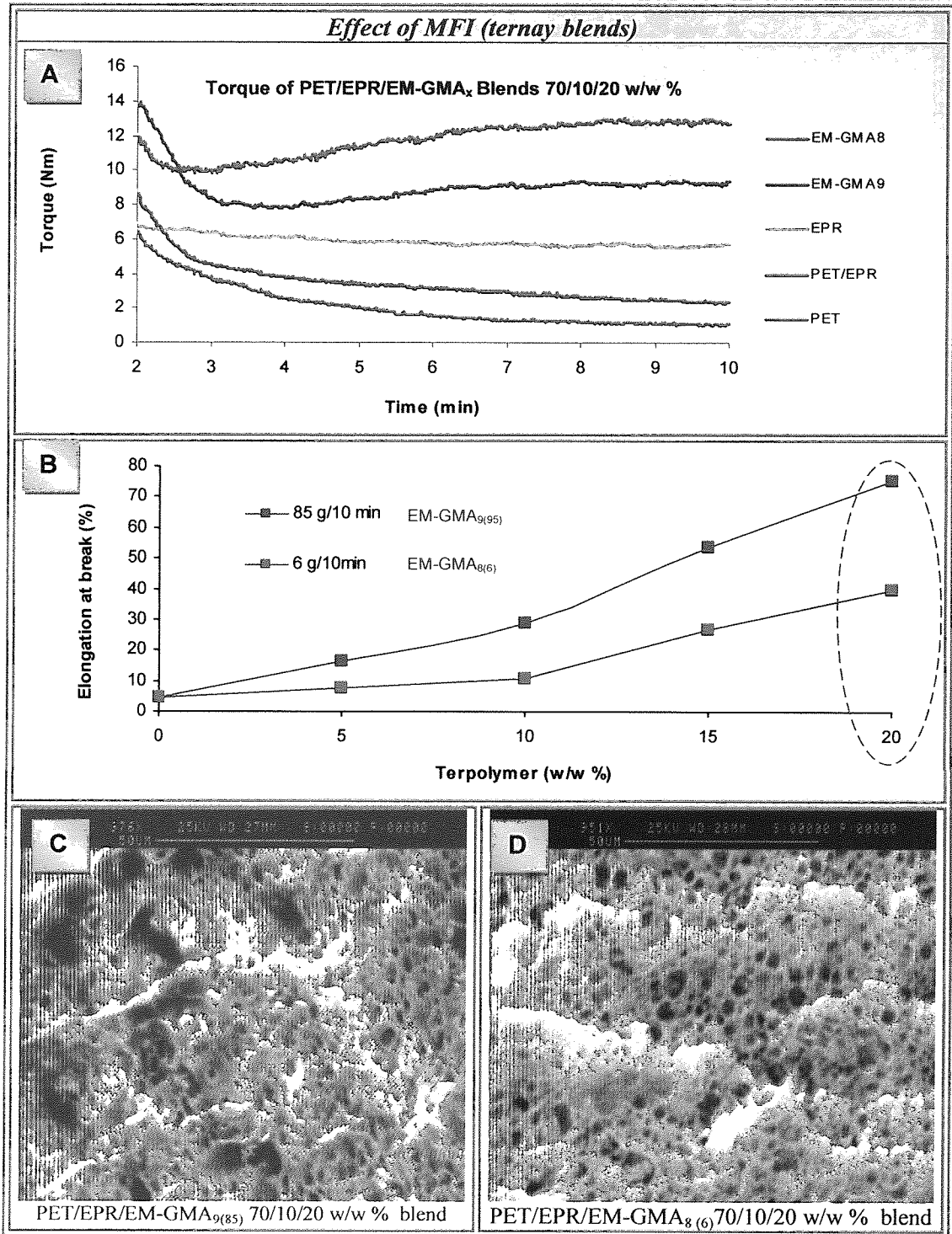


**Figure 5.4.** Effect of viscosity of terpolymer on PET/EPR/EM-GMA<sub>x</sub> ternary blends properties. EM-GMA<sub>8(6)</sub>, GMA=8 %, MFI=6 g/10min, EM-GMA<sub>9(85)</sub>, GMA=9 %, MFI=85 g/min.

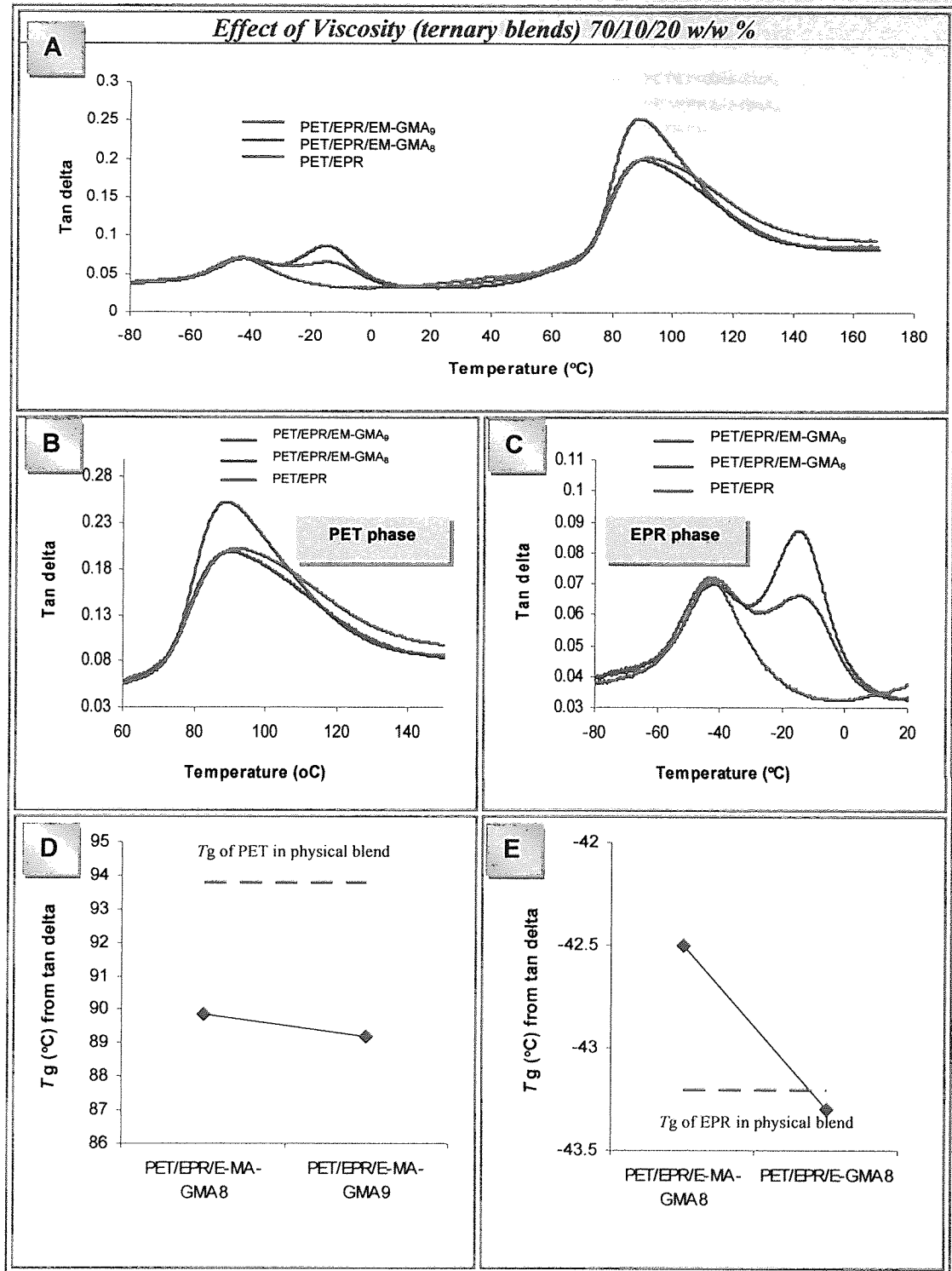


**Figure 5.5.** Effect of GMA content on thermal properties of PET/EPR/EM-GMA<sub>x</sub> 70/10/20 w/w %, see **Table 5.7**. EM-GMA<sub>8(6)</sub>, GMA=8 %, MFI=6 g/10min, EM-GMA<sub>9(85)</sub>, GMA=9 %, MFI=85 g/min.

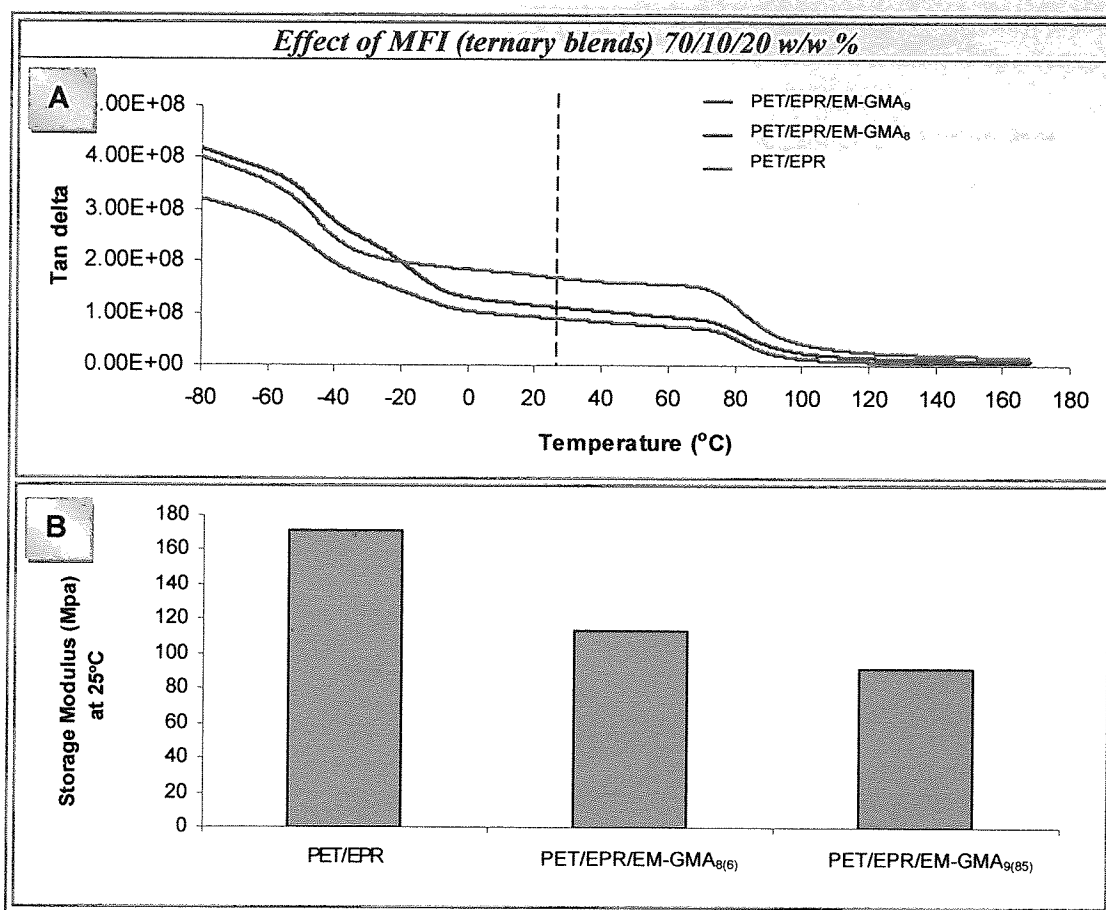


**Figure 5.6.** Effect of GMA content on thermal properties (storage modulus) of PET/EPR/EM-GMA<sub>x</sub> 70/10/20 w/w %, see **Table 5.7**. EM-GMA<sub>8(6)</sub>, GMA=8 %, MFI=6 g/10min, EM-GMA<sub>9(85)</sub>, GMA=9 %, MFI=85 g/min.

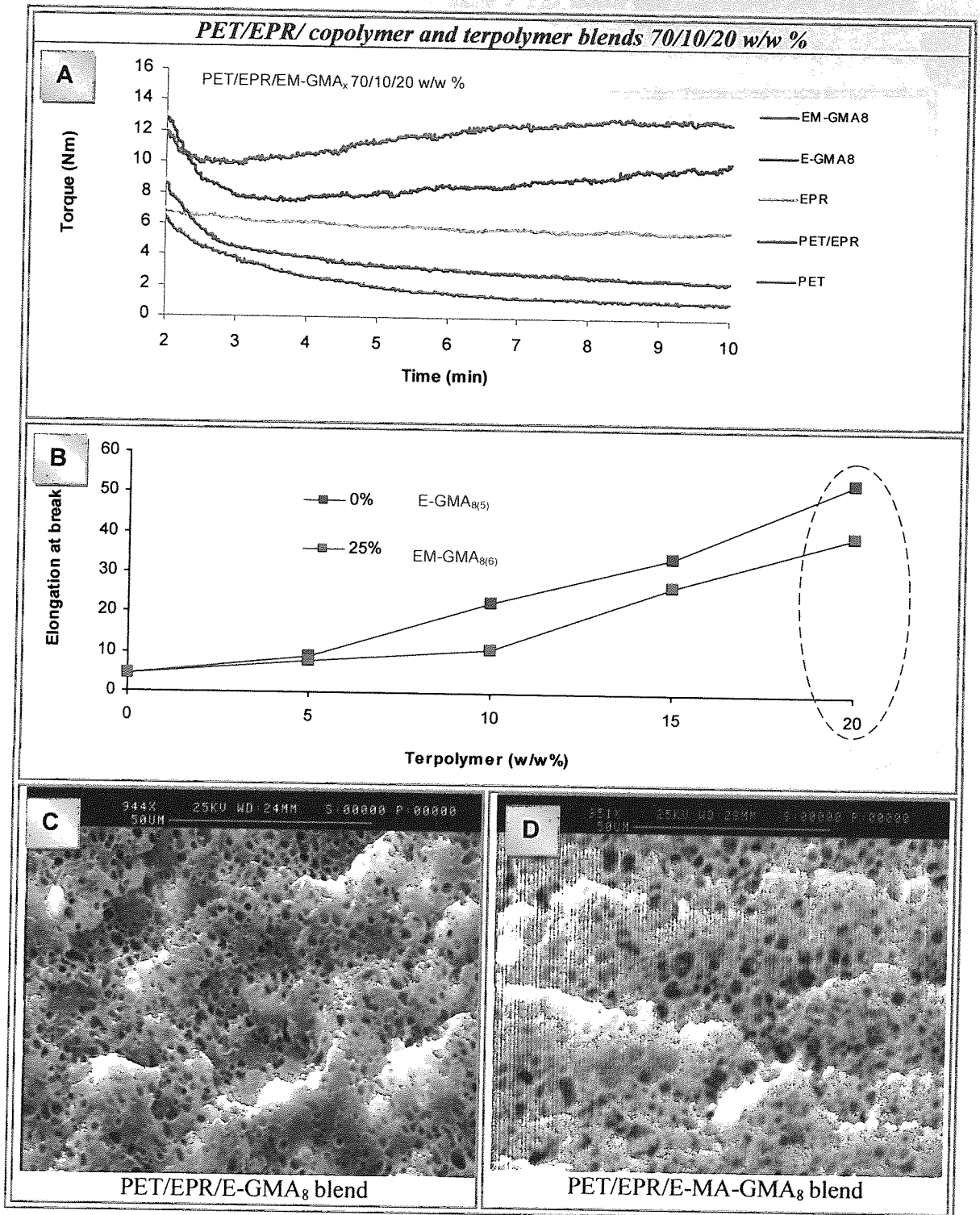


**Figure 5.7.** Effect of copolymer and terpolymer on PET/EPR/EM-GMA<sub>x</sub> ternary blends properties. E-GMA<sub>8(5)</sub>, GMA=8 %, MFI=5 g/10min, 0% ester content, EM-GMA<sub>8(6)</sub>, GMA=9 %, MFI=85 g/min, 25% ester content.

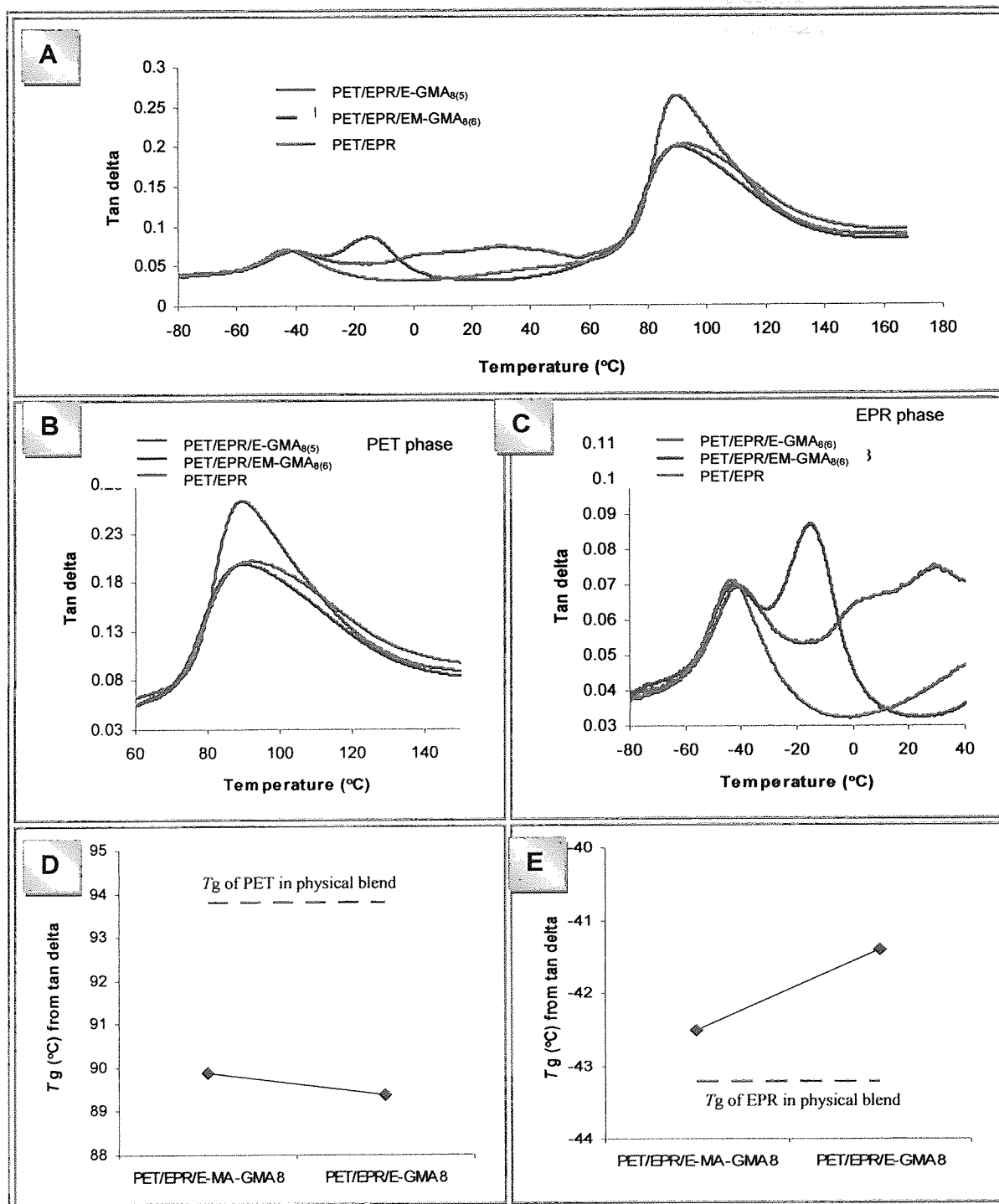


**Figure 5.8.** Effect of copolymer and terpolymer on thermal properties of PET/EPR/EM-GMA<sub>x</sub> 70/10/20 w/w% ternary blends, see **Table 5.9**. E-GMA<sub>8(5)</sub>, GMA=8 %, MFI=5 g/10min, 0% ester content, EM-GMA<sub>8(6)</sub>, GMA=9 %, MFI=85 g/min, 25% ester content.

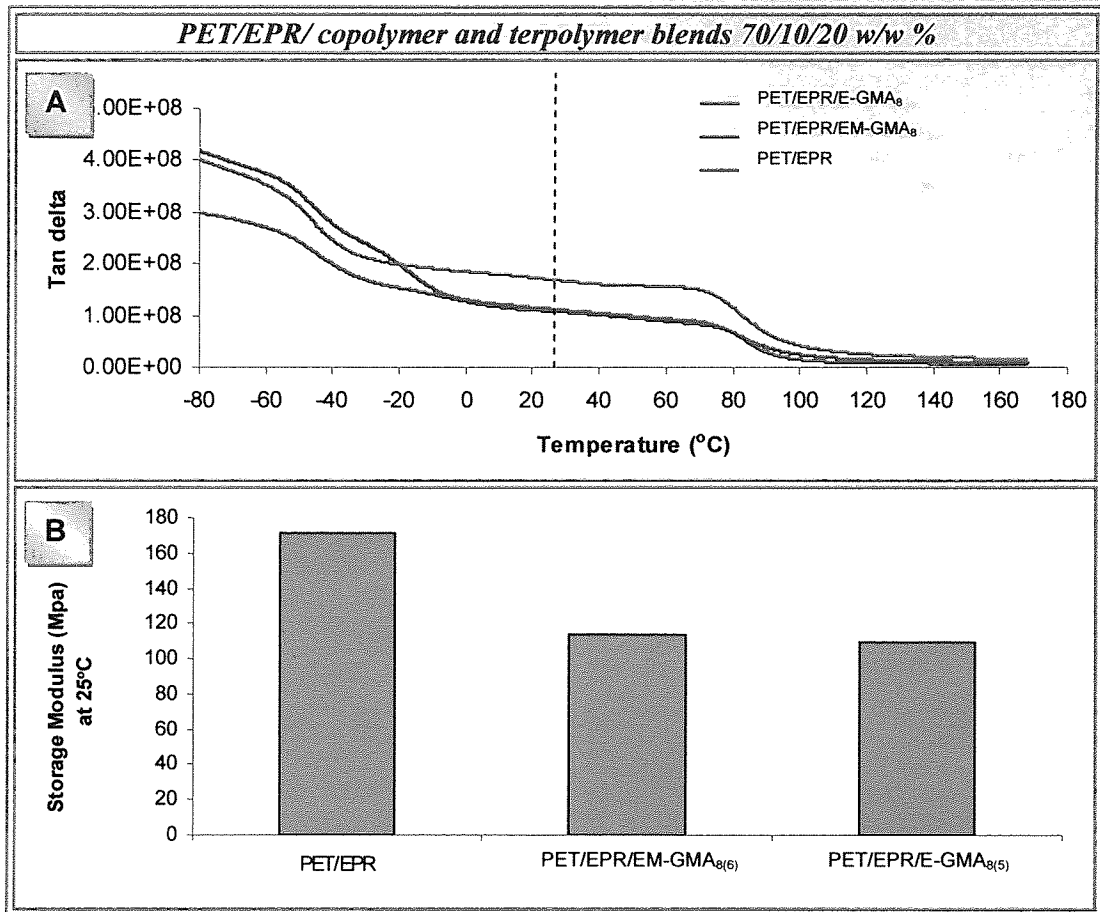


**Figure 5.9.** Effect of copolymer and terpolymer on thermal properties (storage modulus) of PET/EPR/EM-GMAx 70/10/20 w/w % ternary blends, see **Table 5.6**. E-GMA<sub>8(5)</sub>, GMA=8 %, MFI=5 g/10min, 0% ester content, EM-GMA<sub>8(6)</sub>, GMA=9 %, MFI=85 g/min, 25% ester content.



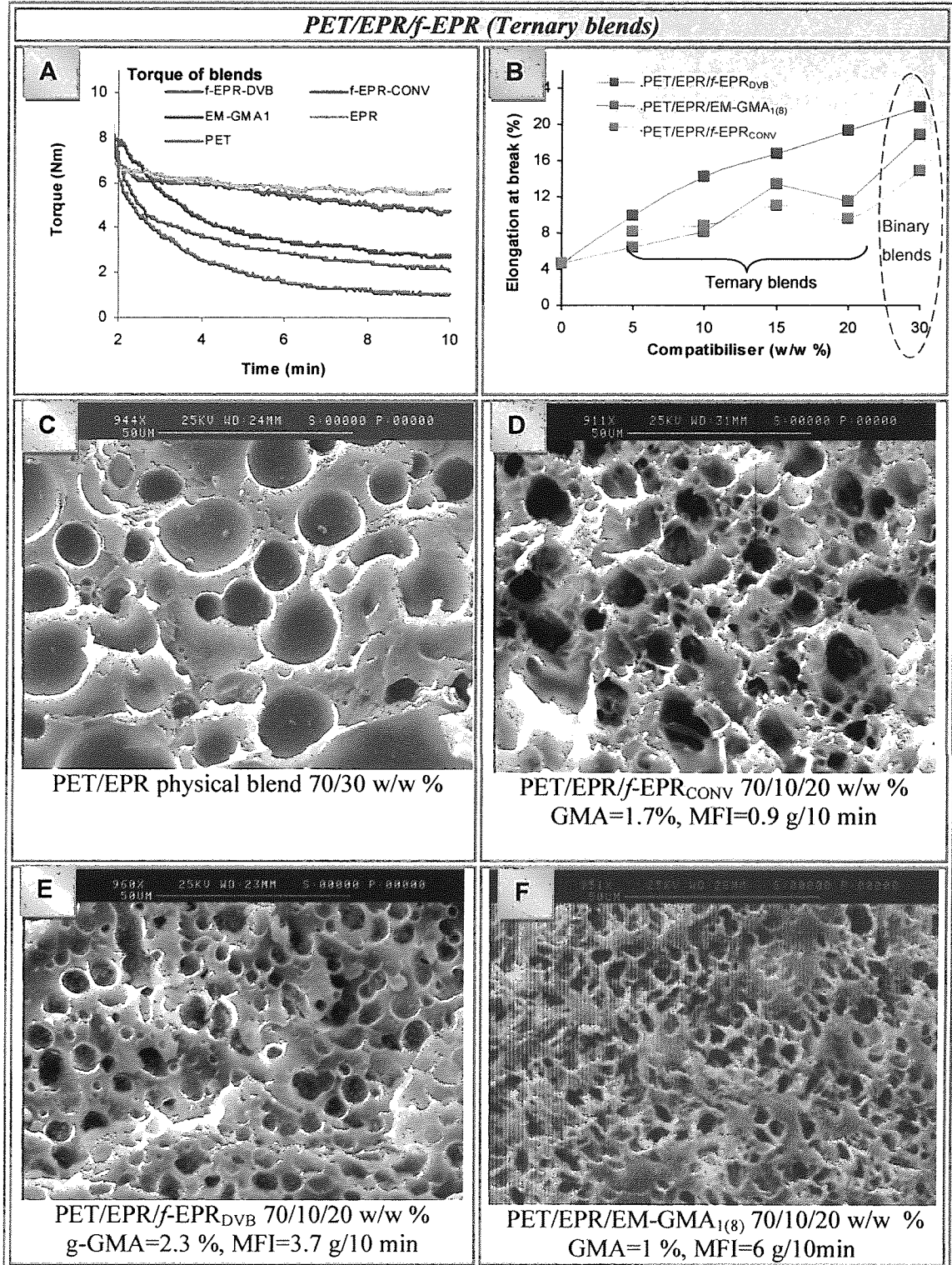


**Figure 5.10.** Effect of *f*-EPR and terpolymer on PET/EPR/*f*-EPR or EM-GMA<sub>1(8)</sub> ternary blends properties. *f*-EPR<sub>DVB</sub>=g-GMA=2.3 wt%, MFI=3.7 g/10min, polyGMA=0%, *f*-EPR<sub>CONV</sub>= g-GMA=1.7 wt%, MFI=0.9 g/10min, polyGMA=0.6%, EM-GMA<sub>1(8)</sub>, GMA=1 %, MFI=8 g/10min.

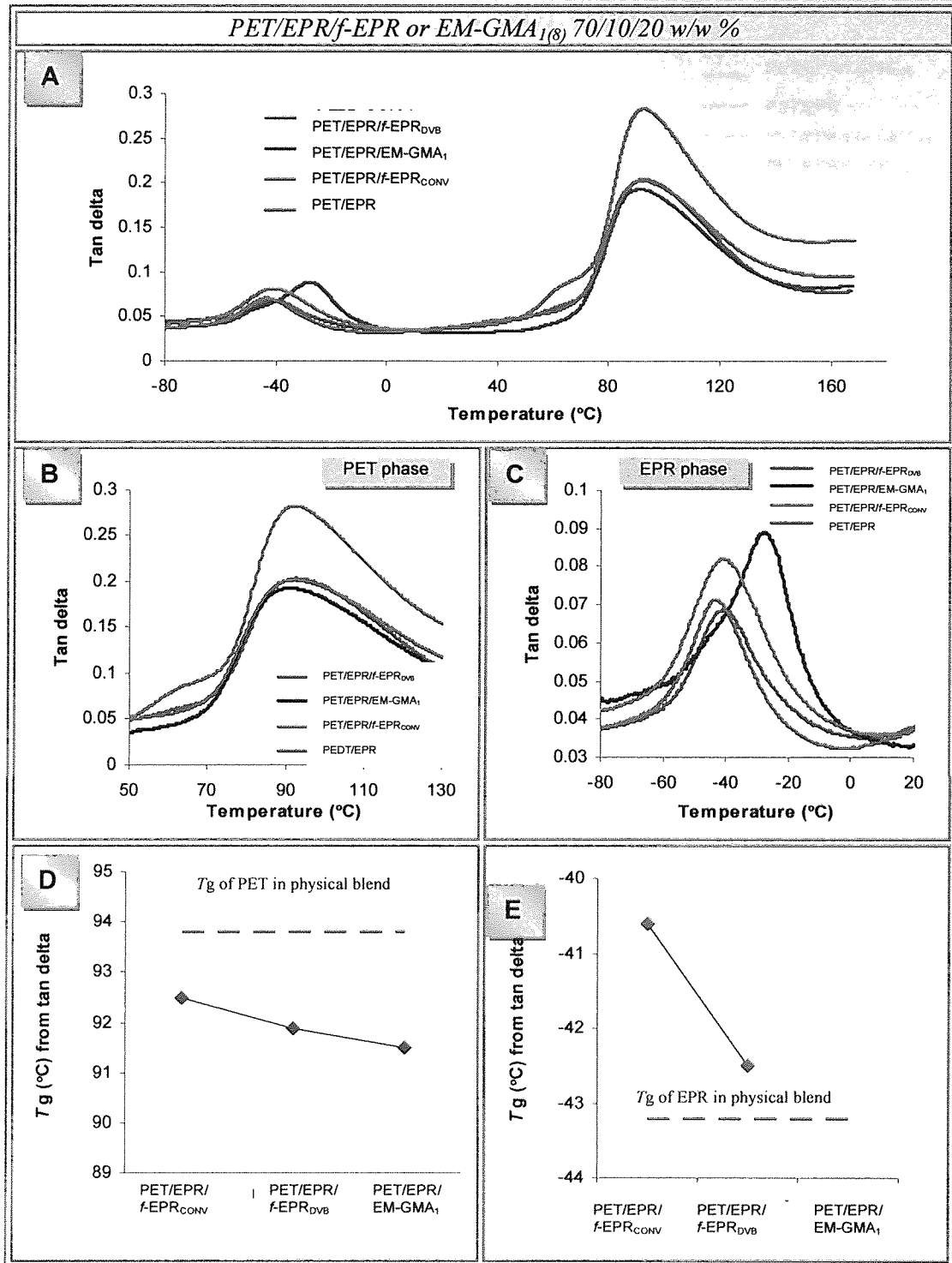


**Figure 5.11.** Effect of *f*-EPR and terpolymer on thermal properties of PET/EPR/*f*-EPR or EM-GMA<sub>1(8)</sub> ternary blends properties, see **Table 5.7**. *f*-EPR<sub>DVB</sub> = *g*-GMA = 2.3 wt%, MFI = 3.7 g/10min, polyGMA = 0%, *f*-EPR<sub>CONV</sub> = *g*-GMA = 1.7 wt%, MFI = 0.9 g/10min, polyGMA = 0.6%, EM-GMA<sub>1(8)</sub>, GMA = 1%, MFI = 8 g/10min.

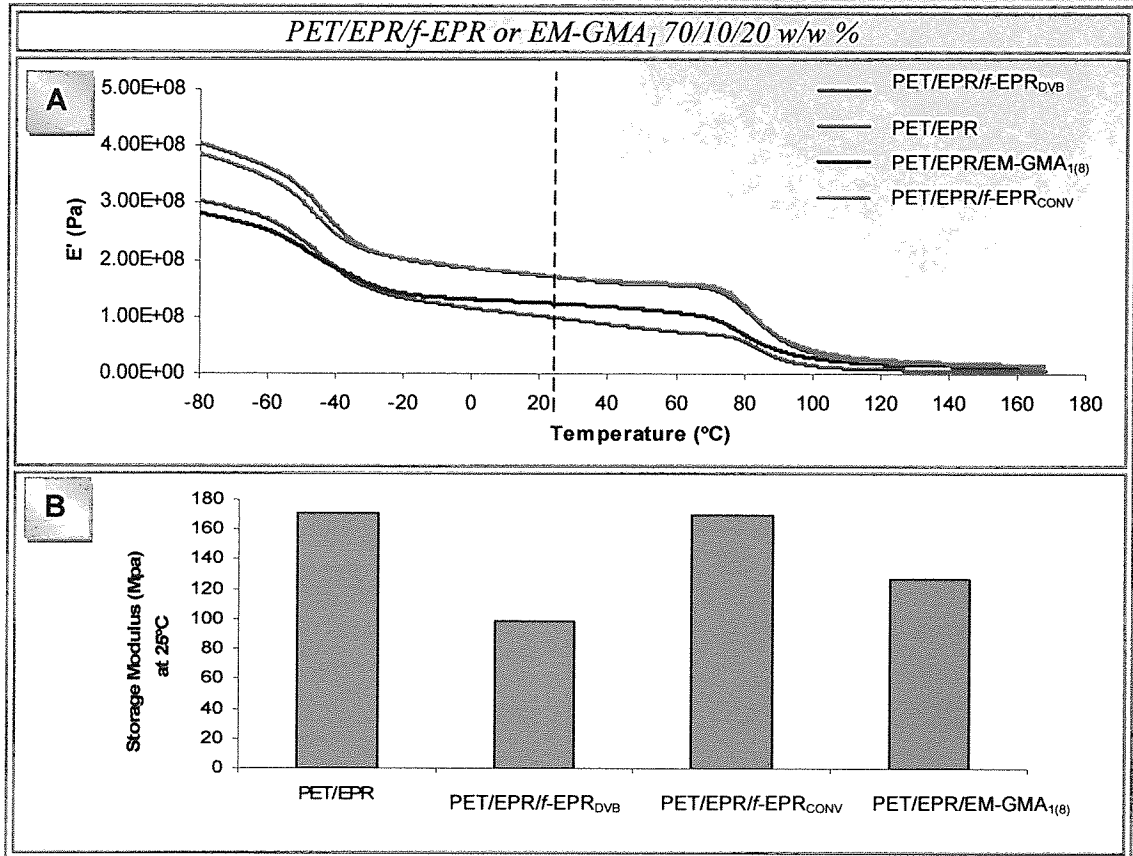


**Figure 5.12.** Effect of *f*-EPR and terpolymer on thermal properties (storage modulus) of PET/EPR/*f*-EPR or EM-GMA<sub>1(8)</sub> ternary blends properties, see **Table 5.7**. *f*-EPR<sub>DVB</sub> = *g*-GMA=2.3 wt%, MFI=3.7 g/10min, polyGMA=0%, *f*-EPR<sub>CONV</sub> = *g*-GMA=1.7 wt%, MFI=0.9 g/10min, polyGMA=0.6%, EM-GMA<sub>1(5)</sub>, GMA=1 %, MFI=8 g/10min.

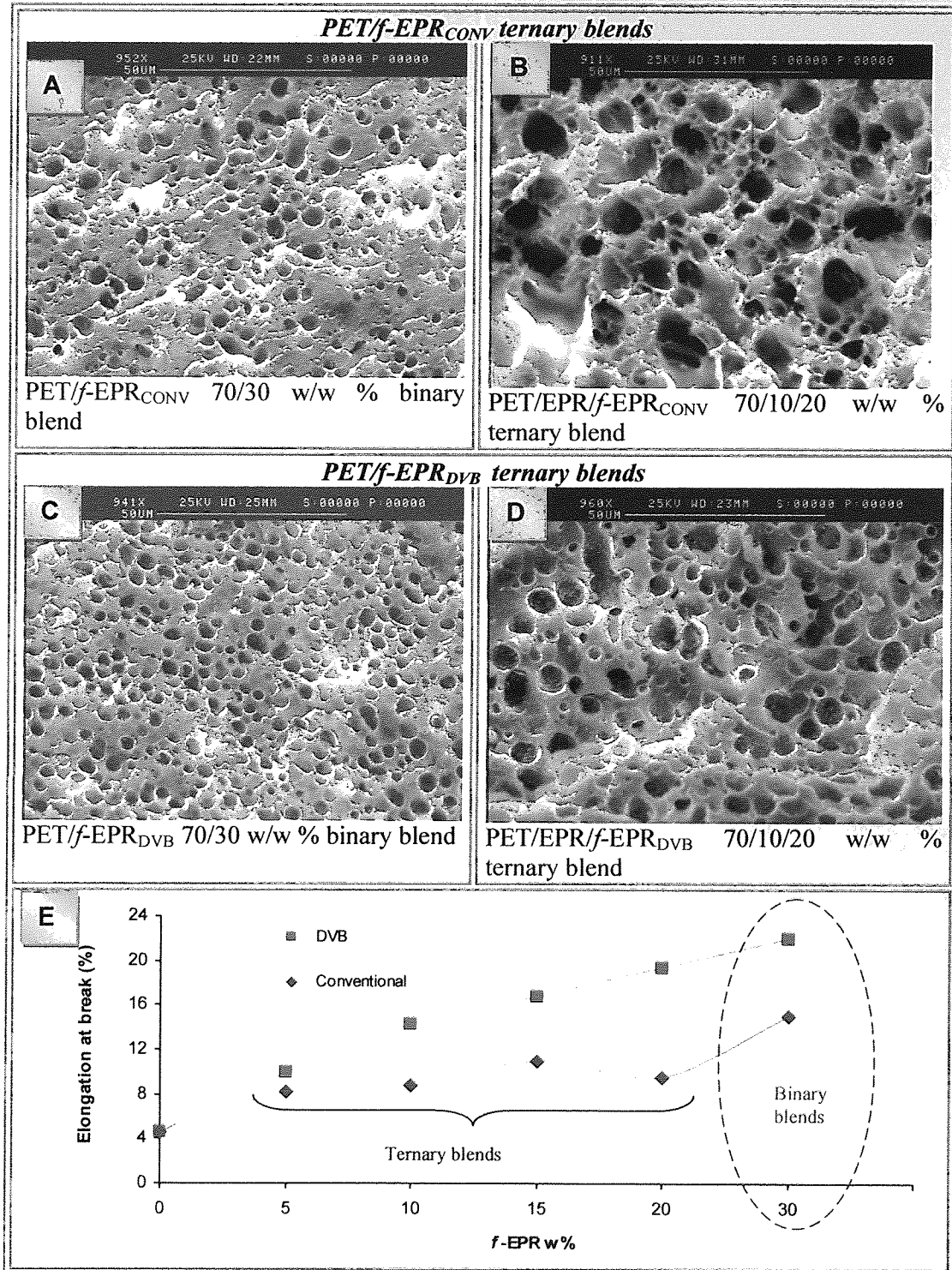


**Figure 5.13.** Comparison between binary PET/*f*-EPR blends and ternary PET/EPR/*f*-EPR blend. Sample of *f*-EPR<sub>DVB</sub>, DG10-(g-GMA=2.3 wt%, MFI=3.7 g/10min), Sample of *f*-EPR<sub>CONV</sub>, G19 (g-GMA=1.7 wt%, MFI=0.9 g/10min).

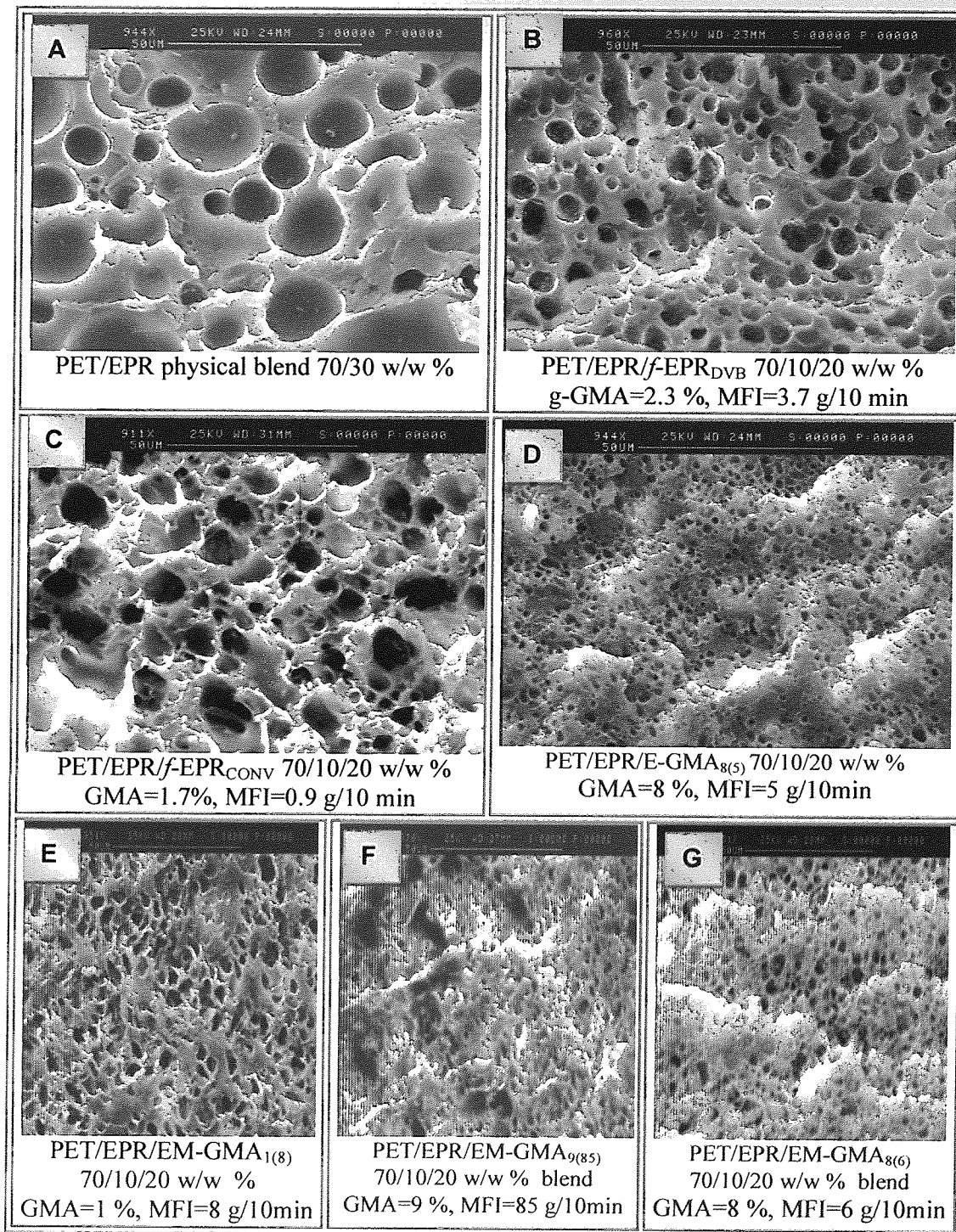


**Figure 5.14:** Morphology of PET/EPR blends compatibilised with different type of compatibilisers.

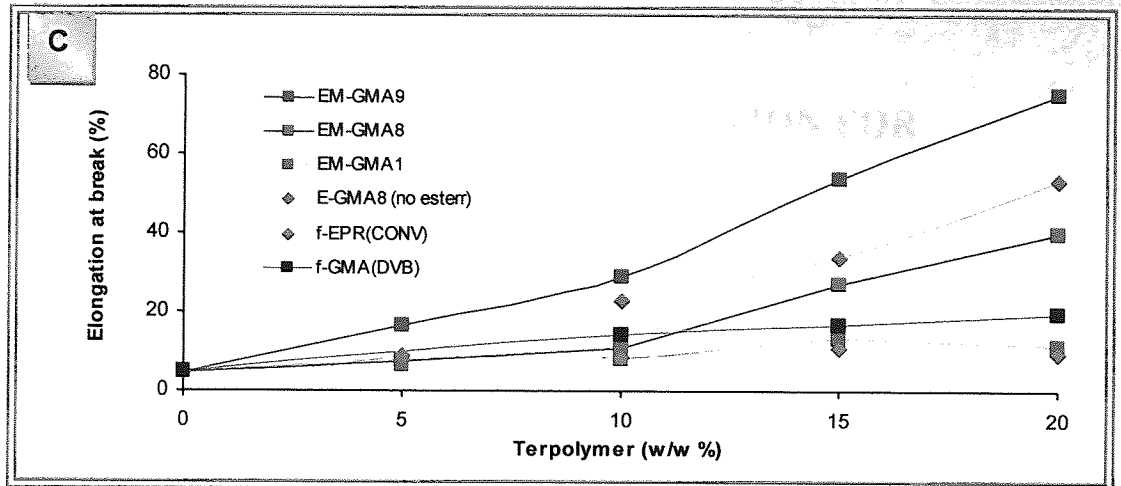


**Figure 5.15.** Tensile properties of ternary PET/EPR blends (PET/Total EPR+compatibiliser 70/30 w/w%) compatibilised with various types of compatibilisers.

## CHAPTER 6

# CONCLUSIONS AND RECOMMENDATION FOR FURTHER WORK

### 6.1 Conclusions

From the results discussed in **Chapters 3 to 5**, several conclusions can be made:

- 6.1.1 The highly reactive comonomer, divinyl benzene (DVB), used in the melt free radical grafting of glycidyl methacrylate (GMA) on EPR (with E:P of 8:2) was shown to give a much higher level of grafting (up to 5 wt%) compared to a similar but conventional system (in the absence of DVB). Another advantages in using the comonomer is that the high GMA grafting level can be achieved at a much lower peroxide concentration compared to the conventional system, thus not contributing to polymer degradation reactions. Further, the amount of polyGMA formed in the EPR-g-GMA<sub>DVB</sub> polymer was found to be negligible (**Figure 3.33, p. 148,**) and this contrasts with the conventional grafting system that gave rise to polyGMA as a consequence of the need to use a much higher peroxide concentration to achieve an increased level of grafting though even under these condition, the overall GMA grafting efficiency remained at a low level and was accompanied by higher levels of polyGMA formation, (**Figure 3.3, p. 148**)
- 6.1.2 The chemical composition of the reaction system had a major effect on the grafting reaction. The use of high GMA/DVB ratio resulted in a significant increase in the extent of grafting, for example a GMA/DVB ratio of 7/3 w/w was shown to give much higher grafting level compared to that of 9/1 w/w ratio (**Figure 3.28, p. 143**). However, this was followed by a decrease in the MFI values of the *f*-EPR<sub>DVB</sub>, (**Figure 3.34, p. 149**) reflecting an increase in branching and crosslinking. The effect of GMA concentration in the presence of DVB gave rise to an increase in the extent of grafting level with only a very small amount of polyGMA formed in the system (**Figure 3.35, p.150**). In contrast, an increase

in the GMA concentration in the conventional system was unfavourable in terms of grafting. Further, in the conventional system, higher GMA concentrations resulted in the formation of a remarkable amount of polyGMA with only a small increase in the extent of the grafting level (**Figure 3.35, p. 150**).

- 6.1.3 The processing conditions had also an important effect on the grafting system. The extent of grafting in the DVB system decreased with increasing the processing temperature. It was found that processing temperature had a great influence on the overall grafting process in both kinetic and thermodynamic aspects. At lower processing temperatures (e.g 170 °C) the grafting level in the DVB system was higher than it was at higher temperatures, e.g at 200 °C (**Figure 3.31, p. 146**). At higher processing temperatures the grafting reaction rate was higher compared to that at lower temperatures, **Figure 3.31, p. 146**).
- 6.1.4 Examining the kinetic of the grafting reactions of DVB and the conventional systems has revealed that the grafting reaction rate in the DVB system was higher compared to the conventional system with the grafting reaction being almost complete in the very early stages of processing (**Figure 3.36, p. 151**), with maximum grafting level achieved in the first 5 minutes. At higher GMA concentration, the rate of the grafting reaction also increased significantly.
- 6.1.5 The microstructure of *f*-EPR was examined using NMR. The graft composition of the conventional *f*-EPR<sub>CONV</sub> (EPR-g-GMA<sub>CONV</sub>) was found to be based on 3 and 4 GMA molecules per graft with similar percentage of the 3 and 4 sequences. The graft distribution across the polymer backbone of the *f*-EPR<sub>CONV</sub> was found to be on average one graft per 636 carbons in the EPR chain (not taking into account the CH<sub>3</sub> groups in the propylene units of EPR). The microstructure for *f*-EPR<sub>DVB</sub> was much more difficult to establish with accuracy due to the complexity of the NMR spectra and the poor solubility of this polymer in all NMR solvents examined even at high temperature. However, it was concluded that for the sample examined which contained high level of g-GMA (of 4.7 wt%), it may contain long (and not short) graft lengths which are



composed of 1 DVB molecule and 14 GMA molecules, but this conclusion has to be treated with caution (Table 3.13, p. 114).

- 6.1.6 The performance of  $f$ -EPR<sub>DVB</sub> having different grafting levels when used as compatibilisers in binary and ternary PET/EPR blends was compared with that of  $f$ -EPR<sub>CONV</sub> systems. It was shown that a blend of PET and  $f$ -EPR<sub>DVB</sub> (70/30 w/w%) containing 2.1 wt% grafted GMA gave the highest elongation at break with finest morphology compared to blends containing higher grafting levels (e.g 3.5 wt%), (Figures 4.17, p. 205 and 4.18, p. 206). Interfacial analysis revealed that the former blend (with 2.1 wt% g-GMA) gave rise to higher extent of interfacial reaction when compared to that determined for the corresponding blend containing 3.5 wt% g-GMA which was also the case when compared with a conventional blend system (containing 1.7 wt% g-GMA), (Figure 4.29, p. 218). The latter conventional blend of PET/ $f$ -EPR<sub>CONV</sub> (70/30 w/w%, blend sample G19) also showed a relatively low elongation at break with coarser morphology, (Figures 4.27, p. 197 and 4.10, p. 198). It was concluded that the reason for the poor blend properties at high GMA grafting level in blends containing of PET/ $f$ -EPR<sub>DVB</sub> was due to higher extent of branching or/and crosslinking that occur in the presence of higher levels of GMA grafting resulting in more difficult dispersion of the rubber phase in the PET matrix. Another reason for the inferior behaviour is the possible unfavourable structure of the GMA grafts (possibly long grafts) when the level of GMA grafting is high as was suggested from the NMR studies, see Chapter 3, Sec 3.3.6, p. 110.
- 6.1.7 Blending PET with EPR-g-GMA<sub>CONV</sub> was found to offer lower extent of compatibilisation at all grafted GMA levels when compared to blends containing  $f$ -EPR<sub>DVB</sub> as judged from their mechanical properties, (Figure 4.18, p. 206 and 4.25, p. 213). This was attributed to the presence of higher level of polyGMA in the conventional blends (Figure 4.27, p. 215). The polyGMA (e.g in 70/30 w/w% PET/ $f$ -EPR<sub>CONV</sub> composition containing 3 % polyGMA) which had adverse effect on the mechanical properties of the blends gave rise also to large domain size resulting in unstable morphology (Figure 4.12D, p. 200). It is concluded that the presence of polyGMA in the blends would compete with the

grafted GMA and react with the carboxylic (-COOH) or hydroxyl (-OH) end groups in PET hence contributing to the observed reduced compatibilisation effect in these blends.

6.1.8 The GMA content in the commercial terpolymers (ethylene methacrylate glycidyl methacrylate, EM-GMA) when examined as compatibilisers for PET/EPR blends had an important role on the level of compatibilisation, at higher GMA content (e.g. 8 wt%), elongation at break and the morphology of the PET/EPR/EM-GMA<sub>8(6)</sub> 70/10/20 w/w% blends was found to be more stable with fine dispersed particles size compared to that of blends containing lower GMA concentration (e.g. 1 wt%), (**Figure 5.1, p. 244**). Low terpolymer viscosity (MFI=85 g/10min) was also shown to give rise to a finer morphology and improved elongation at break (see **Figure 5.4, p. 247**).

6.1.9 Higher compatibilisation effect was found in PET/EPR blends compatibilised with the commercial copolymer ethylene glycidylmethacrylate (E-GMA<sub>8(5)</sub>) was achieved, (**Figure 5.7, p. 259**) as reflected in the observed higher elongation at break when compared to corresponding blends compatibilised with the ester-containing terpolymer EM-GMA<sub>8(6)</sub>. The presence of methacrylate ester groups in the commercial terpolymer EM-GMA (containing similar amount of GMA and same MFI) resulted in low level of compatibilisation due to the possibility of a higher extent of branching and crosslinking resulting from the presence of the ester groups and this would be responsible for the observed lower elongation, and the less favourable morphology observed, (**Figure 5.7, p. 250**). Further, the more bulky structure of the terpolymer compared to the copolymer would give rise to a more difficult migration to the interface, thus lowering the efficiency of compatibilisation. However the morphology of both blends compatibilised with both either the terpolymer or the copolymer were not significantly different, (**Figure 5.7, p. 250**).

6.1.10 Binary blends of PET with *f*-EPR 70/30 w/w % were found to be more highly compatibilised compared to ternary blends of PET/EPR/*f*-EPR. The high compatibilisation achieved in the binary blends is reflected in improved

morphology and mechanical properties, (Figure 5.13, p. 256). This was attributed to the fact that in the binary blends, it is very likely that a higher extent of interfacial reaction may have occurred, as all the rubber phase in this case was functionalised, and this is especially true when the *f*-EPR used was optimised in terms of the level of GMA grafting and its microstructure.

## 6.2 Recommendation for Further Work

- 6.2.1 The use of a highly reactive comonomer, e.g DVB, in the presence of a very small concentration of an initiator was found to give a remarkable improvement in the grafting level of GMA onto ethylene-propylene rubber (EPR) with minimum extent of polyGMA formation, the major side reaction product. It will be useful to determine the generality of this concept by investigating the effectiveness of this highly reactive comonomer on the grafting of other functional monomers and its application in other polyolefins in terms of examining their grafting efficiency and the nature of the competing side reactions.
- 6.2.2 It would be important to carry out the GMA-DVB grafting process in a large scale twin screw extruder (continuous process semi-commercial scale) in order to examine, firstly, whether the GMA-DVB grafting process can be reproduced in the extruder to give a reaction system that has similar characteristics to that obtained in this work using a smaller scale batch mixer, and secondly, to see if one can actually achieve an improved grafting system in the continuous process.
- 6.2.3 It is important to have a better understanding of the effect of the microstructure of EPR-g-GMA<sub>DVB</sub> on the *in situ* interfacial reaction which influences the compatibilisation of polymer blends. A further investigation of the microstructure of the grafted GMA on EPR functionalised in the presence of DVB need to be conducted.

## References

1. S.Al-Malaika, *Reactive Modifiers of Polymer*. 1997, London: Blackie Academic and Professional
2. Tang Lee Han, R.N. Kumar, H.D. Rozman, Mohd. Azemi Md. Noor, *GMA Grafted Sago Starch as a Reactive Component in Ultra Violet Radiation Curable Coatings*. *Carbohydrate Polymers*, 2003. **54**: p. 509–516.
3. S. Al-Malaika, N. Suharty., *Reactive Processing of Polymers: Mechanisms of Grafting Reactions of Functional Antioxidants of Polyolefins in the Presence of a Coagent*. *Polymer Degradation and Stability*, 1995. **49**: p. 77-89.
4. Premamoy Ghosh and Debaprasad Dev, *Processing of Polyethylene: Effect of Peroxide-Induced Graft Copolymerisation of some Acrylic Monomers on Polymer Structure Melt Rheology and Relaxation Behaviour*. *Polymer*, 1998. **34**: p. 1539.
5. C.-H. Kim, K.Y. Cho, J.-K. Park, *Grafting of Glycidyl Methacrylate onto Polycaprolactone: Preparation and Characterization*. *Polymer*, 2001. **42**: p. 5135-5142.
6. C. S. Pande, N. Gupta, *Functionalization of Crosslinked Polystyrene by Radiation-Induced Grafting*. *Journal of Applied Polymer Science*, 1996. **60**: p. 1601-1607.
7. Andres E. Ciolino, M.D.F., Enrique M. Valles, *Melt Grafting of N-Carbamyl Maleamic Acid onto Linear Low-Density Polyethylene*. *Journal of Polymer Science: Part A: Polymer Chemistry*, 2002. **40**: p. 3950-3958.
8. Thomas Browne, M.C., Yoram Cohen, *Graft Polymerization of Vinyl Acetate onto Silica*. *Journal of Applied Polymer Science*, 1992. **44**: p. 671-677.
9. S. Al-Malaika, W. Kong, *Reactive Processing of Polymers: Melt Grafting of Glycidyl Methacrylate on Ethylene Propylene Copolymer in the Presence of a Coagent*. *Journal of Applied Polymer Science*, 2001. **79**: p. 1401–1415.
10. G-H, Hu., J.-J. Flat, M. Lamba, *Chapter 1: Free Radical Grafting of Monomer onto Polymers by Reactive Extrusion: Principles and Applications*. *Reactive Modifiers for Polymers*, ed. S. Al-Malaika. 1997, London: Blackie Academic and Professional.
11. A.R. Bhattacharyya, A.K.Ghosh., A. Misra, *Reactivity Compatibilised Polymer Blends. A Case Study on PA-6/EVA*. *Polym*, 2001. **42**: p. 9143-9154.
12. A.N. Wilkinson, L.Laugel., M.L. Clemens, V.M. Harding, M. Marin, *Phase Structure in Polypropylene/PA6/SEBS Blends*. *Polym*, 1999. **40**: p. 4971-4975.
13. Amiya R. Tripathy, Wenjie Chen, Stephen N. Kukureka, William J. MacKnight, *Novel Poly(butylene terephthalate)/poly(vinyl butyral) Blends Prepared by In Situ Polymerization of Cyclic Poly(butylene terephthalate) Oligomers*. *Polymer*, 2003. **44**: p. 1835–1842.

14. M. Van. Duin, R.J.M. Borggreve, *Chapter 3, Blends of Polyamides and Maleic-Anhydride-Containing Polymers: Interfacial Chemistry and Properties*, in *Reactive Modifiers for polymer*, S. Al-Malaika, Editor. 1997, Blackie Academic and Profesional: London.
15. C.P. O'Brien, J.K.R., M.D. Dadmun, *Reactive Processing with Difunctional Oligomers to Compatibilize Polymer Blends*. *European Polymer Journal*, 2004. **40**: p. 1515-1523.
16. Li-Feng Chen, Betty Wong, W. E. Baker, *Melt Grafting of Glycidyl Methacrylate Onto Polypropylene and Reactive Compatibilization of Rubber Toughened Polypropylene*. *Polymer Engineering and Science*, 1996. **36**: p. 1594.
17. Herve Catier, G.-H.Hu., *Styrene-Assisted Melt Free Radical Grafting of Glycidyl Methacrylate onto Propylene*. *J. Polym. Sci. Part A: Polymer Chemistry*, 1998. **36**: p. 1053.
18. Yi-Jun Sun, G.-H.Hu., and Morand Lambla, *Free Radical Grafting of Glycidyl Methacrylate onto Propylene in a Co-Rotating Twin Screw Extruder*. *J. Appl. Polym. Sci.*, 1995. **57**: p. 1043.
19. Pravitra Chanranupap, S.N., Bhattacharya,, *Reactive Processing of Polyolefins with MAH and GMA in the Presence of Various Additives*. *J. Appl. Polym. Sci.*, 2000. **78**: p. 2405.
20. G. Hu, H. Cartier, *Nondegradative Melt Functionalization of Polypropylene with Glycidyl Methacrylate*. *J. Appl. Polym. Sci*, 1998. **67**: p. 1957.
21. D. C, Clark, W. E. Baker, R. A. Whitney, *Peroxide-Initiated Comonomer Grafting of Styrene and Maleic Anhydride onto Polyethylene: Effect of Polyethylene Microstructure*. *J. Appl. Polym. Sci*, 2001. **79**: p. 96.
22. Norman G. Gaylord, M.M., and Rajendra Metha, *Degradation and Cross-linking of Ethylene-Propylene Copolymer Rubber on Reaction with Maleic Anhydride and/or Peroxide*. *J. Appl. Polym. Sci*, 1987. **33**: p. 2549.
23. S.H.P. Bettini and J.A.M. Agnelli., *Grafting of Maleic Anhydride onto Polypylene by Reactive Processing. II. Effect of Rotor Speed and Reaction Time*. *J. Appl. Polym. Sci*, 1999. **74**: p. 256.
24. U. Anttila, C.V., J. Seppala, *Functionalization of Polyolefins and Elastomers with and Oxazoline Compound*. *J. Appl. Polym. Sci*, 1999. **72**: p. 877
25. Xiaomin Zhang, Z.Y., Lixia, Jinghua Yin, *Grafting of Glycidyl Methacrylate onto Ethylene-Propylene Copolymer: Preparation and Characterization*. *Journal of Applied Polymer Science*, 1996. **61**: p. 2253-2257.
26. Qian Wei, D.C., Elena Galoppini, Mariano Pracella, *Functionalization of LDPE by Melt Grafting with Glycidyl Methacrylate and Reactive Blending with Polyamide-6*. *Macromolecular Chemistry and Physics*, 2003. **204**: p. 1123-1133.

27. Chen-Ming Chen, T.-E.H., Mark O. Liu, *Preparation of Epoxy-Modified Polyethylene by Graft Extrusion and its Applications to Polyphenylene Sulfide Alloys as a Compatibilizer*. *Polymers*, 2008. **68**: p. 1307-1313.
28. S. Al-Malaika, W.Kong, *Reactive Processing of Polymers: Effect of in situ Compatibilisation on Characteristics of Blends of Polyethylene Terephthalate and Ethylene-Propylene Rubber*. *Polymer*, 2005. **46**: p. 209–228.
29. G. Hu, H.C., *Styrene-assisted Melted Free Radical Grafting of Glycidyl Methacrylate onto Polypropylene Rubber*. *J Appl Polym Sci*, 1999. **71**: p. 125.
30. Robert R. Gallucci, Rose C. Going, *Preparation and Reactions of Epoxy Modified Polyethylene*. *J. Appl. Polym. Sci*, 1982. **27**: p. 425.
31. Herve' Cartier, G.-H.-Hu., *Styrene-Assisted Free Radical Grafting of Glycidyl Methacrylate onto Polyethylene in the Melt*. *Journal of Polymer Science: Part A: Polymer Chemistry*, 1998. **36**: p. 2763–2774.
32. B. Wong, W. E. Baker, *Melt Rheology of Grafting Modified Polypropylene*. *Polymer*, 1997. **38**: p. 2781.
33. J.G. Martinez, R. Benavides, C. Guerrero, B.E. Reyes, *UV Sensitisation of Polyethylenes for Grafting of Maleic Anhydride*. *Polymer Degradation and Stability*, 2004. **86**: p. 129-134.
34. Yuncan Zhang, J.C., Huilin Li, *Functionalization of Polyolefins with Maleic Anhydride in Melt State Through Ultrasonic Initiation*. *Polymer*, 2006. **47**: p. 4750–4759.
35. Lianchao Zhu, G.T., Qiang Shi, Chuanlun Cai, Jinghua Yin, *Neodymium Oxide Co-Catalyzed Melt Free Radical Grafting of Maleic Anhydride onto Co-Polypropylene by Reactive Extrusion*. *Reactive & Functional Polymers*, 2006. **66**: p. 984–992.
36. M. Sclavons, M. Laurent, J. Devaux, V. Carlier, *Maleic Anhydride-Grafted Polypropylene: FTIR Study of a Model Polymer Grafted by Ene-Reaction*. *Polymer*, 2005. **46**: p. 8062–8067.
37. Guilherme M.O. Barra, J.S.C., José R. Bertolino, Valdir Soldi, and Alfredo T. Nunes Pires, *Maleic Anhydride Grafting on EPDM: Qualitative and Quantitative Determination*. *J. Braz. Chem. Soc*, 1999. **10**: p. 31-34.
38. A. J. Oostenbrink and R. J. Gaymans, *Maleic Anhydride Grafting on EPDM Rubber in the Melt*. *Polymer*, 1992. **33**: p. 3086-3088.
39. J. Piglowski, I.G., M. Wlazlak, *Oxazoline-Functionalized Hydrogenated Nitrile Rubber as Impact Modifier for Polyamide-6*. *Polymer*, 2000. **41**: p. 3671–3681.
40. T. L. Dimitrova, C. Colletti, F. P. La Mantia, *Melt Free Radical Grafting of an Oxazoline Compound onto HDPE and Its Use as Compatibilizer in PET/HDPE Blends*. *Bulg. J. Phys. ,* 2005. **32**: p. 214–219.

41. Amar Zerroukhi, A.A., Alain Arsac, Nathalie Mignard, Bogdan Marculescu, *Synthesis of A New Oxazoline Monomer and Free Radical Grafting of This Monomer onto ABS*. Polymer Bulletin, 1999. **42**: p. 535-541.
42. S. Lee, O. O. Park, *Preparation of Poly(butylene terephthalate)/Oxazoline Containing Polystyrene Graft Copolymer Through Melt Blending and Their Application as a Compatibiliser in Polycarbonate/Polystyrene Blend*. Polymer, 2001. **42**: p. 6661-6668.
43. N. C. Beck Tan, S.-K. Tai, R. M. Briber, *Morphology Control and Interfacial Reinforcement in Reactive Polystyrene/Amorphous Polyamide Blends*. Polymer, 1996. **37**: p. 3509.
44. Jeziorska, R., *Studies on Reactive Compatibilisation of Polyamide 6/poly(butylene terephthalate) Blends by Low Molecular Weight bis-Oxazoline*. Polymer Degradation and Stability, 2005. **90**: p. 224-233.
45. Tommi Vainio, C.-H.H., Morand Lambla and Jukka V. Seppala, *Functionalized Polypropylene Prepared by Melt Free Radical Grafting of Low Volatile Oxazoline and Its Potential in Compatibilization of PP/PBT Blends*. Journal of Applied Polymer Science, 1996. **61**: p. 843-852.
46. Moad, G., *The synthesis of polyolefin Graft Copolymers by Reactive Extrusion*. Prog. Polym. Sci., 1999. **24**: p. 81-142.
47. Y.X Pang D.M. Jia, H.J. Hu, D.J. Hourston, M. Song, *Effects of a Compatibilizing Agent on the Morphology, Interface and Mechanical Behaviour of Polypropylene/Poly(ethylene terephthalate) Blends*. Polymer, 2000. **41**: p. 357.
48. Xanthos, M., *Chapter 2, Reactive Extrusion, Principle and Practise*. Eds by M. Xanthos. . 1992
49. S. S. Pesetskii, B. Jurkowski, O. A. Makarenko, *Free Radical Grafting of Itaconic Acid and Glycidyl Methacrylate onto PP Initiated by Organic Peroxides*. Journal of Applied Polymer Science, 2002. **86**: p. 64-72.
50. A.H. Hogt, J. Meijer and J. Jelenic, *Chapter 2: Modification of Polypropylene by Organic Peroxides*. Reactive Modifiers for Polymer, ed. S. Al-Malaika. 1997, London: Blackie Academic and Professional.
51. S. Al-Malaika, W.Kong, *Reactive Processing of Polymers: Functionalisation of Ethylene Propylene Diene Terpolymer (EPDM) in the Presence and Absence of a Co-Agent and Effect of Functionalised EPDM on Compatibilisation of Poly(Ethylene Terephthalate)/EPDM Blends*. Polymer Degradation and Stability, 2005. **90**: p. 197-210.
52. Sylvain Augier, S.C., Tania Gagnoli, Elisa Passaglia, Jean-Laurent Pradel, Jean-Jacques Flat, *Coagent Assisted Polypropylene Radical Functionalization: Monomer Grafting Modulation and Molecular Weight Conservation*. Polymer, 2006. **47**: p. 5243-5252.

53. Eddiyanto, *Functionalisation of Polymers: Reactive Processing, Structure and Performance Characteristics*, in *Ph.D Thesis, Polymer Processing and Performance Unit, School of Engineering and Applied Science, Aston University: 2007.*
54. Isabelle Pesneau, Michel F. Champagne, Michel A. Huneaul, Huneaul, *Glycidyl Methacrylate-Grafted Linear Low-Density Polyethylene Fabrication and Application for Polyester/Polyethylene Bonding*. *Journal of Applied Polymer Science*, 2004. **91**: p. 3180-3191.
55. Yongkang Pan, J.R., Dafei Zhou, *Solid-Phase Grafting of Glycidyl Methacrylate onto Polypropylene*, in *J. Appl. Polym. Sci.* 1997. p. 1905.
56. T. Vainio, G. H. Hu, M. Lambla, and J. Seppala, Morand Lambla and Jukka V, *Functionalized Polypropylene Prepared by Melt Free Radical Grafting of Low Volatile Oxazoline and Its Potential in Compatibilization of PP/PBT Blends*. *Journal of Applied Polymer Science*, 1996. **61**: p. 843-852
57. V. M. Hoo, R. A. Whitney, W. E. Baker, *Free Radical Grafting of Co-monomer Systems onto an Ester-containing Polymer*. *Polymer*, 2000. **41**: p. 4367-4371.
58. Abhijit. Jha, Anil K. Bhowmick., *Thermoplastic Blends of Poly(ethylene terephthalate) and Acrylate Rubber: I. Influence of Interaction on Dynamic Mechanical and Tensile Properties*,. *Polymer*, 1997. **38**: p. 4337.
59. Kowalski, R.C., *Chapter 1, Reactive Extrusion, Principle and Practice*, Eds by M. Xanthos. . 1992.
60. R. Scaffaro, L. Botta, F.P. La Mantia, M. Gleria, R. Bertani, F. Samperi, G. Scaltro, *Effect of adding new Phosphazene Compounds to Poly(Butylene Terephthalate)/Polyamide Blends. II: Effect of Different Polyamides on the Properties of Extruded Samples*. *Polymer Degradation and Stability*, 2006. **91** p. 2265-2274.
61. Cristiane Reis Martins, Marco-Aurelio De Paoli, *Antistatic Thermoplastic Blend of Polyaniline and Polystyrene Prepared in a Double-Screw Extruder*. *European Polymer Journal*, 2005. **41**: p. 2867-2873.
62. I. Aravind, P. Albert, C. Ranganathaiah, J.V. Kurian, S. Thomas, *Compatibilizing Effect of EPM-g-MA in EPDM/poly(trimethyleneterephthalate) Incompatible Blends*. *Polymer*, 2004. **45**: p. 4925-4937.
63. Bluma G. Soares, Fabricio F. Alves, Marcia G. Oliverira, Ana C. F. Maria de Fatima S. Lopes, *The Compatibilization of SBR/EVA by Mercaptor-modified EVA*. *European Polymer Journal*, 2001. **37**: p. 1577-1585.
64. Jaehyug Cha, James L. White, *Styrene Grafting onto a Polyolefin in an Internal Mixer and a Twin-Screw Extruder: Experiment and Kinetic Model*. *Polymer Engineering and Science*, 2001. **41**: p. 1238.



65. S. J. Kim, B.S. Shin, J.L. Hong, W.J. Cho, and C.S. Ha, *Reactive Compatibilisation of PBT/EVA Blend by Maleic Anhydride*. Polym, 2001. **42**: p. 4073-4080.
66. Youssef, M.H., *Temperature Dependence of the Degree of Compatibility in SBR-NBR Blends by Ultrasonic attenuation measurements: Influence of Unsaturated Polyester Additive*. Polymer, 2001. **42**: p. 10055.
67. S. Filippi, H.Y., L. Minkova, G. Polacco, M. Talarico, *Reactive Compatibilizer Precursors for LDPE/PA6 Blends, 4. Maleic Anhydride and Glycidyl Methacrylate Grafted SEBS*. Macromol. Mater. Eng, 2004. **289**: p. 512-523.
68. Piyada Charoensirisomboon, M.W., *Reactive PSU/PA Blends: Comparison of Material Prepared by Mini-Twin Screw Extruder and Batch Mixer*. Polymer, 2001. **42**: p. 7009.
69. Brown, S.B., *Chapter 5, Polymer Blends Handbook*, L.A. Utracki, Editor. 2002.
70. Halimatudahliana, H. Ismail, M. Nasir, *Morphology Studies of Uncompatibilized and Compatibilized Polystyrene/Polypropylene Blend*. Polymer Testing, 2002. **21**: p. 263-267.
71. Zhong-Ming Li, Wei Yang, Bang-Hu Xie, Kai-Zhi Shen, Rui Huang, Ming-Bo Yang, *Morphology and Tensile Strength Prediction of in situ Microfibrillar Poly(ethylene terephthalate)/Polyethylene Blends Fabricated via Slit-Die Extrusion-Hot Stretching-Quenching*. Macromol. Mater. Eng. , 2004. **289**: p. 349-354.
72. T.L. Dimitrova, F.P. La Mantia, F. Pilati, M. Toselli, A. Valenza, A. Visco, *On the Compatibilization of PET/HDPE Blends Through a New Class of Copolyesters*. Polymer, 2000. **41**: p. 4817-4824.
73. Brown, S.B., *Chapter 4, Reactive Extrusion, Principle and Practise*. Eds by M. Xanthos. 1992.
74. Charrier, J.-M., *Chapter 3: Polymeric Materials and Processing: Plastics, Elastomer and Composites*. 1991, Munich, Vienna, New York: Henser Publishers.
75. Roberto Scaffaro, Francesco P. La Mantia, Loredana Canfora, Giovanni Polacco, Sara Filippi, Pierluigi Magagnini, *Reactive Compatibilization of PA6/LDPE Blends with an Ethylene-Acrylic Acid Copolymer and a Low Molar Mass Bis-Oxazoline*. Polymer, 2003. **44**: p. 6951-6957.
76. H.A.M van Aerta, G.J.M. van Steenpaala, L. Nelissena, P.J. Lemstraa, J. Liskab, C. Baillyc, *Reactive Compatibilization of Blends of Poly(2,6-dimethyl-1,4-phenylene ether) and Poly(butylene terephthalate)*. Polymer, 2001. **42**: p. 2803-2813.
77. C.K Samios, K.G. Gravalos, N.K. Kalfoglou, *In situ Compatibilization of Polyurethane with Poly(ethylene terephthalate)*. Euro. Polymer J., 2000. **36**: p. 937.

78. Nikos K. Kalfoglou, D.S.S., Joannis K. Kallitis, Jean-Claude Lambert and Luc Van der Stappen, *Comparison of Compatibilizer Effectiveness for PET/HDPE Blends*. *Polymer*, 1995. **36**: p. 4453.
79. W. Hale, H. Keskkula, D.R. Paul, *Compatibilization of PBT/ABS Blends by Methyl Methacrylate-Glycidyl Methacrylate-Ethyl Acrylate Terpolymers*. *Polymer*, 1999. **40**: p. 365-377.
80. Christopher W. Macosko, Hyun K. Jeon, Thomas R. Hoyer, *Reactions at Polymer-Polymer Interfaces for Blend Compatibilization*. *Prog. Polym. Sci.*, 2005. **30**: p. 939-947.
81. Vivek M. Thirtha, Richard L. Lehman, Thomas J. Nosker, *Morphological Effects on Glass Transitions in Immiscible Polymer Blends*. *Mater. Res. Soc. Symp. Proc.* Materials Research Society, 2005. **856E**.
82. J.G. Bonnee and P.S. Hope, *Chapter 3: Compatibilisation and Reactive Blending*. *Polymer Blends and Alloys*, ed. M.J. Folkes and P.S. Hope, 1993, London: Blackie Academic and Professional.
83. Jean-Christophe Lepers, B.D.F., *Interfacial Tension Reduction and Coalescence Suppression in Compatibilized Polymers Blends*. *Material, Interfaces, and Electrochemical Phenomena*, 1999. **45**: p. 887-894.
84. N. C. Liu, H. Q. Xie W. E. Baker., *Comparison of the Effectiveness of Different Basic Functional Groups for the Reactive Compatibilisation of Polymer Blends*. *Polymer*, 1993. **34**: p. 4680-4687.
85. Thai Hoang, Tran Trung, Gohyup Yoo, Joong-Hyun Ahn, Wang-Cheol Zin, Won-Jei Cho, and Chang-Sik Ha, *Compatibilization of SAN/EPDM Blends by Grafting EPDM with Methyl methacrylate*. *Bull. Korean Chem. Soc.*, 2001. **22**: p. 1037.
86. D. E. Mouzakis, N. Papke, J. S. Wu. J. Larger-Kocsis, *Fracture Toughness Assessment of Poly(ethylene terephthalate) Blends with Glycidyl Methacrylate Modified Polyolefin Using Essential Work of Fracture Method*. *Journal of Applied Polymer Science*, 2001. **79**: p. 842-852.
87. Arup R. Bhattacharyya, A.K.G., Ashok Misra, K.-J. Eichhorn, *Reactively Compatibilised Polyamide6/ethylene-co-vinyl acetate Blends: Mechanical Properties and Morphology*. *Polymer*, 2005. **46**: p. 1661.
88. Chunc-Jen Wu, Jen-Feng Kuo, Chuh-Yung Chen, Eamor Woo, *Effects of Reactive Functional Groups in the Compatibilizer on Mechanical Properties of Compatibilized Blends*. *Journal of Applied Polymer Science*, 1994. **52**: p. 1695-1706.
89. S.L. Sun, X.Y. Xu, H.D. Yang, H.X. Zhang, *Toughening of Poly(butylene terephthalate) with Epoxy-Functionalized Acrylonitrile-Butadiene-Styrene*. *Polymer*, 2005. **46**: p. 7632-7643.

90. Wendy Loyens, Gabriel Groeninckx., *Ultimate Mechanical Properties of Rubber Toughened Semicrystalline PET at Room Temperature*. *Polymer*, 2002. **43**: p. 5679–5691.
91. Loyens, G. Groeninckx, *Phase Morphology Development in Reactively Compatibilised Polyethylene Terephthalate/Elastomer Blends*. *Macromol. Chem. Phys*, 2002. **203**: p. 1702-1714
92. P. Martin, C. Gallez, J. Devaux, R. Legras, L. Leemans, M. van Gulp, M. van Duin, *Reactive Compatibilization of Blends of Polybutyleneterephthalate with Epoxide-Containing Rubber. The Effect of the Concentrations in Reactive Functions*. *Polymer*, 2003. **44**: p. 5251-5262.
93. P. Martin, C. Maquet, R. Legras, C. Bailly, L. Leemans, M. van Gulp, M. van Duin, *Conjugated Effects of the Compatibilization and the Dynamic Vulcanization on the Phase Inversion Behavior In Poly(Butylene Terephthalate)/Epoxide Containing Rubber Reactive Polymer Blends*. *Polymer*, 2004. **45**: p. 5111–5125.
94. P. Martin, C. Maquet, R. Legras, C. Bailly, L. Leemans, M. van Gulp, M. van Duin, *Particle-In-Particle Morphology in Reactively Compatibilized Poly(Butylene Terephthalate)/Epoxide-Containing Rubber Blends*. *Polymer*, 2004. **45**: p. 3277-3284
95. P. Martin, J. Devaux, R. Legras, M. van Gulp, M. van Duin, *Competitive Reactions During Compatibilization of Blends of Polybutyleneterephthalate with Epoxide-Containing Rubber*. *Polymer*, 2001. **42**: p. 2463-2478
96. Weng Kong,, *Reactive Processing Methods for Functionalisation of Polymers and In-situ Compatibilisation of Poly(ethylene terephthalate)-based Blends*, in *Ph.D Thesis, Polymer Processing and Performance Unit, School of Engineering and Applied Science*. Aston University, Birmingham, 2001.
97. Mariano Pracella, D.C., *Reactive Compatibilisation of Blends of PET and PP Modified by GMA Grafting*. *Macromol. Symp*, 2003. **198**: p. 161-171.
98. Michel F. Champagne, M.A., Huneault, Claudine Roux, Wilfried Peyrel, *Reactive Compatibilization of Polypropylene/Polyethylene Terephthalate Blends*. *Polymer Engineering and Science*, 1999. **39**: p. 976.
99. Qi-Wei Lu, Christopher W. Macosko, *Comparing the compatibility of various functionalized polypropylenes with thermoplastic polyurethane (TPU)*. *Polymer*, 2004. **45**: p. 1981–1991.
100. G. Gordon Cameron, M. Younus Qureshi., *Free Radical Grafting of Monomers to Polydienes. IV. Kinetics and Mechanism of Methyl Methacrylate Grafting to Polybutadiene* *Journal of Polymer Science: Polymer Chemistry Edition*, 1980. **18**: p. 3149-3161.

101. E. Carone Jr, U. Kopcak, M.C. Goncalves, S.P. Nunes, *In situ Compatibilization of Polyamide 6/Natural Rubber Blends with Maleic Anhydride*. Polym, 2000. **41**: p. 5929-5935.
102. M.B. Coltelli, E. Passaglia, and F.Ciardelli, *One-Step Functionalization and Reactive Blending of Polyolefin/Polyamide Mixtures (EPM/PA6)*. Polym, 2006. **47**: p. 85-97.
103. C. Marco, G. Ellis, M.A. Gomez, J.G. Fatou, J.M. Arribas, I. Campoy, and A. Fontecha, *Rheological Properties, Crystallisation, and Morphology of Compatibilised Blends of Isotactic Polypropylene and Polyamide*. J. Appl. Polym. Sci., 1997. **65**: p. 2665-2677
104. J. Roeder, R.V.B. Oliveira, M.C. Goncalves, V. Soldi, A.T.N. Pires, *Polypropylene/Polyamide-6 Blends: Influence of Compatibilizing Agent on Interface Domains*. Polym. Test, 2002. **21**: p. 815-821.
105. C. Jiang, S. Filippi, P. Magagnini, *Reactive Compatibilizer Precursors for LDPE/PA6 Blends. II: Maleic Anhydride Grafted Polyethylenes*. Polym, 2003. **44**: p. 2411-2422.
106. Y.J. Sun, G.H.Hu., and M. Lambla, *In-situ Compatibilisation of Polypropylene and Poly (Butylene Terephthalate) Polymer Blends by One-Step Reactive Extrusion*. Polym, 1996. **37**: p. 4119-4127.
107. X. Xu, J.Q., J. Yin, Y. Gao, X. Zhang, Y. Ding, Y. Liu, Z. Xin, J. Gao, F. Huang, and Z. Song, *Preparation of Fully Cross-linked CNBR/PP-g-GMA and CNBR/PP/PP-g-GMA Thermoplastic Elastomers and Their Morphology, Structure and Properties*. J. Polym. Sci. B: Polym. Phys., 2004. **42**: p. 1042-1052.
108. J.K. Kim and H. Lee, *The Effect of PS-GMA as An In-Situ Compatibilizer on The Morphology and Rheological Properties of The Immiscible PBT/PS Blends*. Polym, 1996. **37**: p. 305-311.
109. S. L. Sun, Z. Y. Tan, X. F. Xu, C. Zhou, Y. H. Ao, H. X. Zhang, *Toughening of Nylon-6 with Epoxy-Functionalized Acrylonitrile-Butadiene-Styrene Copolymer*. J. Polym. Sci. B: Polym. Phys., 2005. **43**: p. 2170-2180.
110. Yong Tang, Y.H., Lei Song, Ruowen Zong, Zhou Gui, Weicheng Fan, *Preparation and Combustion Properties of Flame Retarded Polypropylene Polyamide-6 Alloys*. Polym. Degrad. Stab, 2006. **91**: p. 234-241.
111. X. Zhang, X.L. Li, D. Wang, Z. Yin, and J. Yin, *Morphology, Thermal Behavior, and Mechanical Properties of PA1010/PP and PA1010/PP- g-GMA Blends*. J. Appl. Polym. Sci, 1997. **64**: p. 1489-1498.
112. Qian Wei, D.C., Mariano Pracella, *Reactive Compatibilization of PA6/LDPE Blends with Glycidyl Methacrylate Functionalized Polyolefins*. Macromol. Chem. Phys, 2005. **206**: p. 777-786.

113. G. Gao, J. Wang, J. Yin, X. Yu, R. Ma, X. Tang, Z. Yin, X. Zhang, *Rheological, Thermal, and Morphological Properties of ABS-PA1010 Blends*. J. Appl. Polym. Sci., 1999. **72**: p. 683-688.
114. M.W. Fowler, W.E. Baker, *Rubber Toughening of Polystyrene Through Reactive Blending*. Polym. Eng. Sci., 1988. **28**: p. 1427-1433.
115. T. Vainio, G.H.Hu, M. Lambla, J. Seppala, *Functionalization of Polypropylene with Oxazoline and Reactive Blending of PP with PBT in a Corotating Twin-Screw Extruder*. J. Appl. Polym. Sci, 1997. **63**: p. 883-894.
116. T. Vainio, G.H.Hu., M. Lambla, and J. Seppala, *Functionalised Polypropylene Prepared by Melt Free Radical Grafting of Low Volatile Oxazoline and Its Potential in Compatibilisation of PP/PBT Blends*. J. Appl. Polym. Sci, 1996. **61**: p. 843-852.
117. Xiaodong Liu, Francesco La Mantia, Roberto Scaffaro, *Oxazoline-Containing Compatibilizers for Polyamide/SAN and Polyamide/ABS Blends*. Journal of Applied Polymer Science, 2002. **86**: p. 449-455.
118. W.Y. Su, Y. Wang, K. Mina, R.P. Quirk, *In situ Copolymerization and Compatibilization of Polyester and Polystyrene Blends. I. Synthesis of Functionalized Polystyrenes and the Reactions with Polyester*. Polym, 2001. **42**: p. 5107-5119
119. V. N. Ignatov, C.C., V. Tartari, R. Pippa and M. Scapin, F. Pilati, C. Berti, M.Toselli, M. Fiorini, *PET/PC Blends and Copolymers by One-Step Extrusion: I. Chemical Structure and Physical Properties of 50/50 Blends*. Polym, 1997. **38**: p. 195- 200.
120. Z. Zhang, Y. Xie and D. Ma., *Relationship Between Miscibility and Chemical Structures in Reactive Blending of Poly(bisphenol A carbonate) and Poly(ethylene terephthalate)*. Eur. Polym. J, 2001. **37**: p. 1961-1966.
121. V. N. Ignatov, C.C., V. Tartariti, R. Pippa, F. Pilati, C. Berti, M. Toselli, M. Fiorini, *Reactive Blending of Commercial PET and PC, with Freshly Added Catalysts*. Polymer, 1996. **37**: p. 5883-5887.
122. T.Y. Bae, K.Y. Park, D.H. Kim, K.D. Suh, *Poly (ethylene terephthalate)/Polypropylene Reactive Blends Through Isocyanate Functional Group*. J. Appl. Polym. Sci, 2001. **81**: p. 1056-1062.
123. J.S. Lee, K.Y. Park, D. Yoo, K.D. Suh, *In situ Compatibilising of PET/PS Blends Through Carbamate Functionalised Reactive Copolymers*. J. Polym. Sci. B. Polym. Phys, 2000. **38**: p. 1396-1404.
124. W.C. Jung, K.Y. Park, J.Y. Kim, K.D. Suh, *Evaluation of Isocyanate Functional Groups as a Reactive Group in the Reactive Compatibilizer*. J. Appl. Polym. Sci, 2003. **88**: p. 2622-2629.

125. S.H. Park, J.S. Lee, K.D. Suh, *Low Density Polyethelene with an Isocyanate Functional Group*. J. Mater. Sci, 1998. **33**: p. 5145-5148.
126. G.Hu, Y.S., and M. Lambla, *Effects of Processing Parameters on the in situ Compatibilisation of Polypropylene and Poly (Butylene Terephthalate) Blends by One-Step Reactive Extrusion*. J. Appl. Polym Sci., 1996. **61**: p. 1039-1047.
127. H. Cartier and G.H. Hu, *Compatibilisation of Polypropylene and Poly (Butylene Terephthalate) Blends by Reactive Extrusion, Effect of the Molecular Structure of a Reactive Compatibiliser*. J. Mater. Sci, 2000: p. 1985.
128. M. Pracella and D. Chionna, *Reactive Compatibilisation of Blends of PET and PP Modified by GMA Grafting*. Macromol. Symp, 2003. **198**: p. 161-172.
129. N. Torres, J. J. Robin, B. Boutevin, *Study of Compatibilization of HDPE–PET Blends by Adding Grafted or Statistical Copolymers*. Journal of Applied Polymer Science, Vol. 81, 2377–2386 (2001), 2001. **81**: p. 2377–2386.
130. H.Yang, M.L., W. Liu, C. Sun, J. Liu, *Morphology and Thermal and Mechanical Properties of PBT/HIPS and PBT/HIPS-G-GMA Blends*. J. Appl. Polym. Sci, 2002. **85**: p. 2600-2608.
131. J.K. Kim, S.K., and C.E. Park, *Compatibilisation Mechanism of Polymer Blends with in situ Compatibiliser* Polym, 1997. **38**: p. 2155-2164.
132. C. Vocke, U. Anttila, M. Heino, P. Hietaoja, J. Seppala, *Use of Oxazoline Functionalized Polyolefins and Elastomers as Compatibilizers for Thermoplastic Blends*, . J. Appl. Polym. Sci, 1998. **70**: p. 1923-1930.
133. M. G. Oliveira, A. C. O. Gomes, M. S. M. Almeida, B.G. Soares, *Reactive Compatibilization of NBR/EPDM Blends by the Combination of Mercapto and Oxazoline Groups*. Macromol. Chem. Phys, 2004. **205**: p. 465-475
134. P. Charoensirisomboon, T. Chiba, K. Torikai, H. Saito, T. Ougizawa, T. Inoue, M. Weber, *Morphology-Interface-Toughness Relationship in Polyamide/Polysulfone Blends by Reactive Processing*. Polym, 1999. **40**: p. 6965-6975.
135. L. Pan, T. Chiba, and T. Inoue, *Reactive Blending of Polyamide with Polyethylene: Pull-Out of In Situ-Formed Graft Copolymers*. Polym, 2001. **42**: p. 8825-8831.
136. S. Filippi, L. Minkova, N. Dintcheva, P. Narducci, P. Magagnini, *Comparative Study of Different Maleic Anhydride Grafted Compatibilizer Precursors Towards LDPE/PA6 blends: Morphology and Mechanical Properties* Polym, 2005. **46**: p. 8054-8061.
137. G. Chen, J. Yang, and J. Liu, *Preparation of HIPS/MA Graft Copolymer and its Compatibilisation in HIPS/PA1010 Blends*. J. Appl. Polym. Sci, 1999. **71**: p. 2017-2025.

138. J. Teng, J.U. Otaigbe, E.P. Taylor, Taylor, *Reactive Blending of Functionalized Polypropylene and Polyamide 6: In situ Polymerization and In situ Compatibilization*. Polym. Eng. Sci., 2004. **44**: p. 648-659.
139. H. Li, T.Chiba, N. Higashida, Y. Yang and T. Inoue, *Polymer-polymer Interface in Polypropylene/polyamide Blends by Reactive Processing*. Polym, 1997. **38**: p. 3921-392
140. S. Jose, S. V. Nair, S. Thomas, J. Karger-Kocsis, *Effect of Reactive Compatibilisation on the Phase Morphology and Tensile Properties of PA12/PP Blends*. J. Appl. Polym. Sci, 2006. **99**: p. 2640-2660.
141. F. Ide and A. Hasegawa., *Studies on Polymer Blend of Nylon 6 and PP or Nylon 6 and PPs Using the Reaction of Polymer*. J. Appl. Polym. Sci, 1974. **18**: p. 963-974.
142. M.V.Duin, M.v.Gurp, L. Leemans, M. Walet, M. Aussems, P. Martin, R. Legras, A.V. Machado, J.A Copas, *Interfacial Chemistry and Morphology of In-Situ Compatibilised PA-6 and PBT Based Blends*. Macromol. Symp, 2003. **198**: p. 135-145.
143. J. M. Lusinchi, B. Boutevin, N. Torres, J. J. Robin, *In Situ Compatibilization of HDPE/PET Blends*. J. Appl. Polym. Sci, 2001. **79**: p. 874-880.
144. H. T. Oyama, T. Kitagawa, T. Ougizawa, T. Inoue, M. Weber, *Novel Application of Reactive Blending: Tailoring morphology of PBT/SAN Blends*. Polym, 2004. **45**: p. 1033-1043
145. V. Tanrattanakul, A. Hiltner and E. Baer, W. G. Perkins and F. L. Massey, A. Moet, *Effect of Elastomer Functionality on Toughened PET*. Polym, 1997. **38**: p. 4117-4125.
146. S.J. Kim, C.J. Kang, S.R. Chowdhury, W.J. Cho, C.S. Ha, *Reactive Compatibilization of the Poly(butylene terephthalate) –EVA Blend by Maleic Anhydride. II. Correlations Among Gel Contents, Grafting Yields, and Mechanical Properties* J. Appl. Polym. Sci, 2003. **89**: p. 1305-1310.
147. S. H. Lee, Jung K. Park, J. H. Han and K. S. Suh, *Space Charge Behaviour in Maleic Anhydride Grafted Polyethylene/ethylene–vinyl–Acetate Copolymer Laminates* J. Phys. D: Appl. Phys, 1997. **30**: p. 1-4.
148. S. Balakrishnan, R. Neelakantan, S.N. Jainsankar, *Effect of Functionality Levels and Compatibility of Polycarbonate Blend with Maleic Anhydride Grafted ABS*. J. Appl. Polym. Sci, 1999. **74**: p. 2102-2110.
149. K. H. Yoon, H.W. Lee, O. O. Park, *Properties of Poly(ethylene terephthalate) and Maleic Anhydride-Grafted Polypropylene Blends by Reactive Processing*. J. Appl. Polym. Sci, 1998. **70**: p. 389-395.
150. Y.T. Shieh, T. N. Liao, F.C. Chang, *Reactive Compatibilization of PP/PBT Blends by a Mixture of PP- g-MA and Epoxy Resin*. J. Appl. Polym Sci., 2001. **79**: p. 2272-2285.

151. Z. Wang, X.W., Z. Gui, Y. Hu, W. Fan, *Thermal and Crystallization Behaviour of Silane-Crosslinked Polypropylene*. Polym. Int, 2005. **54**: p. 442-447.
152. Y. Pietrasanta, J.-J.R., N. Torres, B. Boutevin, *Reactive Compatibilization of HDPE/PET Blends by Glycidyl Methacrylate Functionalized Polyolefins*. Macromol. Chem. Phys., 1999. **200**: p. 142-149.
153. N. Papke, J.K.-K., *Thermoplastic Elastomers Based on Compatibilized Poly(ethylene terephthalate) Blends: Effect of Rubber Type and Dynamic Curing*. Polymer, 2001. **42**: p. 1109-1120.
154. N. M. Larocca, E. Hage Jr., L. A. Pessan, *Effect of Reactive Compatibilization on the Properties of Poly(butylene terephthalate)/Acrylonitrile-Ethylene-Propylene-Diene-Styrene Blends*. Journal of Polymer Science: Part B: Polymer Physics, 2005. **43**: p. 1244-1259.
155. K. Wang, J.W., H. Zeng, *Microstructures and Fracture Behavior of Glass Fiber Reinforced PBT/PC/E-GMA Elastomer Blends—1: Microstructures*. Comp. Sci. Tech, 2001. **61**: p. 1529-1538.
156. C.H. Tsai and F.C. Chang., *Polymer Blend of PBT and PP Compatibilised by Ethylene-co-Glycidyl Methacrylate Copolymers*. J. Appl. Polym. Sci, 1996. **61**: p. 321-332.
157. K. Friedrich, M.E., S. Fakirov, O. Evstatiev, M. Ishii, M. Harrass, *Microfibrillar Reinforced Composites from PET/PP Blends: Processing, Morphology and Mechanical Properties*. Composites Science and Technology, 2005. **65**: p. 107-116.
158. J.C. Lepers, B.D. Favis, S.L. Kent, *Interface-Property Relationships in Biaxially Stretched PP-PET Blends*, . Polym, 2000. **41**: p. 1937-1946.
159. M. Pracella, D.C., A. Pawlak and A. Galeski, *Reactive Mixing of PET and PET/PP Blends with Glycidyl Methacrylate-Modified Styrene-b-(Ethylene-co-Olefin) Block Copolymers*. J. Appl. Polym. Sci, 2005. **98**: p. 2201-2211.
160. G.L. Mantovani, L.B. Canto, E.H. Junior, L.A. Pessan, *Toughening of PBT by ABS, SBS, and HIPS Systems and the Effect of Reactive Functionalised Copolymers*. Macromol. Symp, 2001. **176**: p. 167-180.
161. V. Chiono, S. Filippi, H. Yordanov, L. Minkova and P. Magagnini, *Reactive Compatibilizer Precursors for LDPE/PA6 Blends. III: Ethylene-Glycidyl Methacrylate Copolymer*. Polym, 2003. **44**: p. 2423-2432.
162. E. M. Araujo, E. Hage Jr., A. J. F. Carvalho, *Effect of Compatibilizer in Acrylonitrile-Butadiene-Styrene Toughened Nylon 6 Blends: Ductile-Brittle Transition Temperature*. J. Appl. Polym. Sci, 2003. **90**: p. 2643-2647.
163. E. M. Araujo, E. Hage Jr., A. J. F. Carvalho, *Acrylonitrile-Butadiene-Styrene Toughened Nylon 6: The Influences of Compatibilizer on Morphology and Impact Properties*. J. Appl. Polym. Sci, 2003. **87**: p. 842-847.



164. M. Lazar, L.H., E. Borsig, N. Reichelt, M. Ratzsch, *Course of Degradation and Build-up Reaction in Isotactic Polypropylene During Peroxide Decomposition*. J. Appl. Polym. Sci, 2000. **78**: p. 886-893.
165. E. Borsig, A.F., M. Lazar, *Efficiency of Chemical Cross-Linking of Polypropylene*. J. Macromol. Sci. Chem, 1981. **16**: p. 513-528.
166. T.K. Kang, Y. Kim, W.K. Lee, H.D. Park, W.J. Cho, and C.S. Ha, *Properties of Uncompatibilized and Compatibilized Poly(butylene terephthalate)-LLDPE Blends*. J. Appl. Polym. Sci, 1999. **72**: p. 989-997.
167. M. Pracella, L. Rolla, D. Chionna, A. Galeski, *Compatibilization and Properties of Poly(ethylene terephthalate)/Polyethylene Blends Based on Recycled Materials*. Macromol. Chem. Phys, 2002. **203**: p. 1473-1485.
168. A.N. Wilkinson, M.L. Clemens, V.M. Harding, *The Effects of SEBS-g-Maleic Anhydride Reaction on the Morphology and Properties of Polypropylene/PA6/SEBS Ternary Blends*. Polym, 2004. **45**: p. 5239-5249.
169. B. Ohlsson, H. Hassander, and B. Tornell, *Improved Compatibility Between Polyamide and Polypropylene By The Use of Maleic Anhydride Grafted SEBS*. Polym, 1998. **39**: p. 6705-6714
170. K. Dedecker and G. Groeninckx., *Reactive Compatibilisation of A/(B/C) Polymer Blends Part 1. Investigation of the Phase Morphology Development and Stabilisation*. Polym, 1998. **39**: p. 4985-4992.
171. K. Dedecker and G. Groeninckx *Reactive Compatibilisation of A/(B/C) Polymer Blends Part 2. Analysis of the Phase Inversion Region and the Co-Continuous Phase Morphology*. Polym, 1998. **39**: p. 4993-5000.
172. Y. Ou, Y. Lei, X. Fang and Guisheng Yang, *Maleic Anhydride Grafted Thermoplastic Elastomer as an Interfacial Modifier for Polypropylene/Polyamide 6 Blends*. J. Appl. Polym. Sci, 2004. **91**: p. 1806-1815.
173. A.Kumar and R.K. Gupta, *Chapter 9: Thermodynamics of Polymer Mixtures*. Fundamentals of Polymer. 1998: McGraw-Hill.
174. O. Olabisi, L.M. Robeson and M.T. Shaw, *Chapters 2: Thermodynamic of Polymer-Polymer Miscibility*. Polymer-Polymer Miscibility. 1979, New York: Academic Press.
175. Ultracki, L.A., *Part 1: "Polymer/polymer Miscibility"*, in *Polymer Alloys and Blends and Blends: Thermodynamic and Rheology*,. 1989: p. 2.
176. *PET*, in *Encyclopedia of polymer Science and Technology*. 2007, Wiley Interscience. p. 531.
177. Vegt, A.K.v.d., *Part 1, From polymer to plastics*. 2002.

178. Jean-Michel Charrier, *Polymeric Materials and Processing; Plastics, Elastomer and Composites*. 1991, Munich, Vienna, New York: Hanser Publishers
179. Fried, J.R., *Polymer Science & Technology 2nd Edition*. 2003.
180. Y.S. Hu, V. Prattipati, S. Mehta, D.A. Schiraldi, A. Hiltner, E. Baer, *Improving Gas Barrier of PET by Blending with Aromatic Polyamides*. *Polymer*, 2005. **46**: p. 2685–2698.
181. Susumu Tate, Yhoichi Watanabe, Akira Chiba, *Synthesis of Ultra-High Molecular Weight Poly(ethylene terephthalate) by Swollen-State Polymerization*. *Polymer* 1993 **34**: p. 4974-4977
182. Stearne, J.M.a.W., I. M, *Polymer*, 1969. **4**: p. 1088.
183. S. A. Jabarin, E. A. Lofgren, *Thermal Stability of Polyethylene terephthalate*. Volume 24, Issue 13 , Pages 1056 - 1063, 1984. **24**: p. 1056 - 1063.
184. Francesco P. La Mantia, Michele Vinci, *Recycling poly(ethyleneterephthalate)*. *Polymer Degradation and Stability*, 1994. **45**: p. 121-125.
185. Bronwyn Fox, G.M., Gary van Diepen and Ian Willing, *Characterization of Poly(ethylene terephthalate) and Poly(ethylene terephthalate) Blends*. *Polymer*, 1997. **38**: p. 3035-3043.
186. M. Andrassy, H. J. Mencer, *Molecular Mass Distribution Changes During Processing of Poly(ethylene terephthalate)*. *Polymer Degradation and Stability*, 1993. **41**: p. 77-81.
187. R.K Adams, G.K.H., *Chapter 8, Thermoplastic Elastomers, A Comprehensive Review*, Eds by N. R. Legge, G. Holden, H. E. Schroeder. 1987.
188. P.M. Subramanian, *Poly(ethylene terephthalate) Blends for Permeability Barrier Applications*,. *Polymer. Eng. Sci.*, 1987. **27**: p. 1574.
189. D.R Paul and S. Newman, *Chapter 2: Interfacial Agent ("Compatibilisers") for Polymer Blends*. *Polymer Blends*. Vol. 2. 1978, London: Academic Press.
190. S. Al-Malaika & G. Scott, "Modified Polymers", US Patent 5,382,633 (1995).
191. Ray-Ran, *Product User Manual 5 Series Advanced Melt Flow Systems*.
192. Zhong-Zhen Yu, M.L., Yuchun Oua, Guisheng Yan, *On compatibilization and toughening of a copolyester with a maleated thermoplastic elastomer*. *Polymer*, 2002. **43**: p. 6993–7001.
193. K.H. Yoon, H.W.L., O.O. Park, *Reaction effect on the properties of poly(ethylene terephthalate) and poly(styrene-co-maleic anhydride) blends*. *Polymer*, 2000. **41**: p. 4445–4449.

194. J.F. Ronbinson and K. A. Rubinson, *Comtemporary Chemical Analysis*. 1998: Prentice Hall.
195. Stuart, B., *Polymer Analysis*. 2003.
196. Hu G.-H., C.H., *Styrene-Assisted Melt Free Radical Grafting of Glycidyl Methacrylate onto an Ethylene and Propylene Rubber*. 1999. **71**: p. 125-133.
197. SL Sun, Z.T., MY Zhang, HD Yang and HX Zhang, *Influence of The Degree of Grafting on the Morphology and Mechanical Properties of Blends of Poly(Butylene Terephthalate) and Glycidyl Methacrylate Grafted Poly(Ethylene-Propylene) (EPR)*. *Polym Int*, 2006. **55**: p. 834-842.
198. Herve' Cartier, G.-H.H., *Styrene-Assisted Free Radical Grafting of Glycidyl Methacrylate onto Polyethylene in the Melt*. *J Polym Sci A: Polym Chem*, 1998. **36**: p. 2763-2774
199. N. Papke, J.K.-K., *Determination Methods of the Grafting Yield in Glycidyl Methacrylate-Grafted Ethylene/Propylene/Diene Rubber (EPDM-g-GMA): Correlation Between FTIR and <sup>1</sup>H-NMR Analysis*. *Journal of Applied Polymer Science*, 1999. **74**: p. 2616-2624.
200. Ying Lia, X.-M.X., Bao-Hua Guoa, *Study on Styrene-Assisted Melt Free-Radical Grafting of Maleic Anhydride onto Polypropylene*. *Polymer*, 2001. **42**: p. 3419-3425.
201. N. Torres, J.J.R., B. Boutevin, *Functionalisation of High-Density Polyethylene in the Molten State by Glycidyl Methacrylate Grafting*. *Journal of Applied Polymer Science*, 2001. **81**: p. 581-590.
202. Groninge, R., *Chapter 4, The Extruder as a Polymerisation Reactor for Styrene Based Polymers*, in *Thesis*. 1996.
203. Seong-Heun Cho, J.-B.J., Jee-Hyun Ryu, Kyung-Do Suh, *Preparation of Monodisperse Poly(Divinylbenzene) Macrobeads Via a Drop Breaking and Polymerization Method*. *Colloids and Surfaces A: Physicochem. Eng. Aspects*, 2005. **254**: p. 1-7.
204. A.S. Brar, Gurmeet Singh, Ravi Shankar, *Structural Investigations of Poly(methyl methacrylate) by Two-Dimensional NMR*. *Journal of Molecular Structure*, 2004. **703**: p. 69-81.
205. A.S. Brar, Sunita Hooda, Ashok Kumar Goyal, *Microstructure Determination of 2-Hydroxy Ethyl Methacrylate and Methyl acrylate Copolymers by NMR Spectroscopy*. *Journal of Molecular Structure*, 2007. **828**: p. 25-37.
206. Byung Sun Kim, S.C.K., *Free Radical Grafting of Styrene onto Polyethylene in Intensive Mixer*. *J. Appl. Polym. Sci*, 1998. **69**: p. 1307.
207. Morrison, B., *Organic Chemistry*. 6 ed. 1992, New Jersey: Prentice Hall.

208. Susana Camara, B.C.G., Robert J. Meier, Martin van Duin, Adrian C. Whitwood, *EPR Studies of Peroxide Decomposition, Radical Formation and Reactions Relevant to Crosslinking and Grafting in Polyolefins*. *Polymer*, 2006. **47**: p. 4682-4693.
209. N. C. Liu, H. Q. Xie W. E. Baker, Baker, *Comparison of the Effectiveness of Different Basic Functional Groups for the Reactive Compatibilization of Polymer Blends*. *Polymer*, 1993. **34**: p. 4680-4687.
210. Robbert R. Gallucci, Rose C. Going, *Preparation and Reactions of Epoxy-Modified Polyethylene*. *Journal of Applied Polymer Science*, 1982. **27**: p. 425-437.
211. Sung-Soo Lee, K.-Y.P., Ju-Young Kim, Kyung-Do Suh, *Effect of GMA on Monodisperse Epoxy-Functionalized Polymer Microsphere Particles by Dispersion Copolymerization of Styrene with Glycidyl Methacrylate*. *Journal of Applied Polymer Science*, 2001. **80**: p. 1206-1212.
212. Nobel, A., 2006.
213. Y. Gao, S. Li, Huaming Li, X Wang, *Synthesis and Characterization of Syndiotactic Polystyrene-graft-Poly(glycidyl methacrylate) Copolymer by Atom Transfer Radical Polymerization*. *European Polymer Journal*, 2007. **43**: p. 1258-1266.
214. J.C. Bevington, T.N. Huckerby, *Studies of End-Groups in Polystyrene Using 1H NMR*. *European Polymer Journal*, 2006. **42**: p. 1433-1436.
215. Y. Gao, S.L., Huaming Li, X Wang, *Synthesis of Syndiotactic-Polystyrene-graft-Poly(methyl methacrylate) and Syndiotactic-Polystyrene-graft-Atactic polystyrene by Atom Transfer Radical Polymerization*. *European Polymer Journal*, 2005. **41**: p. 2329-2334
216. G Zheng, C. Pan, *Preparation of Star Polymers Based on Polystyrene or Poly(styrene-*b*-*N*-isopropyl acrylamide) and Divinylbenzene via Reversible Addition-Fragmentation Chain Transfer Polymerization*. *Polymer*, 2005. **46**: p. 2802-2810.
217. V. Schmidt, C. Giacomelli, A. R. Brisson, Redouane Borsali, *Towards an Easy Access to Annexin-A5 Protein Binding Block Copolymer Micelles*. *Materials Science and Engineering C*, 2008. **28** p. 479-488.
218. Armenag H. Dekmejian, Weiqing Weng, Cesar A. Garcia-Franco, Eric J. Markel, *Melt Strength of Blends of Linear Low Density Polyethylene and Comb Polymers*. *Polymer* 2004. **45**: p. 5635-5640.
219. K.L. Fung, Robert K.Y. Li, *Mechanical Properties of Short Glass Fibre Reinforced and Functionalized Rubber-toughened PET Blends*. *Polymer Testing*, 2006. **25**: p. 923-931.

220. Hironori Matsudaa, Bunsow Nagasakab, Tetsuo Asakuraa, *Sequence analysis of poly(ethylene/1,4-cyclohexanedimethylene terephthalate) copolymer using <sup>1</sup>H and <sup>13</sup>C NMR*. *Polymer* 44, 2003: p. 4681–4687.
221. S. Jose, B. Francis, S. Thomas, J. Karger-Kocsis, *Morphology and Mechanical Properties of Polyamide 12/polypropylene Blends in Presence and Absence of Reactive Compatibiliser*. *Polymer*, 2006: p. 1-15.
222. Kostas G. Gravalos, Joannis K. Kallitsis and Nikos K. Kalfoglou, *In situ Compatibilization of Poly(ethylene terephthalate) / Poly (ethylene-co-ethyl acrylate) Blends*. *Polymer* 1995. **36**: p. 1393-1399.
223. Pukanszky, B., *Interfaces and Interphase in Multicomponent Materials: Past, Present, Future*. *Eur Polym J*, 2005. **41**: p. 645-662.
224. M. Mehrabzadeh, K. Hossein Nia., *Impact Modification of Polypropylene by Ethylene Propylene Copolymer-Grafted Maleic Anhydride*. *Journal of Applied Polymer Science*, 1999. **72**: p. 1257-1265.
225. Jin Kon Kim, Hwayong Lee, *The Effect of PS-GMA as an in situ Compatibiliser on the Morphology and Rheology Properties of the Immiscible PBT/PS Blend*. *Polymer* 1996. **37**: p. 305-311.
226. Sara Filippi, H.Y., Liliya Minkova, Giovanni Polacco, Marco Talarico, *Reactive Compatibilizer Precursors for LDPE/PA6 Blends*. *Macromol. Mater. Eng.*, 2004. **289**: p. 512-523.
227. Sanghyo Kim, Jin Kon Kim C. E. Park., *Effect of Molecular Architecture of in-situ Reactive Compatibilizer on the Morphology and Interfacial Activity of an Immiscible Polyolefin/Polystyrene Blend*. *Polymer*, 1997. **38**: p. 1809-1815.
228. O. Moini Jazani, A. Aref Azar., *Blends of Poly(ethylene terephthalate) Bottle Waste with Modified Styrene Butadiene Rubber Through Reactive Mixing*. *Journal of Applied Polymer Science*, 2006. **102**: p. 1615-1623.
229. W.S. Chow, Z.A. Mohd Ishak, J. Karger-Kocsis, A.A. Apostolov, U.S. Ishiaku, *Compatibilizing Effect of Maleated Polypropylene on the Mechanical Properties and Morphology of Injection Molded Polyamide 6/polypropylene/organoclay Nanocomposites*. *Polymer* 2003 **44** p. 7427–7440.
230. Maria-Beatrice Coltelli, E.P., Francesco Ciardelli, *One-Step Functionalization and Reactive Blending of Polyolefin/polyamide Mixtures (EPM/PA6)* *Polymer* 2006 **47**: p. 85–97.
231. Guo-Hua Hu, Yi-Jun Sun, Morand Lambla, *Devolatilazation: A critical Sequential Operation for In Situ Compatibilization Of Immiscible Polymer Blends By One-Step Reactive Extrusion* *Polymer Engineering and Science* 1996. **36**: p. 676-684.

232. E. Borsig, M. van Duin, A.D.G., F. Picchioni, *Long Chain Branching on Linear Polypropylene by Solid State Reactions*. European Polymer Journal, 2008. **44**: p. 200-212.
233. H. K. Jeon, Jin Kon Kim, *Morphology Development with Time for Immiscible Polymer Blends with an In Situ Compatibilizer Under Controlled Shear Conditions*. Polymer, 1998. **39**: p. 6227-6234.
234. Mei-Ling Xue, Y.-L.Y., Hoe H. Chuah, John M. Rhee, Nam Hoon Kim, Joong Hee Lee, *Miscibility and Compatibilization of Poly(trimethylene terephthalate)/Acrylonitrile-Butadiene-Styrene Blends*. European Polymer Journal, 2007. **43**: p. 3826-3837.
235. Xiaodong Xu, J.Q., Jinghua Yin, Ying Gao, Xiaohong Zhang, Yongtao Ding, Yiqun Liu, Zhirong Xin, Jianming Gao, Fan Huang, Zhihai Song, *Preparation of Fully Cross-Linked CNBR/PP-g-GMA and CNBR/PP/PP-g-GMA Thermoplastic Elastomers and Their Morphology, Structure and Properties*. Journal of Polymer Science: Part B: Polymer Physics, 2004. **42**: p. 1042-1052.
236. A.K. Maity, S.F. Xavier, *Rheological Properties of Ethylene-Propylene Block Copolymer and EPDM Rubber Blends using a Torque Rheometer*. European Polymer Journal, 1999. **35**: p. 173-181.
237. Ines Kotter, Wolfgang Grellmann, Thomas Koch, Sabine Seidler, *Morphology-Toughness Correlation of Polypropylene/Ethylene-Propylene Rubber Blends*. Journal of Applied Polymer Science, 2006. **100**: p. 3364-3371.
238. C. A. Orr, J. J. Cernohous, P. Guegan, A. Hirao, H. K. Jeon, C. W. Macosko, *Homogeneous reactive Coupling of Terminally Functional Polymers* Polymers, 2001. **42**: p. 8171-8178.
239. G. E. Schoolenberg, F. Doring, G. Ingenbleek, *Coalescence and Interfacial Tension Measurement for Polymer Melts: Experiments on a PS-PE Model System*. Polymer, 1998. **39**: p. 765-772.
240. Utracki, L.A., *Polymer Alloys and Blends*. 1990, Carl Hanser: New York.
241. Paul, D.R., *Background and Perspective*, in *Polymer Blends*, Eds, D.P.a.S. Newman, Editor. 1978, Academic Press: New York, London.
242. Olagoke Olabisi, Lloyd M. Robeson, Montgomery T. Shaw, *Chapter 4, Polymer-Polymer Miscibility*. 1979, New York: Academic Press.
243. Martin van Duin, Marnix van Gurp, Luc Leemans, Monique Walet, Marcel Aussems, Philippe Martin, Roger Legras, Ana V. Machado, *Interfacial Chemistry and Morphology of In-Situ Compatibilised PA-6 and PBT Based Blends*. Macromol. Symp., 2003. **198**: p. 135-145.

244. G. Bayram, U. Yilmazer, M. Xanthos, *Viscoelastic Properties of Reactive and Non-Reactive Blends of Ethylene-Methyl Acrylate Copolymer with Styrene-Maleic Anhydride Copolymer*. Polymer Engineering and Science, 2001. **41**: p. 262.
245. B. R. Guduri, A. S. Luyt, *Effect of Ethylene Glycidyl Methacrylate Compatibilizer on the Structure and Mechanical Properties of Clay Nanocomposite Modified with Ethylene Vinyl Acetate Copolymer*. J Appl Polym Sci, 2007. **103**: p. 4095-4101.
246. Hong-Sheng Xu, Zhong-Ming Li, Song-Jie Wang, Ming-Bo Yang, *Rheological Behavior of PET/HDPE In Situ Microfibrillar Blends: Influence of Microfibrils' Flexibility*. Journal of Polymer Science: Part B: Polymer Physics, 2007. **45**: p. 1205-1216.
247. Wendy Loyens, Gabriele Groeninckx., *Rubber Toughened Semicrystalline PET: Influence of the Matrix Properties and Test Temperature*. Polymer 2003. **44** p. 123-136